Universidad Autónoma de Madrid

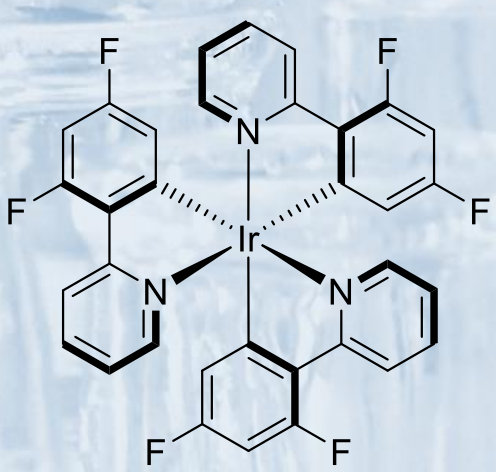

From Molecular Photocatalysis to Organocatalytic Materials

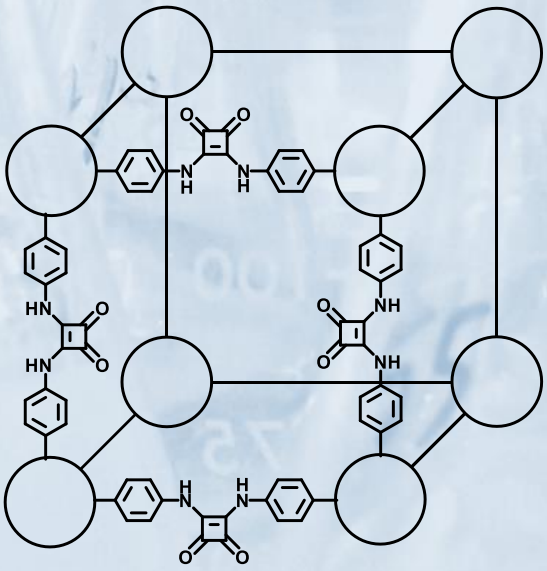

Javier Luis Barrera

Facultad de Ciencias, Departamento de Química Orgánica

Directores:

José Alemán Lara y Rubén Mas Ballesté

Madrid, 2019

Universidad Autónoma de Madrid

Facultad de Ciencias

Departamento de Química Orgánica

Tesis Doctoral

From Molecular Photocatalysis to Organocatalytic Materials

Javier Luis Barrera

Madrid, 2019

La presente tesis ha sido realizada en el Departamento de Química Orgánica de la Universidad Autónoma de Madrid, bajo la supervisión del Dr. José Julián Alemán Lara y del Dr. Rubén Mas Ballesté**.** La financiación de este trabajo ha provenido del Ministerio de Economía y Competitividad (CTQ-2015-64561-R) y del Consejo Europeo de Investigación (ERC-CG, número de contrato 647550).

La tesis se presenta como un compendio de publicaciones. Las publicaciones están distribuidas en dos partes, teniendo cada parte su propia introducción. Además, el documento contiene una introducción general, un resumen de los resultados y unas conclusiones finales comunes a toda la tesis.

El idioma en el que está escrita la tesis es el inglés. Conforme a la normativa, la introducción general y las conclusiones finales están redactadas en español.

Agradecimientos

Ahora que se acerca el final del doctorado, es hora de pararse a reflexionar lo que ha supuesto este periodo, el cual ha sido principio de mi vida laboral y a la vez el final de mi vida como estudiante universitario. Muchas personas han pasado por él, a las cuales me gustaría agradecer su aportación y su apoyo.

Por supuesto a mis padres. Gracias por vuestro apoyo en los estudios desde muy pequeño, ya sea acercándome al cole por la mañana temprano o preguntándome la lección. Vuestra confianza en mí ha sido fundamental para ir avanzando en la vida académica. A mi hermano Enrique y a Edurne, por interesarse siempre en mis avances y a mi hermana Cristina, por su apoyo dentro de casa. A mi abuelo, por transmitirme su experiencia profesional como químico, y a mis dos abuelas.

Creo que es justo continuar esta lista de agradecimientos por aquellas primeras personas que me transmitieron el gusto por la vida académica, el gusto por el simple hecho de aprender y comprender la ciencia y el mundo que nos rodea. Así, encabeza esta lista Javi, mi profesor de Química del Bachillerato, que hizo un trabajo magnífico transmitiendo su asignatura y cuyos apuntes he seguido consultando toda la carrera. Gracias también a esos otros profesores de ciencias del Bachillerato del colegio Patrocinio de San José que sentaron una base muy buena y que me ha sido muy útil durante mi vida académica: Alejandro, Bárbara, Maite, Julián, Mª Luz… No me puedo olvidar de los profesores de asignatura de letras, que sentaron otra base muy importante, las Humanidades, que luego tanto se echa de menos en una carrera de Ciencias: Concha, Fátima, Esther, Jaime, Manuel, Tacha, Nieves…

Y ahora adentrémonos en la vida universitaria. Gracias al grupo de amigos que hicimos durante la carrera. Las risas entre clase y clase, las comidas juntos en la cafetería, las horas encerrados en las peceras resolviendo problemas… era lo que hacía que el día a día en la universidad se hiciera más ameno y daba fuerzas para continuar con los trabajos y estudiar para los exámenes. Aunque el grupo se rompió y a mucho ya no os veo, me acuerdo de vosotros. Gracias a todos: A Laura, por todos los planes que hacía para que nos reuniéramos y por su risa; a Miguel, por poder comentar con él siempre todo tipo de frikadas y datos curiosos; a Guille, porque tan pronto estás teniendo con él una conversación súper profunda y al segundo después estás por los suelos de un ataque de risa; a Roberto, que fue en la gran mayoría de las veces compañero de prácticas y con su calma y simpatía las llevamos muy bien; a Sonia, por todas las conversaciones que compartimos; a Marina, por seguir con nosotros a pesar de su cambio de uni; a Helena, por tantos momentos durante las comidas y por su alegría cuando nos juntábamos. Especialmente a aquellos que después de ser compañeros de carrera nos hemos seguido viendo por la UAM en el mundo del doctorado. A David, por todas aquellas veces que, tanto el grado como en el doctorado, he ido a consultarle alguna duda, y hemos tenido conversaciones de ciencia de calidad; gracias por tu disponibilidad. A Pablo, con el que he pasado muy buenos ratos, que siempre está disponible para enseñarte a hacer una síntesis solvotermal o a intercambiar mil anécdotas, risas y cafés.

A Enrique, por su compañía y amistad en toda mi vida universitaria: grado, máster y doctorado. Eres un ejemplo para mí en cuanto a echarle valor a la vida, perseguir tus sueños, estar a gusto en tu trabajo y trabajar con pasión. Gracias por todo tu apoyo.

A Fernando, compañero desde los 16 años, que son tantas cosas las que tengo que agradecerte que no me caben aquí. Por tu amistad incondicional, por tu confianza en mí, por el apoyo mutuo con las asignaturas de la carrera, por todas las conversaciones de Química que hemos tenido, por todas las veces que he acudido a tu despacho a por ayuda científica o emocional y por todo lo que nos hemos reído juntos y todas las copas en el irlandés.

A dos grandes de la Química Orgánica en la UAM que tuve la suerte de tener de profesores, que la trasmisión de su sabiduría química fue en parte responsable de que acabara haciendo el doctorado: José Luis García Ruano y Juan Carlos Carretero. Gracias también a Ana Martín, que las numerosas visitas que le hice a su despacho para resolver ejercicios fueron claves para remontar la asignatura.

A mis directores de tesis. A José Alemán, le agradezco especialmente que se fijara en mí, que fuese yo a la primera persona que contratase al recibir el proyecto europeo y por todas esas horas en su despacho discutiendo proyectos científicos. A Rubén Mas, por el tiempo que dedicó en mi formación en cálculos computacionales el primer año que le incorporé de director, por confiar es mis valoraciones científicas, y por todas las conversaciones que han ido más allá de la ciencia.

A Alberto Fraile por enseñarme tantas cosas experimentales y por estar disponible ante cualquier duda de Química. A Silvia Cabrera, por su excelente gestión que nos permite llevar a cabo la investigación. A Carmen Maestro, por el interés que muestra en saber cómo estamos y como nos va el doctorado.

A todos mis compañeros de laboratorio. Como este proceso ha sido largo y he vivido un cambio de laboratorio, esta lista es larga.

Primero de todo a Fran. Gracias por enseñarme el primer año a manejarme por el laboratorio, no sé cómo no acabaste harto de que te persiguiera con “Fran, ¿cómo se hace esto?”, “Fran, ¿el vial se pone así?”, “Fran, ayúdame con la columna”. Pero sobre todo gracias por todo el apoyo que me has seguido dando a lo largo de los años. Si algo lamento es que no estuviésemos los últimos años en el mismo laboratorio. Siempre que tenía algún problema en el trabajo, eras al primero al que recurría por tus sabios consejos. Gracias por todas las carcajadas, por compartir tus pensamientos y emociones en cada etapa que has pasado, por tu amistad. Gracias por tu apoyo en los últimos meses con la tesis. Gracias a Sara, la cual ha escuchado también mis movidas y de la cual también he recibido apoyo en la escritura de las tesis.

A Eduardo Rodrigo, uno de los primeros compañeros del L-401, que estando en líneas de investigación diferentes y luego en diferentes grupos de investigación, me demostró desde el primer momento su gran compañerismo. Gracias por tu visita a Regensburg, tu acogida en Mainz, por todas las grandes conversaciones transcendentales o banales que hemos tenido y por el gran apoyo que me has brindado durante la escritura de la tesis, vía Skype o WhatsApp.

A los compañeros con los que llevo desde el principio del doctorado. A Andrea Guerrero, por su simpatía y su súper lucha para que el SFC siempre funcione. Esto también aplicable a Víctor, con el que tengo muchos recuerdos trabajando en el L-305 o echándonos unas risas en las comidas. A Alberto Garrido, por su compañerismo y ayuda incondicional y sobre todo por su gran pasión a la hora de hablar de Química, la cual nos trasmites; gracias por tu revisión de la parte de fotocatálisis de la tesis. A Toni, siempre dispuesto a ayudar o dar apoyo con esa calma que transmite. A Thomas, por ser un ejemplo de perseverancia en el trabajo, de disponibilidad

y por las interesantes charlas sobre Química que hemos tenido. A María Frías, por la confianza que mostró en mí, el apoyo mutuo y por los buenos momentos en el congreso de San Francisco.

A mis compañeros de la sección de Materiales. A Alicia, que tomó el relevo de los MOF-escuaramida, que fue una atenta aprendiz y por su gran sentido del humor. A Alberto López, por su perseverancia y por las conversaciones en el laboratorio de Inorgánica. A Ghazaleh, por la gran confianza que depositó en mí, su capacidad de trabajo y por el compañerismo que nos demostró a todos.

A todos los compañeros que han ido llegando en los últimos años. A Dani, por su gran simpatía y por estar siempre dispuesto a escuchar y hablar de diferentes cosas de la vida. A Jorge, otro transmisor de su gusto por la Química mediante su sentido del humor. A Ana, por su forma metódica de trabajar y sus esfuerzos por sacar una investigación de calidad, y por todo lo que hemos conversado en el laboratorio de la quinta. A Juan y a Noelia, que llegaron con muchas ganas de hacer buenas investigaciones. A Ricardo, que habiendo coincidió con él muy poquito ya me ha mostrado su simpatía.

Guardo con especial cariño recuerdos de los viajes que hice con algunos de vosotros a Copenhague y a Sofía. Gracias también a otras tres chicas, todavía no nombradas, que también hicieron inolvidables estos viajes: Julia, Ana y Sofía.

A Edu, Jorge y Saira, los tres chicos venidos desde México con los que tan bien me los pasé y tanto me reí, tanto fuera como dentro del laboratorio, y que me compartieron muchas cosas de su cultura. A otros muchos que su paso por el laboratorio ha sido más breve pero han dejado su huella. A Lazhar, Houcine, Roberto, Zhara, Fereshte, Fabio, Antonella, Cuauhtémoc… y a muchos otros que no menciono, no por ser menos importantes si no por mi mala memoria. A mis primerísimas compañeras de laboratorio con las que empecé mis andanzas por el L-401: Pamela, Pili, Cristina, Almudena, Diana…

A Raquel, pieza imprescindible en el laboratorio L-305 del módulo 02. Por tu buen trabajo cuidando que no nos falte material, que los reactivos estén correctamente etiquetados y en su armario y que los equipos de análisis estén funcionando correctamente. Hiciste un gran trabajo.

A los alumnos que de un modo u otro he podido supervisar, Víctor Chang y Sandra Bella. Gracias por vuestras ganas de aprender y vuestra confianza en mí.

A todos los “post-doc” que han pasado por el grupo y nos han iluminado de una forma u otra. A Leyre, con la que he coincidido en diferentes etapas de la vida y en todas ellas me ha brindado su experiencia, consejos y muchos buenos momentos. A Wioleta y a Natalia, las primeras que llegaron y que llenaron el grupo con un ambiente multicultural muy guay. A Andrea Gini, por las buenas conversaciones dentro del laboratorio o fuera con una cerveza. A Pipe, por escuchar siempre mis preocupaciones por el futuro y por contarme su experiencia. A Pablo, por su buen humor y sus bromas desde primera hora de la mañana. A Mayka, compañera de mesa, siempre dispuesta a ayudar o a unas risas. A Sara, que habiendo coincidido muy poquito me aportó su apoyo en la recta final de la tesis. A Rafa, por su buen trabajo en proyectos que compartimos y por las discusiones científicas. A Mª Jesús, por su compañía en el Máster y su asesoramiento con la burocracia e impresión de la tesis. A Alicia Moya, por su gran sabiduría química en campos que otros del grupo desconocíamos y por estar siempre dispuesta a tener una buena conversación. A Nacho, con el cual también coincidí en su época de estancia doctoral con nosotros y le agradezco las cosas experimentales que me enseñó.

A la mesa de químicos teóricos (+ inorgánicos), que muchos días me han ayudado a desconectar, a echarme unas risas y a tener conversiones muy interesantes. Aparte de los ya citados, gracias a Arturo, Marcos, Octavio, Paula, Eva, Jorge, Darío, Ransel, Javi…

A Olga García Mancheño, por su acogida para la estancia en Regensburg y permitirme participar en un proyecto que tanto disfruté. Gracias a toda la gente de su grupo por integrarme. A Theresa y a Julia, por transmitir tanta alegría y buen rollo, por su ayuda a adaptarme al laboratorio y por compartir tantos buenos momentos, tanto en Regensburg como en Madrid. Al resto de compañeros del grupo: Dominik, Bastian, Mercedes, Andrea Gini y Qui-Nhi.

A Daniel Maspoch e Inhar Imaz, por la colaboración tan interesante de los MOF-escuaramida y mi breve estancia en Barcelona. A Claudia, por los breves periodos que trabajamos juntos y avanzamos muchísimo en la investigación, y por las muchas birras y conversaciones que nos dio tiempo a compartir.

A tantos amigos de otros muchos sitios, colegio, campamentos, parroquia, etc., que si bien no están directamente relacionados con el doctorado, su apoyo ha sido fundamental estos años y no puedo dejar de mencionarlos: A Juanpy, Frutos, Galo, Juan y Miguel García Valverde, Guillermo Blanco, César, María Trenado, Charlie, Gabriela, Clara, Dani Gonzales, Edu Mandujano, Loreto y Dani, María Santuré y Pablo, Giorgio, Inés, Emilio, Mª Paz…

Y como no podía ser de otra manera a Irene. Son muchas las cosas que te tengo que agradecer, así que centrémonos en lo que tenga que ver con lo académico. Has sido tú la primera en recibir mis alegrías por mis éxitos, como recibir una beca o un proyecto que avanza satisfactoriamente. Pero también has sido tú la primera en recibir mis frustraciones muchos días, en verme decaído porque algo ha salido mal. Las emociones y estados de ánimo que uno tiene durante el doctorado no se quedan en las paredes del laboratorio, si no que se arrastran fuera y has sido tú quien las ha recibido con mucha paciencia. Gracias por todo tu apoyo, cariño y comprensión, has sido mi luz durante esta etapa y me has animado día a día. A mis suegros, a Carmen y a Lucía por su gran acogida. Gracias, Carmen, por ayudarme con el diseño de la portada.

Imágenes de la portada de Kitt_KS (laboratorio) y de ElisaRiva (huella) en Pixabay.

Abreviaturas y acrónimos / Abbreviations and Acronyms

En esta tesis se han empleado las abreviaturas y acrónimos recomendadas en /
In this thesis, the abbreviations and acronyms that have been used are recommended in

"Guidelines for Authors"

(*The Journal of Organic Chemistry*, Standard Abbreviations and Acronyms).

También se han empleado las indicadas a continuación. /
The ones indicated below have also been used.

A	Acceptor
Ad	Adamantyl
BDC	1,4-Benzenedicarboxylic acid
BET	Back electron transfer
bipy	4,4'-Bipyridine
BOX	Bisoxazoline
bpdc	[1,1'-Biphenyl]-4,4'-dicarboxylic acid
bpe	1,2-Bis(4-pyridyl)ethane
BPTA	2,5-Bis(2-propynyloxy)terephthalaldehyde
Cat.	Catalyst
CFL	Compact Fluorescent Lamp
COF	Covalent Organic Framework
CUS	Coordinatively unsaturated metal sites
D	Donor
DA	Donor - Acceptor
DAAn	2,6-Diaminoanthracene
dbda	5,5'-(3,4-Dioxocylcobut-1-ene-1,2-diyl)bis(azanediyl)diisophthalic acid
dFppy	2-(2,4-Difluorophenyl)pyridine
Dha	2,3-Dihydroxyterephthalaldehyde
DIPA	Diisopropylamine

DIPEA	*N*,*N*-Diisopropylethylamine
Dma	2,3-Dimethoxyterephthalaldehyde
DMTP	Dimethoxyterephthaldehyde
DPEphos	Bis[(2-diphenylphosphino)phenyl] ether
dppe	1,2-Bis(diphenylphosphino)ethane
dtbbpy	4,4'-Di-*tert*-butyl-2,2'-dipyridyl
DTBM	Di-*tert*-butylmethoxy
E	Electrophile or Electron withdrawing group
EDG	Electron Donating Group
EnT	Energy Transfer
E_S	Singlet Energy
ESP	Electrostatic Potential
esp	α, α, α', α'-Tetramethyl-1,3-benzenedipropionate
E_T	Triplet Energy
EWG	Electron withdrawing group
Fc	Ferrocene
FFPBA	2-Fluoro-4-formylphenylboronic acid
FPBA	4-Formylphenylboronic acid
FT-IR	Fourier-transform infrared spectroscopy
HAT	Hydrogen atom transfer
Het.	Heterocycle
IBX	2-Iodoxybenzoic acid
INT	Intermediate
IRMOF	Isoreticular MOF
L	Ligand
LA	Lewis acid
L-BCIP	*L*-*N*-*tert*-Butoxycarbonyl-2-(imidazole)-1-pyrrolidine
LC	Ligand centred transition
LED	Light Emitting Diode
LF	Ligand-field transition

LFP	Laser flash photolysis
LG	Leaving group
M	Metal
MLCT	Metal to Ligand Charge Transfer
MOF	Metal-Organic Framework
MS	Mass spectrometry or molecular sieves
o-DCB	*ortho*-Dichlorobenzene
PC	Photocatalyst or Precomplex
Phth	Phthalimide
pin	Pincolato
PMA	Phosphomolybdic acid
PMP	Paramethoxyphenyl
POP	Porous Organic Polymer
ppy	2-Phenylpyridine
Pro	Proline
PTH	10-Phenylphenothiazine
PXRD	Powder X-ray diffraction
PyBOX	Bis(oxazolinyl)pyridine
Q	Quencher
Rh-6G	Rhodamine 6G
SBU	Secondary building unit
SCE	Saturated calomel electrode
SEM	Scanning electron microscopy
Sub	Substrate
TAA	1,3,5,7-Tetraaminoadamantane
TBDPS	*tert*-Butyldiphenylsilyl
t-Bu	*tert*-Butyl
TFPPy	1,3,6,8-Tetrakis(*para*-formylphenyl)pyrene
TGA	Thermogravimetric analysis
TGA-MS	Thermogravimetric analysis – Mass Spectrometry

TMG	Tetramethylguanidine
TPB	Triphenylbenzene
TPDC	[1,1':4',1''-Terphenyl]-4,4''-dicarboxylic acid
Tph	5,10,15,20-Tetrakis(4-aminophenyl)-21*H*,23*H*-porphine
VB	Valence bond

ÍNDICE / INDEX

Part 2: …to Organocatalytic Materials

1. Introducción General

La catálisis química se puede clasificar en dos grandes tipos según la fase en la que están presentes los componentes de la reacción catalizada: catálisis homogénea y catálisis heterogénea. En la catálisis homogénea tanto los reactivos como el catalizador se encuentran en la misma fase, por ejemplo, estando estos componentes presentes como gases o estando disueltos en una misma fase líquida. Por otro lado, la catálisis heterogénea implica el uso de un catalizador en una fase diferente a los reactivos, siendo el ejemplo más típico un catalizador sólido con unos reactivos en fase gas o disueltos en fase líquida.

En la catálisis homogénea, al estar todo presente en la misma fase, suele resultar costosa la purificación de los productos y el catalizador, siendo difícil recuperar el catalizador para reutilizarlo. En cambio, la catálisis heterogénea, al estar el catalizador en una fase diferente al resto de componentes de la reacción, resulta muy fácil recuperarlo (por ejemplo, en el caso de catalizador sólido en fase líquida, se puede recuperar el catalizador por filtración).

La presente tesis doctoral se ha desarrollado en el grupo FRONCAT de la Universidad Autónoma de Madrid, en la cual, siguiendo con la línea de investigación del grupo, se han desarrollado proyectos de catálisis homogénea, concretamente enmarcados dentro la fotocatálisis.

Otra de las líneas de investigación del grupo es la catálisis heterogénea con materiales MOF (Metal-Organic Framework) y COF (Covalent Organic Framework). El objetivo principal de esta línea de investigación es incorporar conceptos y estrategias de catálisis homogénea, como organocatálisis y fotocatálisis, a la catálisis heterogénea con estos materiales. Una segunda parte de esta tesis doctoral se ha dedicado a esta área.

Así, la tesis tiene dos partes, una primera parte de fotocatálisis homogénea y una segunda parte de organocatálisis heterogénea con materiales. El formato de tesis elegido es por compendio de publicaciones. De esta manera, cada una de las dos partes tiene una introducción en la que se exponen conceptos generales del área y se desarrolla el estado en el que se encuentra la investigación y los problemas que se quieren solucionar con la investigación. Después de cada introducción, en cada una de las dos partes se presentan los objetivos, los resúmenes de las publicaciones y las publicaciones en sí que contienen los resultados de las investigaciones llevadas a cabo durante el periodo de doctorado. Cada parte concluye con la sección experimental, directamente tomada del material suplementario de las publicaciones. Puesto que los artículos originales están en inglés, se ha escrito el resto de la tesis en inglés. Cada artículo contiene su sección de conclusiones y además al término de la tesis se recogerán unas conclusiones finales en español.

Fotocatálisis molecular

Tal y como se desarrolla más adelante, los ciclopropanos “dador-aceptor” son anillos de tres miembros que contienen un grupo funcional aceptor de densidad electrónica y un grupo dador de densidad electrónica en posición vecinal directamente unidos al ciclo. Esta disposición les permite experimentar reacciones como las cicloadiciones o las transposiciones, reacciones muy versátiles que permiten construir estructuras cíclicas complejas y que pueden ser

consideradas reacciones de expansión de ciclo, ya que parten de ciclos de tres átomos para llegar a ciclos de cinco átomos.

Si bien es verdad que esta estrategia ha permitido obtener un amplio abanico de carbociclos y heterociclos altamente funcionalizados, también es cierto que tiene ciertas limitaciones. La más notable es que queda impuesto el patrón de sustitución del ciclopropano, debiendo siempre tender, excepto en algunas ocasiones, un grupo funcional dador y otro aceptor en posiciones vecinales, limitando también así el patrón de sustitución de los productos.

Uno de los objetivos que se plantea en esta tesis doctoral es la utilización de la fotocatálisis mediada por luz visible para realizar reacciones de expansión a ciclopropanos que se salgan de la definición "dador-aceptor" y permitan otros patrones de sustitución en sus productos. Puesto que ya han sido desarrollados algunos procesos fotocatalizados para reacciones de cicloadición a ciclopropanos, este trabajo se centrará en reacciones de transposición de ciclopropanos. Además, se buscará desarrollar un método lo más general posible que permita la transposición de ciclopropanos unidos a diferentes tipos de doble enlace.

Este trabajo quedó plasmado en dos publicaciones diferentes que se presentan en esta tesis doctoral. En la primera se recoge la síntesis, mediante un proceso organocatalítico, de los ciclopropanos que servirán como materiales de partida para las reacciones de transposición. En la segunda publicación se expone el trabajo en el que se investiga las reacciones fotocatalizadas de transposición de dichos ciclopropanos.

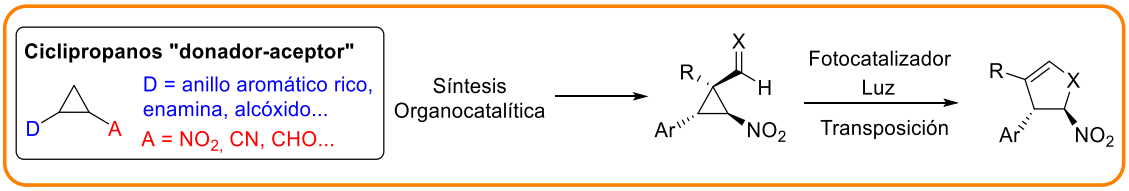

- J. Luis-Barrera, R. Mas-Ballesté, J. Alemán, "One-Pot Asymmetric Synthesis of Cyclopropanes with Quaternary Centers Starting From Bromonitroalkenes under Aminocatalytic Conditions" *ChemPlusChem* **2015**, *80*, 1595-1600.
- J. Luis-Barrera, V. Laina-Martín, T. Rigotti, F. Peccati, X. Solans-Monfort, M. Sodupe, R. Mas-Ballesté, M. Liras, J. Alemán, "Visible-Light Photocatalytic Intramolecular Cyclopropane Ring Expansion" *Angew. Chem. Int. Ed.* **2017**, *56*, 7826 –7830.

También, en esta parte de fotocatálisis homogénea, se plantea la reacción la alilación de Tsuji-Trost, que es un método muy versátil con el cual se pueden construir enlaces C-C, C-N, C-O… y que permite la incorporación de un grupo alilo, con diferentes grados de sustitución, a un nucleófilo. En la gran mayoría de trabajos publicados hasta la fecha es necesario el uso de un catalizador metálico que estabilice el intermedio alílico.

En los casos en los que el producto final puede presentar dos posibles configuraciones en el doble enlace (*Z* y *E*), se observa una fuerte selectividad hacia la obtención del isómero *E* a lo largo de todos los trabajos que han sido publicados hasta la fecha.

Así, existen dos retos a los que se enfrenta la investigación en síntesis orgánica con respecto a las reacciones de alilación a nucleófilos. Uno de ellos es encontrar más métodos que permitan la reacción de alilación sin necesidad de complejos metálicos. El otro es encontrar un método que permita la alilación para la obtención selectiva del isómero *E* o del isómero *Z*. La

propuesta que se hace en esta tesis doctoral para superar estos dos retos al mismo tiempo es el uso de la fotocatálisis.

El trabajo se recoge en la publicación abajo citada, en la cual, como se detallará más adelante, se desarrolla un método de alilación de nucleófilos en el que cambiando los sustituyentes del fotocatalizador y la longitud de onda irradiada se puedo obtener el isómero *E* o el isómero *Z* del producto.

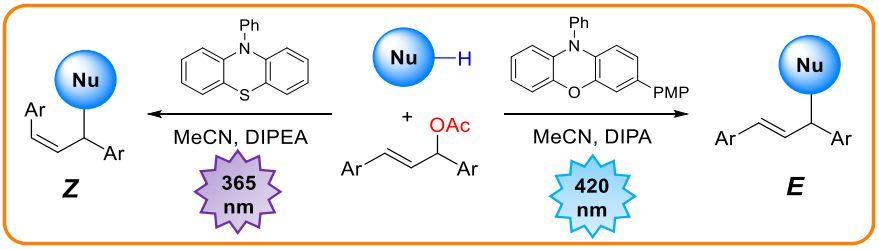

– A. M. Martínez-Gualda, R. Cano, L. Marzo, R. Pérez-Ruiz, J. Luis-Barrera, R. Mas-Ballesté, A. Fraile, V. A. de la Peña O'Shea, J. Alemán, "Chromoselective access to Z- or E- allylated amines and heterocycles by a photocatalytic allylation reaction" *Nat. Commun.* **2019**, *10*, 2634.

Materiales Organocatalíticos

Como se ha mencionado antes, uno de las líneas del grupo de investigación es incorporar conceptos de la organocatálisis clásica homogénea a nuevos materiales para llevarlos al campo de la catálisis heterogénea. Revisando la bibliografía existen dos antecedentes, llevados a cabo por Mirkin y Cohen, en los cuales se ha incorporado el grupo organocatalítico escuaramida a la estructura de materiales MOF. En el MOF llevado a cabo por el grupo de Mirkin, el grupo escuaramida está presente en el 50% de los ligandos del MOF como una ramificación de la estructura del MOF hacia los poros. En cambio, en el MOF realizado por Cohen, la unidad escuaramida es longitudinalmente parte del 100% los ligandos, y por tanto la escuaramida está formando parte de la red central del MOF. Sin embargo, este último MOF tiene la desventaja de que su síntesis es más complicada, debido a que requiere una modificación post-sintética de intercambio de sus centros de metálicos de zinc a cobre. Ambos MOF catalizan eficientemente la alquilación de Friedel-Crafts de indoles.

El propio Cohen hace una interesante reflexión en su publicación en la cual dice que está bien que haya descritos varios MOF con escuaramida con diferentes estructuras, ya que cada uno puedo ser útil en diferentes situaciones. Siguiendo esta línea, nos pareció interesante seguir investigando sobre MOF que contengan escuaramidas, para ampliar el abanico de MOF descritos con este centro catalítico y aportar nuevas ventajas y conceptos a estos materiales. Un posible paso a dar la síntesis de un nuevo MOF en que la escuaramida forme parte de la red principal del material, al igual que el de Cohen, pero que tenga una síntesis más sencilla y no requiera modificaciones post-sintéticas. Además, también consideramos importante el estudio de la acción de estos MOF en otras reacciones, ya que los trabajos de Mirkin y Cohen se centran solo en la Friedel-Crafts. El MOF elegido para servir de base a este propósito es el IRMOF-16.

En la siguiente publicación, la primera de esta tesis doctoral sobre catálisis heterogénea, se describe la síntesis de este MOF análogo al IRMOF-16 con escuaramidas en su estructura y los estudios de catálisis usando dicho MOF en reacciones de apertura de epóxidos.

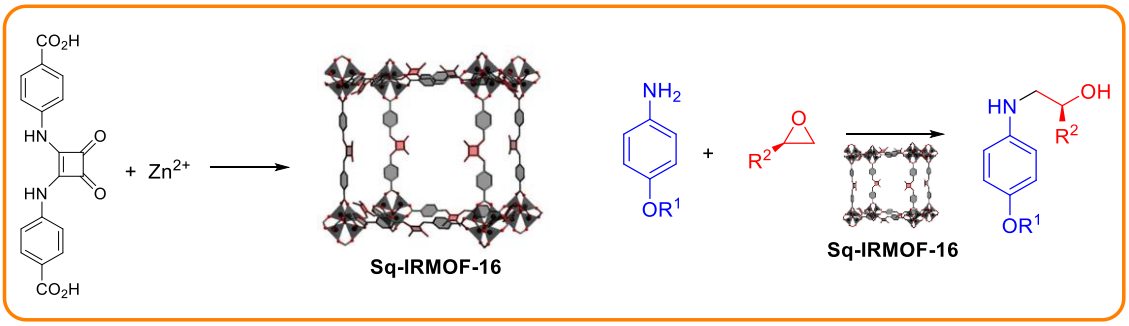

– C. Vignatti, J. Luis-Barrera, V. Guillerm, I. Imaz, R. Mas-Ballesté, J. Alemán, D. Maspoch, "Squaramide-IRMOF-16 Analogue for Catalysis of Solvent-Free, Epoxide Ring-Opening Tandem and Multicomponent Reactions" *ChemCatChem* **2018**, *10*, 3995– 3998.

Como se detallará más adelante, son muchos los trabajos en los que se han incorporado centros organocatalíticos a los materiales COF. En la mayoría de estos trabajos, los grupos funcionales organocatalíticos forman parte de la estructura covalente del COF o están presentes como ramificaciones de la estructura, a la cual están unidos también por enlace covalente. En cambio, existe otra estrategia para funcionalizar los COF, que es la introducción de pequeñas moléculas catalíticas como huéspedes en el interior de los poros del COF y que estas pequeñas moléculas estén ancladas a la estructura del COF por interacciones no covalentes. Esta estrategia ha sido usada para la introducción de pequeños complejos de coordinación o de compuestos inorgánicos. Sin embargo, la introducción de pequeñas moléculas organocatalítcas está por explotar. En vista de esto, nos propusimos como objetivo la funcionalización de un COF mediante interacciones no covalentes con pequeños ácidos y bases orgánicos. Elegimos el COF-300 para llevar a cabo este estudio.

Así, esta tesis doctoral finaliza con la publicación abajo citada, en la cual se describe cómo muestras de COF-300 son funcionalizadas con ácido acético y trietilamina y los estudios de catálisis realizados con estas muestras.

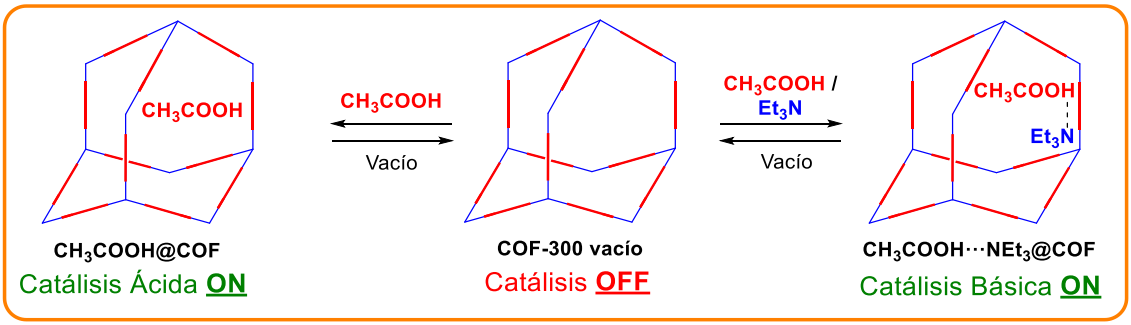

– J. Luis-Barrerra, G. Imani-Shakibaei, J. Heras-Domingo, R. Cano, J. Pérez-Carvajal, I. Imaz, D. Maspoch, X. Solans-Monfort, J. Alemán, R. Mas-Ballesté, "Switching Acidic and Basic Catalysis in a Three-Dimensional Covalent Imine Structure through Supramolecular Functionalization", *J. Catal.* **2019**, enviado.

2. Summary of results

One-Pot Asymmetric Synthesis of Cyclopropanes with Quaternary Centers Starting From Bromonitroalkenes under Aminocatalytic Conditions

J. Luis-Barrera, R. Mas-Ballesté, J. Alemán, *ChemPlusChem* **2015**, *80*, 1595-1600.

The first step of the investigation was to synthesise the chiral formyl cyclopropanes that later will be used as starting materials for the photocatalytic ring expansion reaction.

The cyclopropanes were synthesised through an aminocatalytic one-pot process, consisting in two steps (Scheme 1, top). The first step was the addition of an alkylic aldehyde **1** to a β-Bromo-β-nitrostyrene **2**, catalysed by the Jørgensen-Hayashi catalyst **3**. In this step, the aminocatalyst and the aldehyde condensed and formed an enamine, which undergoes a nucleophilic attack to the bromonitrostyrene by the less hindered face (see **TS-1**), yielding the open intermediate **4** with high enantiomeric excess. In a second step, the base DABCO is added to the reaction media, which deprotonated the α-carbon to the carbonyl group, leading to an intramolecular nucleophilic substitution, obtaining the nitroformylcyclopropanes **5**, with one quaternary centre, which kept the high enantiomeric excess.

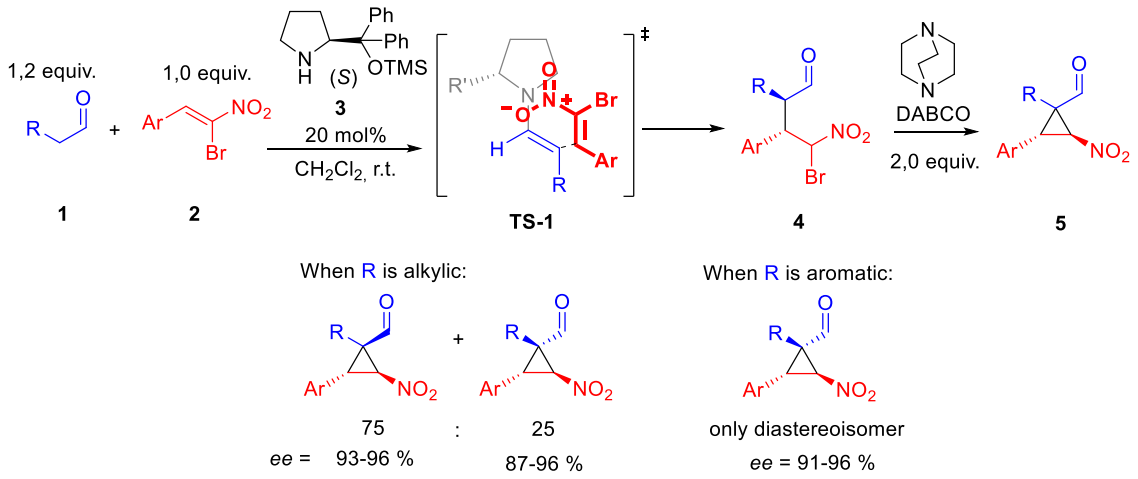

Scheme 1. Enantioselective synthesis of nitrocyclopropanes by organocatalysis.

The scope of the reaction was evaluated, studying how structural changes in the bromonitrostyrene and in the aldehyde affected the reaction. When the group R of the aldehyde **1** was an alkyl group, the cyclopropane product was obtained as a mixture of two diastereoisomers, epimers in the quaternary centre, with a *dr* of 75:25, having both diastereoisomers good enantiomeric excesses, between 87% *ee* and 96% *ee* (Scheme 1, bottom). Curiously, when R group was aromatic, only one diastereoisomer was obtained, with an enantiomeric excess up to 96%. The configuration of this only diastereoisomer, had the same configuration than the minor diastereoisomer in the case of the cyclopropanes with alkyl R group. The use of different bromonitrostyrenes did not affect the reactions, being compatible both electron withdrawing groups and electron donating group in the aromatic ring.

Visible-Light Photocatalytic Intramolecular Cyclopropane Ring Expansion

J. Luis-Barrera, V. Laina-Martín, T. Rigotti, F. Peccati, X. Solans-Monfort, M. Sodupe, R. Mas-Ballesté, M. Liras, J. Alemán, *Angew. Chem. Int. Ed.* **2017**, *56*, 7826 –7830.

Once the nitroformylcyclopropanes **5** had been synthesised, the conditions for the photocatalytic rearrangement were sought. Different photocatalysts were tested, both organic (eosin, rose bengal, metisylacridinium salt…) and inorganic (Ruthenium and Iridium complexes). It was found that only two of them, $Ir(ppy)_3$ and $Ir(dFppy)_3$, were able to carry out the expansion, obtaining dihydrofurane **6** from cyclopropane **5** with good yields. A screening optimization revealed that the optimal conditions for this reaction were the use of 2.5 mol% of the catalyst $Ir(dFppy)_3$ in dichloromethane, irradiating the reaction media with a blue LED (458 nm).

The scope of the reaction was evaluated and all the nitroformylcyclopropanes **5** synthesised in the previous section (and some similar cyclopropanes synthesised with described methods in the literature) were subjected to the reaction conditions, obtaining the dihydrofuranes **5** with good yields (Scheme 2A, top). The reaction was enantiospecific and the enantiomeric excess of the cyclopropanes was kept. The quaternary centre of the cyclopropane **5** was converted in a planar carbon, so although the starting cyclopropane was a mixture of two diastereosiomers (epimers in the quaternary centre), only one diastereoisomer of the dihydrofurane was obtained.

The next step was to explore if this rearrangement could happen with other type of double bonds. Thus, by a Wittig reaction, the carbonyl group of the cyclopropanes was transformed in an alkene group, obtaining nitrovinylcyclopropanes **7**. The conditions for the photocatalytic expansion were carried out in these new cyclopropanes and the reactions took place satisfactorily, obtaining cyclopentenes **8** with good yields and increasing the scope of the reaction (Scheme 2A, bottom).

The reaction mechanism was investigated with both experimental and computational studies. Cyclic voltammetry measurements helped to discard a photoredox mechanism and other observations leaded to conclude that the reaction proceeded through an energy transfer mechanisms of triplet state.

Formylcyclopropanes which did not have a nitro group did not undergo the rearrangement in the reaction conditions. DFT calculations showed that formyl cyclopropanes without the nitro group had a triplet energy much higher in energy than the triplet energy of the photocatalyst, so the energy transfer could not happen. However, the presence of the nitro group stabilizes the triplet, decreasing the triplet energy, making possible the energy transfer.

Finally, the energetic profile was obtained, calculating all the possible intermediates and transitions states, which guided to a mechanism proposal (Scheme 2B). The photocatalyst (PC) is photoexcited to the triplet state. The cyclopropane ($5\text{-}S_0$) reaches the triplet excited state by energy transfer with the photocatalyst ($5\text{-}T_1$). In the triplet state, the cleavage of the three cyclic bonds of the cyclopropane is favourable. The cleavage “a” leads to the open intermediate ($9\text{-}T_1$), which decays to the singlet state and finally cycles in the more stable five-membered ring, the dihydrofurane **6**. The other two possible cleavages, “b” and “c”, of the excited cyclopropane were also calculated, but it was found that the intermediates from these cleavages always evolve to the retro-formation of the cyclopropane **5**.

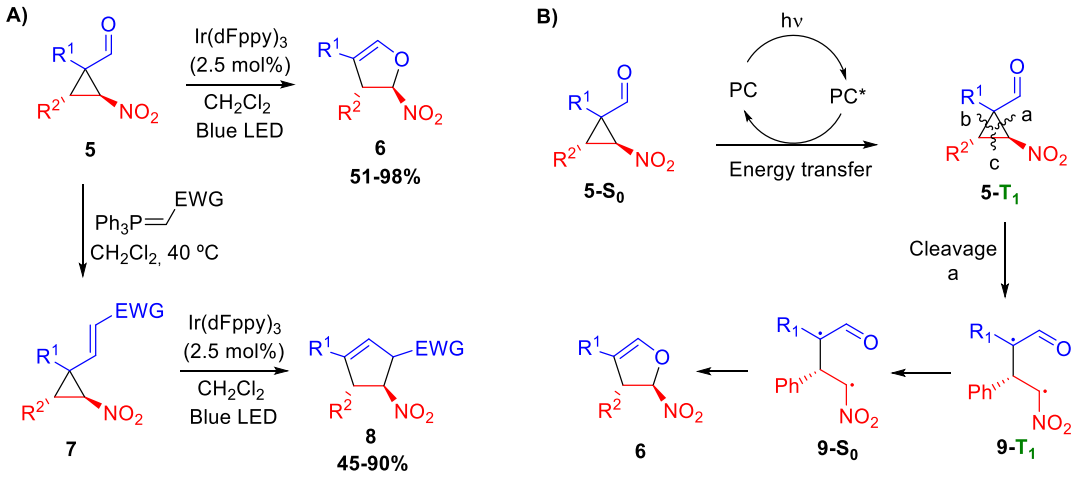

Scheme 2. A) Photocatalytic rearrangement of cyclopropanes. **B**) Mechanism of the reaction.

Chromoselective access to *Z*- or *E*- allylated amines and heterocycles by a photocatalytic allylation reaction

A. M. Martínez-Gualda, R. Cano, L. Marzo, R. Pérez-Ruiz, J. Luis-Barrera, R. Mas-Ballesté, A. Fraile, V. A. de la Peña O'Shea, J. Alemán, *Nat. Commun.* **2019**, *10*, 2634.

The conditions to carry out a photocatalytic allylation reaction of heterocycles **10** were investigated, using the allylic acetate **11** as reagent. Several inorganic and organic photocatalysts were tested, finding that 10-phenyl-10*H*-phenothiazine (PTH) **12a**, under irradiation of UV light (365 nm), catalysed the allylation reaction of a wide range of heterocycles, obtaining the product, **(*Z*)-13**, with high selectivity towards the *Z* isomer (Scheme 3, left).

It was demonstrated that the photocatalyst **12a** has two roles in the reaction. On one hand, it allows the allylation reaction to take place by a photoredox mechanism (that will be detailed later). On the other hand, it leads to the isomerization of the starting material **(*E*)-11** to the *Z* isomer by an energy transfer mechanism, and this configuration is maintained during the course of the reaction, obtaining the *Z* product **(*Z*)-13**. Moreover, the UV light (365 nm) itself is also capable to carry out this isomerization partially.

The phenoxazine photocatalyst **12b** is able to catalyse the allylation reaction, but it does not promote the isomerization. Furthermore, it absorbs visible light, so the use of a blue LED (420 nm) also avoids the isomerization. Thus, the use of this photocatalyst leaded to obtain the allylated heterocycles **13** with high *E* selectivity (Scheme 3, right).

The scope of this reaction was not limited to the allylation of heterocycles. Alcohols and amines could be also allylated using this methodology, with the same selectivity.

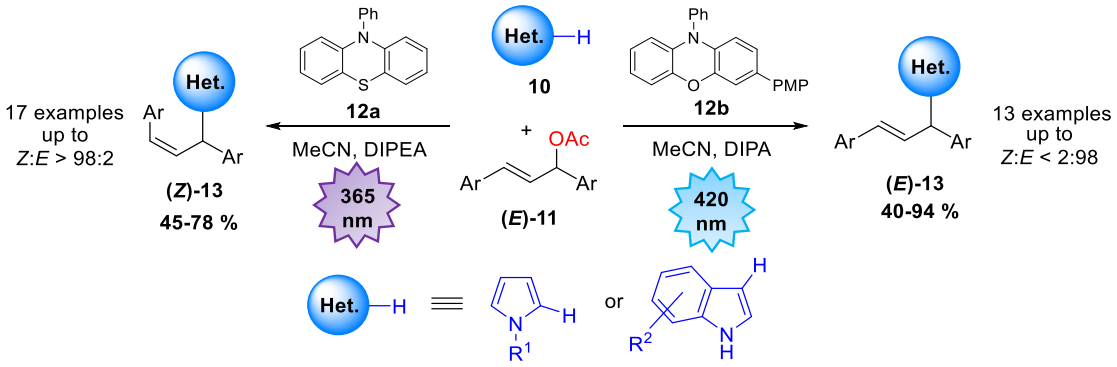

Scheme 3. Diastereo-divergent photocatalytic allylation reaction of heterocycles.

Experimental techniques, like cyclic voltammetries and laser flash photolysis, in combination with DFT calculations, allowed us to make a mechanism proposal (Scheme 4A). It begins with the photoexcitation of the catalyst which reduces the allyl acetate by single electron transfer (SET). This substrate undergoes a scission of the acetate group, rendering and allyl cation intermediate, **INT I**. In a back electron transfer (BET) the intermediate **INT I** is oxidized to the allylic cation **INT II** by the oxidized catalyst ($PC^{\bullet+}$). Finally, the heterocycle attacks to the intermediate **INT II** and, after a rearomatization process the final product is obtained.

Transient absorption spectra provided the most relevant experimental information to validate this mechanism proposal. The transient absorption spectrum (λ_{exc}=355 nm, recorded at 40 ns after de laser pulse) of a mixture of the catalyst **12a** and the allylic acetate (black line, Scheme 4B), shows two peaks, one at 360 nm which corresponds to **INT I**, and other at 490 nm which corresponds **INT II**. When the heterocycle pyrrole is added (red line, Scheme 4B), the peak at 360 nm does not undergo any variation, but in the peak at 490 nm there is a drastic decay in the change in optical density (ΔOD) because the lifetime of the **INT II** decreases. This proves that the heterocycle reacts with the carbocation intermediate **INT II** and not with the radical intermediate **INT I**.

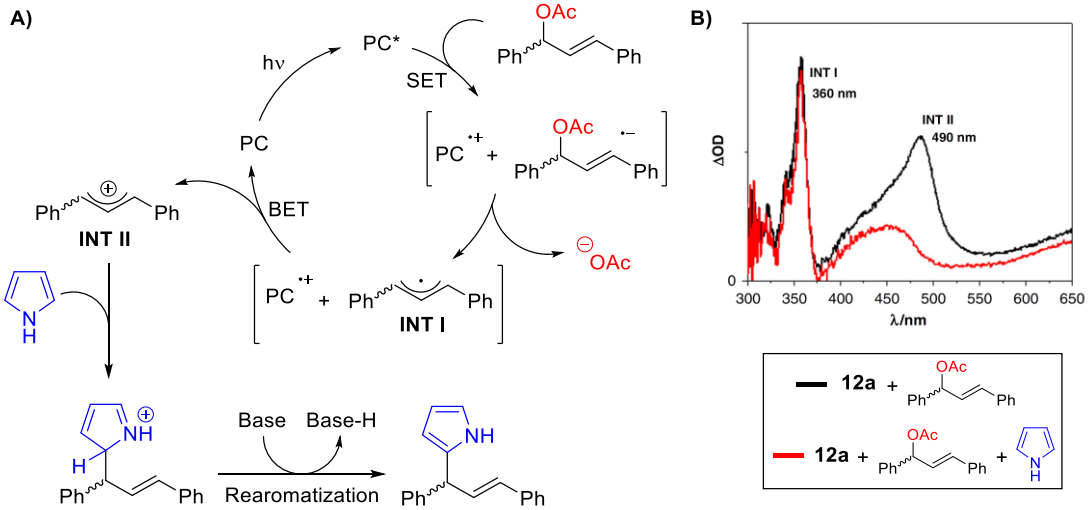

Scheme 4. A) Mechanism of the photocatalytic allylation reaction. **B)** Flash laser photolysis experiments of the reagents.

Squaramide-IRMOF-16 Analogue for Catalysis of Solvent-Free, Epoxide Ring-Opening Tandem and Multicomponent Reactions

C. Vignatti, J. Luis-Barrera, V. Guillerm, I. Imaz, R. Mas-Ballesté, J. Alemán, D. Maspoch, *ChemCatChem* **2018**, *10*, 3995– 3998.

To accomplish the objective of obtaining a MOF with squaramides in its structure, we synthesised the ligand **L1**, which was a linear ditopic dicarboxilate containing a squaramide. This ligand had similar dimensions to tpdc, the ligand of IRMOF-16. The combination of L1 with $Zn(NO_3)_2$ in solvothermal conditions gave rise to the formation of **Sq_IRMOF-16**, which was a MOF analogue to IRMOF-16 which contained squaramide moieties in its backbone (Scheme 5A). The structure of **Sq_IRMOF-16** was simulated, based on the structure of IRMOF-16. The experimental powder X-Ray diffraction pattern was in agreement with the calculated pattern from the simulated structure (Scheme 5B). This MOF did not require any further post-synthetic modification to be used as catalyst.

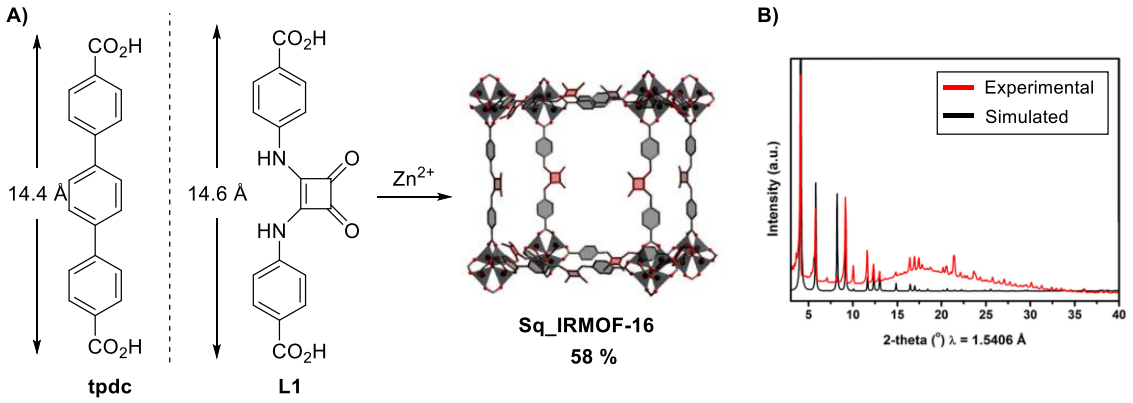

Scheme 5. A) Synthesis of Sq_IRMOF-16. **B)** Experimental and calculated powder X-Ray diffraction pattern of Sq_IRMOF-16.

The catalytic activity of **Sq_IRMOF16** was tested in the opening of epoxides **15** by nucleophilic attack of anilines **14** to form aminoalcohols **16** (Scheme 6A). In this reaction the epoxide is activated by hydrogen-bond interactions. Kinetic studies using differnt anilines **14** and epoxides **15** were carried out, comparing the action of the heterogeneous catalyst **Sq_IRMOF16** (Scheme 6B, solid lines) with the action of the homogeneous squaramide catalyst **C** (Scheme 6B, dashed lines). The molecular squaramide hardly catalysed the reactions due to the self-association. Better results were obtained with **Sq_IRMOF16**, which increased the reaction rate. As can be appreciated in the plot of Scheme 6B, the **Sq_IRMOF16** had better activity when the reagents were smaller, for example, the reaction rate is higher using the small epoxide **15a** (blue or grey solid line) than using the bigger epoxide **15b** (red and orange solid line), which has a long alkyl chain. These results suggested a size selectivity, probably because the reaction occurs inside the pores of the MOF and there is a small diffusion rate of the bulkier reagents within the pores.

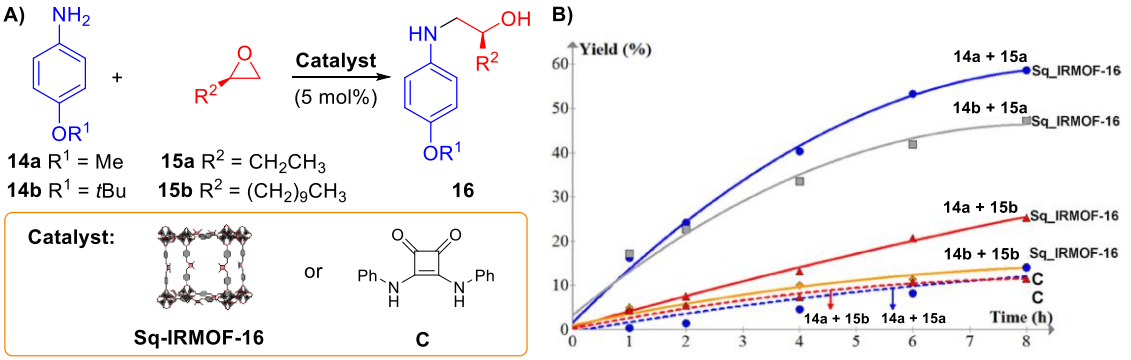

Scheme 6. Kinetics studies of the ring opening of epoxides catalysed by **Sq-IRMOF-16** (solid lines) and squaradime **C** (dashed lines).

The aminoalcohols **16** are the major products at eight hours. However, when the reaction media is allowed to react more time, the aminoalcohols **16** undergo nucleophilic attack to another molecule of epoxide rendering the aminodialcohols **17** (Scheme 7, left) in a tandem process. Therefore, the **Sq-IRMOF16** proved to be useful to synthesise a series of aminodialcohols **17** with good yields. Moreover, it was also possible to do one pot processes with the **Sq-IRMOF16**, in which a first addition of an epoxide molecule was cautiously controlled and then a different epoxide was added to the reaction mixture to obtained di-substituted aminodialcohols **18** (Scheme 7, right).

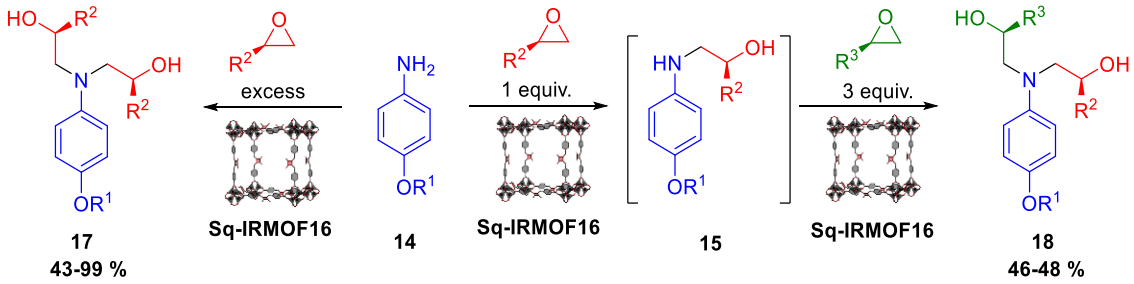

Scheme 7. Tandem and one-pot reactions catalysed by **Sq-IRMOF16**.

Switching Acidic and Basic Catalysis in a Three-Dimensional Covalent Imine Structure through Supramolecular Functionalization

J. Luis-Barrerra, G. Imani-Shakibaei, J. Heras-Domingo, R. Cano, J. Pérez-Carvajal, I. Imaz, D. Maspoch, X. Solans-Monfort, J. Alemán, R. Mas-Ballesté, 2019, submitted to *Journal of Catalysis*.

To make different studies about supramolecular functionalization of a COF, the synthesis of COF-300 was carried out. Two different samples of this material were prepared:

- **a-3**: Amorphous nanoparticles of COF-300. Strictly, this material cannot be considered as a COF, since it is not crystalline, although it has the same building blocks and the same chemical bonds between building blocks.
- **c-3**: Micrometric COF-300 crystals.

Through the treatment of these two materials with acetic acid or trimethylamine, or the use of other techniques like vacuum drying, different samples were prepared:

- **CH_3COOH@a-3** and **CH_3COOH@c-3**: The materials with acetic acid inside the pores.
- **Evacuated a-3** and **Evacuated c-3**: The materials which have been subjected to vacuum drying and do not have organic molecules inside the pores.
- **NEt_3@a-3** and **NEt_3@c-3**: The materials with triethylamine inside the pores.
- **$CH_3COOH\cdots NEt_3$@a-3** and **$CH_3COOH\cdots NEt_3$@c-3**: The materials with both acetic acid and triethylamine inside the pores.

Scheme 8 summarizes the procedures to obtain each material.

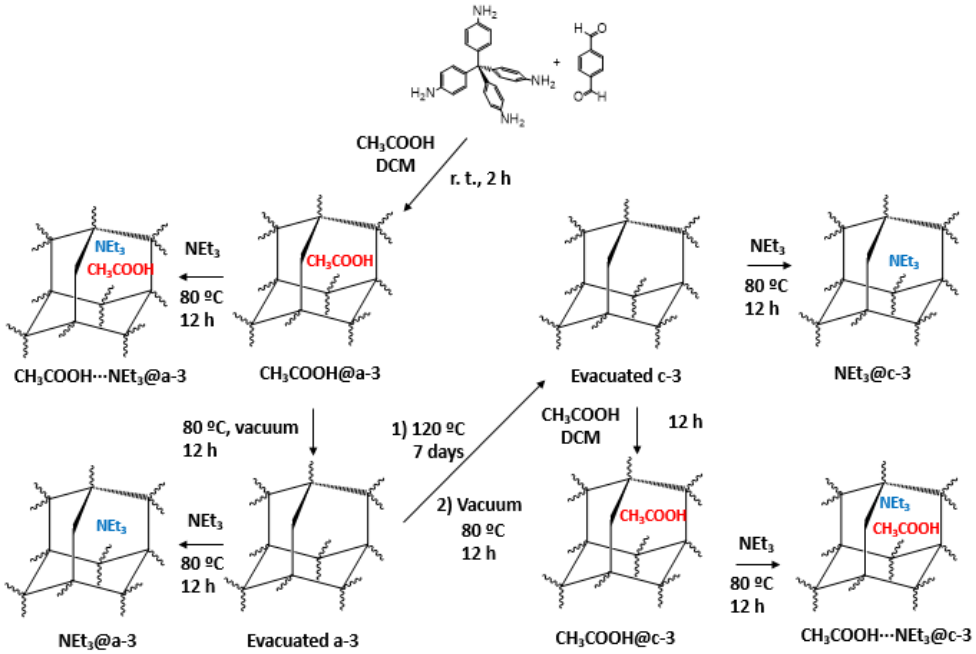

Scheme 8. Preparation of **a-3** and **c-3** and the related supramolecular materials.

Characterization with different techniques (SEM, NMR of solid state, TGA coupled with MS, isotopic labelling, adsorption isotherm, PXRD…) were made to study these materials and to verify that the small molecules of acetic acid and triethylamine were present in each material.

The epoxide opening of amines reaction was selected to test the catalytic activity of the COF with acidic centres (see Scheme 9A) and the Knoevenagel reaction to test the catalytic activity of the COF with basic centres (see Scheme 9B). Important observations were made in the first experiments:

- The materials without catalytic molecules (**Evacuated a-3** and **Evacuated c-3**) hardly catalysed the reactions.
- The material **CH_3COOH@a-3** efficiently catalysed the epoxide opening.
- The materials **NEt_3@a-3** and **$CH_3COOH\cdots NEt_3$@a-3** efficiently catalysed the Knoevenagel condensation. However, the catalysis of **NEt_3@a-3** was due to the leaching of the triethyl amine to the reaction. In the case of **$CH_3COOH\cdots NEt_3$@a-3**, the pair $CH_3COOH\cdots NEt_3$ remains inside the pores during the catalysis, being a case heterogeneous catalysis. It was observed a size selectivity, since the reaction with big aldehydes did not take place.

- The amorphous materials with catalytic molecules (**CH_3COOH@a-3** and **$CH_3COOH\cdots NEt_3$@a-3**) showed better results in the reactions that the crystalline materials with catalytic molecules (**CH_3COOH@c-3** and **$CH_3COOH\cdots NEt_3$@C-3**). This is due to the catalysis happens in the superficial pores of the materials, so the catalysis is higher in the amorphous nanoparticles of **a-3**, which have more surface.

The best materials for the catalysis, **CH_3COOH@a-3** and **$CH_3COOH\cdots NEt_3$@a-3**, were used with synthetic purposes, obtaining different products from the epoxide opening and Knoevenagel products with moderate to good yields (Scheme 9).

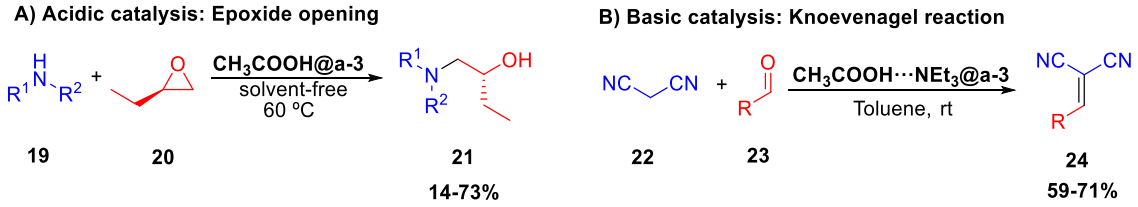

Scheme 9. Reaction catalysed by the materials **CH_3COOH@a-3** and **$CH_3COOH\cdots NEt_3$@a-3.**

DFT calculations with periodic boundary conditions were carried out to study the interaction between the catalytic small molecules and the COF backbone and to elucidate how the catalytic reaction mechanism is inside the pores.

In the **NEt_3@a-3**, the NEt_3 is associated with the COF walls by Van der Waals forces. In the **$CH_3COOH\cdots NEt_3$@a-3**, the CH_3COOH and the NEt_3 are bonded by hydrogen bond (OH···N), and this pair is associated with the COF walls by Van der Waals forces. However, the $CH_3COOH\cdots NEt_3$ has a higher interaction energy with the walls of the COF than the NEt_3, explaining why the latter is easier to leach. Finally, in the case of **CH_3COOH@a-3**, the CH_3COOH is bonded to the COF through a hydrogen bond between the OH and the imine nitrogen of the COF, which has a stronger association energy than in the previous cases.

The intermediates and transitions states of the reactions inside the COF pores were calculated. The intermediates and transitions states starting with the big aldehyde hardly fit in the pores, explaining the size selectivity.

Part 1

From Molecular Photocatalysis…

3. Introduction

3.1. Photocatalysis

3.1.1. General strategies in photochemistry

Photochemistry is the study of chemical reactions that are caused by ultraviolet and visible light. Normally, the reactions that are considered within the field of study of photochemistry are those which are promoted by wavelengths electromagnetic radiation from 200 to 700 nm.[1]

The irradiation of light can be directly carried out to the substrate, in such a way that the substrate reaches an excited state and then evolves to the product (Scheme 10A). Depending of the substrate, the reaction can occur from the excited singlet state, from the excited triplet state or in some cases, from any of them.

The other strategy in photochemistry is the use of a photocatalyst (Scheme 10B).[2] There are several modes of action of the photocatalyst, but all of them begin in the same way: the light is not absorbed by the reactant but by the photocatalyst, which reaches a singlet excited state. Normally, the photocatalyst is a molecule which suffers rapidly an intersystem crossing, reaching the triplet excited state. At this point, there are two general possible ways in which the photocatalyst can act:

- Energy transfer (EnT): the triplet excited state of the photocatalyst is deactivated to the ground singlet state by transferring the energy to the substrate which is thereby raised to the triplet excited state. Then the substrate can evolve to the product.
- Single electron transfer (SET). The photocatalyst in its ground state is normally a bad reductant and a bad oxidant. This scenario totally changes in the excited state. The higher-energy electron can be easily expelled from the molecule, so the photocatalyst can act as a reductant. Simultaneously, in the excited state, the lower-energy hole in the second single occupied orbital may accept an electron, so the photocatalyst can act as oxidant. Therefore, the photocatalyst reduces or oxidizes a component of the reactions (an additive or the substrate itself), generating an anion radical or a cation radical respectively, and then the reaction evolves to the products.

The Scheme 10B shows the most usual case, in which the photocatalyst acts from the triplet excited state. Although less frequently, there are photocatalysts which, after the photoexcitation, do not suffer intersystem crossing and act from the singlet excited state, transferring the singlet excited state to the substrate or suffering processes of single electron

[1] F. A. Carrol, "Perspective on Structure and Mechanism in Organic Chemistry", 2010, John Wiley & Sons, Inc.

[2] a) Tutorial with general concepts of photocatalysis. D. M. Arias-Rotondo, J. K. McCusker, *Chem. Soc. Rev.* **2016**, *45*, 5803—5820. Other reviews about photocatalysis: b) T. Koike, M. Akita, *Inorg. Chem. Front.* **2014**, *1*, 562–576. c) N. A. Romero, D. A. Nicewicz, *Chem. Rev.* **2016**, *116*, 10075−10166. d) M. H. Shaw, J. Twilton, D. W. C. MacMillan, *J. Org. Chem.* **2016**, *81*, 6898−6926. e) H. G. Roth, N. A. Romero, D. A. Nicewicz, *Synlett* **2016**, *27*, 714-723. For a theoretical point of view about photocatalysis: f) T. B. Demissie, K. Ruud, J. H. Hansen, *Organometallics* **2015**, *34*, 4218−4228.

transfer from this state. It is also possible to find photocatalysts that, depending on the reaction conditions and substrates, can act from both singlet or triplet excited states.

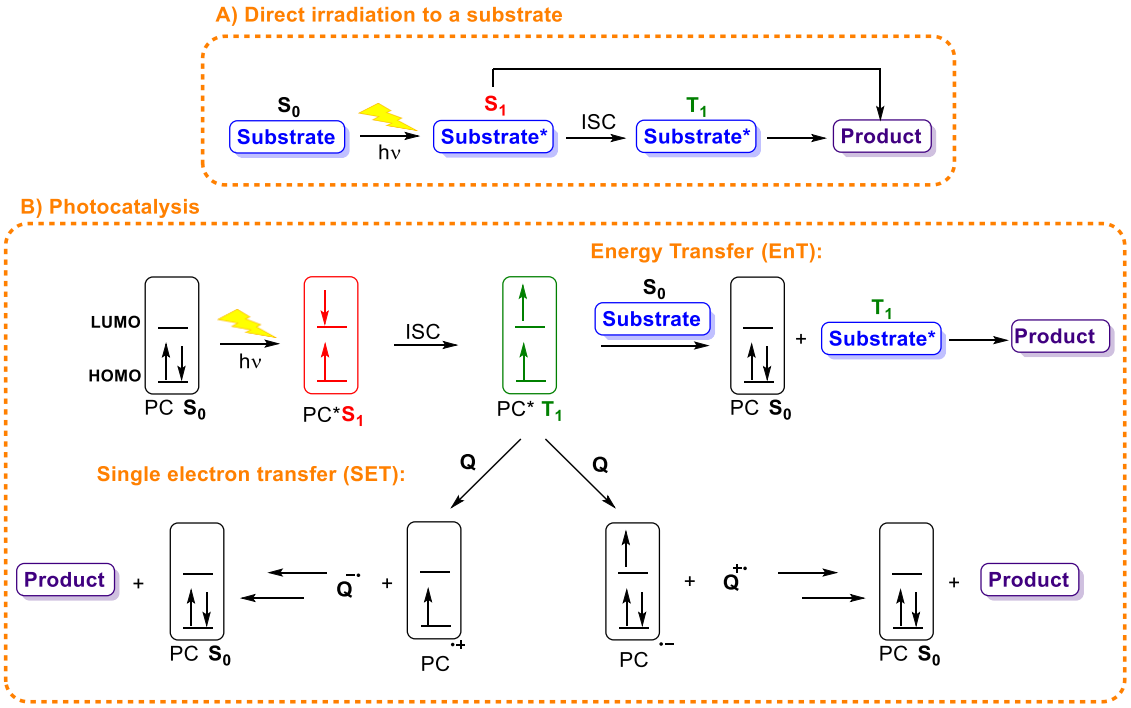

Scheme 10. Photochemical and photocatalysed processes.

Many photocatalysts are molecules whose excited states can be described as charge transfer processes, that is, transitions where the electronic charge is transferred between two parts of the molecule. This process will be described in the next section.

3.1.2. Charge transfer transition

Figure 1 shows the diagram of the typical frontier molecular orbitals of metal polypyridyl complexes commonly used as photocatalysts, like $[Ru(bpy)_3]^{2+}$ or $Ir(ppy)_3$.

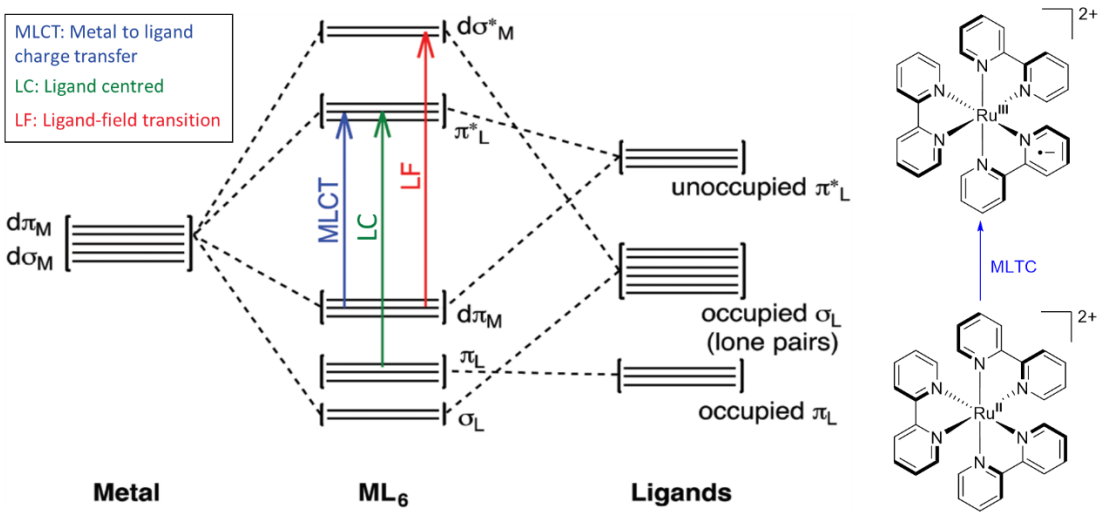

Figure 1. Simplified molecular orbital diagram for an octahedral compound with π–acceptor ligands. Adapted from Ref. 2a with permission from The Royal Society of Chemistry.

The frontier molecular orbitals of this type of compounds are mainly a combination of the *d* orbitals of the metal with the occupied and unoccupied π orbitals and lone pairs of the ligands (Figure 1).[3] These complexes have the peculiarity that the unoccupied orbitals mainly coming from the ligands *π** orbitals are less energetic than the unoccupied orbitals mainly coming from the metal *d* orbitals (Compare π^*_L with $d\sigma^*_M$). As a consequence, the less energetic transition that can be observed in this type of complex is the metal-ligand charge transfer (MLCT) that can be visualized as the promotion of one electron from the metal centre to the ligand. This MLCT transition can be accomplished with visible light, making these complexes very useful for photocatalysis. The singlet $MLCT^1$ state rapidly undergoes intersystem crossing to give the lowest-energy triplet $MLCT^3$ state, whose long life allows the process of energy transfer and single electron transfer shown in Scheme 10 (previous section).

Other common transitions that are usually seen in these complexes are the ligand-centred transitions (LC) and correspond to transitions between orbitals, mainly coming from π and π* ligand orbitals. They can be visualized as promotion of electrons within the ligands and they are normally in the range of UV light.

As an example, Figure 2 shows representative spectra of $Ir(ppy)_3$ complex.[3] The absorption spectrum (solid grey line) has been acquired at 27 °C (300 K). In the range below about 300 nm, the intense bands are related to π-π* transitions, which corresponds to the allowed singlet-singlet ligand centred states (^{1}LC). The broad and unresolved absorption at lower energy, peaking at 376 nm, is assigned to allowed (singlet-singlet) d-π* transitions, corresponding to metal-to-ligand charge transfer states, (^{1}MLCT).

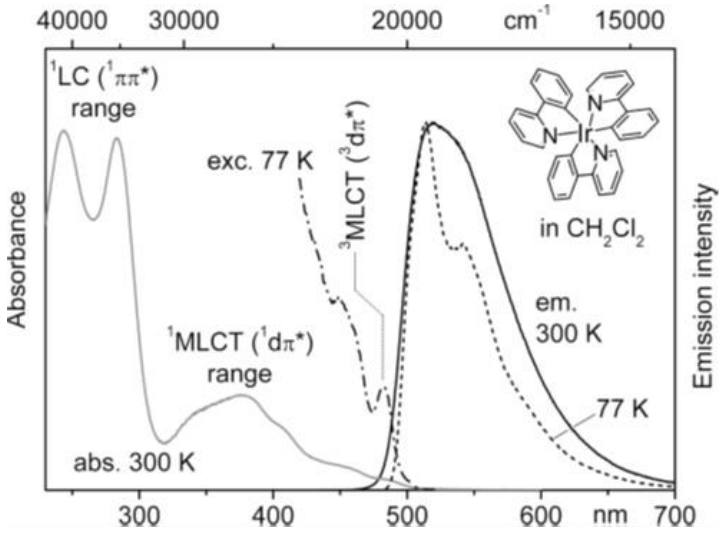

Figure 2. Emission, absorption, and excitation spectra of $Ir(ppy)_3$ in CH_2Cl_2 ($c \approx 2 \cdot 10^{-5}$ mol/L) measured at ambient temperature and 77 K. Emission spectra: λ_{exc}=373 nm. Excitation spectrum: λ_{em}=530 nm. Reprinted with permission from Ref. 3. Copyright 2010 American Chemical Society.

The singlet-triplet transitions are forbidden by spin selection rules and, consequently, are very improbable. However, the high spin-orbit coupling of these complexes makes these transitions more probable, and they can be appreciated even at room temperature with an absorption spectrum. The small band between about 430 nm and 500 nm involves singlet-triplet transitions to ^{3}MLCT states. In fact, the fine structure of this band can be partially distinguished

[3] T. Hofbeck, H. Yersin, *Inorg. Chem.* **2010**, *49*, 9290-9299.

in the excitation spectrum at 77 K taken in this region (Figure 2, dashed points and lines, λ_{em} = 530 nm).

This compound exhibits a very bright phosphorescence with a quantum yield of almost 100%. As opposed to organic molecules, for which special conditions are needed to appreciate their phosphorescence, the emission spectrum of this compound at room temperature corresponds entirely to the emission from the ^{3}MLCT, that is, to the phosphorescence (Figure 2, solid black line). It shows a maximum at 519 nm (55 kcal/mol). Cooling to 77 K leads to a slightly structured spectrum (Figure 2, dashed line) with a dominating peak at 514 nm (56 kcal/mol) and a satellite peak at 541 nm (53 kcal/mol). The excitation spectrum at 77 K overlaps with the emission spectrum in the range of the transitions between the electronic singlet ground state, S_0, and the emitting triplet state, ^{3}MLCT, representing the T_1 state.

All spectra depicted in Figure 2 are carried out in dichloromethane and they are shown in this document because of their didactic interest. However, the most accepted triplet energy for $Ir(ppy)_3$ in the literature is taken from the more energetic maximum of the emission spectrum carried out in a mixture of ethanol and methanol at 77 K, (which is blue-shifted respect to the one in dichloromethane) and the value is 494 nm (E_T = 58 kcal/mol).[4, 12]

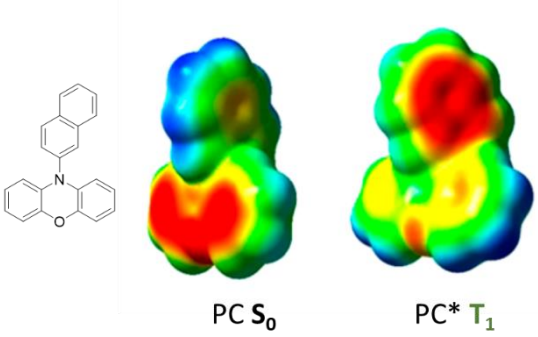

Figure 3. Electrostatic potential (ESP)-mapped electron density *N*-(2-naphthyl)phenoxazine in S_0 and T_1 states. Adapted with permission from Ref. 5. Copyright 2018 American Chemical Society.

Some organic molecules can present charge transfer transitions, for example the *N*-(2-naphthyl)phenoxazine[5] depicted in Figure 3. Electrostatic potential (ESP)-mapped electron density diagrams of its ground state and it first triplet excited state were calculated (Figure 3, red for electron reach regions and blue for electron deficient regions). It can be clearly appreciated a shift of electron density from the phenoxazine core to the 2-naphthyl. The authors came to the conclusion that when this type of molecules can perform charge transfer transitions, they are better photoredox catalysts.

3.1.3. Energy transfer catalysis

Energy transfer is a photophysical process in which an excited state of one molecular entity (the donor, also called the photosensitizer), is deactivated to a lower-lying state by transferring energy to a second molecular entity (the acceptor), which is thereby raised to a higher energy state.[6] In the field of photocatalysis, the photosensitizer is the photocatalyst, and the acceptor is the substrate which needs to reach the excited state to be transformed into the product (Scheme 10).

[4] K. A. King, P. J. Spellane, R. J. Watts, *J. Am. Chem. Soc.* **1985**, *107*, 1431-1432.
[5] B. G. McCarthy, R. M. Pearson, C.-H. Lim, S. M. Sartor, N. H. Damrauer, G. M. Miyake, *J. Am. Chem. Soc.* **2018**, *140*, 5088−5101.
[6] F. Strieth-Kalhoff, M. J. James, M. Teders, L. Pitzer, F. Glorius, *Chem. Soc. Rev.* **2018**, *47*, 7190-7202.

There are two possible mechanisms for the energy transfer (Figure 4):

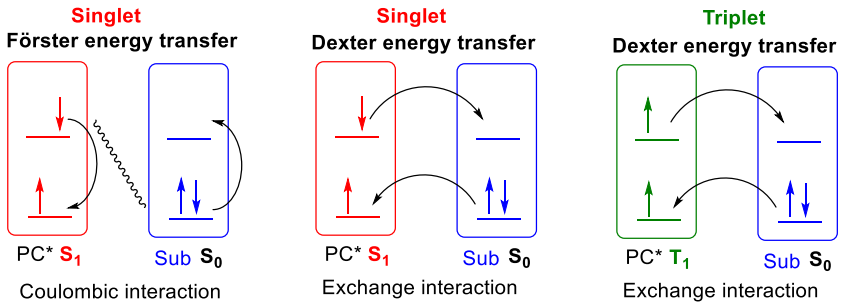

Figure 4. Mechanisms of Energy Transfer.

- **Förster**: Electronic oscillation in the excited state of the photocatalyst induces a dipole and thus electronic oscillation in the ground state of the substrate by charge repulsion through an electromagnetic field. A resonant interaction between the photocatalyst and the substrate would eventually lead to the desired electronic transition, that is, relaxation of the photosensitizer with simultaneous electronic excitation of the substrate. An energy transfer of triplet state cannot be described with Förster's theory.[6]

- **Dexter**: It is a double electron transfer mechanism, as depicted in Figure 4. With this mechanism, both singlet and triplet state can be transferred from the photocatalyst to the substrate.

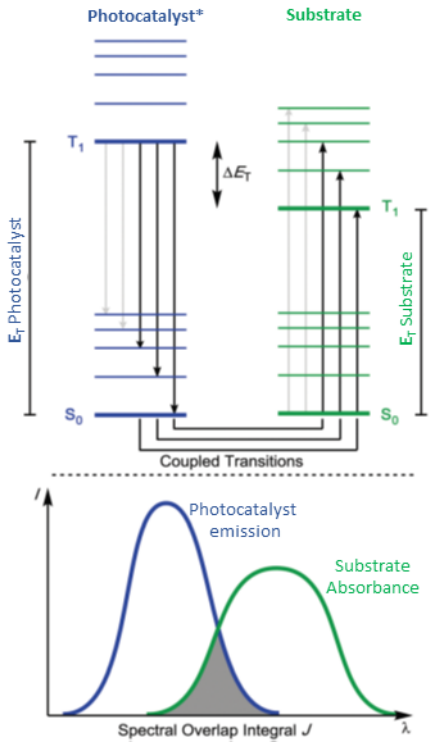

Figure 5. Coupled transitions for Dexter energy transfer and the corresponding spectral overlap integral. Adapted from Ref. 6 with permission from The Royal Society of Chemistry.

Intimate physical contact between the photocatalyst and the substrate is required for Dexter energy transfer to occur since orbital overlap between the two molecules is necessary. The main factor which governs the rate of the Dexter electron transfer is *J*, the spectral overlap integral between the normalized photocatalyst emission spectrum and the normalized substrate absorption spectrum (Figure 5).[6] For the cases when a triplet energy transfer is studied, the photocatalyst emission spectrum would correspond to the phosphorescence spectrum and the substrate absorption spectrum would correspond to the singlet-to-triplet absorption.

In Figure 5 we can observe these two spectra of a theoretical photocatalyst and substrate, their overlap region, and a Jablonski diagram that represents the meaning of this overlap.[6] The values where the two spectra overlap mean that there is a decay in the photocatalyst from the triplet

state to the singlet state that has exactly the same energy as a transition in the substrate from the singlet state to the triplet state, making this transference of energy possible. The bigger this overlap is, the more number of energy transfer events can occur and, consequently, the higher the value of the rate constant. [6]

Unfortunately, singlet-to-triplet absorption spectra are very difficult to obtain. The direct singlet-triplet excitation is forbidden by selection rules and is improbable, so in most of the organic molecules it is not possible to record it. However, it is easy to have an idea of the magnitude of *J*, and therefore the energy transfer efficiency, based on the difference in the triplet excited state energies of the photocatalyst and the substrate: [6]

$$\Delta E_T = E_T(\text{Substrate}) - E_T(\text{Photocatalyst})$$

For $\Delta E_T < 0$, as is the case shown in Figure 5, a large number of coupled transitions exists. It can be assumed that the spectral overlap is large. It is an exergonic energy transfer. [6]

For $\Delta E_T > 0$, coupled transitions only exist from excited vibrational levels of the photocatalyst T_1 states, so the overlap integral depends on thermal population of the T_1 vibrational states. These endergonic energy transfers are more difficult to achieve, and they are negligible when ΔE_T is large. [6]

In 2011, Bach's group carried out a study which perfectly illustrates the potential of the energy transfer photocatalysis. In this work, they studied the intramolecular [2+2] photocycloaddition of 4-substituted quinolones.[7a-b] This reaction could be promoted with UV light which was directly absorbed by the substrate (Scheme 11A).

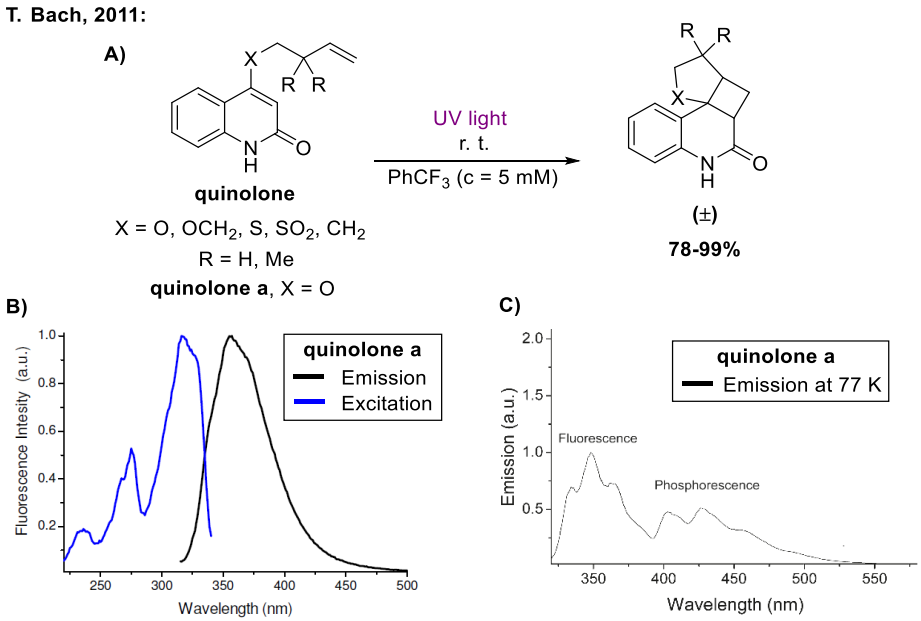

Scheme 11. A) Racemic intramolecular [2+2] photocycloaddition of 4-substituted quinolones. **B)** Emission and excitation spectra at room temperature of **quinolone a**. **C)** Emission spectra at 77 K of **quinolone a**. Adapted with permission from Ref. 7b. Copyright 2011 American Chemical Society.

[7] a) C. Müller, A. Bauer, T. Bach, *Angew. Chem. Int. Ed.* **2009**, *48*, 6640 –6642. b) C. Müller, A. Baurer, M. M. Maturi, M. C. Cuquerella, M. A. Miranda, T. Bach, *J. Am. Chem. Soc.* **2011**, *133*, 16689-16697.

Taking **quinolone a** (X = O) as example, the intersection between its excitation and its emission spectra (Scheme 11B) gives the singlet excited state energy, E_S = 86 kcal/mol (334 nm). When the emission is recorded at cryogenic temperature (-190 °C) in ethanol matrix, partial fine structure of fluorescence can be appreciated and a phosphoresce band appears (Scheme 11C). From the more energetic peak maximum of the phosphorescence band, the triplet state energy is estimated, E_T = 71 kcal/mol (404 nm). Mechanism studies revealed that the substrates reached the singlet excited state after absorption of light, and then they decayed to a triplet excited state through intersystem crossing and, from this latter state, the cycloaddition occurred (see Figure 6, right).

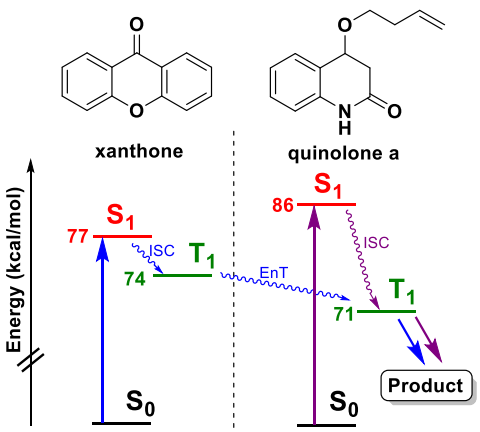

Figure 6. Purple: Direct irradiation. Blue: energy transfer.

The xanthone, which is known to be a good triplet photosensitizer (E_S = 77.4 kcal/mol, 369 nm; E_T = 74.0 kcal/mol, 386 nm),[2c] has a singlet energy lower than **quinolone a** and a triplet energy higher than **quinolone a** (Figure 6). This features makes the xanthone an ideal energy transfer photocatalyst for the reaction, since it can be excited with a lesser energetic light and, once the xanthone decays to the triplet state, it efficiently transfers the triplet state since $\Delta E_T < 0$ (see above). Bach's group developed a photocatalyst consisting in a xanthone motif attached to a chiral skeleton able to coordinate to the quinolone through hydrogen bonds (**catalyst 1**, Scheme 12). The use of this photocatalyst afforded the products with good yields and enantioselectivities.

The mode of action is depicted in Scheme 12, right. The mixture is irradiated with a UV light source (centred in λ = 366 nm) that is efficiently absorbed by the photocatalyst, but not by the substrate. The photocatalyst, which is in the singlet excited state, undergoes intersystem crossing (ISC) to the triplet excited state. Then, the photocatalyst carries out the energy transfer process of the triplet state when it is coordinated to the substrate and, since the cycloaddition is faster than the release of the catalyst, the product is formed in a chiral environment. The fact that the substrate does not absorb the light directly is crucial to avoid the racemic background reaction and, indeed, the product does not reach a total selectivity because of residual direct absorption of the UV light.

Three years later Bach's group developed a similar catalyst bearing a thioxanthone (E_S = 72.4 kcal/mol, 395 nm; E_T = 64.6 kcal/mol, 443 nm)[2c] instead of a xanthone (**catalyst 2**, Scheme 12). This catalyst absorbed the visible light, so they could carry out the same concept employing visible light.[8]

[8] R. Alonso, T. Bach, *Angew. Chem. Int. Ed.* **2014**, *53*, 4368–4371.

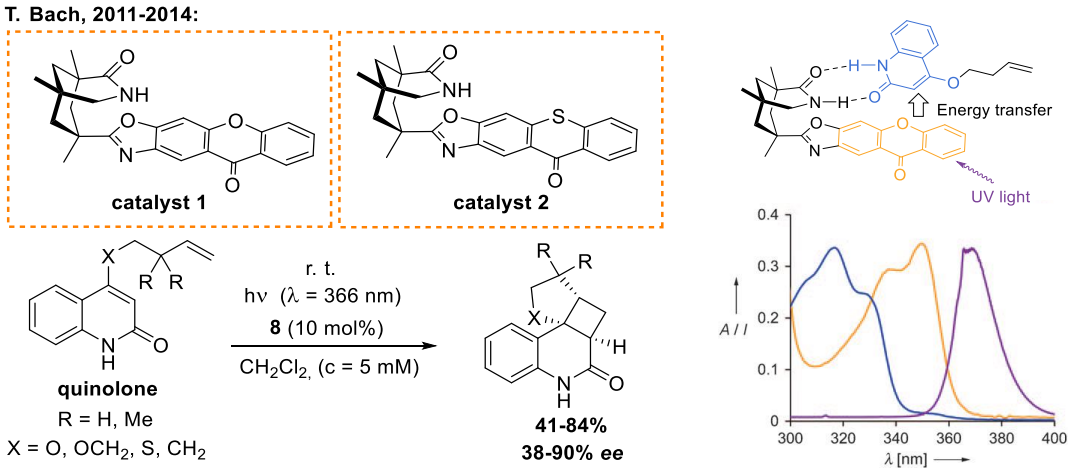

Scheme 12. Left: Catalysed intramolecular [2+2] photocycloaddition of quinolones. Right: Mode of action of catalyst **8**, absorption spectra of quinolone **1a** (blue) and xanthone (orange) and emission spectrum of the irradiation source (purple). Mode of action and spectra adapted from Ref. 7a with permission from John Wiley and Sons.

Other interesting example is the photocatalysed 6π heterocyclization of 2-aryloxyketones, 2-arylthioketones and 2-arylaminoketones developed by M. D. Smith in 2017 (Scheme 13).[9a] This reaction had already been developed by A. G. Schultz in 1978,[9b] irradiating with UV light and without photocatalyst. This direct irradiation presented some disadvantages like a low functional group tolerance, *e.g.*, when the substrate presented a –NMe_2 group in the aromatic ring a photopolymerization took place instead of the heterocyclization.

The substrates have a high singlet energy and they need to absorb UV light to reach the singlet excited state and, after intersystem crossing, reach the triplet excited state. DFT calculations shows that this family of 2-aryloxyketones has a triplet between 58.2 and 62.5 kcal/mol (between 491 and 457 nm respectively), in the range of visible light, but it cannot be reached directly by irradiation because it is a forbidden transition by spin selection rules. Smith's group found that $Ir(dFppy)_3$ was an ideal photosensitizer for this reaction, since it can be excited with visible light and, after ISC, transfer the triplet energy (E_T = 63.5 kcal/mol, 450 nm) to the substrate (ΔET < 0, similar situation to that depicted in Figure 6). The use of visible light allows larger functional group tolerance, so they carried out a broad scope (including the substitution with –NMe_2 group).

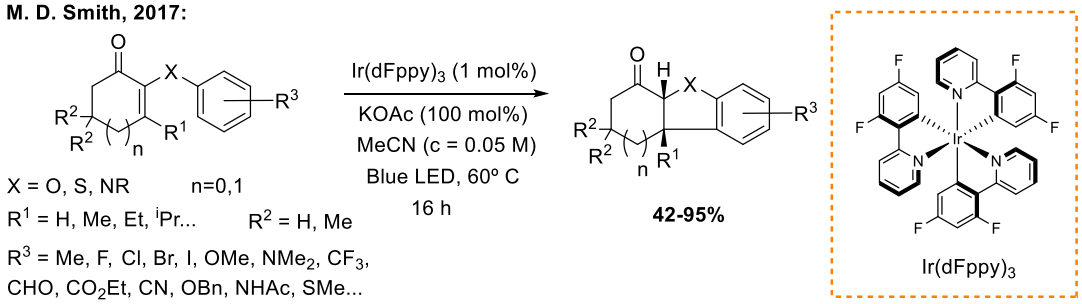

Scheme 13. Triplet energy transfer mediated 6 π heterocyclization.

[9] a) N. Münster, N. A. Parker, L. van Dijk, R. S. Paton, M. D. Smith, *Angew. Chem. Int. Ed.* **2017**, *56*, 9468-9472. b) A. G. Schultz, R. D. Lucci, W. Y. Fu, M. H. Berger, J. Erhardt, W. Hagmann, *J. Am. Chem. Soc*. **1978**, *100*, 2150-2162.

3.1.4. Double bond isomerization

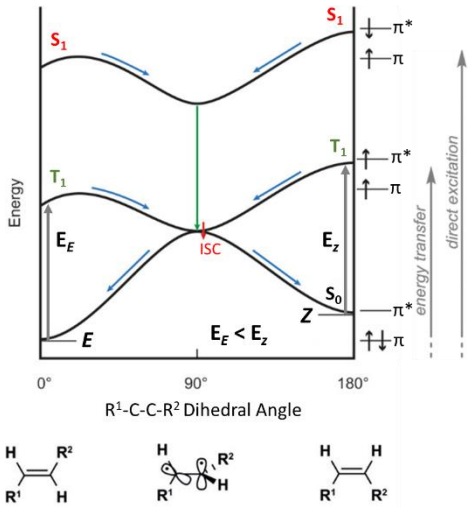

Figure 7. Potencial surfaces of alkenes as functions of dihedral angles. Reproduced from Ref. 10 with permission from Georg Thieme Verlag KG.

The photochemistry and energy transfer catalysis can be applied to the isomerization of *E* alkenes to *Z* alkenes. In the formation of alkenes, the *Z* isomer can be obtained by kinetic control. However, beginning from *E* alkenes, it is impossible to shift the equilibrium to the *Z* alkenes by thermal methods since the *E* isomer is thermodynamically more stable. Photochemical methods are necessary to do this transformation.

The schematic energy surface diagram of an alkene in the coordinate of the dihedral angle of the double bond is shown in Figure 7.[10, 6] In the ground state, the flat geometries of the alkenes *E* and *Z* are minima and the twisted geometry is a maximum. Excitation of an alkene results in the promotion of an electron from a π to a π* orbital, thereby decreasing the bond order, which allows the rotation around the bond axis. Therefore, the potential surface of the excited state (both the singlet and the triplet) completely changes: the flat alkenes geometries are now maxima and the twisted geometry is a minimum. The excitation is vertical, that is, when any of the two isomers of alkene, *Z* or *E*, which are minima, are excited they become maxima and both evolve to the same twisted geometry. Then, the decay to the ground state yields a statistical mixture of *E* and *Z* isomers.

In alkenes conjugated to another π-system the *Z*-isomer triplet structure is specially disfavoured due to non-bonding interactions and steric effects disrupting conjugations, so the excitation energy of the *Z*-alkene is considerably higher than the *E*-alkene excitation energy. With direct excitation, it is possible to select a wavelength that only excites the *E*-alkene but not the *Z* alkene, which results in gradual accumulation of *Z*-alkene. This effect can also be achieved with an energy transfer process, selecting a photosensitizer with an appropriate triplet energy that only excites the *E*-isomer, provoking the gradual accumulation of *Z*-isomer.

The work of Weaver *et al.* in 2014 is an example of how the emergent field of visible light mediated photocatalysis has been used.[11] Through an energy transfer process, they isomerized *E*-cinnamyl derived amines into the *Z* form using $Ir(ppy)_3$ as photocatalyst (Scheme 14).

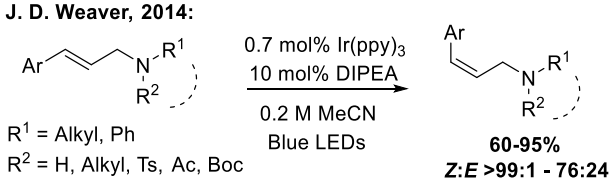

Scheme 14. Photocatalyzed E-Z isomerization of cinnamyl derived amines.

[10] J. B. Metternich, R. Gilmour, *Synlett* **2016**, *27*, 2541–2552.
[11] K. Singh, S. J. Staig, J. D. Weaver, *J. Am. Chem. Soc.* **2014**, *136*, 5275−5278.

3.1.5. Photoredox catalysis

The photoredox catalysis, as it was mentioned above, has emerged as a powerful tool in organic synthesis. Two of the most frequent photocatalysts are $Ir(ppy)_3$ and $[Ru(bpy)_3]^{2+}$ because of their special photophysical characteristics.[12]

For example, $Ir(ppy)_3$ in its ground state is a very bad oxidant ($E½\ Ir^{III}/Ir^{II}$ = -2.19 V)[2b, 13] and a bad reductant ($E½\ Ir^{IV}/Ir^{III}$ = 0.77 V)[2b, 13] (See cyclic voltammetry[14,15] in Figure 8A) . This scenario totally changes in the excited state. As it was depicted in Scheme 10 and Figure 1, $Ir(ppy)_3$ gets a long-lived triplet excited state after a process of absorption, metal-to-ligand charge transfer (MLCT) and intersystem crossing (ISC). The lower-energy hole in the $d\pi_M$ orbital can easily accept one electron and the higher energy electron in the π^*_L orbital can be easily expelled. Therefore, $Ir(ppy)_3$ is a better oxidant and a better reductant in the excited state than in the ground state. The redox potential of the excited states can be obtained from the redox potential in the ground state and the energy of the excited state in the lowest vibrational level of the compound, E_0, with the equations[2a] derived from the thermodynamic cycle[16] depicted in Figure 8B. As seen before, the triplet energy of the $Ir(ppy)_3$ is E_T= 58 kcal/mol (2.5 eV).

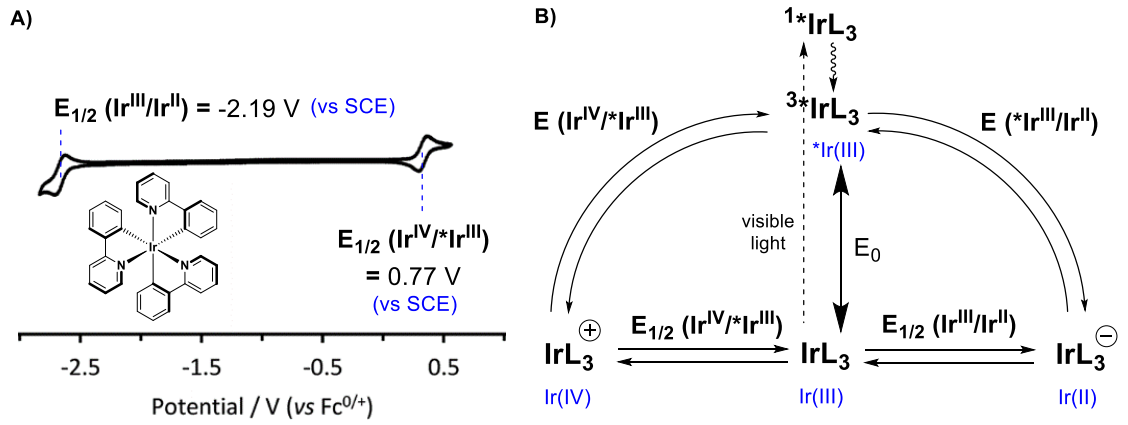

C) $E\ (*Ir^{III}/Ir^{II}) = E_{1/2}\ (Ir^{III}/Ir^{II}) + E_0$ = -2.19 + 2.50 = 0.31 V

$E\ (Ir^{IV}/*Ir^{III}) = E_{1/2}\ (Ir^{IV}/Ir^{III}) - E_0$ = 0.77 - 2.50 = -1.73 V

Figure 8. A) Cyclic voltammetry of $Ir(ppy)_3$. Adapted from Ref. 15 – Published by The Royal Society of Chemistry. **B)** Diagram which correlates the redox potential of the excited and ground state with the energy of the excited state. **C)** Calculations of redox potential in the excited state of $Ir(ppy)_3$. Standard potentials and data calculations from Ref. 2b.

---

[12] a) C. K. Prier, D. A. Rankic, D. W. C. MacMillan, *Chem. Rev.* **2013**, *113*, 5322−5363. b) L. Flamigni, A. Barbieri, C. Sabatini, B. Ventura, F. Barigelletti, *Top. Curr. Chem.* **2007**, *281*, 143-203.

[13] **NOTE:** All the potentials given in this document are potentials vs SCE.

[14] This document gathers cyclic voltammetries from different publications where different reference electrodes are used. The extract potentials written on each graphic are already converted into potentials vs SCE. $V_{SCE} = V^{Fc+/Fc} + 0.51$ V for CH_2Cl_2 and DMF solvents (Ref. 12b)// V_{SCE} = V vs Ag/AgCl KCl (0.1M) + 0.04 V (Ref. 12b)// V_{SCE} = V vs $Ag/AgNO_3$ [0.01M] + 0.298 V (Ref. 5).

[15] E. Kerr, E. H. Doeven, G. J. Barbante, C. F. Hogan, D. J. Hayne, P. S. Donnelly, P. S. Francis *Chem. Sci.* **2016**, *7*, 5271–5279.

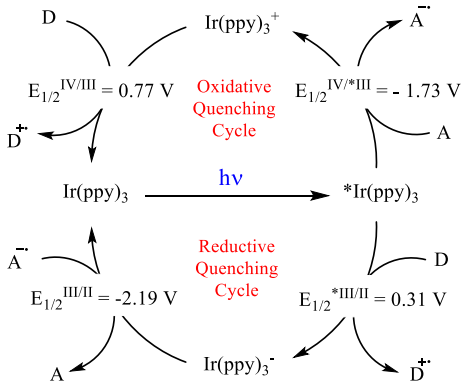

Figure 9. Possible catalytic cycles of $Ir(ppy)_3$.

The redox potentials of $Ir(ppy)_3$* in its excited state (see **Figure 8C**) show that it is a modest oxidant ($E\ ^*Ir^{III}/Ir^{II}$ = 0.31 V)[2b, 13] and an excellent reductant ($E\ Ir^{IV}/^*Ir^{III}$ = -1.73 V).[2b, 13] Therefore, this class of photoredox catalyst can operate through two possible cycles of single electron transfer: the oxidative quenching cycle and the reductive quenching cycle (Figure 9). In the oxidative quenching cycle, once the photocatalyst has been excited with light, it acts as a reductant, reducing an electron acceptor (A), which is called oxidative quencher, and is transformed into a radical anion ($A^{\cdot-}$). The formed oxidized photocatalyst, $Ir(ppy)_3^+$, is now a strong oxidant and accepts one electron from a donor (D), returning to the initial ground state and yielding a radical cation ($D^{\cdot+}$). Alternatively, in the reductive quenching cycle, the excited photocatalyst acts as oxidant and accepts one electron for a donor, which is called reductive quencher. The generated reduced catalyst is now a good reductant and gives one electron to an acceptor. In both cycles the donor or the acceptor can be a reagent, a co-catalyst or the substrate itself.

Two recent examples where we can appreciate iridium complexes acting in the two types of cycles are shown in Scheme 15. In Scheme 15A, it is depicted the enantioselective radical coupling between the α position of an amine with an imine catalysed cooperatively by two catalysts: $Ir(ppy)_3$, which operates through oxidative quenching cycle, and a chiral phosphonium salt.[17] In this reaction, developed by Ooi *et al.* in 2016, the photoexcited iridium ($E\ Ir^{IV}/^*Ir^{III}$ = -1.73 V) reduces the *N*-Ms-benzaldimine ($E_{½}\ R/R^{\cdot-}$ = -1.45 V), rendering a radical anion which is easily coordinated to the positively charged chiral phosphonium. Then, the $Ir(ppy)^+$ ($E_{½}\ Ir^{IV}/Ir^{III}$ = 0.77 V) is able to oxidize the $Ph_2NCH_2SiMe_3$ ($E_{½}\ R^{\cdot+}/R$ = 0.60 V), yielding a radical cation that rapidly releases the trimethylsilylium ion. The formed carbon radical gives the radical coupling with the previously generated radical anion in a chiral environment, forming the product in good enantiomeric excess.

When an iridium complex is required to perform a reductive quenching cycle, normally ligands with electron withdrawing groups are employed, since these ligands make the complex more oxidant.[2a] This can be seen in the decarboxylative hydroalkylation of alkynes carried out by MacMillan's group in 2018 (Scheme 15B),[18] in which they combined an electron poor iridium photocatalyst and a nickel complex. The excited iridium complex ($E\ ^*Ir^{III}/Ir^{II}$ = 1.21 V) oxidized the substrate bearing a carboxylic acid motif, in the case shown in Scheme 15B a protected proline ($E_{½}\ R^{\cdot+}/R$ = 0.95 V). The protected proline suffers deprotonation and CO_2 extrusion and gives a carbon radical. Then, the Ir(II) catalyst ($E_{½}\ Ir^{III}/Ir^{II}$ = -1.37 V) is now able to reduce the Ni(II) complex ($E_{½}\ Ni^{II}/Ni^{I}$ = -1.2 V) to a Ni(I) species. The previously generated carbon radical rapidly engages in an oxidative radical capture with low-valent nickel species. Then, after migratory

[16] A. Singh, K. Teegardin, M. Kelly, K. S. Prasad, S. Krishnan, J. D. Weaver, *J. Organomet. Chem.* **2015**, *776*, 51-59.

[17] a) D. Uraguchi, N. Kinoshita, T. Kizu, T. Ooi, *J. Am. Chem. Soc.* **2015**, *137*, 13768−13771. b) T. Kizu, D. Uraguchi, T. Ooi, *J. Org. Chem.* **2016**, *81*, 6953−6958.

[18] N. A. Till, R. T. Smith, D. W. C. MacMillan, *J. Am. Chem. Soc.* **2018**, *140*, 5701−5705.

insertion of the alkyne, the nickel can promote the coupling to generate the alkene products with good yields.

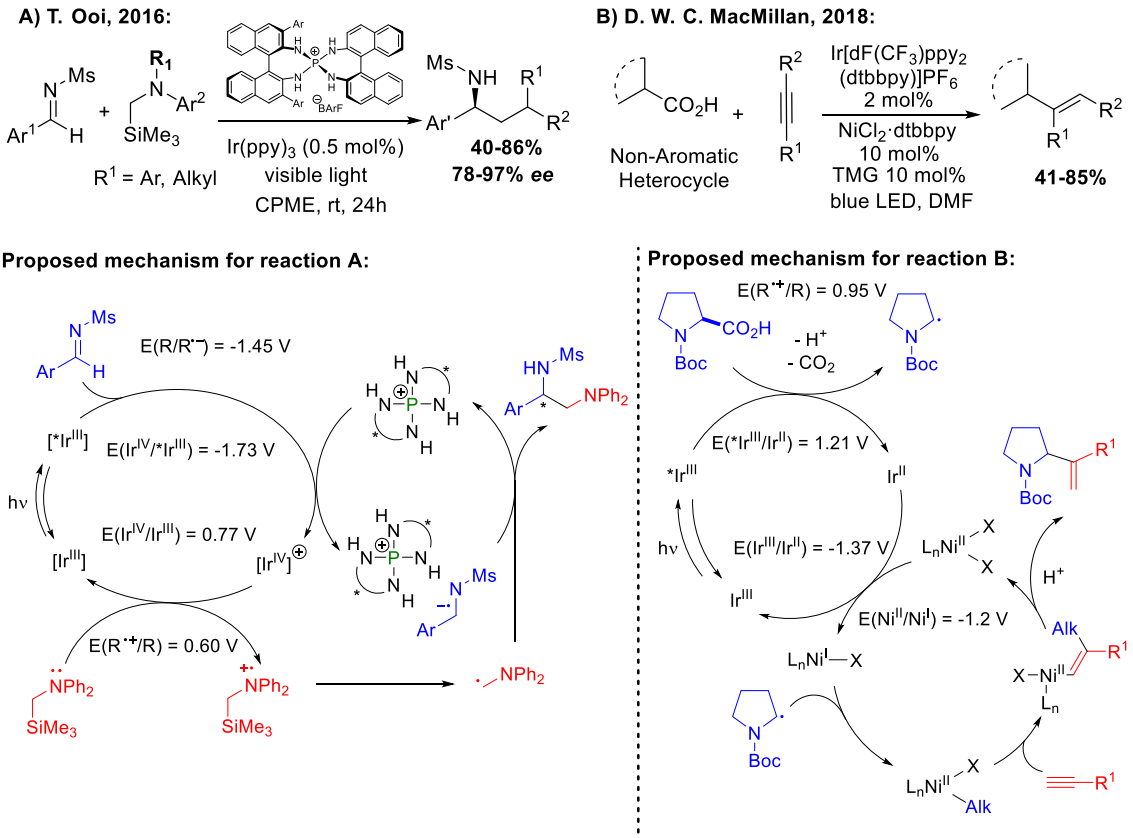

Scheme 15. Recent examples of the use of Iridium complexes as photocatalyst.

As a consequence, the catalysts photophysical properties play an important role in the photoredox reactions and will be analysed in the next section; especially those used in this doctoral thesis.

3.1.6. Photophysical parameters

This section gathers the photophysical parameters (singlet and triplet energies and photoredox potentials of ground and excited states) of the most relevant phtocatalysts used in this doctoral thesis, with the cyclic voltammetries,[13,14] the emission spectra and the calculation directly taken from different publications (Figure 10). In all the cases the singlet energy and the triplet energy are estimated from the maxima of the more energetic peak of fluorescence and phosphorescence emission spectra respectively.

The $Ir(dFppy)_3$ complex[19a-c] absorbance and emission presents similar features as those described for $Ir(ppy)_3$ (see above, section 3.1.2), so all the emission comes from the triplet state. The potentials in the triplet excited state are calculated for the reduction and the oxidation.

The phenylphenothiazine[20a-c] (PTH) and the PMP-phenoxazine[21] usually act as reductants and only potential of the oxidation is calculated. Although they usually act from the triplet state, they might act from the singlet, so potential from both states are calculated. In the case of PMP-phenoxazine, the authors only provide data calculated by DFT for the triplet states.

[19] $Ir(dFppy)_3$: a) Voltammetry from reference 16. Adapted from this reference with permission from Elsevier B. V. b) Absorption and emission spectra from: A. B. Tamayo, B. D. Alleyne, P. I. Djurovich, S. Lamansky, I. Tsyba, N. N. Ho, R. Bau, M. E. Thompson, *J. Am. Chem. Soc.* **2003**, *125*, 7377-7387. Adapted with permission from this reference. Copyright 2003 American Chemical Society. c) Standard potentials and data calculation from reference 2b.

[20] Phenylphenothiazine (PTH): a) Voltammetry from: N. J. Treat, H. Sprafke, J. W. Kramer, P. G. Clark, B. E. Barton, J. R. de Alaniz, B. P. Fors, C. J. Hawker, *J. Am. Chem. Soc.* **2014**, *136*, 16096−16101. Adapted with permission from this reference. Copyright 2014 American Chemical Society. b) Emission spectra from: E. H. Discekici, N. J. Treat, S O. Poelma, K. M. Mattson, Z. M. Hudson, Y. Luo, C. J. Hawker, J. R. de Alaniz, *Chem. Commun.* **2015**, *51*, 11705—11708. Adapted from this reference with permission from The Royal Society of Chemistry. c) Data calculation from reference 2c.

[21] PMP-phenoxazine: Voltammetry, emission spectrum and DFT calculations from reference 5. Adapted with permission from this reference. Copyright 2018 American Chemical Society.

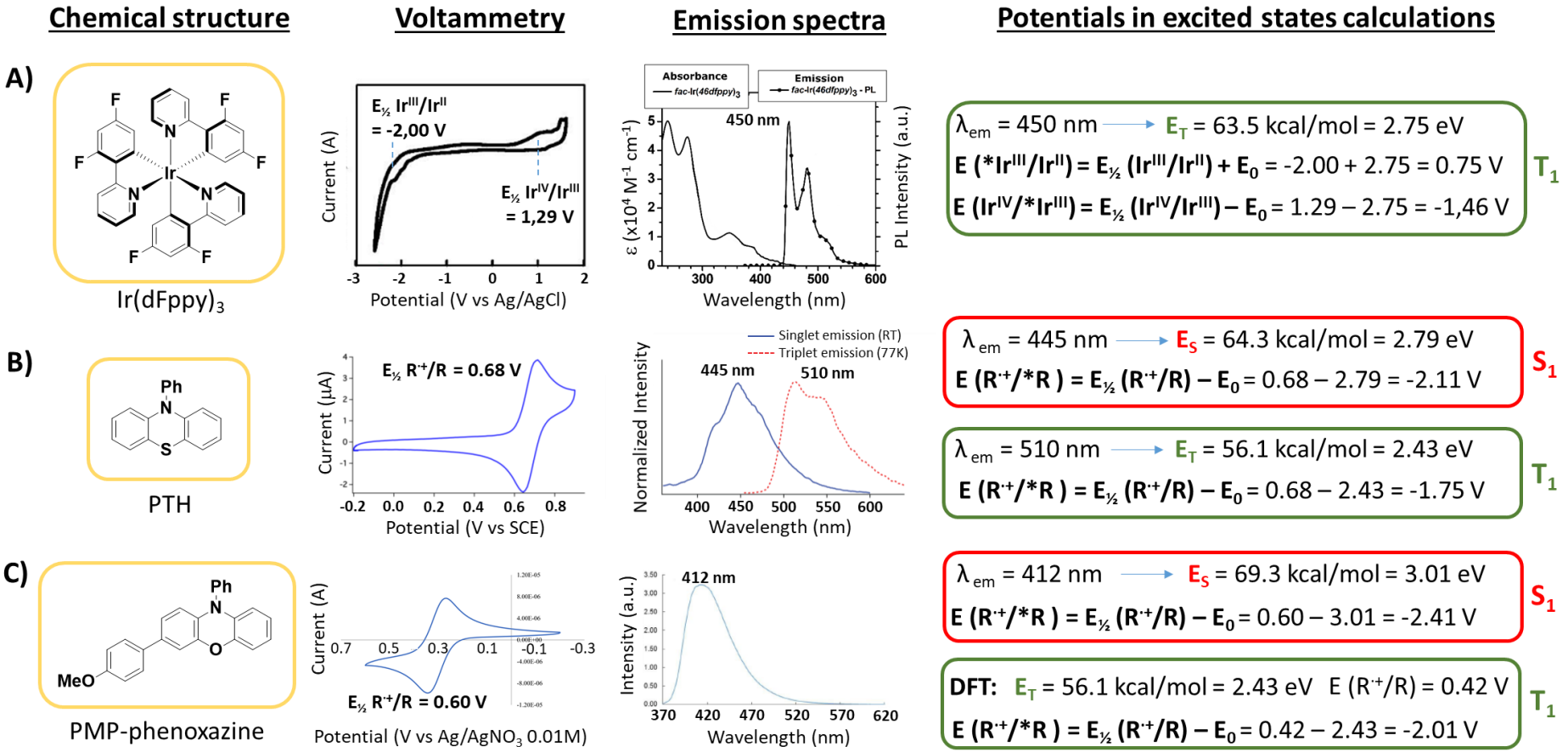

Figure 10. Photophysical parameters of the photocatalysts. The voltammetries, which are reproduced from different publications, have different reference electrodes. The extracted potentials written on each graphic are already converted into potentials vs SCE. V_{SCE} = V vs Ag/AgCl KCl (0.1M) + 0.04 V (Ref. 12b)// V_{SCE} = V vs $Ag/AgNO_3$ [0.01M] + 0.298 V (Ref. 5). All the potentials given in the column on the right are potential vs SCE. For references and permissions, see the footnotes of the previous page.

3.2. Expansion reactions of functionalized cyclopropanes

3.2.1. Reactivity of cyclopropanes and Donor-Acceptor cyclopropanes

Cyclopropanes are very versatile molecules as building blocks in organic synthesis. Their great angle and torsional strain make them very favourable to the ring opening reactions, allowing to construct more complex structures.

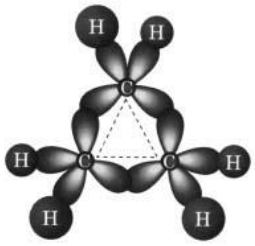

Figure 11. VB orbitals of cyclopropane. Reproduced from Ref. 1 with permission from John Wiley and Sons.

The chemical properties of cyclopropanes can be explained in a simplified way with the valence bond theory. Since carbon atoms forms a triangle, the angle CCC is 60°, which is far from the ideal 109.5° that corresponds to sp^3 hybridization of tetravalent carbons, which makes the angles strained. To improve the overlap, the hybridization is adjusted. The orbitals of the C-C bonds increase their *p* character to reduce the interorbital angle and as a consequence the orbitals of the C-H bond increase their *s* character. Even so, the interorbital angle is now 104°, so the bonding orbitals are not directed along the internuclear axis (Figure 11), making the overlap poor. As a consequence, the electronic density is more concentrated out of this axe.[1]

Due to all these characteristics, the cyclopropane has low thermodynamic stability and increased reactivity with regard to unstrained alkanes. Despite of this increased reactivity, the activation barrier for the ring-opening of cyclopropanes is still high. Functional groups directly attached to cyclopropanes can stabilize the transitions states and intermediates of the ring-opening, modulating their reactivity. A broadly studied strategy for this modulation of reactivity is the use of donor-acceptor cyclopropanes (DA cyclopropanes).[22]

A donor-acceptor cyclopropane (**a**, see Scheme 16) has a functional group capable of stabilizing positive charge (the donor) and a functional group which can stabilize negative charge (acceptor) in vicinal position. This situation allows to decrease the barrier of reactions that proceed through the 1,3-dipole **b**, resulted from the heterolytic cleavage of the bond DC-CA. The possible reactions that these cyclopropanes can experiment are schematically summarized in Scheme 16. The attack of a single electrophile or nucleophile to the donor-acceptor cyclopropane results in an open product. However, cycloadditions and rearrangements, although going through open intermediates, yield cyclic molecules with at least five members in the cycle, so they can be considered as ring expansions. This introduction pretends to focus on ring expansion reactions of cyclopropanes, so only few examples of the former reactions will be given.

[22] For selected reviews see: a) T. F. Schneider, J. Kaschel, D. B. Werz, *Angew. Chem. Int. Ed.* **2014**, *53*, 5504 – 5523. b) M. A. Cavitt, L. H. Phun, S. France, *Chem. Soc. Rev.* **2014**, *43*, 804—818. c) H. K. Grover, M. R. Emmett, M. A. Kerr, *Org. Biomol. Chem.* **2015**, *13*, 655–671. d) S. J. Gharpure, L. N. Nanda, *Tetrahedron Lett.* **2017**, *58*, 711-720. e) B. L. Pagenkopf, N. Vemula, *Eur. J. Org. Chem.* **2017**, 2561–2567.

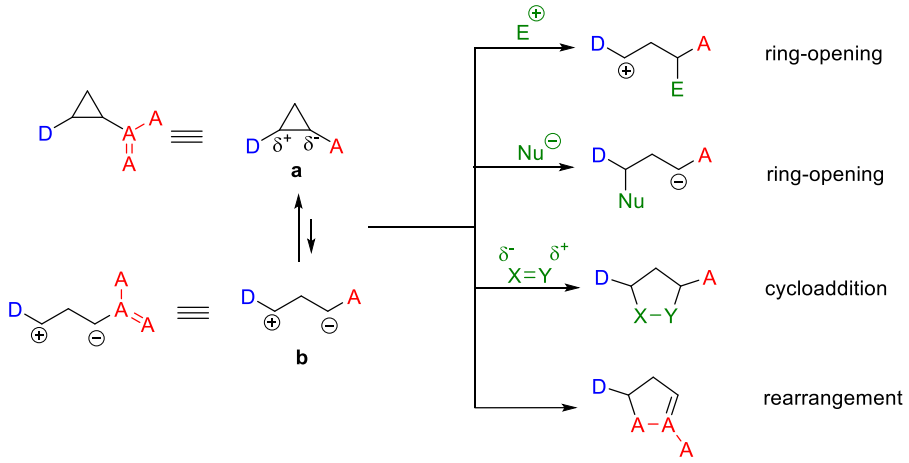

Scheme 16. General reactivity of Donor-Acceptor cyclopropanes.

When enantioenriched products are sought there are two different ways to accomplish them: **enantiospecificity** and **enantioselectivity**. Although these terms are applicable to more organic reactions, it is especially important to distinguish them in this context. In an **enantiospecific** reaction, an enantioenriched cyclopropane is used as starting material, and each enantiomer renders a specific enantiomer of the product, retaining the enantiomeric excess. On the other hand, in an **enantioselective** reaction, the starting material is a racemic cyclopropane and an enantiopure chiral catalyst leads the reaction of the open intermediate to one of the possible enantiomers, generating enantiomeric excess. In the reactions described along this text, the cases where this is not indicated, it is due they are a cases of racemic synthesis or the authors have not checked the enantiospecificity.

3.2.2. Nucleophilic and electrophilic attack to DA cyclopropanes

A very common strategy for the ring opening of cyclopropanes through nucleophilic attack, that can be found in several works in the literature, is the use of cyclopropane with two esters groups in geminal position as double acceptor and an aryl group in vicinal position as donor. In 2013 Johnson *et al.* used a protected indole as nucleophile under a magnesium catalyst with a chiral ligand to render the open product with a new C-C bond with good enantiomeric excess[23a] (Scheme 17A). The employment of phenols,[23b] alkyl or aromatic amines[23c] and thiophenols[23d] as nucleophiles to create C-O, C-N and C-S bonds respectively in the open product can be found in the literature (in the latter case a more complex cyclopropane was used).

The addition of an electrophile to a donor-acceptor cyclopropane can be achieved with a cyclopropane bearing a vinyl group as donor and two ester groups (in some cases ketones or aldehydes) as acceptors. The employment of the appropriate metal catalyst allows the ring opening, forming a metal-allyl complex intermediate, that can attack an electrophile from any of the two allylic reactive carbons, depending of the conditions. In 2008, Oshima's group achieved the boronate addition to the external position of the allylic intermediate with nickel

[23] a) S. M. Wales, M. M. Walker, J. S. Johnson, *Org. Lett.* **2013**, *15*, 2558-2561. b) O. Lifchits, D. Alberico, I. Zakharian, A. B. Charette, *J. Org. Chem.* **2008**, *73*, 6838–6840. c) O. Lifchits, A. B. Charette, *Org. Lett.* **2008**, *10,* 2809-2812. d) M. Yu, B. L. Pagenkopf, *Tetrahedron*, **2003**, *59*, 2765-2771.

catalysis (Scheme 17B).[24a] In 2011 Krische *et al.* developed the enantioselective addition of aldehydes to the inner allylic positions under a chiral iridium complex catalyst (Scheme 17C).[24b]

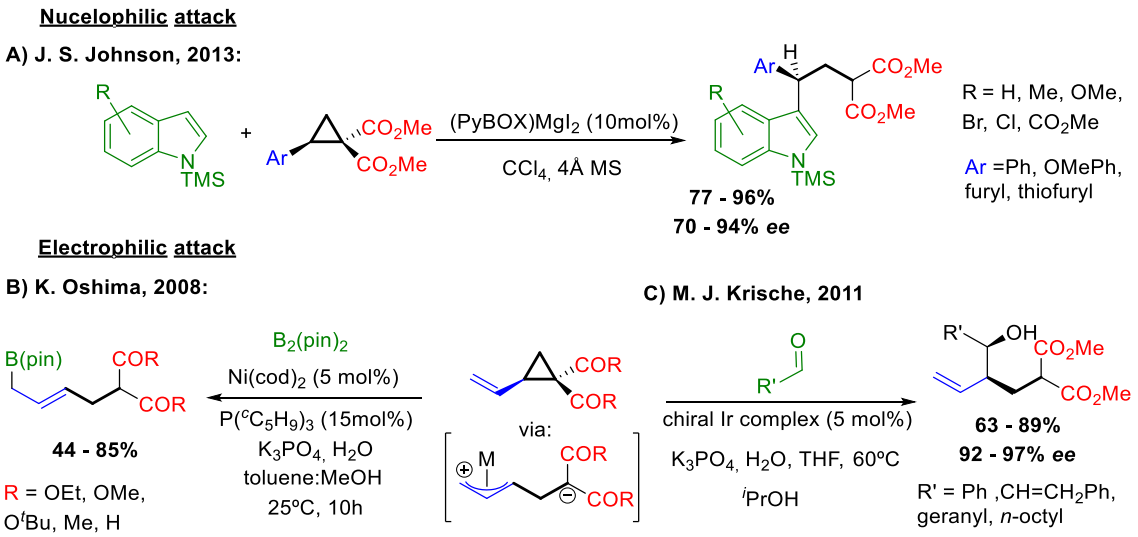

Scheme 17. Examples of ring opening by nucleophilic or electrophilic attack.

3.2.3. Cycloadditions to DA cyclopropanes with hetero-dipolarophiles (C=O, C=N)

There are multiple examples of photocycloadditions to DA cyclopropanes using dipolarophiles bearing C=O and C=N bonds to construct tetrahydrofurans, pyrrolidines or more complex structures.

The cycloaddition of aldehyde and ketones with donor-acceptor cyclopropanes yields tetrahydrofurans. Between the years 2005 and 2012, Johnson *et al.* developed several works of enantiospecific cycloaddition of aldehydes to aryl or alkyl cyclopropanes using Sn^{2+} and Sn^{4+} salts as Lewis acids.[25a-c] In the year 2009, they developed an enantioselective version of this reaction using as catalyst Mg^{2+} with a chiral PyBOX ligand (Scheme 18A).[25d] In 2012, Waser's group used a cyclopropane with a protected amine as donor group for a enantiospecific cycloaddition of ketones (Scheme 18B).[25e]

An elegant strategy was used by Nishibayashi and co-workers to perform this transformation in 2013. They used a cyclopropane with a triple bond group as donor group (Scheme 18C). [26] The ring opening was promoted by the formation of an allenyliden complex with a ruthenium catalyst. An aldehyde or an imine activated by a Lewis acid (BF_3 or Sc^{3+} respectively) reacted with the complex yielding the tetrahydrofuran or pyrrolidine. A very curious method for the cycloaddition of aldehydes with DA cyclopropanes was carried out by Maulide *et al.* in 2016, who used cyclopropanes with a cyclic acetal (Scheme 18D). In the

[24] a) Y. Sumida, H. Yorimitsu, K. Oshima, *Org. Lett.* **2008**, *10,* 4677-4679. b) J. Moran, A. G. Smith, R. M. Carris, J. S. Johnson, M. J. Krische, *J. Am. Chem. Soc*. **2011**, *133*, 18618–18621.

[25] a) P. D. Pohlhaus, J. S. Johnson, *J. Am. Chem. Soc.* **2005**, *127*, 16014-16015; b) P. D. Pohlhaus, J. S. Johnson, *J. Org. Chem.* **2005**, *70*, 1057-1059; c) P. D. Pohlhaus, S. D. Sanders, A. T. Parsons, W. Li, J. S. Johnson, *J. Am. Chem. Soc.* **2008**, *130*, 8642-8650. d) A. T. Parsons, J. S. Johnson, *J. Am. Chem. Soc.* **2009**, *131*, 3122-3123. e) F. Benfatti, F. de Nanteuil, J. Waser, *Chem. Eur. J.* **2012**, *18*, 4844 – 4849.

[26] Y. Miyake, S. Endo, T. Moriyama, K. Sakata, Y. Nishibayashi, *Angew. Chem. Int. Ed.* **2013**, *52*, 1758-1762.

presence of a Lewis acid, this acetal opens forming an oxocarbenium, which acts as acceptor group an promotes the opening of the cyclopropane, allowing the cycloaddition.[27]

The cycloaddition of DA cyclopropanes is not limited to the [3+2]. In 2016 Werz *et al.* described a [3+3] cycloaddition to typical DA cyclopropanes with nitrile imines yielding tetrahydropyridazines (Scheme 18E).[28] The yield was very sensitive to the substituents of the nitrile imine.

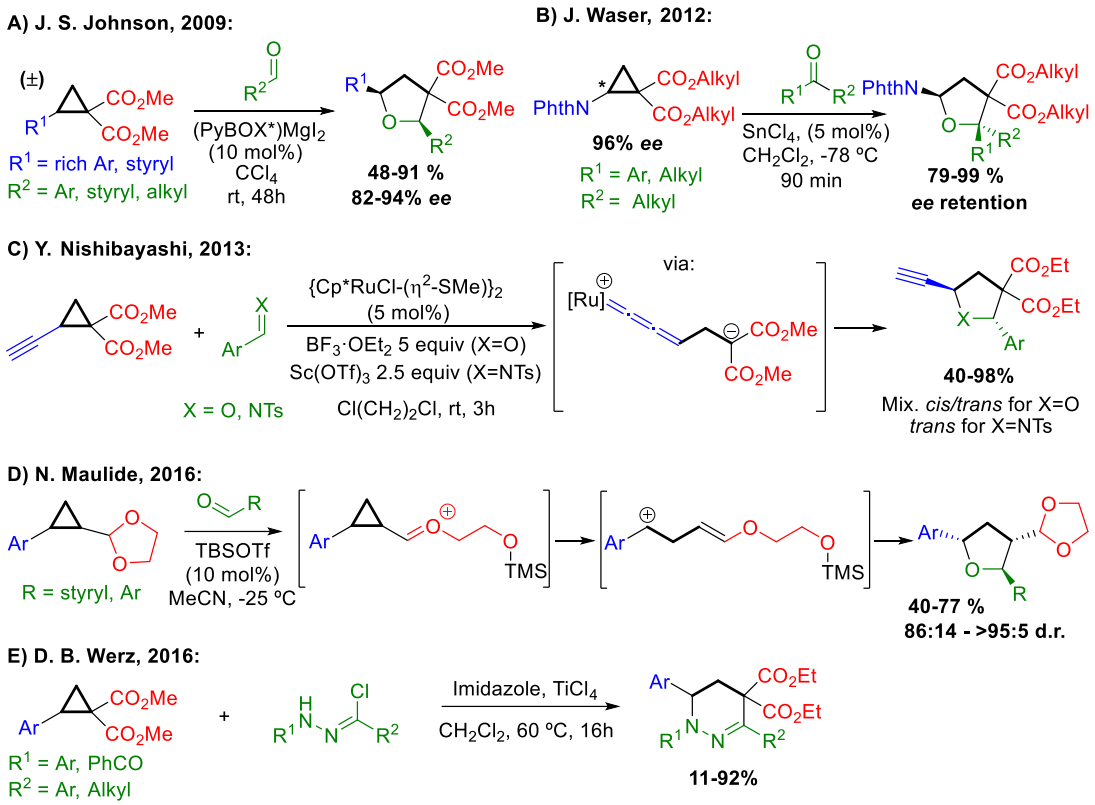

Scheme 18. Intermolecular cycloaddition of DA cyclopropanes with hetero-dipolarophiles.

The intramolecular version of the cycloaddition of a C=O bond was broadly studied in 2010 by Wang *et al.* and they used their methodology for a formal synthesis of the platensimycin (Scheme 19A). [29a] As may be seen, it follows the same strategy as the intermolecular reaction: two esters groups as acceptors, a rich aryl group as donor, a Lewis acid as catalyst and a ketone as dipolarophile. This type of intramolecular cycloaddition can also be found in the total synthesis of the (±)-bruguierol A[29b] and in the synthesis of the core skeleton of komaroviquinone.[29c]

There are more examples in the literature that allow to obtain very interesting structures. In 2008 Kerr's group investigated the synthesis of the bicyclic pyrrolo-isoxazolidines, using cyclopropanes bearing an oxime ether as pending arm (Scheme 19B);[30] the bond N-O of the product could be opened to get highly functionalized pyrroles. In 2015 Wang *et al.* developed a

[27] J. Sabbatani, N. Maulide, *Angew. Chem. Int. Ed*. **2016**, *55*, 6780 –6783.
[28] L. K. B. Garve, M. Petzold, P. G. Jones, D. B. Werz, *Org. Lett.* 2016, *18*, 564−567.
[29] a) S. Xing, W. Pan, C. Liu, J. Ren, Z. Wang, *Angew. Chem. Int. Ed.* **2010**, *49*, 3215 –3218. b) B. Hu, S. Xing, J. Ren, Z. Wang, *Tetrahedron* **2010**, *66*, 5671-5674. c) S. Xing, Y. Li, Z. Li, C. Liu, J. Ren, Z. Wang, *Angew. Chem. Int. Ed.* **2011**, *50*, 12605–12609.
[30] S. K. Jackson, A. Karadeolian, A. B. Driega, M. A. Kerr, *J. Am. Chem. Soc.* **2008**, *130*, 4196-4201

cyclopropane for an intramolecular cycloaddition, having a cobalt-alkyne moiety in the link between the cyclopropane fragment and the carbonyl group. The organometallic moiety was conserved within the bicyclic structure of the product, allowing multiple functionalizations to obtain more complex structures (Scheme 19C).[31]

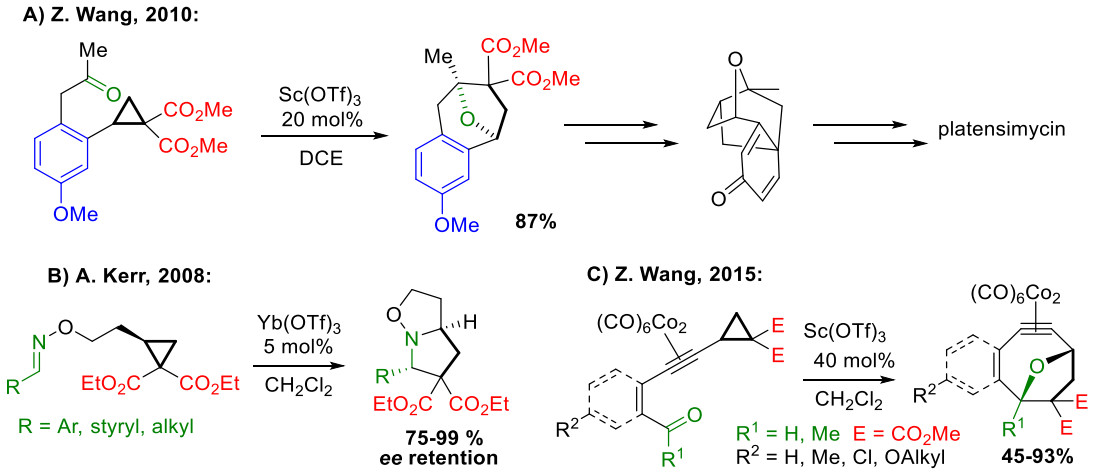

Scheme 19. Intramolecular cycloaddition of DA cyclopropanes bearing hetero-dipolarophiles.

3.2.4. Cycloadditions to DA cyclopropanes with C=C dipolarophiles.

It is possible to find in the literature cycloadditions to DA cyclopropanes where the homo-dipolarophile is an α,β-unsaturated carbonyl compound,[32] but the use of silyl enol ethers as homo-dipolarophiles is much more common.[33] As an example, Scheme 20A shows the enantioselective addition of cyclic silyl enol ether to a prototypic DA cyclopropane to obtain protected hydroxycarbobicycles carried out by Tang and co-workers in 2013.[33c] In 2015 the same author expanded this concept and performed the [4+3] cycloaddition using dienic silyl enol ether (Scheme 20B). [33d]

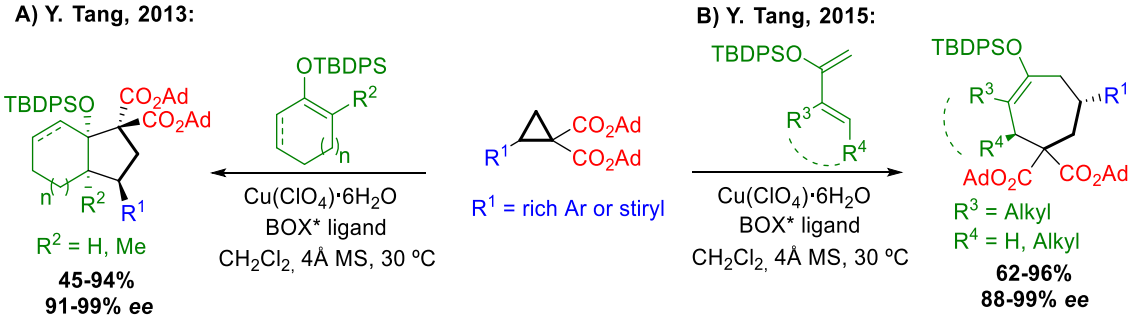

Scheme 20. Intermolecular cycloaddition of DA cyclopropanes with C=C dipolarophiles.

[31] J. Zhang, S. Xing, J. Ren, S. Jiang, Z. Wang, *Org. Lett.* **2015**, *17*, 218−221.
[32] B. M. Trost, P. J. Morris, S. J. Sprague, *J. Am. Chem. Soc.* **2012**, *134*, 17823−17831
[33] a) J.-P. Qu, C. Deng, J. Zhou, X.-L. Sun, Y. Tang, *J. Org. Chem.* **2009**, *74*, 7684–7689. b) F. de Nanteuil, J. Waser, *Angew. Chem. Int. Ed*. **2011**, *50*, 12075 –12079. c) H. Xu, J.-P. Qu, S. Liao, H. Xiong, Y. Tang, *Angew. Chem. Int. Ed.* **2013**, *52*, 4004 –4007. d) H. Xu, J.-L. Hu, L. Wang, S. Liao, Y. Tang, *J. Am. Chem. Soc.* **2015**, *137*, 8006−8009.

In 2013 Whang *et al.* studied several variants of the intramolecular cycloaddition [3+2] of cyclopropanes bearing a pending arm having a double C=C double bond or a diene. They applied this method to the total synthesis of (±)-phyllocladanol and (±)-phyllocladene (Scheme 21).[34]

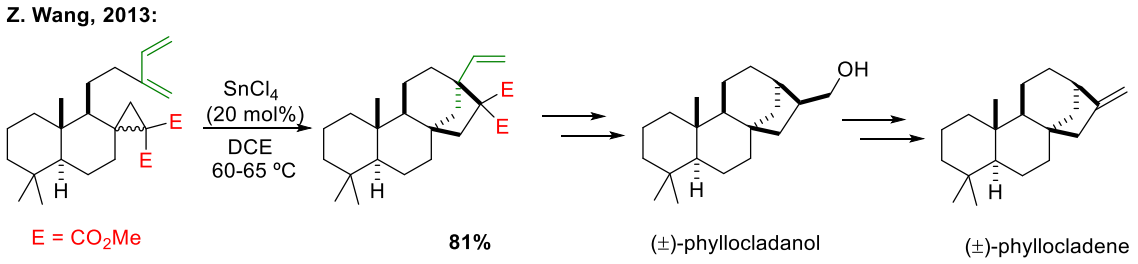

Scheme 21. Intramolecular cycloaddition of DA cyclopropane bearing a C=C dipolarophile.

3.2.5. Organocatalytic methods for cycloadditions to DA cyclopropanes

Despite the presence of donor and acceptor groups in the cyclopropane, in the cycloadditions shown so far, the use of a Lewis acid, normally metallic, is also necessary in most of the cases. Organocatalysis offers different possibilities to open and make cycloadditions to DA cyclopropanes so it deserves a separate section.

One of these possibilities is the combination of a cyclopropylacetaldehyde and a chiral secondary amine catalyst (Scheme 22A). These two molecules condensate and the resulting covalent-bonded intermediate undergoes tautomerization forming a cyclopropylenamine, the real DA cyclopropane. This cyclopropylenamine undergoes easy ring opening to form the open intermediate. The open intermediate is in equilibrium with a dienamine (not shown) which can undergo [2+2] cycloaddition with 3-olefinic oxindoles to form spirocyclobutanes (Scheme 22A, top), reaction developed by K. A. Jørgensen in 2015.[35a] In the next year, using the same combination of the cyclopropylacetaldehyde and an aminocatalyst, Vicario *et al.* carried out a cascade reaction with *o*-aminobenzaldehyde to form pyrrolo[1,2-*a*]quinolones (Scheme 22A, bottom).[35b] In both cases, the bulky substituent (depicted as blue sphere in Scheme 22A) of the amine chiral catalyst led the reaction to enantioenriched products.

Other similar process was performed by Jørgensen and co-workers in 2017.[36] He used a bifunctional chiral catalyst with a thiourea and a Brønsted base, which deprotonated the α-proton of a β-cyclopropylketone. The chiral catalyst led the [3+2] cycloaddition of a nitroalkene to the deprotonated intermediate to form enantioenriched nitrocyclopentanes (Scheme 22B). Other examples of enantioselective cycloaddition to DA cyclopropanes using other types of organocatalyst, such as chiral *N*-heterocycle carbenes, can be found in the literature.[37]

---

[34] W. Zhu, J. Fang, Y. Liu, J. Ren, and Z. Wang, *Angew. Chem. Int. Ed.* **2013**, *52*, 2032 –2037.

[35] a) K. S. Halskov, F. Kniep, V. H. Lauridsen, E. H. Iversen, B. S. Donslund, K. A. Jørgensen, *J. Am. Chem. Soc.* **2015**, *137*, 1685−1691 b) E. Sanchez-Diez, D. L. Vesga, E. Reyes, U. Uria, L. Carrillo, J. L. Vicario, *Org. Lett.* **2016**, *18*, 1270−1273.

[36] J. Blom, A. Vidal-Albalat, J. Jørgensen, C. L. Barløse, K. S. Jessen, M. V. Iversen, K. A. Jørgensen, *Angew. Chem. Int. Ed.* **2017**, *56*, 11831 –11835

[37] L. Prieto, E. Sánchez-Díez, U. Uria, E. Reyes, L. Carrillo, J. L. Vicario, *Adv. Synth. Catal.* **2017**, *359*, 1678-1683.

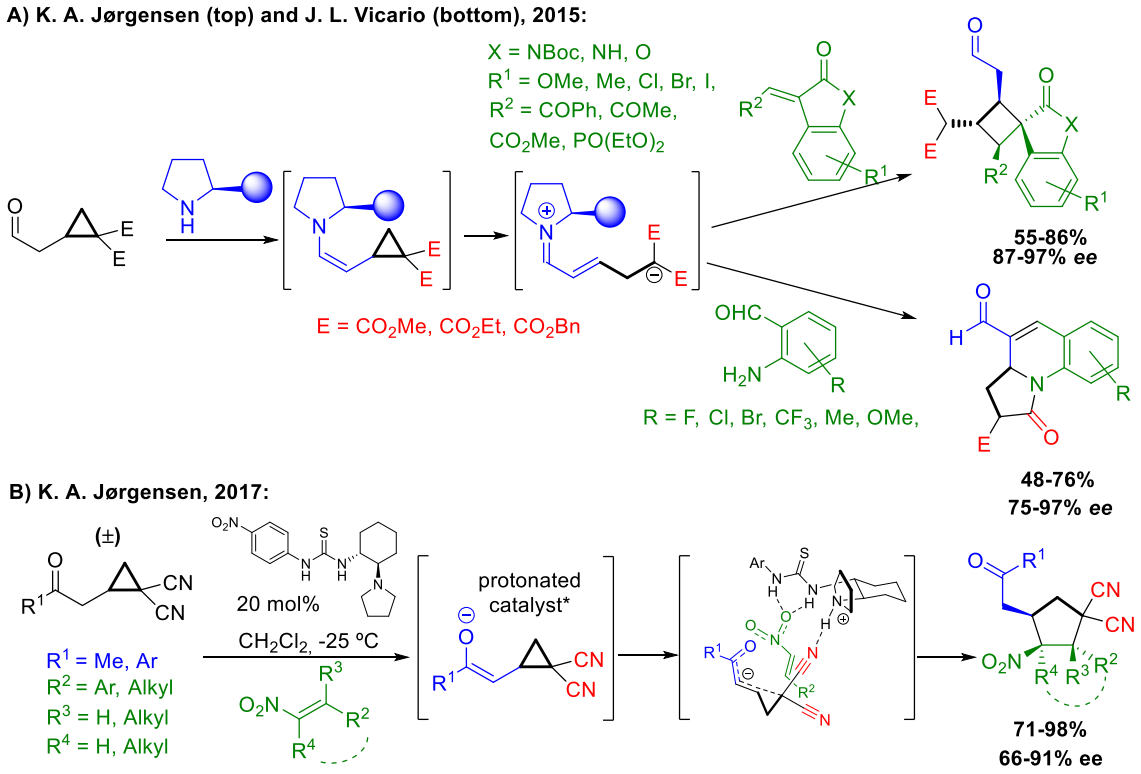

Scheme 22. Organocatalytic cycloadditions to DA cyclopropanes.

3.2.6. Rearrangements of DA cyclopropanes

The rearrangement of a DA cyclopropanes is given between the cyclopropane moiety and a double bond directly attached to the cyclopropane, yielding a cycle of five members (See Scheme 23, right).[38] This double bond is usually part of the acceptor group of the DA cyclopropane. When this group is an imine, aldehyde or ketone the rearrangement is known as Cloke-Wilson reaction.[39] It is important to differentiate the rearrangements from the intramolecular cycloadditions in DA cyclopropanes. In the latter case, there is a linker, normally with three atoms, between the cyclopropane and the dipolarophile. Consequently, when the intramolecular cycloaddition takes place, a bicycle is obtained (see above, Scheme 19 and Scheme 21).

In 2011, Werz *et al.* carried out a very complete computational study where they calculated the activation barrier of the rearrangement of DA cyclopropanes as a function of their donor and acceptor groups.[40] From the graphic of Scheme 23 it can be extracted that thioaldehyde and nitroso groups are the best groups to facilitate the ring expansion. The activation barrier increases if the acceptor group is an aldehyde, ketone, imine or nitro group and finally, the most difficult rearrangement to perform would be those that have esters or carboxylic acids as acceptor. All these rearrangements are calculated for concerted and non-

[38] For a review of cyclopropane rearrangements see: T. Hudlicky, J. W. Reed, *Angew. Chem. Int. Ed.* **2010**, *49*, 4864 – 4876.
[39] a) J. B. Cloke, *J. Am. Chem. Soc.* **1929**, *51*, 1174-1187. b) C. L. Wilson, *J. Am. Chem. Soc.* **1947**, *69*, 3002-3004.
[40] T. F. Schneider, D. B. Werz, *Org. Lett.* **2011**, *13*, 1848-1851.

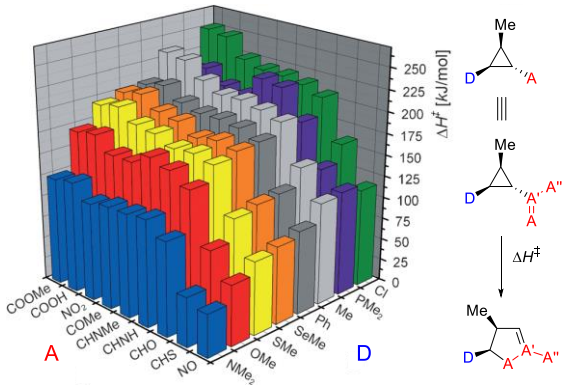

Scheme 23. Activation barrier of DA cyclorpopanes rearrangements. Adapted from Ref. 22a with permission from John Wiley and Sons.

catalysed reactions, but the scenario can change with the use of a catalyst or with more complex cyclopropanes. Functional groups bearing C=C double bond were not studied in this work.

In 2006, Johnson and co-workers developed a DA cyclopropane prone to rearrangement having a vinyl group as donor and two groups as acceptor: one of them was always a ketone and the other one could be a ketone or an ester (Scheme 24A).[41] The rearrangement proceeded via an open allyl complex with a nickel catalyst and then the cyclization was given with the ketone group in an enantiospecific way. The rearrangement never proceeded with the vinyl group, even in the cases that it was conjugated with an ester.

In 2013, Kerr *et al.* carried out the rearrangement of a cyclopropane with a carboxylic acid group. The cyclopropane had an aryl or vinyl group as donor and an extra ester group as acceptor which was lost during the course of the reaction (Scheme 24B).[42] Since the reaction was enantiospecific, this methodology could be used to synthesize the natural product (*R*)-dodecan-4-olide, after a reduction of the double bond of the rearrangement product.

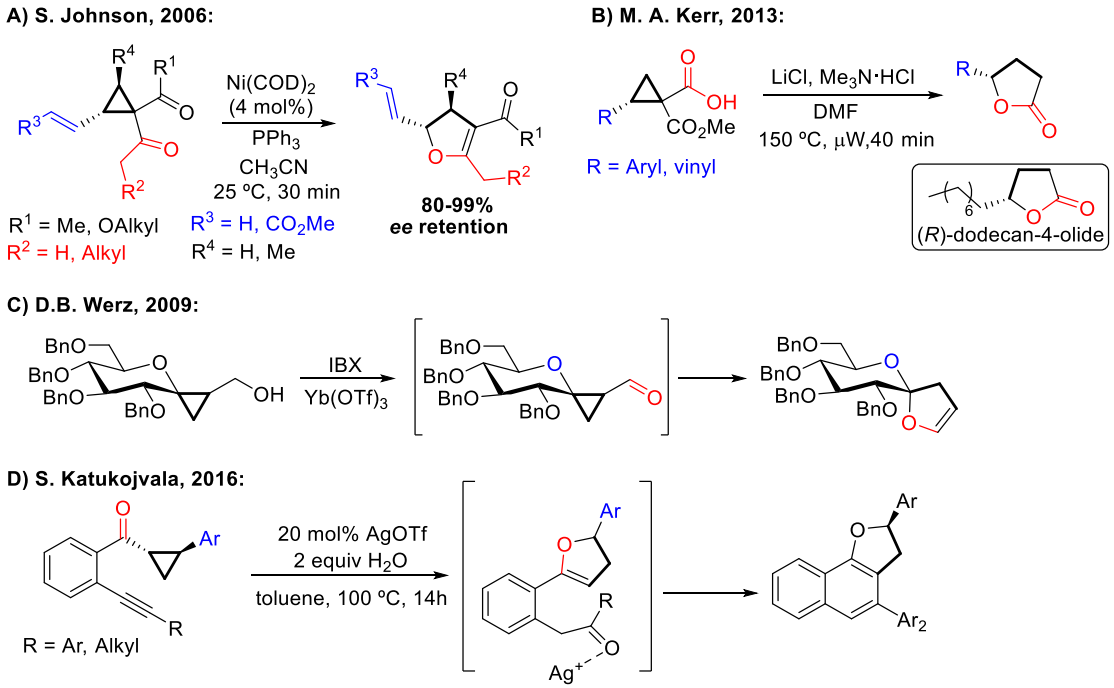

Scheme 24. Rearrangements of DA cyclopropanes with C=O acceptors groups.

[41] R. K. Bowman, J. S. Johnson, *Org. Lett.* **2006**, *8*, 573-576.
[42] H. K. Grover, M. R. Emmett, M.A. Kerr, **2013**, *15*, 4838-4841.

In 2009, Werz's group developed the rearrangement of spiro-formylcyclopropanes to obtain interesting bicyclic structures. [43] As an example, Scheme 24C shows a molecule of protected glucose functionalized with a cyclopropylmethanol forming a spiro compound. When it was oxidized to the corresponding aldehyde it underwent the rearrangement. This methodology was applied to numerous formylcyclopropane spirocycles.

In 2016, Katukojvala and co-workers performed a cascade reaction using 2-ethynylphenyl cyclopropyl ketones (Scheme 24D)[44] where the silver cation has several roles: it promotes the rearrangement of the cyclopropyl ketones motif and the hydration of the triple bond to form the intermediate shown in Scheme 24D and the subsequent Friedel-Crafts to form the final polycycle.

Although less frequently, there are examples of rearrangements of DA cyclopropanes containing a nitrogen in a double bond. However, they are usually cases where the cyclopropane is an intermediate of the reaction. In such a way, in 2013, Werz group, through the reaction of alkenes with α-diazo-α-nitro ethyl acetate, formed nitrocyclopropanes which underwent rearrangement to cyclic nitronates (Scheme 25A).[45a] In the same year, Zhang *et al.* synthesized bicyclic structures of chiral sugar skeletons and cyclopropanes (Scheme 25B); [45b] they added primary amines to these structures, which condensed with the carbonyl group, forming cyclopropylimines. These cyclopropylimines, under the action of $InBr_3$ catalyst, underwent the rearrangement. Finally, an opening of the ring product renders the final polyhydroxylatedalkyl pyrrole, retaining the enantiomeric excess.

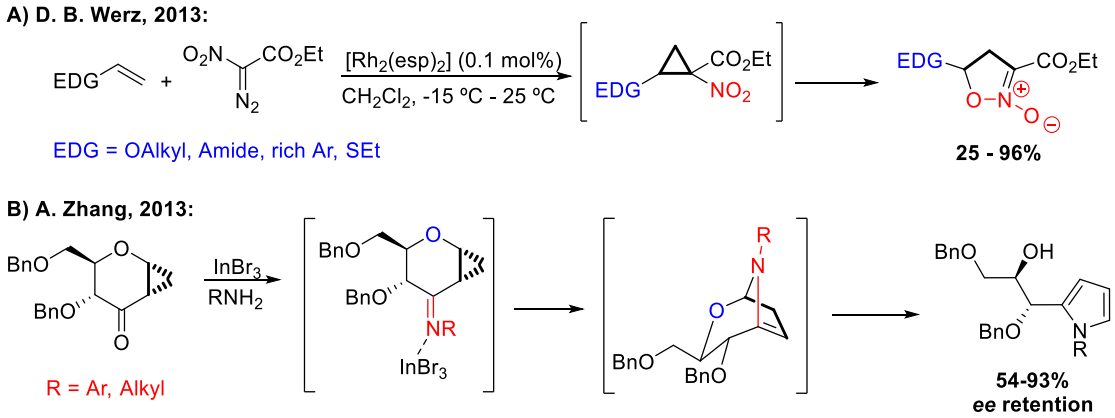

Scheme 25. Rearrangements of DA cyclopropanes with N=O or C=N acceptors groups.

The rearrangements of vinylcyclopropanes, that is, of cyclopropanes bearing a C=C group directly attached, is less frequent than its heteroatomic version, but interesting examples has arisen in the last years. In the case of vinylcyclopropanes, the presence of auxiliary acceptor groups decrease the activation energy of the reaction (see below, Scheme 26). This scenario is opposite to the rearrangements shown in these documents so far, (see above, Scheme 24 and Scheme 25), where the rearrangement is given between the cyclopropane and the double bond of the acceptor group and auxiliary donor groups decreased the activation energy.

[43] C. Brand, G. Rauch, M. Zanoni, B. Dittrich, D. B. Werz, *J. Org. Chem.* **2009**, *74*, 8779–8786.
[44] S. G. Dawande, M. Harode, J. Kalepu, S. Katukojvala, *Chem. Commun.* **2016**, *52*, 13699—13701.
[45] a) C. D. Schmidt, J. Kaschel, T. F. Schneider, D. Kratzert, D. Stalke, D. B. Werz, *Org. Lett.* **2013**, *15*, 6098-6101. b) P. Wang, S. Song, Z. Miao, G. Yang, A. Zhang, *Org. Lett.* **2013**, *15*, 3852-3855.

Several authors have demonstrated that fluorinated vinylcyclopropanes undergo the rearrangement easily due to the acceptor inductive character of this halogen,[46] as can be appreciated in the example shown in Scheme 26A by Z. A. Harrison in 2014.[46b] Actually, this type of rearrangement was discovered in a fluorinated vinylcyclopropane.[47]

In 2017 Trushkov and co-workers developed the Lewis acid catalysed rearrangement of styryl cyclopropanes having two esters groups as acceptors (Scheme 26B); they investigated which metallic Lewis acid was best for each product of the scope.[48] In the previous year Yao *et al.* had applied a similar concept, generating in situ styrylcyclopropanes spirocyclohexadienones, which underwent the rearrangement to the corresponding spirocyclopentene (Scheme 26C).[49] Very recently Ichikawa's group carried out the generation of a vinyl cyclopropane with two fluorines atoms as acceptor groups and a silanolate in geminal position with the vinyl group as an extra donor group (Scheme 26D). Once this cyclopropane was generated in the reaction media, it was only necessary to heat up the mixture to get the final cyclic enolate product.[50]

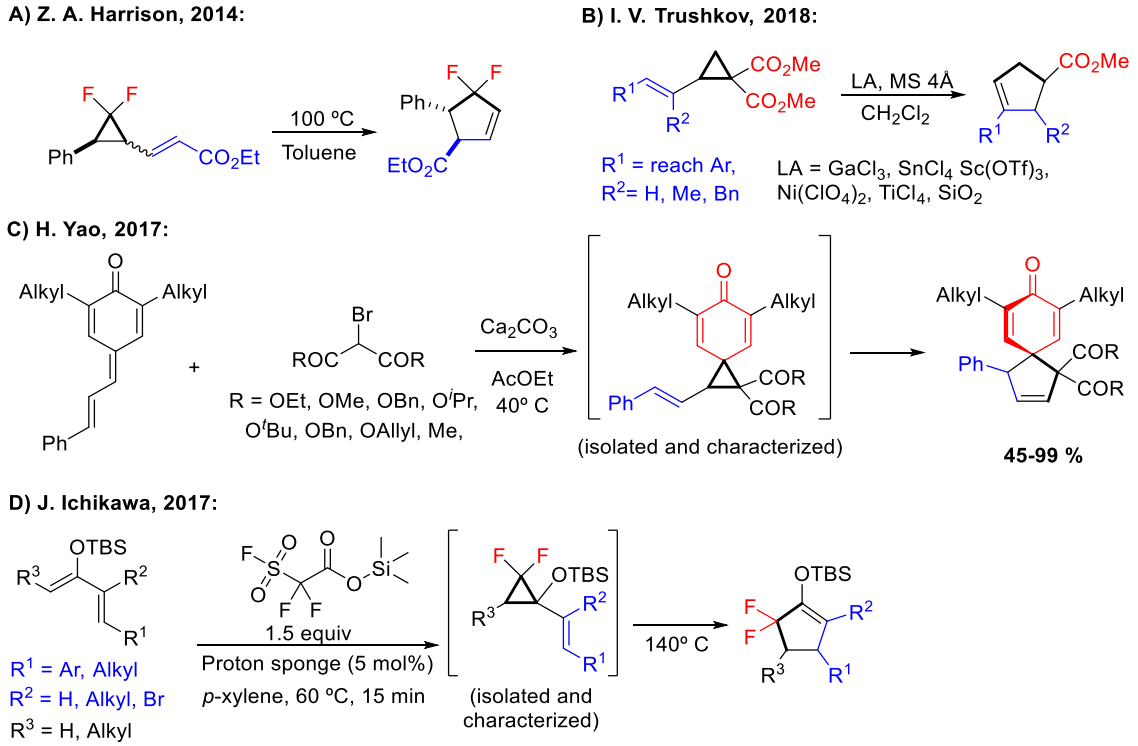

Scheme 26. Rearrangements of vinyl cyclopropanes.

[46] a) B. E. Smart, P. J. Krusic, D. C. Roe, Z.-Y. Yang, *J. Fluorine Chem.* **2002**, *117*, 199-205. b) D. Orr, J. M. Percy, T. Tuttle, A. R. Kennedy, Z. A. Harrison, *Chem. Eur. J.* **2014**, *20*, 14305 – 14316.
[47] N. P. Neureiter, *J. Org. Chem.* **1959**, *24*, 2044-2046.
[48] O. A. Ivanova, A. O. Chagarovskiy, A. N. Shumsky, V. D. Krasnobrov, I. I. Levina, I. V. Trushkov, *J. Org. Chem.* **2018**, *83*, 543−560.
[49] Z. Yuan, K. Gai, Y. Wu, J. Wu, A. Lin, H. Yao, *Chem. Commun.* **2017**, *53*, 3485—3488.
[50] R. Takayama, K. Fuchibe, J. Ichikawa, *Arkivoc* **2018**, *ii*, 72-80.

3.2.7. Organocatalytic rearrangements of DA cyclopropanes

In all the methodologies for the rearrangement of DA cyclopropanes shown so far, when an enantiopure product is obtained, the origin of that enantiomeric excess is none other than the use of enantioenriched starting DA cyclopropanes, which undergo the reaction in an enantiospecific way. That is why an enantioselective rearrangement of cyclopropyl ketones developed by Vicario group in 2018 deserves a special mention. In this work a catalytic chiral phosphoric acid activates the substrate to promote the ring opening event, forms a complex with the polar open intermediate and leads the enantioselective closure (Scheme 27).[51] There are few more examples of organocatalytic rearrangements of DA cyclopropanes in the literature.[52]

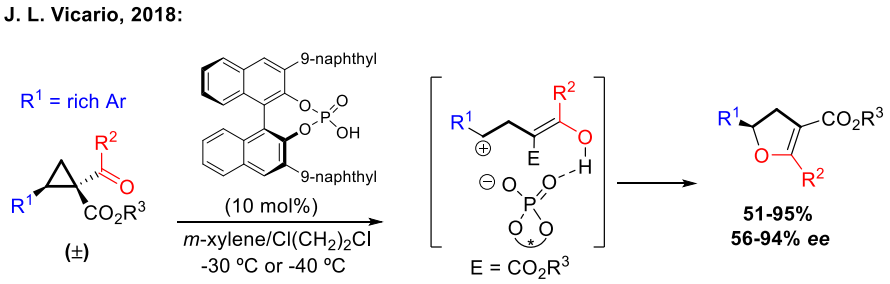

Scheme 27. Enantioselective organocatalysed rearrangement of cyclopropylketones.

3.2.8. Photocatalysis with functionalized cyclopropanes

As we have seen, DA cyclopropanes are very versatile molecules which allows to construct more complex structures through cycloadditions and rearrangement reactions. In most of the cases, the success of the reaction is determined by finding a correct catalyst which interacts with the donor and acceptor groups presented in the cyclopropane. However, the DA cyclopropanes have limitations, since the presence of one acceptor group and one donor group in vicinal positions is necessary in most of the cases, limiting other functional group combinations which could be useful to build other complex structures. Therefore, it is essential to develop ring opening processes, cycloadditions and rearrangements of functionalized cyclopropanes which undergo these reactions through different mechanisms than the polar one to allow other functional group patterns.

The emerging field which offers more possibilities in the quest for new methodologies to manipulate functionalized cyclopropanes is the visible light mediated photocatalysis. There are two important works regarding this topic that were developed before the project of this doctoral thesis (Scheme 28). In 2015 Lu *et al.* published a photocatalysed cycloaddition of styrenes to cyclopropanes bearing in vicinal position a nitro group and an ester group, both acceptor groups (Scheme 28A).[53] The catalytic cycle started with the excitation of the Ru(II) catalyst, which was reduced to Ru(I) by the quencher trimethylamine. Due to the presence of the nitro group, which is easily reduced, the nitrocyclopropane accepts one electron from the Ru(I) by "single electron transfer (SET)" and undergoes ring opening and a stepwise cycloaddition to form

[51] A. Ortega, R. Manzano, U. Uria, L. Carrillo, E. Reyes, T. Tejero, P. Merino, J. L. Vicario, *Angew. Chem. Int. Ed.* **2018**, *57*, 8225 –8229.
[52] J. Zhang, Y. Tang, W. Wei, Y. Wu, Y. Li, J. Zhang, Y. Zheng, S. Xu, *Org. Lett*. **2017**, *19*, 3043−3046
[53] C. Wang, X. Ren, H. Xie, Z. Lu, *Chem. Eur. J.* **2015**, *21*, 9676 – 9680.

nitrocyclopentanes. In the same publication they demonstrate that the nitro group of the products can be easily reduced to the amino group, making this method very versatile to synthesise natural products.

In 2016 Yoon's group utilized a similar strategy for the enantioselective photocatalysed cycloaddition of styrenes (or dienes) to aryl cyclopropyl ketones coordinated with gadolinium (Scheme 28B); the coordination of this Lewis acid makes the ketone motif prone to be reduced. As in the previous case, the excited Ru(II)* was quenched by an alkylamine to Ru(I), which reduced the coordinated cyclopropyl ketone by SET. Since the gadolinium has a PyBOX chiral ligand, the cycloaddition happened in an enantioselective manner and good enantiomeric excesses were obtained in the final product.[54]

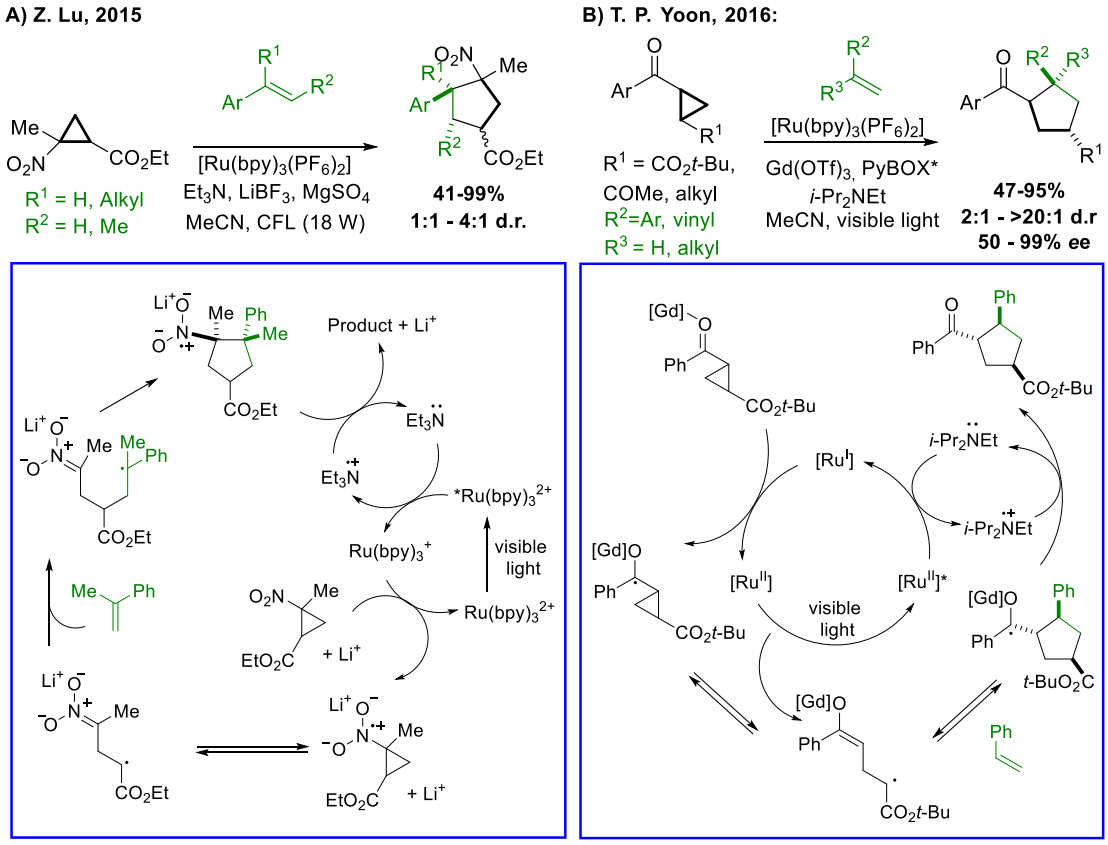

Scheme 28. Visible light mediated photocatalysed cycloadditions to functionalized cyclopropanes and their proposed mechanisms.

As can be seen in both reactions, in photocatalytic processes using cyclopropanes, it is also needed a good combination between the catalysts and the functional groups present in the substrate. The two examples shown in Scheme 28 are cases where photocatalysed cycloaddition are carried out in an intermolecular manner.

[54] A. G. Amador, E. M. Sherbrook, T. P. Yoon, *J. Am. Chem. Soc.* **2016**, *138*, 4722−4725.

3.2.9. Initial hypothesis about photocatalysed cyclopropane rearrangement

Since several intermolecular photocatalysed cycloadditions of cyclopropanes have been already investigated, now it is highly desirable to perform new photocatalysed methodologies for the rearrangement of cyclopropanes bearing doubles bonds. Before 2017, very little information regarding this topic had been published.[55] In 2015 Plietker *et al.* used an iron complex as photocatalyst to carry out the rearrangement of a vinyl cyclopropane ketones (Scheme 29A).[56a] The excited iron complex was coordinated to the C=C double bond and promoted the reaction. In 2016, in Wenger's group, a rearrangement of a simple cyclopropylketone was used to test a new molybdenum (0) isocyanide photoredox catalyst, but the work was not centred on developing the scope of the reaction (Scheme 29B).[56b] In both cases, the rearrangement took place with the C=O double bond of a ketone group, and they did not perform the rearrangement with aldehyde groups or with C=C double bonds.

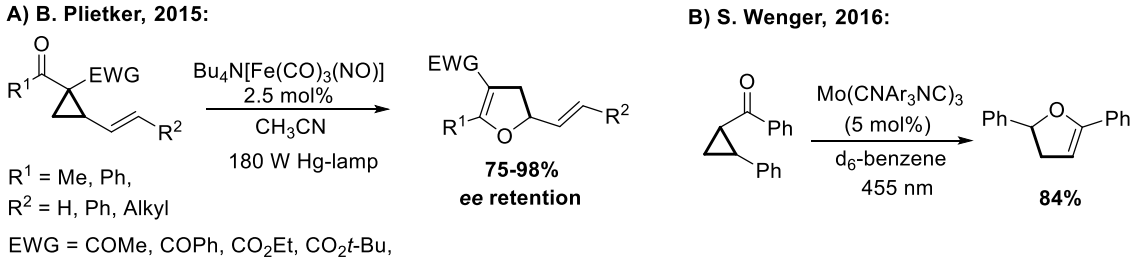

Scheme 29. Photocatalytic rearrangements of cyclopropanes.

Reviewing the literature about rearrangement of donor-acceptor cyclopropanes, it is noteworthy that there are not general methods to do rearrangements to any type of double bond attached to the cyclopropanes. Thus, there are specific methods to do rearrangements that allow the expansion of vinylcyclopropanes (C=C) into cyclopentenes, specific methods for the rearrangements of formylcyclopropanes (C=O) in dihydrofurans, methods for the expansion of iminecyclopropanes (C=N) into dihydropyrroles, etc. Therefore, it would be an interesting goal to develop a unique photocatalytic process that allows the rearrangement of both formylcyclopropanes and vinylcyclopropanes

This would be an important method since a same method would provide access to 2,3-dihydrofuranes and cyclopentenes. These two compounds are very common structures present in a wide number of natural products such as Aflatoxin B1,[57a] Clerodin,[57b] Austocystin A[57c] and Brevifoliol, [57d] among others (Figure 12). They show pharmacological properties, for instance,

---

[55] There are some old examples of rearrangements of cyclopropanes by direct UV light irradiation, for example: L. A. Paquette, G. V. Meehan, R. P. Henzel, and R. F. Eizember, *J. Org. Chem.* **1973**, *38*, 3250-3256.

[56] a) C.-H. Lin, D. Pursley, J. E. M. N. Klein, J. Teske, J. A. Allen, F. Rami, A. Köhn, B. Plietker, *Chem. Sci.* **2015**, *6*, 7034–7043. b) L. A. Bîldt, X. Guo, A. Prescimone, O. S. Wenger, *Angew. Chem. Int. Ed.* **2016**, *55*, 11247 –11250.

[57] a) G. S. Bbosa, D. Kitya, A. Lubega, J. Ogwal-Okeng, W. W. Anokbonggo, D. B. Kyegombe, "Review of the Biological and Health Effects of Aflatoxins on Body Organs and Body Systems, Aflatoxins - Recent Advances and Future Prospects (Chapter 12)", *IntechOpen*, **2013**, 239-265. b) D. H. R. Barton, H. T. Cheung, A. D. Cross, L. M. Jackman, M. Martin-Smith, *J. Chem. Soc.* **1961**, 5061-5072. c) P. S. Steyn, R. Vleggaar, *J. Chem. Soc., Perkin Trans. 1* **1974**, 2250-2256. d) R. Kaur, S. K. Chattopadhyay, A. Chatterjee, O. Prakash, F. Khan, N. Suri, D. Priya, A. K. Saxena, *Med. Chem. Res.* **2014**, *23*, 4138-4148. e) E. Findik, A. Dingil, I. Karaman, Y. Budak, M. Ceylan, *E-Journal of Chemistry*, **2009**, *6*, S53-S58. f) T. G. Kilroy, T. P. O'Sullivan, P. J. Guiry, *Eur. J. Org. Chem.* **2005**, 4929–4949.

they can be antibacterial or antifungal agents.[57e] Furthermore, 2,3-dihydrofurans are important reaction intermediates in the asymmetric synthesis of a wide range of compounds like γ-hydroxyaldehydes, γ-hydroxyketones, γ-lactones, furans and some hydroxyaminoacids.[57f]

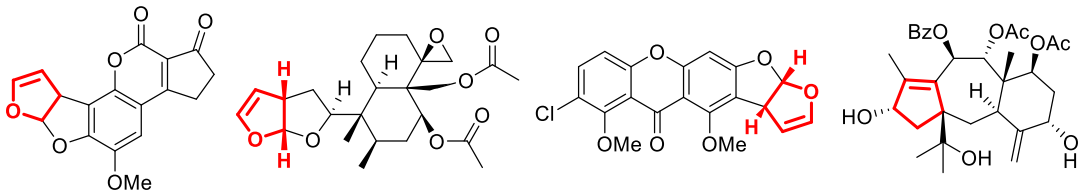

Figure 12. Dihydrofurans and cyclopentenes motifs in natural products.

As it was seen in the previous section, in one of the photocatalytic cycloadditions to cyclopropanes (Scheme 28A), it is essential the presence of a nitro group directly attached to the cyclopropane, since it has the role to accept one electron from the photocatalyst in a "single electron transfer (SET)" process. This data provides a hint that the nitro group can have an important role in reactions of cyclopropanes that proceed through radical or biradical intermediates.[58] Consequently, the nitro group can be required to develop new photocatalytic rearrangements of cyclopropanes.

In view of this background, we considered to develop a photocatalysed rearrangement of formylcyclopropanes and vinylcyclopropanes to obtain enantioenriched dihydrofurans and cyclopentenes. The starting cyclopropane materials will have a nitro group, which we envisage that will be essential for the process. To obtain the final enantioenriched products, we propose to develop a enantiospecific methodology, starting from optically pure cyclopropanes. The broad experience that the research group has in organocatalysis will allow to synthesise these materials with high enantiomeric excess.

The objectives of this part are fully described in Section 4.1.

[58] a) Y. L. Chow, N. Kornblum, "The Chemistry of Amino, Nitroso and Nitro Compoundsand their Derivatives" (Ed.: S. Patai), Wiley, New York, **1982**. b) D. A. Kleier, M. A. Lipton, *J. Mol. Struct. (Theochem)* **1984**, *109*, 39-49.

3.3. Tsuji-Trost reaction

3.3.1. General concepts

The Tsuji-Trost reaction is the substitution of a leaving group (LG) in an allylic position by a nucleophile (Nu).[59] Normally, this reaction is catalysed by a metal complex that causes the leaving group expulsion and forms an allylic metal complex with the substrate, which is attacked by the nucleophile (Scheme 30).[60]

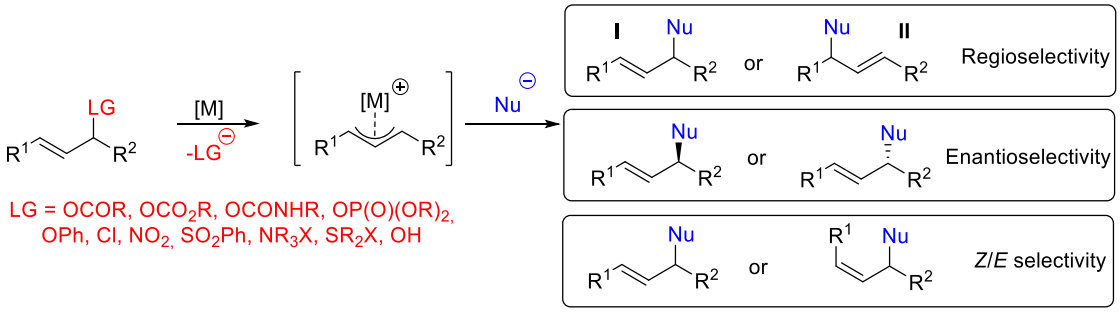

Scheme 30. Tsuji-Trost allylation.

The Tsuji-Trost final product presents several forms of possible isomers, so different types of selectivities can be controlled (Scheme 30):

- Regioselectivity: the nucleophile does not always have to attack the same carbon where the leaving group was. Since the reaction proceeds through an allylic complex where the charge is delocalized, the two terminal carbons of the allylic moiety are prone to suffer the nucleophilic attack.[61] The place of the attack will depend on the nature of the substituents and the nucleophile.
- Enantioselectivity: The nucleophile is bonded to a Csp^3, so if this carbon is not terminal (for example, if in **I**, $R^2 \neq H$) the isomers *R* and *S* can be obtained.
- *Z*/*E* selectivity: The Tsuji-Trost allylic alkylation always renders an alkene, so if the double bond is not terminal (for example, if in **I**, $R^1 \neq H$) the isomers *Z* and *E* can be obtained.

The Tsuji-Trost can proceed through different mechanisms. One of the most typical mechanisms for the Tsuji-Trost catalysed by palladium, a frequent catalyst in this type of reaction, is shown in Scheme 31[59, 60a] (this scheme only considers the formation of regioisomer **I** in *E* configuration): The reaction begins with the coordination of the Pd(0) complex to the double bond of the substrate. The next step is the oxidative addition to form the allylic complex (this step is also called ionization) and it occurs with inversion of configuration, i.e., the palladium centre occupies the opposite face where the leaving group was; depending on the case, the leaving group can become part of the coordination sphere of palladium or can directly abandon the molecule. At this point, two different pathways can happen depending on whether the nucleophile present in the reaction medium is a soft nucleophile[62a] or a hard nucleophile.[62b]

---

[59] J.J. Li, "Name Reactions: A Collection of Detailed Mechanisms and Synthetic Applications", **2002**, Springer.

[60] Reviews about Tsuji-Trost reaction: a) Barry M. Trost, D. L. Van Vranken, *Chem. Rev.* **1996**, *96*, 395-422. b) B. M. Trost, M. L. Crawley, *Chem. Rev.* **2003**, *103*, 2921-2943. c) J. Kleimark, P.-O. Norrby, *Top Organomet. Chem.* **2012**, *38*, 65-94. d) B. M. Trost, Tetrahedron **2015**, *71*, 5708-5733.

[61] B. Plietker, *Angew. Chem. Int. Ed.* **2006**, *45*, 1469 –1473.

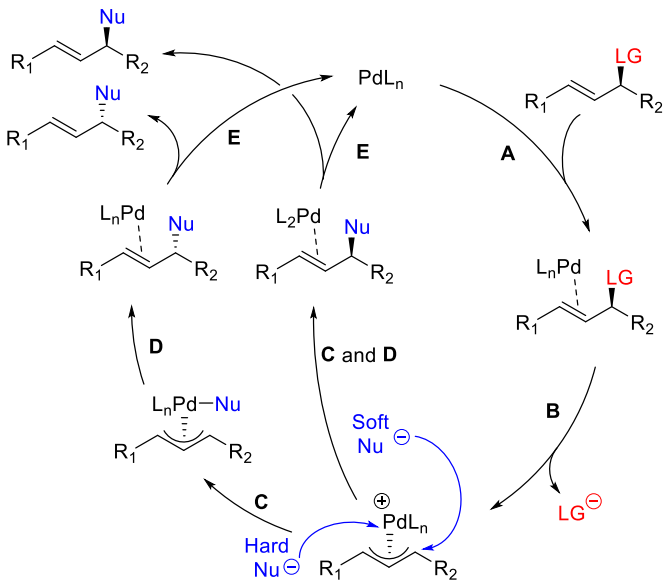

A: Coordination, **B**: oxidative addition, **C**: nucleophilic addition, **D**: reductive elimination, **E**: catalyst release

Scheme 31. Mechanism of Palladium catalysed Tsuji-Trost allylation.

A **soft nucleophile**[62a] directly attacks the carbon atom, entering the opposite face where the palladium is, so the final configuration of the nucleophile is the same as the leaving group had. By contrast, a **hard nucleophile**[62b] first attacks the palladium and then it is transferred to the substrate through reductive elimination. This transference is carried out on the same face where the palladium is, so there is a net inversion of the configuration respect to the original position of the leaving group. These considerations must be taken into account when enantiospecific or enantioselective Tsuji-Trost allylic alkylations are required.[63] The final step in both cases is the release of the catalyst.

Since its discovery by Tsuji[64a] and Trost,[64b] multitude of examples have been developed using different types of nucleophiles and different substituents as leaving groups in the allylic substrate. This introduction aims to show representative examples of the last decade that cover all these variants. The examples will be classified according to the nucleophile used.

The most common leaving groups in these reactions are the acetates and carbonates (LG = $OCOCH_3$, OCO_2CH_3, respectively). They imply very poor atomic economy, since much matter is wasted. From this point of view, the ideal substrate for this reaction is the allylic alcohol (LG = OH), but since the hydroxyl is not a good leaving group, it usually requires harsh conditions.[65] Along this text, some examples where an allylic alcohol has been utilized as a substrate for the Tsuji-Trost allylation will be shown, indicating in each case the factor which allowed to use the hydroxyl as leaving group. In the references of each section, other examples of allylic alcohols as Tsuji-Trost substrates not shown in this text can be found.

[62] a) Soft nucleophile: Nucleophile derived from conjugate acids whose pKa < 25. Also called stabilized nucleophiles, they include malonic esters, α-diketones, 1,1-bissulfonylmethanes, thiols, amines, amides, carboxylates, and alkoxides. b) Hard nucleophile: Nucleophile derived from conjugate acids whose pKa > 25. Also called unstabilized nucleophiles, they include Grignard reagents, alkylzinc halides, and hydride donors such as hydridoborates, hydridostannanes, and formats. Definitions taken from ref. 60a.

[63] This text will not focus in enantiospecific or enantioselective Tsuji-Trost allylation. For a nice discussion about it see reference 60a.

[64] a) J. Tsuji, H. Takahashi, M. Morikawa, *Tetrahedron*, **1965**, *49*, 4387-4388. b) B. M. Trost, T. J. Fullerton, *J. Am. Chem. Soc.* **1973**, *95*, 292–294.

[65] B. Sundararaju, M. Achard, C. Bruneau, *Chem. Soc. Rev.* **2012**, *41*, 4467–4483.

3.3.2. 1,3-Dicarbonyl compounds, enolates and enamines

Since the first reports of Tsuji[64a] and Trost,[64b] the use of 1,3-dicarbonyl compounds as nucleophiles have been exploited over the years to date.[66a-d] In the last years, one of the best examples in terms of enantioselectivity and yield was carried out by Morberg *et al.* in 2016, who used a chiral biphenyl phosphinooxazoline as ligand of the Pd catalyst and obtained in most of the cases more than 99% of enantiomeric excess (Scheme 32A).[66a] They also used alcohols as nucleophiles, but the enantioselectivity decreased (results not shown).

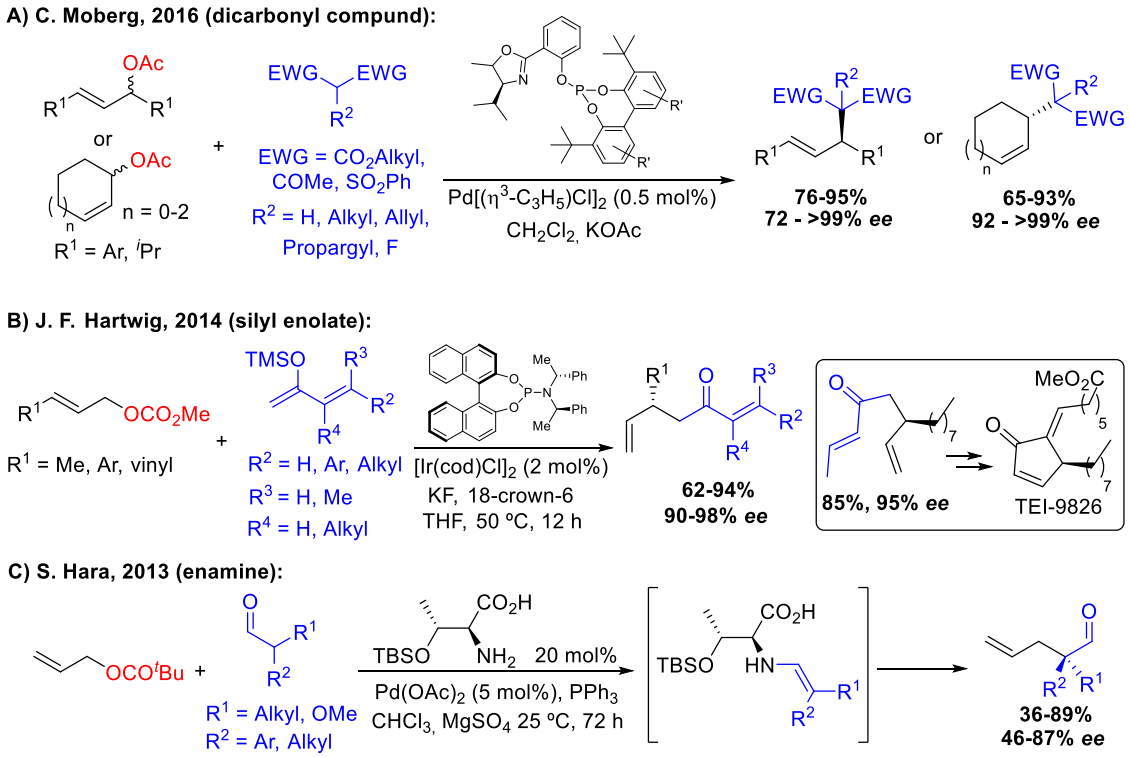

Scheme 32. Tsuji-Trost allylation with dicarbonyl compounds, enolates or enamines as nucleophiles.

The silyl enol ethers are good nucleophiles for the Tsuji-Trost allylation.[67a-f] For example, in 2014 Hartwig and co-workers designed the addition of silyl enolates derived from α,β-unsaturated ketones to allylic carbonates to obtain versatile diunsaturated ketones.[67a] The reaction was catalysed by a chiral iridium complex, transferring good enantiomeric excess to the product (Scheme 32B). Since these diunsaturated ketone products were good substrates for a ring-closing by olefin metathesis, this strategy was used for the synthesis of prostaglandin TEI-9826, an anticancer agent. The chiral iridium catalysed allylation of silyl enol ethers have been

[66] a) R. Bellini, M. Magre, M. Biosca, P.-O. Norrby, O. Pàmies, M. Diéguez, C. Moberg, *ACS Catal.* **2016**, *6*, 1701−1712. Other recent examples using allylic alcohols as substrates: b) R. Blieck, M. S. Azizi, A. Mifleur, M. Roger, C. Persyn, M. Sauthier, H. Bonin, *Eur. J. Org. Chem.* **2016**, 1194–1198. c) Y. Kwon, J. Jung, J. H. Kim, W.-J. Kim, S. Kim, *Asian J. Org. Chem.* **2017**, *6*, 520 – 526. d) S.-B. Tang, X. Zhang, H. F. Tu, S.-L. You, *J. Am. Chem. Soc.* **2018**, *140*, 7737−7742.

[67] a) M. Chen, J. F. Hartwig, *Angew. Chem. Int. Ed.* **2014**, *53*, 8691 –8695. b) M. Chen, J. F. Hartwig, *Angew. Chem. Int. Ed.* **2014**, *53*, 12172 –12176. c) M. Chen, J. F. Hartwig, *J. Am. Chem. Soc.* **2015**, *137*, 13972−13979. d) M. Chen, J. F. Hartwig, *Angew. Chem. Int. Ed.* **2016**, *55*, 11651 –11655. Other recent examples using allylic alcohols as substrates: e) X. Liang, K. Wei, Y.-R. Yang, *Chem. Commun.* **2015**, *51*, 17471—17474. f) J. M. Pérez, C. Maquilón, D. J. Ramón, A. Baeza, Asian, *J. Org. Chem.* **2017**, *6*, 1440 – 1444.

exploited by Hartwig's group in the last years[67b-d], applying the strategy to several types of silyl enol ethers and allylic substrates.

In the first Tsuji's report about these allylations, it is shown that enamines could be used as nucleophiles.[64a] This concept has been applied for the performance of organocatalytic Tsuji-Trost reactions. In 2013, Hara *et al.* carried out the allylation of aldehydes by the combination of two catalytic systems:[68a] the *in situ* enamine formation by condensation of the aldehyde with a chiral amino acid and the formation of an allylic palladium complex, obtaining γ,δ-unsaturated aldehydes with moderate yield and enantioselectivity (Scheme 32C). In the literature, the use of proline derivatives as organocatalysts[68b] or the direct use of enamines[68c] in Tsuji-Trost allylations can also be found.

3.3.3. Phenols, alcohols and amines

Phenols offer several possibilities as nucleophiles[69a-b] since the oxygen can act as the nucleophilic position for an O-allylation, or the ring itself can be the nucleophile for a C-allylation through a Friedel-Crafts reaction. In 2017 Deardorff's group carried out kinetic studies of palladium catalysed Tsuji-Trost allylation of phenols and discovered that the O-allylated product was the first one in being obtained. However, its formation was reversible and it could be isomerized to the most stable C-allylated product.[69a] With this data, they developed a regioselective method and depending of the conditions used, they could obtain any of the two products (Scheme 33A).

One of the broadest scope of alkyl alcohols for the Tsuji-Trost reaction was performed by Xu *et al.* in 2016, in an enantioselective version of the process using a D-Camphor-Based Schiff ligand for the palladium catalyst, obtaining excellent yields and enantioselectivities (Scheme 33B).[70] The work also includes scopes of dicarbonyl compounds and amines as nucleophiles (not shown).

In 2017, Zhang and co-workers utilized a broad scope of alkylic, benzylic and cyclic amines for the Tsuji-Trost allylation.[71] The interest of this work is not only the amine scope but rather the allylic substrates that they used, which have unprotected –OH and $–NH_2$ as leaving groups (Scheme 33C). In the optimization of the reaction they discovered that it only worked with protic solvents, concluding that the mechanism consisted in a cooperative process where the solvent stabilizes the OH or NH_2 as leaving groups and the palladium forms, as other cases, the allylic complex intermediate. The methodology was applied in the one-step synthesis of two drugs, cinnarizine and naftifine, on a gram scale.

[68] a) M. Yoshida, T. Terumine, E. Masaki, S. Hara, *J. Org. Chem*. **2013**, *78*, 10853-10859. b) I. Usui, S. Schmidt, B. Breit, *Org. Lett.* **2009**, *11*, 1453-1456. c) N. Narbon, L. E. Kaim, *Eur. J. Org. Chem*. **2017**, 4242-4246.

[69] a) C. A. Discolo, A. G. Graves, D. R. Deardorff*, J. Org. Chem.* **2017**, *82*, 1034−1045. b) M. Halder, Md. M. Islam, S. Ahammed, Sk. M. Islam, *RSC Adv.* **2016**, *6*, 8282–8289.

[70] Q.-L. Liu, W. Chen, Q.-Y. Jiang, X.-F. Bai, Z. Li, Z. Xu, L.-W. Xu*, ChemCatChem* **2016**, *8*, 1495 – 1499.

[71] J. Jing, X. Huo, J. Shen, J. Fu, Q. Meng, W. Zhang*, Chem. Commun.* **2017**, *53*, 5151—5154.

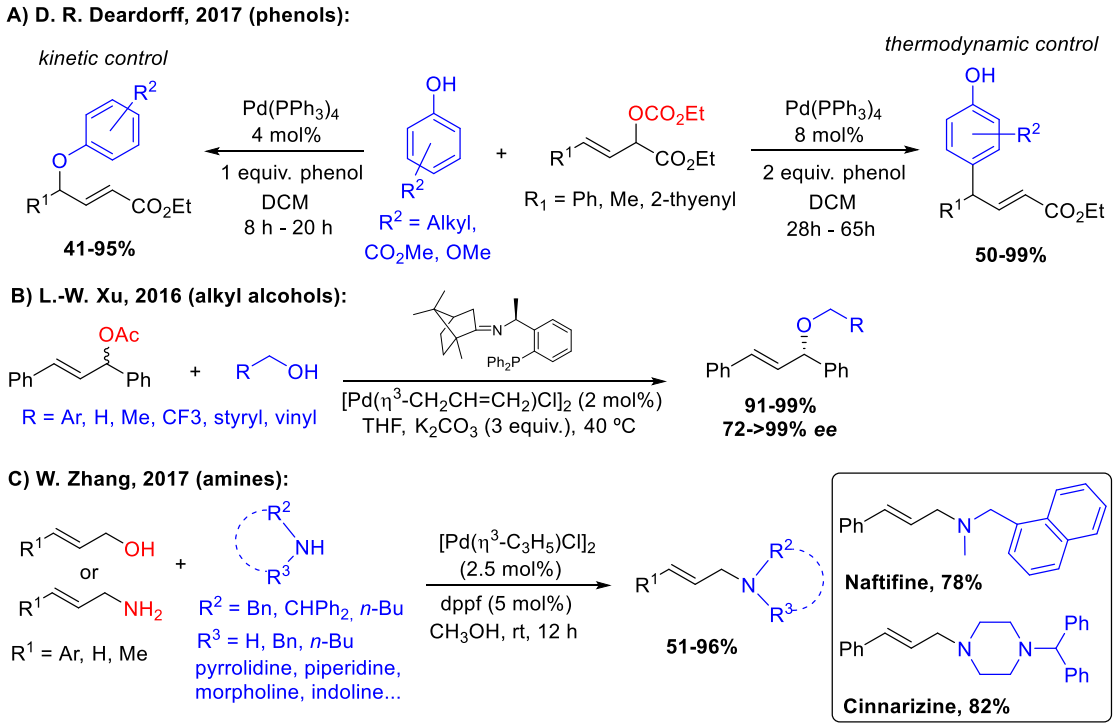

Scheme 33. Tsuji-Trost allylation of phenols, alkyl alcohols and amines.

3.3.4. Aromatic rings

It is well known that the electro enriched aromatic rings and the π-excedent heterocycles are good nucleophiles for the Friedel-Crafts alkylation, so they can also be used for the Tsuji-Trost allylation. Indole derivatives have been extensively used in Tsuji-Trost reactions and big efforts have been done to control the indole position for the allylation. The C-3 position is the most reactive and therefore the easiest to allylate, as it was done by Umani-Ronchi *et al.* in 2004 (Scheme 34A).[72a] An electron-withdrawing substituent decreases the nucleophilicity of the C-3 position relative to that of N-1 position, and increases the acidity of the N-H bond, feature that was used by Hartwig *et al.* in 2009 to carry out an enantioselective allylation in the nitrogen position of the indole (Scheme 34B).[72b] Works in which the C-2 position has been functionalized with a Tsuji-Trost allylation can also be found.[72c]

In the literature there are many works about general methods to carry out the Tsuji-Trost allylation to a big range aromatic ring, which employs metal catalysts based on Mo,[73a] Ru,[73b] Ag[73c] or Ir.[73d-e] Scheme 34C shows a fragment of a work performed by Che's group in 2011, in which they carried out the allylation of different five-membered aromatic heterocycles using

[72] a) M. Bandini, A. Melloni, A. Umani-Ronchi, *Org. Lett.* **2004**, *6*, 3199-3202. b) L. M. Stanley, J. F. Hartwig, *Angew. Chem. Int. Ed.* **2009**, *48*, 7841 –7844. c) J. Y. Lee, H. Ha, S. Bae, I. Han, J. M. Joo, *Adv. Synth. Catal.* **2016**, *358*, 3458 – 3470.

[73] a) A. V. Malkov, S. L. Davis, I. R. Baxendale, W. L. Mitchell, P. Kočovský, *J. Org. Chem.* **1999**, *64*, 2751-2764. b) G. Onodera, H. Imajima, M. Yamanashi, Y. Nishibayashi, M. Hidai, S. Uemura, *Organometallics* **2004**, *23*, 5841-5848. c) G.-Q. Chen, Z.-J. Xu, S. L.-F. Chan, C.-Y. Zhou, C.-M. Che, *Synlett* **2011**, *18*, 2712-2718. d) P. N. Chatterjee, S. Roy, *Tetrahedron* **2012**, *68*, 3776-3785. e) A. K. Maity, P. N. Chatterjee, S. Roy, *Tetrahedron* **2013**, *69*, 942-956.

silver salts as catalysts.[73c] In this work they could use allylic alcohols as starting materials but they had to employ them in excess and they had to apply high temperatures.

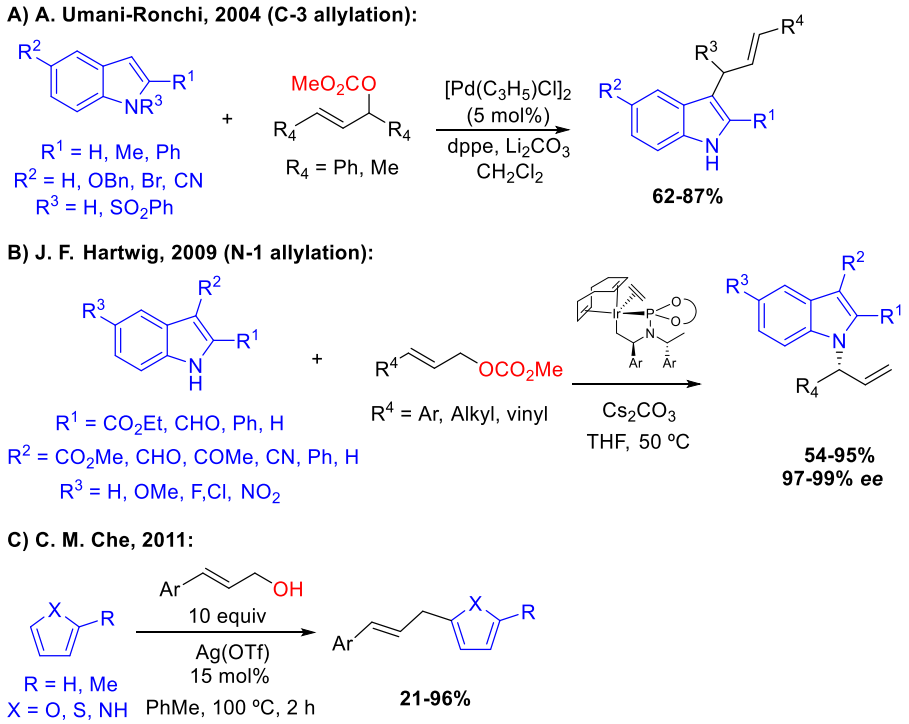

Scheme 34. Tsuji-Trost allylation of heteroaromatic rings.

3.3.5. Other advances in Tsuji-Trost allylation

There are numerous works about the intramolecular version of the Tsuji-Trost allylation, which allows the formation of heterocycles with exocyclic vinyl groups.[74] A good example is the vinylpyrrolidines formation catalysed by a dinuclear Pd-Ti complex, performed by Michaelis *et al* in 2015[75a] (Scheme 35A); the starting material was an allylic alcohol and previous to the addition of the catalyst, thionyl chloride was used to change the hydroxyl by a chlorine, which is a better leaving group. In the same year,Kitamura *et al.* achieved a very interesting intramolecular allylation, since the nucleophilic motif was a carboxylic acid, which is not a common nucleophile in this reaction, to synthesize vinyl lactones (Scheme 35B).[75b] They could use a hydroxyl as leaving group, employing a polar solvent and heating the reaction up, and the chiral ruthenium complex catalyst transferred good enantiomeric excesses to the final product. In both cases the nucleophilic attack was done to the allylic carbon which allows the formation of the most stable five and six membered rings.

[74] A review about intramolecular Tsuji-Trost allylation: J. Cornil, L. Gonnard, C. Bensoussan, A. Serra-Muns, C. Gnamm, C. Commandeur, M. Commandeur, S. Reymond, A. Guérinot, J. Cossy, *Acc. Chem. Res.* **2015**, *48*, 761−773.

[75] a) W. K. Walker, D. L. Anderson, R. W. Stokes, S. J. Smith, D. J. Michaelis, *Org. Lett.* **2015**, *17*, 752−755. b) Y. Suzuki, T. Seki, S. Tanaka, M. Kitamura, *J. Am. Chem. Soc.* **2015**, *137*, 9539−9542.

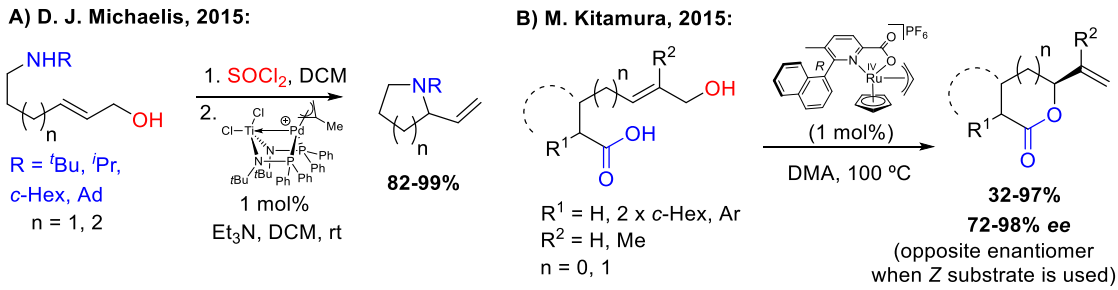

Scheme 35. Intramolecular Tsuji-Trost reactions.

A challenge in the allylation reaction is to break the model of beginning with a substrate bearing a leaving group in an allylic position and being able to use other starting materials. Breit's group achieved successfully this purpose, utilizing terminal allenes (Scheme 36A)[76a] and terminal alkynes (Scheme 36B)[76b] as starting materials. The combination of these substrates with a rhodium complex catalyst gives an allylic complex substrate (as can be appreciated in Scheme 36B), which is a common intermediate with the traditional Tsuji-Trost reactions, allowing the formation of the same allylated products. The example of 2015 is especially interesting, in which they used aromatic hydrazines as nucleophiles with allene substrates, utilizing a chiral rhodium complex catalyst, rendering enantioenriched allylated hydrazines. They demonstrated the versatility of these products which could be condensated with ketones to form enantioenriched *N*-allylated indoles.

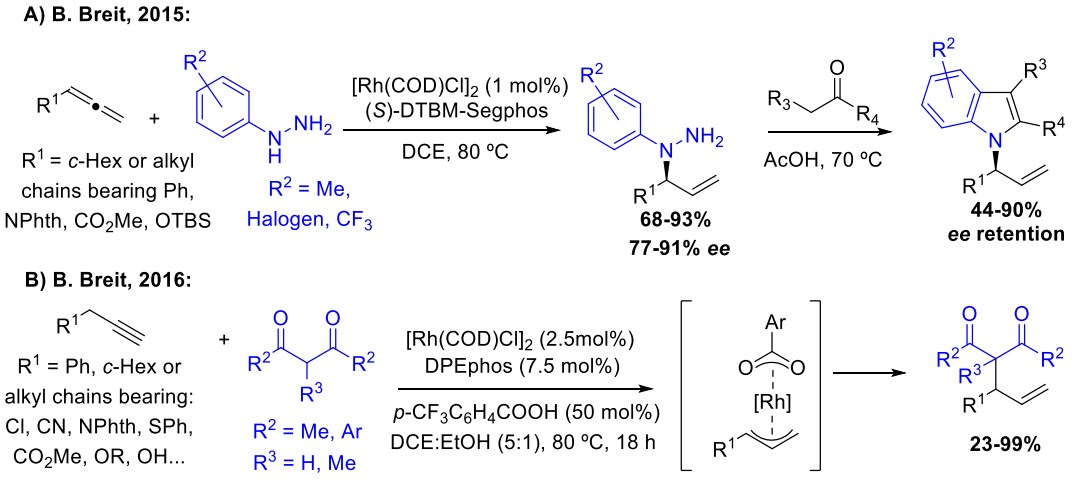

Scheme 36. Alternative starting materials for allylation reactions.

As introduced in different examples in this text, the use of allylic alcohols as starting materials can be accomplished in some specific conditions, such as very polar solvents and high temperature but it is still limited and it cannot always be achieved in all situations. There are research groups which focus their work in developing general methods for the use of allylic alcohols with milder conditions and a broader range of nucleophiles.[77a-b] A good example was the group of Kim in 2017, that found out that *N*,*N*-dimethylacetamide dimethyl acetal (DMADA) activates the allylic alcohols, since it transforms the alcohol into a better leaving group *in situ*

[76] a) K. Xu, T. Gilles, B. Breit, *Nat. Commun.* **2015**, *6*, 7616. b) T. M. Beck, B. Breit, *Org. Lett.* **2016**, *18*, 124−127.

(Scheme 37).[77a] This method is compatible with mild conditions and multiple nucleophiles, such as dicarbonyl compounds, amines, phenols… Although it represents an advance since the allylic alcohols are more easily accessible than other substrates like acetates or carbamates, it cannot be said that it increases the atomic economy of the reaction, since two equivalents of DMADA must be used.

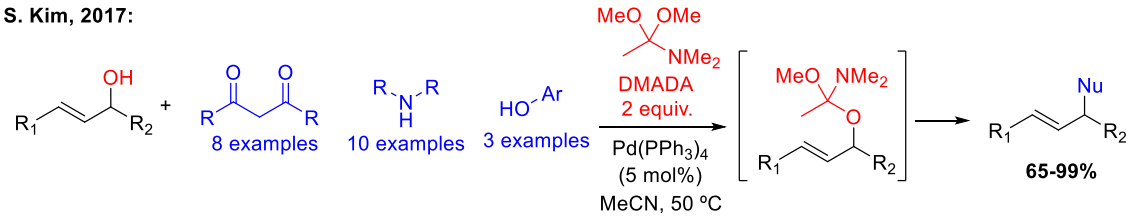

Scheme 37. Other strategy in the Tsuji-Trost allylation.

3.3.6. Initial hypothesis about photocatalysed allylation reaction

As it was introduced, the *Z*/*E* selectivity must be considered in Tsuji-Trost products. Analysing the results presented in this text of the reactions that yield non-terminal alkenes (Schemes 32A, 33A-C, 34A and C, 37A-B), an important conclusion is easily obtained: there is a clear preference for the *E* isomer in the Tsuji-Trost allylation. In fact, most of the authors do not even give importance to this type of selectivity and, since the selectivity is usually complete to the *E* isomer, they do not consider the *Z* isomer obtaining. A few authors just describe that in some products of their scope the *Z* isomer is formed as the minor products, and they treat it as a byproduct (for example, in the allylation of amines by W. Zhang shown in Scheme 33C). An exception is the use of endocyclic *Z*-alkenes as substrates, which renders endocyclic *Z*-alkenes Tsuji-Trost products (Scheme 32A).

The configuration of double bonds plays a central role in the biological properties of different natural and pharmaceutical compounds. For example, (*Z*)-tamoxifen is an antiestrogen that inhibits the development and growth of mammary tumours in rats and is effective in treating estrogen-dependent metastatic breast cancer in humans.[78a] By contrast, the diastereoisomer (*E*)-tamoxifen does not have any clinical uses because it lacks an antiestrogenic effect. Therefore, the ability to control the configuration of a double bond is an extremely important task in the synthetic design of new drugs containing this structural moiety.[78b]

Taking the aforementioned considerations into account, a necessary step to take is the development of a Tsuji-Trost allylation protocol that allows to obtain selectively either the *Z*-isomer or the *E* isomer alkene. Analysing the reactions of this text where *E*-alkenes are obtained again, it can be appreciated that different conditions have been used in each one (different metal catalysts, different ligands, different solvents, different temperature…). If only *E* isomer is obtained utilizing such a broad range of conditions, it will be hard to find specific conditions for the *Z* isomer formation. The emergent field of photocatalysis may be the needed alternative to solve this problem, since photocatalysis has demonstrated that can promote reactions which are very difficult to achieve with traditional thermal methods. Furthermore, a photocatalysed

[77] a) Y. Kwon, J. Jung, J. H. Kim, W.-J. Kim, S. Kim, *Asian J. Org. Chem.* **2017**, *6*, 520 – 526. b) S. Akkarasamiyo, S. Sawadjoon, A. Orthaber, J. S. M. Samec, *Chem. Eur. J.* **2018**, *24*, 3488 – 3498.
[78] a) D. W. Robertson, J. A. Katzenellenbogen, *J. Org. Chem.* **1982**, *47*, 2387-2393. b) L. Marzo, J. Luis-Barrera, R. Mas-Ballesté, J. L. García Ruano, J. Alemán, *Chem. Eur. J.* **2016**, *22*, 16467 – 16477.

allylation could proceed through a totally different mechanism than the thermal one, allowing to avoid the use of the typical metallic complexes; moreover, if the photocatalyst is an organic dye, a metal-free photocatalysed allylation reaction could be developed.

Two articles of photocatalysed Tsuji-Trust allylation have already been published. In one of them, they used a heterogeneous photocatalyst consisting on a MoS2-polypyrrole framework with nanoparticles of Pd absorbed in the pores of the material (Pd@MoS2CPFs).[79a] The Tsuji-Trost reaction studied with this heterogeneous catalyst rendered a terminal alkene, so a possible effect on the stereochemistry of the double bond could not be studied; moreover, this complex catalyst did not avoid the use of metals. In the other work, the photocatalyst was Pd/C supported in a photoactive micellar system;[79b] the reaction can be carried out in water but, again, it does not avoid the use of metals. The Tsuji-Trost allylation studied in this case yields the *E* double bond. A simpler homogeneous Tsuji-Trost allylation is yet to be discovered.

As we have seen in this introduction, different nucleophiles have been used in the thermal Tsuji-Trost allylation over the years. A good point to begin the homogeneous photocatalytic allylation reaction would be the use of pyrroles and indoles, since they are easy nucleophiles to manipulate and they have already been utilized in different photocatalysed transformations. A small revision of this photocatalysed reaction with heterocycles is necessary to extract some clues for trying the photocatalysed allylation of heterocycles.

3.3.7. Photocatalytic arylation of heterocycles

Photocatalysis have been used for the formation of chemical bonds difficult to obtain with other traditional methods, like the Csp^2-Csp^2 bond between two aromatic rings.[80] Scheme 38 shows the bond formation between aryl bromides or heteroaryl bromides and pyrroles using blue light and Rhodamine-6G (Rh-6G) as photocatalyst, reaction developed by König group in the year 2016.[81a-b]

[79] a) J. Liu, X. Mu, Y. Yang, F. Chen, J. Wang, Y. Li, B. Wang, *Applied Catalysis B: Environmental* **2019**, *244*, 356–366. b) M. Billamboz, F. Mangin, N. Drillaud, C. Chevrin-Villette, E. Banaszak-Léonard, C. Len, *J. Org. Chem.* **2014**, *79*, 493−500.

[80] I. Ghosh, L. Marzo, A. Das, R. Shaikh, B. König, *Acc. Chem. Res.* **2016**, *49*, 1566−1577.

[81] a) L. Marzo, I. Ghosh, F. Esteban, B. König, *ACS Catal.* **2016**, *6*, 6780−6784. b) I. Ghosh, B. König, *Angew. Chem. Int. Ed.* **2016**, *55*, 7676 –7679. c) D. P. Hari, P. Schroll, B. König, *J. Am. Chem. Soc.* **2012**, *134*, 2958−2961. d) M. Tobisu, T. Furukawa, N. Chatani, *Chem. Lett.* **2013**, *42*, 1203-1205. e) Y.-X. Liu, D. Xue, J.-D. Wang, C.-J. Zhao, Q.-Z. Zou, C. Wang, J. Xiao, *Synlett* **2013**, *24*, 507-513. f) I. Ghosh, T. Ghosh, J. I. Bardagi, B. König, *Science* **2014**, *346*, 725-728. g) P. Maity, D. Kundu, B. C. Ranu, *Eur. J. Org. Chem.* **2015**, 1727–1734. h) P. Natarajan, A. Bala, S.K. Mehta, K.K. Bhasin, *Tetrahedron* **2016**, *72*, 2521-2526. i) A. Pal, I. Ghosh, S. Sapra, B. König, *Chem. Mater.* **2017**, *29*, 5225−5231. j) L. Buglioni, P. Riente, E. Palomares, M. A. Pericàs, *Eur. J. Org. Chem.* **2017**, 6986–6990.

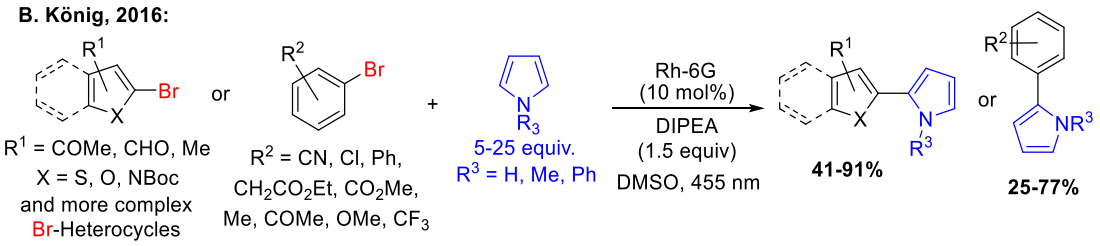

Scheme 38. Photocatalysed Csp^2-Csp^2 bond formation between a bromo-aromatic ring and pyrrole.

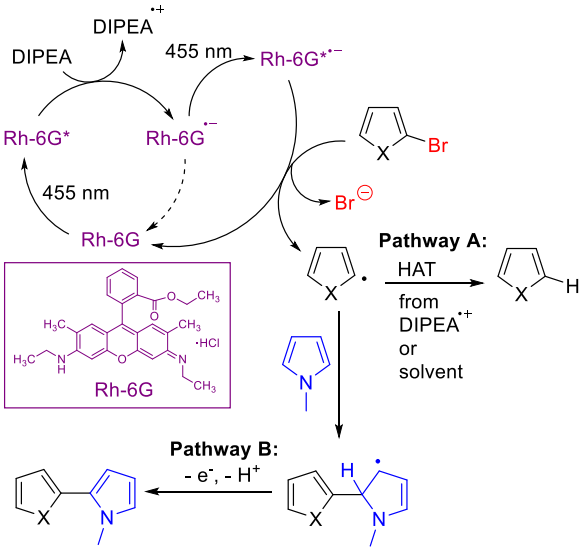

Scheme 39. Mechanism of photocatalysed biheteroaryl formation.

Scheme 39 shows the mechanism proposed by the authors, based on experimental studies, for the coupling between heteroaryl bromides and pyrrole derivatives: The Rh-6G is excited by the blue light and the excited catalyst accepts one electron from the DIPEA, yielding the radical anion $Rh\text{-}6G^{\bullet-}$ and the radical cation $DIPEA^{\bullet+}$. The generated $Rh\text{-}6G^{\bullet-}$ absorbs a second photon, reaching an excited state more reductant which is therefore able to reduce the heteroaryl bromide by single electron transfer, returning to its ground state and yielding the heteroaryl radical by cleavage of the C-Br bond. The heteroaryl radical is so reactive that can suffer hydrogen atom transfer (HAT) from the $DIPEA^{\bullet+}$ or the solvent, yielding the undesired dehalogenated heteroarene (Pathway A). However, when the pyrrole is present in the reaction media, it traps the heteroaryl radical, and after oxidation and rearomatization processes, it forms the biheteroaryl product (Pathway B). Since these two processes are simultaneously working, the pyrrole must be added in a large excess (18 equivalents) to obtain the desired product in good yield. This type of photocatalysed coupling between a generated aryl radical and a pyrrole as trapping reagent has been broadly studied,[81a-j] using different types of catalysts and different leaving groups to form the aryl radical. In most of the cases the big excess of pyrrole is necessary, but there are few authors who succeeded in using just between one and two equivalents.[82]

Since the photocatalysed arylation reaction of heterocycles is a well-known process, *it would be desirable to develop the photocatalysed allylation reaction of these heterocycles*. In this proposed process, the excited photocatalyst might reduce the allylic substrate provoking the cleveage between the leaving group and the allylic motif, yielding a free allylic radical. The pyrrole could trap the allylic radical, and after a process of oxidation and rearomatization, an allylated pyrrole would be obtained (Scheme 40). It is also possible that a more complex mechanism operates in this cycle.

[82] In reference 81c and 81g, big amount of trapping reagent is used, except in the case of pyrroles (2 equivalents). In reference 81h, only one equivalent of all trapping reagents used, including pyrroles, is needed.

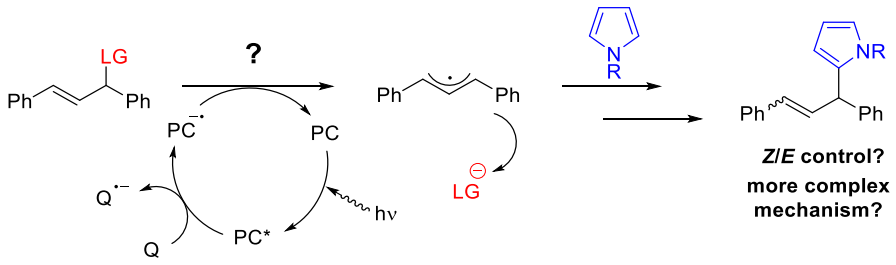

Scheme 40. Proposal of photocatalytic allylation of pyrroles.

There are some reasons to think that in this process a control of the *Z*/*E* selectivity of the product can be achieved:

- The allylic intermediate is free in the reaction medium, unlike in the previous cases, in which is part of a rigid metal complex. The free allylic intermediate could suffer free rotation more easily.
- It is known that appropriate photocatalysts can induce an isomerization of the double bond to the less stable *Z* isomer. Maybe the photocatalyst could have a secondary role of isomerizing either the reactant (that could keep the *Z* configuration until the final product[83]) or the final product itself. This effect could be controlled with the catalyst used and the irradiation source. It would be possible to find a catalyst that promotes the reactions but does not induce the isomerization and another catalyst that both promotes the reaction and induces the isomerization.

The objectives of this part are described in more detail in Section 4.2.

[83] In the next works there are some examples where the authors begin with a *Z* Tusji-Trost substrate and they obtain a *Z* product after the reaction: a) I. Matsuda, S. Wakamatsu, K.-i. Komori, T. Makino, K. Itoh, *Tetrahedron Lett.* **2002**, *43*, 1043–1046. b) C. Cazorla, M. Billamboz, H. Bricout, E. Monflier, C. Len, *Eur. J. Org. Chem.* **2017**, 1078–1085.

4. Objectives

4.1. Photocatalytic Cyclopropane Ring Expansion

The objectives for this part are the following:

1) Organocatalytic enantioselective synthesis of nitro-formylcyclopropanes, which can also be transformed in nitro-vinylcylopropanes

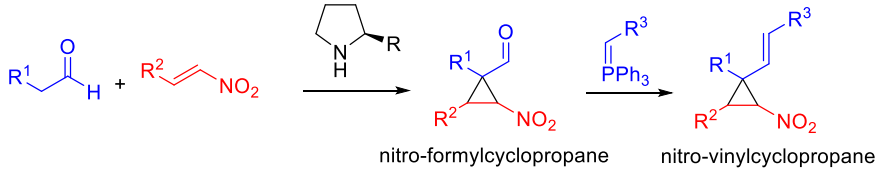

2) Development of a enantiospecific photocatalytic process for the rearrangement of both nitro-formylcyclopropanes and nitro-vinylcylopropanes for the formation of dihydrofuranes and cyclopentenes, respectively.

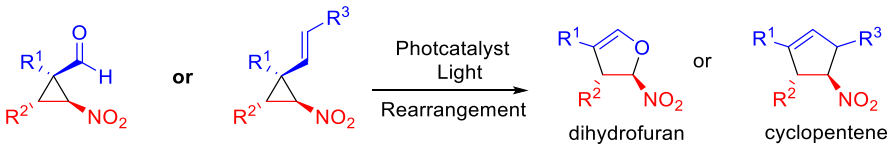

3) Investigation of the reaction mechanism, using both experimental methods and computational calculations. Elucidation of the role of the nitro group and whether it is an energy transfer process or an electron transfer process. Since the rearrangement of cyclopropanes usually undergoes through open intermediates, the energetic profile of all the possible bond cleavages of the cyclopropane will be calculated to clarify the mechanism.

4.2. Photocatalytic allylation reaction

The objectives for this part are the following:

1) Development of a photocatalytic method to carry out the allylation reaction to heterocycles with control of the *Z*/*E* selectivity. Attempts will be done to avoid the use of metals or the use of big excess of the heterocycles.

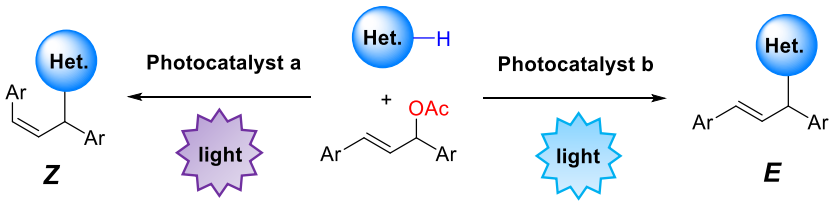

2) Study of the reaction scope: the new allylation method will be carried out using different heterocycles and different allylic substrates, trying to obtain in each case both the *Z* and the *E* isomer. It will be investigated whether the reaction scope can be expanded to other type of nucleophiles, like amines and alcohols.

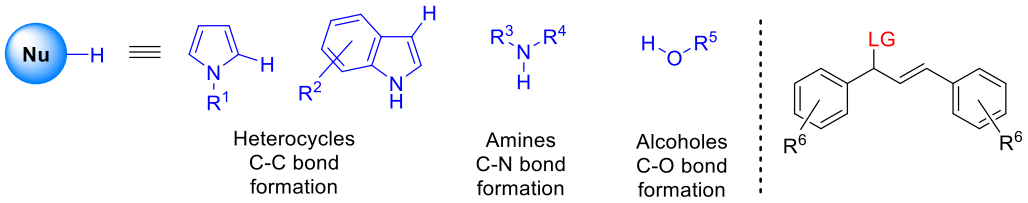

3) Experimental studies of the reaction mechanism. Different techniques will be used:

   a. Analysis of redox potential of all the compounds evolved in the reactions and Stern-Volmer studies. This studies seek to verify an electron transfer mechanisms and to identify what chemical compound is acting as quencher of the excited catalyst.

   b. Transient absorption spectra will be recorded to identify the reaction intermediates and to know if the reaction proceeds through an allylic radical intermediate, an allylic cation intermediate or if both are present in the reaction medium.

4) Computational studies to optimize all the intermediates and transition states evolved in the reaction in order to calculate the reaction profile.

5. Publications

The works done in this doctoral thesis related to molecular photocatalysis are described in the publications shown in this section. They will appear in this order:

1. One-Pot Asymmetric Synthesis of Cyclopropanes with Quaternary Centers Starting From Bromonitroalkenes under Aminocatalytic Conditions

J. Luis-Barrera, R. Mas-Ballesté, J. Alemán, *ChemPlusChem* **2015**, *80*, 1595-1600.

Reprinted with permission from John Wiley and Sons.

2. Visible-Light Photocatalytic Intramolecular Cyclopropane Ring Expansion

J. Luis-Barrera, V. Laina-Martín, T. Rigotti, F. Peccati, X. Solans-Monfort, M. Sodupe, R. Mas-Ballesté, M. Liras, J. Alemán, *Angew. Chem. Int. Ed.* **2017**, *56*, 7826 –7830.

Reprinted with permission from John Wiley and Sons.

3. Chromoselective access to Z- or E- allylated amines and heterocycles by a photocatalytic allylation reaction

A. M. Martínez-Gualda, R. Cano, L. Marzo, R. Pérez-Ruiz, J. Luis-Barrera, R. Mas-Ballesté, A. Fraile, V. A. de la Peña O'Shea, J. Alemán, *Nat. Commun.* **2019**, *10*, 2634.

Open Access Article.

NOTE: Each publication has two indicators for the number of the pages. One of the them indicates the number of the page within the journal. The other one indicates the number of the page within the doctoral thesis.

ChemPubSoc Europe

DOI: 10.1002/cplu.201500320

CHEMPLUSCHEM Communications

One-Pot Asymmetric Synthesis of Cyclopropanes with Quaternary Centers Starting From Bromonitroalkenes under Aminocatalytic Conditions

Javier Luis-Barrera,[a] Ruben Mas-Ballesté,[b] and José Alemán*[a]

Cyclopropanes with a quaternary center are efficiently synthesized starting from bromonitroalkenes and alkyl aldehydes under aminocatalysis, giving good yield, excellent enantioselectivities, and moderate to excellent diastereoselectivities. This work is a novel approach using bromonitroalkenes as starting material instead of the usual synthesis with bromine-activated methylene derivatives. The cyclization process is analyzed by DFT calculations, which suggests an S_N2 mechanism. Theoretical data indicate that diastereoselectivity results from the energetic balance as a consequence of distortion the in trigonal bipyramid transition states and the relative stabilities of both starting rotamers and final products arising from distinct steric repulsions.

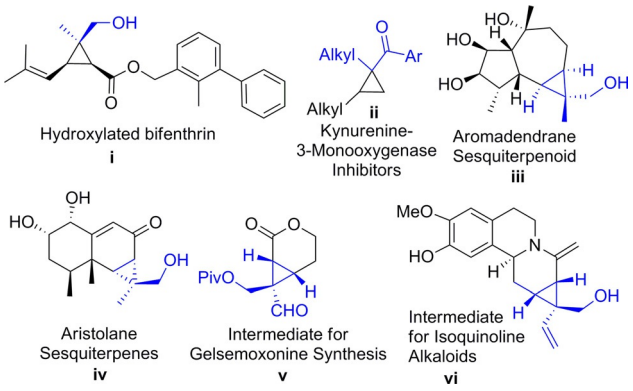

Cyclopropane is the key structural motif of a variety of agrochemical targets, natural products, and biologically active agents. They are also versatile intermediates and building blocks for organic synthesis because of their special reactivity.[1] Especially important are cyclopropane derivatives with asymmetric quaternary centers in their structure. This is because they are present in a large number of insecticides, acaricide derivatives (**i**),[2] and kynurenine-3-monooxygenase inhibitors (**ii**). In addition, they are present in different terpene derivatives such as aromadendrane sesquiterpenoids (**iii**)[3] or aristolane sesquiterpenes (**iv**).[4] They have also been used as intermediates for the synthesis of different products, such as gelsemoxonine (**v**)[5] or isoquinoline alkaloids (**vi**).[6]

In the last 30 years, different enantioselective approaches have been applied for the synthesis of cyclopropane compounds. The most significant and well established involve the metal-catalyzed cyclopropanation of electron-rich alkenes.[7] More recently, new organocatalytic approaches for the enantioselective synthesis of cyclopropanes have been developed.[8] In this latter field, one main approach used (Scheme 1; upper scheme) is based on the cyclopropanation of enones and aldehydes using ylides by Gaunt,[9] MacMillan,[10] and Arvidsson[11] or the use of α,β-unsaturated aldehydes with bromomalonates catalyzed by the Jørgensen–Hayashi catalyst.[12] Taking into account the strategy used by others (Scheme 1; upper scheme), we hypothesized about changing the leaving group (LG) from the nucleophile (Scheme 1; upper scheme) to the electrophilic double bond (Scheme 1; lower scheme). This new approach would allow the organocatalytic synthesis of cyclopropane compounds with asymmetric quaternary centers at the electron-withdrawing group (EWG) position, something not possible with the use of other organocatalytic strategies because the nucleophilic intramolecular reaction is not possible when R′ = alkyl or aryl (see Scheme 1). In this study, we present the synthesis of cyclopropanes containing a quaternary center by using an aminocatalytic approach and bromonitroalkenes as starting material[13] for the introduction of the intermediate bromine leaving group that can be intramolecularly attacked

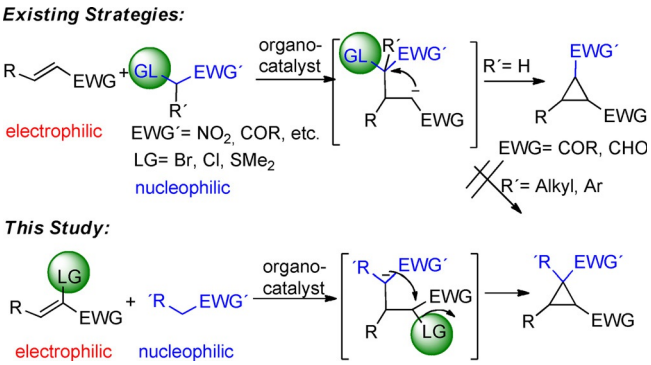

Scheme 1. Cyclopropanation strategies of electron-poor double bonds showing existing strategies and that presented herein.

[a] *J. Luis-Barrera, Dr. J. Alemán*
Module 01, Organic Chemistry Department
Science Faculty, Universidad Autónoma de Madrid
28049, Madrid (Spain)
Website:www.uam.es/jose.aleman
E-mail: Jose.aleman@uam.es

[b] *Dr. R. Mas-Ballesté*
Module 07, Inorganic Chemistry Department
Science Faculty, Universidad Autónoma de Madrid
28049, Madrid (Spain)

Supporting information for this article is available on the WWW under http://dx.doi.org/10.1002/cplu.201500320.

Table 1. Screening of different bases for the synthesis of cyclopropanes **5** in a tandem process.[a]

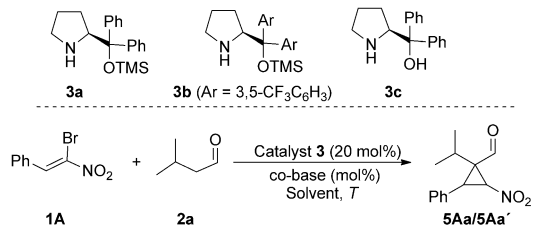

Entry	Cat./Co-base (mol%)	Solvent	Conv.[b]	Yield [%][c]	d.r.	*ee* [%][d]
1	**5a**/none	CH_2Cl_2	15	n.d.	70:30	90
2	**5a**/Et_3N (100)	CH_2Cl_2	78	70	75:25	74
3	**5b**/Et_3N (100)	CH_2Cl_2	n.r.	–	–	–
4	**5c**/Et_3N (100)	CH_2Cl_2	n.r.	–	–	–
5	**5c**/Et_3N (100)	toluene	45	35	74:26	69
6	**5c**/Et_3N (100)	$CHCl_3$	78	44	67:33	61
7	**5c**/Et_3N (100)	DCE	73	48	73:27	69
8	**5c**/Et_3N (100)	DME	88	42	55:45	77
9	**5a**/Py(100)	CH_2Cl_2	n.r.	–	–	–
10	**5a**/DMAP (100)	CH_2Cl_2	n.r.	–	–	–
11	**5a**/DBU (100)	CH_2Cl_2	22	20	91:9	83
12	**5a**/DABCO (100)	CH_2Cl_2	22	20	91:9	87
13	**5a**/DABCO (200)	CH_2Cl_2	50	n.d.	25:75	91

[a] Reaction conditions: all reactions were carried out at 0.2 mmol of **1a**, 0.4 mmol of **2a**, 0.02 mmol of **4a**, 20 mol% of catalyst, and the corresponding co-base was added after 18 h. [b] Conversion of the starting material was determined by ^{1}H NMR spectroscopy for step two. [c] Yield of isolated product. [d] Enantiomeric excess of the major diastereoisomer was determined by SFC on a chiral stationary phase using a Chiralpak IB column. DABCO = 1,4-diazabicyclo[2.2.2]octane, DBU = 1,8-diazabicyclo[5.4.0]undec-7-ene, DCE = dichloroethane, DMAP = 4-dimethylaminopyridine, DME = dimethyl ether, n.d. = not determined, n.r. = no reaction, Py = pyridine, TMS = trimethylsilyl.

Table 2. Screening of different bases for the synthesis of cyclopropanes **5** through a one-pot process.[a]

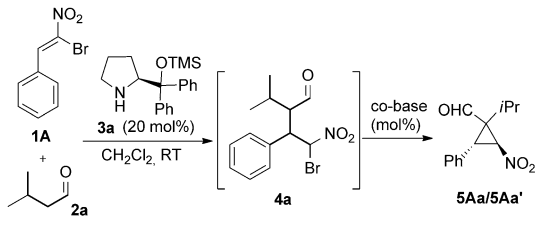

Entry	Co-base (mol%)	Conv. [%][b]	Yield [%][c]	d.r.	*ee* [%][d]
1	–	15	n.a.	70:30	90
2	DBU (100)	72	50	75:25	86
3	DABCO (100)	63	62	73:27	95
4	Et_3N (100)	>99	60	79:21	95
5	**DABCO (200)**	**>99**	**78**	**80:20**	**96**

[a] All reactions were carried out at 0.2 mmol of **1a**, 0.4 mmol of **2a**, 0.02 mmol of **4a**, and the corresponding co-base was added after 18 h. [b] Conversion determined by ^{1}H NMR for the second step. [c] Yield of isolated product. [d] Enantiomeric excess of the major diastereoisomer was determined by SFC on a chiral stationary phase using a Chiralpak IB column. n.a. = not applicable.

to form the final cyclopropane derivatives (Scheme 1; lower scheme).

To identify the optimal reaction conditions, we evaluated the reactivity of the aldehyde **1a** and bromonitrostyrene **2a** using the Jørgensen–Hayashi catalyst **3a** (20 mol%; Table 1, entry 1). As expected, only 15% conversion was observed because the HBr generated during the first catalytic cycle protonated the basic nitrogen of the catalyst **4a** and no further catalytic activity was possible under these conditions.

However, a promising 90% *ee* was obtained for the mixture of diastereoisomers (d.r. = 70:30; Table 1, entry 1). Thus, we hypothesized that the use of a second base would help with the deprotonation and the final cyclopropanation. In fact, the addition of Et_3N increased the conversion to 78% but the enantiomeric excess dropped to 74% *ee* (Table 1, entry 2). To improve

Table 3. Scope for the synthesis of different cyclopropanes.[a]

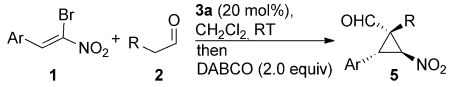

Entry	Ar	R	Yield [%][b]	d.r. [%][c]	*ee* [%][d]
1	Ph-**1A**	*i*Pr-**2a**	78 (**5Aa/5Aa′**)	75:25	96/87
2	Ph-**1A**	*i*Pr-**2a**	80 (**5Aa/5Aa′**)	75:25	95/96
3	*p*MeOC$_6$H$_4$-**1B**	*i*Pr-**2a**	52 (**5Ba/5Ba′**)	75:25	93/95
4	*p*BrC$_6$H$_4$-**1C**	*i*Pr-**2a**	63 (**5Ca/5Ca′**)	70:30	96/91
5	*p*FC$_6$H$_4$-**1D**	*i*Pr-**2a**	71 (**5Da/5Da′**)	71:29	97/92
6	*o*FC$_6$H$_4$-**1E**	*i*Pr-**2a**	53 (**5Ea/5Ea′**)	83:17	96/87
7	*n*Bu-**1F**	*i*Pr-**2a**	n.r.	–	–
8	Ph-**1A**	$CH_3(CH_2)_2$-**2b**	55 (**5Ab/5Ab′**)	60:40	95/94
9	Ph-**1A**	Ph-**2c**	55 (**5Ac′**)	<2:98	95
10	*p*MeOC$_6$H$_4$-**1B**	Ph-**2c**	59 (**5Bc′**)	<2:98	91
11	*p*BrC$_6$H$_4$-**1C**	Ph-**2c**	54 (**5Cc′**)	<2:98	96

[a] All reactions were carried out at 0.2 mmol of **1a**, 0.4 mmol of **2a**, 0.02 mmol of **4a** and 2 equiv of DABCO were added after 18 h. [b] Combined yield of isolated minor and major diastereoisomers. [c] Diastereomeric ratio determined by ^{1}H NMR spectroscopy. [d] Enantiomeric excess of the major and minor diastereoisomers was determined by SFC on a chiral stationary phase using a Chiralpak IB column.

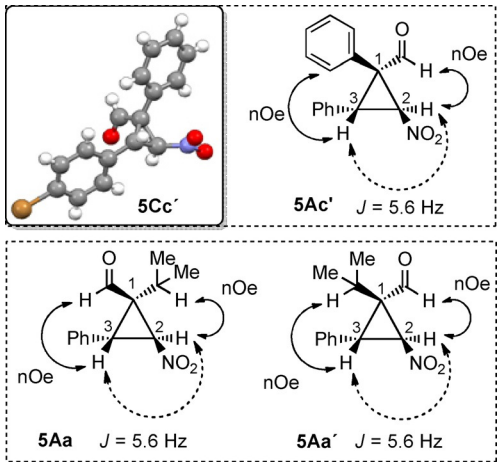

Scheme 2. X-ray analysis of unique diastereoisomer **5Cc′** and NMR nOe analysis of compound **5**.

this outcome, other bulkier catalysts such as **3b** or the hydrogen-bond-type (**3c**) were tested, but no conversion was obtained in both cases (Table 1, entries 3 and 4). Other solvents were then studied, such as toluene, $CHCl_3$, and DCE (Table 1, entries 5–8), in all cases resulting in slightly lower *ee* values. However, in the case of DME, a 77% enantiomeric excess was found with a lower d.r. (55:45; Table 1, entry 8), thus indicating that CH_2Cl_2 was the best solvent in terms of selectivity. Next, we focused on the study of different co-bases (Table 1, entries 9–12). Pyridine and DMAP showed no reactivity (Table 1, entries 9 and 10) whereas DBU and DABCO showed slightly better *ee* values (Table 1, entries 11 and 12). The optimal amount of DABCO was 200 mol% (Table 1, entry 12), and gave 91% *ee* with moderate conversion. This optimization study indicated that some sort of incompatibility must exist between the catalyst **3a**, the substrate (starting material or intermediate), and the co-base.[14] Thus, we decided to study the reaction using a one-pot technique (Table 2).

In fact, when we carried out the reaction in one pot using DBU, the consumption of the starting material increased and a better yield was obtained (compare Table 2, entry 1 with Table 1, entry 11). Other weaker bases such as DABCO or Et_3N gave better results, which were optimal when two equivalents of DABCO were used for step two (Table 2,entry 5). In view of these new conditions, we analyzed the scope of the reaction (Table 3).

First, we studied different nitroalkenes **1** with aldehyde **1a** (Table 3, entries 1–7). The reaction was scaled up (2.0 mmol) without impairing the final enantiomeric excess (Table 3, entry 2). The reaction tolerated different aromatic residues such as electron-donating and electron-withdrawing groups, in all cases resulting in excellent enantioselectivities (Table 3, entries 1–5). The use of *ortho* substituents was also possible without affecting the final *ee* value and was accompanied by a slightly better diastereomeric ratio (Table 3, entry 6). However, the use of the alkyl bromonitroalkene **1e** did not work under the standard conditions (Table 3, entry 7). We then decided to study the reaction with different aldehydes **2**. However, the reaction did work with a less bulky substituent such as the propyl group, and gave slightly lower d.r. but excellent enantioselectivity (Table 3, entry 8). By contrast, a bulkier substituent such as the phenyl group gave a completely diastereoselective reaction with an excellent *ee* value (Table 3, entry 9),[15] which was also valid for other aromatic nitroalkenes (Table 3, entries 10–12) independent of the aromatic residue present.

The absolute configuration of products **5** was determined by X-ray crystallographic analysis of

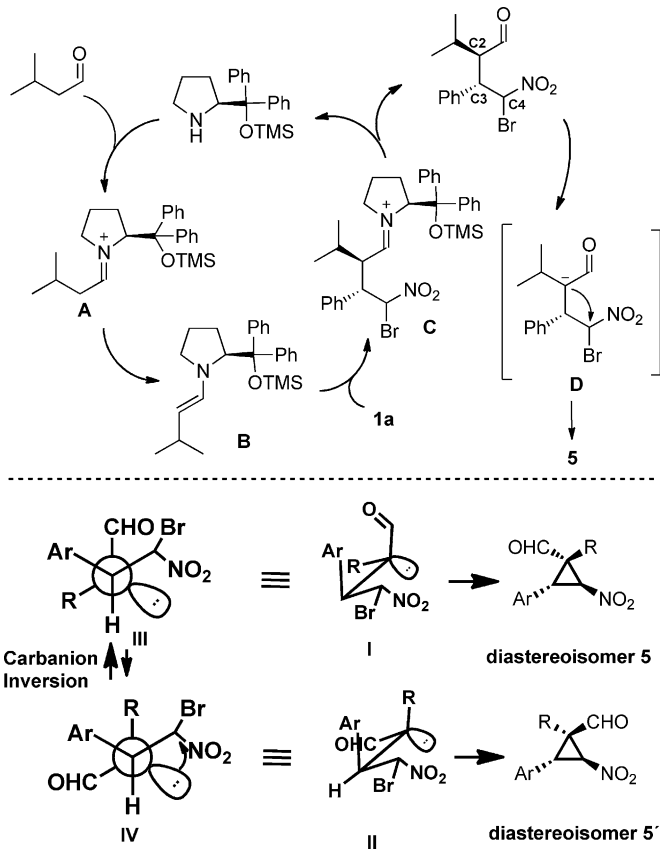

Scheme 3. Proposed mechanism and explanation for the diastereoselectivity obtained in the cyclization reaction (R = Ar or alkyl).

5Cc' (Scheme 2).[16] In addition, the relative configuration of the unique diastereoisomer **5Ac'** was also determined and was in accordance with that described through X-ray analysis. Interestingly, the major diastereoisomer derivative **5Aa** had the op-

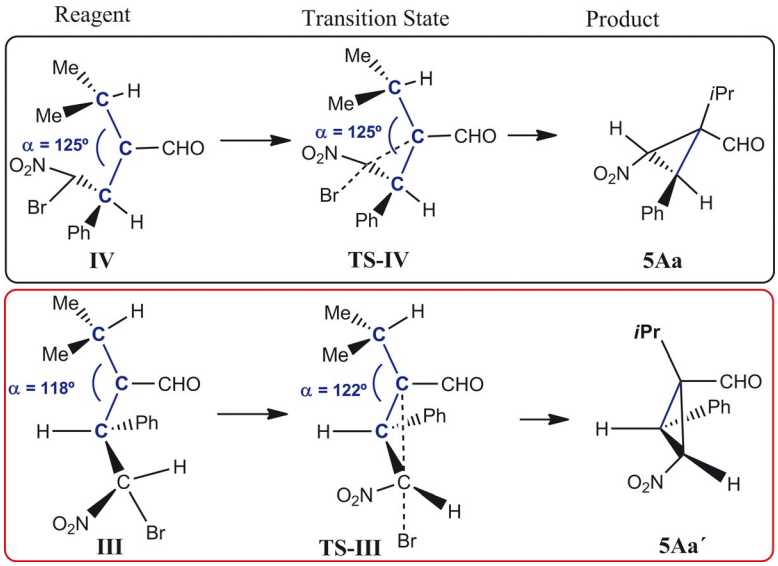

Scheme 4. Energy profile in the formation of diastereoisomers **5Ac** (red box) and **5Ac'** (black box).

posite configuration to the aldehyde center (C1), whereas the minor diastereoisomer was found to have an identical configuration to the diaromatic cyclopropanes (**5 Ac'**, **5 Bc'**, **5 Cc'**). All the spectroscopic parameters (NMR chemical shifts) of the cyclopropanes followed the same pattern. These findings suggest a change in the mechanism in step two when an aromatic ring or an alkyl group is present at C1 of the aldehyde (**1**).

In Scheme 3 we outline a plausible mechanism to explain the enantio- and diastereoselective outcome of the one-pot reaction. The reaction followed the accepted mechanism for an enamine process, and the absolute configuration (C3) fits with the proposed stereochemical model.[17,18] The configuration at C2 is related to the intramolecular attack of the anion formed with the DABCO base whereas the configuration at C4 is related to the acidic proton at this carbon atom and gives a more thermodynamically stable product (NO_2 group in a *trans* configuration to the substituent at C3). To achieve the final cyclization, the σ-orbital with two electrons should be oriented to the σ*-orbital of the C–Br bond (lower part, Scheme 3). To explain the observed diastereoselectivities, we explored a theoretical investigation of the cyclization process from species **III** and **IV** with R = Ph or *i*Pr, by means of DFT calculations using M06 functional.[19] The energy profile found for products **5 Ac/5 Ac'** is shown in Figure 1 whereas that of cyclopropane **5 Aa/5 Aa'** is represented in Figure 2.

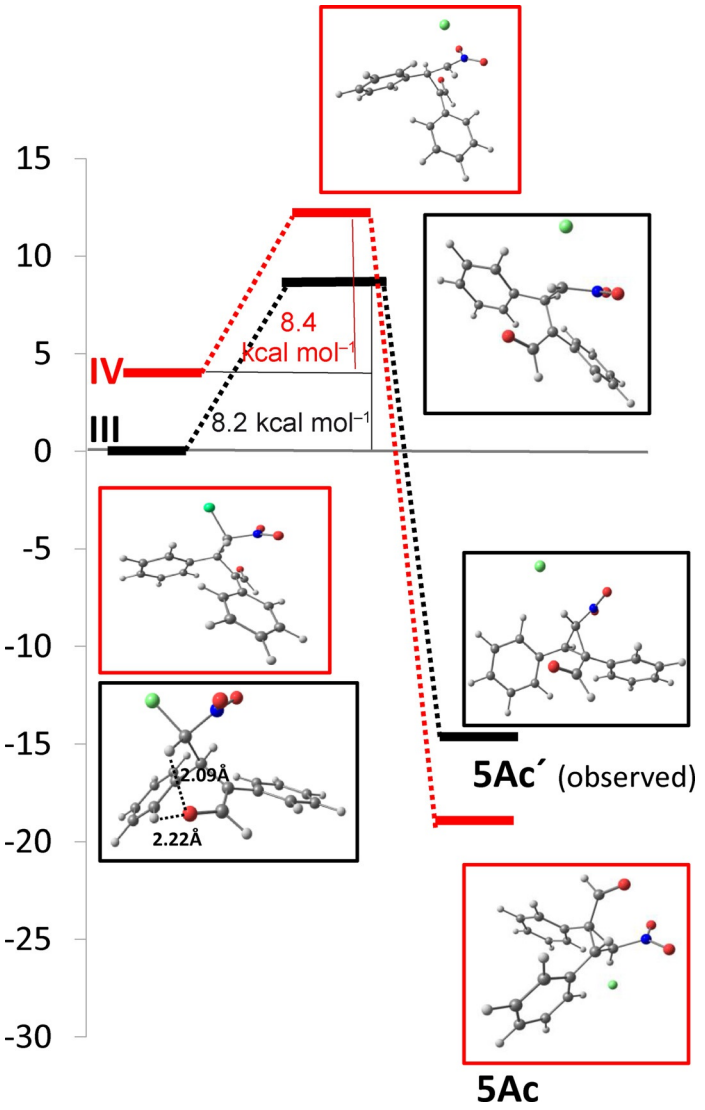

Figure 1. Energy profile in the formation of diastereoisomers **5 Ac** (red box) and **5 Ac'** (black box).

The formation of a cyclopropane ring follows an S_N2 mechanism with a trigonal bipyramid transition state having a high distortion because of the incipient strained three-member ring. A similar activation energy barrier is found for both isomers **5 Ac** and **5 Ac'** (of around 8 kcal mol^{-1}) but isomer **5 Ac** is slightly more exergonic than **5 Ac'** (−15 vs. −19 kcal mol^{-1}; see Figure 1). However, the experimental product observed is less thermodynamically favored. From the energy picture obtained, it can be inferred that the formation of isomer **5 Ac** or **5 Ac'** depends on the initial availability of the starting rotamer **III** or **IV**, respectively. Thus, the selectivity observed obeys the Curtin–Hammet principle, as a consequence of the subtle balance between the different relative energies of the initial rotamers and their very similar activation energies (black line, Figure 1). The greater stability of the starting rotamer **III** is justified because two intramolecular hydrogen bonds are present (see Figure 1) whereas a phenyl/phenyl steric interaction is present in rotamer **IV**.

Formation of **5 Aa** products follows a qualitatively equivalent S_N2 pathway. However, as shown in Figure 2 the energy profiles are significantly different, thus accounting for the different selectivity observed. Two distinct dispositions of isopropyl groups were calculated for the initial rotamers (see the Supporting Information). The energy profile has been computed considering the most stable starting structures that account for **5 Aa** and **5 Aa'**. The rotamer precursor of product **5 Aa** is somehow less stable that its counterpart. However, product **5 Aa** is slightly more stable than **5 Aa'**. Thus, despite the starting rotamers having an energy difference of around 4 kcal mol^{-1}, the lower energy barrier and the lower energy for the final major product (**5 Aa**) determine the reaction's course towards the more stable isomer (red box, Figure 2). The energy balance between reagents and transition states in the phenyl/isopropyl derivatives is the result of different steric repulsions acting on the phenyl/isopropyl units. This proposal is based on the value of angle α shown in Scheme 4. Higher values of this angle in **IV** reveal a major steric repulsive force resulting from phenyl/isopropyl interactions. However, this difference becomes smaller in the transition state because, while the isopropyl group undergoes steric repulsion in TS-**IV** with phenyl fragment, in TS-**III** isopropyl also presents repulsive forces but, in this case, with the -NO_2 group. Thus, while no difference in steric crowding around the isopropyl group is found when going from **IV** to TS-**IV**, there is a significant increase in steric

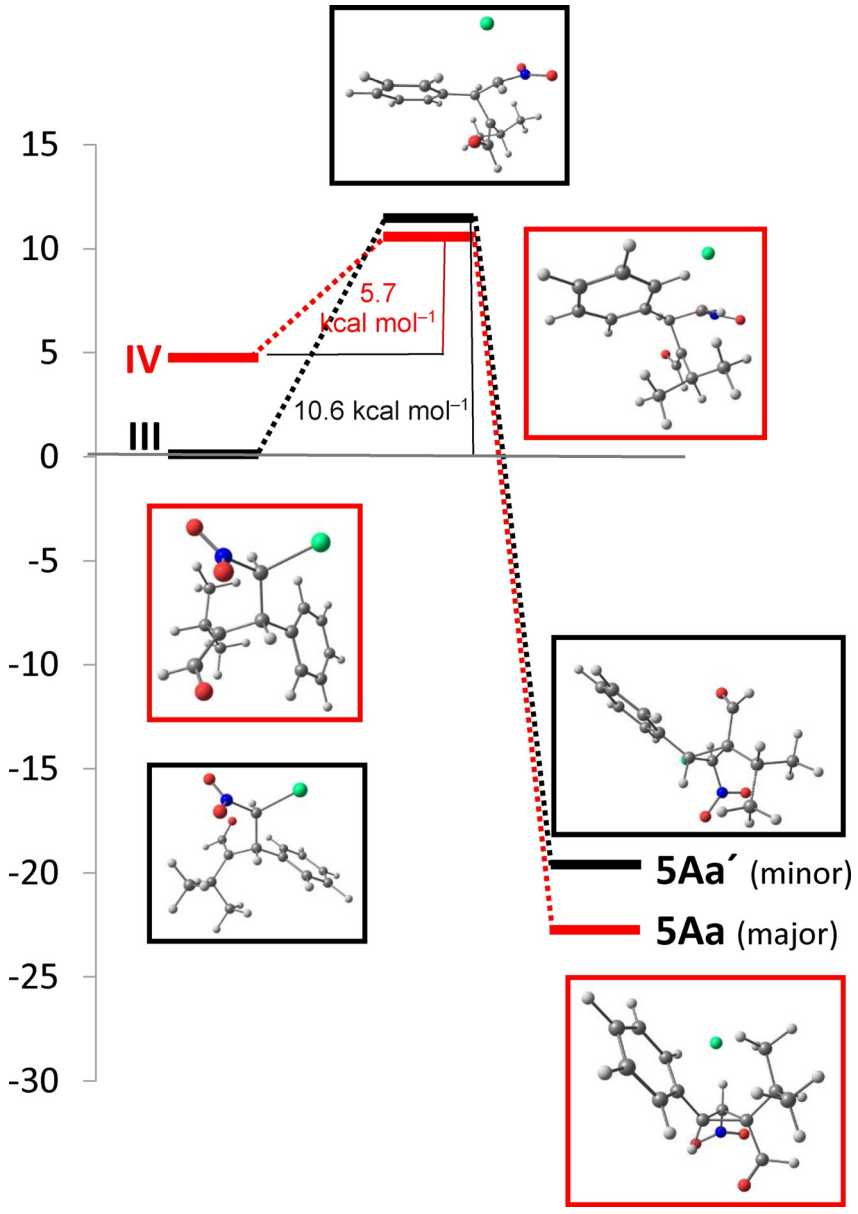

Figure 2. Explanation for the different energy barrier (TS') in the formation of diastereoisomers **5 Aa/5 Aa'**.

repulsion in the process from **III** to TS-**III**. Consequently, the energy becomes very similar in both TS and, considering the different energies of reagents, the activation energy becomes significantly higher for the path from **III** to TS-**III**.

In conclusion, we have developed the asymmetric synthesis of cyclopropanes having a quaternary center using a one-pot reaction resulting in excellent enantioselectivities and good yields. The one-pot reaction is based on a first-step aminocatalytic reaction between aldehydes and bromonitroalkenes and a second-step intramolecular bromo substitution catalyzed by DABCO. We have proposed a plausible mechanism for the one-pot reaction, the enamine and, for the case of the intramolecular bromo substitution, an explanation for the diastereoselectivity based on DFT calculations.

Experimental Section

General procedure for the optically enriched cyclopropanes 5

The corresponding bromonitroalkene **1** (0.2 mmol), aldehyde (0.4 mmol), and (*R*)-α-α-diphenyl-2-pyrrolidinemethanol trimethylsilyl ether (20 mol%) were dissolved in 0.4 mL of CH_2Cl_2. The resulting mixture was stirred at RT overnight (usually 18 h), and then DABCO (2 equiv) was added at RT. Upon completion of the reaction (usually 2–4 h), the solvent was removed under reduced pressure and the residue was purified by flash column chromatography on silica gel (eluent for each case is indicated in the Supporting Information).

(1*S*,2*S*,3*R*)-2-Nitro-1,3-diphenylcyclopropane-1-carbaldehyde (5 Ac)

Following the general procedure described above, the compound was obtained as a yellow oil in 55% yield and 98:2 d.r. (Table 2, entry 10). The crude was product was purified by flash column chromatography on silica gel using cyclohexane/AcOEt (9:1) as eluent. $[\alpha]_D^{20} = +238.7$ ($c = 1.06$, $CHCl_3$); ^{1}H NMR (300 MHz, $CDCl_3$) $\delta = 9.31$ (s, 1H), 7.49–7.32 (m, 10H), 5.67 (d, $J = 5.6$ Hz, 1H), 4.42 ppm (d, $J = 5.6$ Hz, 1H); ^{13}C NMR (75 MHz, $CDCl_3$) $\delta = 193.0$ (CHO), 130.7 (C), 130.2 (C), 129.8 (CH), 129.7 (CH), 129.6 (CH), 129.0 (CH), 128.9 (CH), 128.4 (CH), 67.6 (CH), 52.9 (C), 39.5 ppm (CH); the enantiomeric excess was determined by supercritical fluid chromatography (SFC) on a Chiralpak IB column [CO_2/MeOH (90:10)]; flow rate 3 mL min^{-1}; $\tau_{major} = 2.8$ min, $\tau_{minor} = 3.2$ min; (95% *ee*); EM (TOF-ESI$^-$): elemental analysis calcd (%) for $C_{16}H_{11}O$ [$M-H_2NO_2$]$^-$: 219.0815; found: 219.0825.

Acknowledgements

Financial support from the Spanish Government (CTQ-2012–12168, CTQ-2012–37420-CO2–02) is gratefully acknowledged. J.A. thanks the MICINN for their „Ramón y Cajal" contract. We gratefully acknowledge computational time provided by the CCC (UAM).

Keywords: asymmetric synthesis · cyclopropanes · density functional calculations · organocatalysis · reaction mechanisms

[1] a) H.-U. Reissig, R. Zimmer, *Chem. Rev.* **2003**, *103*, 1151; b) H. N. C. Wong, M.-Y. Hon, C.-H. Tse, Y.-C. Yip, J. Tanko, T. Hudlicky, *Chem. Rev.* **1989**, *89*, 165; c) Z. Goldschmidt, B. Crammer, *Chem. Soc. Rev.* **1988**, *17*, 229; d) H. M. L. Davies, *Tetrahedron* **1993**, *49*, 5203; e) W. A. Donaldson, *Tetrahedron* **2001**, *57*, 8589.

[2] a) S. Sieburth, S. F. Ali, C. M. Langevine, R. H. Tullman, *Bioorg. Med. Chem. Lett.* **1992**, *2*, 1585; b) B. J. Stevenson, J. Bibby, P. Pignatelli, S. Muangnoicharoen, P. M. O'Neill, L. Y. Lian, P. Müller, D. Nikou, A. Steven, J. Hemingway, M. J. Sutcliffe, M. J. I. Paine, *Insect Biochem. Mol. Biol.* **2011**, *41*, 492.

[3] Y.-C. Zhu, G. Wang, J.-K. Liu, *J. Asian Nat. Prod. Res.* **2010**, *12*, 464.

[4] M. Clericuzio, C. Cassino, F. Corana, G. Vidari, *Phytochemistry* **2012**, *84*, 154.

[5] J. Shimokawa, T. Harada, S. Yokoshima, T. Fukuyama, *J. Am. Chem. Soc.* **2011**, *133*, 17634.

[6] H. Takayama, M. Arai, M. Kitajima, N. Aimi, *Chem. Pharm. Bull.* **2002**, *50*, 1141.

[7] For metal catalyzed reactions, see: a) M. Brookhart, W. B. Studabaker, *Chem. Rev.* **1987**, *87*, 411; b) A. Archambeau, F. Miege, C. Meyer, J. Cossy, *Acc. Chem. Res.* **2015**, *48*, 1201; For stereoselective process see stereoselective cyclopropanation reactions: H. Lebel, J.-F. Marcoux, C. Molinaro, A. B. Charette, *Chem. Rev.* **2003**, *103*, 977.

[8] For different reviews, dealing with the topic, see: a) K. Jiang, Y.-C. Chen, *Tetrahedron Lett.* **2014**, *55*, 2049; b) G. Bartoli, G. Bencivenni, R. Dalpozzo, *Synthesis* **2014**, *46*, 979.

[9] C. D. Papageorgiou, M. A. Cubillo de Dios, S. V. Ley, M. J. Gaunt, *Angew. Chem. Int. Ed.* **2004**, *43*, 4641; *Angew. Chem.* **2004**, *116*, 4741.

[10] R. K. Kunz, D. W. C. MacMillan, *J. Am. Chem. Soc.* **2005**, *127*, 3240.

[11] A. Hartikka, P. I. Arvidsson, *J. Org. Chem.* **2007**, *72*, 5874.

[12] For different studies using the Jørgensen–Hayashi catalyst, see: a) R. Rios, H. Sundén, J. Vesely, G. L. Zhao, P. Dziedzic, A. Córdova, *Adv. Synth. Catal.* **2007**, *349*, 1028; b) H. Xie, L. Zu, H. Li, J. Wang, W. Wang, *J. Am. Chem. Soc.* **2007**, *129*, 10886; c) I. Ibrahem, G. L. Zhao, R. Rios, J. Vesely, H. Sundén, P. Dziedzic, A. Córdova, *Chem. Eur. J.* **2008**, *14*, 7867.

[13] For other examples using bromonitroalkenes, see: a) C. Jarava-Barrera, F. Esteban, C. Navarro-Ranninger, A. Parra, J. Alemán, *Chem. Commun.* **2013**, *49*, 2001; b) C. Martín-Santos, C. Jarava-Barrera, A. Parra, F. Esteban, C. Navarro-Ranninger, J. Alemán, *ChemCatChem* **2012**, *4*, 976; c) X. Dou, F. Zhong, Y. Lu, *Chem. Eur. J.* **2012**, *18*, 13945; J.-Y. Pan, X.-S. Li, D.-C. Xu, J.-W. Xie, *Aust. J. Chem.* **2013**, *66*, 1415.

[14] In several examples during the optimization of the tandem process we found the debrominated aldehyde **6Aa**, which can form as a consequence of an attack of the excess of enamine or the co-base on the bromine atom (see scheme below). Moreover, we verified the absolute configuration of the obtained aldehyde, being *2R,3S* configuration, which is in accordance with the obtained in the X-ray analysis (see Scheme 2).

[15] We tried the reaction with the *tert*-butyl group (3,3-dimethylbutanal) but the first Michael addition did not take place.

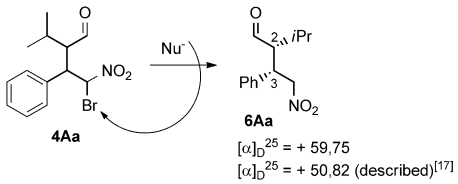

[16] CCDC 1404743 (**5Cc**) contains the supplementary crystallographic data for this paper. These data can be obtained free of charge from The Cambridge Crystallographic Data Centre.

[17] J. M. Betancort, C. F. Barbas III, *Org. Lett.* **2001**, *3*, 3737.

[18] For Reviews on the reaction mechanism under Jorgensen–Hayashi catalysts, see: a) L. Albrecht, J. H. Jiang, K. A. Jørgensen, *Chem. Eur. J.* **2014**, *20*, 358; b) K. L. Jensen, G. Dickmeiss, H. Jiang, L. Albrecht, K. A. Jørgensen, *Acc. Chem. Res.* **2012**, *45*, 248; c) M. Nielsen, D. Worgull, T. Zweifel, B. Gschwend, S. Bertelsen, K. A. Jørgensen, *Chem. Commun.* **2011**, *47*, 632.

[19] Y. Zhao, D. G. Truhlar, *Theor. Chem. Acc.* **2008**, *120*, 215. For more details see the Supporting Information.

Manuscript received: July 16, 2015
Final Article published: August 13, 2015

Photocatalysis

International Edition: DOI: 10.1002/anie.201703334
German Edition: DOI: 10.1002/ange.201703334

Visible-Light Photocatalytic Intramolecular Cyclopropane Ring Expansion

*Javier Luis-Barrera, Víctor Laina-Martín, Thomas Rigotti, Francesca Peccati, Xavier Solans-Monfort, Mariona Sodupe, Rubén Mas-Ballesté, Marta Liras, and José Alemán**

Dedicated to Professor Carmen Navarro Ranninger

Abstract: *Described herein is a new visible-light photocatalytic strategy for the synthesis of enantioenriched dihydrofurans and cyclopentenes by an intramolecular nitro cyclopropane ring expansion reaction. Mechanistic studies and DFT calculations are used to elucidate the key factors in this new ring expansion reaction, and the need for the nitro group on the cyclopropane.*

The [3+2] cycloaddition reactions of donor–acceptor cyclopropanes (DACs), having double bonds, under Lewis acid catalysis are one of the most commonly used methods for the construction of different cycles through ring expansion reactions.[1] Therefore, in the presence of a Lewis acid, 1,3-zwitterions can be generated and trapped by different double bonds, that is C=C, C=N, C=O. Brilliant examples of intermolecular cycloadditions (Scheme 1 a) from the groups of Maulide,[2a] Trushkov,[2b] Tang,[2c] Doyle,[2d] Tomilov,[2e] and Werz[2f–h] have been reported recently, while the group of Wang and others have developed related intramolecular cross-cycloadditions (IMCC; Scheme 1 b).[3]

Visible-light photocatalysis has received significant attention during the last few years because of its ability to achieve bond constructions that are not possible using other procedures.[4] However, although thermal DAC reactions have been studied in the literature, only two examples of intermolecular cyclopropane ring expansion using photocatalysis have been reported.[5] Lu and co-workers have published on the cyclopropane ring opening under visible-light photocatalysis, and its intermolecular addition to a double bond to generate racemic cyclopentanes with a moderate diastereomeric ratio (Scheme 2 a).[5a] More recently, Yoon and co-workers published a very elegant investigation in which photocatalysis is used in combination with a chiral Lewis acid to access cyclopentanes through an intermolecular process (Scheme 2 a).[5b]

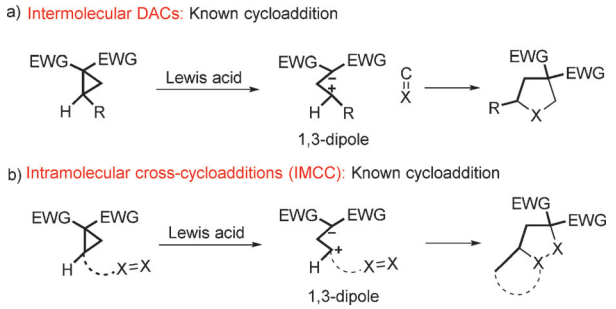

Scheme 1. DAC- and IMCC-type reactions. EWG = electron-withdrawing group.

Based on these investigations, we hypothesized that enantiomerically enriched cyclopropanes could be used as starting materials for the intramolecular visible-light photocatalytic ring expansion, a process that has remained elusive up to now. Very recently, the synthesis of chiral cyclopropanes which contain a chiral center flanked by an aldehyde and a nitro group was reported by our group.[6] We thought that the formation of the chiral intermediate **A**, which could preserve the chiral information to the final product, would be

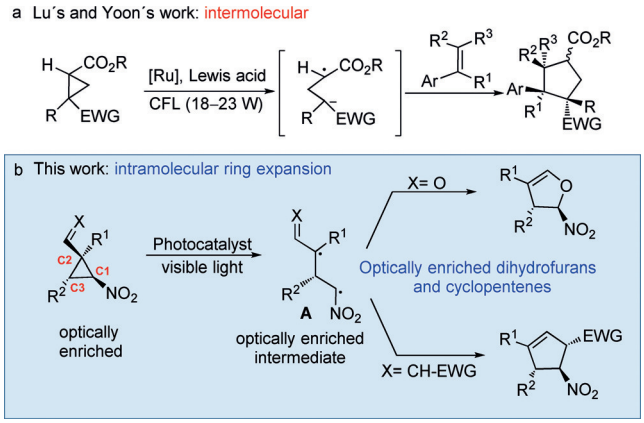

Scheme 2. Different strategies for the intermolecular reaction of cyclopropanes with double bonds and the expansion shown in this work.

[*] J. Luis-Barrera, V. Laina-Martín, T. Rigotti, Prof. Dr. J. Alemán
Organic Chemistry Department, Módulo 1
Universidad Autónoma de Madrid
28049 Madrid (Spain)
E-mail: jose.aleman@uam.es
Homepage: http://www.uam.es/jose.aleman
Dr. F. Peccati, Prof. Dr. X. Solans-Monfort, Prof. Dr. M. Sodupe
Departament de Química, Universidad Autónoma de Barcelona
08193 Bellaterra (Spain)
Prof. Dr. R. Mas-Ballesté
Inorganic Chemistry Deparment, Universidad Autónoma de Madrid
28049 Madrid (Spain)
Dr. M. Liras
Imdea Energy Institute
28935 Móstoles (Madrid)

Supporting information for this article can be found under: https://doi.org/10.1002/anie.201703334.

an appropriate strategy for its intramolecular expansion reaction (Scheme 2b). This approach is challenging because two other plausible C–C bond ruptures might take place (C2–C3 and C3–C1), but only the C1–C2 bond breaking will lead to **A** for the expansion reaction. This ring enlargement (C1–C2 cleavage) stands in contrast to the common expansion of DACs (C2–C3 cleavage).[3e,f] Therefore, the first visible-light photocatalytic strategy for the synthesis of enantioenriched dihydrofurans and cyclopentenes,[7] by an intramolecular cyclopropane expansion reaction is presented.

First, we studied the expansion of the aldehyde **1a** to **2a** (for structures see Table 1) using different photocatalysts such as acridinium salts, eosin Y, and different iridium and ruthenium complexes. Only two iridium complexes were active, and **3b** [Ir(dFppy)$_3$] allowed higher conversion than **3a** [Ir(ppy)$_3$], with CH_2Cl_2 as the best solvent and irradiation of blue light into the reaction media, through a glass bar, thus achieving full conversion of **2a** after 4 hours (see the Supporting Information for full optimization of reaction conditions). The scope of the reaction was studied with different cyclopropanes (**1**[8]; Table 1). Regarding R^2, different aromatic groups, having substitutions at the *para* position, and alkyl groups were studied. Excellent yields for the compounds **2a–c** were achieved. In addition, different R^1 groups were studied, thus showing that the reaction takes place with primary alkyl groups (**2d**), aromatics (**2e** and **2f**), and hydrogen (**2g** and **2h**).[9] In all cases, we observed similar final *ee* values for the products **2** as those for the reactants **1** (*ee* value within parentheses), thus indicating that no loss of stereochemical information at C3 was observed. The absolute configuration of the starting material **1f** was unequivocally determined by its X-ray diffraction structure (see structure in Table 1).[10]

To expand the scope of the reaction, we studied cyclopropanes bearing a double bond instead of an aldehydic group (Table 2). Firstly, the aldehydes **1** were treated with different commercially available Wittig reagents to give the cyclopropane starting materials **4** (see the Supporting Information). The reaction worked with the cyclopropane **4a** to give **5a**, with a good *ee* value, by using the same reaction conditions as those used for the expansion of the aldehydes **1**, but with slightly longer reaction times compared to that of the aldehydes. Substrates with other aromatic residues, such as methoxy and bromo substituents (**4b** and **4c**), also underwent the ring expansion reaction in moderate to good yields. Other groups at R^1, such as *n*Pr (**4d**), were also tolerated. Unexpectedly, the aromatic group at R^1 (**4e**) did not yield the desired product **5e**. Other double bonds bearing benzyl esters (**4f**), ketones (**4g**), or nitriles (**4h**) also worked, giving moderate to good yields, without any loss in the final enantioselectivity. The absolute configuration of the starting material **4c** was unequivocally determined by its X-ray diffraction structure (see structure in Table 2).[10]

Furthermore, the photocatalytic cyclopropanation expansion reaction worked with other functional groups (Scheme 3). When the reaction was performed with the ketone **6**, the reaction was much slower (3 days) in comparison with the aldehyde derivatives **1**, yielding **7** in moderate yield. The α-keto-ester **8** was more reactive (24 h), thus giving the trisubstituted dihydrofuran **9** in good yield.

Table 1: Different ring expansions of **1** using the photocatalyst **3b**.[a]

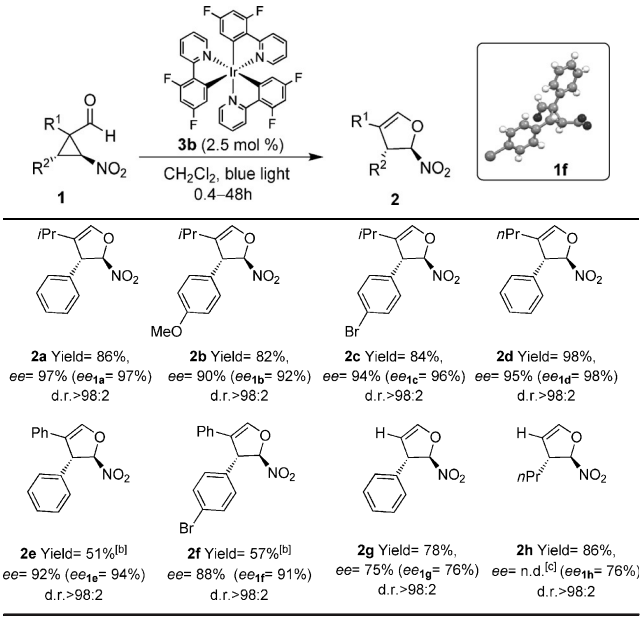

[a] All the reactions were performed at 0.1 mmol scale of **1** in 1.0 mL CH_2Cl_2. The *ee* value of the starting cyclopropane **1** (given within parentheses) and final dihydrofurans (**2**) were determined by SFC. Yield of product isolated after flash chromatography. [b] Yield based on conversion as determined by ^{1}H NMR spectroscopy. [c] The *ee* value could not be determined by SFC, although possess optical rotation activity.

Table 2: Different ring expansion of **4** using the photocatalyst **3b**.[a]

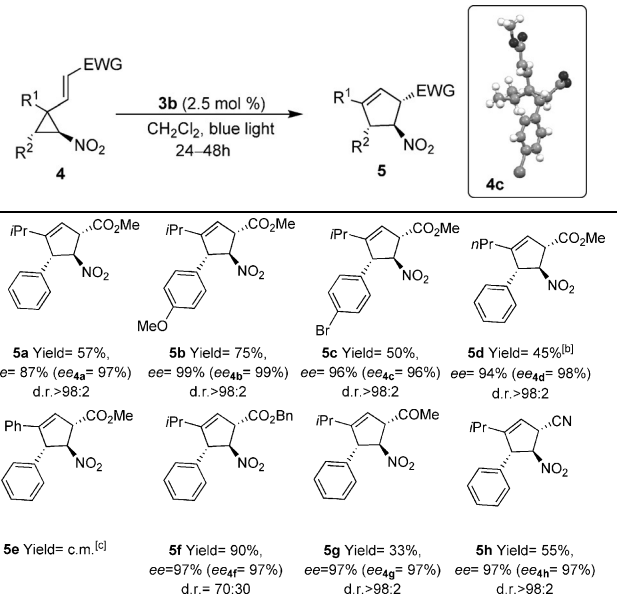

[a] All the reactions were performed at 0.1 mmol scale of **4** in 1.0 mL CH_2Cl_2. The *ee* value of the starting material cyclopropane **4** (given within parentheses) and the final cyclopentenes **5** were determined by SFC. Yield of product isolated after flash chromatography. [b] Yield based on conversion as determined by ^{1}H NMR spectroscopy. [c] Complex mixture.

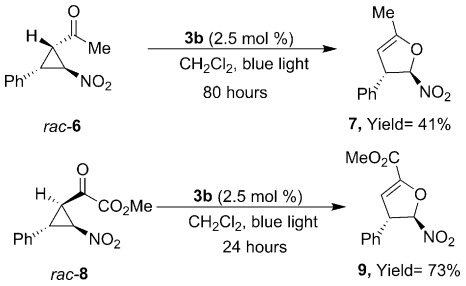

Scheme 3. Reaction with ketone and α-ketoester cyclopropane derivatives.

To understand this process, we carried out additional experiments and DFT(M06/6-31+G(d,p)) calculations,[11a] including the SMD implicit solvent model[11b] (see the Supporting Information for details). The process starts with the excitation of the photocatalyst **3b** to **3b*** using visible-light irradiation. To evaluate the possibility of a photo-redox mechanism, cyclic voltammetry measurements were carried out for **1a** and compared with the reported redox potentials for the excited state of **3b**[12] (see the Supporting Information). Electrochemical characterization rules out photocatalytic oxidation as a mechanism of activation since no oxidation features below +1.5 V (vs. Ag/AgCl) were observable in the cyclic voltammogram of **1a**. However, one irreversible reduction of **1a** at half-wave potential of −1.06 V (vs. Ag/AgCl) was observed. Although photoreduction of **1a** by **3b*** ($Ir^{4+}/Ir^{3+*} = -1.39$ V vs. Ag/AgCl) would be possible, we found that the use of Eosin Y as a photo reductor catalyst [$E°(EY^{+}/EY^{*}) = -1.11$ V vs. Ag/AgCl[4d]] did not result in any conversion (see the Supporting Information). Furthermore, despite the higher reducing power of [$Ir(ppy)_3$] (**3a**) in its excited state [$E°(Ir^{4+}/Ir^{3+*}) = -1.67$ V vs. Ag/AgCl], the conversion into the observed product using **3a** is very poor in comparison with the results obtained with **3b** (27% vs. >98%; see the Supporting Information). Therefore, an energy-transfer process should be considered as an alternative mechanism.[13] Considering that we did not observe any overlap in the emission of the photocatalyst **3b** ($\lambda_{max} = 453$ nm) and the absorption of the nitrocyclopropane **1a** ($\lambda_{max} = 229$ nm; see the Supporting Information), the energy-transfer process from **3b*** to the substrate should proceed through a Dexter-type mechanism (instead of a Forster pathway). Such a mechanism implies that triplet spin state in the substrate is induced by short distance interaction with the triplet excited state of photocatalyst. Indeed, the calculated values of singlet–triplet gap in **1a** and the emission energy of **3a** are in good agreement (see below). In a quest for evidence of an energy-transfer mechanism, the cyclopropane **8** was irradiated with UV light ($\lambda_{max} = 365$ nm), and the expansion reaction was observed with a moderate conversion (23%) after 24 hours. Although a value of the quantum yield less than one does not exclude a possible radical-chain mechanism, we measured the Φ of the reaction of **1a** in the presence of **3b** (see the Supporting Information). The observed value ($\Phi = 0.05$) could suggest that a radical-chain propagation is not taking place.

Considering that changes in R^1, R^2, and CHO/CH=EWG did not suppress the observed reactivity, we hypothesized that the nitro group must play a key role in the photocatalytic activation of cyclopropane. Indeed, when the nitro group was substituted by an ester or a ketone (**10** and **11**; see Figure 1),

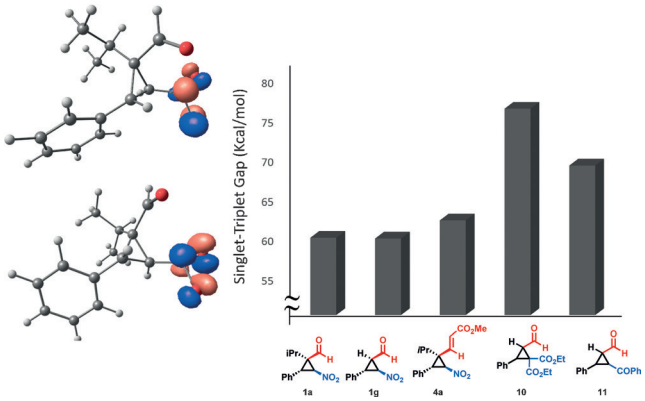

Figure 1. SOMO orbitals calculated for triplet state of **1a** (left) and singlet–triplet energy gap for a range of cyclopropane reagents (right).

the reaction under visible-light photocatalytic conditions did not take place, thus indicating that the presence of the nitro group is essential for the ring-expansion process. With the aim of gaining a deeper insight into this point, the singlet–triplet Gibbs energy gap was calculated for **1a** and other related structures where the nitro group was substituted by different functional groups (Figure 1). Interestingly, the lowest singlet–triplet gaps are computed for molecules enclosing the nitro group. In fact, such an energetic difference between the spin states of the organic reagent, reasonably matches the reported emission energy for **3b** (ca. 60 kcal mol^{-1}).[12] Certainly, when the nitro group is substituted by COPh or two esters, the gap substantially increases (>70 kcal mol^{-1}), thus hindering the photocatalytic process, which is in agreement with the absence of reactivity of **10** and **11**. The two SOMO orbitals of the triplet state are localized on the NO_2 group, in agreement with the role of such a fragment on lowering the excitation energy of the reagent.

The first step is the opening of the cyclopropane ring that leads to the formation of the first biradical ^{3}**IIa** (Figure 2, right). Three C–C bond breaks are possible (paths a, b, or c), and give three different isomers (^{3}**IIa**, ^{3}**IIb**, and ^{3}**IIc**). Ring expansion from ^{3}**IIa** enables the final observed five-membered ring isomer (**2a**) whereas that from ^{3}**IIb** would lead to the five-membered ring ^{1}**IVb** which is not observed experimentally. Finally, ^{3}**IIc** is an unproductive pathway because of the disposition of the aldehyde group. Product formation through pathways a and b requires the conformational change from ^{3}**II** to another biradical, ^{3}**III**, to properly orient the reacting groups before ring closure occurs. This ring closure implies a spin crossing from the triplet to the singlet state and can occur either before or after ^{3}**II**→^{3}**III** interconversion. To understand the reaction mechanism, we explored the reactivity of **1a** as a representative example (for **4a**, see the

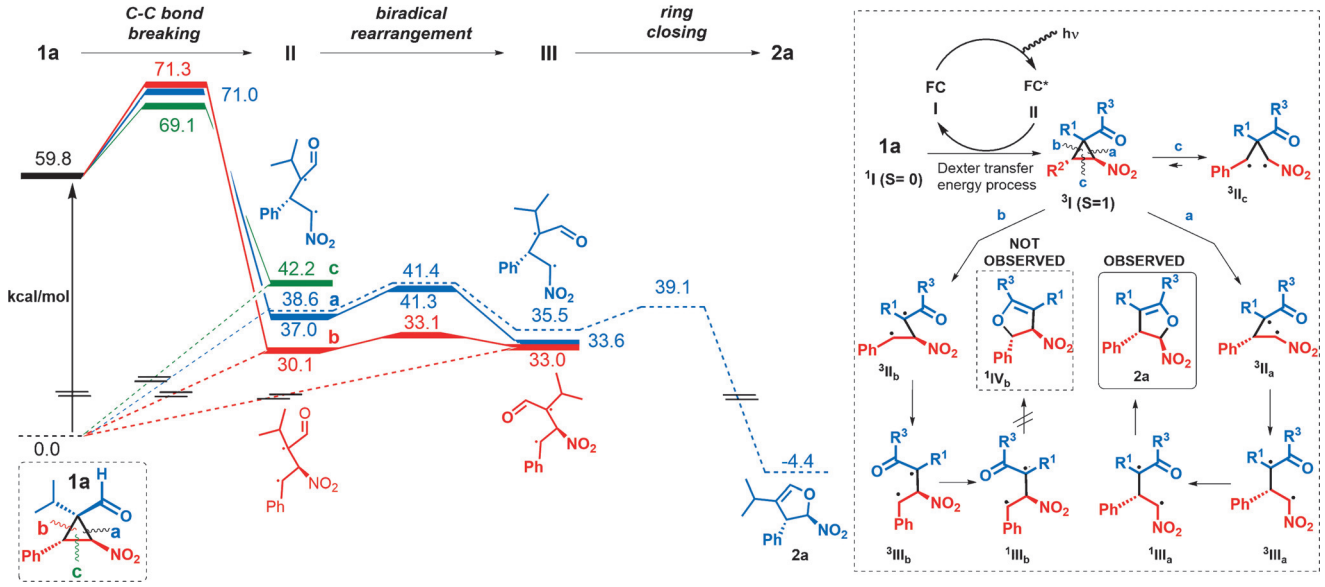

Figure 2. Gibbs energy profile calculated for reaction pathway from **1a** to **2a** (left). Solid lines correspond to species in the triplet state, whereas dashed lines refer to the energies of the spin-corrected singlet state.[11c] Possible reaction pathways of triplet excited state of **1a** (right).

Supporting Information), considering both the triplet and open-shell singlet states for all biradical intermediates.

Figure 2 shows the Gibbs energy profiles for pathways a, b, and c of **1a**. The three possible C–C cleavages are kinetically and thermodynamically favored. Energy barriers are low (9–12 kcal mol^{-1}) and the reaction ΔG ranges from −18 to −30 kcal mol^{-1}. Noteworthy, the most stable biradical corresponds to ^{3}**IIb**. In these species, the radical character lies at the two carbon centers which are able to better stabilize the unpaired electrons: the tertiary carbon atom presents the stabilizing CHO group and the benzyl carbon atom (see the Supporting Information for details). However, this cleavage pathway would lead to the ring expansion product ^{1}**IVb** which is not experimentally observed (Figure 2), thereby indicating that other factors determine the observed reactivity. In particular, the evolution of intermediates ^{3}**IIa** and ^{3}**IIb** differs significantly. That is, although for both intermediates the Gibbs energy barrier for the biradical rearrangement (^{3}**II**→ ^{3}**III**) is low, this process is exergonic for path a and endergonic for path b. This data suggests that ^{3}**IIIa** would be a more long-lived species than ^{3}**IIa**, whereas the opposite is expected for pathway b. Moreover, open-shell singlet-state optimizations of ^{1}**IIa** and ^{1}**IIIa** yield to two minima with very similar geometries and energetics to those of the triplet states. ^{1}**IIa** evolves to reactants in an essentially barrierless process, whereas ^{1}**IIIa** leads to the final product observed, after overcoming a low-energy barrier of 3.6 kcal mol^{-1}. This process suggests that spin crossing probably occurs after biradical rearrangement, that is, at geometries close to that of ^{3}**IIIa**. In contrast, all attempts to locate open-shell singlet-state structures for **IIb** and **IIIb** collapsed to reactants, thus suggesting that spin crossing always leads to the initial reactants.[14] Thus, spin crossing in pathway b appears to be unproductive, and is in agreement with the non-observation of ^{1}**IVb** as the resulting product[15] and the low value of the quantum yield.

The calculations suggest that the key point is that the biradical intermediates of pathway a can evolve into products, whereas those of pathway b can only return to reactants. This difference seems to originate from three key points: 1) The biradical rearrangement is only exergonic for pathway a, and favors the species which leads to the final product. It suggests that it is more likely that spin crossing occurs after biradical rearrangement. 2) There is almost no overlap between the carbon p orbitals of both species (**IIa** and **IIIa**) involved in the formation of dihydrofuran in pathway a, and is in contrast to the overlap observed in **IIb**. Furthermore, the S^2 expectation value obtained for open-shell singlets is around 1. Indeed, this value is observed for **IIa** and **IIIa**, whereas in the case of **IIb** the calculated value is 0.86 (Figure 3). Consequently, the latter intermediate exhibits a smaller biradical character. Therefore, after spin-crossing in pathway b the reactant is easily recovered, but not the product, which requires a larger electronic reorganization. 3) The partial charges of the atoms involved in the new C–O bond formation in the ring-closure step are both negative for **IIIb**, and they present opposite signs in **IIIa** (Figure 3). That is, the NO_2 electron-withdrawing character induces a positive charge on the carbon atom directly bonded to it, thus resulting in a Coloumbic attraction in **IIIa** with the negatively charged oxygen fragment. Therefore, this could favor the orientation of the reacting fragments and overall facilitate the reaction along pathway a.

In conclusion, a new visible-light photocatalytic strategy for the synthesis of enantioenriched dihydrofurans and cyclopentenes by an intramolecular cyclopropane ring expansion reaction has been developed. This process proceeds under mild reaction conditions, achieving good to excellent yields with excellent enantioselectivities in the final products. Moreover, DFT calculations have been carried out to elucidate the role of the nitro group and the origin of product selectivity.

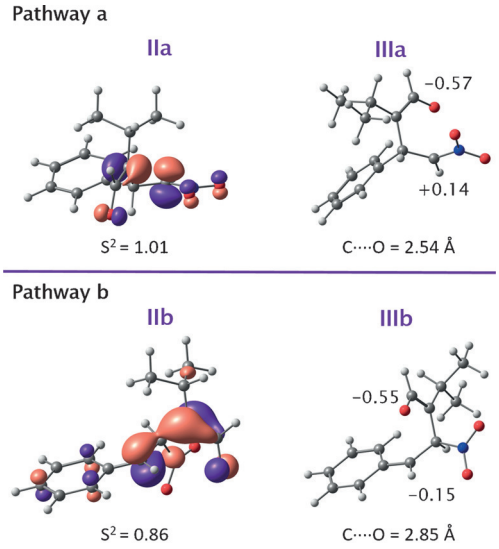

Figure 3. Lowest-energy singly occupied orbital of the unrestricted broken shell singlet at the ^{3}**IIa** and ^{3}**IIb** geometries (left). Partial charges of the oxygen and carbon atoms involved in the formation of the five-membered ring in the ^{3}**IIIa** and ^{3}**IIIb** structures (right).

Acknowledgments

The Spanish Government (CTQ2015-64561-R, CTQ2014-59544-P) and the European Research Council (ERC-CG, contract number: 647550) are acknowledged. We acknowledge the generous allocation of computing time at the CCC (UAM). V.L.-M. and M.L. thank the UAM and MINECO for a predoctoral fellowship-UAM and Ramon y Cajal contract, respectively. X.S.-M. is grateful for a Professor Agregat Serra-Húnter position and M.S. financial support from an ICREA award.

Conflict of interest

The authors declare no conflict of interest.

Keywords: density functional calculations · small ring systems · photocatalysis · reaction mechanisms · ring expansion

How to cite: *Angew. Chem. Int. Ed.* **2017**, *56*, 7826–7830
Angew. Chem. **2017**, *129*, 7934–7938

[1] For recent review, see: T. F. Schneider, J. Kaschel, D. B. Werz, *Angew. Chem. Int. Ed.* **2014**, *53*, 5504; *Angew. Chem.* **2014**, *126*, 5608.

[2] For intermolecular processes, see e.g.: a) J. Sabbatani, N. Maulide, *Angew. Chem. Int. Ed.* **2016**, *55*, 6780; *Angew. Chem.* **2016**, *128*, 6892; b) O. A. Ivanova, E. M. Budynina, V. N. Khrusta-lev, D. A. Skvortsov, I. V. Trushkov, M. Y. Melnikov, *Chem. Eur. J.* **2016**, *22*, 1223; c) H. Xu, J.-L. Hu, L. Wang, S. Liao, Y. Tang, *J. Am. Chem. Soc.* **2015**, *137*, 8006; d) Q.-Q. Cheng, Y. Qian, P. Y. Zavalij, M. P. Doyle, *Org. Lett.* **2015**, *17*, 3568; e) D. D. Borisov, R. A. Novikov, Y. V. Tomilov, *Angew. Chem. Int. Ed.* **2016**, *55*, 12233; *Angew. Chem.* **2016**, *128*, 12421; f) L. K. B. Garve, M. Petzold, P. G. Jones, D. B. Werz, *Org. Lett.* **2016**, *18*, 564.

[3] For a recent review of intramolecular cyclopropane expansion, see: a) M. A. Cavitt, L. H. Phun, S. France, *Chem. Soc. Rev.* **2014**, *43*, 804. For some selected references, see: b) J. Zhang, S. Xing, J. Ren, S. Jiang, Z. Wang, *Org. Lett.* **2015**, *17*, 218; c) W. Zhu, J. Fang, Y. Liu, J. Ren, Z. Wang, *Angew. Chem. Int. Ed.* **2013**, *52*, 2032; *Angew. Chem.* **2013**, *125*, 2086; d) Y. Bai, W. Tao, J. Ren, Z. Wang, *Angew. Chem. Int. Ed.* **2012**, *51*, 4112; *Angew. Chem.* **2012**, *124*, 4188; e) C. Brand, G. Rauch, M. Zanoni, B. Dittrich, D. B. Werz, *J. Org. Chem.* **2009**, *74*, 8779; f) T. F. Schneider, J. Kaschel, S. I. Awan, B. Dittrich, D. B. Werz, *Chem. Eur. J.* **2010**, *16*, 11276.

[4] For some selected reviews in photocatalysis, see: a) C. Prier, D. Rankic, D. W. C. MacMillan, *Chem. Rev.* **2013**, *113*, 5322; b) J. M. R. Narayanam, C. R. J. Stephenson, *Chem. Soc. Rev.* **2011**, *40*, 102; c) N. A. Romero, D. A. Nicewicz, *Chem. Rev.* **2016**, *116*, 10075.

[5] a) C. Wang, X. Ren, H. Xie, Z. Lu, *Chem. Eur. J.* **2015**, *21*, 9676; b) A. G. Amador, E. M. Sherbrook, T. P. Yoon, *J. Am. Chem. Soc.* **2016**, *138*, 4722.

[6] J. Luis-Barrera, R. Mas-Balleste, J. Alemán, *ChemPlusChem* **2015**, *80*, 1595.

[7] For examples, see: a) D. H. R. Barton, H. T. Chung, A. D. Gross, L. M. Jackman, M. Martin-Smith, *J. Chem. Soc.* **1961**, 5061; b) R. B. von Dreele, G. R. Pettit, R. H. Ode, R. E. Perdue, J. D. White, P. S. Manchand, *J. Am. Chem. Soc.* **1975**, *97*, 6236; c) R. Kaur, S. K. Chattopadhyay, A. Chatterjee, O. Prakash, F. Khan, N. Suri, D. Priya, A. K. Saxena, *Med. Chem. Res.* **2014**, *23*, 4138.

[8] The absolute configuration at C2 with aromatic groups of the starting material **1** possess opposite configuration to those with hydrogen or alkyls groups. See Ref. [6] and the Supporting Information for more details.

[9] The synthesis of cyclopropanes **1g** and **1h** were obtained following procedures described in the literature, see: a) J. Vesely, G.-L. Zhao, A. Bartoszewicz, A. Córdova, *Tetrahedron Lett.* **2008**, *49*, 4209.

[10] CCDC 1404743 (**1f**) and 1529711 (**4c**) contain the crystallographic data. These data can be obtained free of charge from The Cambridge Crystallographic Data Centre. Because the chiral center configuration supporting R^2 did not change during the ring expansion process, we assumed the same configuration at this carbon atom in the final product **2** or **5**, whereas the configuration of the α-nitro carbon atom (C1) and α-EWG carbon atom in products **5** were confirmed by ^{1}H NMR experiments (see the Supporting Information).

[11] a) Y. Zhao, D. G. Truhlar, *Theor. Chem. Acc.* **2008**, *120*, 215; b) A. V. Marenich, C. J. Cramer, D. G. Truhlar, *J. Phys. Chem. B* **2009**, *113*, 6378; c) K. Yamaguchi, F. Jensen, A. Dorigo, K. N. Houk, *Chem. Phys. Lett.* **1988**, *149*, 537.

[12] T. B. Demissie, K. Ruud, J. H. Hansen, *Organometallics* **2015**, *34*, 4218.

[13] For a related study, see: T. R. Blum, Z. D. Miller, D. M. Bates, I. A. Guzei, T. P. Yoon, *Science* **2016**, *354*, 1391.

[14] The unique transition state leading to ^{1}**IVb**, one that we have been able to locate, is a closed-shell singlet which connects **1a** with ^{1}**IVb** and can be associated with a high-energy barrier ($\Delta G^{\neq} = 34.2$ kcal mol^{-1}) by a thermal process.

[15] To understand why racemization processes are not taking place with pathways b and c, we also calculated the unproductive racemization pathways (see the Supporting Information). Interestingly, all intermediates that would involve a loss of enantioselectivity are higher in energy than the most stable biradical, ^{3}**II**, of each pathway by between 2.9 and 8.5 kcal mol^{-1}.

Manuscript received: March 31, 2017
Revised manuscript received: April 28, 2017
Accepted manuscript online: May 10, 2017
Version of record online: June 6, 2017

nature COMMUNICATIONS

ARTICLE

https://doi.org/10.1038/s41467-019-10441-4 OPEN

Chromoselective access to *Z*- or *E*- allylated amines and heterocycles by a photocatalytic allylation reaction

Ana María Martínez-Gualda[1], Rafael Cano[2], Leyre Marzo[1], Raúl Pérez-Ruiz[3], Javier Luis-Barrera[1], Rubén Mas-Ballesté[2,4], Alberto Fraile[1,4], Víctor A. de la Peña O'Shea[5] & José Alemán[1,4]

The most useful strategies for the alkylation of allylic systems are related to the Tsuji–Trost reaction or the use of different Lewis acids. Herein we report a photocatalytic approach for the allylation reaction of a variety of nucleophiles, such as heteroarenes, amines and alcohols. This method is compatible with a large variety of pyrroles and indoles, containing different substituents such as electron-withdrawing and electron-donating groups, unprotected nitrogen atoms and bromo derivatives. Moreover, this methodology enables the chromoselective synthesis of *Z*- or *E*-allylated compounds. While the use of UV-light irradiation has allowed the synthesis of the previously inaccessible *Z*-allylated products, *E*-isomers are prepared simply by changing both the light source to the visible region, and the catalytic system. Based on mechanistic and photochemical proofs, laser flash photolysis studies and DFT calculations, a rational mechanism is presented.

[1] Organic Chemistry Department, Módulo 1, Universidad Autónoma de Madrid, 28049 Madrid, Spain. [2] Inorganic Chemistry Department, Módulo 7, Universidad Autónoma de Madrid, 28049 Madrid, Spain. [3] Departamento de Química, Universitat Politècnica de València, Camino de Vera s/n, 46022 Valencia, Spain. [4] Institute for Advanced Research in Chemical Sciences (IAdChem), Universidad Autónoma de Madrid, Madrid 28049, Spain. [5] Photoactivated Processes Unit, IMDEA Energy, Av. Ramón de la Sagra 3C, 28935 Móstoles, Madrid, Spain. Correspondence and requests for materials should be addressed to J.A. (email: jose.aleman@uam.es)

The preparation of allyl-substituted compounds has attracted a special interest due to their utility as building blocks in organic synthesis[1–3]. The Tsuji–Trost reaction[4] is one of the most powerful methodologies for the alkylation of allylic systems, which is commonly catalyzed by palladium, and the allylic position is usually activated by a halide, an acetate, or a carbonate (eq. a, Fig. 1) and affords exclusively the *E*-isomer. The high selectivity and the general scope of this reaction makes it one of the most prominent Csp^3–Csp^3 bond formation methodologies[5]. Indoles and pyrroles are versatile and useful heterocycles for the synthesis of a large variety of biologically active compounds and natural products[6]. Different authors have reported the allylation of indoles at the C-3 position via the Tsuji–Trost reaction in a racemic manner[7–12]. However, although this methodology is very important, to the best of our knowledge, no photocatalytic approaches for the allylation of heterocycles have been reported so far.

Over the past decade, photocatalysis has emerged as a powerful tool for the construction of new bonds that are difficult to obtain using other established procedures[13–31]. A large number of photocatalytic methodologies have been described for the formation of new Csp^2–Csp^2 bonds. In particular, the arylation of (hetero)-aromatic rings, usually pyrroles, under different photocatalytic systems has been recently reported[32–40]. However, one of the major problems related to this photocatalytic arylation is the large excess of the heterocycle required in this reaction (24–40 equiv.). Although the photocatalytic heteroatomatic ring arylation has been extensively studied, the photoallylation of heterocycles remains an elusive process.

We hypothesize that the reduction of the allylic derivative by a photocatalyst with the adequate redox potential would result in the appropriate intermediate, which will allow the functionalization of the allylic position. There are two prerequisites to achieve this goal: (i) the development of a photocatalytic system able to activate the C–O bond; (ii) since an unsaturation is present, it is necessary to control the isomerization of the double bond (*Z* or *E*).

In this work, we present a chromoselective photocatalytic allylation of heteroaromatic rings, using smooth conditions and short reaction times to access the *Z*- or *E*-double bonds, depending on the reaction conditions (eq. b, Fig. 1). In addition, mechanistic and photochemical proofs, DFT calculations, and laser flash photolysis studies enabled us to postulate a plausible mechanistic pathway.

Results

Optimization of the model reaction. Based on the previous photocatalytic arylation reactions[32–40], we started the screening of the reaction using the acetate allylic derivative **1a** and pyrrole **2a** (18 equiv.) in the presence of different photocatalysts **3** under light irradiation (Table 1). Transition-metal-based photocatalysts (**3a–3b**) failed to promote the formation of the allylated heterocycle (entries 1 and 2). Several photoorganocatalysts with different reductive power (**3c–3f**) were tested, but only the 10-phenyl-10*H*-phenothiazine (PTH) (**3e**) gave the *Z*-allylated pyrrole **4a** with low conversion under 420-nm LED irradiation (entries 3–6). Encouraged by these results, we used an irradiation source with a wavelength closer to the maximum absorption of PTH (entry 7). Pleasantly, using a 365-nm LED, **4a** was obtained with a 65% conversion. In the absence of a photocatalyst, light, and both, the allylation did not proceed (entries 8–10), confirming the photocatalytic nature of this transformation. Different solvents were then evaluated, and the best result was obtained using CH_3CN (entries 7 and 11–14). In order to decrease the amount of heterocycle, the reaction was carried out using 10 and 2 equivalents of **2a** (entries 15 and 16) and **4a** was obtained with a good yield of 58% in only 3 h, using just two equivalents of the heterocycle. The use of inorganic bases (Na_2CO_3, LiOAc) afforded the final product, although with moderate yield, due to the lower solubility of such bases in acetonitrile (entries 17 and 18).

Substrate scope. Having established the best conditions (Table 1, entry 16), we performed the scope of the reaction (Table 2). With *N*-methyl pyrrole, the allylic derivative **4b** was obtained with a better yield than **4a** and with a similar selectivity for the *Z*-isomer. Other substituents were tolerated at the *N*-atom of the pyrrole (**4c** and **4d**) with excellent *Z*/*E* selectivity (up to 96:4) and with a slight decrease for the phenyl derivative **4c**. Indoles without protecting groups at the nitrogen were also employed, keeping the high selectivity for the *Z*-isomers, and with better yields than with the pyrroles (compare **4e** and **4f** with **4a** and **4b**). Electron-donating groups (EDGs) were well tolerated at different positions of the indole ring (**4g**, **4h,** and **4i**) as well as electron-withdrawing groups (EWG) at the aromatic ring (**4j**). A methyl substituent next to the indolinic nitrogen (**4k**) or the reactive C-3 center (**4l**)

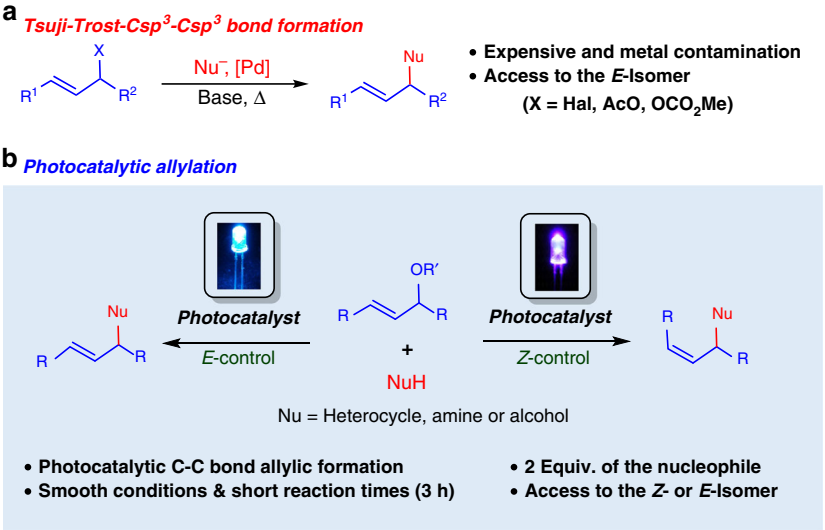

Fig. 1 The photocatalytic allylation reaction. **a** Precedents in the Tsuji–Trost allylation and **b** this work

Table 1 Optimization of the photocatalytic allylation reaction[a]

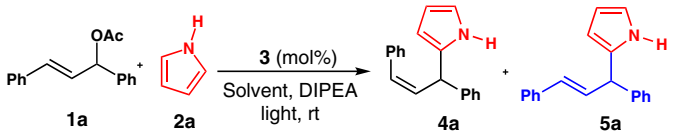

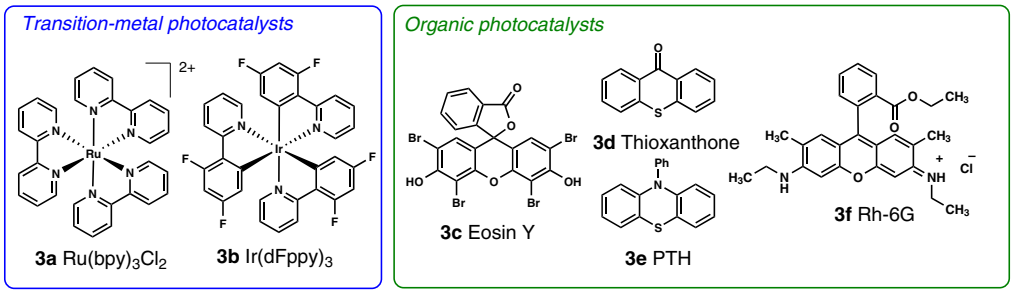

Entry	3 (mol%)	Light (nm)	Solvent	Pyrrole (equiv.)	t (h)	4a:5a[b]
1	**3a** (5)	420	MeCN	18	1	n.r.
2	**3b** (5)	420	MeCN	18	1	n.r.
3	**3c** (5)	530	MeCN	18	1	n.r.
4	**3d** (5)	420	MeCN	18	1	n.r.
5	**3e** (5)	420	MeCN	18	1	100:0 (5%)[c]
6	**3f** (10)	455	MeCN	18	41	n.r.
7	**3e** (5)	365	MeCN	18	1	100:0 (65%)[c]
8	**3e** (5)	-	MeCN	18	1	n.r.
9	-	365	MeCN	18	1	n.r.
10	-	-	MeCN	18	1	n.r.
11	**3e** (5)	365	DMSO	18	1	100:0 (61%)[c]
12	**3e** (5)	365	DMF	18	1	100:0 (49%)[c]
13	**3e** (5)	365	Toluene	18	1	100:0 (21%)[c]
14	**3e** (5)	365	DCM	18	1	100:0 (10%)[c]
15	**3e** (5)	365	MeCN	10	3	94:6 (86%)[c]
16	**3e (5)**	**365**	**MeCN**	**2**	**3**	**94:6 (91%)[c,d]**
17[e]	**3e** (5)	365	MeCN	2	3	80:20 (33%)[c]
18[f]	**3e** (5)	365	MeCN	2	3	78:22 (28%)[c]

[a]Conditions: **1a** (0.1 mmol), **2a** (see table), DIPEA (0.5 mmol), and catalyst (mol%) in the solvent indicated (1.0 mL)
[b]Measured by ^{1}H-NMR
[c]Conversion in the crude mixture
[d]Optimized conditions highlighted in bold
[e]Reaction carried out under standard conditions but using Na_2CO_3 (0.5 mmol) instead of DIPEA
[f]Reaction carried out under standard conditions but using LiOAc (0.5 mmol) instead of DIPEA

did not have a negative influence on the reactivity, obtaining both in very good yields and high selectivity. Remarkably, the presence of Br at the 5-position (**4m**) was also well tolerated under the presence of the high-reducing photocatalyst **3e**. The scope of the allylic derivative was also evaluated. Electron-rich (**4n**, **4o,** and **4p**) as well as electron-poor aromatic rings (**4q**) worked with excellent selectivities (up to > 98:2). We then studied the influence of the leaving group at the allylic position (R group in **1a**). The reaction worked with other leaving groups such as benzoate, carbamate, or carbonate, which were suitable for this process. However, the reaction with the hydroxyl group did not proceed, because of its higher reduction potential (−2.52 V vs. SCE) compared with the other activated allylic alcohols (E = −2.06 to −2.35 V vs. SCE, see Suplementary Note 4 for cyclic voltammetry).

After obtaining these good results with the *Z*-isomer, our next objective was the development of a photocatalytic variant to obtain the corresponding *E*-isomers. To achieve this goal, we analyzed the conditions that avoided the isomerization of the reagent **1a**. A sample containing *E*-**1a** in MeCN was irradiated for 3 h under different reaction conditions (Fig. 2). Without the use of the photocatalyst under 365-nm irradiation, we found a mixture of 60/40 *E*/*Z*-**1a**, while in the presence of **3e**, this isomerization to *Z*-**1a** was complete (Fig. 2). According to theoretical calculations, photosensitization and subsequent isomerization of *E*-**1a** by the photocatalyst is feasible, while photosensitization and subsequent isomerization of *Z*-**1a** cannot take place (see Supplementary Information Fig. 25). The absorption spectra of *E*-**1a** at the reaction conditions revealed a significant absorption at 365 nm (see Supplementary Information Fig. 8), while at 420 nm, it was negligible, suggesting that the reaction must be carried out in the visible-light region to avoid isomerization. Under 420-nm irradiation, only 5% of the *E*-**1a** was isomerized to the *Z*-isomer after 3 h. Therefore, a photocatalyst with high reduction potential (≥2.35 V vs. SCE) and absorption in the visible-light region is required. The phenoxazine **3g**, that meets all these criteria[41], resulted in only a small amount of *Z*-**1a** at 420-nm irradiation after 3 h (Fig. 2). Therefore, under these conditions (using photocatalyst **3g** and 420-nm irradiation), it should be possible to avoid the isomerization step and selectively form *E*-allylated products **5**.

Table 2 Scope of the allylation reaction for the synthesis of *Z*-isomers with pyrroles and indoles under catalyst 3e[a,b]

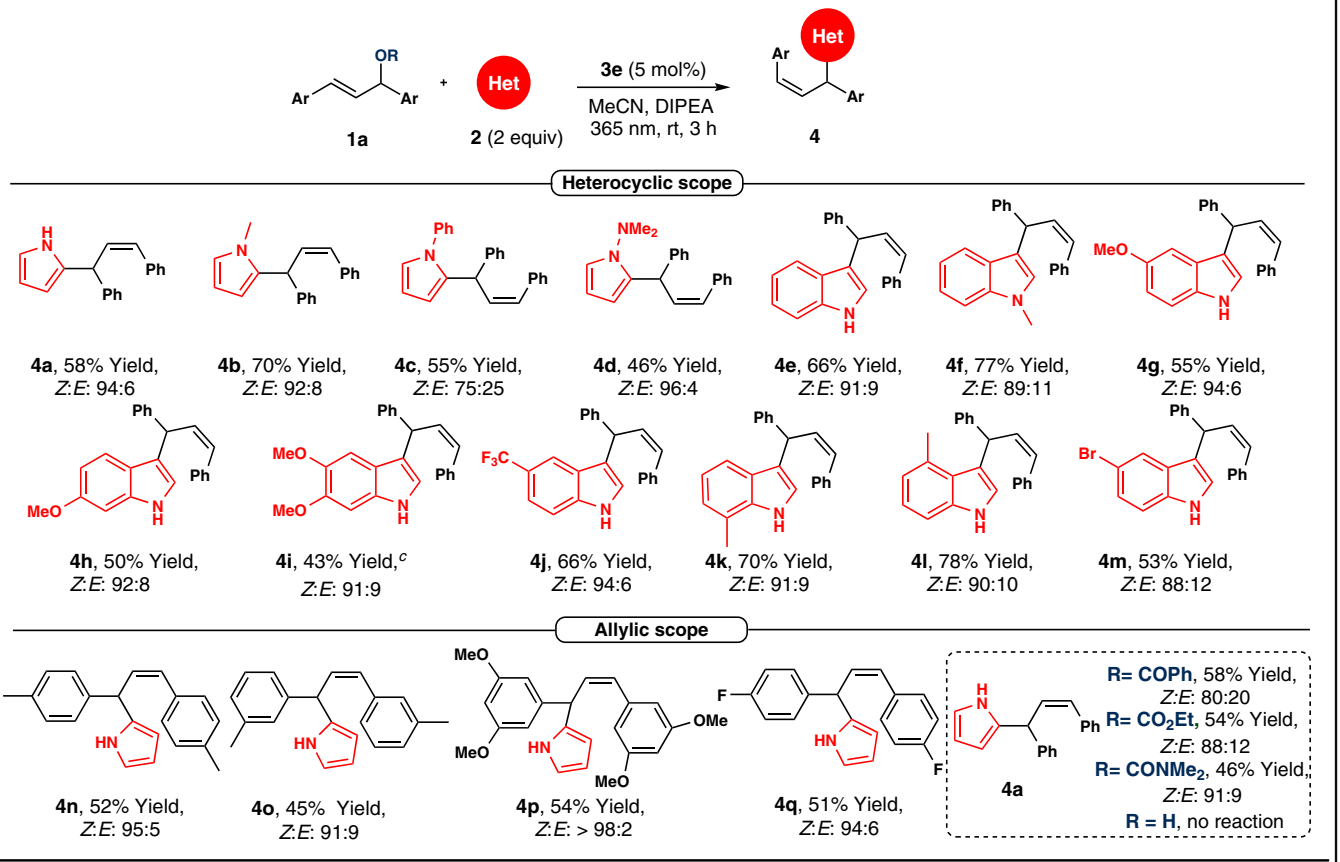

[a]Conditions: **1** (0.1 mmol), **2** (0.2 mmol), DIPEA (0.5 mmol), and **3e** (5 mol%) in MeCN (1.0 mL)
[b]Isolated yields after flash chromatography
[c]Combined isolated yield along with the C2-allylated compound

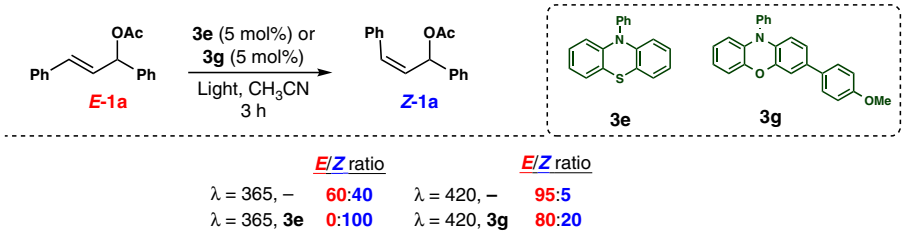

Fig. 2 Isomerization studies. Isomerization proofs of *E*-**1a** under different catalysts (**3e** and **3g**) and different irradiation wavelengths

To our delight, when carrying out the reaction between the allylic derivative **1a** and pyrrole (**2a**) in the presence of the photocatalyst **3g** under 420-nm irradiation, the allylated product *E*-**5a** was obtained with a good yield as the major isomer (Table 3). Other *N*-substituted pyrroles were also employed and maintained the same selectivity (**5b–5c**). Only compound **5d** was obtained as a complex mixture. The reaction with indoles afforded even better yield and selectivity than pyrroles (**5e** and **5f**). Unprotected indolinic nitrogen as well as different substituents were tolerated, from EDGs (**5g–i**) to EWGs (**5j**), methyl (**5k–l**), or bromo derivatives (**5m**), obtaining in all cases good yields (67–92%) and excellent selectivities (up to > 98:2). The isomerization of the final product **5e** under 420-nm irradiation was also studied, obtaining a *Z*/*E* mixture 30/70 after 3 h of irradiation, without the photocatalyst, while in the presence of the photocatalyst **3g,** a *Z*/*E* mixture 20/80 was obtained. The final product is present in the reaction in higher concentrations only after 2 h of reaction. Therefore, the irradiation time is not enough to produce its isomerization, which explains the obtention of the *E*-isomer as the major one.

Mechanistic studies. The proposed reaction mechanism is outlined in Fig. 3a. After light absorption by the photocatalyst under LED irradiation ($\lambda = 365$ or 420 nm), single-electron transfer (SET) takes place from its S_1 excited state ($E_{S1} = 3.2$ eV, see Supplementary Information Figs. 11 and 12) to **1a**. Steady-state and time-resolved fluorescence quenching studies in the

Table 3 Scope of the allylation reaction for the synthesis of *E*-isomers with pyrroles and indoles under catalyst 3g[a,b]

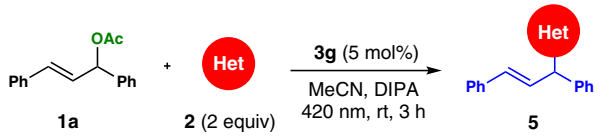

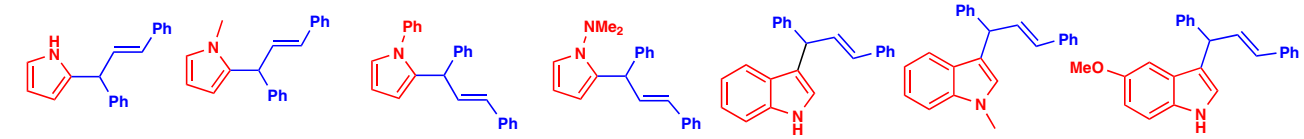

5a, 71% Yield, *Z*:*E*: 5:95

5b, 40% Yield, *Z*:*E*: 10:90 (6h)

5c, 59% Yield, *Z*:*E*: 8:92

5d, complex mixture

5e, 78% Yield, *Z*:*E*: 4:96

5f, 94% Yield, *Z*:*E*: 7:93

5g, 73% Yield, *Z*:*E*: 6:94

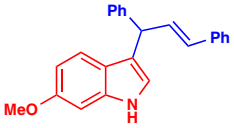

5h, 73% Yield,[c] *Z*:*E*: 6:94

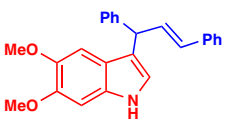

5i, 83% Yield,[c] *Z*:*E*: 6:94

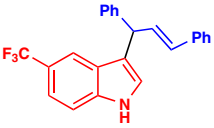

5j, 67% Yield, *Z*:*E*: 13:87

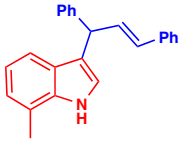

5k, 92% Yield, *Z*:*E*: 4:96

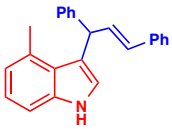

5l, 69% Yield, *Z*:*E*: <2:98

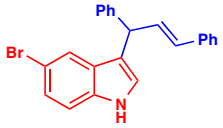

5m, 76% Yield, *Z*:*E*: 17:83

[a] Conditions: **1a** (0.1 mmol), **2** (0.2 mmol), DIPA (0.5 mmol), and **3g** (5 mol%) in MeCN (1.0 mL)
[b]Isolated yields after flash chromatography
[c]Combined isolated yield along with the C2-allylated compound

presence of **1a** afforded a quenching rate constant of $k_q(S_1) = 4.7 \times 10^9\ M^{-1}\ s^{-1}$ (see Supplementary Information Fig. 9a), indicating that the radical ion pair ($\mathbf{PC}^{\bullet+} + \mathbf{1a}^{\bullet-}$) formation occurs at nearly diffusion rate. In addition, SET from the excited singlet state would be an exergonic process, taking into account the free energy change ($\Delta G_{ET} = -4.0$ kcal mol^{-1}) associated with the electron transfer (see Supplementary Note 4 for Rehm–Weller equation).

Importantly, photooxidation of DIPEA ($E_{ox} = 0.94$ V vs. SCE)[42], DIPA ($E_{ox} = 1.17$ V vs. SCE)[43], or pyrrole ($E_{ox} = 1.04$ V vs. SCE)[44] by **PC** S_1 excited state could not occur, taking into account the oxidation power of **3e** and **3g** ($E_{(Pc^*/Pc^{\bullet-})} = -0.3$ V vs. SCE for **3e** and **3g**, see Supplementary Note 4), and was further confirmed by fluorescent-quenching studies (see Fig. 3b). The fate of such reduced species has been investigated by DFT calculations, considering both *Z*- and *E*-isomers (Fig. 3d). Initial single-electron transfer process from the photocatalyst (**PC**) to **1a** generates the radical cation $\mathbf{PC}^{\bullet+}$ and the radical anion $\mathbf{1a}^{\bullet-}$, that evolves through the C–O bond scission to afford acetate anion and the radical intermediate **I** (**INT I**). This step is a very exergonic process (−22 or −21.3 kcal mol^{-1}) and proceeds through a very shallow kinetic barrier ($E_a = 1.4$ or 3.2 kcal mol^{-1}). Then, the oxidation of **INT I** by the oxidized photocatalyst ($\mathbf{PC}^{\bullet+}$), results in the regeneration of the photocatalyst (**PC**) and formation of a carbocationic intermediate **II** (**INT II**) (Fig. 3d). Such electron transfer is calculated as a thermodynamically favorable process (−8.7 or −11.8 kcal mol^{-1}). The calculated energetic barriers for *E* to *Z* isomerizations for radical or carbocation intermediates **I** and **II** rule out this process from such transient species (see Supplementary Information Fig. 28). Formation of this carbocation **INT II** was experimentally confirmed, carrying out the reaction in the presence of H_2O^{18} as the nucleophile obtaining the isotopically labeled compound **7** (Fig. 3c). In addition, when two nonsymmetric allylic derivatives bearing different aryl groups were studied, an equimolecular mixture of products was obtained (see Supplementary Fig. 30, compounds **6** and **6′**), indicating that the reaction takes places through a common intermediate. Then, a Friedel–Crafts reaction between the carbocation **INT II** and pyrrole takes place, generating the protonated intermediate **III** (**INT III**). This step is also theoretically found exergonic (−14 or −26.3 kcal mol^{-1}) and kinetically favorable ($E_a = 3.8$ kcal mol^{-1}). A final rearomatization by deprotonation of **INT III** gives the final product (Fig. 3d). For such deprotonation, both DIPEA and the anion acetate (formed during the reaction) would act as a base through very exergonic processes (see entries 16 and 17 from Table 1 for reactions in the presence of Na_2CO_3 and LiOAc).

In order to gain a better understanding of the reaction mechanism, laser flash photolysis (LFP) measurements have been carried out. Excitation of **3g** at 355 nm results in two peaks at 468 and 530 nm at 40 ns after the laser pulse, which are assigned to the **3g** radical cation ($\mathbf{3g}^{\bullet+}$) and the excited triplet state of **3g** ($^3\mathbf{3g}^*$), respectively (Fig. 4a, black line, for further details, see also Supplementary Note 2). This experiment was performed in the presence of **1a** to identify the possible transient reaction intermediates (Fig. 4a, red line). Two new absorption bands at 360 and 490 nm are clearly observed, which correspond to intermediates **I** and **II**, respectively, based on literature data[45]. The lifetime of the carbocation **INT II** also depends on the nucleophilicity of the anionic leaving group (see Supplementary Information Fig. 4). In order to check whether formation of **INT II** and **INT I** is instantaneous with the laser pulse, additional LFP experiments of **3g** in the presence of increasing amounts of **1a** were performed (Fig. 4c and d). Generation of **INT II** is practically instantaneous even at lower concentration of **1a** (Fig. 4d), whereas lifetimes of **INT I** are not affected by higher amounts of **1a** (Fig. 4c). This result suggests that SET from $\mathbf{3g}^*$ to **1a** at

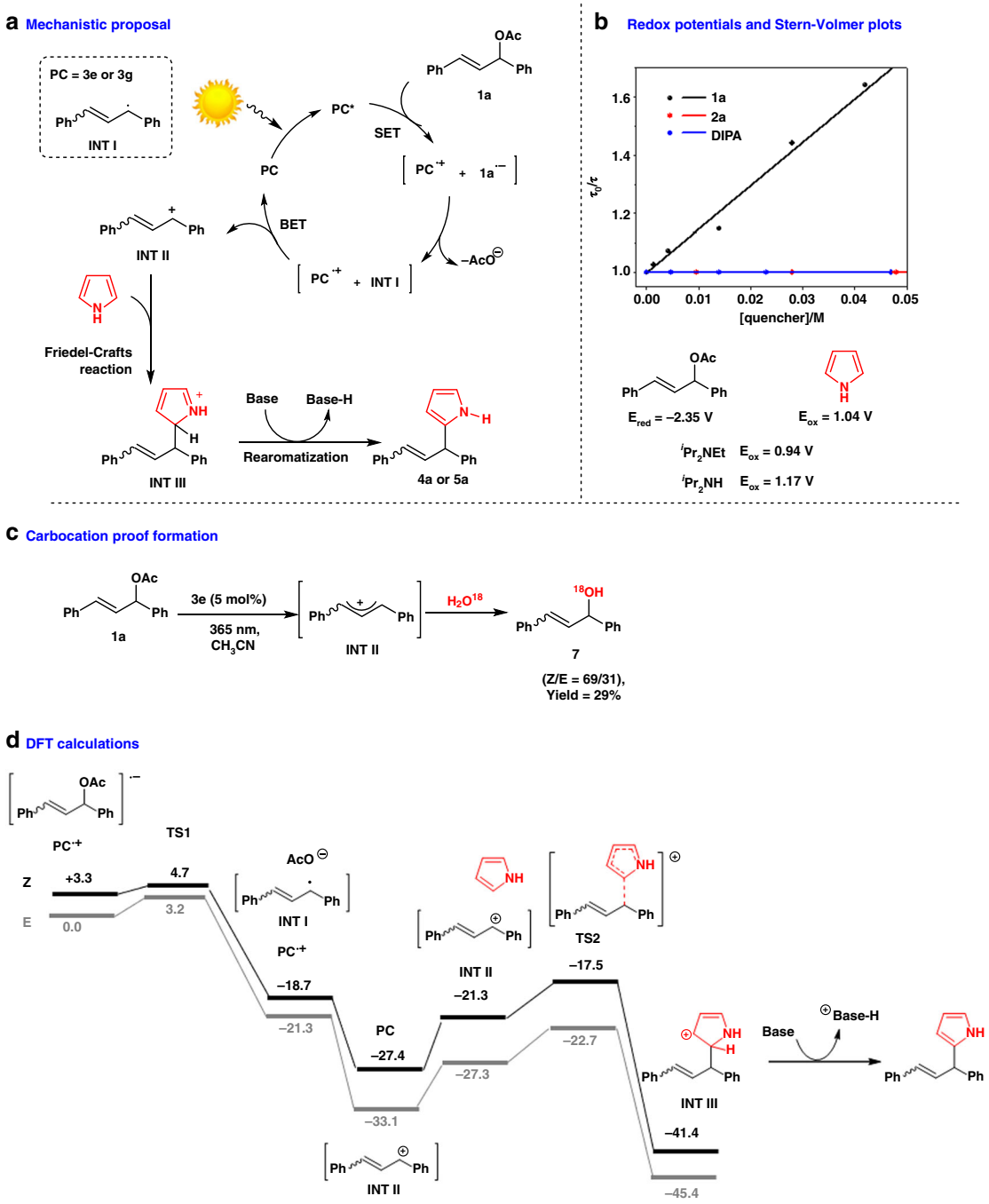

Fig. 3 Mechanistic studies. **a** Mechanistic proposal for the photoallylation. **b** Redox potentials and Stern–Volmer plots of the time-resolved fluorescence quenching of **3g** with **1a**, pyrrole, and DIPA (DIPA = diisopropylamine). **c** Reaction of **1a** with H_2O^{18} under standard reaction conditions. **d** For DFT calculations, geometry optimizations were performed using the M06-2X functional in combination with the 6-311G** basis set

diffusion control rate (see Supplementary Information Fig. 9) gives rise to the contact radical ion pair at this singlet stage (Fig. 3a). All processes in the contact radical ion pairs undergo in the sub-nanosecond scale[46]. Fast acetate release from $\mathbf{1a}^{\bullet-}$ led to **INT I**, which is still in close contact with $\mathbf{3g}^{\bullet+}$. At this point, **INT I** undergoes an ultrafast back electron transfer with $\mathbf{3g}^{\bullet+}$ restoring **3g** and generating **INT II,** whose amount is slightly dependent on the concentration of **1a** in the sample (Fig. 4d). In addition, $\mathbf{3g}^{\bullet+}$ and **INT I** can split up, forming the corresponding free $\mathbf{3g}^{\bullet+}$ and free **INT I**, that are detected in the LFP experiments with lifetimes in the microsecond scale (Fig. 4a, red line). Once the detection of both intermediates **I** and **II** by LFP has been established, the question arises whether **INT I** or **INT II** (radical or carbocation) would react with a trapping agent (Fig. 4e and transient absorption spectrum in Fig. 4b). Addition of pyrrole to a **3g**/**1a** mixture results only in a marked decrease of the **INT II** lifetime (Fig. 4g), while the band corresponding to **INT I** (360 nm) is not affected (Fig. 4f). Therefore, this experiment clearly corroborated with the previous data (Fig. 3) that the carbocation **INT II** is the reactive intermediate in our reaction. A quantum yield of 1.5% was found, suggesting a

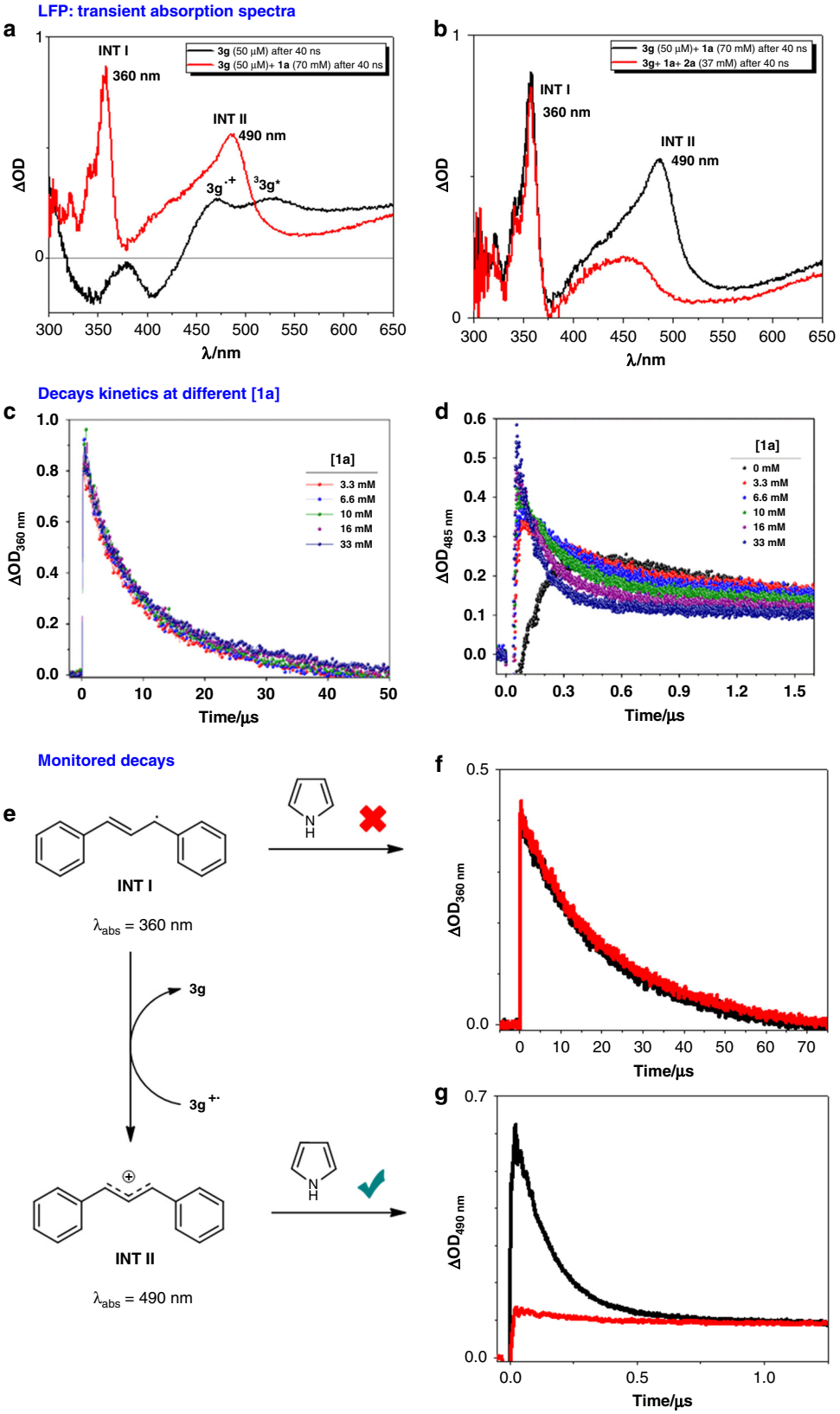

Fig. 4 Laser flash photolysis ($\lambda_{exc} = 355$ nm, MeCN/Ar) experiments. **a** Transient absorption spectra recorded at 40 ns after the laser pulse of **3g** (50 mM) without **1a** (black), with 70 mM of **1a** (red). **b** Transient absorption spectra recorded at 40 ns after the laser pulse of **3g** (50 mM) with 70 mM of **1a** (black) and with 35 mM of **2a** (red). **c** Decay kinetics at 360 nm after 355-nm LFP of **3g** (50 μM) in the presence of increasing amounts of **1a**. **d** Decay kinetics at 485 nm after 355-nm LFP of **3g** (50 μM) in the presence of increasing amounts of **1a**. **e** Scheme of the formation of intermediate **II** from intermediate **I** and their reaction with **2a**. **f** Lifetime of **INT I**: decays monitored at 360 nm of **3g** (50 mM) and **1a** (70 mM) (black line) and in the presence of **2a** (37 mM) (red line). **g** Lifetime of **INT II**: decays monitored at 490 nm of **3g** (50 mM) and **1a** (70 mM) (black line) and in the presence of **2a** (37 mM) (red line)

Table 4 Scope of the allylation reaction with amines and alcohols for the synthesis of *Z*-isomers under photocatalyst 3e[a,b]

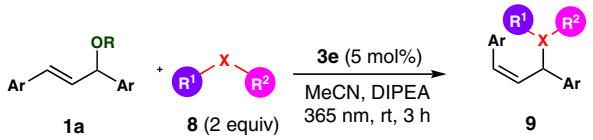

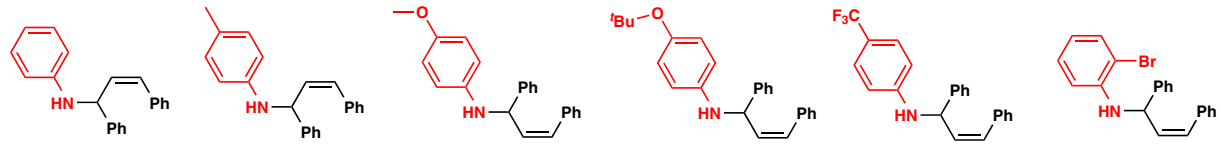

9a, 61% Yield, *Z*:*E*: 87:13 | **9b**, 48% Yield, *Z*:*E*: 76:24 | **9c**, 77% Yield, *Z*:*E*: 36:64 | **9d**, 53% Yield, *Z*:*E*: 65:35 | **9e**, 76% Yield, *Z*:*E*: 88:12 | **9f**, 67% Yield, *Z*:*E*: 84:16

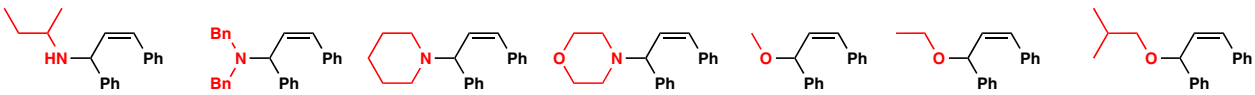

9g, 61% Yield, *Z*:*E*: 93:7 | **9h**, 77% Yield, *Z*:*E*: 85:15 | **9i**, 68% Yield, *Z*:*E*: 91:9 | **9j**, 76% Yield, *Z*:*E*: 94:6 | **9k**, 76% Yield, *Z*:*E*: 88:12 | **9l**, 69% Yield, *Z*:*E*: 86:14 | **9m**, 66% Yield, *Z*:*E*: 86:14

[a] Conditions: **1a** (0.1 mmol), **2** (0.2 mmol), DIPEA (0.5 mmol), and **3g** (5 mol%) in MeCN (1.0 mL)
[b]Isolated yields after flash chromatography

photocatalytic process without a significant radical chain propagation[47].

Scope with alcohols and amines. Once that we proved that the reaction takes place through a carbocation intermediate formation, we decided to study other nucleophiles to prove the generality of our protocol. Allylic amines are very useful compounds that can be employed as building blocks for the synthesis of amino acids, alkaloids, and carbohydrate derivatives[48–50]. Moreover, this structure is present in numerous natural products and drugs with antifungal, antibacterial, and anti-inflammatory action[51–53]. Different amines were tried under UV irradiation in order to obtain the *Z*-allylated amines which are not accessible by other methodologies (Table 4). Aniline gave the corresponding *Z*-allylated amine **9a** with high selectivity. Aromatic amines with EDGs were well tolerated (**9b–d**) with moderate selectivity, whereas anilines with EWGs gave significant better yield (**9e**) and *Z*/*E* ratio. In addition, the presence of Br at the aromatic ring was tolerated without detecting the corresponding reduced product (**9f**). Aliphatic primary and secondary amines were also suitable for the reaction conditions (**9g–h**). Cyclic allylated amine **9i** was obtained in good selectivity (*Z*:*E* = 91:9) and good yield. Moreover, the use of morpholine as a nucleophile can be employed for the synthesis of **9j** with excellent selectivity. The preparation of allylic ethers has a great interest, as they are also present in numerous pharmaceuticals and natural products[54–57]. For this reason, alcohols were employed as nucleophiles, obtaining *Z*-allylated ethers with good yields and good selectivities (**9k–m**)[58].

Using the visible-light irradiation conditions and photocatalyst **3g** with amines and alcohols is possible to obtain the corresponding *E*-isomers (Table 5). Aromatic amines gave the corresponding allylated compounds with high selectivities and good yields with EDGs (**10b–d**) and EWGs (**10e**), or *ortho*-bromo substituents (**10f**). Aliphatic primary (**10g**) and secondary amines (**10h–j**) were employed, keeping in all the cases high *Z*/*E* selectivity. Moreover, allylated ethers can also be obtained under visible-light irradiation with excellent selectivities (**10k–m**). A similar mechanistic scenario was found for amines and alcohols, using *p*-toluidine **8b** as a nucleophile in the LFP and photochemical mechanistic probes (see Supplementary Fig. 9).

Discussion

In summary, a chromoselective photocatalytic approach for the allylation of indoles, pyrroles, amines, and alcohols has been developed. This approach represents a photocatalytic allylation reaction for the synthesis of demand of *Z*- or *E*-isomers, with only two equivalents of the desired nucleophile. Therefore, under UV-light irradiation *Z*-allylated products are obtained, while the *E*-isomer is simply prepared by changing both the light source to the visible region, and the catalytic system. DFT calculations, photochemical proofs, and mechanistic experiments indicate that the most plausible mechanism involves a nucleophilic attack to an allyl-cation intermediate.

Methods

Procedure for the preparation of *Z*-allylic compounds. A vial equipped with a magnetic stir bar and fitted with a Teflon screw cap septum was charged with the corresponding allylic compound **1** (0.1 mmol), the corresponding heterocycle, amine, or alcohol (0.2 mmol), *N*-phenyl phenothiazine (1.4 mg, 5 mol%), DIPEA (86 µL, 0.5 mmol), and acetonitrile (1 mL). The reaction was degassed with three freeze–pump–thaw cycles. The vial was then backfilled with N_2 and stirred under 365-nm LED irradiation (8.2460 W m^{-2} intensity; approximate distance was 2 cm from the vial) at 20 °C. After 3 h, the vial was opened, the solvent evaporated, and the crude product was purified by column chromatography to give the corresponding products **4** or **9**.

Table 5 Scope of the allylation reaction with amines and alcohols for the synthesis of *E*-isomers under photocatalyst 3g[a,b]

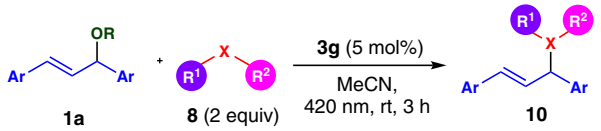

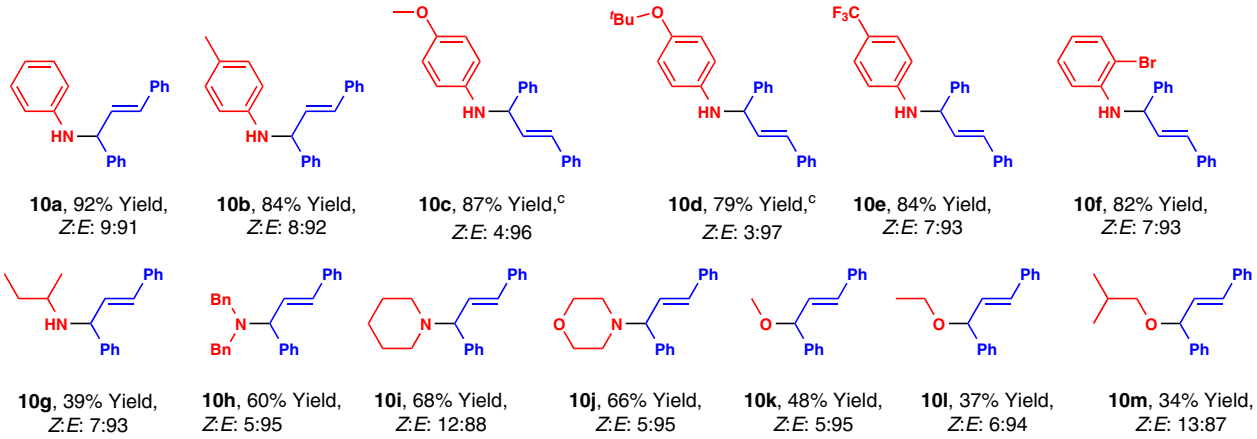

[a] Conditions: **1a** (0.1 mmol), **8** (0.2 mmol), and **3g** (5 mol%) in MeCN (1.0 mL)
[b]Isolated yields after flash chromatography
[c]Reaction performed by adding DIPEA (0.5 mmol)

Procedure for the preparation of *E*-allylic compounds. A vial equipped with a magnetic stir bar and fitted with a Teflon screw cap septum was charged with the corresponding allylic compound **1** (0.1 mmol), the corresponding heterocycle, amine, or alcohol (0.2 mmol), 3-(4-methoxyphenyl)-10-phenyl-10H-phenoxazine (1.7 mg, 5 mol%), DIPA (70 µL, 0.5 mmol, only base is needed for reactions with heterocycles as nucleophile), and acetonitrile (1 mL). The reaction was degassed with three freeze–pump–thaw cycles. The vial was then backfilled with N_2 and stirred under 420-nm LED irradiation (18.3396 W m^{-2} intensity; approximate distance was 2 cm from the vial) at room temperature. After 3 h, the vial was opened, the solvent evaporated, and the crude product was purified by column chromatography to give the corresponding products **5** or **10**.

Data availability

The authors declare that all data supporting the findings of this study are available within the article and Supplementary Information files, and also are available from the corresponding author upon reasonable request.

Received: 30 November 2018 Accepted: 13 May 2019
Published online: 14 June 2019

References

1. Trost, B. M. & Strege, P. E. Asymmetric induction in catalytic allylic alkylation. *J. Am. Chem. Soc.* **99**, 1649–1651 (1977).
2. Trost, B. M. New rules of selectivity: allylic alkylations catalyzed by palladium. *Acc. Chem. Res.* **13**, 385–393 (1980).
3. Tsuji, J., Minami, I. & Shimizu, I. Palladium-catalyzed allylation of ketones and aldehydes with allylic carbonates via silyl enol ethers under neutral conditions. *Chem. Lett.* **12**, 1325–1326 (1983).
4. Trost, B. M. & Van Vranken, D. L. Asymmetric transition metal-catalyzed allylic alkylations. *Chem. Rev.* **96**, 395–422 (1996).
5. De Meijere, A., Diederich, F. (eds) *Metal-Catalyzed Cross-coupling Reactions*, 2nd edn (Wiley, Weinheim, 2008).
6. D'Ischia, A., Napolitano, A. & Pezella, A. Pyrroles and their Benzo Derivatives: Application. in *Comprehensive Heterocyclic Chemistry III* (eds Katritzky, A. R., Ramsden, C. A., Scriven, E. F. V. & Taylor, R. J. K.) 353–386 (Elsevier Science, Amsterdam, 2008).
7. Malkov, A. V., Davis, S. L., Baxendale, I. R., Mitchell, W. L. & Kočovsky, P. Molybdenum(II)-catalyzed allylation of electron-rich aromatics and heteroaromatics. *J. Org. Chem.* **64**, 2751–2764 (1999).
8. Bandini, M., Melloni, A. & Umani-Ronchi, A. New versatile Pd-catalyzed alkylation of indoles via nucleophilic allylic substitution: controlling the regioselectivity. *Org. Lett.* **6**, 3199–3202 (2004).
9. Kimura, M., Futamata, M., Mukai, R. & Tamaru, Y. Pd.catalyzed C3-selective allylation of indoles with allyl alcohols promoted by triethylborane. *J. Am. Chem. Soc.* **127**, 4592–4593 (2005).
10. Stanley, L. M. & Hartwig, J. F. Iridium-catalyzed regio- and enantioselective *N*-allylation of indoles. *Angew. Chem. Int. Ed.* **48**, 7841–7844 (2009).
11. Xu, K., Gilles, T. & Breit, B. Asymmetric synthesis of *N*-allylic indoles via regio- and enantioselective allylation of aryl hydrazines. *Nat. Commun.* **6**, 7616 (2015).
12. Lee, J. Y., Ha, H., Bae, S., Han, I. & Joo, J. M. Catalytic C-2 allylation of indoles by electronic modulation of the indole ring and its application to the synthesis of functionalized carbazoles. *Adv. Synth. Catal.* **358**, 3458–3470 (2016).
13. Narayanam, J. M. R. & Stephenson, C. R. J. Visible light photoredox catalysis: applications in organic synthesis. *Chem. Soc. Rev.* **40**, 102–113 (2011).
14. Prier, C. K., Rankic, D. A. & MacMillan, D. W. C. Visible light photoredox catalysis with transition metal complexes: applications in organic synthesis. *Chem. Rev.* **113**, 5322–5363 (2013).
15. Meggers, E. Asymmetric catalysis activated by visible light. *Chem. Commun.* **51**, 3290–3301 (2015).
16. Ravelli, D., Protti, S. & Fagnoni, M. Carbon-carbon bond forming reactions via photogenerated intermediates. *Chem. Rev.* **116**, 9850–9913 (2016).
17. Skubi, K. L., Blum, T. R. & Yoon, T. P. Dual catalysis strategies in photochemical synthesis. *Chem. Rev.* **116**, 10035–10074 (2016).
18. Pitre, S. P., McTiernan, C. D. & Scaiano, J. C. Understanding the kinetics and spectroscopy of photoredox catalysis and transition-metal-free alternatives. *Acc. Chem. Res.* **49**, 1320–1330 (2016).
19. Tellis, J. C. et al. Single-electron transmetalation via photoredox/nickel dual catalysis: unlocking a new paradigm for sp^3-sp^2 cross-coupling. *Acc. Chem. Res.* **49**, 1429–1439 (2016).
20. Gentry, E. C. & Knowles, R. R. Synthetic applications of proton-coupled electron transfer. *Acc. Chem. Res.* **49**, 1546–1556 (2016).
21. Hernandez-Perez, A. C. & Collins, S. Heteroleptic Cu-based sensitizers in photoredox catalysis. *Acc. Chem. Res.* **49**, 1557–1565 (2016).
22. Goddard, J.-P., Ollivier, C. & Fensterbank, L. Photoredox catalysis for the generation of carbon centered radicals. *Acc. Chem. Res.* **49**, 1924–1936 (2016).

23. Morris, S. A., Wang, J. & Zheng, N. The prowess of photogenerated amine radical cations in cascade reactions: from carbocycles to heterocycles. *Acc. Chem. Res.* **49**, 1957–1968 (2016).
24. Fabry, D. C. & Rueping, M. Merging visible light photoredox catalysis with metal catalyzed C-H activations: on the role of oxygen and superoxide ions as oxidants. *Acc. Chem. Res.* **49**, 1969–1979 (2016).
25. Majek, M. & von Wangelin, A. J. Mechanistic perspectives on organic photoredox catalysis for aromatic substitutions. *Acc. Chem. Res.* **49**, 2316–2327 (2016).
26. Shaw, M. H., Twilton, J. & MacMillan, D. W. C. Photoredox catalysis in organic chemistry. *J. Org. Chem.* **81**, 6898–6926 (2016).
27. Zhou, W.-J., Zhang, Y.-H., Gui, Y.-Y., Sun, L. & Yu, D.-G. Merging transition-metal catalysis with photoredox catalysis: an environmentally friendly strategy for C-H functionalization. *Synthesis* **50**, 3359–3378 (2018).
28. Garrido-Castro, A. F., Carmen Maestro, M. & Alemán, J. Asymmetric induction in photocatalysis—discovering a new side to light-driven chemistry. *Tetrahedron Lett.* **59**, 1286–1294 (2018).
29. Marzo, L., Pagire, S. K., Reiser, O. & König, B. Visible-light photocatalysis: does it make a difference in organic synthesis. *Angew. Chem. Int. Ed.* **57**, 10034–10072 (2018).
30. Wang, C.-S., Dixneuf, P. H. & Soule, J.-F. Photoredox catalysis for building C-C bonds from C(sp^2)-H bonds. *Chem. Rev.* **118**, 7532–7585 (2018).
31. Hari, D. P. & König, B. The photocatalyzed Meerwein arylation: classic reaction of aryl diazonium salts in a new light. *Angew. Chem. Int. Ed.* **52**, 4734–4743 (2013).
32. Ghosh, I., Marzo, L., Das, A., Shaikh, R. & König, B. Visible-light mediated photoredox catalytic arylation reactions. *Acc. Chem. Res.* **49**, 1566–1577 (2016).
33. Hari, D. P., Schroll, P. & König, B. Metal-free, visible-light-mediated direct C-H arylation of heteroarenes with aryl diazonium salts. *J. Am. Chem. Soc.* **134**, 2958–2961 (2012).
34. Ghosh, I., Ghosh, T., Bardagi, J. I. & König, B. Reduction of aryl halides by consecutive visible light-induced electron transfer processes. *Science* **346**, 725–728 (2014).
35. Meyer, A. U., Slanina, T., Yao, C.-J. & König, B. Metal-free perfluoroarylation by visible light photoredox catalysis. *ACS Catal.* **6**, 369–375 (2016).
36. Ghosh, I. & König, B. Chromoselective photocatalysis: controlled bond activation through light-color regulation of redox potentials. *Angew. Chem. Int. Ed.* **55**, 7676–7679 (2016).
37. Marzo, L., Ghosh, I., Esteban, F. & König, B. Metal-free photocatalyzed cross coupling of bromoheteroarenes with pyrroles. *ACS Catal.* **6**, 6780–6784 (2016).
38. Kalyani, D., McMurtrey, K. B., Neufeldt, S. R. & Sanford, M. S. Room-temperature C-H arylation: merger of Pd-catalyzed C-H functionalization and visible-light photocatalysis. *J. Am. Chem. Soc.* **133**, 18566–18569 (2011).
39. Zoller, J., Fabry, D. C. & Rueping, M. Unexpected dual role of titanium dioxide in the visible light heterogeneous catalysed C-H arylation of heteroarenes. *ACS Catal.* **5**, 3900–3904 (2015).
40. Maity, P., Kundu, D. & Ranu, B. C. Multigram four-step synthesis of 1,4,7-triazacyclononanes with $2R_a/R_bN$-functionalization pattern by starting from diethylenetriamine. *Eur. J. Org. Chem.* **2015**, 1727–1734 (2015).
41. McCarthy, B. G. et al. Structure-property relationships for tailoring phenoxazines as reducing photoredox catalysts. *J. Am. Chem. Soc.* **140**, 5088–5101 (2018).
42. Roth, H. G., Romero, N. A. & Nicewicz, D. A. Experimental and calculated electrochemical potentials of common organic molecules for applications to single-electron redox chemistry. *Synlett* **27**, 714–723 (2016).
43. Adenier, A., Chehimi, M. M., Gallardo, I., Pinson, J. & Vila, N. Electrochemical oxidation of aliphatic amines and their attachment to carbon and metal surfaces. *Langmuir* **20**, 8243–8253 (2004).
44. Garrido-Castro, A. F., Choubane, H., Daaou, M., Maestro, M. C. & Alemán, J. Asymmetric radical alkylation of *N*-sulfinimines under visible light photocatalytic conditions. *Chem. Commun.* **53**, 7764–7767 (2017).
45. Miranda, M. A., Perez-Prieto, J., Font-Sanchis, E., Kónya, K. & Scaiano, J. C. Flash photolysis of 1,3-dichloro-1,3-diphenylpropane in polar solvents: generation of a stabilized γ-chloropropyl cation, subsequent formation of a propenyl cation, and nucleophilic trapping of both cations. *J. Phys. Chem. A* **102**, 5724–5727 (1998).
46. Mattay, J. & Vondenhof, M. Contact and solvent-separated radical ion pairs in organic. In *Photoinduced electron transfer III. Topics in Current Chemistry* (Ed. Mattay, J.) 219–255 (Springer, Heidelberg, 1991).
47. Kuhn, H. J., Braslavsky, S. E. & Schmidt, R. Chemical actinometry (IUPAC technical report). *Pure Appl. Chem.* **76**, 2105–2146 (2004).
48. Cheikh, R. B., Chaabouni, R., Laurent, A., Mison, P. & Nafti, A. Synthesis of primary allylic amines. *Synthesis* 685−700 (1983).
49. Johannsen, M. & Jørgensen, K. A. Allylic amination. *Chem. Rev.* **98**, 1689–1708 (1998).
50. Trost, B. M. & Crawley, M. L. Asymmetric transition-metal-catalyzed allylic alkylations: applications in total synthesis. *Chem. Rev.* **103**, 2921–2943 (2003).
51. Petranyi, G., Ryder, N. S. & Stutz, A. Allylamine derivatives: new class of synthetic antifungal agents inhibiting fungal squalene epoxidase. *Science* **224**, 1239–1241 (1984).
52. Stutz, A. Allylamine derivatives—a new class of active substances in antifungal chemotherapy. *Angew. Chem. Int. Ed.* **26**, 320–328 (1987).
53. Nanavati, S. M. & Silverman, R. B. Mechanisms of inactivation of *gamma*-aminobutyric acid aminotransferase by the antiepilepsy drug *gamma*-vinyl GABA (vigabatrin). *J. Am. Chem. Soc.* **113**, 9341–9349 (1991).
54. Mizuguchi, E. & Achiwa, K. Chiral palladium complex-catalyzed synthesis of optically active vinylchroman. *Chem. Pharm. Bull.* **45**, 1209–1211 (1997).
55. Nicolaou, K. C. et al. Natural product-like combinatorial libraries based on privileged structures. 1. General principles and solid-phase synthesis of benzopyrans. *J. Am. Chem. Soc.* **122**, 9939–9953 (2000).
56. Cao, B., Park, H. & Joullié, M. M. Total synthesis of Ustiloxin D. *J. Am. Chem. Soc.* **124**, 520–521 (2002).
57. Ishibashi, H., Ishihara, K. & Yamamoto, H. A new artificial cyclase for polyprenoids: enantioselective total synthesis of (−)-chromazonarol, (+)-8-*epi*-puupehedione, and (−)-11′-deoxytaondiol methyl ether. *J. Am. Chem. Soc.* **126**, 11122–11123 (2004).
58. Pochetti, G. et al. Structural insight into peroxisome proliferator-activated receptor γ binding of two ureidofibrate-like enantiomers by molecular dynamics, cofactor interaction analysis, and site-directed mutagenesis. *J. Med. Chem.* **53**, 4354–4366 (2010).

Acknowledgements

Financial support from the Spanish Government (CTQ2015-64561-R), CCC-UAM (computing time), and ERC (ERC-CG, 647550, 648319) is acknowledged. L.M., R.P-R, and R.C. thank CAM for the "Atracción de Talento" fellowship. The authors thank "Comunidad de Madrid" and European Structural Funds for their financial support to FotoArt-CM project (S2018/NMT-4367). We thank Miguel Ángel Miranda for helpful discussions about photochemical mechanisms.

Author contributions

A.M.M-G and A.F. carried out the optimization and scope of the reaction. R.C. and J.L-B. carried out the scope of the reaction. L.M. performed the photocatalytic studies for mechanism elucidation. R.P-R. and V.A.P. performed the Laser Flash Photolysis studies. R.M-B. carried out the DFT-computational studies. J.A. conceived the project and prepared the paper, which was edited by all other authors.

Additional information

Supplementary Information accompanies this paper at https://doi.org/10.1038/s41467-019-10441-4.

Competing interests: The authors declare no competing interests.

Reprints and permission information is available online at http://npg.nature.com/reprintsandpermissions/

Journal peer review information: *Nature Communications* thanks anonymous reviewer(s) for their contribution to the peer review of this work.

Publisher's note: Springer Nature remains neutral with regard to jurisdictional claims in published maps and institutional affiliations.

6. Experimental Section

The experimental section is directly taken from the documents “Supporting Information” of each publication.

Each Supporting Information appears in the same order as the publications

In each Supporting Information the section “Cartesian Coordinates of DFT optimized structures” is not shown in this doctoral thesis. NMR spectra and chiral chromatograms are only shown for representative compounds.

The complete documents “Supporting Information”, with all NMR spectra, chiral chromatograms and Cartesian coordinates are compiled on the CD enclosed.

CHEMPLUSCHEM

Supporting Information

One-Pot Asymmetric Synthesis of Cyclopropanes with Quaternary Centers Starting From Bromonitroalkenes under Aminocatalytic Conditions

Javier Luis-Barrera,[a] Ruben Mas-Ballesté,[b] and José Alemán*[a]

cplu_201500320_sm_miscellaneous_information.pdf

Table of Contents

1. General Experimental Details

Tetrahydrofuran, toluene, acetonitrile and dichloromethane were purified by passing through a Pure Solv™ column drying system from Innovative Technology, Inc. Additionally, dichloromethane and toluene were dried using activated 4Å molecular sieves and stored under argon. Dry-*tert*-butylmethylether was acquired from commercial sources. 4Å Molecular sieves, 1.6-2.5 mm of particle size, were activated by microwave (700W) (3 x 30 sec) and subsequent cycles of vacuum/argon.

NMR spectra were acquired on a Bruker 300 spectrometer, running at 300, and 75 MHz for ^{1}H and ^{13}C, respectively. Chemical shifts (δ) are reported in ppm relative to residual solvent signals ($CDCl_3$, 7.26 ppm for 1H NMR and 77.2 ppm for ^{13}C NMR respectively). ^{13}C NMR spectra were acquired on a broad band decoupled mode. The following abbreviations are used to describe peak patterns when appropriate: s (singlet), d (doublet), t (triplet), q (quartet), quint (quintet), sept (septuplet), m (multiplet), br (broad). Mass Spectrometry (MS) was registered in a spectrometer *GCT AgilentTechnologies 6890N* using Electronic Impact (E.I.) and electrospray (ESI+).

For thin layer chromatography (TLC) silica gel plates with fluorescence indicator 254 nm were used and compounds were visualized by irradiation with UV light and/or by treatment with a solution of phosphomolybdic acid in EtOH followed by heating. Flash column chromatography was performed using pore 60 Å, 40-63 μm silica gel and compressed air. Celite® 512 medium was used for some filtration.

Hexane and EtOAc were used without previous purification. Optical rotation was recorded in cells with 10 cm path length. The specific solvents and concentrations (in g/100 mL) are indicated.

SFC-HPLC analysis was performed with chiral columns (25 cm) using the given conditions.

All Aldehydes **2,** catalysts **3**, and co-bases were purchased from commercial suppliers without further purification. All Bromonitroalquenes **1** were synthesized following a standard procedure.[1]

[1]M. Ganesh, I. N. N. Namboothiri, *Tetrahedron* **2007**, *63*, 11973.

2. General procedure for the optically enriched cyclopropanes 5.

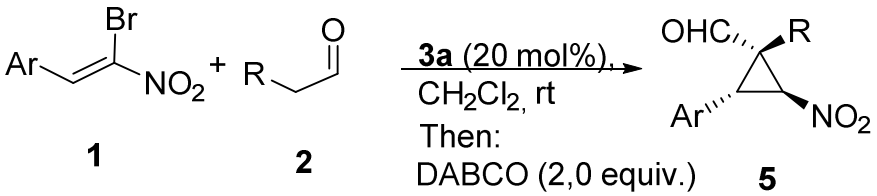

1 **2** **5**

The corresponding bromonitroalkene **1** (0.2 mmol), aldehyde **2** (0.4 mmol) and (*R*)-α-α-diphenyl-2-pyrrolidinemethanol trimethylsilyl ether (20 mol%) were dissolved in 0.4 mL of CH_2Cl_2 an. The resulting mixture was stirred at room temperature overnight (usually 18h), and 2 equivalent of DABCO were added at rt. Upon completion (usually 18 h), the solvent was removed under reduced pressure and the residue was purified by flash column chromatography (eluent indicated in each case).

(1*R*/1*S*,2*S*,3*R*)-1-Isopropyl-2-nitro-3-phenylcyclopropane-1-carbaldehyde (5Aa/5Aa').

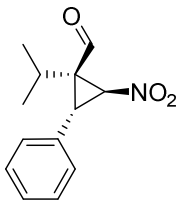

Following the general procedure described above, the compound was obtained in 78% yield and d.r. = 75:25 as a yellow oil **(Entry 1, Table 3)**. The crude was purified by flash column chromatography using 6:1 cyclohexane:AcOEt as eluent. $[\alpha]^{20}_D$ = + 7.0 (*c* = 1.02, $CHCl_3$)

Major diastereoisomer: ^{1}H-NMR (300 MHz, $CDCl_3$) δ 9.67 (s, 1H), 7.38-7.26 (m, 5H), 4.81 (d, *J* = 5.6 Hz, 1H), 4.17 (d, *J* = 5.6 Hz, 1H), 1.31 (d, *J* = 6.7 Hz, 3H), 1.21 (quint, *J* = 6.7 Hz, 1H), 0.85 (d, *J* = 6.7 Hz, 3H).

^{13}C-NMR (75 MHz, $CDCl_3$) δ 195.1 (CHO), 130.6 (C), 128.9 (CH), 128.5 (CH), 128.4 (CH), 69.3 (CH), 51.5 (C), 38.5 (CH), 28.9 (CH), 19.8 (CH_3), 17.7 (CH_3).

The enantiomeric excess was determined by SFC using Chiralpak IA column [CO_2/MeOH (97:3)]; flow rate 3 ml/min; τ_{major} = 4.1 min, τ_{minor} = 5.8 min. (*ee* = 96 %)

Minor diastereoisomer: ^{1}H-NMR (300 MHz, $CDCl_3$) δ 9.37 (s, 1H), 7.38-7.15 (m, 5H), 5.42 (d, *J* = 5.6 Hz, 1H), 3.72 (d, *J* = 5.6 Hz, 1H), 2.14 (quint, *J* = 7.1 Hz, 1H), 1.59 (d, *J* = 7.1 Hz, 3H), 1.10 (d, *J*= 7.1 Hz, 3H).

^{13}C-NMR (75 MHz, $CDCl_3$) δ 195.1 (CHO), 130.8 (C), 128.8 (CH), 128.5 (CH), 128.1 (CH), 68.0 (CH), 51.6 (C), 40.3 (CH), 28.2 (CH), 20.3 (CH_3), 19.3 (CH_3).

The enantiomeric excess was determined by SFC using Chiralpak IA column [CO_2/MeOH (97:3)]; flow rate 3 ml/min; τ_{major} = 2.7 min, τ_{minor} = 2.6 min. (*ee* = 87 %)

EM (TOF-ESI$^+$): calculated for $C_{13}H_{15}NO_3Na$ $[M+Na]^+$: 256.0944; found: 256.0947.

(1*R*/1*S*,2*R*,3*S*)-1-Isopropyl-2-(4-methoxyphenyl)-3-nitrocyclopropane-1-carbaldehyde (5Ba/5Ba´)

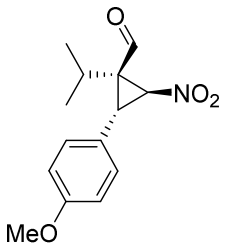

Following the general procedure described above, the compound was obtained in 52% yield and d.r. = 75:25 as a yellow oil **(Entry 3, Table 3)**. The crude was purified by flash column chromatography using 6:1 cyclohexane:AcOEt as eluent. $[\alpha]^{20}_D$ = +18.3 (*c* = 1.2, $CHCl_3$).

Major diastereoisomer: ^{1}H-NMR (300 MHz, $CDCl_3$) δ 9.63 (s, 1H), 7.18 (d, *J* = 8.6 Hz, 2H), 6.89 (d, *J* = 8.6 Hz, 2H), 4.75 (d, *J* = 5.6 Hz, 1H), 4.11 (d, *J* = 5.6 Hz, 1H), 3.81 (s, 3H), 1.30 (d, *J* = 6.7 Hz, 3H), 1.23-1.16 (m, 1H), 0.85 (d, *J* = 6.7 Hz, 3H).

^{13}C-NMR (75 MHz, $CDCl_3$)δ 195.4 (CHO), 159.6 (C), 129.6 (CH), 122.3 (C), 114.3 (CH), 69.7 (CH), 55.3 (CH_3) 51.5 (C), 38.1 (CH), 28.9 (CH), 19.7 (CH_3), 17.7 (CH_3).

The enantiomeric excess was determined by SFC using Chiralpak ID column [CO_2/MeOH (98:2)]; flow rate 3 ml/min; τ_{major} = 7.3 min, τ_{minor} = 6.5 min. (*ee* = 93 %)

Minor diastereoisomer: ^{1}H-NMR (300 MHz, $CDCl_3$) δ 9.37 (s, 1H), 7.08 (d, *J* = 8.6 Hz, 2H), 6.82 (d, *J* = 8.6 Hz, 2H), 5.38 (d, *J* = 5.6 Hz, 1H), 3.77 (s, 3H), 3.66 (d, *J* = 5.6 Hz, 1H), 2.12 (quint,*J* = 7.1 Hz, 1H), 1.58 (d, *J* = 7.1 Hz, 3H), 1.08 (d, *J* = 7.1Hz, 3H).

^{13}C-NMR (75 MHz, $CDCl_3$)δ 194.6 (CHO), 159.3 (C), 129.6 (CH), 122.7 (C), 114.2 (CH), 68.2 (CH), 55.3 (CH_3) 51.8 (C), 39.9 (CH), 28.1 (CH), 20.03 (CH_3), 19.3 (CH_3).

The enantiomeric excess was determined by SFC using Chiralpak ID column [CO_2/MeOH (98:2)]; flow rate 3 ml/min; τ_{major} = 4.2 min, τ_{minor} = 4.6 min. (*ee* = 95 %)

EM (TOF-ESI$^+$): calculated for $C_{14}H_{17}NO_4Na$ $[M+Na]^+$: 286.1049; found: 286.1056.

(1*R*/1*S*,2*R*,3*S*)-2-(4-Bromophenyl)-1-isopropyl-3-nitrocyclopropane-1-carbaldehyde (5Ca/5Ca')

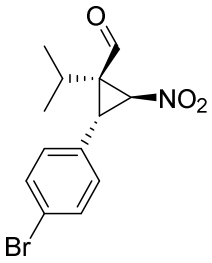

Following the general procedure described above, the compound was obtained in 63% yield and d.r. = 70:30 as a yellow oil **(Entry 4, Table 3)**. The crude was purified by flash column chromatography using 6:1 cyclohexane:AcOEt as eluent. $[\alpha]^{20}_D$ = +6.3 (*c* = 0.35, $CHCl_3$).

Major diastereoisomer: ^{1}H-NMR (300 MHz, $CDCl_3$) δ 9.66 (d, *J* = 1.2 Hz,1H), 7.51 (d, *J* = 8.2 Hz, 2H), 7.15 (d, *J* = 8.2 Hz, 2H), 4.75 (d, *J* = 5.5 Hz, 1H), 4.10 (d, *J* = 5.5 Hz, 1H), 1.32 (d, *J* = 6.8 Hz, 3H), 1.22-1.16 (m, 1H), 0.85 (d, *J* = 6.8 Hz, 3H)

^{13}C-NMR (75 MHz, $CDCl_3$)δ 194.7 (CHO), 132.1 (CH), 130.1(CH), 129.7 (C), 122.5 (C), 69.0 (CH), 51.3 (C), 37.6 (CH), 28.9 (CH), 19.8 (CH_3), 17.8 (CH_3).

The enantiomeric excess was determined by SFC using Chiralpak IA column [CO_2/MeOH (90:10)]; flow rate 3 ml/min; τ_{major} = 4.2 min, τ_{minor} = 8.4 min.(*ee* = 96%).

Minor diastereoisomer: ^{1}H-NMR (300 MHz, $CDCl_3$) δ 9.45 (s,1H), 7.44 (d, *J* = 8.1 Hz, 2H), 7.03 (d, *J* = 8.1 Hz, 2H), 5.39 (d, *J* = 5.6 Hz, 1H), 3.65 (d, *J* = 5.6 Hz, 1H), 2.14 (quint,*J* = 7.1 Hz, 1H), 1.58 (d, *J* = 7.1 Hz, 3H), 1.10 (d, *J* = 7.1 Hz, 3H).

^{13}C-NMR (75 MHz, $CDCl_3$) δ 194.2 (CHO), 131.9 (CH), 130.2 (CH), 129.1 (C), 122.2 (C), 67.9 (CH), 51.6 (C), 39.7 (CH), 28.1 (CH), 20.3 (CH_3), 19.4 (CH_3).

The enantiomeric excess was determined by SFC using Chiralpak IA column [CO_2/MeOH (90:10)]; flow rate 3 ml/min; τ_{major} = 3.4 min, τ_{minor} = 3.0 min. (*ee* = 91%)

EM (TOF-ESI$^+$): calculated for $C_{13}H_{14}NO_3BrNa$ $[M+Na]^+$: 334.0049; found: 334.0063.

(1*R*/1*S*,2*R*,3*S*)-2-(4-Fluorophenyl)-1-isopropyl-3-nitrocyclopropane-1-carbaldehyde (5Da/5Da´)

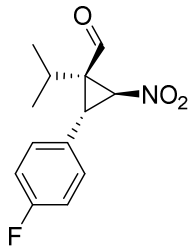

Following the general procedure described above, the compound was obtained in 71% yield and d.r. = 71:29 as a yellow oil **(Entry 5, Table 3)**. The crude was purified by flash column chromatography using 6:1 cyclohexane:AcOEt as eluent. $[\alpha]^{20}_D$ = - 6.1 (*c* = 0.54, $CHCl_3$).

Major diastereoisomer: ^{1}H-NMR (300 MHz, $CDCl_3$) δ 9.66 (d, *J* = 1.0 Hz, 1H), 7.27-7.23 (m, 2H), 7.16-6.97 (m, 2H), 4.76 (d, *J* = 5.5 Hz, 1H), 4.13 (d, *J* = 5.5 Hz, 1H), 1.32 (d, *J* = 6.8 Hz, 3H), 1.22-1.13 (m, 1H), 0.86 (d, *J* = 6.8 Hz, 3H).

^{13}C-NMR (125 MHz, $CDCl_3$) δ 194.9 (CHO), 162.5 (d, J_{C-F} = 246.9 Hz, C), 130.2 (d, J_{C-F} = 8.3 Hz, CH), 126.4 (d, J_{C-F}= 3.3 Hz, C), 116.0 (d, J_{C-F} = 21.7 Hz, CH), 69.4 (CH), 51.3 (C), 37.6 (CH), 28.9 (CH), 19.8 (CH_3), 17.8 (CH_3).

The enantiomeric excess was determined by SFC using Chiralpak IA column [CO_2/MeOH (90:10)]; flow rate 3 ml/min; τ_{major} = 2.4 min, τ_{minor} = 3.5 min. (*ee* = 97 %)

Minor diastereoisomer: ^{1}H-NMR (300 MHz, $CDCl_3$) δ 9.44 (s, 1H), 7.27-7.23(m, 2H), 7.16-6.97(m, 2H), 5.39 (d, *J* = 5.7 Hz, 1H), 3.68 (d, *J* =5.7 Hz, 1H), 2.19-2.10 (quint, *J* =7.2 Hz, 1H), 1.59 (d, *J* = 7.2 Hz, 3H), 1.10 (d, *J* =7.2 Hz, 3H).

^{13}C-NMR (125 MHz, $CDCl_3$)δ 194.4 (CHO), 162.3 (d, J_{C-F} = 246.4 Hz, C), 130.3 (d, J_{C-F} = 8.3 Hz, CH), 126.5 (d, J_{C-F}= 3.3 Hz, C), 115.8 (d, J_{C-F} = 21.8 Hz, CH), 68.1 (CH), 51.6 (C), 39.7 (CH), 28.0 (CH), 20.4 (CH_3), 19.4 (CH_3).

The enantiomeric excess was determined by SFC using Chiralpak IA column [CO_2/MeOH (90:10)]; flow rate 3 ml/min; τ_{major} = 1.9 min, τ_{minor} = 1.8 min. (*ee*= 92%).

EM (TOF-ESI$^+$): calculated for $C_{13}H_{14}NO_3FNa$ $[M+Na]^+$: 274.0849; found: 274.0860.

(1*R*/1*S*,2*S*,3*S*)-2-(2-Fluorophenyl)-1-isopropyl-3-nitrocyclopropane-1-carbaldehyde (5Ea/5Ea´)

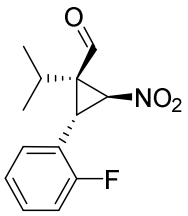

Following the general procedure described above, the compound was obtained in 53% yield and d.r. = 83:17 as a yellow oil **(Entry 6, Table 3)**. The crude was purified by flash column chromatography using 6:1 cyclohexane:AcOEt as eluent. $[\alpha]^{20}_D$ = +7.5 (*c* = 0.93, $CHCl_3$).

Major diastereoisomer: ^{1}H-NMR (300 MHz, $CDCl_3$) δ 9.68 (s, 1H), 7.39-7.10 (m, 4H), 4.83 (d, *J* = 5.7 Hz, 1H), 4.15 (d, *J* = 5.7 Hz, 1H), 1.31 (d, *J* = 6.9 Hz, 3H), 1.18-1.14 (m, 1H), 0.88 (d, *J* = 6.9 Hz, 3H).

^{13}C-NMR (125 MHz, $CDCl_3$)δ 195.0 (CHO), 161.8 (d, J_{C-F} = 246.7 Hz, C), 130.4 (d, J_{C-F} = 8.2 Hz, CH), 129.2 (d, J_{C-F} = 2.9 Hz, CH), 124.4 (d, J_{C-F} = 3.7 Hz, CH), 118.6(d, J_{C-F} = 14.2 Hz, C), 116.0 (d, J_{C-F} = 21.1 Hz, CH), 68.8 (d, J_{C-F} = 1.8 Hz, CH), 50.5 (C), 33.3 (d, J_{C-F} = 4.4 Hz, CH), 29.5 (CH), 19.9 (CH_3), 17.4 (d, J_{C-F} = 1.7 Hz, CH_3).

The enantiomeric excess was determined by SFC using Chiralpak IA column [CO_2/MeOH (95:5)]; flow rate 3 ml/min; τ_{major} = 2.8 min, τ_{minor} = 3.8 min. (*ee* = 96%)

Minor diastereoisomer: ^{1}H-NMR (300 MHz, $CDCl_3$) δ 9.57 (s, 1H), 7.39-7.10 (m, 4H), 5.35 (d, *J* = 5.6 Hz, 1H), 3.62 (d, *J* = 5.6 Hz, 1H), 2.20-2.11 (m, 1H), 1.60 (d, *J* = 7.0 Hz, 3H), 1.11 (d, *J* = 7.0 Hz, 3H).

^{13}C-NMR (125 MHz, $CDCl_3$)δ 194.2 (CHO), 161.2 (d, J_{C-F} = 245.6 Hz, C), 130.2 (d, J_{C-F} = 3.0 Hz, CH), 130.1 (d, J_{C-F} = 8.3 Hz, CH), 124.3 (d, J_{C-F} = 3.7 Hz, CH), 118.7(d, J_{C-F} = 14.2 Hz, C), 115.6 (d, J_{C-F} = 21.1 Hz, CH), 67.6 (CH), 50.4 (C), 34.6 (d, J_{C-F} = 3.8 Hz, CH), 28.1 (CH), 19.8 (d, J_{C-F} = 2.7 Hz, CH_3), 19.7 (CH_3).

The enantiomeric excess was determined by SFC using Chiralpak IA column [CO_2/MeOH (95:5)]; flow rate 3 ml/min; τ_{major} = 2.0 min, τ_{minor} = 1.8 min. (*ee* = 87%)

EM (TOF-ESI$^+$): calculated for $C_{13}H_{14}NO_3FNa$ $[M+Na]^+$: 274.0849; found: 274.0861.

(1*R*/1*S*,2*S*,3*R*)-2-Nitro-3-phenyl-1-propylcyclopropane-1-carbaldehyde (5Ab/5Ab')

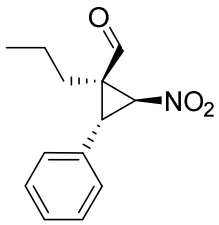

Following the general procedure described above, the compound was obtained in 73% yield and d.r. = 60:40 as a brown oil **(Entry 8, Table 3)**. The crude was purified by flash column chromatography using 6:1 cyclohexane:AcOEt as eluent. $[\alpha]^{20}_D$ = +19.6 (*c* = 1.35, $CHCl_3$).

Major diastereoisomer: ^{1}H-NMR (300 MHz, $CDCl_3$) δ 9.57 (s, 1H), 7.39-7.18 (m, 5H), 4.87 (d, *J* = 5.6 Hz, 1H), 4.17 (d, *J* = 5.6 Hz, 1H), 1.74-1.27 (m, 4H), 0.79 (d, *J* = 7.3 Hz, 3H).

^{13}C-NMR (75 MHz, $CDCl_3$) δ 195.0 (CHO), 130.6 (C), 129.0 (CH), 128.5 (CH), 128.2 (CH), 69.3 (CH), 48.0 (C), 37.9 (CH), 28.5 (CH_2), 19.8 (CH_2), 13.9 (CH_3).

The enantiomeric excess was determined by SFC using Chiralpak IA column [CO_2/MeOH (97:3)]; flow rate 1 ml/min; τ_{major} = 8.2 min, τ_{minor} = 8.7 min.(*ee* = 95 %)

Minor diastereoisomer: ^{1}H-NMR (300 MHz, CDCl3) δ 9.03 (s,1H), 7.39-7.18 (m, 5H), 5.35 (d, *J* = 5.6 Hz, 1H), 3.78 (d, *J* = 5.6 Hz, 1H), 2.23-1.97 (m ,2H), 1.74-1.27 (m, 2H), 0.99 (t, *J* = 7.3 Hz, 3H).

^{13}C-NMR (75 MHz, $CDCl_3$)δ 195.2 (CHO), 130.9 (C), 129.0 (CH), 128.5 (CH), 128.2 (CH), 67.5 (CH), 47.7 (C), 39.1 (CH), 28.5 (CH_2), 20.7 (CH_2), 14.0 (CH_3).

EM (TOF-ESI$^+$): calculated for $C_{13}H_{15}O$ $[M-NO_2]^+$: 187.1117; found: 187.1115.

(1*R*,2*S*,3*R*)-2-Nitro-1,3-diphenylcyclopropane-1-carbaldehyde (5Ac')

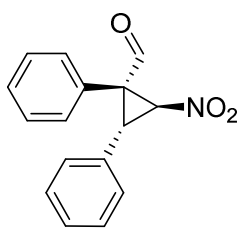

Following the general procedure described above, the compound was obtained in 55% yield and d.r.> 98:2 as a yellow oil **(Entry 9, Table 3)**. The crude was purified by flash column chromatography using 9:1 cyclohexane:AcOEt as eluent. $[\alpha]^{20}_D$ = +238.7 (*c* = 1.06, $CHCl_3$).

^{1}H-NMR (300 MHz, CDCl3) δ 9.31 (s, 1H), 7.49-7.32 (m, 10H), 5.67 (d, *J* = 5.6 Hz, 1H), 4.42 (d, *J* = 5.6 Hz, 1H)

^{13}C-NMR (75 MHz, $CDCl_3$)δ 193.0 (CHO), 130.7 (C), 130.2 (C), 129.8 (CH), 129.7 (CH), 129.6 (CH), 129.0 (CH), 128.9 (CH), 128.4 (CH), 67.6 (CH), 52.9 (C), 39.5 (CH).

The enantiomeric excess was determined by SFC using Chiralpak IB column [CO_2/MeOH (90:10)]; flow rate 3 ml/min; τ_{major} = 2.8 min, τ_{minor} = 3.2 min. (*ee* = 95%)

EM (TOF-ESI$^-$): calculated for $C_{16}H_{11}O$ [M-H_2NO_2]$^-$: 219.0815; found: 219.0825.

(1*R*,2*R*,3*S*)-2-(4-Methoxyphenyl)-3-nitro-1-phenylcyclopropane-1-carbaldehyde (5Bc')

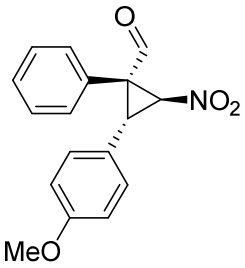

Following the general procedure described above, the compound was obtained in 59% yield and d.r. > 98:2 as a yellow oil **(Entry 10, Table 3**). The crude was purified by flash column chromatography using 9:1 cyclohexane:AcOEt as eluent. $[\alpha]^{20}_D$ = +196.2 (*c* = 1.2, $CHCl_3$).

^{1}H-NMR (300 MHz, CDCl3) δ 9.30 (s, 1H), 7.48-7.40 (m, 5H), 7.25 (d, *J* = 9.0 Hz, 2H), 6.90 (d, *J* = 8.6 Hz, 2H), 5.63 (d, *J* = 5.6 Hz, 1H), 4.37 (d, *J* = 5.6 Hz, 1H)

^{13}C-NMR (75 MHz, $CDCl_3$)δ 193.2 (CHO), 159.5(C), 130.8 (C), 130.0 (CH), 129.8 (CH), 129.6 (CH), 129.5 (CH), 122.0 (C), 114.4 (CH), 67.8 (CH), 55.3 (CH_3), 53.1 (CH), 39.1 (CH).

The enantiomeric excess was determined by SFC using Chiralpak ID column [CO_2/MeOH (90:10)]; flow rate 3 ml/min; τ_{major} = 3.9 min, τ_{minor} = 3.3 min. (*ee* = 91%)

EM (TOF-ESI$^+$): calculated for $C_{17}H_{15}O_2$ [M-NO_2]$^+$: 251.1066; found: 251.1066.

(1*R*,2*R*,3*S*)-2-(4-Bromophenyl)-3-nitro-1-phenylcyclopropane-1-carbaldehyde (5Cc')

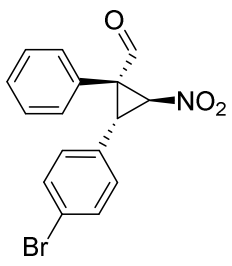

Following the general procedure described above, the compound was obtained in 54% yield and d.r.> 98:2 as a white solid **(Entry 11, Table 3)**. The crude was purified by flash

column chromatography using 9:1 cyclohexane:AcOEt as eluent. $[\alpha]^{20}_D$ = +241.5 (*c* = 0.81, $CHCl_3$).

^{1}H-NMR (300 MHz, $CDCl_3$) δ 9.34 (s, 1H), 7.52-7.40 (m, 7H), 7.20 (d, *J* = 8.3 Hz, 2H), 5.62 (d, *J* = 5.6 Hz, 1H), 4.35 (d, *J* = 5.6 Hz, 1H).

^{13}C-NMR (75 MHz, $CDCl_3$)δ 192.9 (CHO), 132.1(CH), 130.5 (CH), 130.5 (C), 129.8 (CH), 129.7 (CH), 129.6 (CH), 129.2 (C), 122.5 (C), 67.5 (CH), 52.8 (C), 38.9 (CH).

The enantiomeric excess was determined by SFC using Chiralpak ID column [CO_2/MeOH (90:10)]; flow rate 3 ml/min; τ_{major} = 4.5 min, τ_{minor} = 3.3 min (*ee* = 96 %).

EM (TOF-ESI$^-$): calculated for $C_{17}H_{16}BrClNO_4$ $[M+MeOH+Cl]^-$: 411.9956; found: 411.9952.

(2R,3S,4*S*/4*R*)-4-bromo-2-isopropyl-4-nitro-3-phenylbutanal (4Aa)

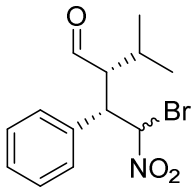

The bromonitroalkene **1A** (0.2 mmol), aldehyde **2a** (0.4 mmol) and (*R*)-α-α-diphenyl-2-pyrrolidinemethanol trimethylsilyl ether (20 mol%) were dissolved in 0.4 mL of CH_2Cl_2. The resulting mixture was stirred at room temperature overnight. Upon completion (18 h), the solvent was removed under reduced pressure and the residue was purified by flash column chromatography using 20:1 hexane:AcOEt as eluent. The compound was obtained in 80% yield and d.r. 64:36 as a yellow oil. It has an 18% of cyclopropane **5Aa**/**5Aa'** as an inseparable impurity.

The spectra data is given as a mixture of the signals of the two diastereoisomers.

^{1}H-NMR (300 MHz, $CDCl_3$) δ 10.04 (d, *J* = 1.9 Hz, 1H), 9.98 (d, *J* = 1.1 Hz, 2H), 7.37-7.12 (m, 10H), 6.71 (d, *J* = 4.4 Hz, 1H), 6.44 (d, *J* = 5.5 Hz, 1H), 4.16 (dd, *J* = 10.9, 4.4 Hz, 1H), 3.96 (dd, *J* = 10.7, 5.5 Hz, 1H), 3.25-3.18 (m, 2H), 1.84-1.67(m, 2H), 1.20 (d, *J* = 7.3 Hz, 3H), 1.12 (d, *J* = 7.3 Hz, 3H), 0.79 (d, *J* = 7.0 Hz, 3H), 0.75 (d, *J* = 7.0 Hz, 3H).

^{13}C-NMR (75 MHz, $CDCl_3$) δ 204.9 (CHO), 204.7 (CHO), 134.1 (C), 132.9 (C), 129.4 (CH), 129.3 (CH), 129.1 (CH), 129.1 (CH), 129.0 (CH), 128.9 (CH), 87.5 (CH), 83.7 (CH), 58.7 (CH), 57.7 (CH), 50.4 (CH), 47.7 (CH), 29.2 (CH), 28,4 (CH), 22.0 (CH_3), 21.9 (CH_3), 17.2 (CH_3), 16.7 (CH_3).

EM (TOF-ESI$^+$): calculated for $C_{13}H_{16}NO_3NaBr$: $[M+Na]^+$ 336.0205; found: 336.0219.

(2R,3S)-2-isopropyl-4-nitro-3-phenylbutanal (6Aa)

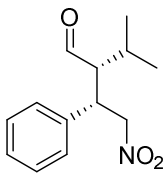

The product was obtained as a byproduct in the reaction of entry 11 of **Table 1**. The compound was obtained in 30% yield and d.r. > 98:2 as a brown oil. The crude was purified by flash column chromatography using 20:1 hexane:AcOEt as eluent. $[\alpha]^{20}_D$ = +59.75 (*c* = 0.9, $CHCl_3$). The absolute configuration was established comparing this value with the described value in the literature[2], which was $[\alpha]^{20}_D$ = + 50,82 (*c* = 0.9, $CHCl_3$).

^{1}H-NMR (300 MHz, $CDCl_3$) δ 9.93 (d, *J* = 2.3 Hz, 1H), 7.37-7.29 (m, 3H), 7.20-7.18 (m, 2H), 4.67 (dd, *J* = 12.5 Hz, 4.5 Hz, 1H), 4.57 (dd, *J* = 12.5 Hz, 10.1 Hz, 1H) 3.90 (td, *J* = 10.1 Hz, 4.5 Hz, 1H), 2.80-2.74 (m, 1H), 1.76-1.79 (m, 1H), 1.10 (d, *J* = 7.1 Hz, 3H), 0.88 (d, *J* = 7.1 Hz, 3H).

[2] J. M. Betancort, C. F. Barbas III, *Org. Lett.* **2001,** *3*, 3737.

3. NMR spectra and HPLC chromatograms

^{1}H-NMR (300 MHz, $CDCl_3$) **(5Aa/5Aa')**

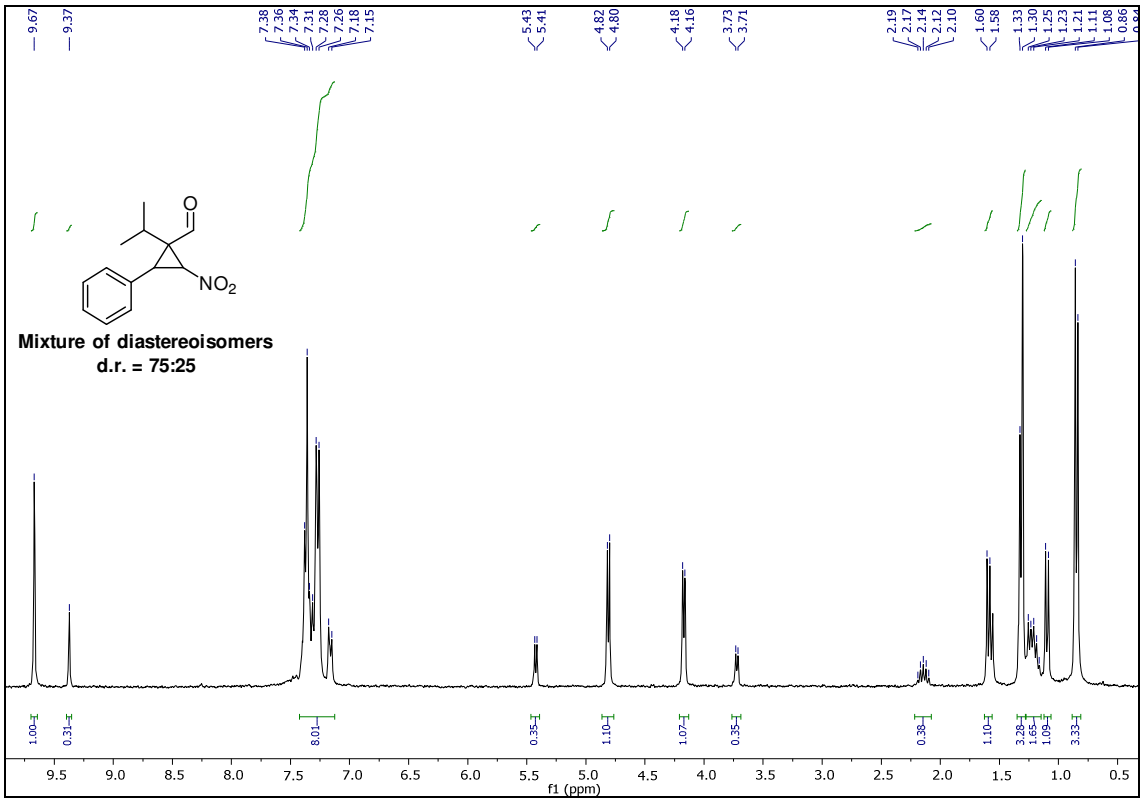

^{13}C-NMR (75 MHz, $CDCl_3$) **(5Aa/5Aa')**

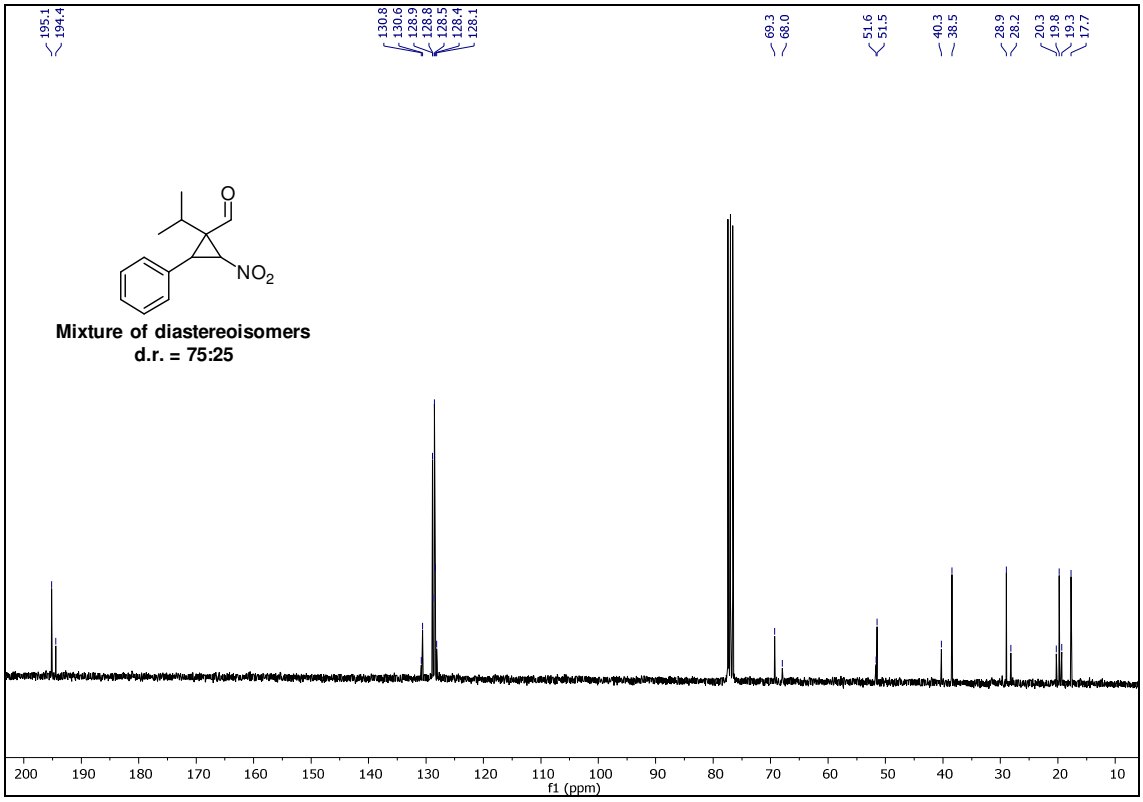

Chromatogram of racemic **(5Aa/5Aa')**

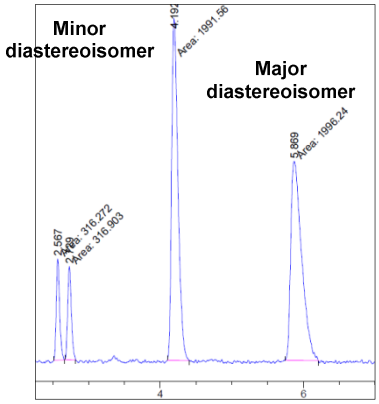

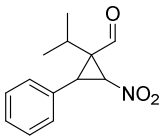

Peak #	RetTime [min]	Type	Width [min]	Area [mAU*s]	Height [mAU]	Area %
1	2.567	MM	0.0546	316.27188	96.59939	6.8443
2	2.729	MM	0.0594	316.90295	88.85853	6.8579
3	4.192	MM	0.1024	1991.55811	324.08603	43.0983
4	5.869	MM	0.1762	1996.23877	188.86168	43.1995
Totals :				4620.97171	698.40562	

Chromatogram of enantiomerically enriched **(5Aa/5Aa')**

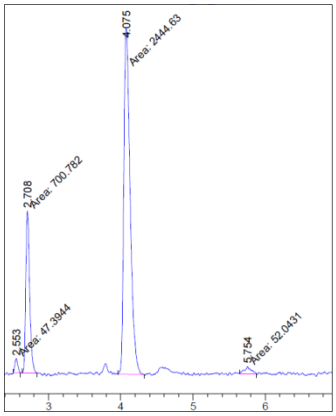

Peak #	RetTime [min]	Type	Width [min]	Area [mAU*s]	Height [mAU]	Area %
1	2.553	MM	0.0472	47.39437	16.71939	1.4606
2	2.708	MM	0.0617	700.78198	189.23622	21.5967
3	4.075	MM	0.1008	2444.63184	404.21512	75.3388
4	5.754	MM	0.1043	52.04310	8.31464	1.6039
Totals :				3244.85129	618.48537	

^{1}H-NMR (300 MHz, $CDCl_3$) **(5Ac')**

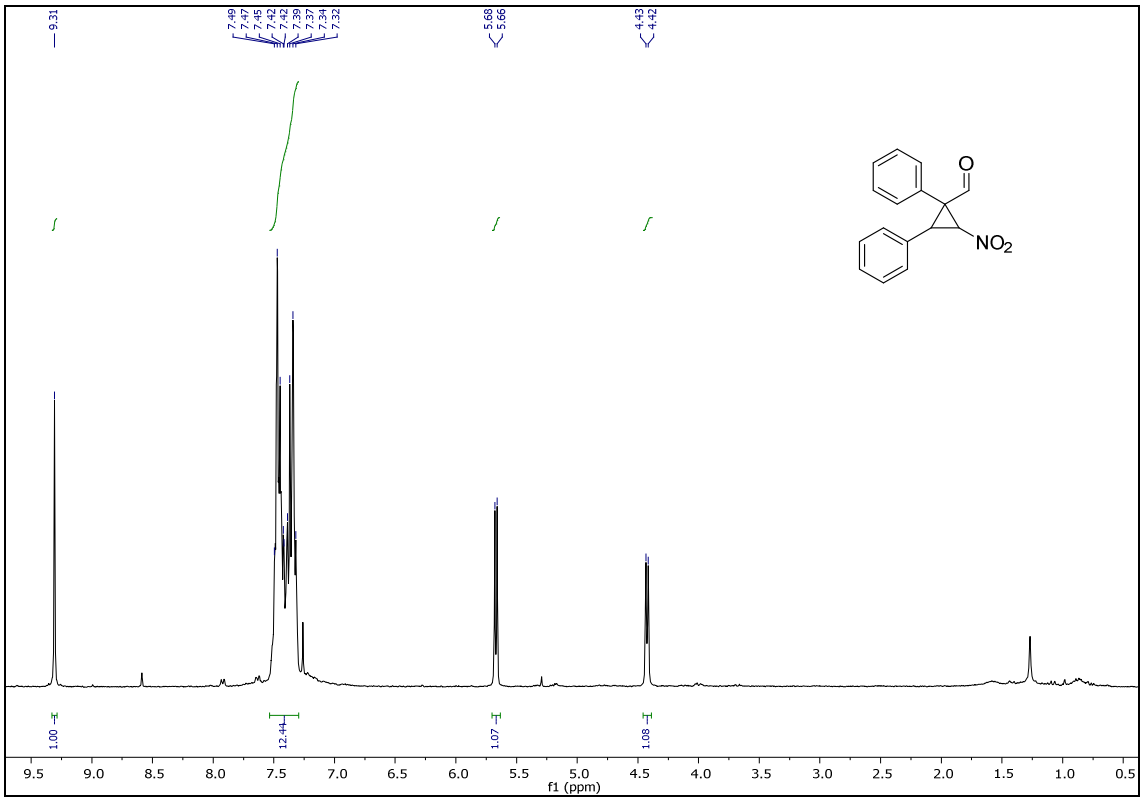

^{13}C-NMR (75 MHz, $CDCl_3$) **(5Ac')**

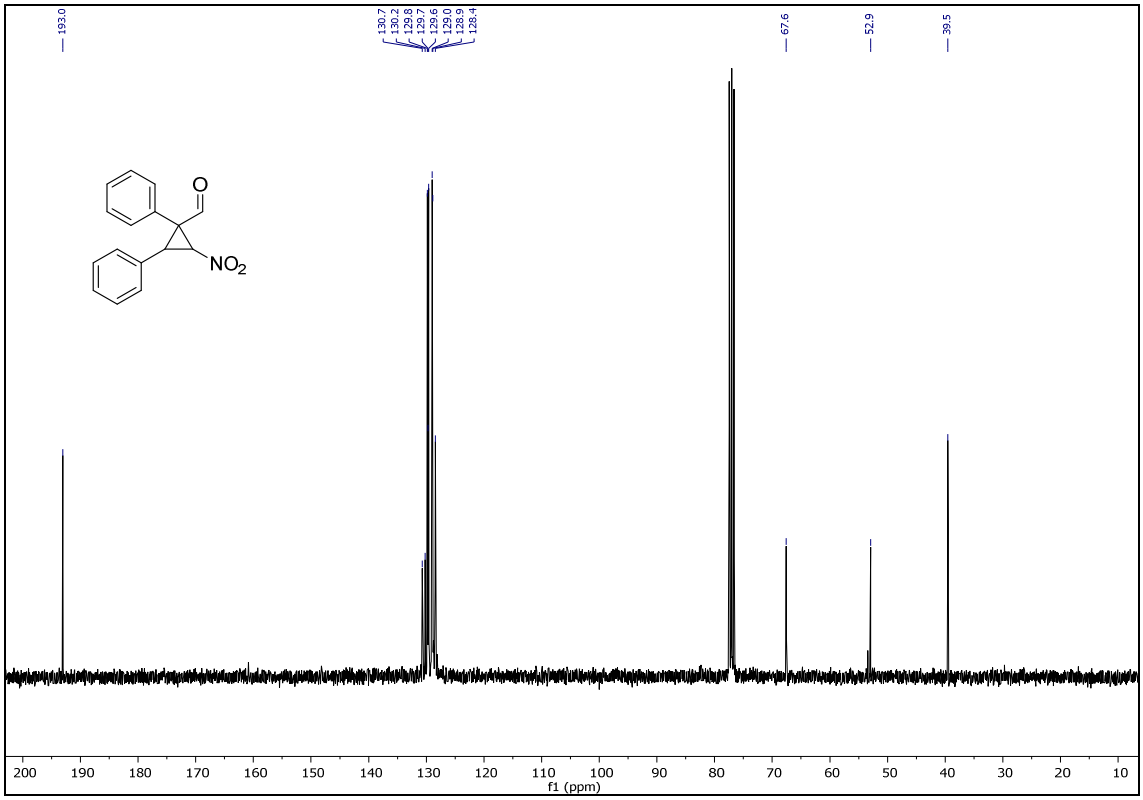

Chromatogram of racemic **(5Ac')**

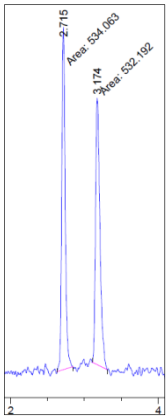

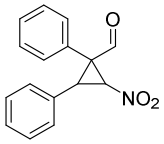

Peak #	RetTime [min]	Type	Width [min]	Area [mAU*s]	Height [mAU]	Area %
1	2.715	MM	0.0540	534.06293	164.95387	50.0877
2	3.174	MM	0.0691	532.19183	128.27612	49.9123
Totals :				1066.25476	293.23000	

Chromatogram of enantiomerically enriched **(5Ac')**

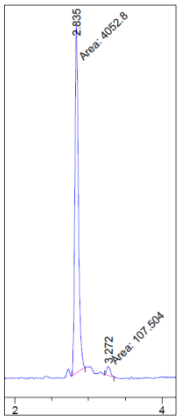

Peak #	RetTime [min]	Type	Width [min]	Area [mAU*s]	Height [mAU]	Area %
1	2.835	MM	0.0557	4052.79517	1212.17151	97.4159
2	3.272	MM	0.0571	107.50436	31.38448	2.5841
Totals :				4160.29952	1243.55599	

^{1}H-NMR (300 MHz, $CDCl_3$) **(4Aa)**

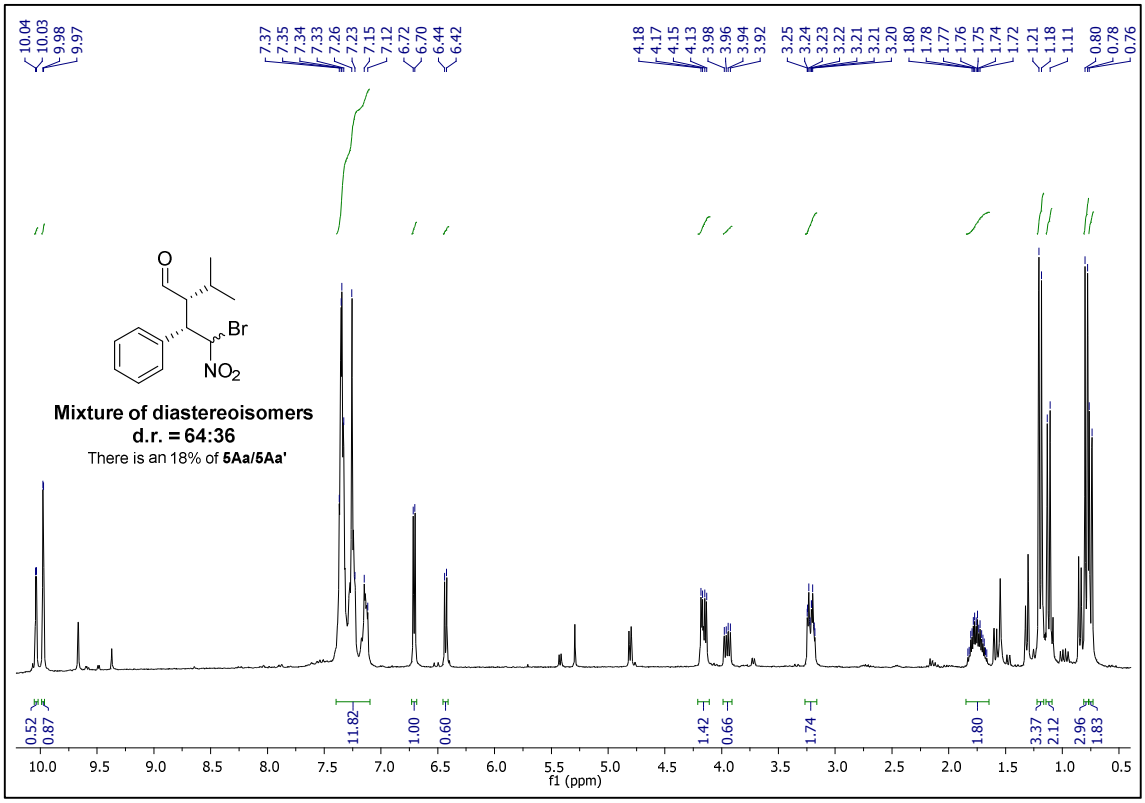

^{13}C-NMR (75 MHz, $CDCl_3$) **(4Aa)**

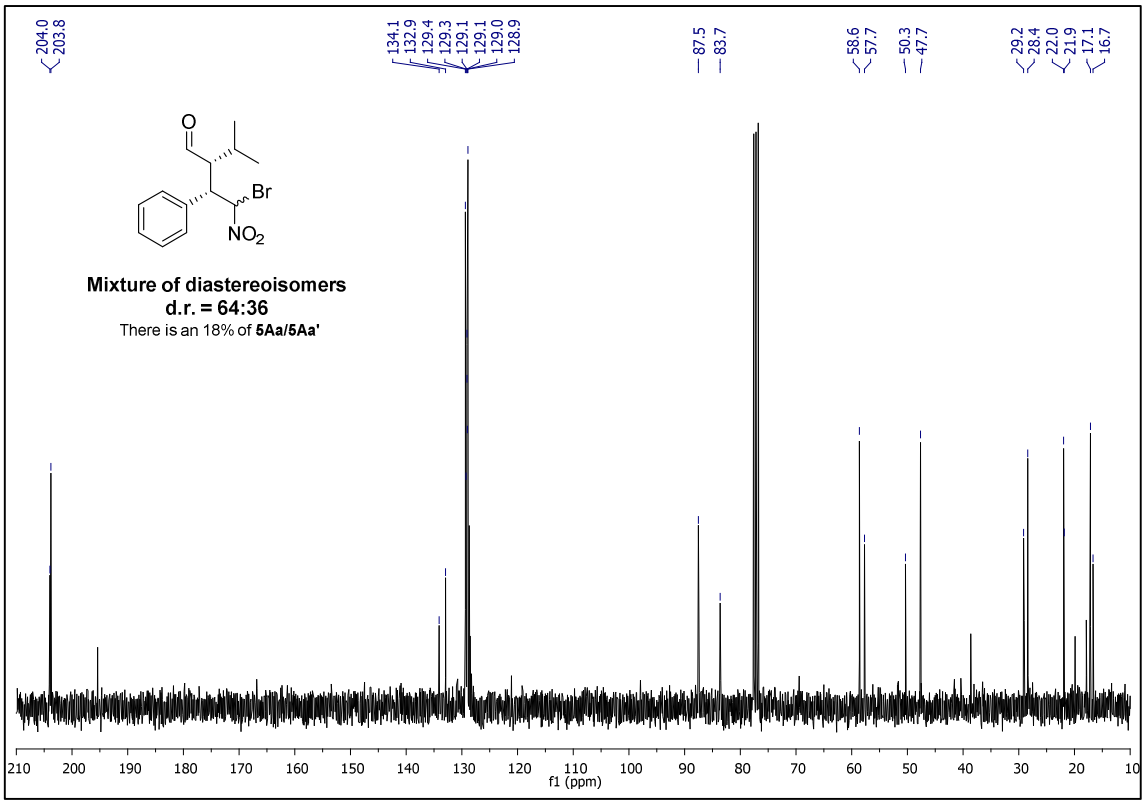

^{1}H-NMR (300 MHz, $CDCl_3$) **(6Aa)**

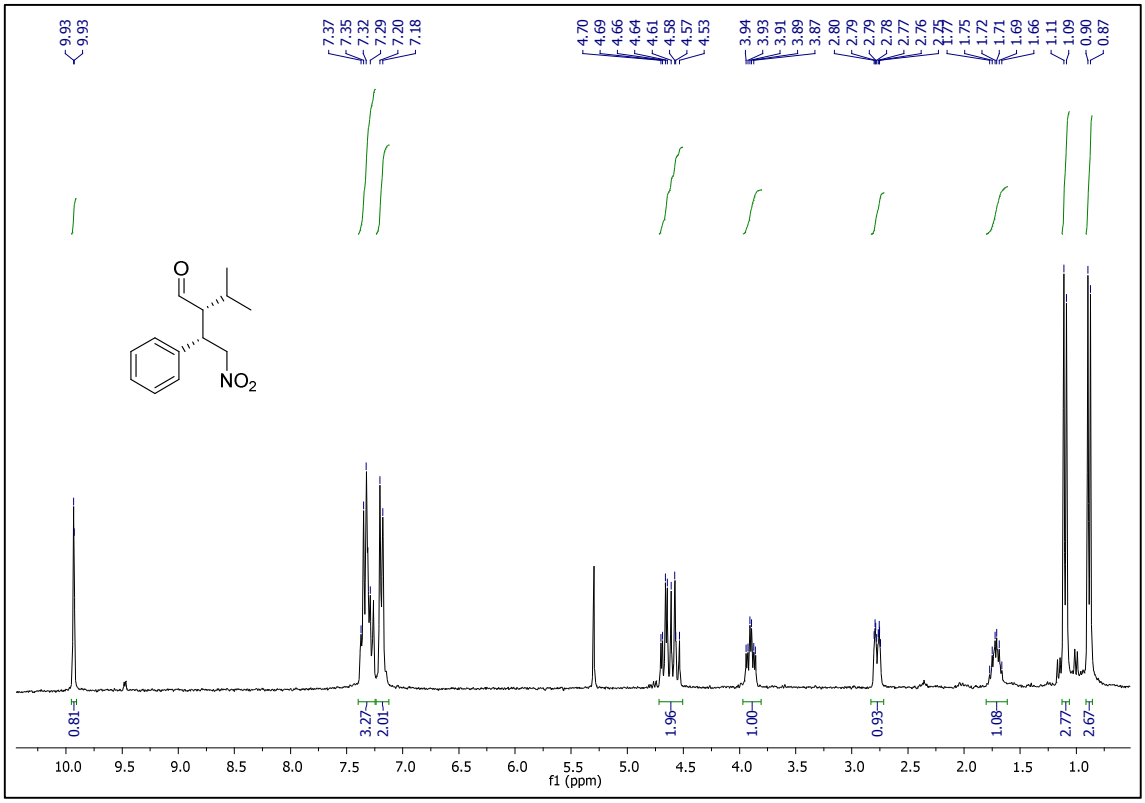

4. nOe signals

We took a mixture of the two diastereoisomer of **5Aa/5Aa'** (d.r. = 73:27) and we did several NMR spectra irradiating the signals of both diastereoisomers in order to see the nOe signals. Here, we present the spectra[3] in two groups: firstly, the spectra in which we irradiated the signals of the mayor diastereoisomer (**5Aa**); then, the spectra in which we irradiated the signals of the minor diastereoisomer (**5Aa'**). In both cases the original spectrum without irradiation is given for comparison.

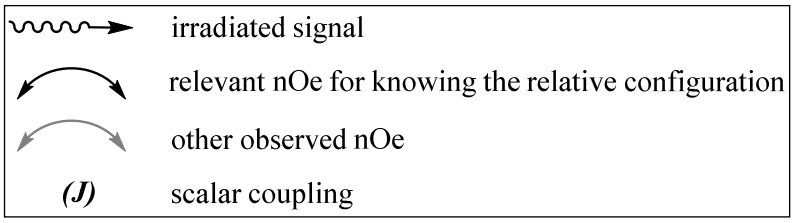

[3] The spectra are presented as the difference between the original spectrum and the irradiated spectrum.

Irradiated spectra of mayor diastereiosmer (**5Aa**)

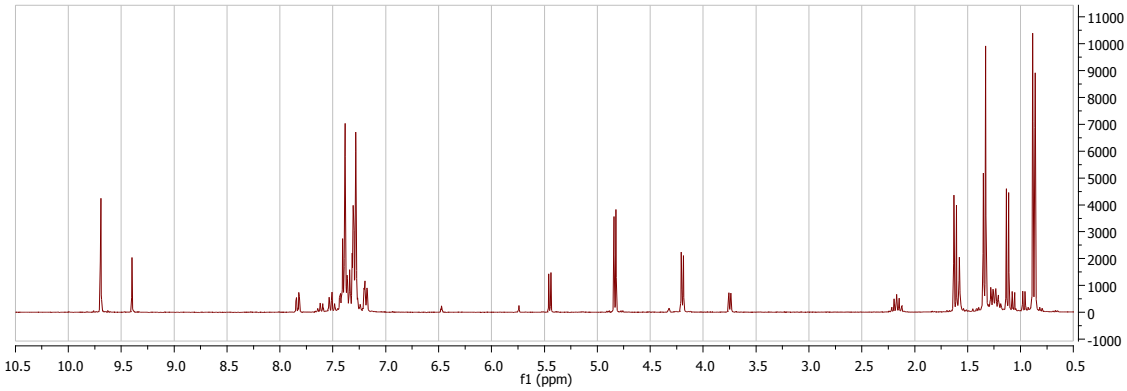

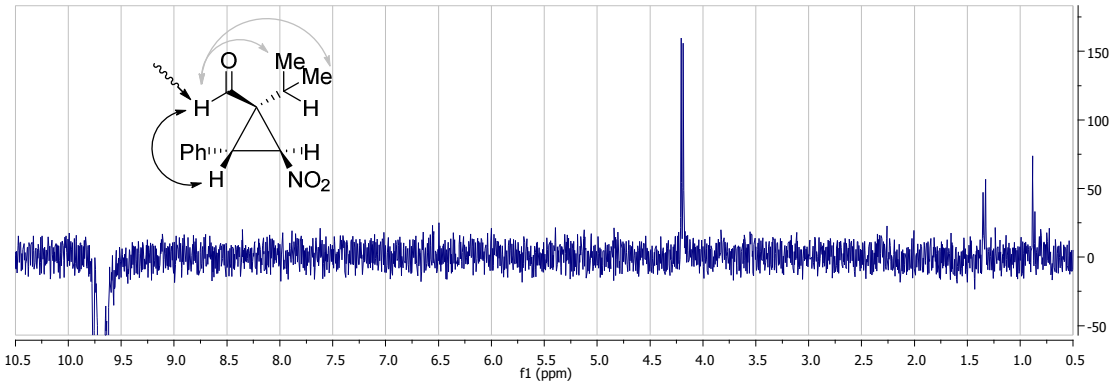

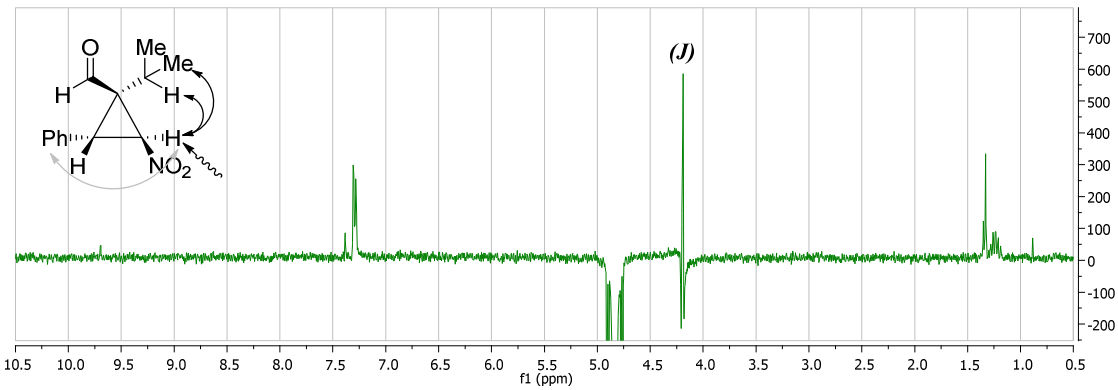

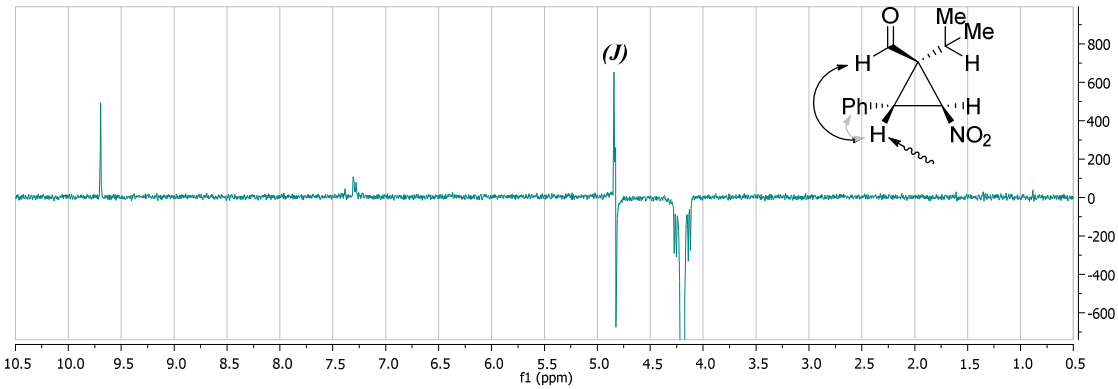

Irradiated spectra of minor diastereisomer (**5Aa'**)

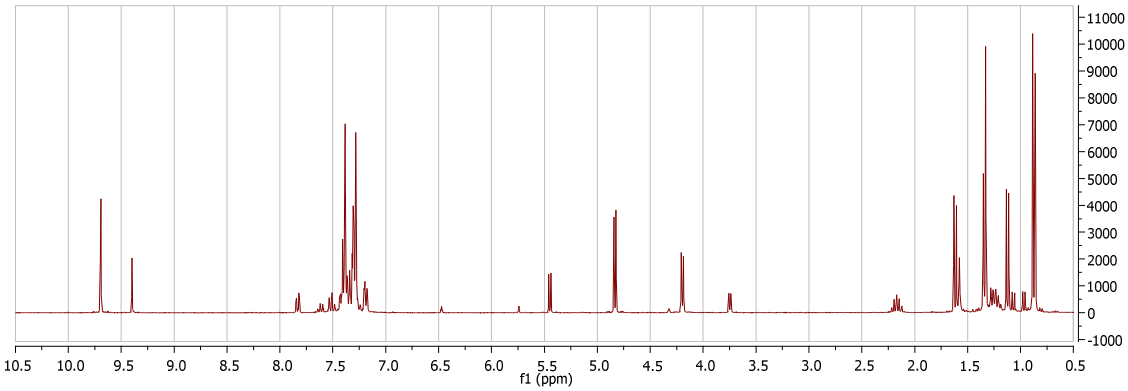

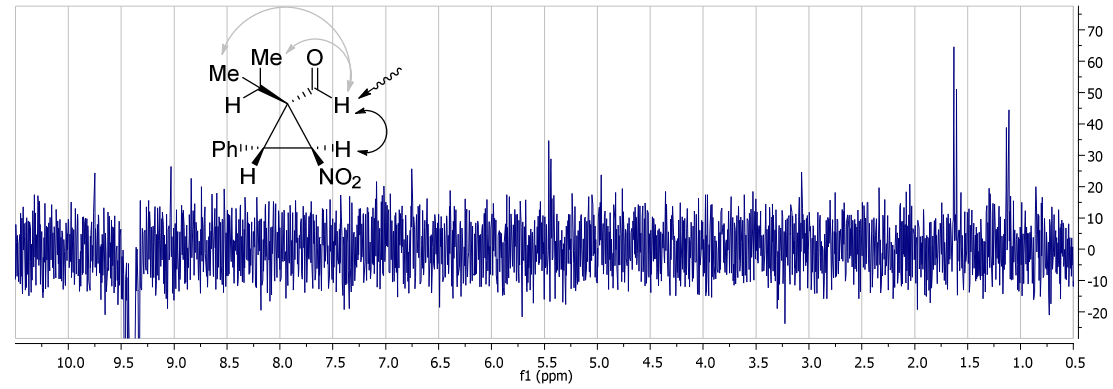

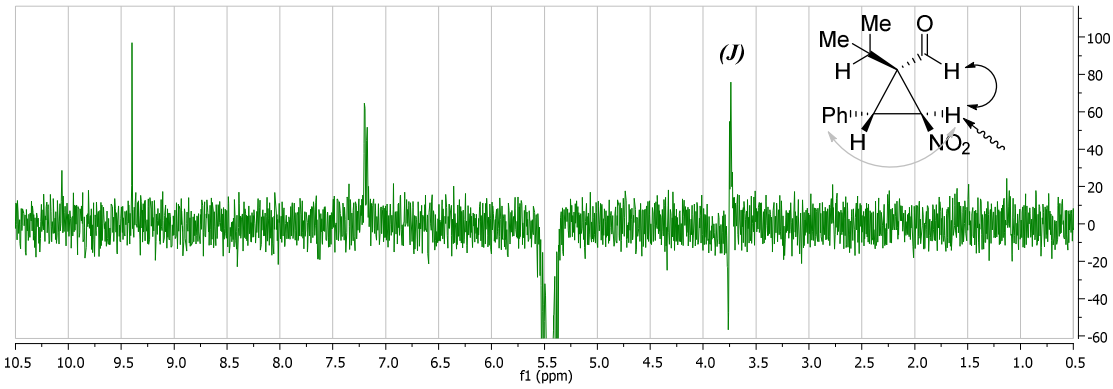

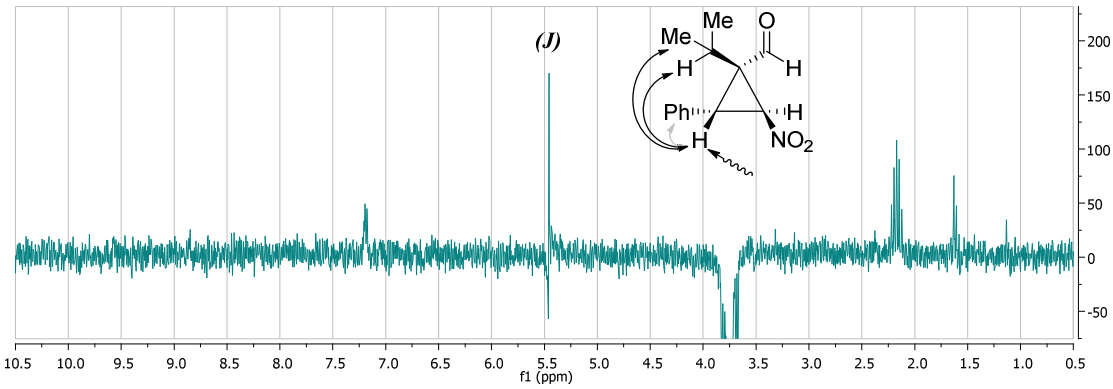

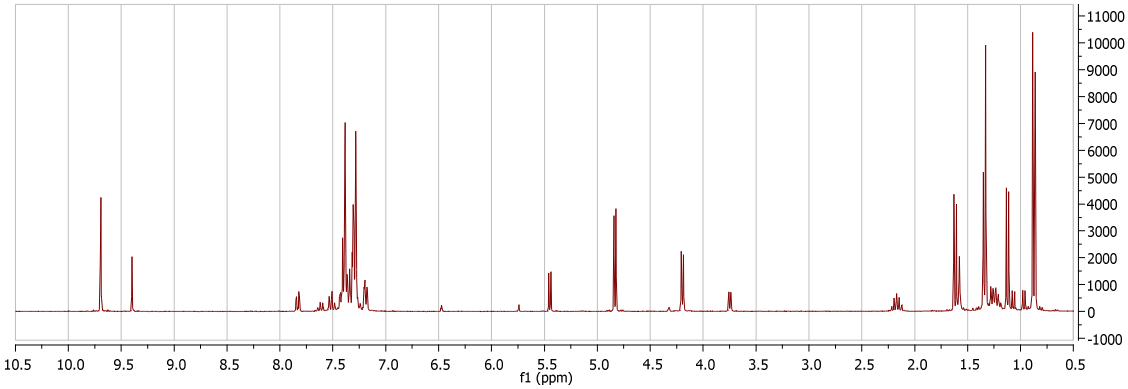
11000
10000
9000
8000
7000
6000
5000
4000
3000
2000
1000
0
-1000
10.5 10.0 9.5 9.0 8.5 8.0 7.5 7.0 6.5 6.0 5.5 5.0 4.5 4.0 3.5 3.0 2.5 2.0 1.5 1.0 0.5
f1 (ppm)

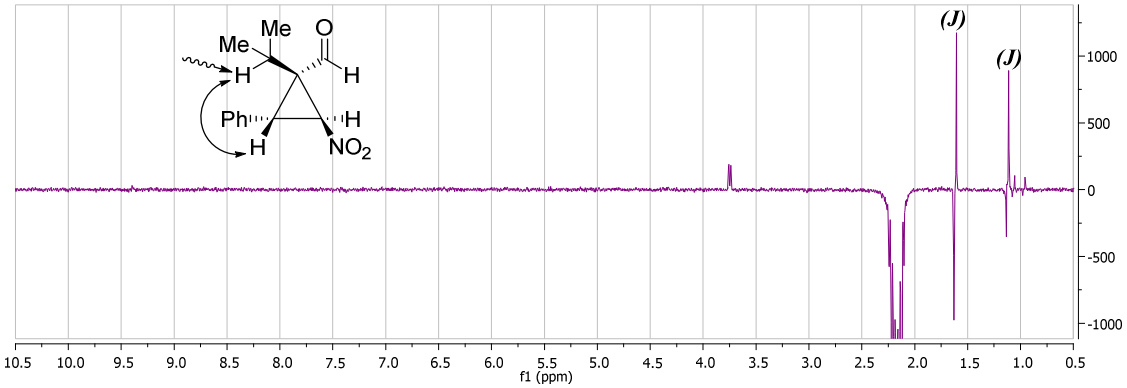
Me
O
Me
H
H
Ph
H
H
NO2
(J)
(J)
1000
500
0
-500
-1000
10.5 10.0 9.5 9.0 8.5 8.0 7.5 7.0 6.5 6.0 5.5 5.0 4.5 4.0 3.5 3.0 2.5 2.0 1.5 1.0 0.5
f1 (ppm)

Here we present the irradiated spectra of **5Ac'**. The relative configuration deduced from the observed nOe signals is in agreement with the configuration obtained with X-ray diffraction for the cyclopropane **5Cc'**.

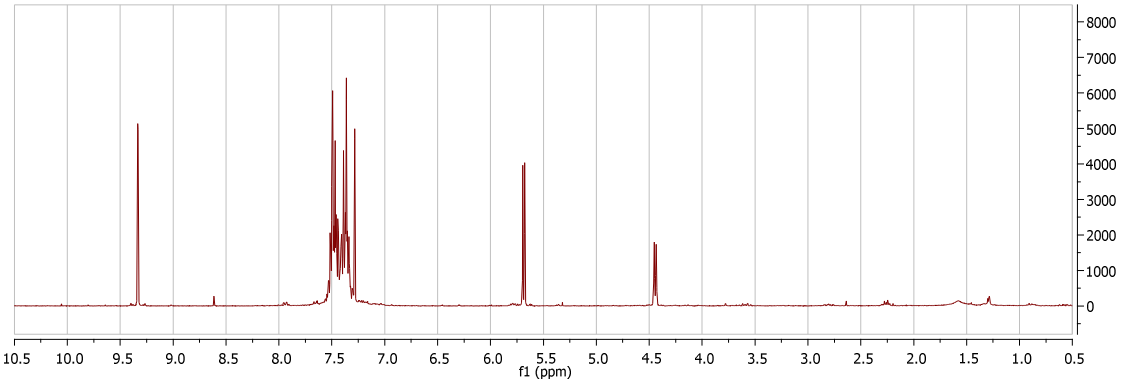

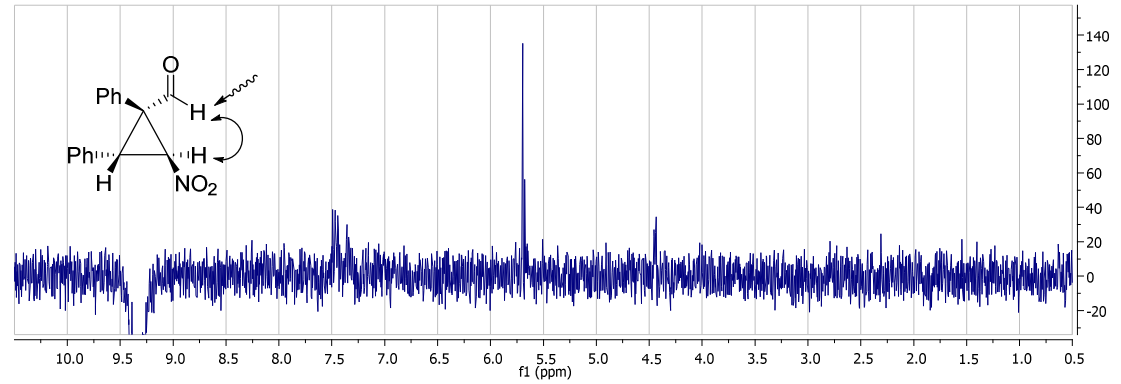

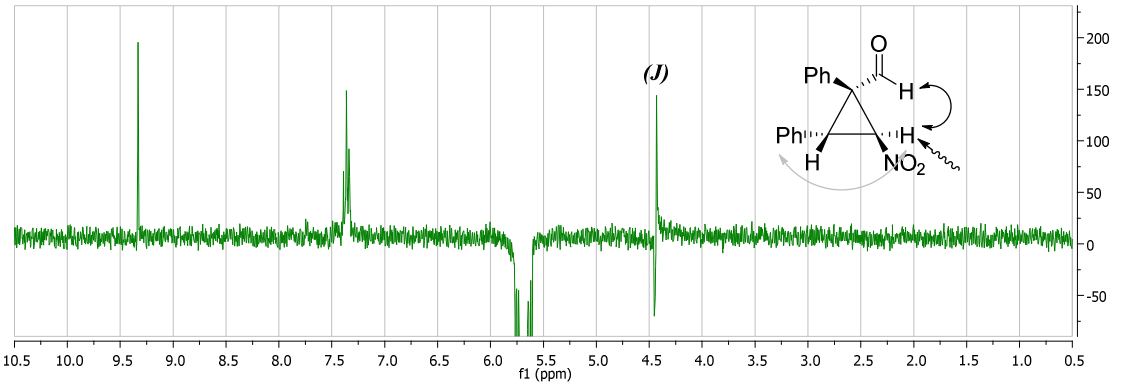

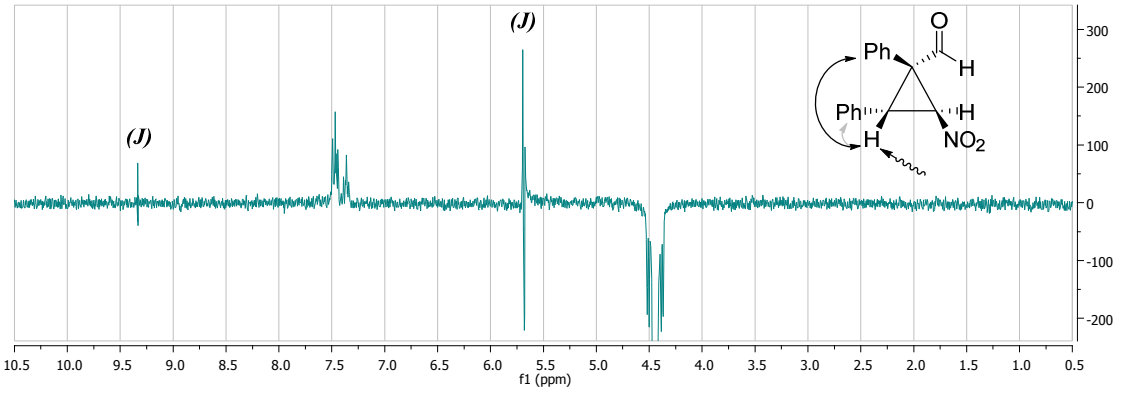

4. Computational details

General Methods for DFT calculations

Quantum chemistry calculations were carried out using the density functional theory (DFT). In particular, geometry optimizations were performed using the M06 functional[4] in combination with the 6-31G(d,p) basis set including dichloromethane (ε = 8.93) solvent effects with the solvation model density (SMD) continuum solvation model.[5] Harmonic vibrational frequencies have been also evaluated at the same level to characterize minima and transition states in the potential energy surface. Transition states have been connected to products by optimization of geometries slightly modified from the transition states. More accurate values of the energy were obtained with the same functional and solvent correction by employing the larger 6-311++G(d,p) basis over the geometry previously optimized. All the energies given in the text are the Gibbs energies in solution found at that level of theory, which were calculated by adding thermal and entropic corrections to the SMD energies. All the calculations were performed using the Gaussian09 program.[6]

[4] Y. Zhao and D.G. Truhlar *Theor Chem Account*, **2006**, *120* 215

[5] Marenich, A. V.; Cramer, C. J.; Truhlar, D. G. *J. Phys. Chem. B* **2009**, *113*, 6378−6396.

[6] Frisch, M. J.; Trucks, G. W.; Schlegel, H. B.; Scuseria, G. E.; Robb, M. A.; Cheeseman, J. R.; Scalmani, G.; Barone, V.; Mennucci, B.; Petersson, G. A.; Nakatsuji, H.; Caricato, M.; Li, X.; Hratchian, H. P.; Izmaylov, A. F.; Bloino, J.; Zheng, G.; Sonnenberg, J. L.; Hada, M.; Ehara, M.; Toyota, K.; Fukuda, R.; Hasegawa, J.; Ishida, M.; Nakajima, T.; Honda, Y.; Kitao, O.; Nakai, H.; Vreven, T.; Montgomery, J. A., Jr.; Peralta, J. E.; Ogliaro, F.; Bearpark, M.; Heyd, J. J.; Brothers, E.; Kudin, K. N.; Staroverov, V. N.; Kobayashi, R.; Normand, J.; Raghavachari, K.; Rendell, A.; Burant, J. C.; Iyengar, S. S.; Tomasi, J.; Cossi, M.; Rega, N.; Millam, N. J.; Klene, M.; Knox, J. E.; Cross, J. B.; Bakken, V.; Adamo, C.; Jaramillo, J.; Gomperts, R.; Stratmann, R. E.; Yazyev, O.; Austin, A. J.; Cammi, R.; Pomelli, C.; Ochterski, J. W.; Martin, R. L.; Morokuma, K.; Zakrzewski, V. G.; Voth, G. A.; Salvador, P.; Dannenberg, J. J.; Dapprich, S.; Daniels, A. D.; Farkas, Ö.; Foresman, J. B.; Ortiz, J. V.; Cioslowski, J.; Fox, D. J. Gaussian 09, Revision A.1; Gaussian, Inc.: Wallingford, CT, 2009

Thermodynamic evaluation of different phenyl-Isopropyl reactive species generated by rotation of isopropyl group

For the starting compounds that are intermediate precursors to the cyclopropane products containing phenyl and isopropyl groups, two different dispositions of $CH(CH_3)_2$ fragments have been considered. Below are represented the optimized structures and the energy values found. Structures inside frames are the most stable ones, and therefore, the considered starting points in the mechanism proposed.

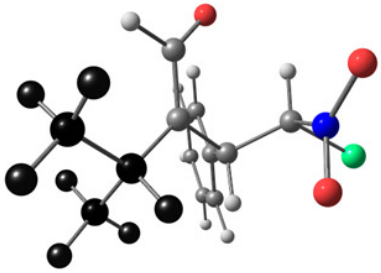

IV (^{i}Pr) (less stable)
-3358.3502797 (+ 0.4 kcal/mol)

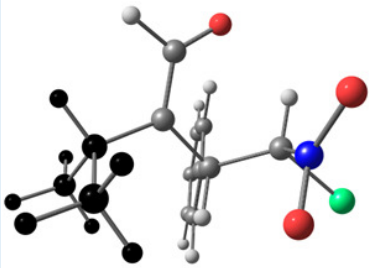

IV (^{i}Pr)
-3358.350889 (0.0Kcal/mol)

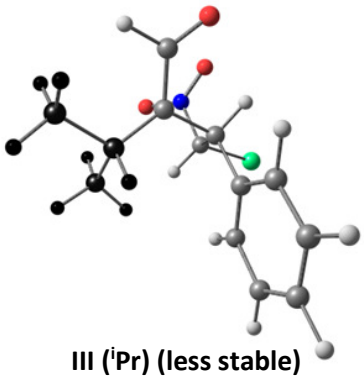

III (^{i}Pr) (less stable)
-3358.341786 (+5.7 Kcal/mol)

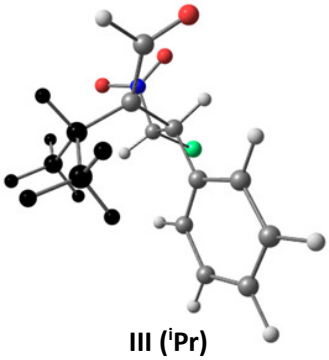

III (^{i}Pr)
-3358.344781 (+3.8 Kcal/mol)

Angewandte Chemie
Eine Zeitschrift der Gesellschaft Deutscher Chemiker

Supporting Information

Visible-Light Photocatalytic Intramolecular Cyclopropane Ring Expansion

*Javier Luis-Barrera, Víctor Laina-Martín, Thomas Rigotti, Francesca Peccati, Xavier Solans-Monfort, Mariona Sodupe, Rubén Mas-Ballesté, Marta Liras, and José Alemán**

anie_201703334_sm_miscellaneous_information.pdf

Table of Contents

1. General Methods and Starting Materials

Toluene, acetonitrile and dichloromethane were purified by passing through a Pure Solv™ column drying system from Innovative Technology, Inc. N,N-Dimethylformamide (DMF), nitromethane, dimethylsulfoxide (DMSO), and chloroform were acquired from commercial sources. All photocatalysts **3** were purchased from commercial suppliers without further purification. For thin layer chromatography (TLC) silica gel plates with fluorescence indicator 254 nm were used and compounds were visualized by irradiation with UV light and/or by treatment with a solution of phosphomolybdic acid in EtOH followed by heating. Flash column chromatography was performed using pore 60 Å, 40-63 μm silica gel and compressed air. Celite® 512 medium was used for some filtration. Cyclohexane and Ethyl Acetate were acquired from commercial sources and were used without previous purification. Optical rotation was recorded in cells with 10 cm path length; the specific solvents and concentrations (in g/100 mL) are indicated. NMR spectra were acquired on a *Bruker Avance 300 MHz spectrometer*, running at 300 and 75 MHz for ^{1}H and ^{13}C, respectively (In some indicated cases they were acquired on a *Bruker DRX 500 MHz*, running at 500 and 125 MHz). Chemical shifts (δ) are reported in ppm relative to residual solvent signals ($CDCl_3$, 7.26 ppm for ^{1}H NMR and 77.2 ppm for ^{13}C NMR respectively). ^{13}C NMR spectra were acquired on a broad band decoupled mode. The following abbreviations are used to describe peak patterns when appropriate: s (singlet), d (doublet), t (triplet), q (quartet), quint (quintet), sept (septuplet), m (multiplet), bs (broad singlet). Different methods have been used for measuring the exact mass (indicated for each case): MS (ESI) (Electrospray mass spectroscopy) acquired with an *Agilent Technologies 6120 Quadrupole LC/MS*; MS (EI) (Electron Ionization mass spectroscopy) acquired with an *Agilent Technologies 5977B MSD*, in these two techniques *MassWorks software ver. 4.0.0.0 (Cerno Bioscience*) was used for the formula identification. *MassWorks* is a MS calibration software which calibrates for isotope profile as well as for mass accuracy allowing highly accurate comparisons between calibrated and theoretical spectra;[1] MS (TOF-ESI) (Electrospray mass spectroscopy with Time-of-flight detector) acquired with *QSTAR ABSciex.*

Enantiomeric excess was determined with Supercritical Fluid Chromatography (SFC) with chiral columns. The chromatograms were acquired with an *Agilent Technologies 1260*

[1] a) Y. Wang, M. Gu, *Anal. Chem.* **2010**, *82*, 7055-7062. b) Y. Wang, Methods for Operating MS Instrument Systems, United States Patent No. 6,983,213, **2006**. c) N. Ochiaia, K. Sasamoto, K. MacNamara, *Journal of Chromatography A*, **2012**, *1270*, 296-304. d) H.-P. Ho, R.-Y. Lee, C.-Y. Chen, S.-R. Wang, Z.-G. Li, M.-R. Lee, *Rapid Commun. Mass Spectrom.* **2011**, *25*, 25-32.

Infinity with a *SFC module* and a UV-vis detector with chiral columns Chiralpack IA, IB-3, IC, ID-3, IG-3 (see in each case).

Optically enriched nitrocyclopropanecarbaldehydes **1a**, **1b**, **1c**, **1d**, **1e, 1g** and **1f** were synthesized following a procedure described in the literature by us,[2] and **1g**-**1h** [3] and *rac*-**8**[4] by others**.**

[2] J. Luis-Barrera, R. Mas-Ballesté, J. Alemán, *ChemPlusChem* **2015**, *80*, 1595-1600.
[3] J. Vesely, G.-L. Zhao, A. Bartoszewicz, A. Córdova, *Tetrahedron Lett.* **2008***, 49*, 4209-4212
[4] H. Yu, Q. Wang, Y. Wang, H. Song, Z. Zhou, C. Tang, *Chem. Asian J.* **2013**, *8*, 2859-2863

2. Screening of different conditions in the ring-expansion process

General procedure for the optimization: The corresponding photocatalyst **3** (0.025 mmol), was transferred to a Schlenk tube followed by cyclopropane **1a** (0.1mmol) dissolved in 1 mL of the corresponding solvent. The mixture was degassed by "freeze-pump-thaw" cycles (x3). The reaction was irradated with a household light bulb and was stirred during the indicated time. The conversion was meassured by ^{1}H-NMR.

Table S1. Screening of different photocatalyst **3** in the ring-expansion process.

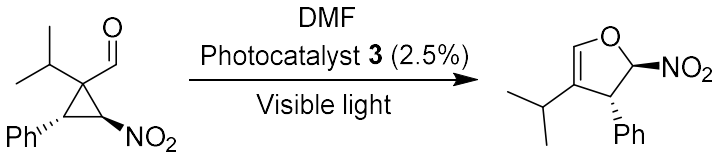

1a **2a**

Entry	Photocatalyst	Conversion (4h)	Conversion (21h)
1	$Ir(ppy)_3$ **3a**	11%	27%
2	$Ir(dFppy)_3$ **3b**	18%	>98%
3	$Ir(ppy)_2(bpy)PF_6$ **3c**	-[a]	-[a]
4	$Ir\{dF(CF_3)ppy\}_2(dtbbpy)PF_6$ **3d**	-[a]	-[a]
5	$Ru(bpy)Cl_2$ **3e**	-[a]	-[a]
6	$AcrMesClO_4$ **3f**	-[a]	-[a]
7	Eosyn Y **3g**	-[a]	-[a]
8	Rose Bengal **3h**	-[a]	-[a]

[a] The cyclopropane **1a** was unaltered recovered.

First, we studied the reaction with the aldehyde **1a** using different photocatalysts such as acridinium salts, eosin Y and different iridium and ruthenium complexes (see Table S1.). Only two iridium complexes were active, and **3b** ($Ir(dFppy)_3$) allowed higher conversion than **3a** ($Ir(ppy)_3$) at the same reaction conditions (entries 1 and 2, Table S2). Different solvents were studied (entries 3-8). The conversion to **2a** in DMF was higher (>98 % after 21 hours) than when using some of the standard solvents used in photochemistry, such as CH_3CN, $MeNO_2$ and DMSO. Interestingly, better results were achieved using dichloromethane (entry 8), resulting in full conversion to dihydrofurane **2a**. Different wavelengths were also studied, using **3b** as catalyst

and CH_2Cl_2 as solvent (entries 9, 10). Blue-light (λ_{max}= 450 nm) increased the reaction rate (compare entries 8 and 10). The reaction time was improved when the light was directly irradiated into the reaction media through a glass bar, achieving full conversion after 4h (entry 11, see S.I. for more details). In this case, the catalyst loading was reduced to 1 mol %, but 21 hours were needed to obtain full conversion (entry 12). In all the cases, we observed complete diastereoselectivity (d.r.>98:2).

Table S-2. Optimization of reaction conditions for the ring-expansion reaction.[a]

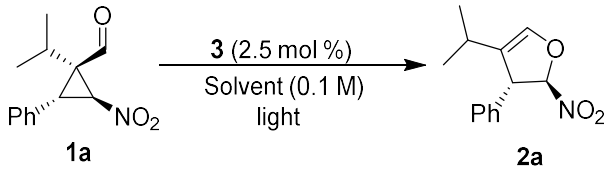

1a 2a

Entry	Catalyst	Solvent	Light	Conversion (%)[b] (4h)	Conversion (%)[b] (21h)
1	**3a**	DMF	White light	11	27
2	**3b**	DMF	White light	18	>98
3	**3b**	CH_3CN[c]	White light	<5	25
4	**3b**	CH_3NO_2[c]	White light	5	24
5	**3b**	DMSO	White light	18	66
6	**3b**	Toluene	White light	25	83
7	**3b**	$CHCl_3$	White light	13	58
8	**3b**	CH_2Cl_2	White light	36	>98
9	**3b**	CH_2Cl_2	Black light	10	39
10	**3b**	CH_2Cl_2	Blue leds	50	>98
11	**3b**	**CH_2Cl_2**	**Blue[d] light[e]**	**>98**	**-**
12	**3b**[e]	CH_2Cl_2	Blue[d] light[e,f]	74	>98

[a] All the reactions were performed at 0.1 mmol scale in 1.0 mL solvent. [b] Determined by ^{1}H NMR analysis of the crude mixture after 4 and 21 hours. [c] Starting Material **1a** partially insoluble in this solvent [d] Blue light irradiated in the reaction media via glass bar (see next section for more details). [e] 1 mol % of catalyst was used.

Structure of photocatalysts used in the Table S1

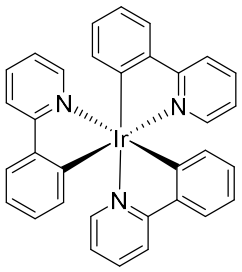

3a $Ir(ppy)_3$

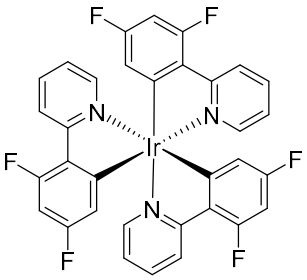

3b $Ir(dFppy)_3$

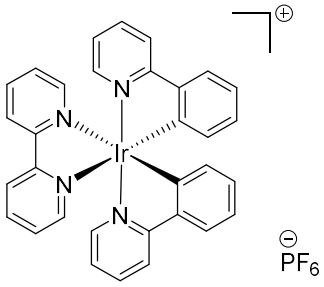

3c $Ir(ppy)_2(bpy)PF_6$

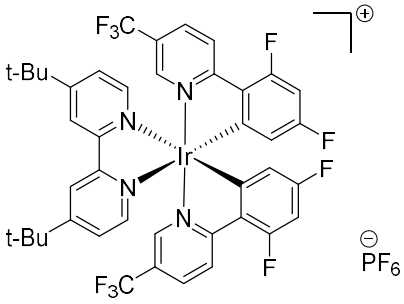

3d $Ir\{dF(CF_3)ppy\}_2(dtbbpy)PF_6$

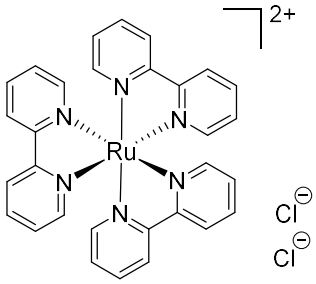

3e $Ru(bpy)_3Cl_2$

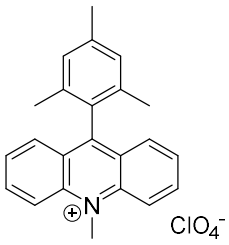

3f $(Acr\text{-}Mes)ClO_4$

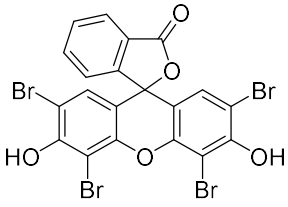

3h Esosin Y

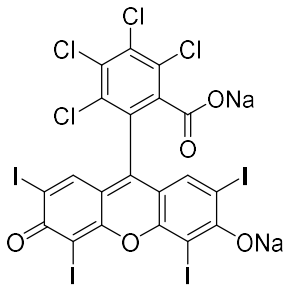

3h Rose Bengal

3. Irradiation system.

In the optimized reaction conditions, the blue light is irradiated inside de solution using the next system. A glass bar transmits the blue light from the LED to the reaction media.

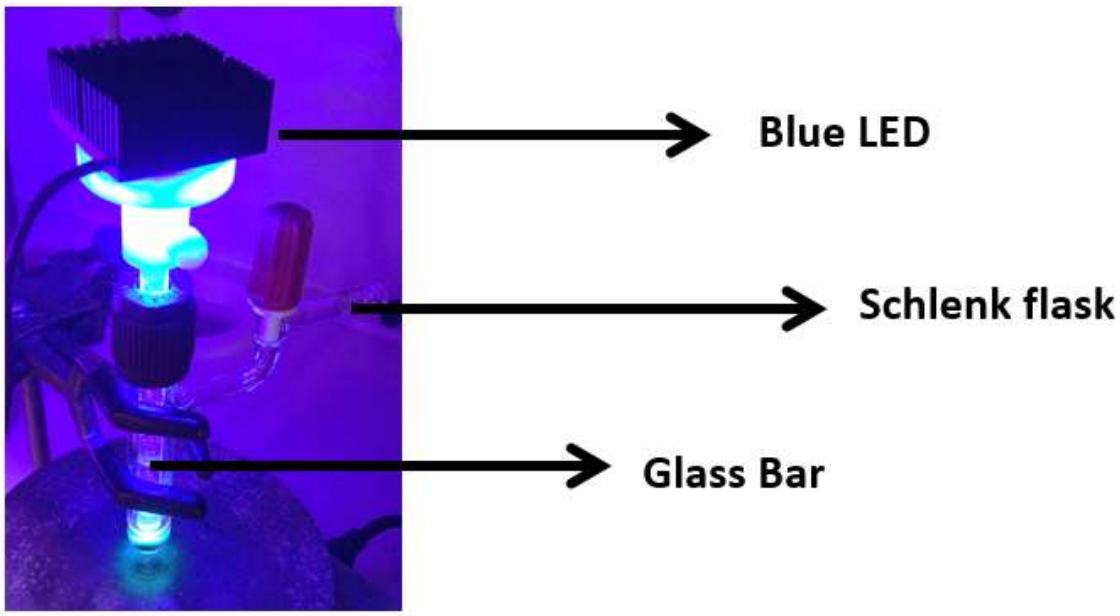

4. Synthesis and characterization data of dihydrofuranes 2

General procedure for the synthesis of dihydrofuranes (2)

The photocatalyst tris[2-(4,6-difluorophenyl)pyridinato-C2,N]iridium(III) **3b** (0.0025 mmol), was transferred to a Schlenk tube followed by the corresponding nitrocyclopropanecarbaldehyde **1** (0.1 mmol) dissolved in 1 mL of CH_2Cl_2. The mixture was degassed by "freeze-pump-thaw" cycles (x3), the photoreactor (blue LEDs) was switched on and the reaction mixture was stirred during the indicated time. In the end, after removal of the solvent, the crude mixture was purified through filtration over Celite 512® or by flash chromatography (cyclohexane : ethyl acetate).

(2*R*,3*R*)-4-Isopropyl-2-nitro-3-phenyl-2,3-dihydrofuran (2a)

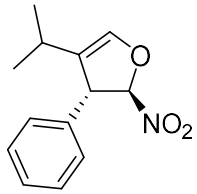

2a

The product was obtained following the general procedure starting from **1a** after 4h of irradiation. The final filtration over celite afforded the pure product **2a** as a pale yellow oil (86% yield). $[\alpha]^{20}_D$ = - 213.1 (*c* = 0.765, $CHCl_3$). **^{1}H-NMR:** δ 7.42-7.32 (m, 3H), 7.26-7.20 (m, 2H), 6.45 (t, *J* = 1.6 Hz, 1H), 5.72 (d, *J* = 1.9 Hz, 1H), 4.30 (m, 1H), 2.22-2.06 (m, 1H), 1.05 (d, *J* = 6.8 Hz, 3H), 0.94 (d, *J* = 6.9 Hz, 3H) ppm. **^{13}C-NMR:** δ 138.8, 137.5, 129.3, 128.3, 127.5, 127.0, 111.9, 57.3, 24.3, 21.9, 20.9 ppm. **MS (EI):** calculated for $C_{13}H_{14}O^+$ $[M -H,-NO_2]^+$: 186.1039; found: 186.1029. The enantiomeric excess was determined by SFC using a Chiralcell IA column: CO_2/MeOH 97:3, flow rate 3.0 mL/min, τ_{major} = 1.95 min, τ_{minor} = 2.45 min, **ee** = 97%.

(2*R*,3*R*)-4-Isopropyl-3-(4-methoxyphenyl)-2-nitro-2,3-dihydrofuran (2b)

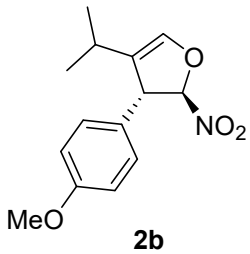

2b

The product was obtained following the general procedure starting from **1b** after 4h of irradiation. The crude reaction mixture was purified by flash chromatography affording the product **2b** as a pale yellow oil (82% yield). $[\alpha]^{20}_D$ = - 181.2 (*c* = 0.46, $CHCl_3$). **^{1}H-NMR:** δ 7.14 (d, *J* = 8.6 Hz, 2H), 6.90 (d, *J* = 8.6 Hz, 2H), 6.42 (d, *J* = 1.4 Hz, 1H), 5.68 (d, *J* = 1.6 Hz, 1H), 4.25 (m, 1H), 3.74 (s, 3H), 2.22-2.06 (m, 1H), 1.04 (d, *J* = 6.8 Hz, 3H), 0.94 (d, *J* = 6.9 Hz, 3H) ppm. **^{13}C-NMR:** δ 138.6, 130.1, 129.4, 128.6, 127.0, 114.6, 112.1, 56.7, 55.3, 24.3, 21.9, 20.9 ppm. **MS (TOF-ESI):** calculated for $C_{14}H_{17}O_2^+$ $[M -NO_2]^+$: 217.1223; found: 217.1221. The enantiomeric excess was determined by SFC using a Chiralcell IA column: CO_2/MeOH 97:3, flow rate 3.0 mL/min, τ_{major} = 2.47 min, τ_{minor} = 3.04 min, **ee** = 90%.

(2*R*,3*R*)-3-(4-Bromophenyl)-4-isopropyl-2-nitro-2,3-dihydrofuran (2c)

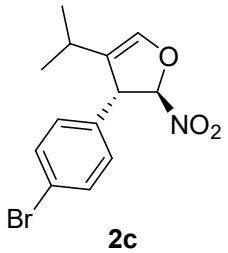

2c

The product was obtained following the general procedure starting from **1c** after 4h of irradiation. The final filtration over Celite afforded the pure product **2c** as a pale yellow oil (84% yield). $[\alpha]^{20}_{D}$ = - 97.9 (*c* = 0.58, $CHCl_3$). **^{1}H-NMR:** δ 7.52 (d, *J* = 8.5 Hz, 2H), 7.12 (d, *J* = 8.4 Hz, 2H), 6.46 (t, *J* = 1.6 Hz, 1H), 5.67 (d, *J* = 1.8 Hz, 1H), 4.27 (m, 1H), 2.21-2.06 (m, 1H), 1.04 (d, *J* = 6.8 Hz, 3H), 0.94 (d, *J* = 6.9 Hz, 3H) ppm. **^{13}C-NMR:** δ 139.2, 136.5, 132.4, 129.1, 126.6, 122.4, 111.3, 56.7, 24.3, 21.9, 20.9 ppm. **MS (EI):** calculated for $C_{13}H_{13}BrO^+$ [M -H,-NO_2]$^+$: 264.0144; found: 264.0198. The enantiomeric excess was determined by SFC using a Chiralcell IA column: CO_2/MeOH 97:3, flow rate 3.0 mL/min, τ_{major} = 2.83 min, τ_{minor} = 3.40 min, **ee** = 94%.

(2*R*,3*R*)-2-Nitro-3-phenyl-4-propyl-2,3-dihydrofuran (2d)

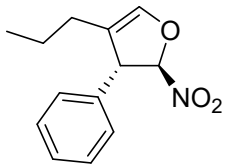

2d

The product was obtained following the general procedure starting from **1d** after 4h of irradiation. The final filtration over Celite afforded the pure product **2d** as a pale yellow oil (98% yield). $[\alpha]^{20}_{D}$ = - 191.4 (*c* = 0.84, $CHCl_3$). **^{1}H-NMR:** δ 7.36-7.27 (m, 3H), 7.20-7.12 (m, 2H), 6.40 (m, 1H), 5.66 (d, *J* = 1.8 Hz, 1H), 4.15 (m, 1H), 1.92-1.72 (m, 2H), 1.42-1.18 (m, 2H), 0.78 (t, *J* = 7.3 Hz, 3H) ppm. **^{13}C-NMR:** δ 139.7, 137.2, 129.3, 128.3, 127.5, 120.2, 111.6, 58.1, 25.9, 20.8, 13.6 ppm. **MS (TOF-ESI):** calculated for $C_{13}H_{15}O$ [M-NO_2]$^+$: 187.1117; found: 187.1115. The enantiomeric excess was determined by SFC using a Chiralcell IA column: CO_2/MeOH 97:3, flow rate 3.0 mL/min, τ_{major} = 2.16 min, τ_{minor} = 2.85 min, **ee** = 95%.

(*2R,3R*)-2-Nitro-3,4-diphenyl-2,3-dihydrofuran (2e)

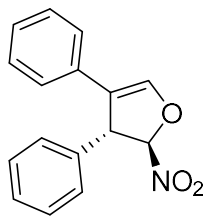

2e

The product was obtained following the general procedure starting from **1e** after 20 minutes, and the crude was purified by FC (9:1 cyclohexane : ethyl acetate), affording the pure product as a yellow oil (51% yield based on a conversion of 52% by ^{1}H-NMR). $[\alpha]^{20}_{D}$ = - 180.5 (*c* = 0.60, $CHCl_3$). **^{1}H-NMR:** δ 7.40 – 7.13 (m, 11H), 5.80 (d, *J* = 1.7 Hz, 1H), 4.81 (t, *J* = 1.7 Hz, 1H) ppm. **^{13}C-NMR:** δ 141.5, 137.1, 130.3, 129.6, 128.9, 128.7, 127.6 (x2), 125.6, 120.2, 111.9, 56.7 ppm. **MS (EI):** calculated for $C_{16}H_{12}O^+$ [M -H, -NO_2]$^+$: 220.0883; found: 220.0926. The enantiomeric excess was determined by SFC using a Chiralcell IA column: CO_2/MeOH 90:10, flow rate 2.0 mL/min, τ_{major} = 4.5 min, τ_{minor} = 5.3 min, **ee** = 92%.

(*2R,3R*)-3-(4-Bromophenyl)-2-nitro-4-phenyl-2,3-dihydrofuran (2f)

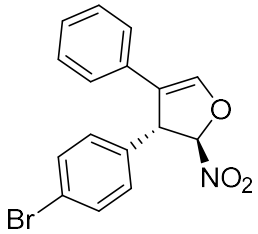

2f

The product was obtained following the general procedure starting from **1e** after 20 minutes, and the crude was purified by FC (9:1 cyclohexane : ethyl acetate), affording the pure product as a yellow oil (57% yield based on a conversion of 60% by ^{1}H-NMR). **$[\alpha]^{20}_D$** = - 26.5 (*c* = 0.23, $CHCl_3$). **^{1}H-NMR:** δ 7.51 (d, *J* = 8.5 Hz, 2H), 7.28 – 7.10 (m, 8H), 5.76 (d, *J* = 1.7 Hz, 1H), 4.78 (bs, 1H) ppm. **^{13}C-NMR:** δ 141.6, 135.9, 132.7, 129.8, 129.2, 128.9, 127.7, 125.4, 122.7, 119.7, 111.3, 55.9 ppm. **MS (EI):** calculated for $C_{16}H_{11}OBr^+$ [M -H, -NO_2]$^+$: 297.9988; found: 298.0061. The enantiomeric excess was determined by SFC using a Chiralcell IB-3 column: CO_2/MeOH 97:3, flow rate 2.0 mL/min, τ_{minor} = 2.0 min, τ_{major} = 2.5 min, **ee** = 88%.

(2*R*,3*S*)-2-Nitro-3-phenyl-2,3-dihydrofuran (2g)

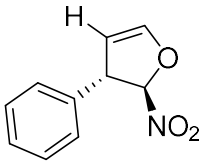

2g

Following the general procedure described above, the compound was obtained in 78% yield as a yellow oil (time 21h). The crude was purified by flash column chromatography cyclohexane:AcOEt (9:1 → 7:3) as eluent. $[\alpha]^{20}_D$ = - 81.7 (*c* = 0.75, $CHCl_3$). **^{1}H-NMR:** δ 7.44-7.31 (m, 3H), 7.30-7.24 (m, 2H), 6.77 (t, *J* = 2.3 Hz, 1H), 5.80 (d, *J* = 2.1 Hz, 1H), 5.41 (t, *J* = 2.8 Hz, 1H), 4.45 (q, *J* = 2.2 Hz, 1H). **^{13}C-NMR**: δ 145.8, 137.9, 129.2, 128.4, 127.2, 110.9, 105.3, 55.5. **MS (EI):** calculated for $C_{10}H_8O^+$ [M –H, -NO_2]$^+$: 144.0570; found: 144.0560. The enantiomeric excess was determined by SFC using Chiralpak IA column [CO_2/MeOH (97:3)]; flow rate 3 ml/min; τ_{major} = 2.7 min, τ_{minor} = 3.1 min. (*ee* = 76 %).

(2*R*,3*R*)-2-Nitro-3-propyl-2,3-dihydrofuran (2h)

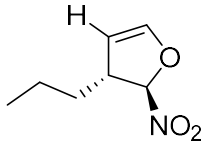

2h

Following the general procedure described above, the compound was obtained in 86% yield as a yellow oil (time 48h). The crude was purified by flash column chromatography using 9:1 cyclohexane:AcOEt as eluent in 86% yield. $[\alpha]^{20}_D$ = - 11.2 (*c* = 0.60, $CHCl_3$). **^{1}H-NMR:** δ 6.51 (t, *J* = 2.3 Hz, 1H), 5.67 (d, *J* = 2.1 Hz, 1H), 5.22 (t, *J* = 2.8 Hz, 1H), 3.26 – 3.17 (m, 1H), 1.55 – 1.39 (m, 4H) 0.97 (t, *J* = 7.0 Hz, 3H). **^{13}C-NMR:** δ 144.6, 109.8, 105.9, 50.5, 36.0, 19.8, 13.8. The enantiomeric excess could not be determined because the lack of UV active groups of **2h**. However, the optical activity of the sample demonstrates that the compuound **2h** is enantiomerically enriched. **MS (EI):** calculated for $C_7H_{11}O^+$ [M, -NO_2]$^+$: 111.0804; found: 111.0881.

6. Synthesis and characterization data of vinylcyclopropanes 4

General procedure for the synthesis of vinylcyclopropanes (4)

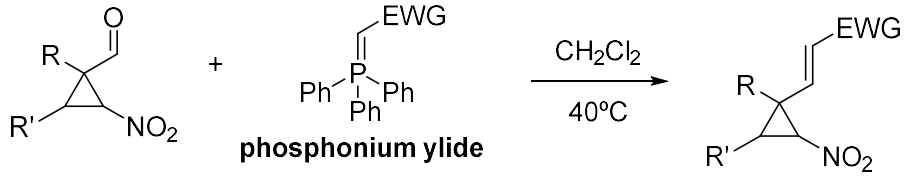

In a vial charged with a magnetic stir bar the corresponding nitrocyclopropane **1g** (0.2 mmol) and the phosphonium ylide (0.4 mmol) were dissolved in 2 mL of dry CH_2Cl_2. The reaction was stirred at 40ºC during 24h. Then, the solvent was evaporated under reduced pressure and the crude reaction mixture was purified by FC (cyclohexane : ethyl acetate).

Methyl (*E*)-3-((*1R/1S,2S,3R*)-1-isopropyl-2-nitro-3-phenylcyclopropyl)acrylate (4a)

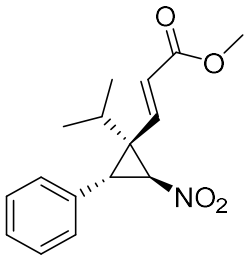

4a

The product was obtained following the general procedure starting from **1a** and methyl (triphenylphosphoranylidene)acetate and the crude was purified by FC (15:1 cyclohexane : ethyl acetate), affording the pure product as a yellow oil (66% yield, *d.r.* = 72:28). **$[\alpha]^{20}_D$** = + 41.5 (*c* = 4.05, $CHCl_3$). **Major diastereomer (*1R,2S,3R*) ^{1}H-NMR:** δ 7.52 – 7.33 (m, 5H), 7.08 (d, *J* = 15.7 Hz, 1H), 6.36 (d, *J* = 15.7 Hz, 1H), 4.86 (d, *J* = 4.9 Hz, 1H), 3.91 (m, 4H), 1.46 – 1.31 (m, 1H), 1.26 (d, *J* = 6.6 Hz, 3H), 0.79 (d, *J* = 6.5 Hz, 3H) ppm. **^{13}C-NMR:** δ 165.9, 139.6, 132.0, 128.7, 128.5, 127.8, 127.2, 69.0, 51.9, 46.6, 37.7, 30.7, 19.5, 18.4 ppm. **Minor diastereomer (*1S,2S,3R*) ^{1}H-NMR:** δ 7.52 – 7.33 (m, 5H), 6.83 (d, *J* = 15.8 Hz, 1H), 5.96 (d, *J* = 15.8 Hz, 1H), 5.02 (d, *J* = 5.0 Hz, 1H), 3.79 (s, 3H), 3.64 (d, *J* = 5.1 Hz, 1H), 2.27 (hept, *J* = 7.0 Hz, 1H), 1.39 (d, *J* = 6.9 Hz, 3H), 1.00 (d, *J* = 6.8 Hz, 3H) ppm. **^{13}C-NMR:** δ 165.9, 140.8, 132.2, 128.8, 128.1, 127.7, 126.1, 69.5, 51.8, 46.9, 38.1, 31.0, 19.9, 18.9 ppm. **MS (TOF-ESI):** calculated for $C_{16}H_{20}NO_4^+$ $[M+H]^+$: 290.1386; found: 290.1394.

Methyl (*E*)-3-((*1R/1S,2R,3S*)-1-isopropyl-2-(4-methoxyphenyl)-3-nitrocyclopropyl)acrylate (4b)

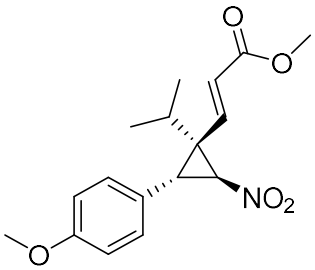

4b

The product was obtained following the general procedure starting from **1b** and methyl (triphenylphosphoranylidene)acetate and the crude was purified by FC (9:1 cyclohexane : ethyl acetate), affording the pure product as a yellow oil (84% yield, *d.r.* = 75:25). **$[\alpha]^{20}_D$** = + 19.2 (*c* = 0.64, $CHCl_3$). **Major diastereomer (*1R,2S,3R*) ^{1}H-NMR:** δ 7.32 – 6.84 (m, 4H), 6.98 (d, *J* = 15.7 Hz, 1H), 6.24 (d, *J* = 15.7 Hz, 1H), 4.70 (d, *J* = 4.9 Hz, 1H), 3.85 (s, 3H), 3.82 (s, 3H), 3.77 (d, *J* = 4.8 Hz, 1H), 1.32 – 1.21 (m, 1H), 1.17 (d, *J* = 6.5 Hz, 3H), 0.71 (d, *J* = 6.5 Hz, 3H) ppm. **^{13}C-NMR:** δ 165.9, 159.2, 139.7, 129.6, 127.0, 123.8, 114.2, 69.4, 55.3, 51.8, 46.6, 37.6, 30.6, 19.5, 18.5 ppm. **Minor diastereomer (*1S,2S,3R*) ^{1}H-NMR:** δ 7.32 – 6.84 (m, 4H), 6.75 (d, *J* = 15.8 Hz, 1H), 5.86 (d, *J* = 15.8 Hz, 1H), 4.87 (d, *J* = 5.0 Hz, 1H), 3.82 (s, 3H), 3.72 (s, 3H), 3.50 (d, *J* = 5.0 Hz, 1H), 2.16 (hept, *J* = 6.8 Hz, 1H), 1.32 – 1.21 (m, 3H), 0.91 (d, *J* = 6.8 Hz, 3H) ppm. **^{13}C-NMR:** δ 165.5, 159.1, 141.0, 129.3, 125.9, 124.2, 114.1, 69.8, 55.2, 51.7, 46.9, 38.4, 30.9, 19.9, 18.9 ppm. **MS (TOF-ESI):** calculated for $C_{17}H_{21}NO_5Na^+$ $[M+Na]^+$: 342.1311; found: 342.1314.

Methyl (*E*)-3-((*1R,2R,3S*)-2-(4-bromophenyl)-1-isopropyl-3-nitrocyclopropyl)acrylate (4c)

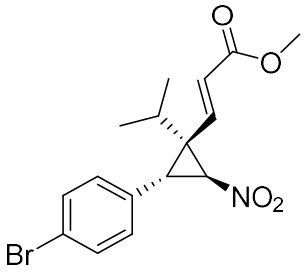

4c

The product was obtained following the general procedure starting from **1c** and methyl (triphenylphosphoranylidene)acetate and the crude was purified by FC (9:1 cyclohexane : ethyl acetate), affording the pure product as an orange oil (62% yield). **$[\alpha]^{20}_D$** = + 49.3 (*c* = 7.40, $CHCl_3$). **^{1}H-NMR:** δ 7.56 – 7.09 (m, 4H), 6.93 (d, *J* = 15.7 Hz, 1H), 6.20 (d, *J* = 15.7 Hz, 1H), 4.69 (d, *J* = 4.9 Hz, 1H), 3.78 (s, 3H), 3.73 (d, *J* = 4.8 Hz, 1H), 1.28 – 1.17 (m, 1H), 1.14 (d, *J* = 6.0 Hz, 3H), 0.67 (d, *J* = 6.3 Hz, 3H) ppm. **^{13}C-NMR:** δ 165.7, 139.1, 131.9, 131.1, 130.1, 127.3, 121.9, 68.9, 51.9, 46.5, 37.0, 30.8, 19.4, 18.5 ppm. **MS (TOF-ESI):** calculated for $C_{16}H_{19}NO_4Br^+$ $[M+H]^+$: 368.0491; found: 368.0490.

Methyl (*E*)-3-((*1R/1S,2S,3R*)-2-nitro-3-phenyl-1-propylcyclopropyl)acrylate (4d)

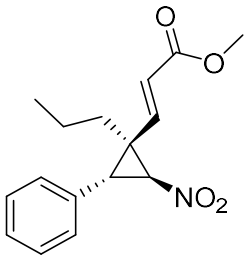

4d

The product was obtained following the general procedure starting from **1d** and methyl (triphenylphosphoranylidene)acetate and the crude was purified by FC (9:1 cyclohexane : ethyl acetate), affording the pure product as a colorless oil (42% yield, *d.r.* = 51:49). **$[\alpha]^{20}_D$** = + 52.7 (*c* = 0.62, $CHCl_3$). **Major diastereomer (*1R,2S,3R*) ^{1}H-NMR:** δ 7.32 – 7.02 (m, 5H), 6.93 (d, *J* = 15.9 Hz, 1H), 5.85 (d, *J* = 15.9 Hz, 1H), 4.69 (d, *J* = 5.2 Hz, 1H), 3.72 - 3.67 (m, 4H), 1.52 – 1.07 (m, 4H), 0.67 (t, *J* = 7.1 Hz, 3H) ppm. **^{13}C-NMR:** δ 166.2, 144.6, 132.0, 129.0, 128.9, 128.5, 123.7, 70.2, 51.8, 41.4, 39.0, 32.6, 19.4, 13.9 ppm. **Minor diastereomer (*1S,2S,3R*) ^{1}H-NMR:** δ 7.32 – 7.02 (m, 5H), 6.25 (d, *J* = 15.9 Hz, 1H), 6.03 (d, *J* = 15.8 Hz, 1H), 4.77 (d, *J* = 5.2 Hz, 1H), 3.58 (s, 3H), 3.54 (d, *J* = 5.3 Hz, 1H), 1.85 (t, *J* = 8.2 Hz, 2H), 1.52 – 1.07 (m, 2H), 0.89 (t, *J* = 7.3 Hz, 3H) ppm. **^{13}C-NMR:** δ 165.9, 143.6, 132.4, 128.9, 128.4, 127.9, 123.2, 70.1, 51.7, 41.5, 39.2, 31.9, 19.9, 14.0 ppm. **MS (TOF-ESI):** calculated for $C_{16}H_{20}NO_4^+$ $[M+H]^+$: 290.1386; found: 290.1397.

Methyl (*E*)-3-((1S,2S,3R)-2-nitro-1,3-diphenylcyclopropyl)acrylate (4e)

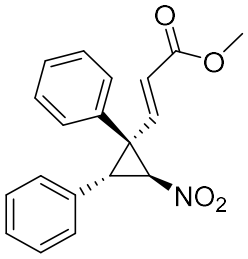

4e

The product was obtained following the general procedure starting from **1e** and methyl (triphenylphosphoranylidene)acetate and the crude was purified by FC (15:1 cyclohexane : ethyl acetate), affording the pure product as a yellow oil (54% yield). **$[\alpha]^{20}_D$** = + 183.2 (*c* = 3.75, $CHCl_3$). **^{1}H-NMR**: δ 7.38 – 7.19 (m, 10H), 6.30 (d, *J* = 15.5 Hz, 1H), 5.34 (d, *J* = 15.5 Hz, 1H), 5.05 (d, *J* = 5.2 Hz, 1H), 4.15 (d, *J* = 5.2 Hz, 1H), 3.51 (s, 3H) ppm. **^{13}C-NMR:** δ 164.1, 144.8, 132.5, 130.4, 127.8, 127.6, 127.5, 127.2, 127.0, 126.6, 123.0, 68.7, 49.9, 44.5, 36.7 ppm. **MS (TOF-ESI):** calculated for $C_{19}H_{17}NO_4Na^+$ $[M+Na]^+$: 346.1049; found: 346.1036.

Benzyl (*E*)-3-((*1R,2S,3R*)-1-isopropyl-2-nitro-3-phenylcyclopropyl)acrylate (4f)

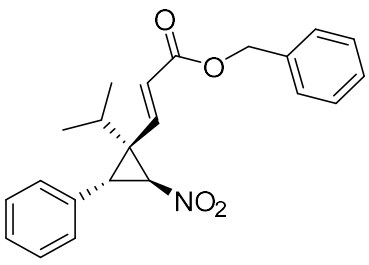

4f

The product was obtained following the general procedure starting from **1a** and benzyl(triphenylphosphoranylidene)acetate and the crude was purified by FC (19:1 cyclohexane : ethyl acetate), affording the pure product as a colorless oil (59% yield). **$[\alpha]^{20}_D$** = + 28.9 (*c* = 2.47, $CHCl_3$). **^{1}H-NMR:** δ 7.45 – 7.19 (m, 10H), 7.00 (d, *J* = 15.7 Hz, 1H), 6.27 (d, *J* = 15.7 Hz, 1H), 5.22 (d, *J* = 1.0 Hz, 2H), 4.72 (d, *J* = 4.9 Hz, 1H), 3.78 (d, *J* = 4.9 Hz, 1H), 1.24 (m, 1H), 1.13 (d, *J* = 6.6 Hz, 3H), 0.65 (d, *J* =

6.5 Hz, 3H) ppm. **^{13}C-NMR:** δ 165.3, 140.1, 135.8, 132.0, 128.8, 128.7, 128.6, 128.5, 127.9, 127.3, 69.1, 66.8, 46.8, 37.9, 30.8, 19.6, 18.5 ppm. **MS (EI):** calculated for $C_{22}H_{22}O_2^+$ [M –H, -NO_2]$^+$: 318.1614; found: 318.1688.

(*E*)-4-((1*S*,2*S*,3*R*)-1-Isopropyl-2-nitro-3-phenylcyclopropyl)but-3-en-2-one (4g)

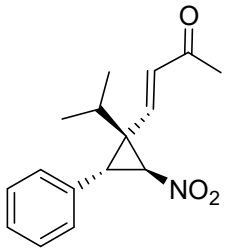

4g

The product was obtained following a modification of the general procedure starting from **1a** and stirring the reaction mixture for 96h at 110°C in 3mL of toluene with the 1-(triphenylphosphoranylidene)-2-propanone (3 eq). The crude was then purified by FC over Iatrobeads (cyclohexane : ethyl acetate), affording the pure product as a single diastereoisomer, since only the minor diastereosiomer of the starting cyclopropanecarbaldehyde reacted (48% yield based on a conversion of 23% by ^{1}H-NMR). **[α]$^{20}_D$** = + 61.583 (*c* = 0.695, $CHCl_3$). **^{1}H-NMR:** δ 7.34-7.24 (m, 3H), 7.10-7.04 (m, 2H), 6.48 (d, *J* = 16.1 Hz, 1H), 6.07 (d, *J* = 16.0 Hz, 1H), 4.90 (d, *J* = 5.0 Hz, 1H), 3.54 (d, *J* = 5.0 Hz, 1H), 2.23-2.11 (m, 1H), 2.08 (s, 3H), 1.26 (d, *J* = 6.9 Hz, 3H), 0.88 (d, *J* = 6.8 Hz, 3H) ppm. **^{13}C-NMR:** δ 196.6, 139.1, 134.9, 132.2, 128.7, 128.1, 127.8, 69.5, 46.8, 38.8, 30.9, 27.6, 19.9, 19.0 ppm. **MS (EI):** calculated for $C_{16}H_{19}NO_3^+$ [M]$^+$: 273.1359; found: 273.1312.

(*E*)-3-((*1R/1S,2S,3R*)-1-Isopropyl-2-nitro-3-phenylcyclopropyl)acrylonitrile (4h)

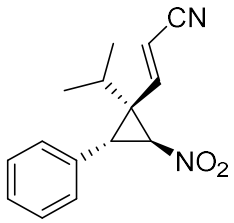

4h

The product was obtained following the general procedure starting from **1a** and (trimethylphosphoranylidene)acetonitrile and the crude was purified by FC (19:1 cyclohexane : ethyl acetate), affording the pure product as a colorless oil (76% yield, *d.r.* = 93:7). **[α]$^{20}_D$** = + 38.4 (*c* = 4.29, $CHCl_3$). **Major diastereomer (*1R,2S,3R*) ^{1}H-NMR:** δ 7.39 – 7.28 (m, 3H), 7.11 – 7.04 (m, 2H), 6.43 (d, *J* = 16.5 Hz, 1H), 5.30 (d, *J* = 16.5 Hz, 1H), 4.83 (d, *J* = 5.1 Hz, 1H), 3.54 (d, *J* = 5.1 Hz, 1H), 2.23 – 2.07 (m, 1H), 1.24 (d, *J* = 7.0 Hz, 3H), 0.90 (d, *J* = 6.8 Hz, 3H) ppm. **^{13}C-NMR:** δ 147.6, 131.5, 129.2, 128.3, 128.1, 116.1, 105.7, 69.0, 47.0, 38.7, 31.1, 19.9, 19.0 ppm. **Minor diastereomer (*1S,2S,3R*) ^{1}H-NMR:** δ 7.39 – 7.28 (m, 3H), 7.11 – 7.04 (m, 2H), 6.72 (d, *J* = 16.3 Hz, 1H), 5.75 (d, *J* = 16.1 Hz, 1H), 4.72 (d, *J* = 4.8 Hz, 1H), 3.74 (d, *J* = 4.9 Hz, 1H), 1.14 – 1.06 (m, 4H), 0.68 (d, *J* = 6.6 Hz, 3H) ppm. **MS (TOF-ESI):** calculated for $C_{15}H_{17}N_2O_2^+$ [M+H]$^+$: 257.1284; found: 257.1280.

Methyl (*E*)-3-((1*S*/1*R*,2*R*,3*S*)-2-nitro-3-phenylcyclopropyl)acrylate (4i)

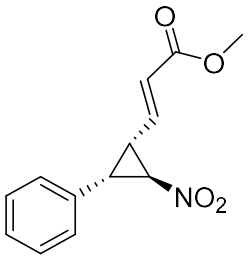

4i

The enantiomeric excess of **1g** was determined through derivatization to **4i.** The product was obtained following the general procedure starting from **1g** and methyl (triphenylphosphoranylidene)acetate and the crude was purified by FC (9:1 cyclohexane : ethyl acetate), affording the pure product as a yellow oil (86% yield, *d.r.* = 59:41). **Major diastereoisomer (1*S*,2*R*,3*S*): ^{1}H-NMR:** δ 7.40-7.30 (m, 3H), 7.24-7.18 (m, 2H), 6.23 (dd, *J* = 15.6, 9.8 Hz, 1H), 6.10 (d, *J* = 15.6 Hz, 1H), 4.79 (t, *J* = 3.8 Hz, 1H), 3.72-3.64 (m, 1H), 3.68 (s, 3H), 3.13 (td, *J* = 10.4, 3.4 Hz, 1H). **^{13}C-NMR (125 MHz, CD_3Cl):** δ 165.8, 140.5, 131.9, 129.2, 128.9, 128.4, 125.1, 65.2, 51.9, 35.3, 33.3. The enantiomeric excess was determined by HPLC using Chiralpak IB column [Hexanes/Isopropanol (95:5)]; flow rate 1 ml/min; τ_{major} = 15.2 min, τ_{minor} = 15.8 min. (*ee* = 76 %) $[\alpha]^{20}_{D}$ = + 19.1 (*c* = 0.59, $CHCl_3$). **Minor diastereoisomer (1*R*,2*R*,3*S*): ^{1}H-NMR:** δ 7.41-7.30 (m, 3H), 7.17-7.10 (m, 2H), 7.01 (dd, *J* = 15.7, 9.5 Hz, 1H), 6.16 (d, *J* = 15.7 Hz, 1H), 4.80 (dd, *J* = 8.2, 4.5 Hz, 1H), 3.76 (s, 3H), 3.55 (dd *J* = 7.7, 4.5 Hz, 1H), 2.63 (q, *J* = 8.1 Hz, 1H). **^{13}C-NMR:** δ 165.8, 139.9, 134.8, 129.2, 128.3, 126.8, 125.6, 67.0, 51.9, 34.4, 34.3. The enantiomeric excess was determined by HPLC using Chiralpak IB column [Hexanes/Isopropanol (95:5)]; flow rate 1 ml/min; $\boldsymbol{\tau_{major}}$ = 45.8 min, $\boldsymbol{\tau_{minor}}$ = 20.7 min. (*ee* = 76 %). $[\alpha]^{20}_{D}$ = + 27.7 (*c* = 0.59, $CHCl_3$) (for a diastereomeric mixture 1*S*:1*R* of 24:76) **MS (ESI):** calculated for $C_{13}H_{13}NO_4Na^+$ $[M+Na]^+$: 270.0737; found: 270.0740.

Benzyl (*E*)-3-((1*R*,2*R*,3*S*)-2-nitro-3-phenylcyclopropyl) (4j)

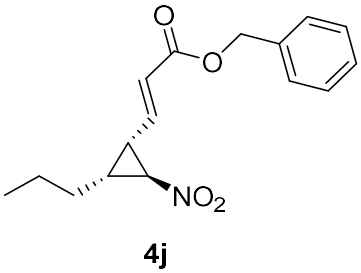

4j

The enantiomeric excess of **1h** was determined through derivatization to **4j**. The product was obtained following the general procedure starting from **1h** and benzyl(triphenylphosphoranylidene)acetate and the crude was purified by FC (19:1 cyclohexane : ethyl acetate), affording the pure product as a colorless oil (45% yield). **^{1}H-NMR:** δ 7.35 (s, *J* = 11.4 Hz, 5H), 6.61 (dd, *J* = 15.5, 9.8 Hz, 1H), 6.14 (d, *J* = 15.5 Hz, 1H), 5.19 (s, 2H), 4.20 (t, *J* = 3.6 Hz, 1H), 2.84 (td, *J* = 9.8, 3.6 Hz, 1H), 2.42 – 2.29 (m, 1H), 1.58 – 1.39 (m, 4H), 0.73 (t, *J* = 6.7 Hz, 3H) ppm. **^{13}C-NMR:** δ 165.3, 141.2, 135.7, 128.6, 128.4, 128.3, 124.9, 66.5, 65.9, 32.1, 31.9, 28.4, 21.8, 13.5 ppm. **MS (EI):** calculated for $C_{16}H_{18}O_2^+$ [M, –H, $–NO_2$]$^+$: 242.1301; found: 242.1311. The enantiomeric excess was determined by SFC using a Chiralcell IA column: CO_2/MeOH 97:3, flow rate 3.0 mL/min, $\boldsymbol{\tau_{major}}$ = 4.5 min, $\boldsymbol{\tau_{minor}}$ = 5.3 min, **ee** = 75%.

6. Synthesis and characterization data of cyclopentenes 5

General procedure for the synthesis of cyclopentenes (5)

To a schlenk tube charged with a magnetic stir bar were added tris[2-(4,6-difluorophenyl)pyridinato-C2,N]iridium(III) (0.0025 mmol) and the corresponding vinylcyclopropane **4** (0.1 mmol) dissolved in 2.0 mL of dry CH_2Cl_2. Then, a freeze-pump-thaw degasification was carried out and the reaction was stirred in the presence of blue light until complete conversion was observed by ^{1}H-NMR. After that, the solvent was evaporated under reduced pressure and the crude reaction mixture was purified by FC (cyclohexane : ethyl acetate) using Iatrobeads silica gel or filtration over celite.

Methyl (*1S,4S,5S*)-3-isopropyl-5-nitro-4-phenylcyclopent-2-ene-1-carboxylate (5a)

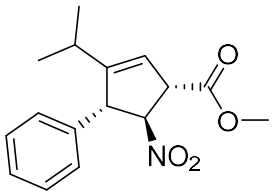

5a

The product was obtained following the general procedure starting from **4a** after 24h, and the crude was purified by FC (9:1 cyclohexane : ethyl acetate), affording the pure product as a yellow oil (57% yield). **$[\alpha]^{20}_D$** = - 60.4 (*c* = 1.40, $CHCl_3$). **^{1}H-NMR:** δ 7.32 – 7.08 (m, 5H), 5.49 (m, 1H), 5.32 (t, *J* = 5.8 Hz, 1H), 4.34 (d, *J* = 6.0 Hz, 1H), 4.28 – 4.23 (m, 1H), 3.73 (s, 3H), 1.90 (m, 1H), 0.99 (d, *J* = 6.7 Hz, 3H), 0.84 (d, *J* = 7.0 Hz, 3H) ppm. **^{13}C-NMR:** δ 171.6, 152.9, 139.8, 129.1, 128.2, 127.8, 118.5, 93.7, 58.2, 54.3, 52.7, 27.5, 21.1, 20.4 ppm. **MS (TOF-ESI):** calculated for $C_{16}H_{19}NO_4Na^+$ $[M+Na]^+$: 312.1206; found: 312.1201. The enantiomeric excess was determined by SFC using a Chiralcell IG-3 column: CO_2/MeOH 98:2, flow rate 2.0 mL/min, τ_{major} = 2.8 min, τ_{minor} = 3.0 min, **ee** = 87%.

Methyl (*1S,4S,5S*)-3-isopropyl-4-(4-methoxyphenyl)-5-nitrocyclopent-2-ene-1-carboxylate (5b)

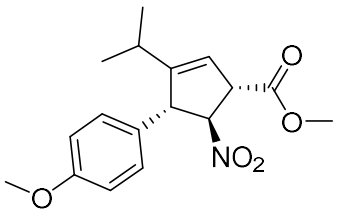

5b

The product was obtained following the general procedure starting from **4b** after 24h, and the crude was purified by FC (9:1 cyclohexane : ethyl acetate), affording the pure product as a yellow oil (75% yield). **$[\alpha]^{20}_D$** = - 31.2 (c = 0.34, $CHCl_3$). **^{1}H-NMR:** δ 7.09 (d, *J* = 8.7 Hz, 2H), 6.88 (d, *J* = 8.6 Hz, 2H), 5.54 (bs, 1H), 5.34 (t, *J* = 5.9 Hz, 1H), 4.35 (d, *J* = 5.8 Hz, 1H), 4.30 – 4.24 (m, 1H), 3.80 (s, 3H), 3.79 (s, 3H), 2.03 – 1.95 (m, 1H), 1.06 (d, *J* = 6.6 Hz, 3H), 0.90 (d, *J* = 7.0 Hz, 3H) ppm. **^{13}C-NMR:** δ 171.6, 159.2, 153.0, 131.7, 129.3, 118.2, 114.4, 93.9, 57.7, 55.3, 54.1, 52.7, 27.5, 21.0, 20.4 ppm. **MS (TOF-ESI):** calculated for $C_{17}H_{21}NO_5Na^+$ $[M+Na]^+$: 342.1317; found: 342.1320. The enantiomeric excess was

determined by SFC using a Chiralcell IA column: CO_2/MeOH 97:3, flow rate 3.0 mL/min, τ_{major} = 2.2 min, τ_{minor} = 3.1 min, **ee** = 99%.

Methyl (*1S,4S,5S*)-4-(4-bromophenyl)-3-isopropyl-5-nitrocyclopent-2-ene-1-carboxylate (5c)

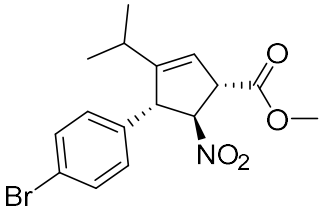

5c

The product was obtained following the general procedure starting from **4c** after 24h, and the crude was purified by FC (9:1 cyclohexane : ethyl acetate), affording the pure product as a yellow oil (50% yield). $[\alpha]^{20}_D$ = - 9.5 (*c* = 0.20, $CHCl_3$). **^{1}H-NMR:** δ 7.32 – 7.08 (m, 4H), 5.49 (m, 1H), 5.32 (t, *J* = 5.8 Hz, 1H), 4.34 (d, *J* = 6.0 Hz, 1H), 4.28 – 4.23 (m, 1H), 3.73 (s, 3H), 1.90 (m, 1H), 0.99 (d, *J* = 6.7 Hz, 3H), 0.84 (d, *J* = 7.0 Hz, 3H) ppm. **^{13}C-NMR:** δ 171.6, 152.9, 139.8, 129.1, 128.2, 127.8, 118.5, 93.7, 58.2, 54.3, 52.7, 27.5, 21.1, 20.4 ppm. **MS (TOF-ESI):** calculated for $C_{16}H_{18}NO_4NaBr^+$ $[M+Na]^+$: 390.0311; found: 390.0316. The enantiomeric excess was determined by SFC using a Chiralcell IC column: CO_2/MeOH 98:2, flow rate 2.0 mL/min, τ_{minor} = 6.6min, τ_{minor} = 7.0 min, **ee** = 96%.

Methyl (*1S,4S,5S*)-5-nitro-4-phenyl-3-propylcyclopent-2-ene-1-carboxylate (5d)

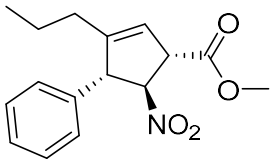

5d

The product was obtained following the general procedure starting from **4d** after 48h, and the crude was purified by FC (9:1 cyclohexane : ethyl acetate), affording the pure product as a yellow oil (45% yield yield based on conversion by ^{1}H-NMR). $[\alpha]^{20}_D$ = - 34.2 (*c* = 0.74, $CHCl_3$). **^{1}H-NMR:** δ 7.42 – 7.08 (m, 5H), 5.58 (bs, 1H), 5.40 (t, *J* = 5.6 Hz, 1H), 4.36 – 4.28 (m, 2H), 3.79 (s, 3H), 1.92 – 1.71 (m, 2H), 1.49 – 1.31 (m, 2H), 0.84 (t, *J* = 7.3 Hz, 3H) ppm. **^{13}C-NMR:** δ 171.6, 146.9, 139.6, 129.1, 128.1, 127.9, 120.2, 93.4, 59.2, 54.5, 52.7, 31.1, 20.2, 13.7 ppm. **MS (TOF-ESI):** calculated for $C_{16}H_{19}NO_4Na^+$ $[M+Na]^+$: 312.1206; found: 312.1195. The enantiomeric excess was determined by SFC using a Chiralcell IG-3 column: CO_2/MeOH 90:10, flow rate 3.0 mL/min, τ_{major} = 1.0 min, τ_{minor} = 1.1 min, **ee** = 94%.

Benzyl (*1S,4S,5S*)-3-isopropyl-5-nitro-4-phenylcyclopent-2-ene-1-carboxylate (5f)

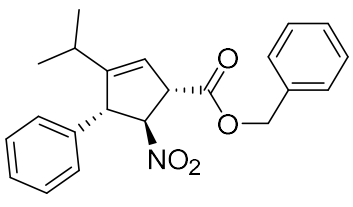

5f

The product was obtained following the general procedure starting from **4a** after 24h, and the crude was purified by FC (19:1 cyclohexane : ethyl acetate), affording the pure product as a yellow oil (90% yield, *d.r.* = 2:1). $[\alpha]^{20}_D$ = - 100.0 (*c* = 0.66, $CHCl_3$). **Major diastereoisomer (1*S*,4*S*,5*S*): ^{1}H-NMR:** δ 7.42 –

7.27 (m, 8H), 7.18 – 7.14 (m, 2H), 5.58 (dd, *J* = 3.8, 2.1 Hz, 1H), 5.40 (t, *J* = 5.7 Hz, 1H), 5.22 (d, *J* = 1.9 Hz, 2H), 4.41 (d, *J* = 1.9 Hz, 1H), 4.35 (ddd, *J* = 5.8, 3.8, 2.1 Hz, 1H), 1.97 (m, 1H), 1.05 (d, *J* = 6.8 Hz, 3H), 0.90 (d, *J* = 6.8 Hz, 3H) ppm. **^{13}C-NMR:** δ 171.1, 153.2, 139.9, 135.4, 129.2, 128.8, 128.7, 128.4, 128.3, 118.7, 93.8, 67.6, 58.4, 54.7, 29.9, 27.7, 21.2, 20.6 ppm. The enantiomeric excess was determined by SFC using a Chiralcell IG-3 column: CO_2/MeOH 95:5, flow rate 2.0 mL/min, τ_{major} = 4.0 min, τ_{minor} = 4.7 min, **ee** = 97%. **Minor diastereoisomer (1*R*,4*S*,5*S*): ^{1}H-NMR:** δ 7.41 – 7.18 (m, 10H), 5.74 – 5.67 (m, 1H), 5.16 – 5.09 (m, 3H), 4.64 (d, *J* = 5.4 Hz, 1H), 4.21 – 4.13 (m, 1H), 2.10 – 1.97 (m, 1H), 1.06 (d, *J* = 6.8 Hz, 3H), 0.89 (d, *J* = 6.8 Hz, 3H) ppm. **MS (EI):** calculated for $C_{22}H_{22}O_2^+$ [M –H, -NO_2]$^+$: 318.1614; found: 318.1595

1-((4*S*,5*S*)-3-Isopropyl-5-nitro-4-phenylcyclopent-2-en-1-yl)ethan-1-one (5g)

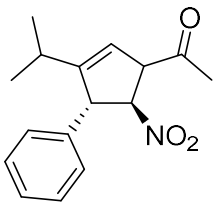

5g

The product was obtained following the general procedure starting from **4g** after 2h of irradiation. The crude was purified by FC (cyclohexane : ethyl acetate) affording the pure product as a pale yellow oil (33% yield). **[α]$^{20}_{D}$** = - 49.1 (*c* = 0.38, $CHCl_3$). **^{1}H-NMR:** δ 7.39-7.28 (m, 3H), 7.17-7.11 (m, 2H), 5.57 (dd, *J* = 3.7, 1.9 Hz, 1H), 5.49 (t, *J* = 5.4 Hz, 1H), 4.45 (d, *J* = 5.3 Hz, 1H), 4.34 (dd, *J* = 4.9, 1.9 Hz, 1H), 2.37 (s, 3H), 2.05-1.90 (m, 1H), 1.05 (d, *J* = 6.7 Hz, 3H), 0.92 (d, *J* = 6.9 Hz, 3H). **^{13}C-NMR:** δ 203.7, 153.4, 139.9, 129.0, 128.2, 127.7, 117.7, 91.8, 62.8, 57.7, 28.8, 27.5, 21.1, 20.5. **MS (EI):** calculated for $C_{16}H_{18}O^+$ [M -H,-NO_2]$^+$: 226.1352; found: 226.1334. The enantiomeric excess was determined by SFC using a Chiralcell IA column: CO_2/MeOH 98:2, flow rate 2.0 mL/min, τ_{major} = 3.86 min, τ_{minor} = 4.16 min, **ee** = 97%.

(*1S,4S,5S*)-3-Isopropyl-5-nitro-4-phenylcyclopent-2-ene-1-carbonitrile (5h)

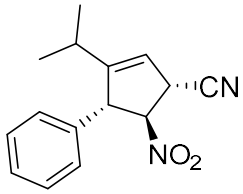

5h

The product was obtained following the general procedure starting from **4h** after 24h, and the crude was purified by FC (9:1 cyclohexane : ethyl acetate), affording the pure product as a colorless oil (55% yield). **[α]$^{20}_{D}$** = - 37.2 (*c* = 2.03, $CHCl_3$). **^{1}H-NMR:** δ 7.50 – 7.07 (m, 5H), 5.54 (bs, 1H), 5.15 (t, *J* = 5.0 Hz, 1H), 4.43 (d, *J* = 5.0 Hz, 2H), 2.11 – 2.02 (m, 1H), 1.10 (d, *J* = 6.7 Hz, 3H), 0.92 (d, *J* = 7.0 Hz, 3H). **^{13}C-NMR:** δ 155.9, 138.0, 129.5, 128.5, 127.9, 118.0, 115.8, 93.9, 58.5, 38.8, 27.7, 20.9, 20.3. **MS (EI):** calculated for $C_{15}H_{16}N^+$ [M -NO_2]$^+$: 210.1277; found: 210.1325. The enantiomeric excess was determined by SFC using a Chiralcell IA column: CO_2/MeOH 97:3, flow rate 2.0 mL/min, τ_{major} = 4.0 min, τ_{minor} = 4.3 min, **ee** = 97%.

7. Synthesis and characterization data of compounds *rac*-6, 7 and 9

1-((1*S,2*S**,3*S**)-2-Nitro-3-phenylcyclopropyl)ethan-1-one (*rac*-6)**

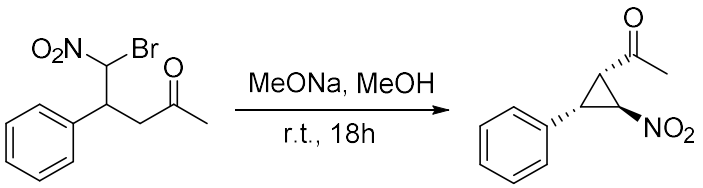

rac-**6**

The product was obtained following a modification of a procedure described in the literature, using a different base.[5] To a round-bottom flask charged with a magnetic stir bar and a solution of 1.1 mmol of sodium methoxide in 12 mL of methanol was added the 5-bromo-5-nitro-4-phenylpentan-2-one[6] (1.22 mmol) dissolved in 3 mL of methanol. The reaction was stirred at room temperature during 18h. Then, the solvent was evaporated under reduced pressure and the crude reaction mixture was purified by FC (cyclohexane 9:1 ethyl acetate) (Yield = 30 %) . **^{1}H-NMR:** δ 7.40 – 7.28 (m, 3H), 7.18 – 7.12 (m, 2H), 4.66 (dd, *J* = 8.6, 4.6 Hz, 1H), 3.74 (dd, *J* = 7.8, 4.6 Hz, 1H), 2.86 – 2.78 (m, 1H), 2.39 (s, 3H). **13C-NMR:** δ 198.2, 134.5, 129.0, 128.2, 126.7, 66.2, 38.6, 31.6, 30.8 ppm. **MS (EI):** calculated for $C_{11}H_{11}O^+$ $[M - NO_2]^+$: 159.0804; found: 159.0816.

(*2R,*3S**)-5-Methyl-2-nitro-3-phenyl-2,3-dihydrofuran (7)**

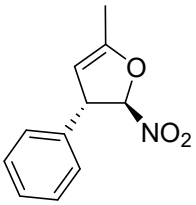

7

The product was obtained following the general procedure for the synthesis of dihydrofuranes starting from ***rac*-6** after 80 hours, and the crude was purified by FC (19:1 cyclohexane : ethyl acetate), affording the pure product as a colorless oil (41% yield). **^{1}H-NMR (CD_2Cl_2):** δ 7.34 – 7.16 (m, 5H), 5.69 (d, *J* = 1.9 Hz, 1H), 4.96 – 4.93 (m, *J* = 2.7, 1.3 Hz, 1H), 4.32 – 4.28 (m, 1H), 2.02 (t, *J* = 1.5 Hz, 3H) ppm. **^{13}C-NMR (CD_2Cl_2):** δ 156.6, 139.5, 129.5, 128.5, 127.6, 111.9, 100.2, 56.9, 13.4 ppm. **MS (EI):** calculated for $C_{11}H_{10}O^+$ $[M-NO_2]^+$: 158.0726; found: 158.0689.

[5] J. Lv, J. Zhang, Z. Lin, Y. Wang, Chem. Eur. J.

[6] For the synthesis of the intermediate ketone, see: Dong, L.; Lu, R.; Du, Q.; Zhang J.; Liu; S.; Xuan, Y.; Yan, M. *Tetrahedron* **2009**, *65*, 4124-4129.

Methyl (3*S*,4R)-4-nitro-3-phenylcyclopent-1-ene-1-carboxylate (9)**

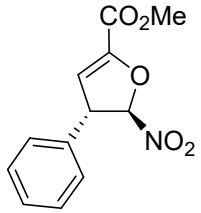

9

The compound was obtained following the general procedure for the synthesis of dihydrofuranes starting from *rac*-**8** and after 24h of irradiation. The crude product was purified over celite to obtain the pure product as a pale yellow oil (73% yield). **^{1}H-NMR:** δ 7.45-7.35 (m, 3H), 7.27-7.22 (m, 2H), 6.28 (d, *J* = 3.1 Hz, 1H), 5.92 (d, *J* = 2.3 Hz, 1H), 4.60-4.55 (m, 1H), 4.93 (s, 3H) **^{13}C-NMR:** δ 158.8, 148.0, 136.2, 129.5, 128.9, 127.2, 114.2, 110.4, 56.3, 52.8 **MS (TOF-ESI):** calculated for $C_{12}H_{11}NO_5Na$ $[M+Na]^+$: 272.0529; found: 272.0526.

8. Studies of the photocatalytic mechanism

8.1 Absorption and emission spectra

Two mechanism are possible for the energy transfer process (Foster or Dexter). In order to distinguish between the two mechanisms, the phosphorescence emission spectrum of the photocatalyst **3b** and the cyclopropane **1a** absorption were measured (**Figures S1** and **S2)**.

The phosphorescence emission spectrum of the photocatalyst (c = 1.25 mM, CH_2Cl_2, irradiating at 453 nm) presents a broad emission band between 450 nm and 600 nm approximately with the maximum in 482 nm (**Figure S1**)

The UV-visible absorption spectrum of the cyclopropane **1a** (c = 0.25 mM, CH_2Cl_2) presents an intense band with a maximum in 246 nm and a shoulder in 300 nm (**Figure S2**). However, it does not present any absorption between 450 nm and 600 nm (the emission of the photocatalyst **3a**). Therefore, both spectra do not overlap and it can be concluded that the reaction does not proceed through a Foster type mechanism and it goes through a Dexter type mechanism.

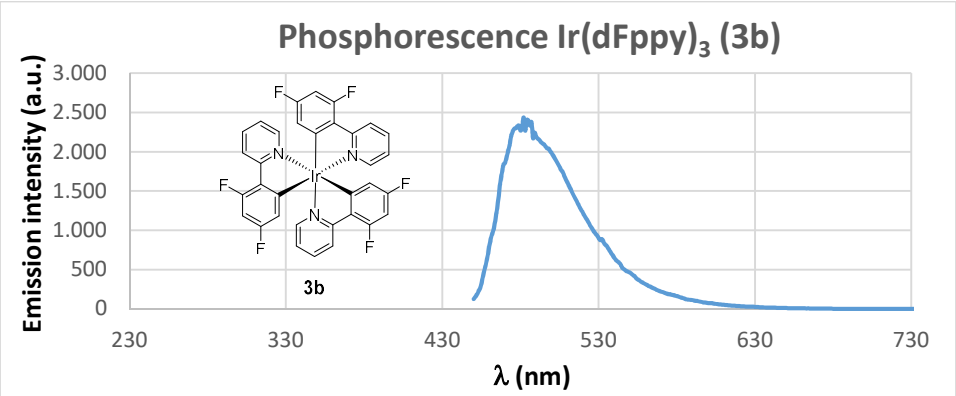

Figure S1. (c = 1.25 mM, CH_2Cl_2, irradiating at 453 nm)

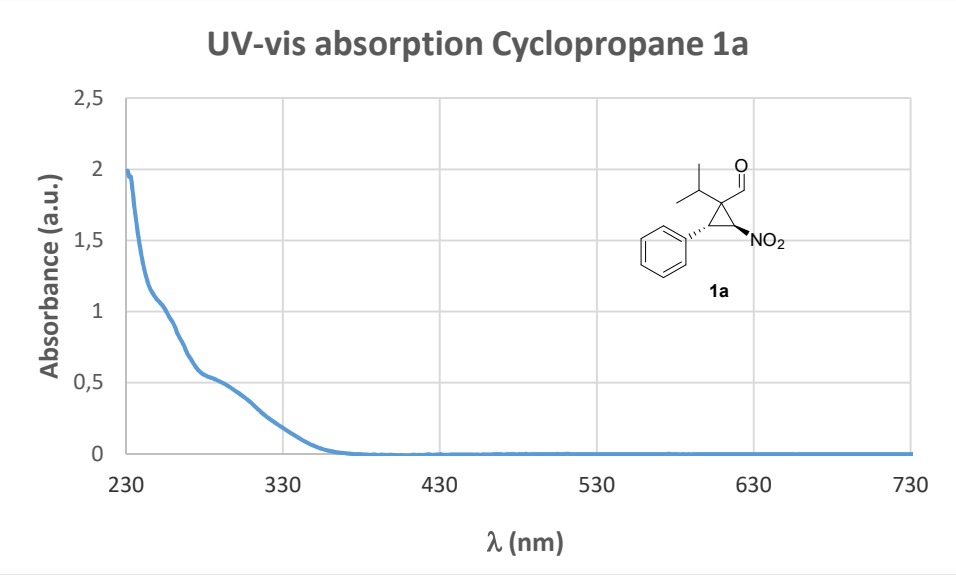

Figure S2. (c = 0.25 mM, CH_2Cl_2)

8.2 Cyclic voltammetry

A cyclic voltammetry was measured at 50mV/sec from a solution 1mM of cyclopropane **1a** in CH_2Cl_2 containing $N(Bu)_4PF_6$ (0.1M) as inert electrolyte (**Figure S3**). A three electrode system was used composed by a glassy carbon as working electrode (3mm of diameter), a platinum bar as counter electrode and a Ag/AgCl reference electrode. In **Figure S3** are indicated the potentials for the $Ir^{3+}*/Ir^{2+}$ reduction and the $Ir^{3+}*/Ir^{4+}$ oxidation of the catalyst $Ir(dFppy)_3$ (**3b**). Red bar indicates oxidation processes that could be the result of electron transfer from photocatalyst **3b** in the excited state. Brown bar indicates reduction processes that could be the result of electron transfer from photocatalyst **3b** in the excited state. The potential for the oxidation in the excited state of $Ir(ppy)_3$ (**3a**) and of Eosyn Y are also indicated.

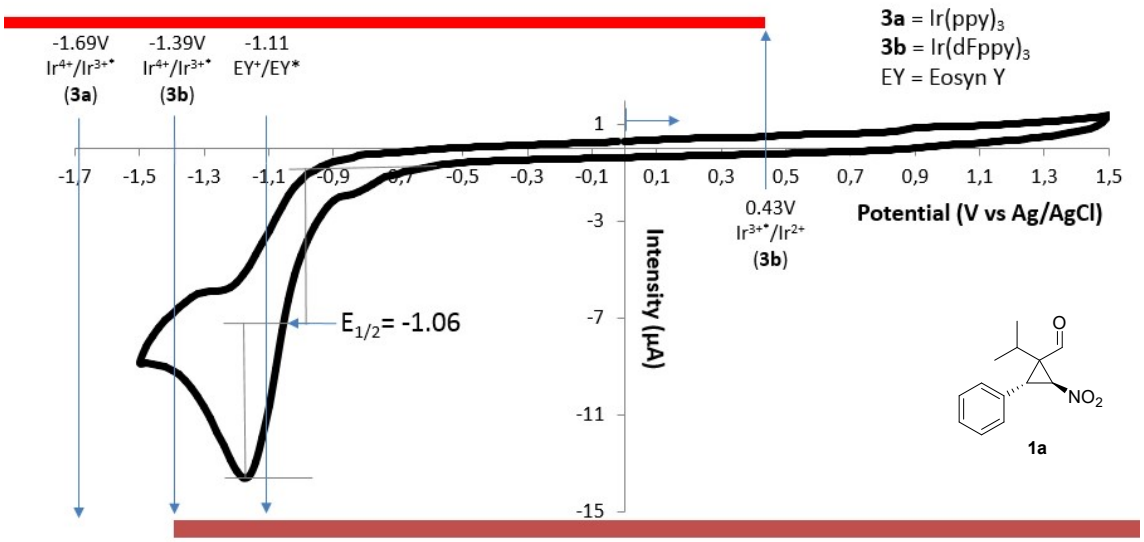

Figure S3. Cyclic voltammetry of cyclopropane **1a**.

8.3 Quantum Yield Measurement

A solution of ferrioxalate was chosen as actinometer following the procedure described by the IUPAC (subcommittee on photochemistry).[7] The procedure is based on the decomposition under irradiation of ferric ions to ferrous ions which are complexed by 1,10-phenanthroline. This photochemical transformation has a known quantum yield and the complexation of Fe^{2+} with 1,10-phenanthroline can be monitored by UV-Visible absorption since its extinction coefficient at 510 nm is known (ε =11100 M^{-1} cm^{-1}). Therefore, the moles transformed can be related with the moles of photons absorbed by the equation [1].

$$\Phi = \frac{\#\text{mol transformed}}{\#\text{photons absorved}} \qquad [1]$$

The complete procedure should be done under a red safe-light environment. Green crystals of $K_3[Fe(C_2O_4)_3]\cdot 3H_2O$ were prepared using the following procedure: 55.0 g of potassium oxalate monohydrate were dissolved in 80 mL of water at 90° C, then, 16.2 g of $FeCl_3$ were added to the solution and it was stirred for 10 minutes while cooling to room temperature. The precipitate was filtered and recrystallized in water (Yield = 50%). It is kept in the dark. 0.006, 0.012, or 0.15 M solutions can be used for actinometry. In this case we chose a concentration of 0.012 M.
The solutions were prepared and stored in a dark laboratory as follows:

- **Potassium ferrioxalate solution 0.012 M**: 59.0 mg of $K_3[Fe(C_2O_4)]\cdot 3H_2O$ and 28 µL of H_2SO_4 were added into a 10 mL volumetric flack and filled to the mark with Milli-Q water.
- **1,10-phenanthroline 0.01 M**: 100 mg of 1,10-phenantroline monohydrate were added to 50 mL volumetric flask and filled to the mark with MilliQ water.
- **Buffer solution**: 4.94 g of NaOAc and 1 mL of H_2SO_4 were added to 100 mL volumetric flask and filled to the mark with MilliQ water
- **Model reaction solution**: The photocatalyst tris[2-(4,6-difluorophenyl)pyridinato-C2,N]iridium(III) **3b** (3.8 mg, 0.00478 mmol) was transferred to a Schlenk tube, followed by a nitrocyclopropanecarbaldehyde **1a** solution (44.9 mg, 0.192 mmol in 1.92 mL of CH_2Cl_2). The mixture was degassed by "freeze-pump-thaw" cycles (x3).

Actinometry procedure: Due to the reactor setup, the simultaneous irradiation of both the actinometer solution and model reaction is not feasible. However, the stability of the irradiation

[7] H. J. Kuhn, S. E. Braslavsky, R. Schmidt, *Pure Appl. Chem.* **2004**, *76*, 2105–2146.

light was checked through radiometer measurements (from spectro-radiometer equipment Stellarnet model Blue-Wave UV-NB50). Therefore, we assumed that consecutive measurements of both actinometer and model reaction are comparable. In addition, using the same spectrometer, the LED source spectrum was measured, detecting a maximum wavelength of emission of 458 nm (**Figure S4**).

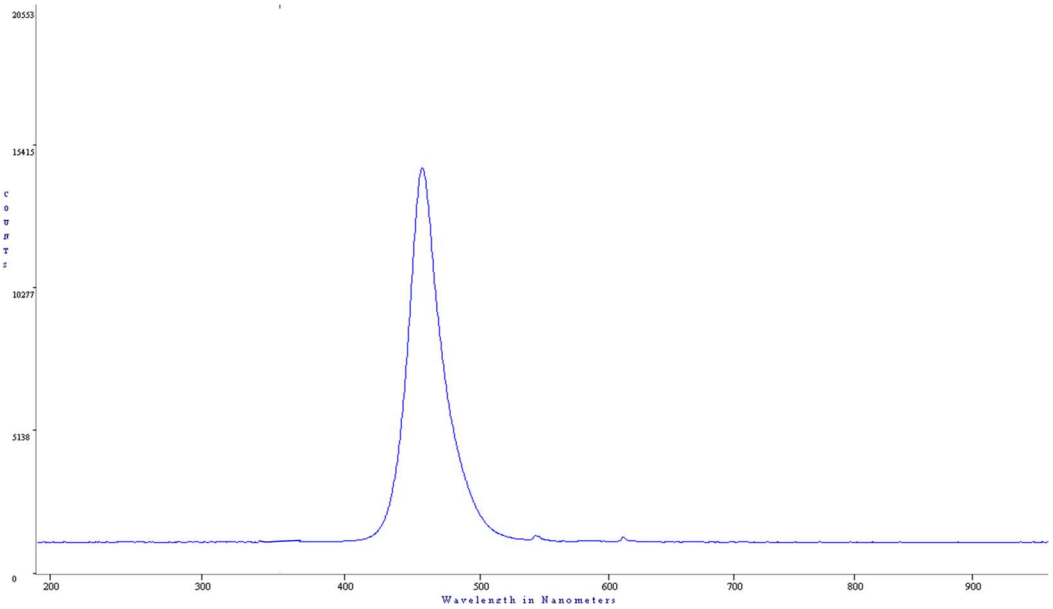

Figure S4. Emission spectrum of the blue LED of the photochemical reactor (λ_{max}= 458 nm).

2 mL of potassium ferrioxalate solution (0.012 M) were introduced into the photoreactor under dark conditions while being stirred. Then, the blue LED was switched on. Every 30 s the light was switched off and a 0.1 mL aliquot was taken. To each aliquot, 2 mL of buffer solution and 0.5 mL of 1,10-phenanthroline 0.01M were added and the final volume was raised to 10 mL with MilliQ water. As a blank sample, a solution was prepared with 0.1 mL of potassium ferrioxalate solution (0.012 M) before irradiation, 2 mL of buffer solution and 0.5 mL of 1,10-phenanthroline 0.01M in a 10 mL of volumetric flask filled with water until the mark. The absorbance spectrum of each sample was monitored at 510 nm, using an Agilent 8453 spectrometer. The absorbance to each time was related with the photochemically produced Fe^{2+} ions across the Lambert-Beer Law (Equation [2]).

$$moles\ Fe^{+2} = \frac{V_1 \cdot V_3 \cdot \Delta A(510\ nm)}{10^3 \cdot V_2 \cdot b \cdot \varepsilon(510\ nm)} \qquad [2]$$

where V_1 is the irradiated volume (noting that the initial volume is 2 mL but it changes as the aliquots are taken); V_2 is the aliquot volume (0.1 mL), V_3 is the final volume after addition of 1,10-phenanthroline and buffer (10 mL), b is referred to the optical pathway (1 cm) and ε (510 nm)

is the extinction coefficient of the complex formed by Fe(II) and 1,10-phenanthroline (*ca.* 11100 M^{-1} cm^{-1}).

The moles of Fe^{2+} formed (x) are plotted as a function of time (t).

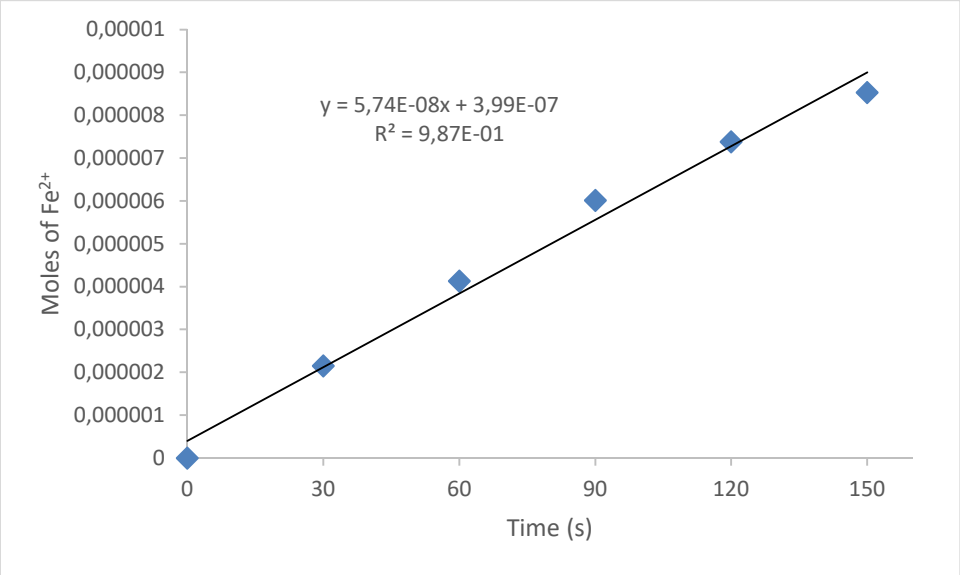

The slope of this line (dx/dt) was correlated to the moles of incident photons by unit of time ($q^0_{n,p}$) using the following equation [3]:

$$q^0_{n,p} = \frac{dx/dt}{\phi(\lambda)\cdot[1-10^{-A(\lambda)}]} \qquad [3]$$

Where ϕ (λ) is the quantum yield of the actinometer reaction at the irradiated wavelength, in this case being 1.12 at 458 nm for 0.01 M dilution[7] (note that a similar value (ca. 1.1 for 0.012 M dilution) is reported by M. Monalti, et. al. in *Chemical Actinometry Handbook of photochemistry*[8]) and A(λ) is the absorbance of the actinometer solution (ferrioxalate) at the irradiated wavelength (458 nm). The absorbance at 458 nm was measured with an Agilent 8453 spectrometer using a quartz cuvette with 1 cm of optical pathway, obtaining a value of 0.140.

Therefore, the moles of incident photons by unit of time ($q^0_{n,p}$) was determined as $1.85\cdot10^{-7}$ einstein s^{-1}.

The kinetics of the reaction under study were done as follows: the photoreactor (blue LEDs) was switched on and the reaction mixture was stirred. Every 30 minutes an aliquot of 0.15 mL was taken from the reaction mixture, opening the system under nitrogen flux. The solvent of the aliquot was removed under reduced pressure and a ^{1}H-NMR spectrum in $CDCl_3$ was acquired to evaluate the conversion.

[8] M. Monalti, A. Credi, L. Prodi, M. T. Gandolfi, *Chemical Actinometry. Handbook of Photochemistry. 3rd Ed*, **2006**.

Knowing the initial molar concentration, the determination of the moles of photo-converted product is possible. Plotting the moles of product versus the irradiation time, the slope *dx/dt* can be related with the quantum yield across the equation [3] being equal to $(q_{n,p}^{0}) \cdot \phi(\lambda) \cdot \left[1 - 10^{-A(\lambda)}\right]$.

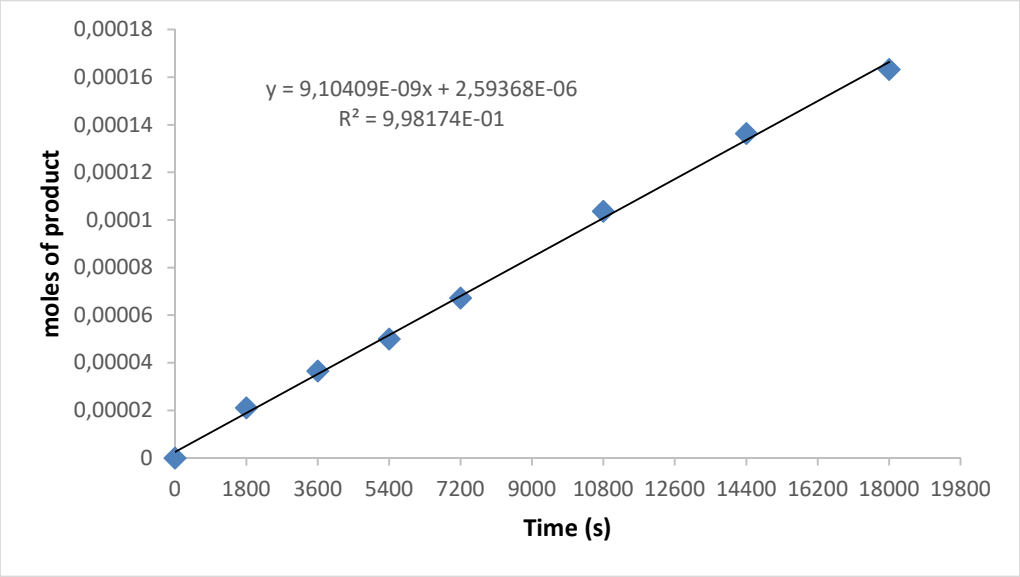

Therefore, the quantum yield at the wavelength of irradiation ϕ(458 nm) can be calculated once A (458 nm) is determined. To measure A(458 nm), a model reaction solution was added to a 1 cm optical pathway cuvette and the UV-Visible spectrum was recorded, using an Agilent 8453 spectrometer. The absorbance at 458 nm was 1.728. Then, the quantum yield at 458 nm of the intramolecular cyclopropane ring expansion of compound **1a** photocatalized by **3b** was calculated as **0.05**. *As the value of ϕ(458 nm) is less than one we can discard a radical chain growth process in the mechanism for the intramolecular cyclopropane ring expansion of* **1a**.

8.4 Other reactions (Cyclopropanes 10 and 11)

The procedure for the synthesis of cyclopropanes **10** and **11** and the results for their photocatalytic expansion are presented in this section. As it can be observed, the formylcyclopropanes **10** and **11**, which does not have a nitro group attached to the ring, did not react when they were set under the optimal conditions for the photocatalytic expansion.

8.4.1 Diethyl (*2R*,3S**)-2-formyl-3-phenylcyclopropane-1,1-dicarboxylate (10)

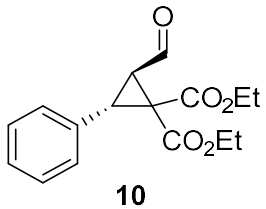

10

Prepared following a modified procedure reported in the literature.[9] To a mixture of bromomalonate diethyl ester (0.62 mmol), 2,6-lutidine (0.66 mmol) and (*S*)-(–)-α,α-Diphenyl-2-pyrrolidinemethanol trimethylsilyl ether (0.062 mmol) in CH_2Cl_2 (2.5 mL) at room temperature was added cinnamaldehyde (0.14 mmol). The resulting mixture was stirred for 48 hours and purified by flash chromatography obtaining 157 mg of pure product (87% yield). NMR spectra in accordance with those reported in the literature.[10] **^{1}H-NMR:** δ 9.50 (d, *J* = 4.7 Hz, 1H), 7.38-7.25 (m, 5H), 4.43-4.22 (m, 2H) 3.97 (q, J = 7.1 Hz, 2H), 3.87 (d, *J* = 7.5 Hz, 1H), 3.42 (dd, *J* = 7.4, 4.8 Hz, 1H), 1.34 (t, *J* = 7.1 Hz, 3H), 0.97 (d, *J* = 7.1 Hz, 3H).

[9] H. Xie, L. Zu, H. Li, J. Wang, W. Wang, *J. Am. Chem. Soc.*, **2007**, *129*, 10886-10894
[10] I. Ibrahem, G.-L. Zhao, R. Rios, J. Vesely, H. Sundén, P. Dziedzic, A. Córdova, *Chem. Eur. J.* **2008**, 14, 7867-7879

^{1}H-NMR (300 MHz, $CDCl_3$) (**10**)

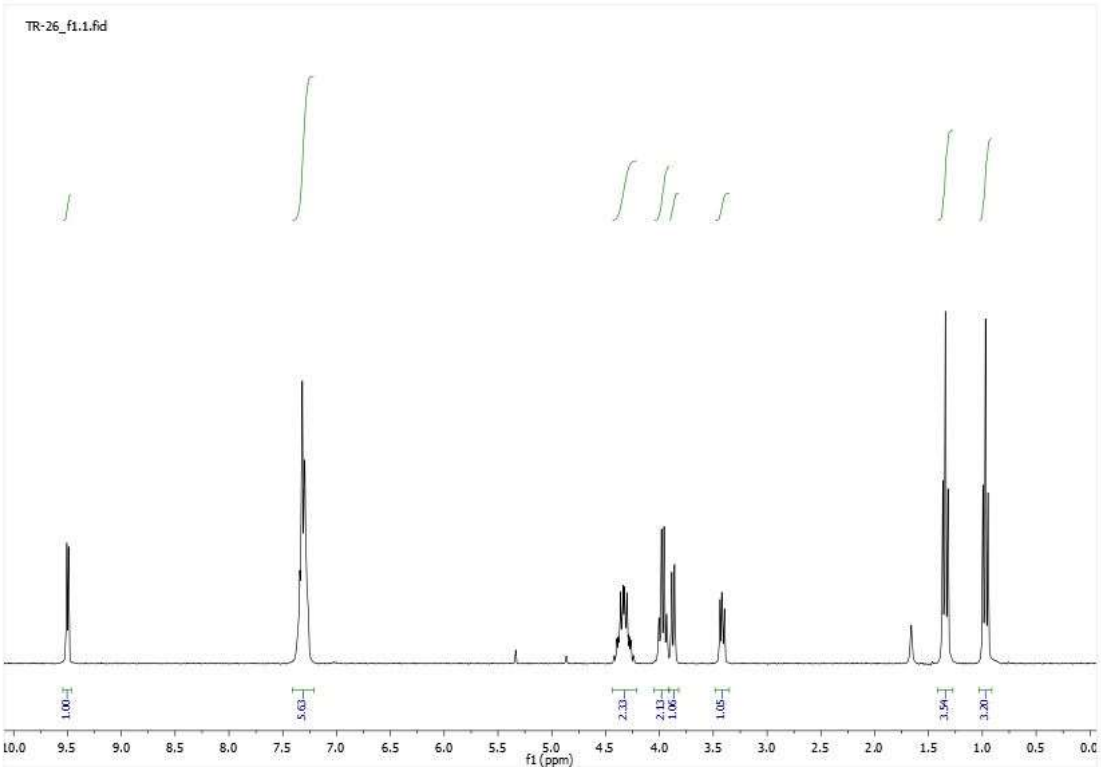

8.4.2 Reaction of 10 under photocatalytic conditions

The photocatalytic ring-expansion reaction was performed following the general procedure for the dihydrofuranes synthesis but failed over the above described standard conditions.

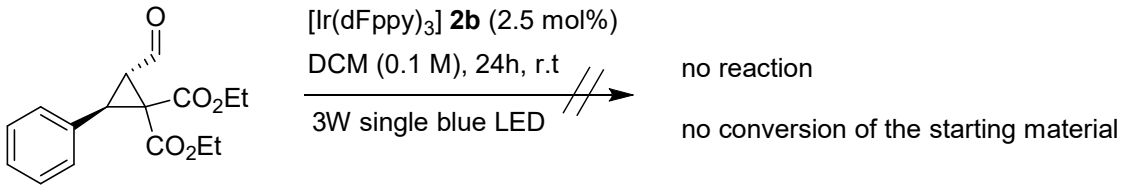

10

8.4.3 (*1R*,2R*,3R)-2-Benzoyl-3-phenylcyclopropane-1-carbaldehyde (11).**

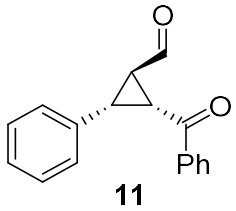

11

Prepared a following a modified procedure reported in the literature.[11] To a solution of CH_2Cl_2 (1.0 mL) were added cinnamaldehyde (0.49 mmol), 2-Chloroacetophenone (1.5 mmol), (*S*)-(–)-α,α-Diphenyl-2-pyrrolidinemethanol trimethylsilyl ether (0.10 mmol) and triethylamine (0.50 mmol). The reaction mixture was stirred at room temperature for 19 hours and the solvent removed under vacuum. Then, after flash chromatography 49.9 mg of the pure product were obtained as a yellow solid (41% yield). NMR spectra in accordance with those reported in the literature. **^{1}H-NMR**: δ (ppm) 9.87 (d, *J* = 2.8 Hz, 1H), 8.04-7.84 (m, 2H), 7.59.7.52 (m, 1H), 7.49-7.41 (m, 2H), 7.24-7.16 (m, 5H), 3.68 (dd, *J* = 10.0, 4.9 Hz, 1H), 3.61-3.54 (m, 1H), 3.43 (dd, *J* = 10.0, 6.2 Hz, 1H).

^{1}H-NMR (300 MHz, $CDCl_3$) (**11**)

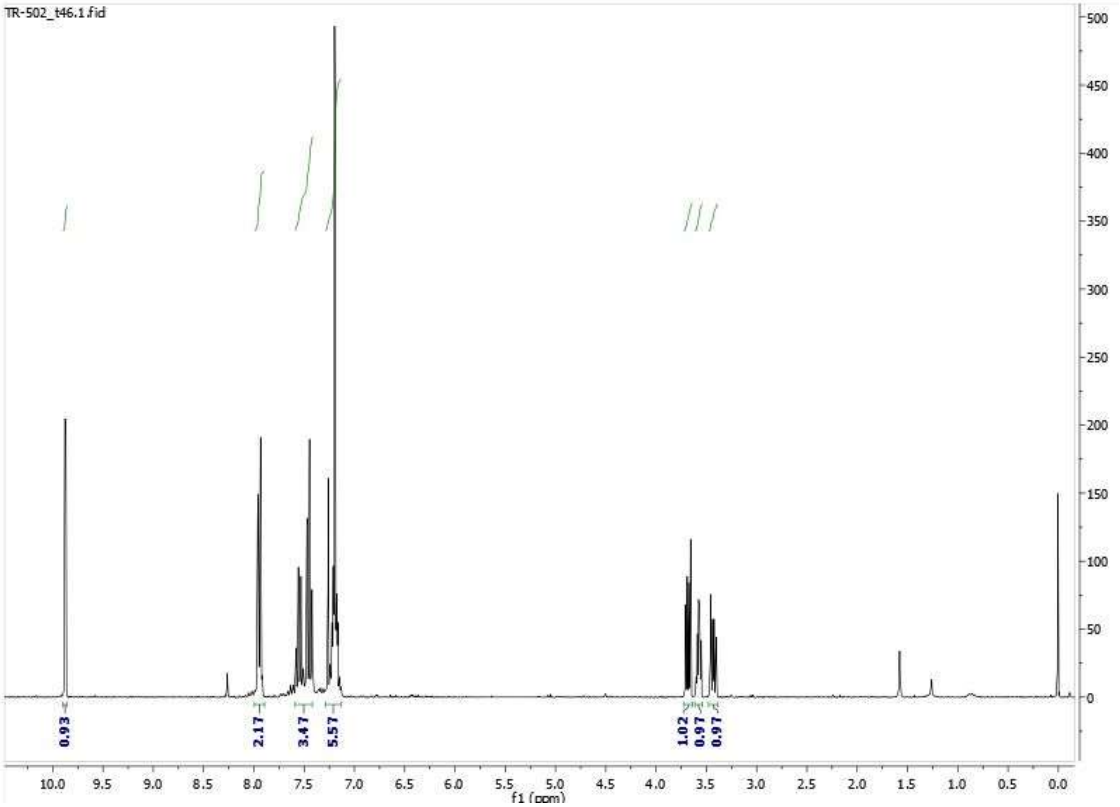

[11] W. Li, X. Li, T. Ye, W. Wu, X. Liang, J. Ye, *Tetrahedron Lett.*, **2011**, *52*, 2715-2718

8.4.4 Reaction of 10 under photocatalytic conditions

The photocatalytic ring-expansion reaction was performed following the general procedure for the dihydrofuranes synthesis but failed over the above described standard conditions.

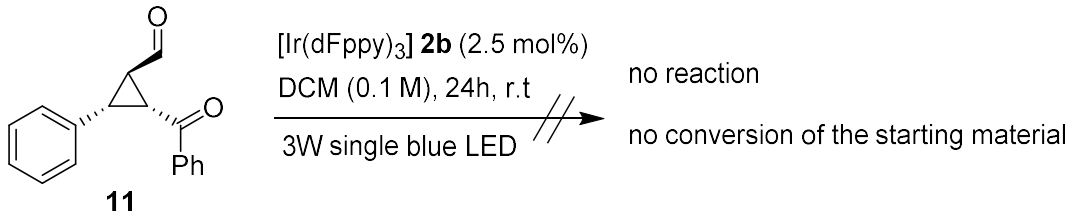

11

9. NMR spectra and chiral chromatograms

9.1 Dihydrofuranes 2

^{1}H-NMR (300 MHz, $CDCl_3$) (**2a**)

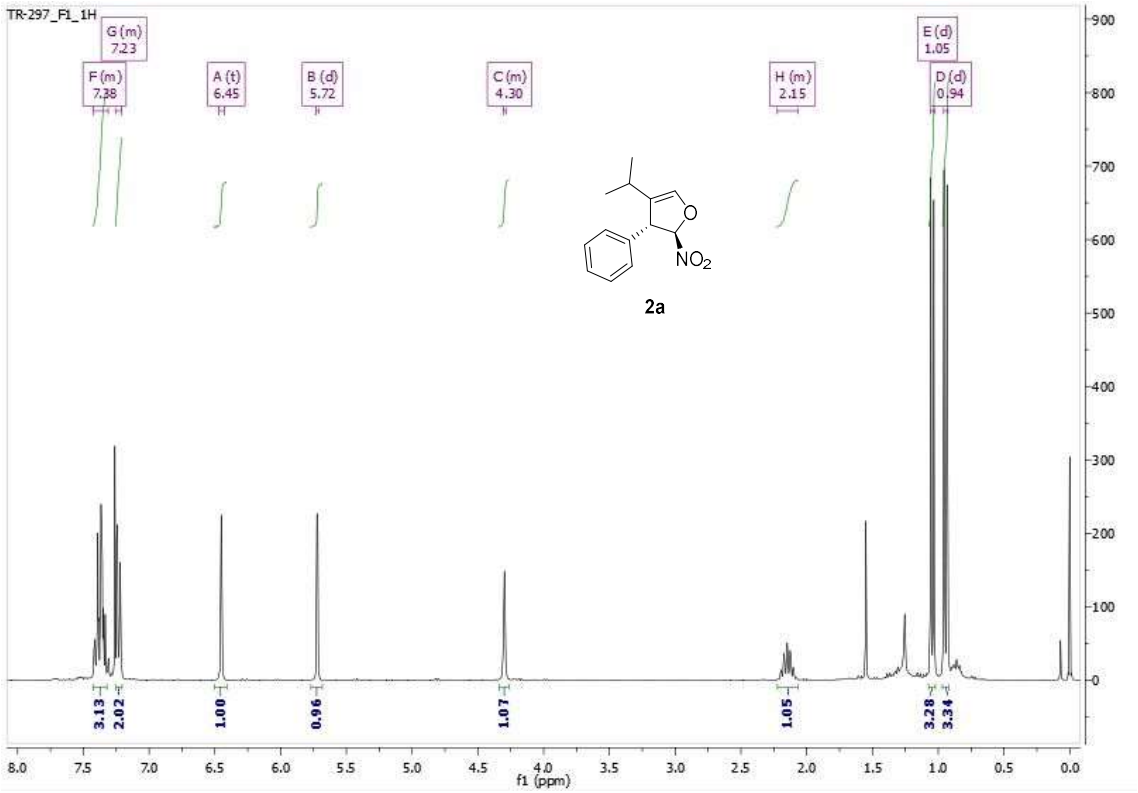

^{13}C-NMR (75 MHz, $CDCl_3$) (**2a**)

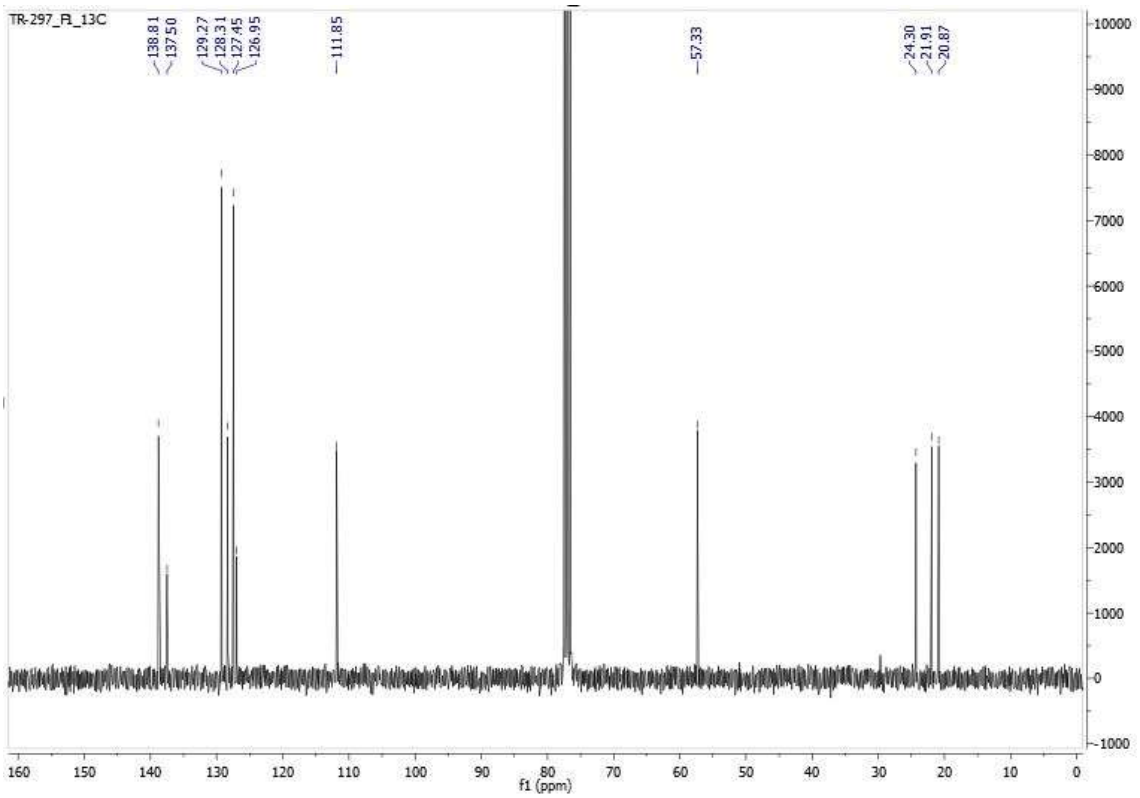

Chromatogram of racemic (**2a**)

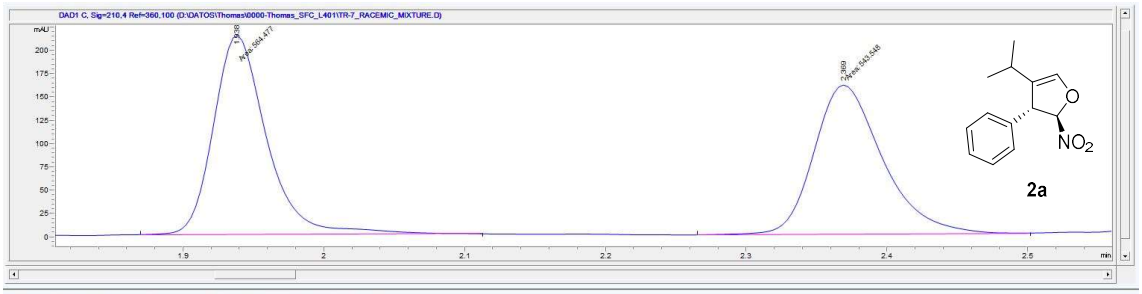

#	Time	Type	Area	Height	Width	Area%	Symmetry
1	1.938	MM	564.5	214.4	0.0439	50.944	0.752
2	2.369	MM	543.5	160.3	0.0565	49.056	0.741

Chromatogram of enantiomerically enriched (**2a**)

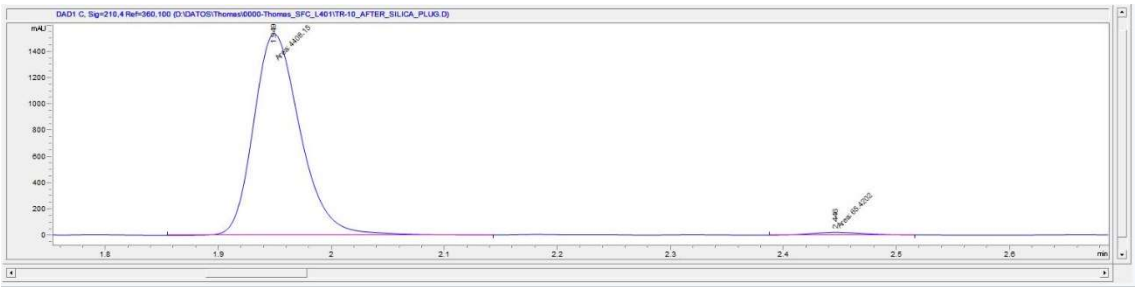

#	Time	Type	Area	Height	Width	Area%	Symmetry
1	1.949	MM	4408.1	1540.9	0.0477	98.538	0.76
2	2.446	MM	65.4	20.2	0.0539	1.462	0.832

^{1}H-NMR (300 MHz, $CDCl_3$) (**2e**)

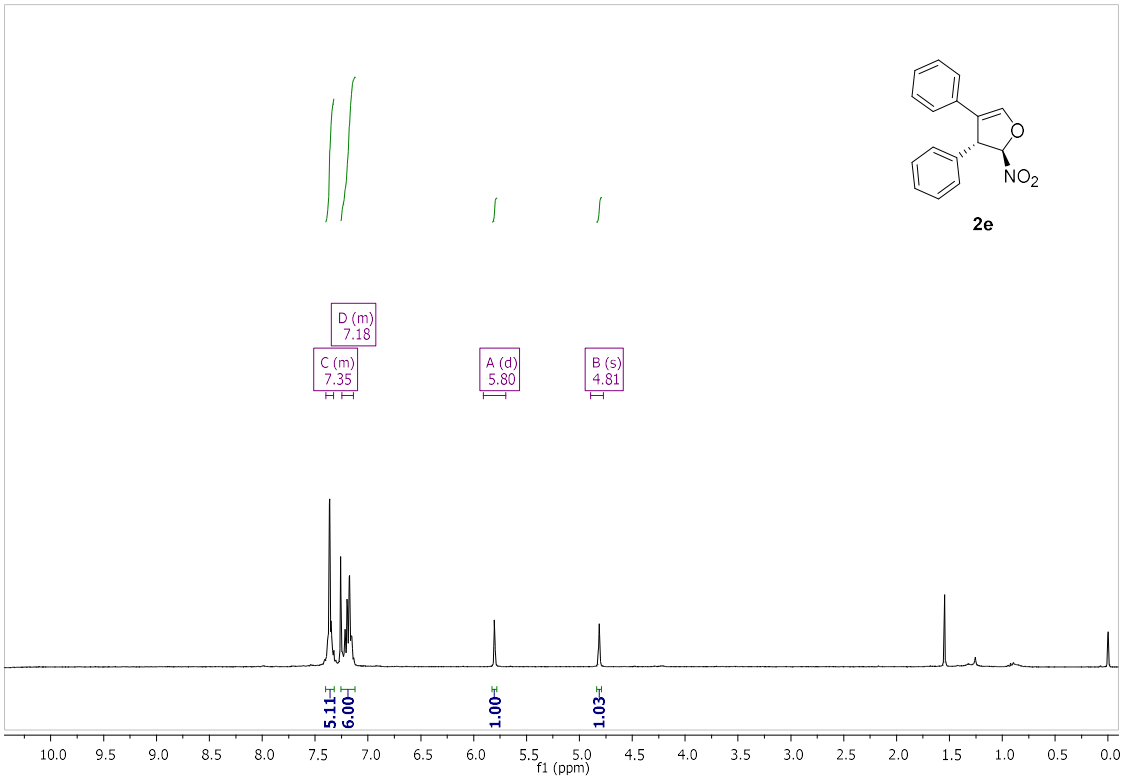

^{13}C-NMR (75 MHz, $CDCl_3$) (**2e**)

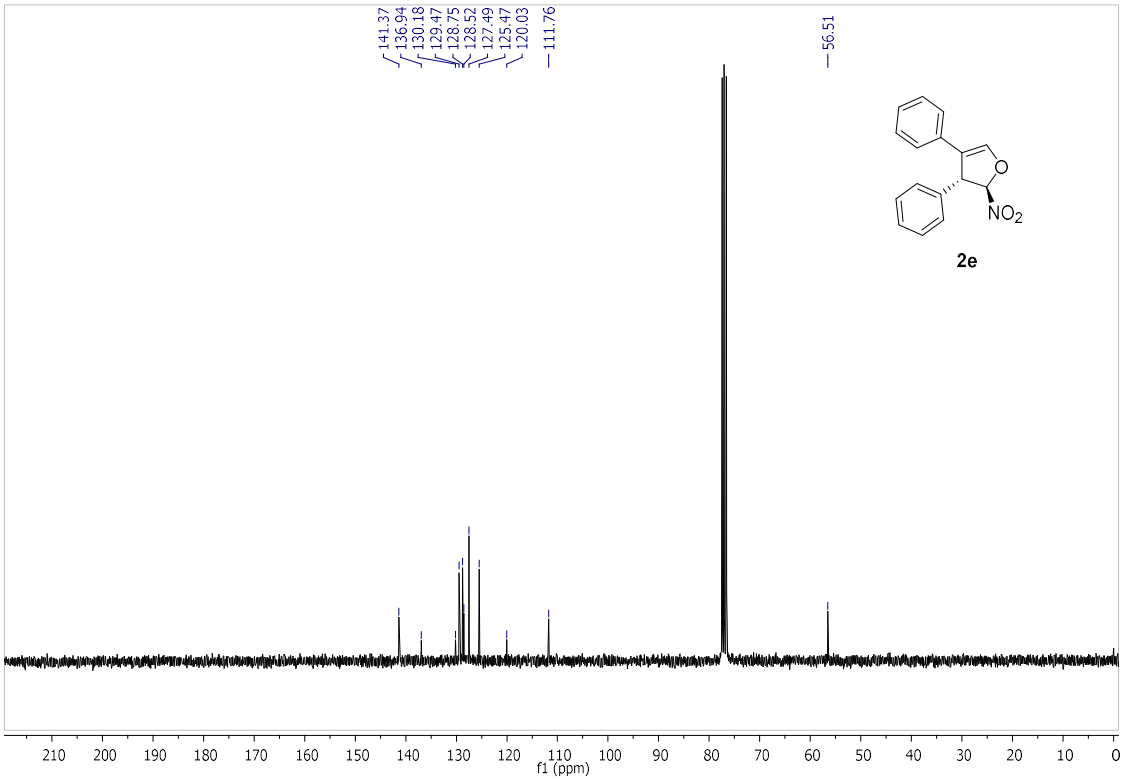

Chromatogram of racemic (**2e**)

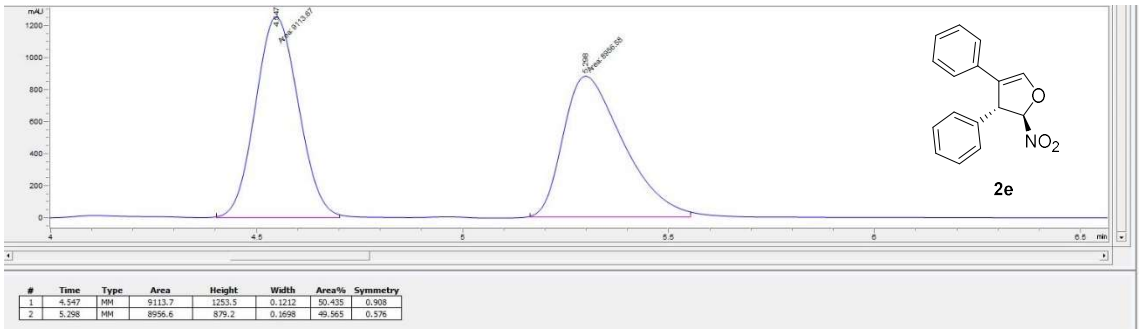

#	Time	Type	Area	Height	Width	Area%	Symmetry
1	4.547	MM	9113.7	1253.5	0.1212	50.435	0.908
2	5.298	MM	8956.6	879.2	0.1698	49.565	0.576

Chromatogram of enantiomerically enriched (**2e**)

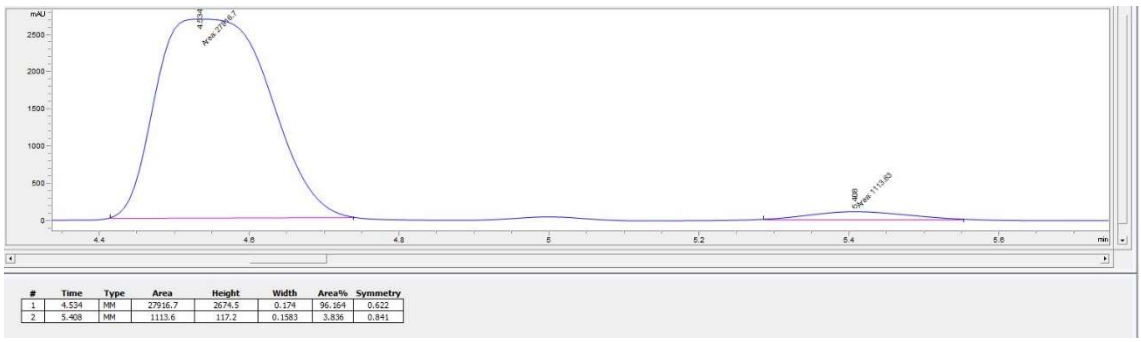

#	Time	Type	Area	Height	Width	Area%	Symmetry
1	4.534	MM	27916.7	2674.5	0.174	96.164	0.622
2	5.408	MM	1113.6	117.2	0.1583	3.836	0.841

9.2 Vinylciclopropanes 4

^{1}H-NMR (300 MHz, $CDCl_3$) (**4a**)

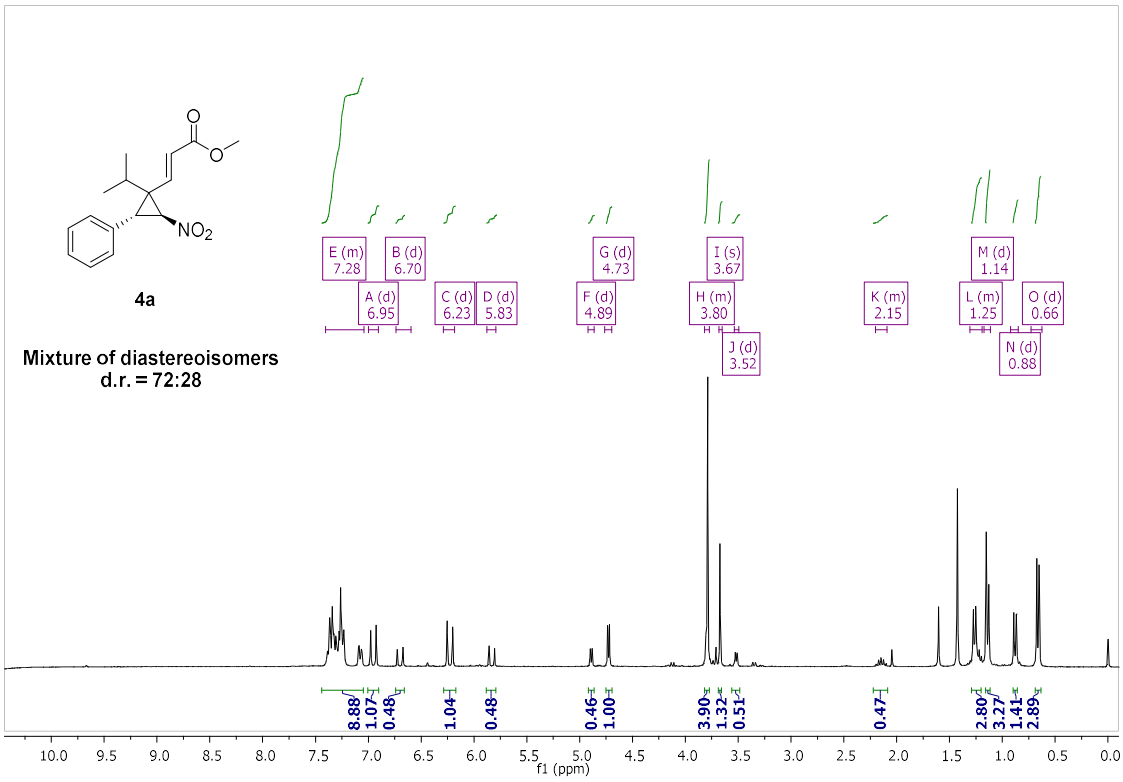

^{13}C-NMR (75 MHz, $CDCl_3$) (**4a**)

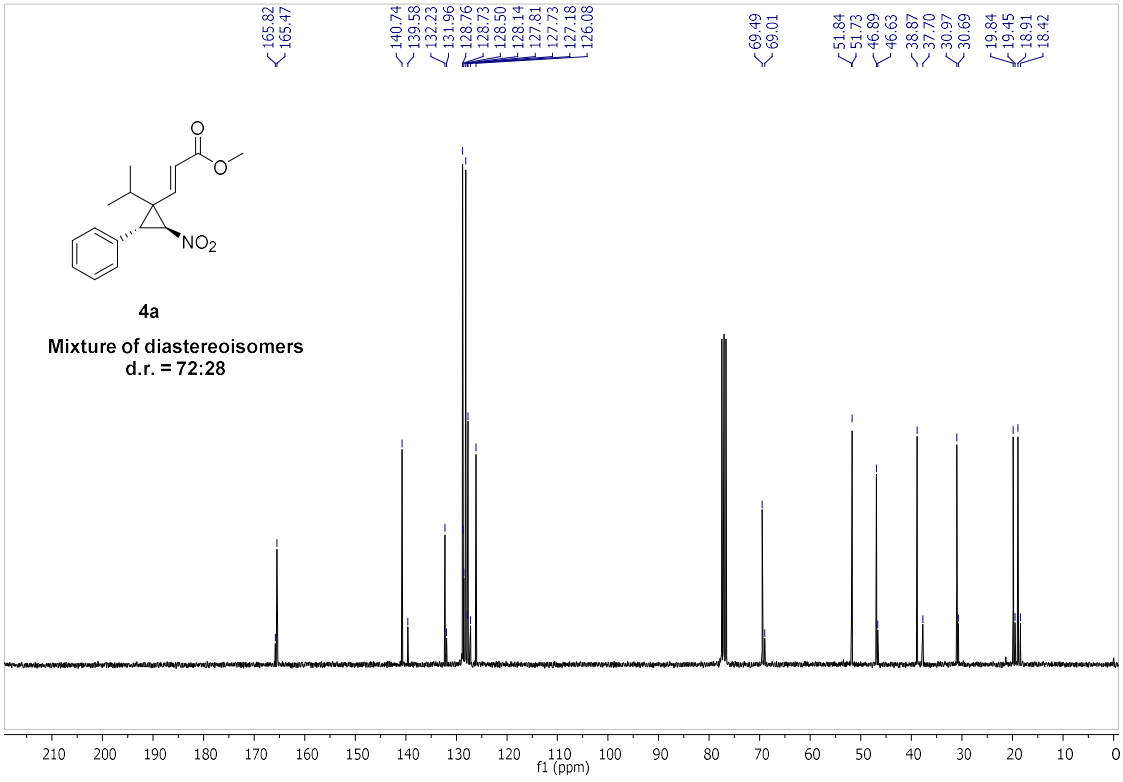

^{1}H-NMR (300 MHz, $CDCl_3$) (**4e**)

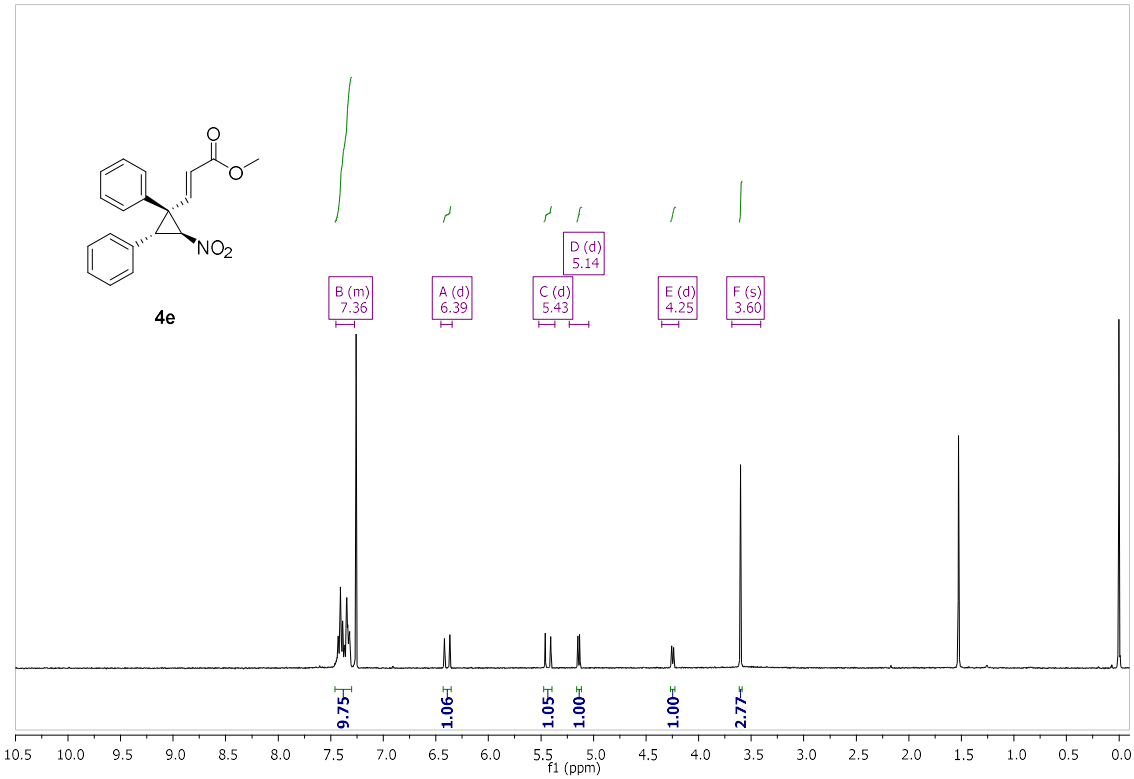

^{13}C-NMR (75 MHz, $CDCl_3$) (**4e**)

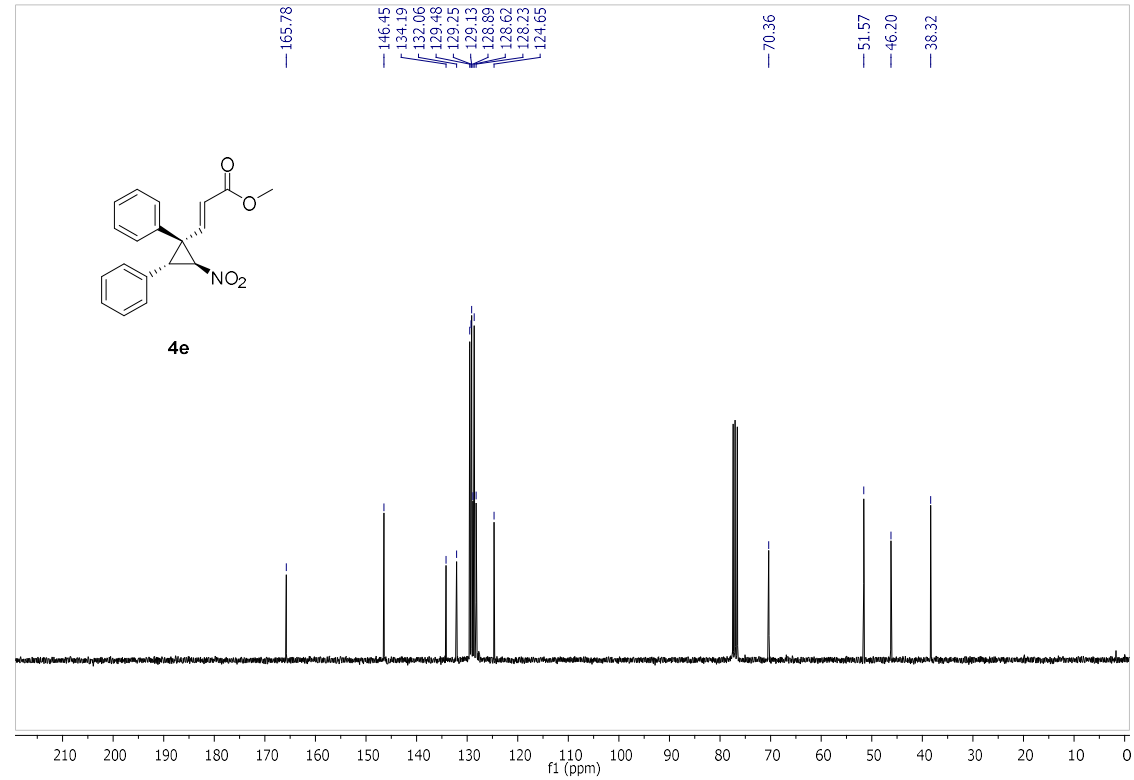

9.3 Cyclopentenes 5

^{1}H-NMR (300 MHz, $CDCl_3$) (**5a**)

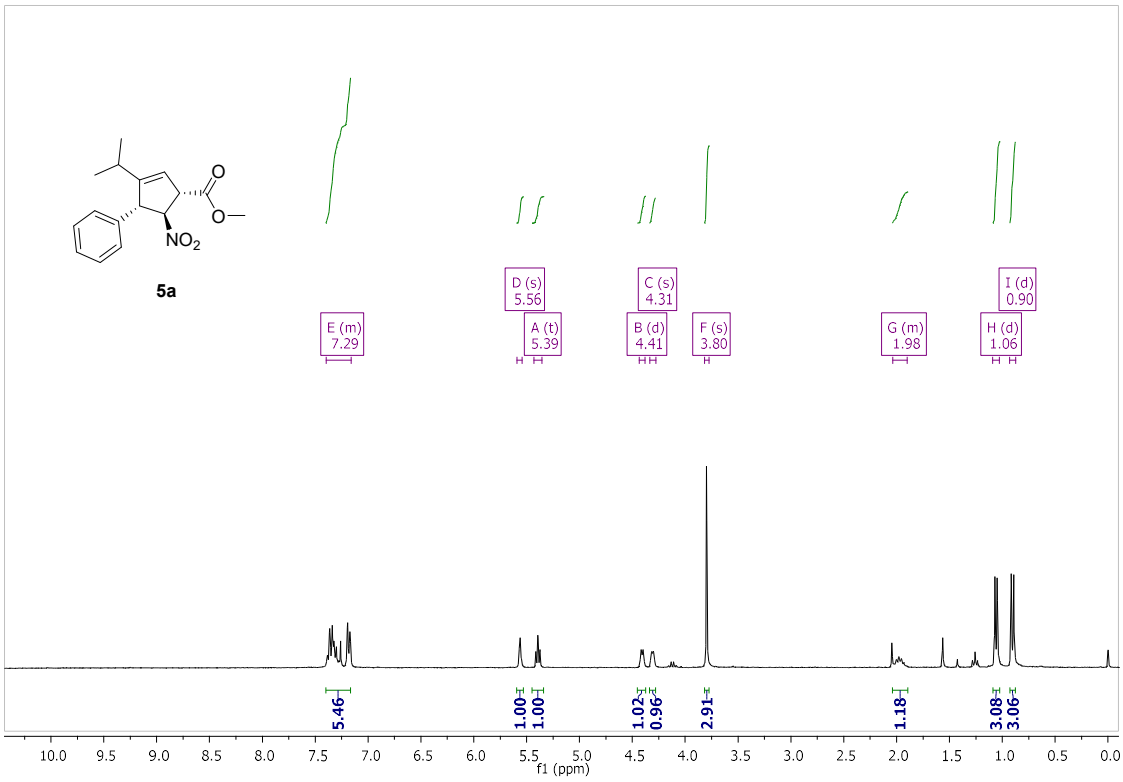

^{13}C-NMR (75 MHz, $CDCl_3$) (**5a**)

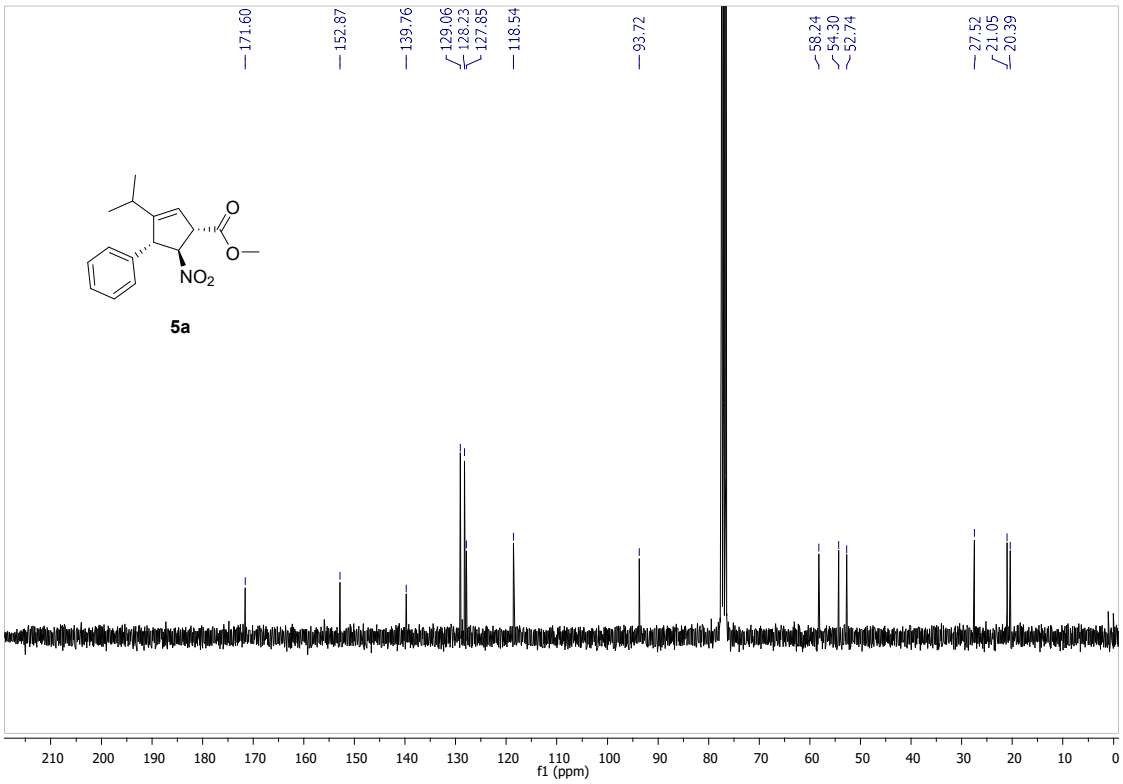

Chromatogram of racemic (**5a**)

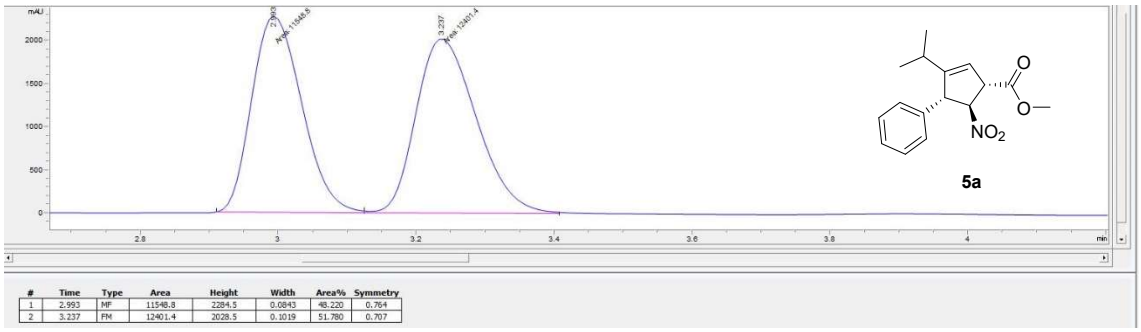

#	Time	Type	Area	Height	Width	Area%	Symmetry
1	2.993	MF	11548.8	2284.5	0.0843	48.220	0.764
2	3.237	FM	12401.4	2028.5	0.1019	51.780	0.707

Chromatogram of enantiomerically enriched (**5a**)

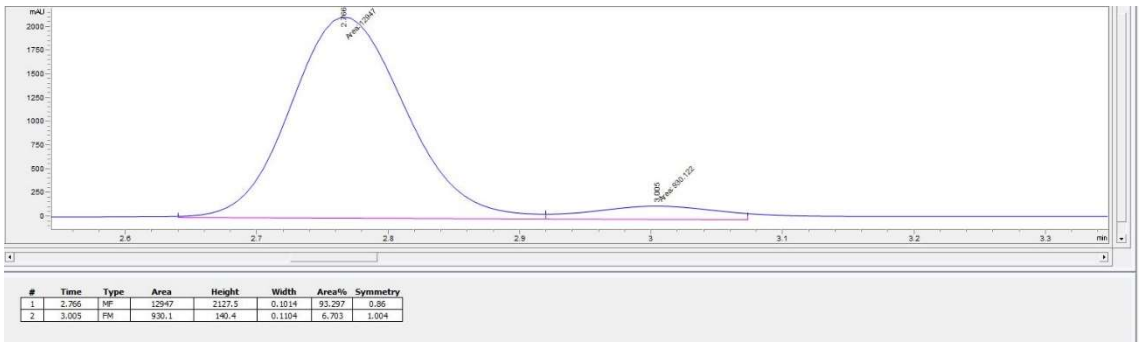

#	Time	Type	Area	Height	Width	Area%	Symmetry
1	2.766	MF	12947	2127.5	0.1014	93.297	0.86
2	3.005	FM	930.1	140.4	0.1104	6.703	1.004

9.5 nOeSY spectrum of compound 2a

The absolute configuration of starting material **1f** was unequivocally determined by its X-ray diffraction structure. We assumed that there were no changes in the configuration at C-R^2 through the expansion process (See **Scheme S1**). The C-NO_2 configurations was determined by bidimensional spectrum nOeSY of **2a**.

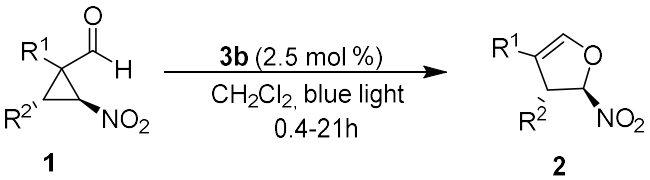

1 **2**

Scheme S1

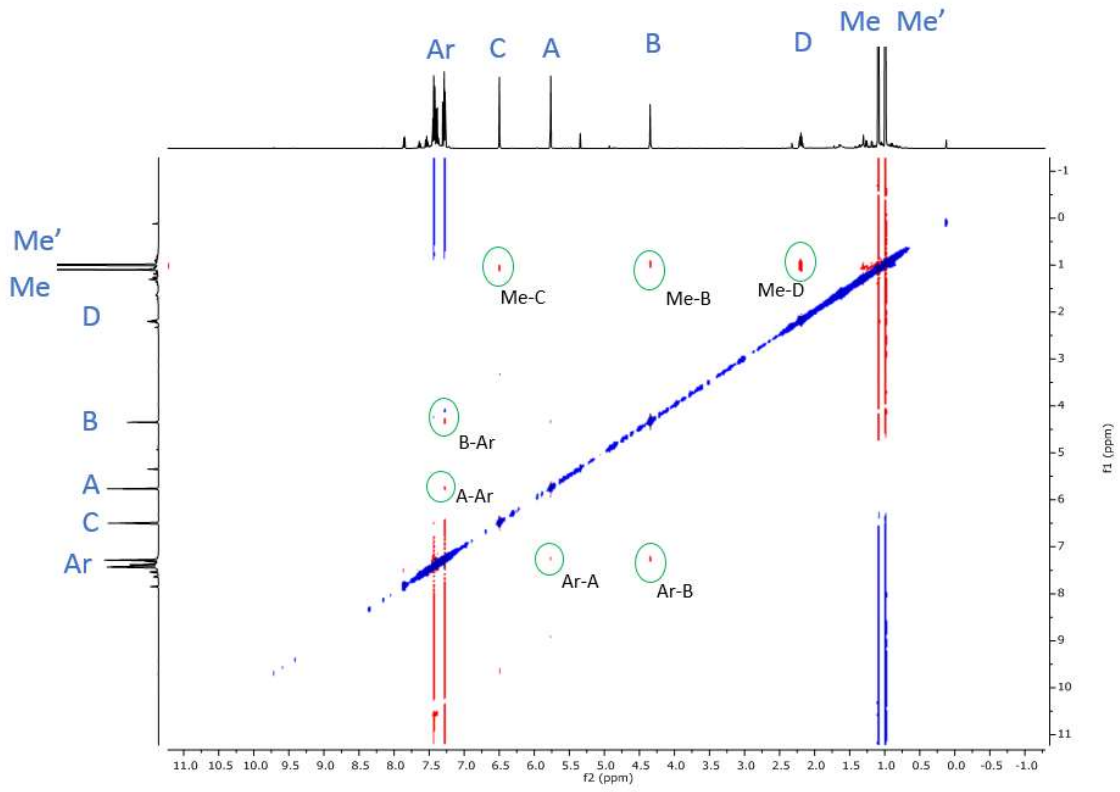

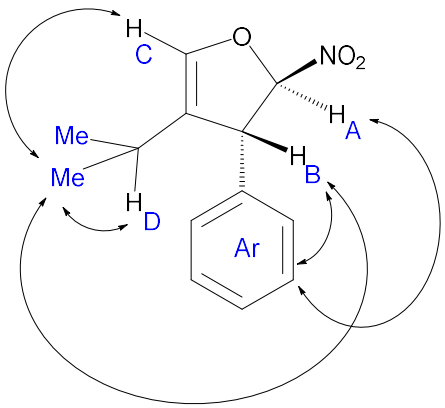

9.6 nOe spectra of compound 5a

The absolute configuration of the starting material **4c** was unequivocally determined by its X-ray diffraction structure. We assumed that there were no changes in the configuration at C-R^2 through the expansion process (See **Scheme S2**). The C-NO_2 and C-EWG configurations were determined by several NMR spectra irradiating some of the signals of compound **5a** in order to determine the nOe signals.

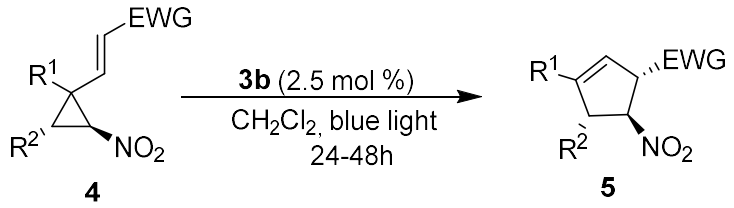

Scheme S2

^{1}H-NMR (300 MHz, $CDCl_3$) (**5a**)

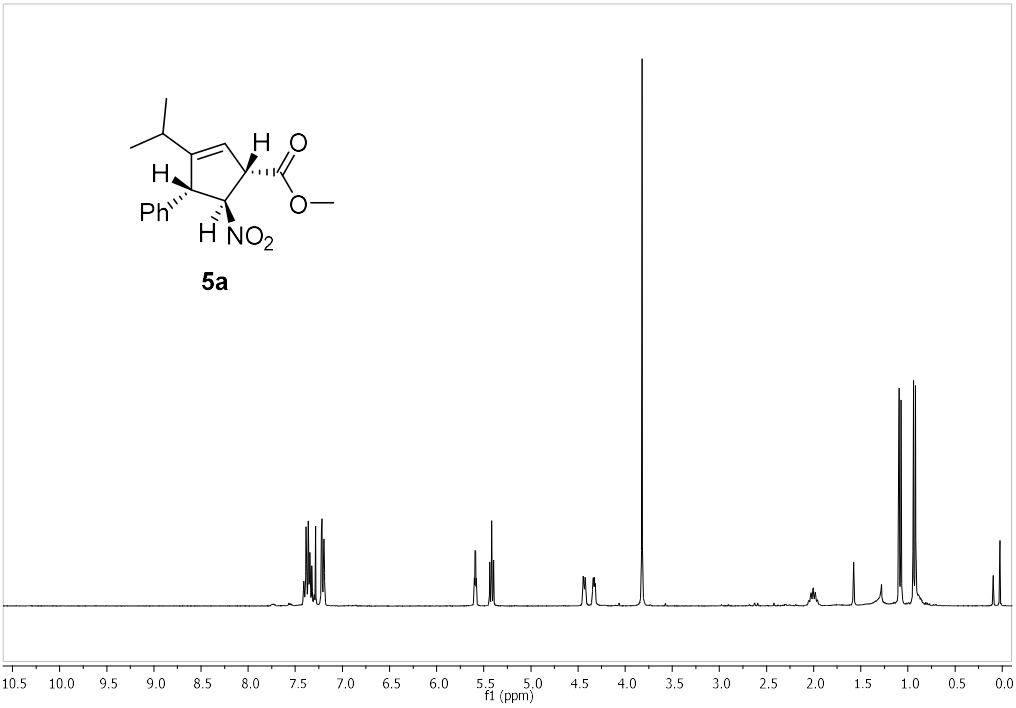

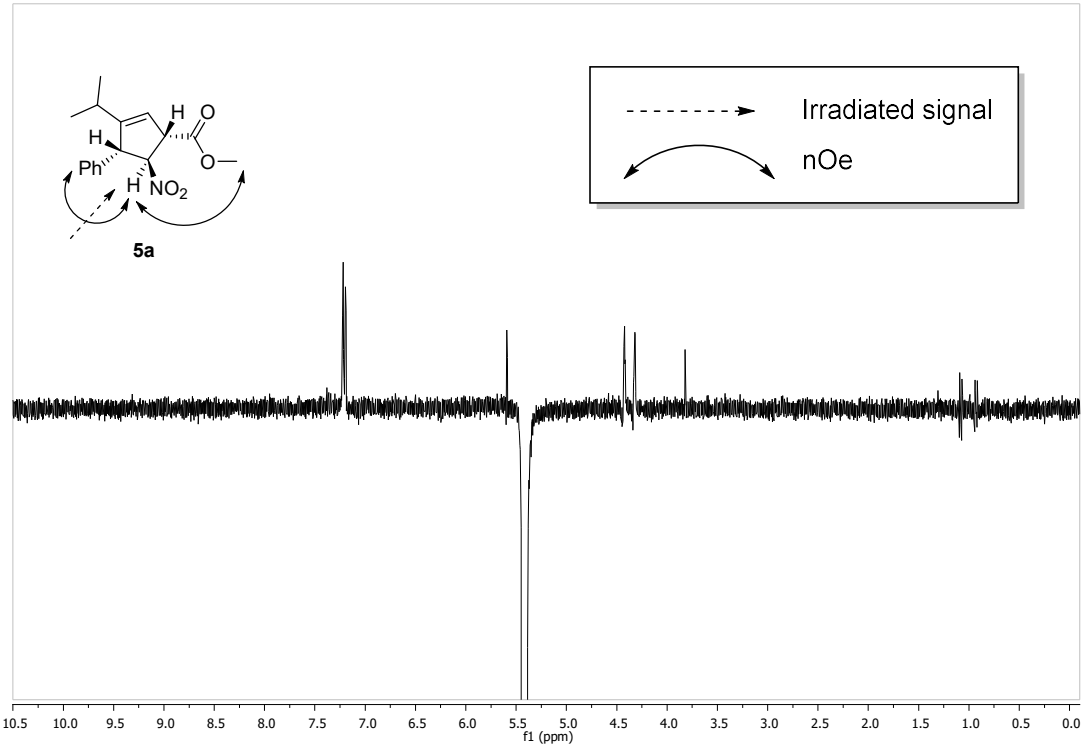
Irradiated signal
nOe
5a
10.5 10.0 9.5 9.0 8.5 8.0 7.5 7.0 6.5 6.0 5.5 5.0 4.5 4.0 3.5 3.0 2.5 2.0 1.5 1.0 0.5 0.0
f1 (ppm)

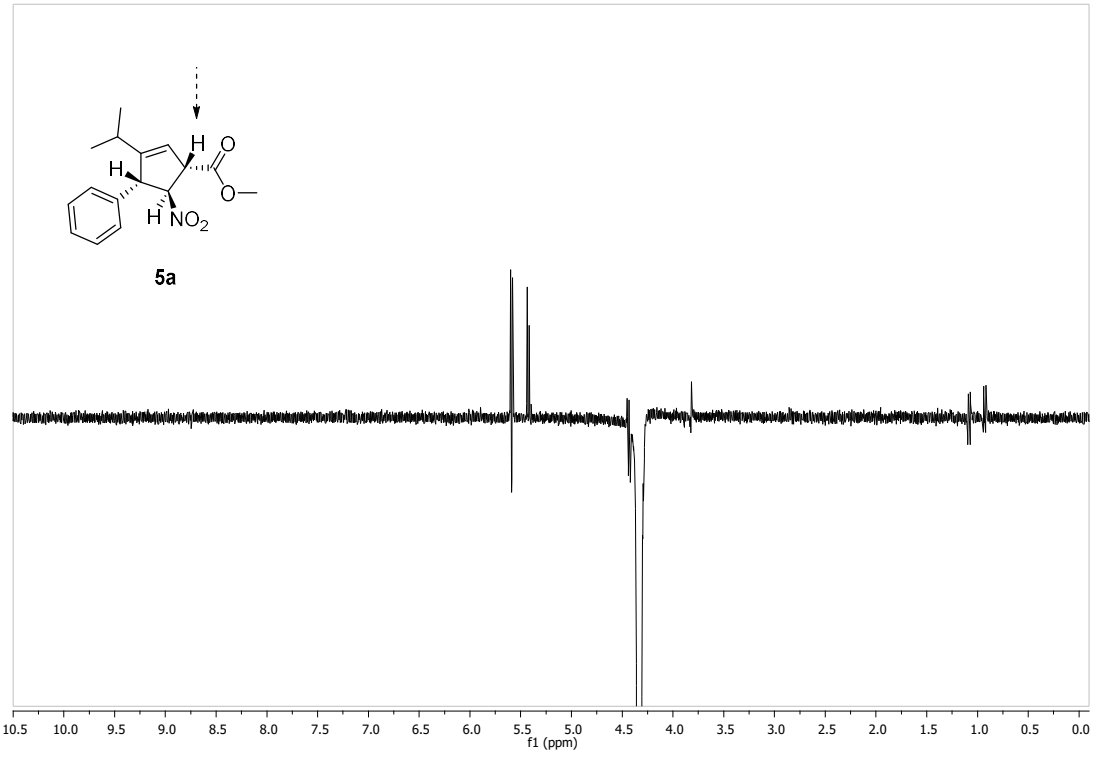
5a
10.5 10.0 9.5 9.0 8.5 8.0 7.5 7.0 6.5 6.0 5.5 5.0 4.5 4.0 3.5 3.0 2.5 2.0 1.5 1.0 0.5 0.0
f1 (ppm)

10. Computational Calculations

10.1 General Methods

The calculations presented in this work were performed with the Gaussian09 package[12] using the M06 functional[13] and a 6-31+G(d,p) basis set.[14] Solvation effects were included using the SMD implicit model[15] with dichloromethane (ε = 8.9) as solvent. All optimizations were performed without any geometrical constraint and the nature of all intermediates and transition states was verified by vibrational analysis. IRC calculations were performed to ensure the interconnected minima. The spin contamination introduced when performing unrestricted broken symmetry calculations was corrected according to Yamaguchi's approximate spin projection method.[16]

[12] Gaussian 09, Revision D.01, M. J. Frisch, G. W. Trucks, H. B. Schlegel, G. E. Scuseria, M. A. Robb, J. R. Cheeseman, G. Scalmani, V. Barone, B. Mennucci, G. A. Petersson, H. Nakatsuji, M. Caricato, X. Li, H. P. Hratchian, A. F. Izmaylov, J. Bloino, G. Zheng, J. L. Sonnenberg, M. Hada, M. Ehara, K. Toyota, R. Fukuda, J. Hasegawa, M. Ishida, T. Nakajima, Y. Honda, O. Kitao, H. Nakai, T. Vreven, J. A. Montgomery, Jr., J. E. Peralta, F. Ogliaro, M. Bearpark, J. J. Heyd, E. Brothers, K. N. Kudin, V. N. Staroverov, T. Keith, R. Kobayashi, J. Normand, K. Raghavachari, A. Rendell, J. C. Burant, S. S. Iyengar, J. Tomasi, M. Cossi, N. Rega, J. M. Millam, M. Klene, J. E. Knox, J. B. Cross, V. Bakken, C. Adamo, J. Jaramillo, R. Gomperts, R. E. Stratmann, O. Yazyev, A. J. Austin, R. Cammi, C. Pomelli, J. W. Ochterski, R. L. Martin, K. Morokuma, V. G. Zakrzewski, G. A. Voth, P. Salvador, J. J. Dannenberg, S. Dapprich, A. D. Daniels, O. Farkas, J. B. Foresman, J. V. Ortiz, J. Cioslowski, and D. J. Fox, Gaussian, Inc., Wallingford CT, **2013.**

[13] Y. Zhao & D.G. Truhlar **2006,** Theor. Chem. Account ,*120*, 215.

[14] W. J. Hehre, R. Ditchfield, and J. A. Pople, **1972**, J. Chem. Phys., *56*, 2257.

[15] A.V. Marenich, C. J. Cramer, and D. G. Truhlar **2009**, J. Phys. Chem. B, *113*, 6378.

[16] K. Yamaguchi, F. Jensen, A. Dorigo and K. N. Houk, **1988**, Chem. Phys. Lett., *149*, 537.

10.2 DFT results for the reactivity of 4a

The reaction pathways associated with **4a** (**Figure S5**) are similar to those of **1a**, with a few particularities. The cyclopropane opening is thermodynamically favorable for the three pathways and presents low energy barriers (from 3.3 to 9.8 kcal mol^{-1}). The resulting most stable biradical is again ^{3}**IIb**, the one that could evolve to the not observed isomer ^{1}**IVb**. This superior stability can be associated, also in this case, with the fact that in ^{3}**IIb** the substituents of the carbons supporting the unpaired electrons allows a better stabilization of the radical character (see below). However, this clearly shows that the nature of the final product does not depend neither on the facility for C-C bond breaking of the cyclopropane nor on the stability of the generated birradical. In particular, ^{3}**IIb** does not require any rearrangement to favor the 5-membered ring closing process, but the ^{1}**IIb** open shell minimum is much more stable than ^{3}**IIb**. This correlates with a S^2 value of 0.73 and an important overlap between the two monoocupied orbitals. Therefore, we expect that pathway **b** would never allow the required electronic reorganization for the formation of products and would always return to reactants. On the other hand, intermediate rearrangement from ^{3}**IIa** is needed to favor the formation of the final product, but, similarly to the case of **1a**, the ^{3}**IIa** to ^{3}**IIIa** rearrangement is kinetically very easy and exergonic (ΔG = -3.4 kcal mol^{-1}). This suggests that ^{3}**IIIa** may become the major intermediate. Moreover, although we could not localize ^{1}**IIa** (all our attempts evolved directly to the initial reactants), ^{1}**IIIa** has essentially the same Gibbs energy as the triplet state (^{3}**IIIa**). This is due to the lack of overlap between the orbitals bearing the unpaired electrons as shown by the S^2 value of about 1 and suggests that the open shell singlet may be stable enough to further evolve to products. This occurs by overcoming a very small Gibbs energy barrier of 2.0 kcal mol^{-1}, and indicates that only when the spin crossing occurs after rearrangement, the cyclopentene product will be formed. In this view, the same three key points seem to apply in the reactivity of **4a**. Only for pathway **a**: i) the birradical rearrangement is exergonic; ii) there is essentially no overlap between the monooccupied orbitals in the birradicals, and iii) atomic charges of opposite sign on the atoms involved in the formation of the new bond presents electrostatic attraction.

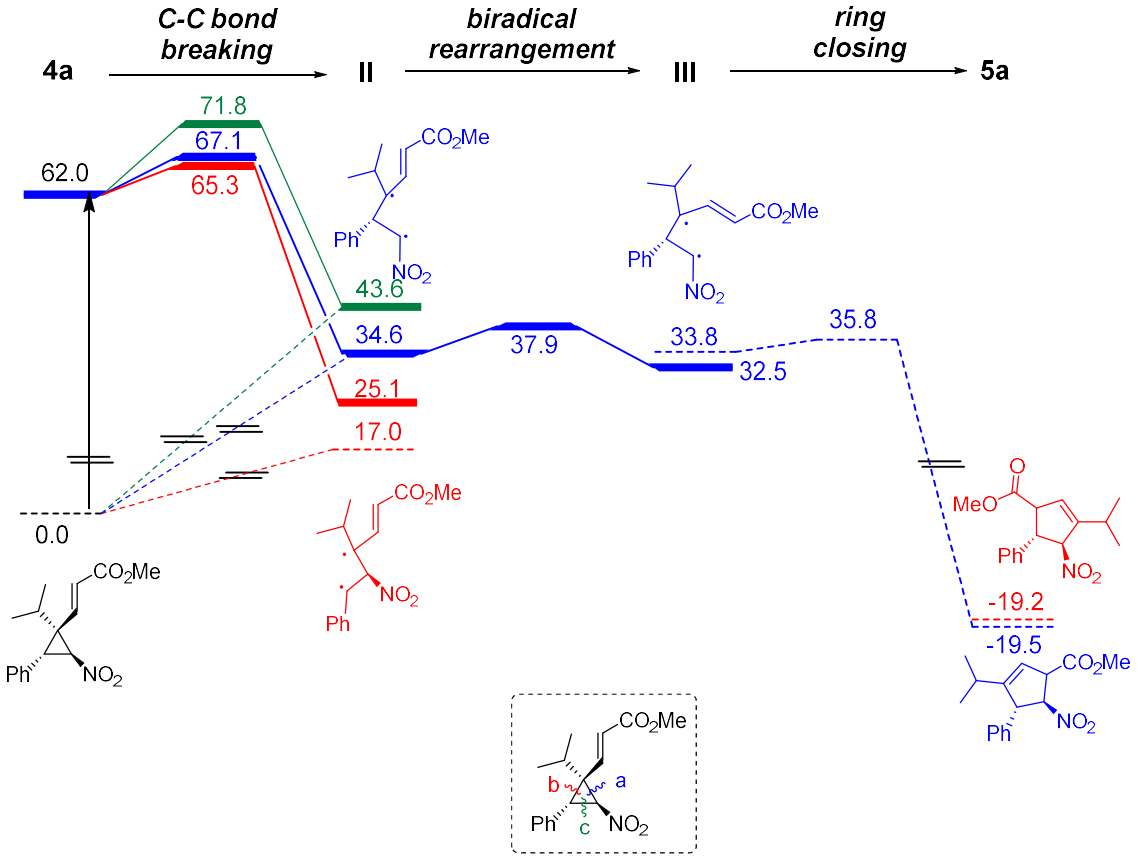

Figure S5. Gibbs Energy profile calculated for the reaction pathway from **4a** to **5a**. Solid lines correspond to species in the triplet state, whereas dashed lines refer to the energies of spin-corrected singlet state.

10.3 Analysis of the biradical stability

With the aim of understanding the relative stabilities of birradical **^{3}IIa**, **^{3}IIb** and **^{3}IIc** in the reacticity of both **1a** and **4a**, we computed the homolytic C-H bond cleavage energy in models of the fragments that can support the unpaired electrons in intermediates **^{3}IIa**, **^{3}IIb** and **^{3}IIc**. These models were constructed considering the groups in C1, C2 and C3 (Scheme 2) and replacing the rest of the opened cyclopropane by a methyl (see **Figure S6**). The goal is to analyse the differences in C-H bond dissociation energies induced by the presence of nitro, phenyl, isopropyl, carbonyl and ester groups and compare these values with the relative stabilities of the intermediates.

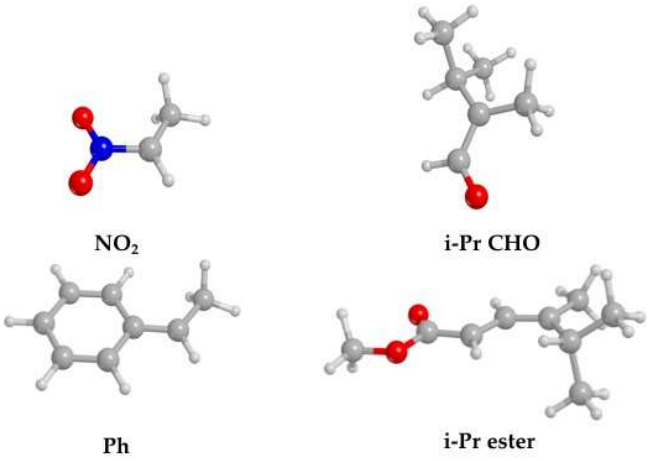

Figure S6. Simple secondary and tertiary radicals.

The lowest C-H bond dissociation energies are obtained for the tertiary carbon bearing an *i*Pr and either an ester or a carbonyl fragment, intermediate C-H dissociation energies are obtained for the fragment containing the Ph group and the largest values are associated with the carbon containing the NO_2 (see **Table S2**). This can be attributed to a larger stabilization of the resulting radical in the tertiary carbon rather than in the secondary phenyl or nitro containing fragments. Interestingly, the lowest in energy birradical intermediate **^{3}IIb** of **1a** has one unpaired electron on the tertiary carbon with *i*Pr and carbonyl fragments and the other on the secondary carbon with the phenyl. Similarly, for **4a** the most stable intermediate has the unpaired electrons on the *i*Pr ester and Ph fragments. In both cases, this corresponds to the isomer that localizes the unpaired electrons on the two more stabilizing fragments and shows that the stabilization of each radical separately has a predominant role. This is further confirmed by the relative stability of **^{3}IIa** and **^{3}IIc**, as well as the energy differences of the three intermediates. On one hand,

intermediate ^{3}**IIc** is always the highest energy isomer and it always corresponds to the situation in which two unpaired electrons are localized on the least stabilizing fragments. On the other hand, the energy difference between isomers matches reasonably well with the relative energies of the separated fragments.

Table S2. C-H bond cleavage energy (in kcal mol^{-1}) corresponding to the generation of the radicals reported in **Figure S6**. Potential energy (**E**), enthalpy (**H**) and Gibbs free energy (**G**) are reported.

	ΔE	ΔH	ΔG
NO_2	100.0	92.6	84.5
*i*PrCHO	89.4	82.9	74.4
Ph	92.2	85.1	76.8
*i*Pr ester	83.7	77.3	69.5

10.4 Study of the rotation of intermediates

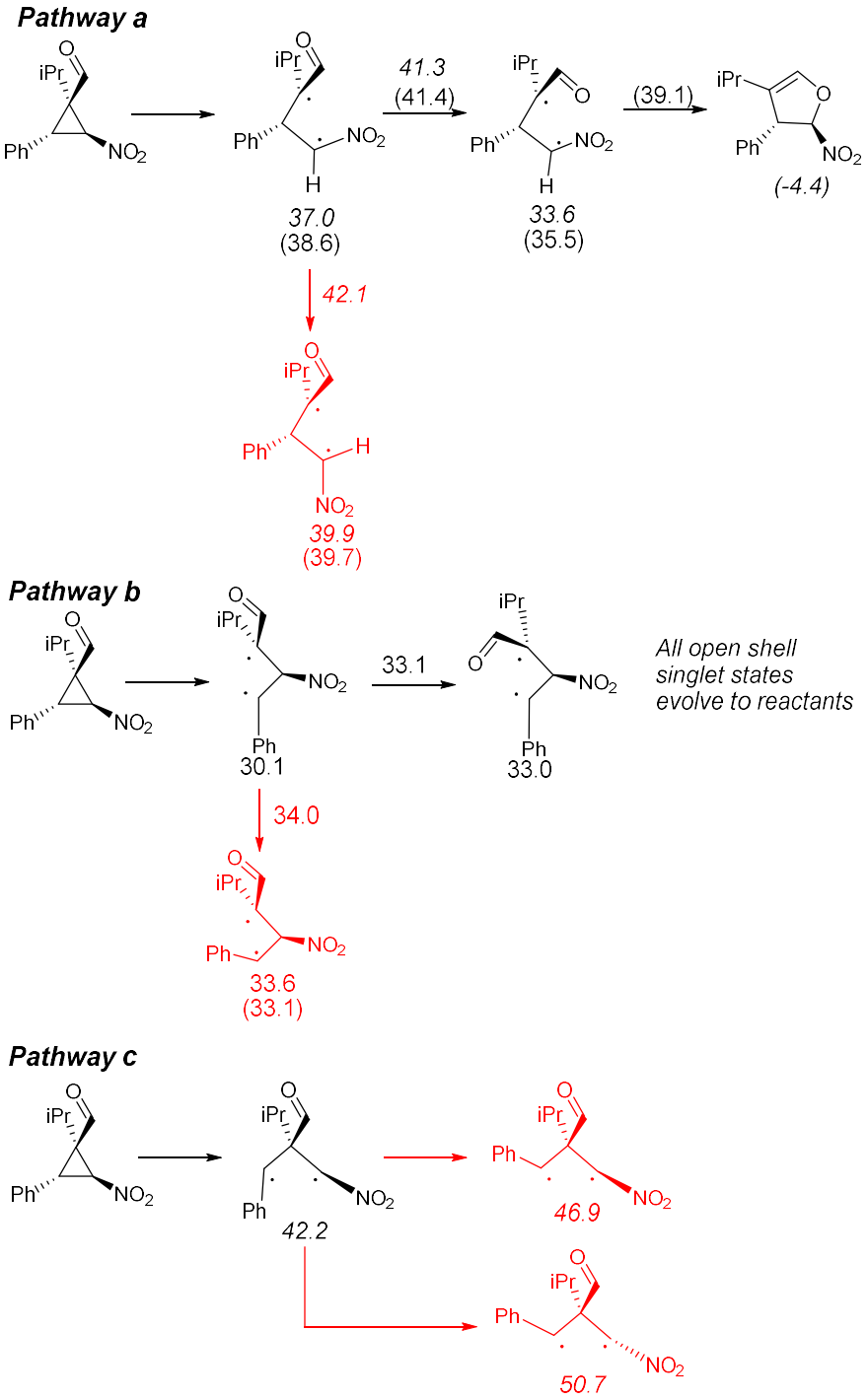

Scheme S3. Gibbs energies (kcal mol^{-1}) of the less stable rotamers of birradical **II** intermediate of each pathway (red structures). Pathways involving the most stable rotamers (in black) are also included for comparison. Values in italic corresponds to the triplet state, while the energetics of the singlet state is given in parenthesis.

Supplementary Information

Chromoselective Access to *Z*- or *E*- Allylated Amines and Heterocycles by a Photocatalytic Allylation Reaction

Ana María Martínez-Gualda, et al

Supplementary Methods.

General Experimental Details

The solvents employed in the reactions were used without any further purification. The reactions were carried out in vials and stirred with a magnetic bar under inert atmosphere.

NMR spectra were acquired on a Bruker 300 spectrometer, running at 300 and 75 MHz for ^{1}H and ^{13}C, respectively. Chemical shifts (δ) are reported in ppm relative to residual solvent signals ($CDCl_3$, 7.26 ppm for ^{1}H NMR and 77.00 ppm for ^{13}C NMR). ^{13}C NMR spectra were acquired on a broadband decoupled mode. The following abbreviations are used to describe peak patterns when appropriate: s (singlet), d (doublet), t (triplet), q (quartet), quint (quintet), sept (septuplet), m (multiplet), br (broad).

Analytical thin layer chromatography (TLC) was performed using pre-coated aluminium-backed plates, with fluorescence indicator to 254 nm, and visualized by ultraviolet irradiation. Purification of reaction products was carried out by flash chromatography (FC).

High Resolution Mass Spectra (HRMS) were acquired on a spectrometer Agilent Technologies 5977B MSD using electron ionization (EI) making use of the MassWorks software ver. 4.0.0.0. (Cerno Bioscience) for the formula identification. MassWorks is a MS calibration software, which calibrates for isotope profile as well as for mass accuracy allowing highly accurate comparisons between calibrated and theoretical spectra.[1],[2],[34] Obtained data are expressed in mass/charge (m/z) units.

Commercially available reagents and catalyst were used without further purification.

Supplementary Notes 1.

Synthesis of allylic derivatives (1)

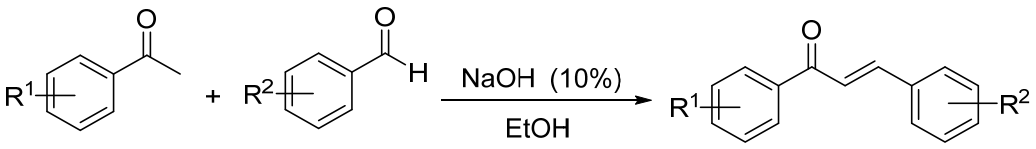

To a stirred solution of the corresponding ketone (5 mmol) in EtOH (14 mL), an aqueous solution of NaOH 10% (6 mL) was added dropwise at 0 ºC. After 5 min, the corresponding aldehyde was added dropwise and the mixture allowed to stir at room temperature until

complete conversion (4-6 h). After reaction completion, the mixture was diluted with water (10 mL). If the chalcone was precipitated at this stage, it was filtered and washed with water and with the minimum amount of EtOH, dried and used in the next step without further purification. If the chalcone was not precipitated, the reaction mixture was extracted three times with DCM (10 mL). The combined organic phases were dried over $MgSO_4$ and the solvent evaporated under reduced pressure. The crude oil was used in the next step without further purification.

(*E*)-1,3-di-*p*-tolylprop-2-en-1-one

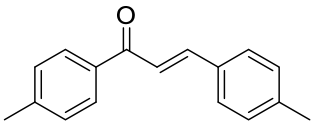

From 1-(*p*-tolyl)ethan-1-one (0.66 mL, 5 mmol) and 4-methylbenzaldehyde (0.59 mL, 5 mmol), following the general procedure, (*E*)-1,3-di-*p*-tolylprop-2-en-1-one (1.180 g, 4.99 mmol) was obtained in 99% yield as a white solid. Spectroscopic data are in agreement with the published data.[5] **^{1}H-NMR (300 MHz, $CDCl_3$)** δ 7.94 (d, *J* = 6.7 Hz, 2H), 7.80 (d, *J* = 15.5 Hz, 1H), 7.60 – 7.35 (m, 3H), 7.35 – 7.20 (m, 4H), 2.45 (s, 3H), 2.40 (s, 3H).

(*E*)-1,3-di-*m*-tolylprop-2-en-1-one

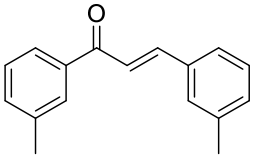

From 1-(*m*-tolyl)ethan-1-one (0.68 mL, 5 mmol) and 3-methylbenzaldehyde (0.59 mL, 5 mmol), following the general procedure, (*E*)-1,3-di-*m*-tolylprop-2-en-1-one (1.044 g, 4.42 mmol) was obtained in 88% yield as a pale yellow oil. Spectroscopic data are in agreement with the published data.[6] **^{1}H-NMR (300 MHz, $CDCl_3$)** δ 7.85 – 7.75 (m, 3H), 7.55 – 7.37 (m, 5H), 7.35 – 7.28 (m, 1H), 7.25 – 7.20 (m, 1H), 2.45 (s, 3H), 2.41 (s, 3H).

(*E*)-1,3-bis(3,5-dimethoxyphenyl)prop-2-en-1-one

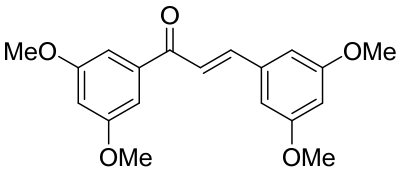

From 1-(3,5-dimethoxyphenyl)ethan-1-one (901.0 mg, 5 mmol) and 3,5-dimethoxybenzaldehyde (831.0 mg, 5 mmol), following the general procedure, (*E*)-1,3-bis(3,5-dimethoxyphenyl)prop-2-en-1-one (1.412 g, 4.30 mmol) was obtained in 86% yield as a white solid. Spectroscopic data are in agreement with the published data.[7] **^{1}H-NMR (300 MHz, $CDCl_3$)** δ 7.72 (d, *J* = 15.7 Hz, 1H), 7.41 (d, *J* = 15.6 Hz, 1H), 7.14 (d, *J* = 2.4 Hz, 2H), 6.78 (d, *J* = 2.4 Hz, 2H), 6.68 (t, *J* = 2.2 Hz, 1H), 6.53 (t, *J* = 2.2 Hz, 1H), 3.87 (s, 6H), 3.85 (s, 6H).

(*E*)-1,3-bis(4-fluorophenyl)prop-2-en-1-one

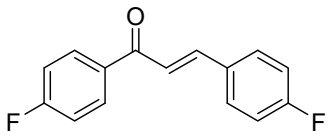

From 1-(4-fluorophenyl)ethan-1-one (0.61 mL, 5 mmol) and 4-fluorobenzaldehyde (0.54 mL, 5 mmol), following the general procedure, (*E*)-1,3-bis(4-fluorophenyl)prop-2-en-1-one (927 mg, 3.80 mmol) was obtained in 76% yield as a white solid. Spectroscopic data are in agreement with the published data.[8] **^{1}H-NMR (300 MHz, $CDCl_3$)** δ 8.10 – 8.00 (m, 2H), 7.79 (d, *J* = 15.8 Hz, 1H), 7.70 – 7.60 (m, 2H), 7.44 (d, *J* = 15.8, 1H), 7.25 – 7.08 (m, 4H).

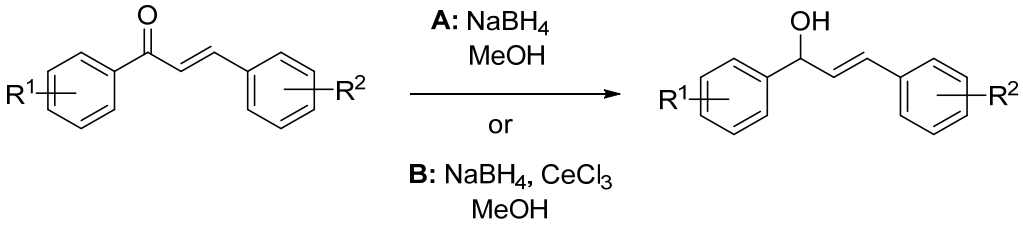

Procedure **A** for chalcone reduction: To a stirred solution of the corresponding chalcone (1.5 mmol) in MeOH (3 mL) at 0 ºC, $NaBH_4$ (114 mg, 3 mmol) was added portionwise. The mixture was then stirred at room temperature for 6 h. The reaction was quenched with water (3 mL) and extracted with DCM (3 x 10 mL). The combined organic phases were dried over $MgSO_4$ and the solvent evaporated under reduced pressure. The crude was used in the next step without further purification.

Procedure **B** for chalcone reduction: To a stirred solution of the corresponding chalcone (3.5 mmol) and $CeCl_3$ (106 mg, 4.2 mmol) in MeOH (15 mL) at 0 ºC, $NaBH_4$ (161 mg, 4.2 mmol) was added portionwise. The mixture was then stirred at room temperature for 30 min. The reaction was quenched with water (15 mL) and extracted with DCM (3 x 20 mL). The combined organic phases were dried over $MgSO_4$ and the solvent evaporated under reduced pressure. The crude was used in the next step without further purification.

(*E*)-1,3-di-*p*-tolylprop-2-en-1-ol

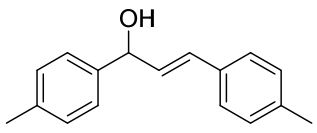

From (*E*)-1,3-di-*p*-tolylprop-2-en-1-one (1.11 g, 4.70 mmol), following the general procedure **A**, (*E*)-1,3-di-p-tolylprop-2-en-1-ol (554 mg, 2.32 mmol) was obtained in 50% yield as a colorless oil. Spectroscopic data are in agreement with the published data.[6] **^{1}H-NMR (300 MHz, $CDCl_3$)** δ 7.37 – 7.28 (m, 4H), 7.22 – 7.08 (m, 4H), 6.65 (d, *J* = 15.7 Hz, 1H),

6.33 (dd, *J* = 15.8, 6.5 Hz, 1H), 5.40 – 5.32 (m, 1H), 2.36 (s, 3H), 2.33 (s, 3H), 1.95 (d, *J* = 3.6 Hz, 1H).

(*E*)-1,3-di-*m*-tolylprop-2-en-1-ol

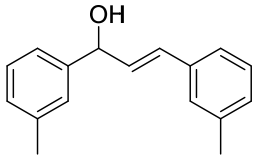

From (*E*)-1,3-di-*m*-tolylprop-2-en-1-one (1.040 g, 4.42 mmol), following the general procedure **B**, (*E*)-1,3-di-*m*-tolylprop-2-en-1-ol (823 g, 3.46 mmol) was obtained in 78% yield as a pale yellow oil. Spectroscopic data are in agreement with the published data.[9] **^{1}H-NMR (300 MHz, $CDCl_3$)** δ 7.30 – 7.05 (m, 8H), 6.67 (dd, *J* = 15.8, 1.2 Hz, 1H), 6.37 (dd, *J* = 15.8, 6.5 Hz, 1H), 5.35 (d, *J* = 6.6 Hz, 1H), 2.37 (s, 3H), 2.33 (s, 3H), 1.99 (s, 1H).

(*E*)-1,3-bis(3,5-dimethoxyphenyl)prop-2-en-1-ol

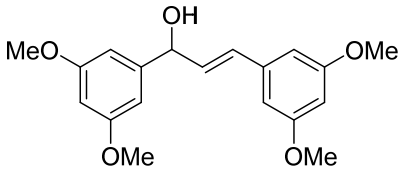

From (*E*)-1,3-bis(3,5-dimethoxyphenyl)prop-2-en-1-one (1.334 g, 4.07 mmol), following the general procedure **B**, (*E*)-1,3-bis(3,5-dimethoxyphenyl)prop-2-en-1-ol (897 mg, 2.72 mmol) was obtained in 67% yield as a white solid. **^{1}H-NMR (300 MHz, $CDCl_3$)** δ 6.62 (d, *J* = 15.8 Hz, 1H), 6.60 (d, *J* = 2.1 Hz, 2H), 6.55 (d, *J* = 2.3 Hz, 2H), 6.40 (t, *J* = 2.3 Hz, 1H), 6.37 (t, *J* = 2.1 Hz, 1H), 6.33 (dd, *J* = 15.8, 6.4 Hz, 1H), 5.33 – 5.30 (m, 1H), 3.80 (s, 6H), 3.79 (s, 6H), 2.04 – 2.00 (m, 1H). **^{13}C-NMR (75 MHz, $CDCl_3$)** δ 161.0 (2C), 160.9 (2C), 145.3, 138.5, 131.7, 130.6, 104.7 (2C), 104.2 (2C), 100.2, 99.7, 75.0, 55.4 (2C), 55.3 (2C). **HRMS (EI$^+$)** calculated for $C_{19}H_{22}O_4$ [M-O]$^+$: 314.1513, found: 314.1518.

(*E*)-1,3-bis(4-fluorophenyl)prop-2-en-1-ol

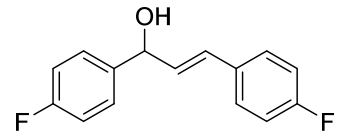

From 1-(4-fluorophenyl)ethan-1-one (927 mg, 3.8 mmol), following the general procedure **A**, (*E*)-1,3-bis(4-fluorophenyl)prop-2-en-1-ol (697 mg, 2.83 mmol) was obtained in 75% yield as a colorless oil. Spectroscopic data are in agreement with the published data.[9] **^{1}H-NMR (300 MHz, $CDCl_3$)** δ 7.42 – 7.32 (m, 4H), 7.10 – 6.95 (m, 4H), 6.64 (d, *J* = 15.8 Hz, 1H), 6.27 (dd, *J* = 15.8, 6.5 Hz, 1H), 5.40 – 5.30 (m, 1H), 1.99 (d, *J* = 3.5 Hz, 1H).

(*E*)-1-(4-fluorophenyl)-3-phenylprop-2-en-1-ol

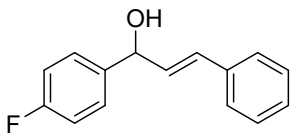

From (*E*)-1-(4-fluorophenyl)-3-phenylprop-2-en-1-one (339 mg, 1.5 mmol), following the general procedure **A**, (*E*)-1-(4-fluorophenyl)-3-phenylprop-2-en-1-ol (314.6 mg, 1.38 mmol) was obtained in 92% yield as a colorless oil. Spectroscopic data are in agreement with the published data.[10] **^{1}H-NMR (300 MHz, $CDCl_3$)** δ 7.45 – 7.23 (m, 7H), 7.10 – 7.03 (m,

2H), 6.69 (d, *J* = 15.8 Hz, 1H), 6.36 (dd, *J* = 15.9, 6.5 Hz, 1H), 5.42 – 5.36 (m, 1H), 2.02 (d, *J* = 3.2 Hz, 1H).

(*E*)-3-(4-fluorophenyl)-1-phenylprop-2-en-1-ol

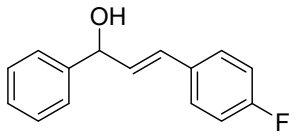

From (*E*)-3-(4-fluorophenyl)-1-phenylprop-2-en-1-one (339 mg mL, 1.5 mmol), following the general procedure **A**, (*E*)-3-(4-fluorophenyl)-1-phenylprop-2-en-1-ol (304.1 mg, 1.34 mmol) was obtained in 89% yield as a colorless oil. Spectroscopic data are in agreement with the published data.[10] **^{1}H NMR (300 MHz, $CDCl_3$)** δ 7.46 – 7.30 (m, 7H), 7.05 – 6.95 (m, 2H), 6.66 (d, *J* = 15.8 Hz, 1H), 6.31 (dd, *J* = 15.9, 6.5 Hz, 1H), 5.42 – 5.36 (m, 1H), 2.02 (d, *J* = 3.5 Hz, 1H).

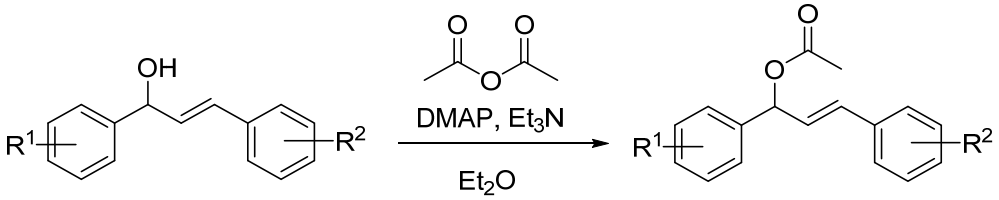

To a vigorously stirred solution of the corresponding alcohol (3 mmol), DMAP (13 mg, 0.097 mmol) and Et_3N (1.31 mL, 9.4 mmol) in Et_2O (7 mL) at 0 ºC, acetic anhydride was added dropwise (0.87 mL, 9.1 mmol). The reaction was stirred at room temperature for 2 h. The reaction mixture was quenched with sat. solution of $NaHCO_3$ (10 mL). The organic phase was separated and the aq. layer extracted with EtOAc (3 x 10 mL). The combined organic phases were dried over $MgSO_4$ and the solvent evaporated under reduced pressure. The crude was used in the next step without further purification.

(*E*)-1,3-di-*p*-tolylallyl acetate (1b)

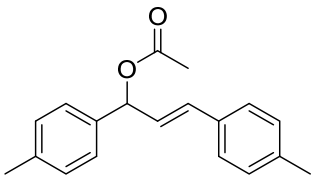

From (*E*)-1,3-di-*p*-tolylprop-2-en-1-ol (520 mg, 2.20 mmol), following the general procedure, (*E*)-1,3-di-*p*-tolylallyl acetate (**1b**) (500 mg, 1.78 mmol) was obtained in 81% yield as a pale yellow oil. Spectroscopic data are in agreement with the published data.[11] **^{1}H-NMR (300 MHz, $CDCl_3$)** δ 7.33 – 7.24 (m, 4H), 7.18 (d, *J* = 7.9 Hz, 2H), 7.10 (d, *J* = 7.7 Hz, 2H), 6.59 (d, *J* = 15.7 Hz, 1H), 6.40 (d, *J* = 6.9 Hz, 1H), 6.29 (dd, *J* = 15.7, 6.8 Hz, 1H), 2.35 (s, 3H), 2.32 (s, 3H), 2.11 (s, 3H).

(*E*)-1,3-di-*m*-tolylallyl acetate (1c)

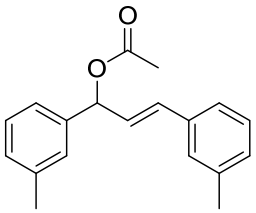

From (*E*)-1,3-di-*m*-tolylprop-2-en-1-ol (823 mg, 3.46 mmol), following the general procedure, (*E*)-1,3-di-*m*-tolylallyl acetate (**1c**) (812 mg, 2.9 mmol) was obtained in 84% yield as a pale yellow oil. Spectroscopic data are in agreement with the published data.[12] **^{1}H-NMR (300 MHz, $CDCl_3$)** δ 7.30 – 7.03 (m, 8H), 6.61 (d, *J* = 15.3 Hz, 1H), 6.41 (d, *J* = 6.9 Hz, 1H), 6.33 (dd, *J* = 15.5, 6.8 Hz, 1H), 2.37 (s, 3H), 2.33 (s, 3H), 2.14 (s, 3H).

(*E*)-1,3-bis(3,5-dimethoxyphenyl)allyl acetate (1d)

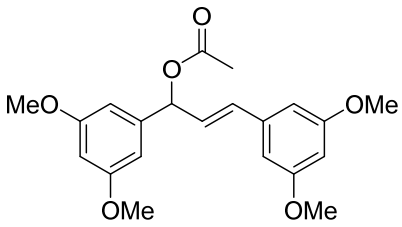

From (*E*)-1,3-bis(3,5-dimethoxyphenyl)prop-2-en-1-ol (897 mg, 2.72 mmol), following the general procedure, (*E*)-1,3-bis(3,5-dimethoxyphenyl)allyl acetate (**1d**) (925 mg, 2.49 mmol) was obtained in 91% yield as a pale yellow oil. **^{1}H-NMR (300 MHz, $CDCl_3$)** δ 6.56 (d, *J* = 15.4 Hz, 1H), 6.55 (d, *J* = 2.3 Hz, 2H), 6.53 (d, *J* = 2.3 Hz, 2H), 6.41 (t, *J* = 2.3 Hz, 1H), 6.37 (t, *J* = 2.3 Hz, 1H), 6.34 (d, *J* = 6.9 Hz, 1H), 6.28 (dd, *J* = 15.3, 6.8 Hz, 1H), 3.80 (s, 6H), 3.78 (s, 6H), 2.14 (s, 3H). **^{13}C-NMR (75 MHz, $CDCl_3$)** δ 169.9, 161.0 (2C), 160.9 (2C), 141.5, 138.2, 132.7, 127.8, 105.0 (2C), 104.8 (2C), 100.5, 99.9, 75.9, 55.39 (2C), 55.36 (2C), 21.3. **HRMS (EI^+)** calculated for $C_{19}H_{22}O_4$ $[M-C_2H_3O_2+H]^+$: 314.1513, found: 314.1512.

(*E*)-1,3-bis(4-fluorophenyl)allyl acetate (1e)

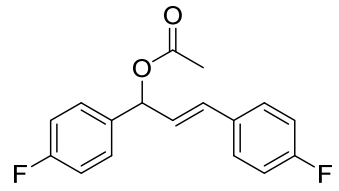

From (*E*)-1,3-bis(4-fluorophenyl)prop-2-en-1-ol (697 mg, 2.8 mmol), following the general procedure, (*E*)-1,3-bis(4-fluorophenyl)allyl acetate (**1e**) (674 mg, 2.34 mmol) was obtained in 84% yield as a pale yellow oil. **^{1}H-NMR (300 MHz, $CDCl_3$)** δ 7.45 – 7.32 (m, 4H), 7.11 – 6.97 (m, 4H), 6.58 (d, *J* = 15.8 Hz, 1H), 6.40 (d, *J* = 6.7 Hz, 1H), 6.24 (dd, *J* = 15.8, 6.7 Hz, 1H), 2.13 (s, 3H). **^{13}C-NMR (75 MHz, $CDCl_3$)** δ 169.9, 162.6 (d, $^1J_{C\text{-}F}$ = 247.7 Hz), 162.5 (d, $^1J_{C\text{-}F}$ = 247.0 Hz), 135.0 (d, $^4J_{C\text{-}F}$ = 3.1 Hz), 132.2 (d, $^4J_{C\text{-}F}$ = 3.3 Hz), 131.6, 128.9 (d, $^3J_{C\text{-}F}$ = 8.2 Hz, 2C), 128.3 (d, $^3J_{C\text{-}F}$ = 8.1 Hz, 2C), 127.1 (d, $^5J_{C\text{-}F}$ = 2.3 Hz), 115.6 (d, $^2J_{C\text{-}F}$ = 21.7 Hz, 4C), 75.4, 21.3. **^{19}F-NMR (282 MHz, $CDCl_3$)** δ -113.5, -113.7. **HRMS (ESI^+)** calculated for $C_{17}H_{14}F_2O_2$ $[M]^+$: 288.0956, found: 288.0950.

(*E*)-1-(4-fluorophenyl)-3-phenylallyl acetate (1j)

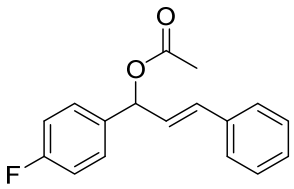

From (*E*)-1-(4-fluorophenyl)-3-phenylprop-2-en-1-ol (314.6 mg, 1.38 mmol), following the general procedure, (*E*)-1-(4-fluorophenyl)-3-phenylallyl acetate (**1j**) (309 mg, 1.14 mmol) was obtained in 83% yield as a pale yellow oil. **^{1}H-NMR (300 MHz, $CDCl_3$)** δ 7.43 – 7.25 (m, 7H), 7.43 – 7.25 (m, 2H), 6.62 (d, *J* = 15.7 Hz, 1H), 6.42 (d, *J* = 6.8 Hz, 1H), 6.32 (dd, *J* = 15.7, 6.6 Hz, 1H), 2.14 (s, 3H). **^{13}C-NMR (75 MHz, $CDCl_3$)** δ 169.9, 162.5 (d, $^{1}J_{C\text{-}F}$ = 246.9 Hz), 136.0, 135.1 (d, $^{4}J_{C\text{-}F}$ = 3.3 Hz), 132.7, 128.9 (d, $^{3}J_{C\text{-}F}$ = 8.3 Hz, 2C), 128.6 (2C), 128.4, 127.2, 126.7 (2C), 115.5 (d, $^{2}J_{C\text{-}F}$ = 21.6 Hz, 2C), 75.4, 21.3. **^{19}F-NMR (282 MHz, $CDCl_3$)** δ -113.8. **HRMS (EI^{+})** calculated for $C_{17}H_{15}FO_2$ [M]$^{+}$: 270.1051, found: 270.1042.

(*E*)-3-(4-fluorophenyl)-1-phenylallyl acetate (1k)

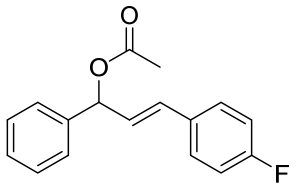

From (*E*)-3-(4-fluorophenyl)-1-phenylprop-2-en-1-ol (304.1 mg, 1.34 mmol) following the general procedure, (*E*)-3-(4-fluorophenyl)-1-phenylallyl acetate (**1k**) (288 mg, 1.07 mmol) was obtained in 80% yield as a colorless oil. **^{1}H-NMR (300 MHz, $CDCl_3$)** δ 7.44 – 7.30 (m, 7H), 7.05 – 6.95 (m, 2H), 6.60 (d, *J* = 15.7 Hz, 1H), 6.42 (d, *J* = 6.7 Hz, 1H), 6.26 (dd, *J* = 15.8, 6.8 Hz, 1H), 2.14 (s, 3H). **^{13}C-NMR (75 MHz, $CDCl_3$)** δ 170.0, 162.6 (d, $^{1}J_{C\text{-}F}$ = 247.6 Hz), 139.1, 132.3 (d, $^{4}J_{C\text{-}F}$ = 3.4 Hz), 131.4, 128.6 (2C), 128.3 (d, $^{3}J_{C\text{-}F}$ = 8.4 Hz, 2C), 128.2, 127.3 (d, $^{5}J_{C\text{-}F}$ = 2.3 Hz), 127.0 (2C), 115.5 (d, $^{2}J_{C\text{-}F}$ = 21.7 Hz, 2C), 76.1, 21.3. **^{19}F-NMR (282 MHz, $CDCl_3$)** δ -113.7. **HRMS (EI^{+})** calculated for $C_{17}H_{15}FO_2$ [M]$^{+}$: 270.1051, found: 270.1056.

Synthesis of 1f:

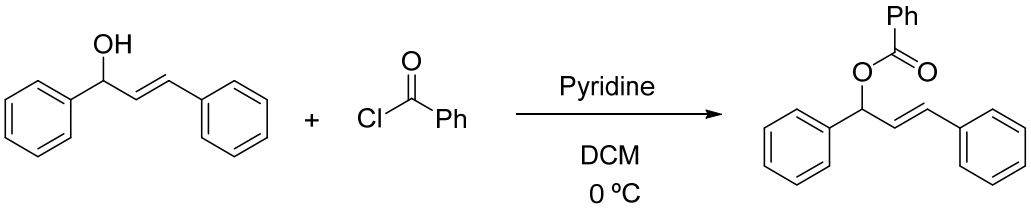

To a stirred solution of (*E*)-1,3-diphenylprop-2-en-1-ol (210 mg, 1 mmol) and pyridine (0.23 mL, 2.8 mmol) in DCM (5 mL) was added benzoyl chloride (0.33 mL, 2.8 mmol) dropwise at 0 ºC, and the mixture was stirred at room temperature for 12 h. The reaction was quenched by the addition of water (5 mL). The aqueous phase was extracted with Et_2O (4 x 8 mL). The combined organic phases were washed successively with 10% HCl (15 mL), sat. $NaHCO_3$ (15 mL), brine (15 mL) and water (15 mL), dried over $MgSO_4$ and the solvent evaporated under reduced pressure. The crude was purified by column chromatography. Eluent: Cyclohexane:AcOEt (9:1).

(*E*)-1,3-diphenylallyl benzoate (1f)

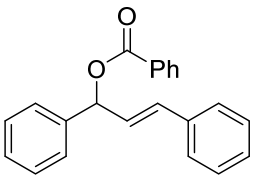

(*E*)-1,3-diphenylallyl benzoate (**1f**) (288 mg, 0.56 mmol) was obtained in 56% yield as a white solid. Spectroscopic data are in agreement with the published data.[13] **^{1}H-NMR (300 MHz, $CDCl_3$)** δ 8.19 – 8.09 (m, 2H), 7.60 – 7.20 (m, 13H), 6.73 (d, *J* = 16.0 Hz, 1H), 6.70 (d, *J* = 6.7 Hz, 1H), 6.47 (dd, *J* = 15.9, 6.7 Hz, 1H).

Synthesis of 1g:

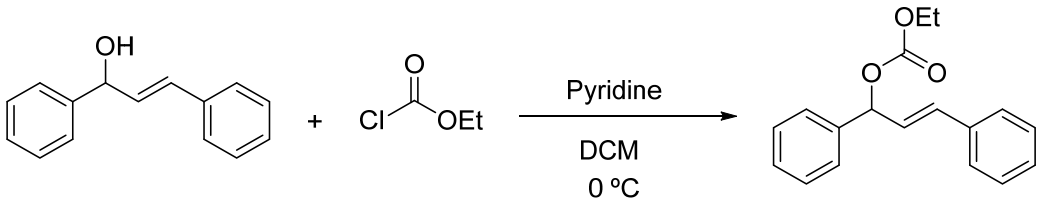

To a stirred solution of (*E*)-1,3-diphenylprop-2-en-1-ol (315 mg, 1.5 mmol) and pyridine (0.13 mL, 1.65 mmol) in DCM (6 mL) was added ethyl chloroformate (0.26 mL, 2.7 mmol) dropwise at 0 ºC. After 3 h stirring at room temperature, 1M HCl (4.5 mL) was added. The mixture was extracted with DCM (3 x 5 mL). The combined organic phases were washed with 1M HCl (8 mL), dried over $MgSO_4$ and the solvent evaporated under reduced pressure. The crude was used in the next step without further purification.

(*E*)-1,3-diphenylallyl ethyl carbonate (1g)

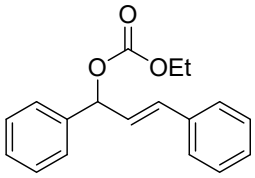

(*E*)-1,3-diphenylallyl ethyl carbonate (**1g**) (257 mg, 0.92 mmol) was obtained in 61% yield as a colorless oil. Spectroscopic data are in agreement with the published data.[14] **^{1}H-NMR (300 MHz, $CDCl_3$)** δ 7.46 – 7.26 (m, 10H), 6.69 (d, *J* = 15.7 Hz, 1H), 6.37 (dd, *J* = 15.7, 6.9 Hz, 1H), 6.26 (d, *J* = 6.9 Hz, 1H), 4.21 (q, *J* = 7.2, Hz, 1H), 4.20 (q, *J* = 7.2, Hz, 1H) 1.31 (t, *J* = 7.2 Hz, 3H).

Synthesis of 1h

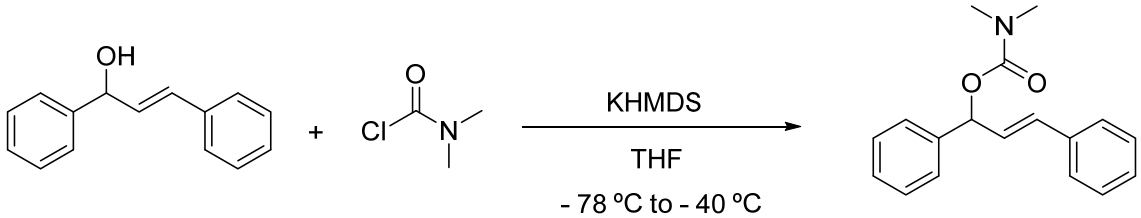

To a stirred solution of (*E*)-1,3-diphenylprop-2-en-1-ol (315 mg, 1.5 mmol) in THF (6 mL) was added dropwise a solution of potassium hexamethyldisilazide (1.83 mL, 1.65 mmol) in THF (1M) at – 78 ºC. After 10 min stirring at – 78 ºC, a solution of dimethyl carbamoyl chloride (0.15 mL, 1.65 mmol) in THF (3 mL) was added. The mixture was then stirred

at – 40 ºC during 1 h. The mixture was poured into a mixture of THF (1.5 mL) and acetic acid (1.5 mL). The aqueous phase was extracted with Et_2O (3 x 5 mL). The combined organic phases were washed with water (5 mL) and brine (1.5 mL), dried over $MgSO_4$ and the solvent evaporated under reduced pressure. The crude was used in the next step without further purification.

(*E*)-1,3-diphenylallyl dimethylcarbamate (1h)

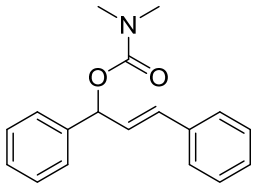

(*E*)-1,3-diphenylallyl dimethylcarbamate (**1h**) (380 mg, 0.92 mmol) was obtained in 90% yield as a yellow oil. **^{1}H-NMR (300 MHz, $CDCl_3$)** δ 7.45 – 7.20 (m, 10H), 6.67 – 6.58 (m, 1H), 6.46 – 6.30 (m, 2H), 3.02 (s, 3H), 2.94 (s, 3H). **^{13}C-NMR (75 MHz, $CDCl_3$)** δ 175.4, 155.7, 140.0, 136.4, 132.0, 128.51 (2C), 128.48 (2C), 128.45, 127.9, 126.9 (2C), 126.7 (2C), 76.96, 36.5, 35.9. **HRMS (EI^+)** calculated for $C_{18}H_{19}NO_2^+$ $[M]^+$: 281.1410, found: 281.1470.

General procedure for the preparation of *N*-phenyl phenothiazine catalyst (3e)

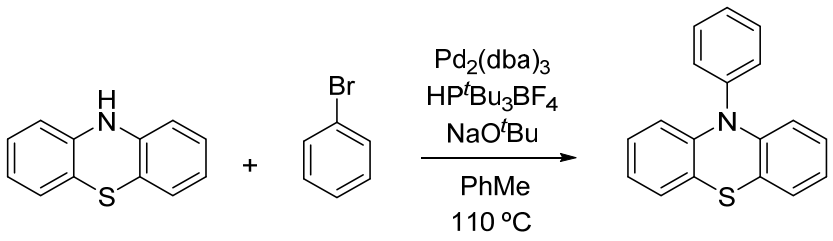

Phenothiazine (1.99 g, 10 mmol) and 1-bromobenzene (1 mL, 11 mmol) were dissolved in toluene (10 mL). $Pd_2(dba)_3$ (275 mg) and $HP^tBu_3BF_4$ (145 mg) were added and the mixture was stirred for 10 min under N_2 atmosphere. NaO^tBu (1.11 g) was added and the mixture stirred under N_2 atmosphere at 110 ºC for 48 h. After cooling to room temperature, the resulting mixture was diluted with DCM (20 mL) and filtered through a pad of celite®. The celite pad was washed with DCM (3 x 10 mL). The solvent was evaporated under reduced pressure and the crude purified by column chromatography. Eluent: Cyclohexane:AcOEt (98:2). White solid (2.477 g, 9 mmol, 90% yield). Spectroscopic data are in agreement with the published data.[15] **^{1}H-NMR (300 MHz, $CDCl_3$)** δ 7.65 – 7.55 (m, 2H), 7.50 – 7.45 (m, 1H), 7.42 – 7.35 (m, 2H), 7.05 – 7.00 (m, 2H), 6.90 – 6.75 (m, 4H), 6.25 – 6.15 (m, 2H).

General procedure for the preparation of 3-(4-methoxyphenyl)-10-phenyl-10*H*-phenoxazine catalyst (3g)

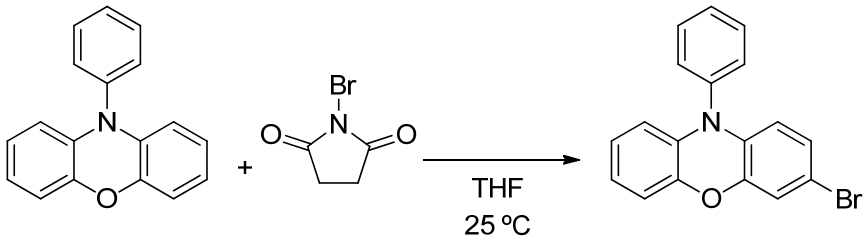

Phenyl-10-phenoxazine (1.0 g, 3.86 mmol) was dissolved in THF (168 mL) and the flask was covered in aluminum foil. *N*-bromosuccinimide (0.706 g, 3.97 mmol) was added portionwise over thirty minutes. The reaction was stirred at room temperature until disappearance of the phenyl-10-phenoxazine followed by TLC. Then, THF was removed under reduced pressure. The reaction was re-dissolved in DCM, washed with de-ionized water once and brine twice, dried over magnesium sulfate and concentrated under reduced pressure. The crude product was collected as a red oil and the crude purified by column chromatography. Eluent: Cyclohexane:DCM (15:1). White solid (2.477 g, 9 mmol, 90% yield). Spectroscopic data are in agreement with the published data.[16] **^{1}H-NMR (300 MHz, $CDCl_3$)** δ 7.69 – 7.60 (m, 2H), 7.58 – 7.48 (m, 1H), 7.40 – 7.30 (m, 2H), 6.85 (ddd, *J* = 4.7, 2.2, 0.9 Hz, 1H), 6.77 – 6.60 (m, 4H), 6.00 – 5.93 (m, 1H), 5.86 – 5.77 (m, 1H).

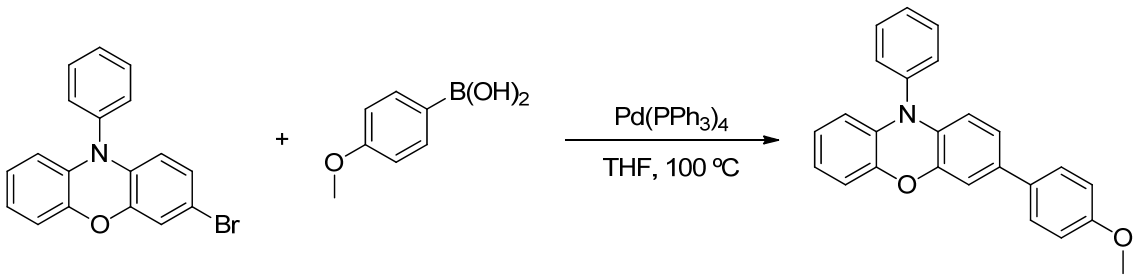

3-Bromophenyl-10-phenoxazine (0.373 g, 1.1 mmol) and 4-methoxyphenyl boronic acid (0.334 g, 2.2 mmol) were added to a storage tube and cycled between vacuum and nitrogen three times before dried and degassed THF (8.00 mL) was added. Once all reagents were dissolved, a 2.00 M aqueous solution of K_2CO_3 (8.00 mL), which had been sparged with nitrogen, was added. In a separate Schlenk flask, tetrakis(triphenylphosphine) palladium (0.102 g, 0.088 mmol) was dissolved in THF (8.00 mL) under inert atmosphere. The solution of $Pd(PPh_3)_4$ was then added to the reaction mixture and the reaction was heated at 100 °C for 48 h, before it was exposed to oxygen and allowed to cool to room temperature. The reaction mixture was concentrated under reduced pressure, diluted with DCM/hexanes, and passed through a short plug of silica. The solution was then moved to a separatory funnel, washed with de-ionized water once and brine twice. The solution was dried over magnesium sulfate, concentrated under

vacuum, and recrystallized using DCM/methanol at -25 °C. The product was collected via vacuum filtration as a white solid (0.162 g, 0.444 mmol, 40% yield). Spectroscopic data are in agreement with the published data.[16] **^{1}H-NMR (300 MHz, C_6D_6)** δ 7.48 – 7.37 (m, 2H), 7.24 – 7.18 (m, 3H), 7.17 – 6.99 (m, 3H), 6.97 – 6.77 (m, 4H), 6.57 (td, *J* = 7.6, 1.6 Hz, 2H), 6.17 – 6.02 (m, 2H), 3.39 (s, 3H).

General procedure for the preparation of *Z*-allylic compounds (4)

A vial equipped with a magnetic stir bar and fitted with a teflon screw cap septum was charged with the corresponding allylic compound **1** (0.1 mmol), the corresponding heterocycle **2** (0.2 mmol), *N*-phenyl phenothiazine (1.4 mg, 5 mol%), DIPEA (86 μL, 0.5 mmol) and acetonitrile (1 mL). The reaction was degassed with three freeze-pump-thaw cycles. The vial was then backfilled with N_2 and stirred under 365 nm LEDs irradiation (8.2460 W/m^2 intensity; approximate distance was 2 cm from the vial) at 20 ºC. After 3 h the vial was opened, the solvent evaporated and the crude purified by column chromatography.

(*Z*)-2-(1,3-diphenylallyl)-1*H*-pyrrole (4a)

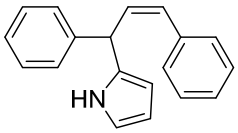

4a

From (*E*)-1,3-diphenylallyl acetate (25.2 mg, 0.1 mmol) and pyrrole (13.9 μL, 0.2 mmol), following the general procedure, compound **4a** (15.0 mg, 0.058 mmol) was obtained in 58% yield (*Z*:*E* ratio = 94:6) as a brownish oil. The crude product was purified by column chromatography. Eluent: Pentane:AcOEt (95:5). **^{1}H-NMR (300 MHz, $CDCl_3$)** δ 7.78 (br s, 1H), 7.36 – 7.21 (m, 10H), 6.71 – 6.67 (m, 1H), 6.66 (d, *J* = 11.5 Hz, 1H), 6.16 (m, 1H), 6.05 (dd, *J* = 11.4, 10.3 Hz, 1H), 6.01 – 5.98 (m, 1H), 5.18 (d, *J* = 10.3 Hz, 1H). **^{13}C-NMR (75 MHz, $CDCl_3$)** δ 142.9, 136.7, 133.6, 132.6, 129.6, 128.8 (2C), 128.7 (2C), 128.3 (2C), 128.1 (2C), 127.1, 126.8, 117.1, 108.4, 106.5, 43.3. **HRMS (EI$^+$)** calculated for $C_{19}H_{17}N$ [M]$^+$: 259.1356, found: 259.1375.

(*Z*)-2-(1,3-diphenylallyl)-1-methyl-1*H*-pyrrole (4b)

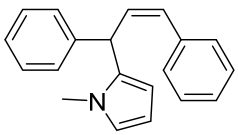

4b

From (*E*)-1,3-diphenylallyl acetate (25.2 mg, 0.1 mmol) and 1-methylpyrrole (16.2 μL, 0.2 mmol), following the general procedure, compound **4b** (19.2 mg, 0.070 mmol) was obtained in 70% yield (*Z*:*E* ratio = 92:8) as an orange oil. The crude product was purified by column chromatography. Eluent: Hexane:DCM (2:1). **^{1}H-NMR (300 MHz, $CDCl_3$)** δ 7.35 – 7.20 (m, 8H), 7.18 – 7.10 (m, 2H), 6.65 – 6.54 (m, 2H), 6.14 - 6.09 (m, 1H), 6.06 – 5.95 (m, 2H), 5.13 (d, *J* = 10.1 Hz, 1H), 3.24 (s, 3H). **^{13}C-NMR (75 MHz, $CDCl_3$)** δ 143.2, 137.0, 134.2, 133.2, 128.7 (2C), 128.6 (2C), 128.5, 128.3 (2C), 127.8 (2C), 127.0,

126.5, 122.0, 107.3, 106.6, 42.3, 33.9. **HRMS (EI$^+$)** calculated for $C_{20}H_{19}N$ $[M]^+$: 273.1512, found: 273.1505.

(*Z*)-2-(1,3-diphenylallyl)-1-phenyl-1*H*-pyrrole (4c)

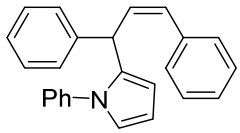

4c

From (*E*)-1,3-diphenylallyl acetate (25.2 mg, 0.1 mmol) and 1-phenylpyrrole (28.6 mg, 0.2 mmol), following the general procedure, compound **4c** (18.3 mg, 0.055 mmol) was obtained in 55% yield (*Z*:*E* ratio = 75:25) as a yellow oil. The crude product was purified by column chromatography. Eluent: Hexane:DCM (5:1). *Z*-isomer: **^{1}H-NMR (300 MHz, $CDCl_3$)** δ 7.40 – 7.05 (m, 12H), 7.03 – 6.95 (m, 3H), 6.79 – 6.74 (m, 1H), 6.50 (d, *J* = 11.3 Hz, 1H), 6.28 (m, 1H), 6.24 – 6.20 (m, 1H), 6.01 (dd, *J* = 11.3, 10.2 Hz, 1H), 5.13 (d, *J* = 10.2 Hz, 1H). **^{13}C-NMR (75 MHz, $CDCl_3$)** δ 143.9, 139.9, 136.8, 135.3, 133.6, 129.4, 128.7 (2C), 128.5 (2C), 128.3 (2C), 128.1 (2C), 127.7 (2C), 127.1, 126.8, 126.5 (2C), 126.2, 122.1, 108.2, 108.0, 41.8. **HRMS (EI$^+$)** calculated for $C_{25}H_{21}N$ $[M]^+$: 335.1669, found: 335.1642.

E-isomer: **^{1}H-NMR (300 MHz, $CDCl_3$)** δ 7.35 – 7.04 (m, 4.5H), 6.79 – 6.76 (m, 0.3H), 6.52 (dd, *J* = 15.8, 7.0 Hz, 0.3H), 6.29 – 6.23 (m, 0.3H), 6.17 – 6.09 (m, 0.6H), 4.76 (d, *J* = 7.0 Hz, 0.3H). **^{13}C-NMR (75 MHz, $CDCl_3$)** δ 142.5, 140.1, 137.3, 134.6, 132.0, 130.7, 128.8 (2C), 128.41 (2C), 128.36 (2C), 128.2 (2C), 127.4, 127.2, 126.9 (2C), 126.33, 126.29 (2C), 122.4, 108.6, 108.0, 46.3.

(*Z*)-2-(1,3-diphenylallyl)-*N*,*N*-dimethyl-1*H*-pyrrol-1-amine (4d)

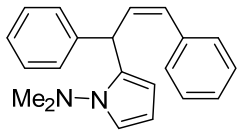

4d

From (*E*)-1,3-diphenylallyl acetate (25.2 mg, 0.1 mmol) and 1-(dimethylamino)pyrrole (24.2 μL, 0.2 mmol), following the general procedure, compound **4d** (14 mg, 0.046 mmol) was obtained in 46% yield (*Z*:*E* ratio = 96:4) as a colorless oil. The crude product was purified by column chromatography. Eluent: Hexane:DCM (5:1). **^{1}H-NMR (300 MHz, $CDCl_3$)** δ 7.35 – 7.20 (m, 7H), 7.18 – 7.10 (m, 3H), 6.88 (dd, *J* = 3.1, 1.8 Hz, 1H), 6.56 (d, *J* = 11.3 Hz, 1H), 6.15 (t, *J* = 3.4 Hz, 1H), 6.08 (t, *J* = 11.0 Hz, 1H), 5.92 (dd, *J* = 3.8, 1.8 Hz, 1H), 5.44 (d, *J* = 10.5 Hz, 1H), 2.47 (br s, 6H). **^{13}C-NMR (75 MHz, $CDCl_3$)** δ 144.3, 137.3, 134.2, 133.6, 128.8 (2C), 128.4, 128.2 (2C), 128.0 (2C), 127.8 (2C), 126.7, 125.9, 111.9, 106.4, 102.8, 47.5 (2C), 41.3. **HRMS (EI$^+$)** calculated for $C_{19}H_{16}N$ $[M-C_2H_6N]^+$: 258.1277, found: 258.1266.

(*Z*)-3-(1,3-diphenylallyl)-1*H*-indole (4e)

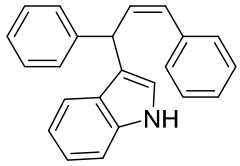

4e

From (*E*)-1,3-diphenylallyl acetate (25.2 mg, 0.1 mmol) and indole (23.4 mg, 0.2 mmol), following the general procedure, compound **4e** (20.7 mg, 0.066 mmol) was obtained in 66% yield (*Z*:*E* ratio = 91:9) as a colorless oil. The crude product was purified by column chromatography. Eluent: Hexane:DCM (1:1). **^{1}H-NMR (300 MHz, $CDCl_3$)** δ 7.95 (br s, 1H), 7.38 – 7.12 (m, 13H), 7.04 – 6.93 (m, 2H), 6.63 (d, *J* = 11.4 Hz, 1H), 6.14 (dd, *J* = 11.3, 10.3 Hz, 1H), 5.42 (d, *J* = 10.2 Hz, 1H). **^{13}C-NMR (75 MHz, $CDCl_3$)** δ 144.2, 137.1, 136.8, 134.4, 128.7 (2C), 128.5 (2C), 128.4, 128.3 (2C), 128.1 (2C), 126.9, 126.6, 126.3, 122.3, 122.1, 120.0, 119.3, 119.0, 111.1, 41.8. **HRMS (EI$^+$)** calculated for $C_{23}H_{19}N$ [M]$^+$: 309.1512, found: 309.1501.

(*Z*)-3-(1,3-diphenylallyl)-1-methyl-indole (4f)

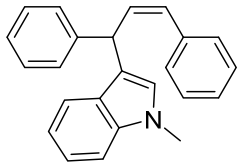

4f

From (*E*)-1,3-diphenylallyl acetate (25.2 mg, 0.1 mmol) and *N*-methylindole (26.2 μL, 0.2 mmol), following the general procedure, compound **4f** (25.3 mg, 0.077 mmol) was obtained in 77% yield (*Z*:*E* ratio = 89:11) as a colorless oil. The crude product was purified by column chromatography. Eluent: Hexane:DCM (3:1). **^{1}H-NMR (300 MHz, $CDCl_3$)** δ 7.32 – 7.15 (m, 13H), 6.99 – 6.91 (m, 1H), 6.87 (s, 1H), 6.62 (d, *J* = 11.4 Hz, 1H), 6.13 (dd, *J* = 11.4, 10.3 Hz, 1H), 5.42 (d, *J* = 10.3 Hz, 1H), 3.75 (s, 3H). **^{13}C-NMR (75 MHz, $CDCl_3$)** δ 144.4, 137.5, 137.1, 134.6, 128.8 (2C), 128.5 (2C), 128.30, 128.28 (2C), 128.1 (2C), 127.01, 126.97, 126.9, 126.2, 121.6, 120.0, 118.7, 117.4, 109.2, 41.7, 32.7. **HRMS (EI$^+$)** calculated for $C_{24}H_{21}N$ [M]$^+$: 323.1669, found: 323.1664.

(*Z*)-3-(1,3-diphenylallyl)-5-methoxy-1*H*-indole (4g)

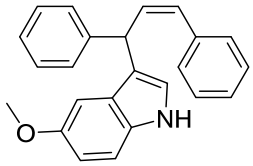

4g

From (*E*)-1,3-diphenylallyl acetate (25.2 mg, 0.1 mmol) and 5-methoxyindole (29.4 mg, 0.2 mmol), following the general procedure, compound **4g** (18.6 mg, 0.055 mmol) was obtained in 55% yield (*Z*:*E* ratio = 94:6) as a colorless oil. The crude product was purified by column chromatography. Eluent: Hexane:DCM (1:2). **^{1}H-NMR (300 MHz, $CDCl_3$)** δ 7.88 (br s, 1H), 7.35 – 7.20 (m, 11H), 6.95 (d, *J* = 2.6 Hz, 1H), 6.85 – 6.77 (m, 1H), 6.64 (d, *J* = 11.4 Hz, 1H), 6.58 (d, *J* = 2.4 Hz, 1H), 6.13 (dd, *J* = 11.1, 10.5 Hz, 1H), 5.39 (d, *J* = 10.4 Hz, 1H), 3.62 (s, 3H). **^{13}C-NMR (75 MHz, $CDCl_3$)** δ 153.7, 144.0, 137.1, 134.4, 131.8, 128.8 (2C), 128.5 (2C), 128.4, 128.3 (2C), 128.1 (2C), 127.0, 126.9, 126.3, 122.9, 118.9, 112.3, 111.7, 101.6, 55.6, 41.7. **HRMS (EI$^+$)** calculated for $C_{24}H_{21}NO$ [M]$^+$: 339.1618, found: 339.1604.

(*Z*)-3-(1,3-diphenylallyl)-6-methoxy-1*H*-indole (4h)

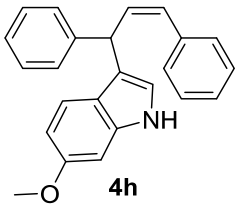

4h

From (*E*)-1,3-diphenylallyl acetate (25.2 mg, 0.1 mmol) and 6-methoxyindole (29.4 mg, 0.2 mmol), following the general procedure, compound **4h** (17.0 mg, 0.050 mmol) was obtained in 50% yield (*Z*:*E* ratio = 92:8) as a brownish oil. The crude product was purified by column chromatography. Eluent: Hexane:DCM (1:3). **^{1}H-NMR (300 MHz, $CDCl_3$)** δ 7.87 (br s, 1H), 7.36 – 7.24 (m, 10H), 7.03 (d, *J* = 8.7 Hz, 1H), 6.91 (dd, *J* = 2.4, 1.1 Hz, 1H), 6.85 (d, *J* = 2.3 Hz, 1H), 6.63 (dd, *J* = 8.7, 2.3 Hz, 1H), 6.62 (d, *J* = 11.3 Hz, 1H), 6.12 (dd, *J* = 11.4, 10.2 Hz, 1H), 5.37 (d, *J* = 10.3 Hz, 1H), 3.81 (s, 3H). **^{13}C-NMR (75 MHz, $CDCl_3$)** δ 156.5, 144.2, 137.6, 137.1, 134.5, 128.7 (2C), 128.5 (2C), 128.4, 128.3 (2C), 128.1 (2C), 126.9, 126.3, 121.1, 121.0, 120.5, 119.0, 109.2, 94.7, 55.6, 41.9. **HRMS (EI$^+$)** calculated for $C_{24}H_{21}NO$ $[M]^+$: 339.1618, found: 339.1616.

(*Z*)-3-(1,3-diphenylallyl)-5,6-dimethoxy-1*H*-indole (4i)

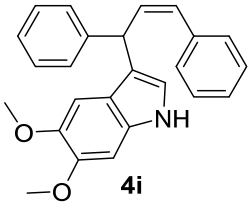

4i

From (*E*)-1,3-diphenylallyl acetate (25.2 mg, 0.1 mmol) and 5,6-dimethoxyindole (35.4 mg, 0.2 mmol), following the general procedure, compound **4i** (6.6 mg, 0.018 mmol) was obtained in 18% yield (*Z*:*E* ratio = 91:9) as a yellow oil. The crude product was purified by column chromatography. Eluent: Hexane:DCM (1:1). **^{1}H-NMR (300 MHz, $CDCl_3$)** δ 7.82 (br s, 1H), 7.36 – 7.23 (m, 10H), 6.86 (s, 1H), 6.84 (dd, *J* = 2.4, 1.1 Hz, 1H), 6.64 (d, *J* = 11.4 Hz, 1H), 6.52 (s, 1H), 6.12 (dd, *J* = 11.4, 10.3 Hz, 1H), 5.37 (d, *J* = 10.4 Hz, 1H), 3.88 (s, 3H), 3.65 (s, 3H). **^{13}C-NMR (75 MHz, $CDCl_3$)** δ 147.1, 144.7, 144.0, 137.2, 134.5, 130.9, 128.8 (2C), 128.5 (2C), 128.33, 128.29 (2C), 128.1 (2C), 126.9, 126.3, 120.7, 119.5, 119.1, 101.5, 94.5, 56.2, 56.1, 41.7. **HRMS (EI$^+$)** calculated for $C_{25}H_{23}NO_2$ $[M]^+$: 369.1723, found: 369.1707.

The C2-allylated compound was obtained as a side-product:

(*Z*)-2-(1,3-diphenylallyl)-5,6-dimethoxy-1*H*-indole (4i')

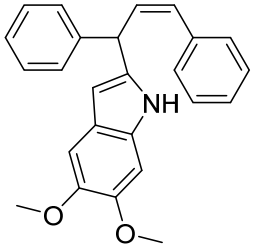

4i'

Compound **4i'** (9.3 mg, 0.027 mmol) was obtained in 25% yield as a yellow oil. The crude product was purified by column chromatography. Eluent: Hexane:DCM (1:1). **^{1}H-NMR (300 MHz, $CDCl_3$)** δ 7.59 (br s, 1H), 7.34 – 7.22 (m, 10H), 7.02 (s, 1H), 6.78 (s, 1H), 6.71 (d, *J* = 11.3 Hz, 1H), 6.29 – 6.25 (m, 1H), 6.10 (dd, *J* = 11.3, 10.1 Hz, 1H), 5.28 (d, *J* = 10.2 Hz, 1H), 3.90 (s, 3H), 3.86 (s, 3H). **^{13}C-NMR (75 MHz, $CDCl_3$)** δ 146.6, 145.1, 142.4, 139.1, 136.6, 132.0, 130.5, 130.1, 128.9 (2C), 128.7 (2C), 128.4 (2C), 128.2 (2C), 127.2, 127.0, 121.2, 102.3, 100.9,

94.5, 56.4, 56.2, 44.0. **HRMS (ESI$^+$)** calculated for $C_{25}H_{23}NO_2$ $[M]^+$: 369.1723, found: 369.1707.

(*Z*)-3-(1,3-diphenylallyl)-5-(trifluoromethyl)-1*H*-indole (4j)

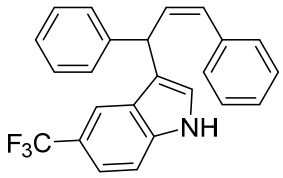

4j

From (*E*)-1,3-diphenylallyl acetate (25.2 mg, 0.1 mmol) and 5-(trifluoromethyl)indole (37.0 mg, 0.2 mmol), following the general procedure, compound **4j** (25.2 mg, 0.066 mmol) was obtained in 66% yield (*Z*:*E* ratio = 94:6) as an orange oil. The crude product was purified by column chromatography. Eluent: Hexane:DCM (3:1). **^{1}H-NMR (300 MHz, $CDCl_3$)** δ 8.15 (br s, 1H), 7.47 (s, 1H), 7.41 – 7.37 (m, 2H), 7.34 – 7.22 (m, 10H), 7.04 (dd, *J* = 2.5, 1.2 Hz, 1H), 6.67 (d, *J* = 11.2 Hz, 1H), 6.12 (dd, *J* = 11.4, 10.3 Hz, 1H), 5.41 (d, *J* = 10.4 Hz, 1H). **^{13}C-NMR (75 MHz, $CDCl_3$)** δ 143.5, 138.0, 136.9, 133.8 (2C), 129.0, 128.7 (2C), 128.4 (2C), 128.0 (2C), 127.1, 126.6, 126.3, 126.0, 125.8 (q, $^1J_{C\text{-}F}$ = 231.6 Hz), 123.8, 121.8, (q, $^2J_{C\text{-}F}$ = 31.8 Hz), 120.4, 118.9 (q, $^3J_{C\text{-}F}$ = 3.3 Hz), 117.6 (d, $^3J_{C\text{-}F}$ = 4.2 Hz), 111.3, 41.4. **^{19}F-NMR (282 MHz, $CDCl_3$)** δ -60.3. **HRMS (EI$^+$)** calculated for $C_{24}H_{18}NF_3$ $[M]^+$: 387.0617, found: 387.0618.

(*Z*)-3-(1,3-diphenylallyl)-7-methyl-1*H*-indole (4k)

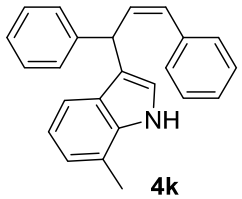

4k

From (*E*)-1,3-diphenylallyl acetate (25.2 mg, 0.1 mmol) and 7-methylindole (39.2 mg, 0.2 mmol), following the general procedure, compound **4k** (26.2 mg, 0.070 mmol) was obtained in 70% yield (*Z*:*E* ratio = 91:9) as a colorless oil. The crude product was purified by column chromatography. Eluent: Hexane:DCM (3:1). **^{1}H-NMR (300 MHz, $CDCl_3$)** δ 7.87 (br s, 1H), 7.35 – 7.20 (m, 10H), 7.08 – 7.00 (m, 2H), 6.96 (d, *J* = 6.5 Hz, 1H), 6.90 (d, *J* = 7.4 Hz, 1H), 6.62 (d, *J* = 11.4 Hz, 1H), 6.13 (dd, *J* = 11.5, 10.2 Hz, 1H), 5.42 (d, *J* = 10.1 Hz, 1H), 2.46 (s, 3H). **^{13}C-NMR (75 MHz, $CDCl_3$)** δ 144.3, 137.1, 136.4, 134.5, 128.7 (2C), 128.5 (2C), 128.4, 128.3 (2C), 128.1 (2C), 126.9, 126.2, 126.1, 122.6, 122.0, 120.2, 119.53, 119.45, 117.7, 41.9, 16.6. **HRMS (EI$^+$)** calculated for $C_{23}H_{18}N$ $[M\text{-}CH_3]^+$: 308.1434, found: 309.1403.

(*Z*)-3-(1,3-diphenylallyl)-4-methyl-1*H*-indole (4l)

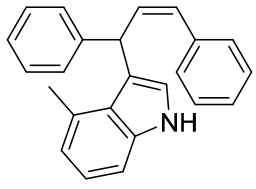

4l

From (*E*)-1,3-diphenylallyl acetate (25.2 mg, 0.1 mmol) and 4-methylindole (26.2 μL, 0.2 mmol), following the general procedure, compound **4l** (25.1 mg, 0.078 mmol) was obtained in 78% yield (*Z*:*E* ratio = 90:10) as a brownish oil. The crude product was purified by column chromatography. Eluent: Hexane:DCM (2:1). **^{1}H-NMR (300 MHz, $CDCl_3$)** δ 8.08 (br s, 1H), 7.35 – 7.20 (m, 9H), 7.15 – 7.10 (m, 3H), 7.09 – 7.03 (m, 1H), 6.76 (d, *J* = 7.1 Hz, 1H), 6.57 (d, *J* = 11.3 Hz, 1H), 6.08 (dd, *J* =

11.1, 10.3 Hz, 1H), 5.75 (d, *J* = 10.1 Hz, 1H), 2.25 (s, 3H). **^{13}C-NMR (75 MHz, CDCl$_3$)** δ 146.0, 137.1, 135.7, 131.3, 128.8 (2C), 128.4 (2C), 128.33, 128.27 (2C), 128.0 (2C), 127.6, 126.9, 126.3, 126.1, 122.8, 122.2, 121.2, 119.4, 109.0, 42.3, 20.3. **HRMS (EI$^+$)** calculated for $C_{24}H_{21}N$ [M]$^+$: 323.1669, found: 309.1675.

(*Z*)-5-bromo-3-(1,3-diphenylallyl)-1*H*-indole (4m)

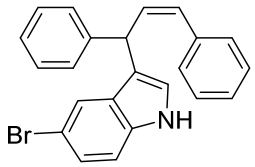

4m

From (*E*)-1,3-diphenylallyl acetate (25.2 mg, 0.1 mmol) and 5-bromoindole (39.2 mg, 0.2 mmol), following the general procedure, compound **4m** (20.3 mg, 0.053 mmol) was obtained in 53% yield (*Z*:*E* ratio = 88:12) as a brownish oil. The crude product was purified by column chromatography. Eluent: Hexane:DCM (2:1). **^{1}H-NMR (300 MHz, CDCl$_3$)** δ 8.00 (br s, 1H), 7.32 – 7.19 (m, 13H), 6.98 (d, *J* = 2.5 Hz, 1H), 6.64 (d, *J* = 11.4 Hz, 1H), 6.10 (dd, *J* = 11.4, 10.3 Hz, 1H), 5.35 (d, *J* = 10.3 Hz, 1H). **^{13}C-NMR (75 MHz, CDCl$_3$)** δ 143.7, 136.9, 135.4, 133.9, 128.8, 128.7 (2C), 128.6 (2C), 128.4 (2C), 128.3, 127.9 (2C), 127.1, 126.5, 125.0, 123.4, 122.5, 118.9, 112.7, 122.5, 41.5. **HRMS (EI$^+$)** calculated for $C_{23}H_{18}NBr$ [M]$^+$: 387.0617, found: 387.0618.

(*Z*)-2-(1,3-di-*p*-tolylallyl)-1*H*-pyrrole (4n)

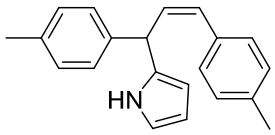

4n

From **1b** (28 mg, 0.1 mmol) and pyrrole (14 μL, 0.2 mmol), following the general procedure, compound **4n** (15 mg, 0.052 mmol) was obtained in 52% yield (*Z*:*E* ratio = 95:5) as a brownish oil. The crude product was purified by column chromatography. Eluent: Pentane:AcOEt (98:2). **^{1}H-NMR (300 MHz, CDCl$_3$)** δ 7.80 (br s, 1H), 7.24 – 7.12 (m, 8H), 6.70 – 6.67 (m, 1H), 6.62 (d, *J* = 11.3 Hz, 1H), 6.19 – 6.16 (m, 1H), 6.04 – 5.96 (m, 2H), 5.16 (d, *J* = 10.3 Hz, 1H), 2.36 (s, 3H), 2.35 (s, 3H). **^{13}C-NMR (75 MHz, CDCl$_3$)** δ 140.0, 136.8, 136.4, 133.9, 132.2, 129.5 (2C), 129.3, 129.0 (2C), 128.6 (2C), 128.0 (2C), 126.6, 117.0, 108.4, 106.3, 43.0, 21.2, 21.0. **HRMS (EI$^+$)** calculated for $C_{21}H_{21}N$ [M]$^+$: 287.1669, found: 287.1670.

(*Z*)-2-(1,3-di-*m*-tolylallyl)-1*H*-pyrrole (4o)

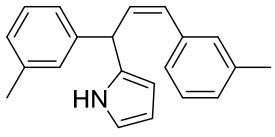

4o

From **1c** (28.0 mg, 0.1 mmol) and pyrrole (14 μL, 0.2 mmol), following the general procedure, compound **4o** (13 mg, 0.045 mmol) was obtained in 45% yield (*Z*:*E* ratio = 91:9) as a pale yellow oil. The crude product was purified by column chromatography. Eluent: Pentane:AcOEt (98:2). **^{1}H-NMR (300 MHz, CDCl$_3$)** δ 7.79 (br s, 1H), 7.25 – 7.18 (m, 2H), 7.13 – 7.01 (m, 6H), 6.69 – 6.67 (m, 1H), 6.62 (d, *J* = 11.4 Hz, 1H), 6.18 – 6.15 (m, 1H), 6.05 (dd, *J* = 11.4, 10.3 Hz, 1H), 6.00 – 5.96 (m, 1H), 5.14 (d, *J* = 10.3 Hz, 1H), 2.33 (s, 6H). **^{13}C-NMR (75 MHz, CDCl$_3$)** δ 142.9, 138.4, 137.8,

136.7, 133.8, 132.6, 129.6, 129.5, 128.8, 128.7, 128.2, 127.8, 127.6, 125.7, 125.2, 117.0, 108.4, 106.3, 43.3, 21.5, 21.4. **HRMS (EI$^+$)** calculated for $C_{21}H_{21}N$ $[M]^+$: 287.1669, found: 287.1664.

(*Z*)-2-(1,3-bis(4-methoxyphenyl)allyl)-1*H*-pyrrole (4p)

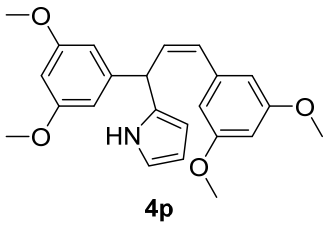

4p

From **1d** (37.2 mg, 0.1 mmol) and pyrrole (14 μL, 0.2 mmol), following the general procedure, compound **4p** (20.3 mg, 0.054 mmol) was obtained in 54% yield (*Z*:*E* ratio = 100:0) as a pale yellow oil. The crude product was purified by column chromatography. Eluent: Pentane:AcOEt (85:15). **^{1}H-NMR (300 MHz, $CDCl_3$)** δ 7.84 (br s, 1H), 6.70 – 6.65 (m, 1H), 6.60 (d, *J* = 11.3 Hz, 1H), 6.45 (d, *J* = 2.3 Hz, 2H), 6.42 (d, *J* = 2.3 Hz, 1H), 6.38 (t, *J* = 2.3 Hz, 1H), 6.36 (t, *J* = 2.3 Hz, 2H), 6.15 (q, *J* = 2.9 Hz, 1H), 6.05 (dd, *J* = 11.3, 10.1 Hz, 1H), 6.04 – 6.00 (m, 1H), 5.11 (d, *J* = 10.0 Hz, 1H), 3.76 (s, 6H), 3.72 (s, 6H). **^{13}C-NMR (75 MHz, $CDCl_3$)** δ 161.1 (2C), 160.6 (2C), 145.3, 138.6, 133.2, 132.7, 129.8, 117.1, 108.4, 106.7 (2C), 106.4, 106.2 (2C), 99.7, 98.8, 55.30 (2C), 55.25 (2C), 43.7. **HRMS (EI$^+$)** calculated for $C_{23}H_{25}NO_4$ $[M]^+$: 379.1778, found: 379.1777.

(*Z*)-2-(1,3-bis(4-fluorophenyl)allyl)-1*H*-pyrrole (4q)

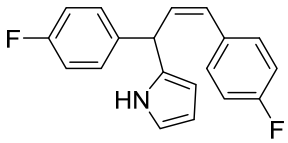

4q

From **1e** (28.8 mg, 0.1 mmol) and pyrrole (14 μL, 0.2 mmol), following the general procedure, compound **4q** (15.0 mg, 0.051 mmol) was obtained in 51% yield (*Z*:*E* ratio = 94:6) as a colorless oil. The crude product was purified by column chromatography. Eluent: Pentane:AcOEt (98:2). **^{1}H-NMR (300 MHz, $CDCl_3$)** δ 7.80 (br s, 1H), 7.26 – 7.14 (m, 4H), 7.07 – 6.98 (m, 4H), 6.74 – 6.70 (m, 1H), 6.62 (d, *J* = 11.3 Hz, 1H), 6.20 – 6.16 (m, 1H), 6.03 – 5.96 (m, 2H), 5.10 (d, *J* = 10.2 Hz, 1H). **^{13}C-NMR (75 MHz, $CDCl_3$)** δ 162.0 (d, $^1J_{C\text{-}F}$ = 246.8 Hz), 161.8 (d, $^1J_{C\text{-}F}$ = 245.5 Hz), 138.5 (d, $^4J_{C\text{-}F}$ = 3.2 Hz), 133.1, 132.6 (d, $^4J_{C\text{-}F}$ = 3.3 Hz), 132.4, 130.3 (d, $^3J_{C\text{-}F}$ = 8.0 Hz, 2C), 129.5 (d, $^3J_{C\text{-}F}$ = 7.9 Hz, 2C), 128.7, 117.4, 115.6 (d, $^2J_{C\text{-}F}$ = 21.3 Hz, 2C), 115.3 (d, $^2J_{C\text{-}F}$ = 21.4 Hz, 2C), 108.5, 106.6, 42.6. **^{19}F-NMR (282 MHz, $CDCl_3$)** δ -114.7, -115.9. **HRMS (EI$^+$)** calculated for $C_{19}H_{15}NF_2$ $[M]^+$: 295.1167, found: 295.1175.

General procedure for the preparation of *E*-allylic compounds (5)

A vial equipped with a magnetic stir bar and fitted with a teflon screw cap septum was charged with the corresponding allylic compound **1** (0.1 mmol), the corresponding heterocycle (0.2 mmol), 3-(4-methoxyphenyl)-10-phenyl-10*H*-phenoxazine (1.7 mg, 5

mol%), DIPA (70 μL, 0.5 mmol) and acetonitrile (1 mL). The reaction was degassed with three freeze-pump-thaw cycles. The vial was then backfilled with N_2 and stirred under 420 nm LEDs irradiation (18.3396 W/m^2 intensity; approximate distance was 2 cm from the vial) at room temperature. After 3 h the vial was opened, the solvent evaporated and the crude purified by column chromatography.

(*E*)-2-(1,3-diphenylallyl)-1*H*-pyrrole (5a)

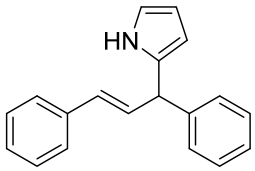

5a

From (*E*)-1,3-diphenylallyl acetate (25.2 mg, 0.1 mmol) and pyrrole (13.9 μL, 0.2 mmol), following the general procedure, compound **5a** (18.4 mg, 0.071 mmol) was obtained in 71% yield (*Z*:*E* ratio = 5:95) as a brownish oil. The crude product was purified by column chromatography. Eluent: Hexane:DCM (1:1). Spectroscopic data are in agreement with the published data.[17] **^{1}H-NMR (300 MHz, $CDCl_3$)** δ 7.88 (br s, 1H), 7.39 – 7.20 (m, 10H), 6.76 – 6.69 (m, 1H), 6.60 (dd, *J* = 15.8, 7.6 Hz, 1H), 6.43 (d, *J* = 15.8 Hz, 1H), 6.19 – 6.16 (m, 1H), 5.99 – 5.95 (m, 1H), 4.87 (d, *J* = 7.6 Hz, 1H).

(*E*)-2-(1,3-diphenylallyl)-1-methyl-1*H*-pyrrole (5b)

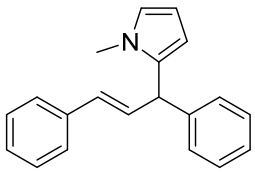

5b

From (*E*)-1,3-diphenylallyl acetate (25.2 mg, 0.1 mmol) and 1-methylpyrrole (16.2 μL, 0.2 mmol), following the general procedure, compound **5b** (10.8 mg, 0.040 mmol) was obtained in 40% yield (*Z*:*E* ratio = 10:90) as a yellow oil. The crude product was purified by column chromatography. Eluent: Hexane:DCM (1:3). **^{1}H-NMR (300 MHz, $CDCl_3$)** δ 7.40 – 7.15 (m, 10H), 6.63 – 6.56 (m, 2H), 6.25 (d, *J* = 15.7 Hz, 1H), 6.12 – 6.07 (m, 1H), 5.97 – 5.93 (m, 1H), 4.85 (d, *J* = 7.0 Hz, 1H), 3.40 (s, 3H). **^{13}C-NMR (75 MHz, $CDCl_3$)** δ 137.3, 133.7, 131.5, 130.9, 128.6, 128.54 (2C), 128.48 (2C), 128.4 (2C), 127.3, 126.6, 126.3 (2C), 122.2, 107.9, 106.5, 46.7, 34.0. **HRMS (EI$^+$)** calculated for $C_{20}H_{19}N$ [M]$^+$: 273.1512, found: 273.1516.

(*E*)-2-(1,3-diphenylallyl)-1-phenyl-1*H*-pyrrole (5c)

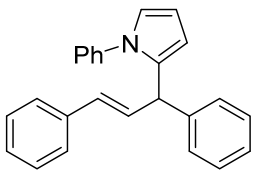

5c

From (*E*)-1,3-diphenylallyl acetate (25.2 mg, 0.1 mmol) and 1-phenylpyrrole (28.6 mg, 0.2 mmol), following the general procedure, compound **5c** (19.9 mg, 0.059 mmol) was obtained in 59% yield (*Z*:*E* ratio = 8:92) as an orange oil. The crude product was purified by column chromatography. Eluent: Hexane:DCM (4:1). **^{1}H-NMR (300 MHz, $CDCl_3$)** δ 7.35 – 7.04 (m, 15H), 6.79 – 6.76 (m, 1H), 6.52 (dd, *J* = 15.8, 7.0 Hz, 1H), 6.29 – 6.23 (m, 1H), 6.17 – 6.09 (m, 2H), 4.76 (d, *J* = 7.0 Hz, 1H). **^{13}C-NMR (75 MHz, $CDCl_3$)** δ 142.5, 140.1, 137.3, 134.6, 132.0, 130.7, 128.8 (2C), 128.41 (2C), 128.36 (2C), 128.3 (2C), 127.4, 127.2, 126.9 (2C), 126.33, 126.28 (2C),

122.4, 108.6, 108.0, 46.3. **HRMS (EI$^+$)** calculated for $C_{25}H_{21}N$ [M]$^+$: 335.1669, found: 335.1282.

(*E*)-3-(1,3-diphenylallyl)-1*H*-indole (5e)

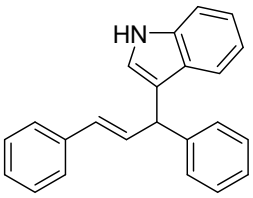

5e

From (*E*)-1,3-diphenylallyl acetate (25.2 mg, 0.1 mmol) and indole (23.4 mg, 0.2 mmol), following the general procedure, compound **5e** (23.7 mg, 0.078 mmol) was obtained in 78% yield (*Z*:*E* ratio = 4:96) as a brownish oil. The crude product was purified by column chromatography. Eluent: Hexane:DCM (6:1). Spectroscopic data are in agreement with the published data.[18] **^{1}H-NMR (300 MHz, $CDCl_3$)** δ 7.97 (br s, 1H), 7.42 (d, *J* = 8.0 Hz, 1H), 7.38 – 7.14 (m, 12H), 7.02 (t, *J* = 7.5 Hz, 1H), 6.92 – 6.87 (m, 1H), 6.73 (dd, *J* = 15.8, 7.3 Hz, 1H), 6.43 (d, *J* = 15.8 Hz, 1H), 5.12 (d, *J* = 7.4 Hz, 1H).

(*E*)-3-(1,3-diphenylallyl)-1-methyl-indole (5f)

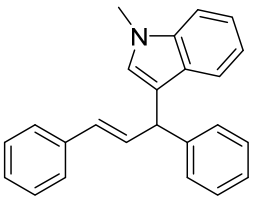

5f

From (*E*)-1,3-diphenylallyl acetate (25.2 mg, 0.1 mmol) and *N*-methylindole (26.2 μL, 0.2 mmol), following the general procedure, compound **5f** (30.4 mg, 0.094 mmol) was obtained in 94% yield (*Z*:*E* ratio = 7:93) as a yellow oil. The crude product was purified by column chromatography. Eluent: Hexane:DCM (6:1). Spectroscopic data are in agreement with the published data.[19] **^{1}H-NMR (300 MHz, $CDCl_3$)** δ 7.42 (d, *J* = 8.0 Hz, 1H), 7.35 – 7.18 (m, 12H), 7.01 (m, 1H), 6.76 – 6.66 (m, 2H), 6.43 (d, *J* = 15.8 Hz, 1H), 5.11 (d, *J* = 7.3 Hz, 1H), 3.72 (s, 3H).

(*E*)-3-(1,3-diphenylallyl)-5-methoxy-1*H*-indole (5g)

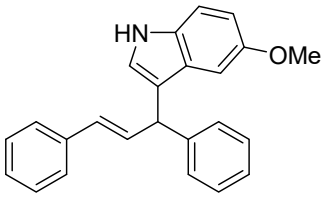

5g

From (*E*)-1,3-diphenylallyl acetate (25.2 mg, 0.1 mmol) and 5-methoxyindole (29.4 mg, 0.2 mmol), following the general procedure, compound **5g** (24.8 mg, 0.073 mmol) was obtained in 73% yield (*Z*:*E* ratio = 6:94) as a yellow oil. The crude product was purified by column chromatography. Eluent: Hexane:DCM (1:1). Spectroscopic data are in agreement with the published data.[17] **^{1}H-NMR (300 MHz, $CDCl_3$)** δ 7.90 (br s, 1H), 7.39 – 7.19 (m, 11H), 6.89 (dd, *J* = 2.5, 1.0 Hz, 1H), 6.85 – 6.81 (m, 2H), 6.71 (dd, *J* = 15.8, 7.3 Hz, 1H), 6.44 (d, *J* = 15.7 Hz, 1H), 5.07 (d, *J* = 7.3 Hz, 1H), 3.71 (s, 3H).

(*E*)-3-(1,3-diphenylallyl)-6-methoxy-1*H*-indole (5h)

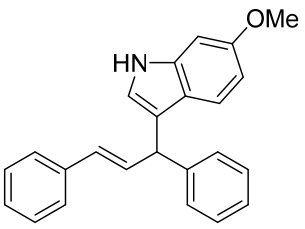

5h

From (*E*)-1,3-diphenylallyl acetate (25.2 mg, 0.1 mmol) and 6-methoxyindole (29.4 mg, 0.2 mmol), following the general procedure, compound **5h** (7.5 mg, 0.021 mmol) was obtained in 22% yield (*Z*:*E* ratio = 6:94) as a yellow oil. The crude product was purified by column chromatography. Eluent: Hexane:DCM (3:1). Spectroscopic data are in agreement with the published data.[20] **^{1}H-NMR (300 MHz, $CDCl_3$)** δ 7.88 (br s, 1H), 7.39 – 7.19 (m, 11H), 6.86 (d, *J* = 2.3 Hz, 1H), 6.81 (dd, *J* = 2.4, 1.1 Hz, 1H), 6.74 – 6.65 (m, 2H), 6.44 (d, *J* = 15.8 Hz, 1H), 5.07 (d, *J* = 7.5 Hz, 1H), 3.83 (s, 3H).

The C2-allylated compound was obtained as a side-product:

(*E*)-2-(1,3-diphenylallyl)-6-methoxy-1*H*-indole (5h')

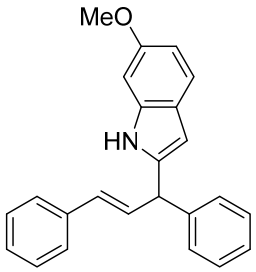

5h'

From (*E*)-1,3-diphenylallyl acetate (25.2 mg, 0.1 mmol) and 6-methoxyindole (29.4 mg, 0.2 mmol), following the general procedure, compound **5h'** (17.3 mg, 0.051 mmol) was obtained in 51% yield as a yellow oil. The crude product was purified by column chromatography. Eluent: Hexane:DCM (3:1). **^{1}H-NMR (300 MHz, $CDCl_3$)** δ 7.72 (br s, 1H), 7.43 – 7.20 (m, 11H), 6.79 – 6.77 (m, 1H), 6.75 (dd, *J* = 8.5, 2.3 Hz, 1H), 6.65 (dd, *J* = 15.8, 7.4 Hz, 1H), 6.48 (d, *J* = 15.9 Hz, 1H), 6.24 – 6.21 (m, 1H), 4.99 (d, *J* = 7.4 Hz, 1H), 3.81 (s, 3H). **^{13}C-NMR (75 MHz, $CDCl_3$)** δ 156.1, 141.5, 138.9, 137.0, 136.9, 131.8, 130.4, 128.8 (2C), 128.6 (2C), 128.5 (2C), 127.6, 127.1, 126.4 (2C), 122.7, 120.8, 109.5, 101.2, 94.5, 55.7, 48.5. **HRMS (EI$^+$)** calculated for $C_{24}H_{21}NO_3$ [M]$^+$: 339.1618, found: 339.1627.

(*E*)-3-(1,3-diphenylallyl)-5,6-dimethoxy-1*H*-indole (5i)

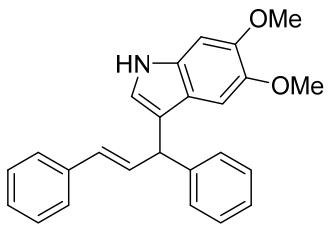

5i

From (*E*)-1,3-diphenylallyl acetate (25.2 mg, 0.1 mmol) and 5,6-dimethoxyindole (35.4 mg, 0.2 mmol), following the general procedure, compound **5i** (12.2 mg, 0.033 mmol) was obtained in 33% yield (*Z*:*E* ratio = 6:94) as a yellow oil. The crude product was purified by column chromatography. Eluent: Hexane:DCM (2:1). Spectroscopic data are in agreement with the published data.[21] **^{1}H-NMR (300 MHz, $CDCl_3$)** δ 7.83 (s, 1H), 7.39 – 7.27 (m, 8H), 7.23 – 7.18 (m, 2H), 6.88 – 6.86 (m, 1H), 6.79 – 6.76 (m, 2H), 6.70 (dd, *J* = 15.8, 7.3 Hz, 1H), 6.45 (d, *J* = 15.9 Hz, 1H), 5.05 (d, *J* = 7.3 Hz, 1H), 3.90 (s, 3H), 3.74 (s, 3H).

The C2-allylated compound was obtained as a side-product:

(*E*)-2-(1,3-diphenylallyl)-5,6-dimethoxy-1*H*-indole (5i')

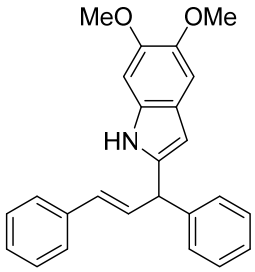

5i'

Compound **5i'** (18.5 mg, 0.050 mmol) was obtained in 50% yield as a yellow oil. The crude product was purified by column chromatography. Eluent: Hexane:DCM (2:1). **^{1}H-NMR (300 MHz, $CDCl_3$)** δ 7.68 (br s, 1H), 7.41 – 7.29 (m, 10H), 7.01 (s, 1H), 6.81 (s, 1H), 6.65 (dd, *J* = 15.8, 7.5 Hz, 1H), 6.48 (d, *J* = 15.8 Hz, 1H), 6.20 – 6.18 (m, 1H), 4.99 (d, *J* = 7.4 Hz, 1H), 3.90 (s, 3H), 3.87 (s, 3H). **^{13}C-NMR (75 MHz, $CDCl_3$)** δ 146.6, 145.1, 141.6, 138.7, 136.9, 131.7, 130.5, 128.8 (2C), 128.6 (2C), 128.5 (2C), 128.2, 127.6, 127.1, 126.4 (2C), 121.2, 102.3, 101.1, 94.5, 56.4, 56.2, 48.5. **HRMS (EI$^+$)** calculated for $C_{10}H_{10}NO_2$ [M – $C_{15}H_{13}$]$^+$: 176.0706, found: 176.0702.

(*E*)-3-(1,3-diphenylallyl)-5-(trifluoromethyl)-1*H*-indole (5j)

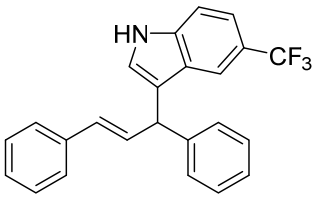

5j

From (*E*)-1,3-diphenylallyl acetate (25.2 mg, 0.1 mmol) and 5-(trifluoromethyl)indole (37.0 mg, 0.2 mmol), following the general procedure, compound **5j** (25.9 mg, 0.067 mmol) was obtained in 67% yield (*Z*:*E* ratio = 13:87) as an brownish oil. The crude product was purified by column chromatography. Eluent: Hexane:DCM (1:1). **^{1}H-NMR (300 MHz, $CDCl_3$)** δ 8.15 (br s, 1H), 7.70 (s, 1H), 7.41 – 7.39 (m, 2H), 7.38 – 7.19 (m, 10H), 7.00 (dd, *J* = 2.3, 0.7 Hz, 1H), 6.69 (dd, *J* = 15.8, 7.3 Hz, 1H), 6.42 (d, *J* = 15.9 Hz, 1H), 5.13 (d, *J* = 7.2 Hz, 1H). **^{13}C-NMR (75 MHz, $CDCl_3$)** 142.8, 137.9, 137.3, 132.0, 131.0, 128.6 (2C), 128.5 (2C), 128.4 (2C), 127.4 (q, $^{1}J_{C\text{-}F}$ = 244.5 Hz), 127.3, 126.7, 126.3 (2C), 126.2, 124.2, 122.0 (q, $^{2}J_{C\text{-}F}$ = 31.8 Hz), 119.8, 119.0 (q, $^{3}J_{C\text{-}F}$ = 3.5 Hz), 117.5 (q, $^{3}J_{C\text{-}F}$ = 4.4 Hz), 111.4, 45.9. **^{19}F-NMR (282 MHz, $CDCl_3$)** δ -60.3. **HRMS (ESI$^+$)** calculated for $C_{24}H_{18}NF_3$ [M]$^+$: 377.1386, found: 377.1387.

(*E*)-3-(1,3-diphenylallyl)-7-methyl-1*H*-indole (5k)

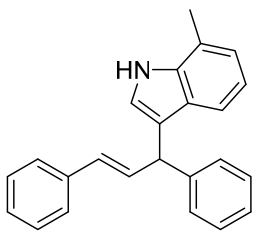

5k

From (*E*)-1,3-diphenylallyl acetate (25.2 mg, 0.1 mmol) and 7-methylindole (26.2 mg, 0.2 mmol), following the general procedure, compound **5k** (29.8 mg, 0.092 mmol) was obtained in 92% yield (*Z*:*E* ratio = 4:96) as an orange oil. The crude product was purified by column chromatography. Eluent: Hexane:DCM (2:1). Spectroscopic data are in agreement with the published data.[22] **^{1}H-NMR (300 MHz, $CDCl_3$)** δ 7.89 (br s, 1H), 7.38 – 7.18 (m, 11H),

7.00 – 6.94 (m, 2H), 6.92 – 6.88 (m, 1H), 6.72 (dd, *J* = 15.8, 7.4 Hz, 1H), 6.43 (d, *J* = 15.8 Hz, 1H), 5.11 (d, *J* = 7.3 Hz, 1H), 2.47 (s, 3H).

(*E*)-3-(1,3-diphenylallyl)-4-methyl-1*H*-indole (5l)

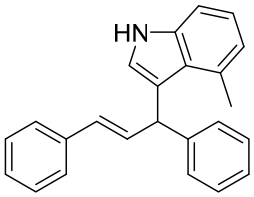

5l

From (*E*)-1,3-diphenylallyl acetate (25.2 mg, 0.1 mmol) and 4-methylindole (26.2 mg, 0.2 mmol), following the general procedure, compound **5l** (22.3 mg, 0.069 mmol) was obtained in 69% yield (*Z*:*E* ratio = 0:100) as a brownish oil. The crude product was purified by column chromatography. Eluent: *c*-Hexane:DCM (9:1). Spectroscopic data are in agreement with the published data.[23] **^{1}H-NMR (300 MHz, $CDCl_3$)** δ 8.04 (br s, 1H), 7.38 – 7.27 (m, 8H), 7.25 – 7.18 (m, 3H), 7.07 (t, *J* = 7.7 Hz, 1H), 6.87 (d, *J* = 2.6 Hz, 1H), 6.80 (d, *J* = 7.2 Hz, 1H), 6.75 (dd, *J* = 15.9, 6.5 Hz, 1H), 6.24 (d, *J* = 15.9 Hz, 1H), 5.46 (d, *J* = 6.5 Hz, 1H), 2.53 (s, 3H).

(*E*)-5-bromo-3-(1,3-diphenylallyl)-1*H*-indole (5m)

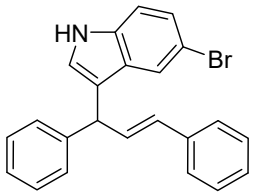

5m

From (*E*)-1,3-diphenylallyl acetate (25.2 mg, 0.1 mmol) and 5-bromoindole (39.2 mg, 0.2 mmol), following the general procedure, compound **5m** (29.9 mg, 0.076 mmol) was obtained in 76% yield (*Z*:*E* ratio = 17:83) as a brownish oil. The crude product was purified by column chromatography. Eluent: Hexane:DCM (2:1). Spectroscopic data are in agreement with the published data.[22] **^{1}H-NMR (300 MHz, $CDCl_3$)** δ 8.05 (br s, 1H), 7.55 (s, 1H), 7.40 – 7.20 (m, 12H), 6.93 (dd, *J* = 2.4, 0.9 Hz, 1H), 6.69 (dd, *J* = 15.8, 7.2 Hz, 1H), 6.41 (d, *J* = 15.9 Hz, 1H), 5.07 (d, *J* = 7.1 Hz, 1H).

General procedure for the preparation of *Z*-allylic compounds (9)

A vial equipped with a magnetic stir bar and fitted with a teflon screw cap septum was charged with the corresponding allylic compound **1** (0.1 mmol), the corresponding amine or alcohol **8** (0.2 mmol), *N*-phenyl phenothiazine (1.4 mg, 5 mol%), DIPEA (86 μL, 0.5 mmol) and acetonitrile (1 mL). The reaction was degassed with three freeze-pump-thaw cycles. The vial was then backfilled with N_2 and stirred under 365 nm LEDs irradiation (8.2460 W/m^2 intensity; approximate distance was 2 cm from the vial) at 20 ºC. After 3 h the vial was opened, the solvent evaporated and the crude purified by column chromatography.

(*Z*)-*N*-(1,3-diphenylallyl)aniline (9a)

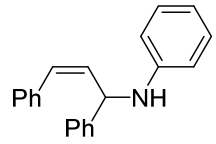

9a

From (*E*)-1,3-diphenylallyl acetate (25.2 mg, 0.1 mmol) and aniline (19 μL, 0.2 mmol), following the general procedure, compound **9a** (17.4 mg, 0.061 mmol) was obtained in 61% yield (*Z*:*E* ratio = 87:13) as a colorless oil. The crude product was purified by column chromatography. Eluent: Hexane:DCM (2:1). **^{1}H-NMR (300 MHz, $CDCl_3$)** δ 7.47 – 7.42 (m, 2H), 7.39 – 7.26 (m, 8H), 7.11 – 7.04 (m, 2H), 6.72 – 6.64 (m, 2H), 6.49 – 6.42 (m, 2H), 5.82 (dd, *J* = 11.4, 9.4 Hz, 1H), 5.40 (d, *J* = 9.3 Hz, 1H), 4.13 (br s, 1H). **^{13}C-NMR (75 MHz, $CDCl_3$)** δ 146.8, 142.7, 136.5, 133.2, 131.2, 129.1 (2C), 128.9 (2C), 128.8 (2C), 128.5 (2C), 127.5 (2C), 127.0 (2C), 117.6, 113.5 (2C), 55.5. **HRMS (EI$^+$)** calculated for $C_{21}H_{19}N$ $[M]^+$: 285.1517, found: 285.1520.

(*Z*)-*N*-(1,3-diphenylallyl)-4-methylaniline (9b)

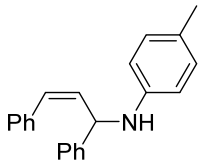

9b

From (*E*)-1,3-diphenylallyl acetate (25.2 mg, 0.1 mmol) and *p*-toluidine (21.4 mg, 0.2 mmol), following the general procedure, compound **9b** (14.3 mg, 0.048 mmol) was obtained in 48% yield (*Z*:*E* ratio = 76:24) as a light yellow oil. The crude product was purified by column chromatography. Eluent: DCM. **^{1}H-NMR (300 MHz, $CDCl_3$)** δ 7.46 – 7.41 (m, 2H), 7.39 – 7.26 (m, 8H), 6.89 (d, *J* = 8.0 Hz, 2H), 6.68 (d, *J* = 11.4 Hz, 1H), 6.38 (d, *J* = 8.4 Hz, 2H), 5.81 (dd, *J* = 11.4, 9.4 Hz, 1H), 5.37 (d, *J* = 9.4 Hz, 1H), 4.08 (br s, 1H), 2.20 (s, 3H). **^{13}C-NMR (75 MHz, $CDCl_3$)** δ 144.6, 142.9, 136.6, 133.4, 131.0, 129.6 (2C), 128.81 (2C), 128.75 (2C), 128.4 (2C), 127.4 (2C), 127.0 (2C), 126.8, 113.7 (2C), 55.7, 20.4. **HRMS (EI$^+$)** calculated for $C_{22}H_{21}N$ $[M]^+$: 299.1669, found: 299.1674.

(*Z*)-*N*-(1,3-diphenylallyl)-4-methoxyaniline (9c)

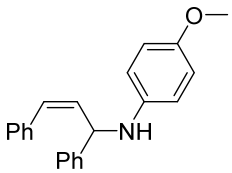

9c

From (*E*)-1,3-diphenylallyl acetate (25.2 mg, 0.1 mmol) and 4-methoxyaniline (24.6 mg, 0.2 mmol), following the general procedure, compound **9c** (24.2 mg, 0.077 mmol) was obtained in 77% yield (*Z*:*E* ratio = 36:64) as a yellow oil. The crude product was purified by column chromatography. Eluent: DCM. **^{1}H-NMR (300 MHz, $CDCl_3$)** δ 7.43 – 7.40 (m, 2H), 7.37 – 7.20 (m, 8H), 6.75 – 6.70 (m, 2H), 6.69 – 6.56 (m, 3H), 5.80 (dd, *J* = 11.3, 9.6 Hz, 1H), 5.31 (d, *J* = 9.4 Hz, 1H), 3.88 (br s, 1H), 3.69 (s, 3H). **^{13}C-NMR (75 MHz, $CDCl_3$)** δ 152.2, 142.9, 141.1, 136.6, 133.6, 131.0, 128.81, 128.76 (2C), 128.65, 128.4 (2C), 127.4 (2C), 127.0 (2C), 114.9 (2C), 114.8 (2C), 56.3, 55.7. **HRMS (EI$^+$)** calculated for $C_{22}H_{21}NO$ $[M]^+$: 315.1623, found: 315.1623.

(*Z*)-4-(*tert*-butoxy)-*N*-(1,3-diphenylallyl)aniline (9d)

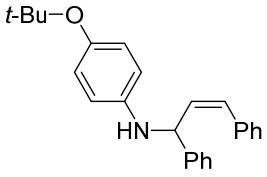

9d

From (*E*)-1,3-diphenylallyl acetate (25.2 mg, 0.1 mmol) and 4-*tert*-butoxyaniline (33 mg, 0.2 mmol), following the general procedure, compound **9d** (18.8 mg, 0.053 mmol) was obtained in 53% yield (*Z*:*E* ratio = 65:35) as a yellow oil. The crude product was purified by column chromatography. Eluent: DCM. **^{1}H-NMR (300 MHz, $CDCl_3$)** δ 7.50 – 7.46 (m, 2H), 7.42 – 7.23 (m, 8H), 6.73 and 6.35 (AA'BB' system, 4H), 6.70 (d, *J* = 11.4 Hz, 1H), 5.83 (dd, *J* = 11.5, 9.4 Hz, 1H), 5.33 (d, *J* = 9.3 Hz, 1H), 3.98 (br s, 1H), 1.28 (s, 9H). **^{13}C-NMR (75 MHz, $CDCl_3$)** δ 146.6, 143.2, 142.9, 136.5, 133.6, 131.1, 128.8 (2C), 128.7 (2C), 128.4 (2C), 127.1 (2C), 126.6, 126.4, 125.2 (2C), 113.8 (2C), 77.7, 56.2, 28.7 (3C). **HRMS (EI$^+$)** calculated for $C_{25}H_{27}NO$ $[M]^+$: 357.2093, found: 357.2034.

(*Z*)-*N*-(1,3-diphenylallyl)-4-(trifluoromethyl)aniline (9e)

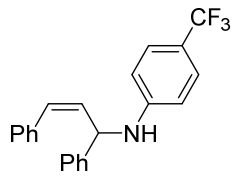

9e

From (*E*)-1,3-diphenylallyl acetate (25.2 mg, 0.1 mmol) and 4-(trifluoromethyl)aniline (25.1 μL, 0.2 mmol), following the general procedure, compound **9e** (27.2 mg, 0.076 mmol) was obtained in 76% yield (*Z*:*E* ratio = 88:12) as a colorless oil. The crude product was purified by column chromatography. Eluent: Hexane:DCM (3:1). **^{1}H-NMR (300 MHz, $CDCl_3$)** δ 7.49 – 7.28 (m, 12H), 6.75 (d, *J* = 11.4 Hz, 1H), 6.44 (d, *J* = 8.7 Hz, 2H), 5.81 (dd, *J* = 11.4, 9.3 Hz, 1H), 5.42 (d, *J* = 9.3 Hz, 1H), 4.46 (br s, 1H). **^{13}C-NMR (75 MHz, $CDCl_3$)** δ 149.2, 141.8, 136.2, 132.1, 131.9, 129.0 (2C), 128.7 (2C), 128.5 (2C), 127.8, 127.7, 126.89 (q, $^{2}J_{C\text{-}F}$ = 35.1 Hz), 126.89 (2C), 126.5 (q, $^{3}J_{C\text{-}F}$ = 4.3, 3.8 Hz, 2C), 121.3 (q, $^{1}J_{C\text{-}F}$ = 282.1 Hz), 112.6 (2C), 55.2. **^{19}F-NMR (282 MHz, $CDCl_3$)** δ -61.1. . **HRMS (EI$^+$)** calculated for $C_{22}H_{18}F_3N$ $[M]^+$: 353.1391, found: 353.1373.

(*Z*)-2-bromo-*N*-(1,3-diphenylallyl)aniline (9f)

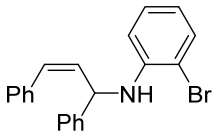

9f

From (*E*)-1,3-diphenylallyl acetate (25.2 mg, 0.1 mmol) and 2-bromoaniline (21.8 μL, 0.2 mmol), following the general procedure, compound **9f** (24.4 mg, 0.067 mmol) was obtained in 67% yield (*Z*:*E* ratio = 84:16) as a colorless oil. The crude product was purified by column chromatography. Eluent: Hexane:DCM (3:1). **^{1}H-NMR (300 MHz, $CDCl_3$)** δ 7.45 – 7.26 (m, 11H), 6.95 (ddd, *J* = 8.5, 7.4, 1.5 Hz, 1H), 6.72 (d, *J* = 11.4 Hz, 1H), 6.53 (td, *J* = 7.6, 1.5 Hz, 1H), 6.27 (dd, *J* = 8.2, 1.5 Hz, 1H), 5.82 (dd, *J* = 11.4, 9.4 Hz, 1H), 5.42 (dd, *J* = 9.4, 5.7 Hz, 1H), 4.82 (d, *J* = 5.9 Hz, 1H). **^{13}C-NMR (75 MHz, $CDCl_3$)** δ 143.6, 142.0, 136.4, 132.5, 132.3, 131.6, 129.0 (2C), 128.7 (2C), 128.5 (2C), 128.3, 127.62,

127.56, 126.9 (2C), 118.1, 112.8, 109.9, 55.5. **HRMS (EI$^+$)** calculated for $C_{21}H_{18}BrN$ $[M]^+$: 363.0623, found: 363.0623.

(*Z*)-*N*-(1,3-diphenylallyl)butan-2-amine (9g)

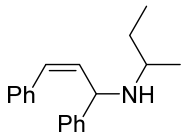

9g

From (*E*)-1,3-diphenylallyl acetate (25.2 mg, 0.1 mmol) and *sec*-butylamine (20.2 μL, 0.2 mmol), following the general procedure, compound **9g** (16 mg, 0.061 mmol) was obtained in 61% yield (*Z*:*E* ratio = 93:7) as an orange oil. The crude product was purified by column chromatography. Eluent: DCM: MeOH (4:1). **^{1}H-NMR (300 MHz, $CDCl_3$)** δ 7.46 – 7.26 (m, 10H), 6.63, 6.57 (2 x d, *J* = 11.7 Hz, 1H), 5.85, 5.80 (2 x dd, *J* = 11.6, 9.8 Hz, 1H), 4.82 (d, *J* = 9.8 Hz, 1H), 2.58, 2.50 (2 x q, *J* = 6.2 Hz, 1H), 2.11 (br s, 1H), 1.37 – 1.14 (m, 2H), 1.01, 0.86 (2 x d, *J* = 6.3 Hz, 2H), 0.85, 0.76 (2 x t, *J* = 7.4 Hz, 3H). **^{13}C-NMR (75 MHz, $CDCl_3$)** δ 137.1, 130.1, 129.8, 128.7 (2C), 128.6 (2C), 128.2 (2C), 127.4, 127.3 (2C), 127.2, 127.02, 127.00, 56.9, 56.6, 51.6, 51.4, 29.6, 29.4, 19.9, 19.8, 10.3, 10.1. **HRMS (EI$^+$)** calculated for $C_{19}H_{23}N$ $[M]^+$: 265.1830, found: 265.1830.

(*Z*)-*N*,*N*-dibenzyl-1,3-diphenylprop-2-en-1-amine (9h)

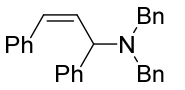

9h

From (*E*)-1,3-diphenylallyl acetate (25.2 mg, 0.1 mmol) and dibenzylamine (38.5 μL, 0.2 mmol), following the general procedure, compound **9h** (30.1 mg, 0.077 mmol) was obtained in 77% yield (*Z*:*E* ratio = 85:15) as a colorless oil. The crude product was purified by column chromatography. Eluent: Hexane:DCM (2:1). **^{1}H-NMR (300 MHz, $CDCl_3$)** δ 7.67 – 7.59 (m, 2H), 7.45 – 7.28 (m, 4H), 7.17 – 7.11 (m, 12H), 7.07 – 6.99 (m with d at 7.03, *J* = 11.8 Hz, 3H), 6.09 (dd, *J* = 11.8, 10.4 Hz, 1H), 4.85 (d, *J* = 10.5 Hz, 1H), 3.72 and 3.42 (AB System, *J* = 13.4 Hz, 4H). **^{13}C-NMR (75 MHz, $CDCl_3$)** δ 142.3, 139.8 (2C), 136.8, 133.9, 128.8 (4C), 128.5 (2C), 128.3 (2C), 128.23 (2C), 128.18 (2C), 127.9 (4C), 127.8, 127.03, 126.97, 126.6 (2C), 58.7, 53.6 (2C). **HRMS (EI$^+$)** calculated for $C_{15}H_{13}$ $[M]^+$ $[M - C_{14}H_{14}N]^+$: 193.1012, found: 193.1019.

(*Z*)-1-(1,3-diphenylallyl)piperidine (9i)

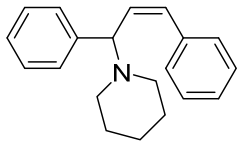

9i

From (*E*)-1,3-diphenylallyl acetate (25.2 mg, 0.1 mmol) and piperidine (20.0 μL, 0.2 mmol), following the general procedure, compound **9i** (18.7 mg, 0.068 mmol) was obtained in 68% yield (*Z*:*E* ratio = 91:9) as a pale yellow oil. The crude product was purified by column chromatography. Eluent: Pentane:AcOEt (98:2). Spectroscopic data are in agreement with the published data.[24] **^{1}H-NMR (300 MHz, $CDCl_3$)** δ 7.40 – 7.20 (m, 10H), 6.62 (d, *J* = 11.7 Hz, 1H), 5.95 (dd, *J* = 11.7, 10.1 Hz, 1H), 4.24 (d, *J* = 10.1 Hz, 1H),

2.54 – 2.40 (m, 2H), 2.25 (dt, *J* = 11.0, 5.3 Hz, 2H), 1.56 – 1.47 (m, 4H), 1.43 – 1.35 (m, 2H).

(*Z*)-4-(1,3-diphenylallyl)morpholine (9j)

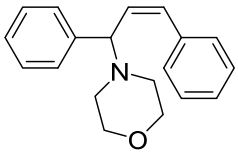

9j

From (*E*)-1,3-diphenylallyl acetate (25.2 mg, 0.1 mmol) and morpholine (17.0 μL, 0.2 mmol), following the general procedure, compound **9j** (20.0 mg, 0.076 mmol) was obtained in 76% yield (*Z*:*E* ratio = 94:6) as a white solid. The crude product was purified by column chromatography. Eluent: Cyclohexane:AcOEt (95:5). Spectroscopic data are in agreement with the published data.[24] **^{1}H-NMR (300 MHz, $CDCl_3$)** δ 7.40 – 7.20 (m, 10H), 6.66 (d, *J* = 11.7 Hz, 1H), 5.91 (dd, *J* = 11.7, 10.1 Hz, 1H), 4.23 (d, *J* = 10.1 Hz, 1H), 3.65 (t, *J* = 4.7 Hz, 4H), 2.52 (dt, *J* = 11.5, 4.7 Hz, 2H), 2.28 (dt, *J* = 11.5, 4.7 Hz, 2H).

(*Z*)-(3-methoxyprop-1-ene-1,3-diyl)dibenzene (9k)

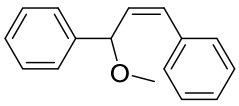

9k

From (*E*)-1,3-diphenylallyl acetate (25.2 mg, 0.1 mmol) and methanol (8.0 μL, 0.2 mmol), following the general procedure, compound **9k** (17.0 mg, 0.076 mmol) was obtained in 76% yield (*Z*:*E* ratio = 88:12) as a yellow oil. The crude product was purified by column chromatography. Eluent: Cyclohexane: DCM (95:5). **^{1}H-NMR (300 MHz, $CDCl_3$)** δ 7.44 – 7.23 (m, 10H), 6.75 (d, *J* = 11.6 Hz, 1H), 5.87 (dd, *J* = 11.6, 9.3 Hz, 1H), 5.07 (d, *J* = 9.3 Hz, 1H), 3.27 (s, 3H). **^{13}C-NMR (75 MHz, $CDCl_3$):** δ 141.2, 136.7, 132.3, 132.0, 128.8 (2C), 128.6 (2C), 128.3 (2C), 127.8, 127.3, 127.0 (2C), 78.9, 55.9. **HRMS (EI$^+$)** calculated for $C_{16}H_{16}O$ $[M]^+$: 224.1196, found: 224.1188.

(*Z*)-(3-ethoxyprop-1-ene-1,3-diyl)dibenzene (9l)

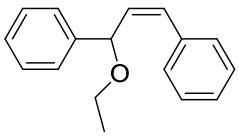

9l

From (*E*)-1,3-diphenylallyl acetate (25.2 mg, 0.1 mmol) and ethanol (12.0 μL, 0.2 mmol), following the general procedure, compound **9l** (16.4 mg, 0.069 mmol) was obtained in 69% yield (*Z*:*E* ratio = 86:14) as a yellow oil. The crude product was purified by column chromatography. Eluent: Cyclohexane:DCM (95:5). **^{1}H-NMR (300 MHz, $CDCl_3$)** δ 7.43 – 7.23 (m, 10H), 6.71 (d, *J* = 11.6 Hz, 1H), 5.88 (dd, *J* = 11.6, 9.4 Hz, 1H), 5.19 (d, *J* = 9.4 Hz, 1H), 3.50 (dq, *J* = 9.1, 7.0 Hz, 1H), 3.34 (dq, *J* = 9.1, 7.0 Hz, 1H), 1.19 (t, *J* = 7.0 Hz, 3H). **^{13}C-NMR (75 MHz, $CDCl_3$):** δ 141.7, 136.7, 132.7, 132.0, 128.8 (2C), 128.6 (2C), 128.2 (2C), 127.6, 127.2, 127.0 (2C), 77.2, 63.5, 15.4. **HRMS (EI$^+$)** calculated for $C_{17}H_{18}O$ $[M]^+$: 238.1352, found: 238.1336.

(*Z*)-(3-isobutoxyprop-1-ene-1,3-diyl)dibenzene (9m)

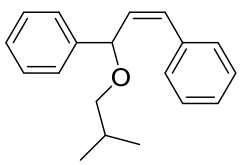

9m

From (*E*)-1,3-diphenylallyl acetate (25.2 mg, 0.1 mmol) and 2-methylpropan-1-ol (18.0 μL, 0.2 mmol), following the general procedure, compound **9m** (17.6 mg, 0.066 mmol) was obtained in 66% yield (*Z*:*E* ratio = 86:14) as a yellow oil. The crude product was purified by column chromatography. Eluent: Cyclohexane: DCM (95:5). **^{1}H-NMR (300 MHz, $CDCl_3$)** δ 7.44 – 7.24 (m, 10H), 6.72 (d, *J* = 11.6 Hz, 1H), 5.85 (dd, *J* = 11.6, 9.4 Hz, 1H), 5.16 (d, *J* = 9.4 Hz, 1H), 3.21 (dd, *J* = 9.0, 6.5 Hz, 1H), 3.05 (dd, *J* = 8.9, 6.7 Hz, 1H), 1.92 – 1.79 (m, 1H), 0.91 (d, *J* = 6.6 Hz, 3H), 0.89 (d, *J* = 6.6 Hz, 3H). **^{13}C-NMR (75 MHz, $CDCl_3$):** δ 141.8, 136.7, 132.7, 131.6, 128.8 (2C), 128.5 (2C), 128.2 (2C), 127.6, 127.2, 126.9 (2C), 77.3, 75.1, 28.6, 19.6 (2C). **HRMS (EI$^+$)** calculated for $C_{19}H_{22}O$ $[M]^+$: 266.1665, found: 266.1669.

General procedure for the preparation of *E*-allylic compounds (10)

A vial equipped with a magnetic stir bar and fitted with a teflon screw cap septum was charged with the corresponding allylic compound **1** (0.1 mmol), the corresponding amine or alcohol (0.2 mmol), 3-(4-methoxyphenyl)-10-phenyl-10*H*-phenoxazine (1.7 mg, 5 mol%) and acetonitrile (1 mL). The reaction was degassed with three freeze-pump-thaw cycles. The vial was then backfilled with N_2 and stirred under 420 nm LEDs irradiation (18.3396 W/m^2 intensity; approximate distance was 2 cm from the vial) at room temperature. After 3 h the vial was opened, the solvent evaporated and the crude purified by column chromatography.

(*E*)-*N*-(1,3-diphenylallyl)aniline (10a)

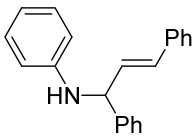

10a

From (*E*)-1,3-diphenylallyl acetate (25.2 mg, 0.1 mmol) and aniline (19 μL, 0.2 mmol), following the general procedure, compound **10a** (26.4 mg, 0.092 mmol) was obtained in 92% yield (*Z*:*E* ratio = 9:91) as a colorless oil. The crude product was purified by column chromatography. Eluent: Hexane:DCM (2:1). Spectroscopic data are in agreement with the published data.[25] **^{1}H-NMR (300 MHz, $CDCl_3$)** δ 7.48 – 7.25 (m, 10H), 7.20 – 7.12 (m, 2H), 6.75 – 6.61 (m, 4H), 6.41 (dd, *J* = 15.8, 6.1 Hz, 1H), 5.10 (d, *J* = 5.7 Hz, 1H), 4.16 (br s, 1H). **HRMS (EI$^+$)** calculated for $C_{21}H_{19}N$ $[M]^+$: 285.1517, found: 285.1520.

(*E*)-*N*-(1,3-diphenylallyl)-4-methylaniline (10b)

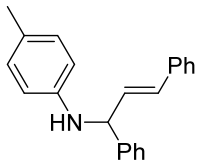

10b

From (*E*)-1,3-diphenylallyl acetate (25.2 mg, 0.1 mmol) and *p*-toluidine (21.4 mg, 0.2 mmol), following the general procedure, compound **10b** (25.5 mg, 0.084 mmol) was obtained in 84% yield (*Z*:*E* ratio = 8:92) as a colorless oil. The crude product was purified by column chromatography. Eluent: Hexane:DCM (3:1). Spectroscopic data are in agreement with the published data.[26] **^{1}H-NMR (300 MHz, $CDCl_3$)** δ 7.47 – 7.41 (m, 2H), 7.39 – 7.25 (m, 8H), 6.96 and 6.56 (AA'BB' system, 4H), 6.63 (d, *J* = 15.7 Hz, 1H), 6.39 (dd, *J* = 15.8, 6.1 Hz, 1H), 5.06 (d, *J* = 6.2 Hz, 1H), 4.18 (br s, 1H), 2.22 (s, 3H).

(*E*)-*N*-(1,3-diphenylallyl)-4-methoxyaniline (10c)

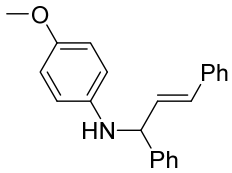

10c

From (*E*)-1,3-diphenylallyl acetate (25.2 mg, 0.1 mmol) and 4-methoxyaniline (24.6 mg, 0.2 mmol), following the general procedure and adding DIPEA (86 μL, 0.5 mmol), compound **10c** (27.8 mg, 0.087 mmol) was obtained in 87% yield (*Z*:*E* ratio = 4:96) as a yellow oil. The crude product was purified by column chromatography. Eluent: DCM. Spectroscopic data are in agreement with the published data.[26] **^{1}H-NMR (300 MHz, $CDCl_3$)** δ 7.45 – 7.39 (m, 2H), 7.37 – 7.19 (m, 8H), 6.73 and 6.59 (AA'BB' system, 4H), 6.61 (d, *J* = 16.1 Hz, 1H), 6.38 (dd, *J* = 15.8, 6.2 Hz, 1H), 5.00 (d, *J* = 6.2 Hz, 1H), 3.86 (br s, 1H), 3.71 (s, 3H).

(*E*)-4-(*tert*-butoxy)-*N*-(1,3-diphenylallyl)aniline (10d)

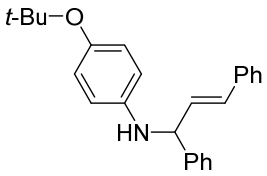

10d

From (*E*)-1,3-diphenylallyl acetate (25.2 mg, 0.1 mmol) and 4-*tert*-butoxyaniline (33 mg, 0.2 mmol), following the general procedure and adding DIPEA (86 μL, 0.5 mmol), compound **10d** (28.8 mg, 0.079 mmol) was obtained in 79% yield (*Z*:*E* ratio = 3:97) as a yellow oil. The crude product was purified by column chromatography. Eluent: DCM. **^{1}H-NMR (300 MHz, $CDCl_3$)** δ 7.45 – 7.40 (m, 2H), 7.38 – 7.17 (m, 8H), 6.78 and 6.53 (AA'BB' system, 4H), 6.61 (d, *J* = 15.9 Hz, 1H), 6.38 (dd, *J* = 15.8, 6.3 Hz, 1H), 5.01 (d, *J* = 6.2 Hz, 1H), 3.95 (br s, 1H), 1.26 (s, 9H). **^{13}C-NMR (75 MHz, $CDCl_3$)** δ 146.7, 143.6, 142.4, 136.8, 131.2, 131.0, 128.8 (2C), 128.6 (2C), 127.7, 127.5, 127.2 (2C), 126.5 (2C), 125.3 (2C), 113.9 (2C), 77.7, 61.4, 28.7 (3C). **HRMS (EI$^+$)** calculated for $C_{25}H_{27}NO$ $[M]^+$: 357.2093, found: 357.2087.

(*E*)-*N*-(1,3-diphenylallyl)-4-(trifluoromethyl)aniline (10e)

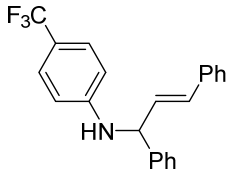

10e

From (*E*)-1,3-diphenylallyl acetate (25.2 mg, 0.1 mmol) and 4-(trifluoromethyl)aniline (25.1 μL, 0.2 mmol), following the general procedure, compound **10e** (30.1 mg, 0.084 mmol) was obtained in 84% yield (*Z*:*E* ratio = 7:93) as a yellow solid. The crude product was purified by column chromatography. Eluent: Hexane:DCM (3:1). Spectroscopic data are in agreement with the published data.[27] **^{1}H-NMR (300 MHz, $CDCl_3$)** δ 7.44 – 7.21 (m, 12H), 6.67 – 6.55 (m, 3H), 6.37 (dd, *J* = 15.8, 6.1 Hz, 1H), 5.12 (m, 1H), 4.42 (d, *J* = 5.1 Hz, 1H).

(*E*)-2-bromo-*N*-(1,3-diphenylallyl)aniline (10f)

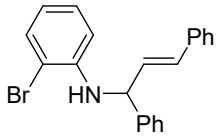

10f

From (*E*)-1,3-diphenylallyl acetate (25.2 mg, 0.1 mmol) and 2-bromoaniline (21.8 μL, 0.2 mmol), following the general procedure, compound **10f** (30.2 mg, 0.082 mmol) was obtained in 82% yield (*Z*:*E* ratio = 7:93) as a light yellow oil. The crude product was purified by column chromatography. Eluent: Hexane:DCM (3:1). **^{1}H-NMR (300 MHz, $CDCl_3$)** δ 7.45 – 7.40 (m, 3H), 7.39 – 7.33 (m, 4H), 7.32 – 7.26 (m, 3H), 7.25 – 7.21 (m, 1H), 7.06 (ddd, *J* = 8.5, 7.3, 1.5 Hz, 1H), 6.63 – 6.52 (m, 3H), 6.40 (dd, *J* = 15.9, 6.1 Hz, 1H), 5.13 (t, *J* = 5.5 Hz, 1H), 4.81 (d, *J* = 5.0 Hz, 1H). **^{13}C-NMR (75 MHz, $CDCl_3$)** δ 144.0, 141.5, 136.5, 132.4, 131.5, 130.2, 129.0 (2C), 128.6 (2C), 128.4, 127.8, 127.7, 127.1 (2C), 126.6 (2C), 118.2, 112.9, 110.0, 60.5. **HRMS (EI$^+$)** calculated for $C_{21}H_{18}BrN$ $[M]^+$: 363.0623, found: 363.0623.

(*E*)-*N*-(1,3-diphenylallyl)butan-2-amine (10g)

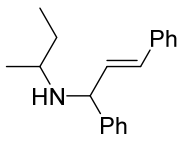

10g

From (*E*)-1,3-diphenylallyl acetate (25.2 mg, 0.1 mmol) and *sec*-butylamine (20.2 μL, 0.2 mmol), following the general procedure, compound **10g** (10.3 mg, 0.039 mmol) was obtained in 39% yield (*Z*:*E* ratio = 7:93) as an orange oil. The crude product was purified by column chromatography. Eluent: DCM: MeOH (6:1). **^{1}H-NMR (300 MHz, $CDCl_3$)** δ 7.40 – 7.24 (m, 10H), 6.55, 6.50 (2 x d, *J* = 15.7 Hz, 1H), 6.32, 6.27 (2 x dd, *J* = 15.7, 6.7 Hz, 1H), 4.51, 4.48 (2 x d, *J* = 6.6 Hz, 1H), 2.64, 2.56 (2 x q, *J* = 6.3 Hz, 1H), 1.85 (br s, 1H), 1.54 – 1.32 (m, 2H), 1.07, 1.04 (2 x d, *J* = 6.3 Hz, 3H), 0.89, 0.86 (2 x t, *J* = 7.4 Hz, 3H). **^{13}C-NMR (75 MHz, $CDCl_3$)** δ 137.1, 130.0, 129.9, 128.63 (2C), 128.55 (2C), 128.48, 128.47, 127.39, 127.35, 127.29 (2C), 127.13, 127.12, 126.4 (2C), 62.43, 62.43, 51.4, 51.2, 29.8, 29.5, 20.1, 19.9, 10.17, 10.15. **HRMS (EI$^+$)** calculated for $C_{19}H_{23}N$ $[M]^+$: 265.1830, found: 265.1830.

(*E*)-*N*,*N*-dibenzyl-1,3-diphenylprop-2-en-1-amine (10h)

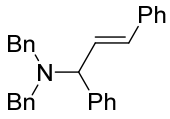

10h

From (*E*)-1,3-diphenylallyl acetate (25.2 mg, 0.1 mmol) and dibenzylamine (38.5 μL, 0.2 mmol), following the general procedure, compound **10h** (23.4 mg, 0.060 mmol) was obtained in 60% yield (*Z*:*E* ratio = 5:95) as a colorless oil. The crude product was purified by column chromatography. Spectroscopic data are in agreement with the published data.[28] Eluent: Hexane:DCM (3:1). **^{1}H-NMR (300 MHz, $CDCl_3$)** δ 7.57 – 7.52 (m, 2H), 7.45 – 7.40 (m, 6H), 7.38 – 7.30 (m, 7H), 7.29 – 7.21 (m, 5H), 6.57 – 6.41 (m, 2H), 4.44 (d, *J* = 6.7 Hz, 1H), 3.73 and 3.61 (AB system, *J* = 13.8 Hz, 4H).

(*E*)-1-(1,3-diphenylallyl)piperidine (10i)

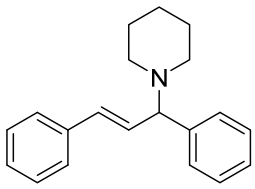

10i

From (*E*)-1,3-diphenylallyl acetate (25.2 mg, 0.1 mmol) and piperidine (20.0 μL, 0.2 mmol), following the general procedure, compound **10i** (18.8 mg, 0.068 mmol) was obtained in 68% yield (*Z*:*E* ratio = 12:88) as a pale yellow solid. The crude product was purified by column chromatography. Eluent: Pentane:AcOEt (98:2). Spectroscopic data are in agreement with the published data.[29] **^{1}H-NMR (300 MHz, $CDCl_3$)** δ 7.42 – 7.15 (m, 10H), 6.52 (d, *J* = 15.8 Hz, 1H), 6.34 (dd, *J* = 15.8, 8.6 Hz, 1H), 3.81 (d, *J* = 8.6 Hz, 1H), 2.55 – 2.45 (m, 2H), 2.40 – 2.28 (m, 2H), 1.62 – 1.51 (m, 4H), 1.47 – 1.39 (m, 2H).

(*E*)-4-(1,3-diphenylallyl)morpholine (10j)

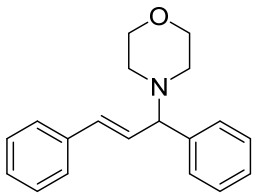

10j

From (*E*)-1,3-diphenylallyl acetate (25.2 mg, 0.1 mmol) and morpholine (17.0 μL, 0.2 mmol), following the general procedure, compound **10j** (18.4 mg, 0.066 mmol) was obtained in 66% yield (*Z*:*E* ratio = 5:95) as a yellow oil. The crude product was purified by column chromatography. Eluent: Cyclohexane:AcOEt (98:2). Spectroscopic data are in agreement with the published data.[29] **^{1}H-NMR (300 MHz, $CDCl_3$)** δ 7.44 – 7.16 (m, 10H), 6.56 (d, *J* = 15.8 Hz, 1H), 6.28 (dd, *J* = 15.8, 8.9 Hz, 1H), 3.78 (d, *J* = 8.9 Hz, 1H), 3.70 (t, *J* = 4.6 Hz, 4H), 2.62 – 2.50 (m, 2H), 2.38 (dt, *J* = 11.6, 4.6 Hz, 2H).

(*E*)-(3-methoxyprop-1-ene-1,3-diyl)dibenzene (10k)

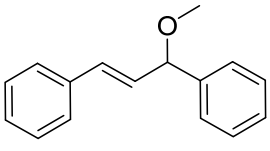

10k

From (*E*)-1,3-diphenylallyl acetate (25.2 mg, 0.1 mmol) and methanol (8.0 μL, 0.2 mmol), following the general procedure, compound **10k** (10.8 mg, 0.048 mmol) was obtained in 48% yield (*Z*:*E* ratio = 5:95) as a yellow oil. The crude product was purified

by column chromatography. Eluent: Cyclohexane:DCM (95:5). Spectroscopic data are in agreement with the published data.[30] **^{1}H-NMR (300 MHz, $CDCl_3$)** δ 7.42 – 7.35 (m, 6H), 7.35 – 7.19 (m, 4H), 6.63 (d, *J* = 15.9 Hz, 1H), 6.28 (dd, *J* = 15.9, 7.0 Hz, 1H), 4.80 (d, *J* = 7.0, 1H), 3.38 (s, 3H).

(*E*)-(3-ethoxyprop-1-ene-1,3-diyl)dibenzene (10l)

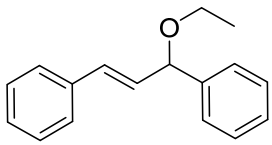

10l

From (*E*)-1,3-diphenylallyl acetate (25.2 mg, 0.1 mmol) and ethanol (12.0 μL, 0.2 mmol), following the general procedure, compound **10l** (8.8 mg, 0.037 mmol) was obtained in 37% yield (*Z*:*E* ratio = 6:94) as a yellow oil. The crude product was purified by column chromatography. Eluent: Cyclohexane: DCM (95:5). Spectroscopic data are in agreement with the published data.[30] **^{1}H-NMR (300 MHz, $CDCl_3$)** δ 7.44 – 7.18 (m, 10H), 6.60 (d, *J* = 15.8 Hz, 1H), 6.31 (dd, *J* = 15.8, 7.0 Hz, 1H), 4.92 (d, *J* = 7.0 Hz, 1H), 3.59 (dq, *J* = 9.1, 7.0 Hz, 1H), 3.48 (dq, *J* = 9.1, 7.0 Hz, 1H), 1.26 (t, *J* = 7.0 Hz, 3H).

(*E*)-(3-isobutoxyprop-1-ene-1,3-diyl)dibenzene (10m)

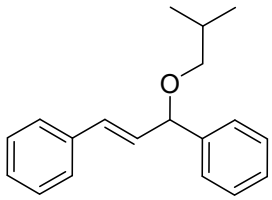

10m

From (*E*)-1,3-diphenylallyl acetate (25.2 mg, 0.1 mmol) and 2-methylpropan-1-ol (18.0 μL, 0.2 mmol), following the general procedure, compound **10m** (9.1 mg, 0.034 mmol) was obtained in 34% yield (*Z*:*E* ratio = 13:87) as a yellow oil. The crude product was purified by column chromatography. Eluent: Cyclohexane: DCM (95:5). Spectroscopic data are in agreement with the published data.[31] **^{1}H-NMR (300 MHz, $CDCl_3$)** δ 7.45 – 7.20 (m, 10H), 6.61 (d, *J* = 15.9 Hz, 1H), 6.29 (dd, *J* = 15.9, 6.9 Hz, 1H), 4.89 (d, *J* = 6.9 Hz, 1H), 3.30 (dd, *J* = 8.8, 6.7 Hz, 1H), 3.18 (dd, *J* = 8.8, 6.7 Hz, 1H), 2.02 – 1.87 (m, 1H), 0.94 (d, *J* = 6.7 Hz, 6H).

Supplementary Notes 2.

Laser flash photolysis studies of the reaction with photocatalysts 3e and 3g:

The employed laser flash photolysis equipment (λ_{exc} = 355 nm, power = 300-500 μJ/pulse) is based on a pump-probe setup purchased from Edinburgh Co (LP980-K). The pump source is an optical parametric oscillator (OPO) pumped by the third harmonic of a Nd:YAG laser (EKSPLA). The wavelength can be set from 210 nm to about 2600 nm, with a pulse width of about 5 nm using an OPO mod. NT342A-10 with an UV extension NT242 with typical pulse duration of 5 ns. A pulsed xenon flash lamp (150 W) is employed as detecting light source. A monochormator (TMS302-A, grating 150

lines/mm) disperses the probe light after it has passed the sample. The probe light is then passed on to a PMT detector (Hamamatsu Photonics) to obtain the temporal resolved picture. The time resolution in each window is about 10 % of the temporal window width. All components are controlled by the software L900 provided by Edinburgh.

Laser flash photolysis of a solution 50 µM of **3g** in CH_3CN under inert atmosphere resulted in the formation of two new peaks at 468 nm and 530 nm (Supplementary Figure 1a) that were assigned to the radical cation **[3g]**$^{\cdot+}$ and the triplet excited state ^{3}**[3g]*** respectively (Supplementary Figure 1a). The latest was confirmed by disappearance of this band under aerobic conditions, due to triplet quenching by oxygen (Supplementary Figure 1b).

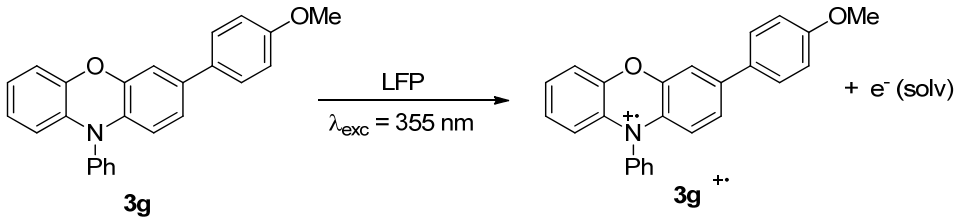

a) b)

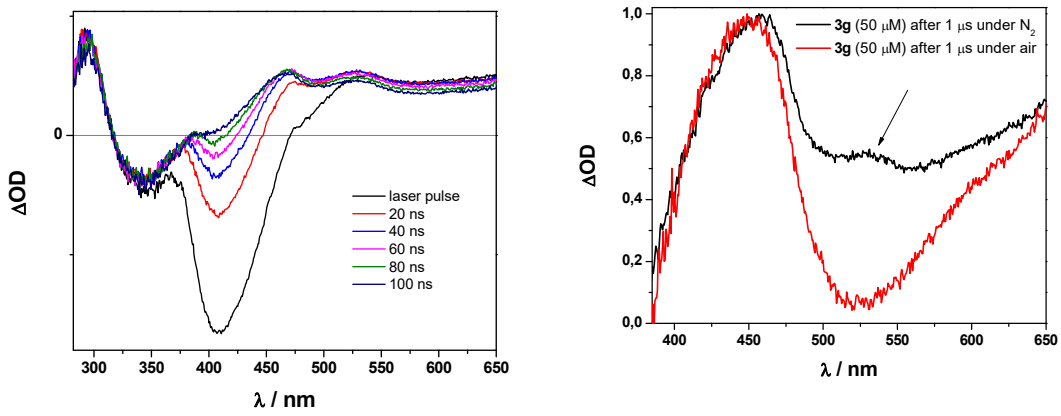

Supplementary Figure 1: **Reaction with photocatalyst 3g:** Laser flash photolysis (λ_{exc} = 355 nm, MeCN/Ar) experiments. a) Transient absorption spectra recorded at different times after the laser pulse of **3g** (50 µM); b) Transient absorption spectra recorded at 1 µs after the laser pulse of **3g** (50 mM) under N_2 (black) or under air (red).

Laser flash photolysis (λ_{exc} = 355 nm) of a solution containing **3g** (50 µM) and **1a** (70 mM) gave rise to the formation of two new intense peaks at 360 nm and 490 nm (see Supplementary Figure 2a), that were assigned to the radical intermediate **I** (**INT I**) and

the carbocation **II** (**INT II**) on the basis of the reported data (For the transient absorption spectrum of **I** and **II** see [32]). Thus, after single electron transfer (SET) from the singlet excited state (^{1}**3g***) to **1a** at diffusion-controlled rate ($k_q(S_1)$ = 4.9 x 10^9 $M^{-1}s^{-1}$), the corresponding radical ion pair (**3g**$^{\cdot+}$------**1a**$^{\cdot-}$) is generated. Fast acetate release from the **1a**$^{\cdot-}$ led to the formation of **INT I** which is still in contact with the radical cation of **3g** (**3g**$^{\cdot+}$----**INT I)** At this point, two pathways could take place. On one hand, ultra-fast back electron transfer (BET) occurs between the **3g** radical cation (**3g**$^{\cdot+}$) and **INT I**, restoring **3g** to its ground state and generating free **INT II** which has been successfully observed by LFP (λ_{abs} = 490 nm, Supplementary Figure 2b). In order to whether **INT II** comes from **INT I** we have performed additional LFP experiments of **3g** in the presence of increasing amounts of **1a** (Supplementary Figure 2 c and d). Generation of **INT II** is practically instantaneous even at lower concentrations of **1a** Supplementary Figure 2d) whereas lifetimes of **INT I** is not affected by higher amounts of **1a** (Supplementary Figure 2c), what is indicating that the BET process undergoes in the sub-nanosecond scale (as well as the SET and the C-O bond scission).[33] The other possible evolution pathway of (**3g**$^{\cdot+}$----**INT I)** is that they diffuse apart (escape process), forming their corresponding free radical ion and free radical, respectively. These two stable species are actually detected by the LPF experiments with lifetimes in the microsecond scale (see Supplementary Figure 2b and c) and it seems that they do not interact (see Supplementary Figure 2b and c).

a)

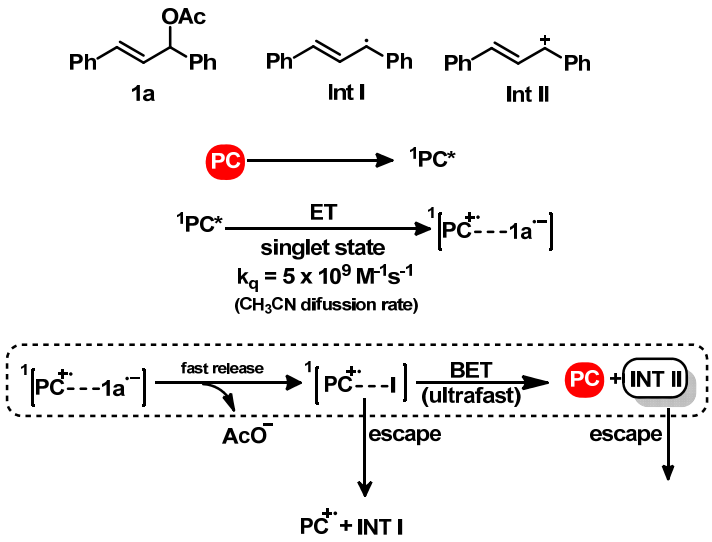

b)

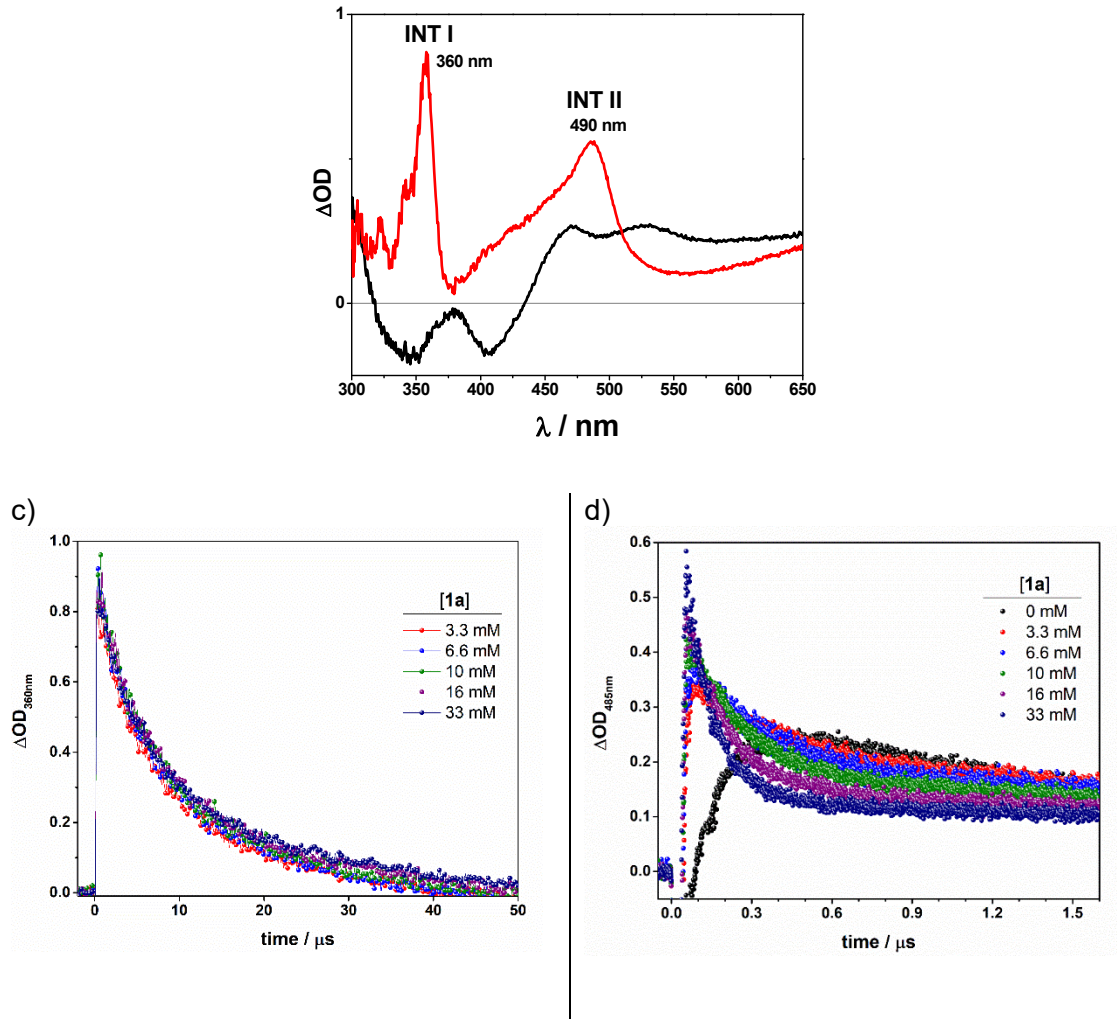

Supplementary Figure 2. a) Proposed reaction mechanism; b) Transient absorption spectra recorded 40 ns after the laser pulse (λ_{exc} = 355 nm, MeCN/Ar) of **3g** (50 μM) without **1a** (black), with 70 mM of **1a** (red); c) Normalized decays monitored at 357 nm of **3g** (50 mM), with increasing concetrations of 1a; d) Normalized decays monitored at 485 nm of **3g** (50 mM), with increasing concetrations of **1a.**

Having established the formation of **INT I** and **INT II**, the question arises whether nucleophiles such as pyrrole (**2a**) or *p*-toluidine (**8b**) are capable of reacting with these intermediates, which would require direct quenching of **INT I** or **INT II** by **2a** (or **8b**). In fact, addition of **2a** (37 mM) or **8b** (40 mM) to the **3g**/**1a** mixture resulted in a totally disappearance of the band at 490 nm, while the band at 360 nm is not affected (Supplementary Figure 3), clearly confirming that **INT II** is the reactive species.

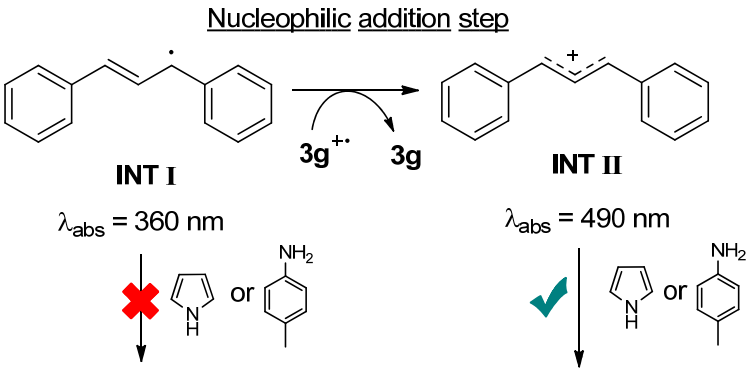

a) Reaction with pyrrole **2a**

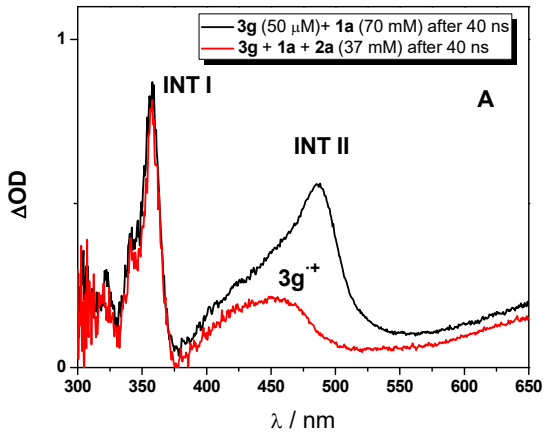

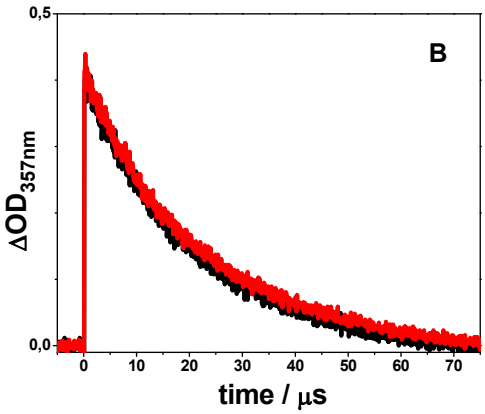

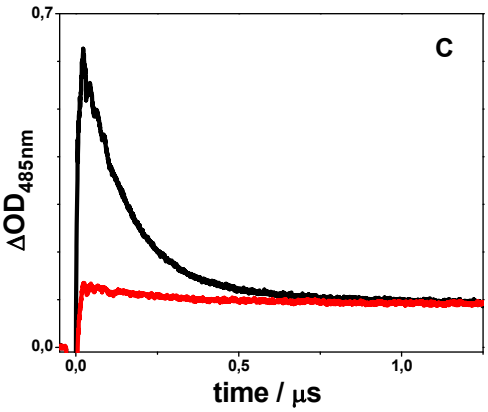

b) Reaction with *p*-toluidine **8b**

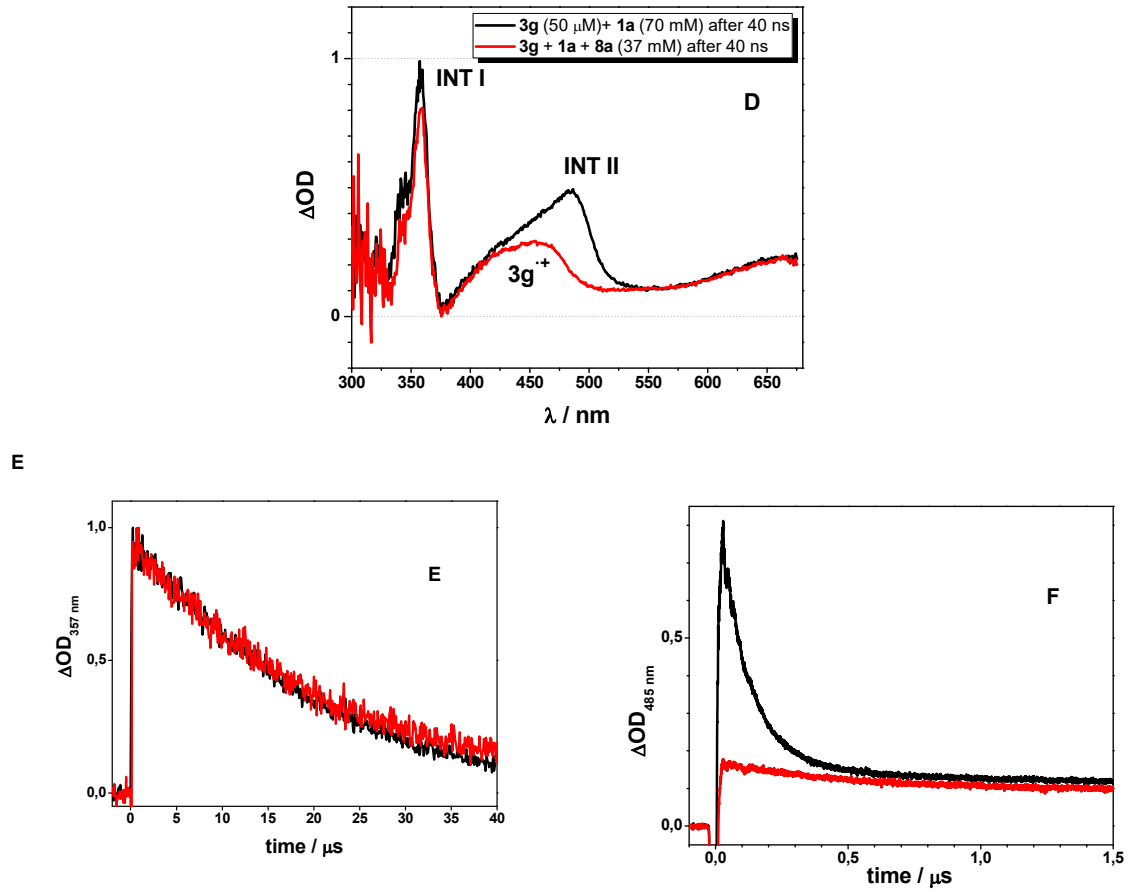

Supplementary Figure 3. a) LFP of the quenching with pyrrole **2a**: A: Transient absorption spectra recorded 40 ns after the laser pulse (λ_{exc} = 355 nm, MeCN/Ar) of **3g** (50 μM) with 70 mM of **1a** (black), and in the presence of **2a** (40 m M) (red). B: Decay at 357 nm of **3g** (50 mM) and **1a** (70 mM) (black) and in the presence of **2a** (37 mM) (red). C: Decay at 490 nm of **3g** (50 mM) and **1a** (70 mM) (black) and in the presence of **2a** (37 mM) (red); b) LFP of the quenching with *p*-toluidine **8b**: D: Transient absorption spectra recorded 40 ns after the laser pulse (λ_{exc} = 355 nm, MeCN/Ar) of **3g** (50 μM) with 70 mM of **1a** (black), and in the presence of **8b** (37 mM) (red). E: Decay at 357 nm of **3g** (50 mM) and **1a** (70 mM) (black) and in the presence of **8b** (37 mM) (red). F: Decay at 490 nm of **3g** (50 mM) and **1a** (70 mM) (black) and in the presence of **8b** (37 mM) (red).

Laser flash photolysis (λ_{exc} = 355 nm) of a solution containing **3g** (50 μM) and the **allylic benzoate 1** (70 mM) was also performed in order to compare the lifetime of the carbocation compared to the one obtained with the allylic acetate (Supplementary Figure 4). The experiment gave rise to the formation of the same two intense peaks at 360 nm and 490 nm (see Supplementary Figure 4b), corresponding again to the radical

intermediate **I** (**INT I**) and the carbocation **II** (**INT II**). Supplementary Figure 4b shows a comparison of the life time of **INT II** formed from the allylic acetate **1a** and the carbocation formed from the **allylic benzoate 1**. As it can be seen, the life time of the carbocation is dependent on the nucleophilic character of the anion released after the SET step. In the presence of a more nucleophilic anion (AcO^-) the life time of **INT II** is shorter than in the presence of the less nucleophilic benzoate ($PhOCO^-$).

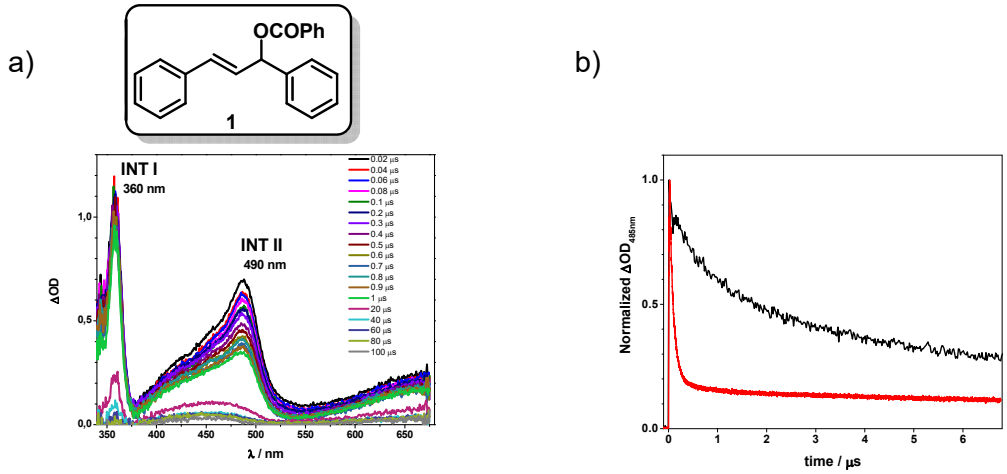

Supplementary Figure 4. a) Transient absorption spectra of **3g** (50 mM) and 70 mM of **"allylic benzoate 1"** recorded at different times after the laser pulse; b) Normalized decays monitored at 485 nm of **3g** (50 mM), with 70 mM of "**allylic benzoate 1**" (black), or with 70 mM of **1a** (red).

Reaction with photocatalyst 3e:

Laser flash photolysis (λ_{exc} = 355 nm) of a solution 50 µM of **3e** in CH_3CN under inert atmosphere resulted in the formation of two a new peak at 460 nm corresponding to the triplet excited state ^{3}**[3g]**, confirmed by disappearance of the signal when carrying out the experiment under air (Supplementary Figure 5).

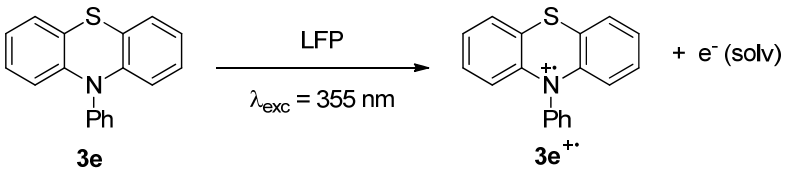

a) b)

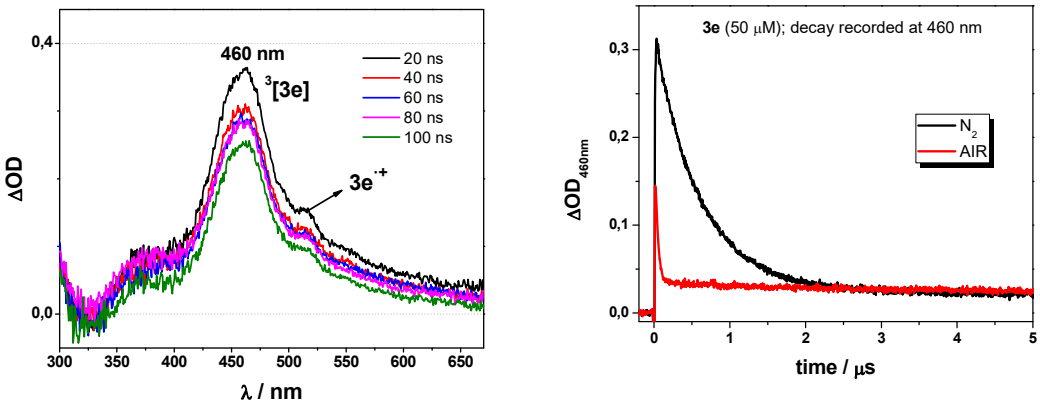

Supplementary Figure 5: a) Transient absorption spectra recorded at different times after the laser pulse of **3e** (50 μM) in CH_3CN; b) Decay at 460 nm of **3e** (50 mM) under N_2 (black) and under air (red).

Laser flash photolysis (λ_{exc} = 355 nm) of a solution containing **3e** (50 μM) and **1a** (70 mM) revealed the formation of two new absorption bands at 360 nm and 490 nm corresponding, as in the previous case, to the formation of the radical intermediate **I** (**INT I**) and the carbocation **II** (**INT II**) (see Supplementary Figure 6a).[32]

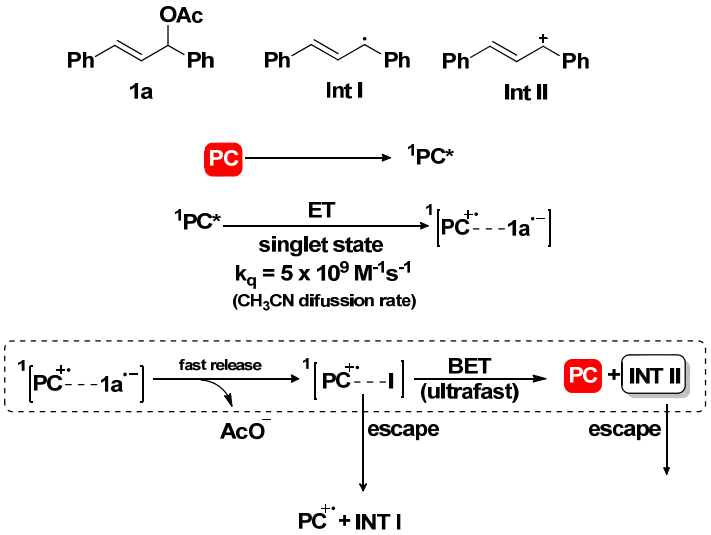

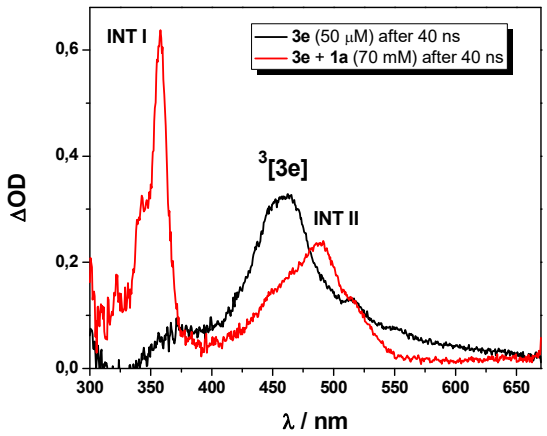

Supplementary Figure 6. Transient absorption spectra recorded 40 ns after the laser pulse (λ_{exc} = 355 nm, MeCN/Ar) of **3e** (50 μM) without **1a** (black) and with **1a** (70 mM, red).

As in the reaction with photocatalyst **3g** (Supplementary Figure 7), in the presence of pyrrole **2a** (37 mM) or *p*-toluidine **8b** (40 mM), the transient absorption spectrum shows disappearance of the peak at 490 nm while the band at 360 nm is not affected, confirming that the reactive intermediate is the carbocation intermediate **II** (**INT II**).

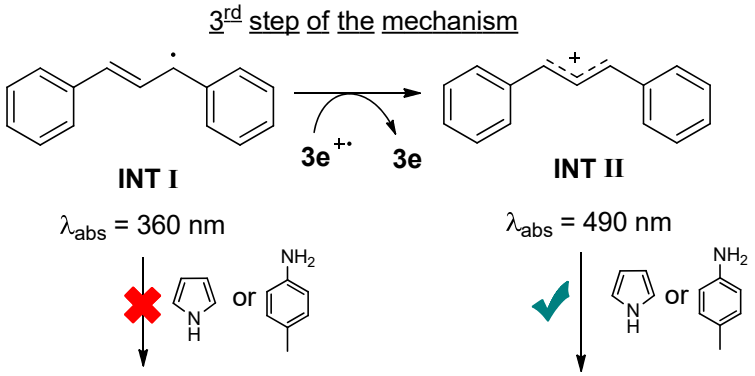

a) Reaction with pyrrole **2a**

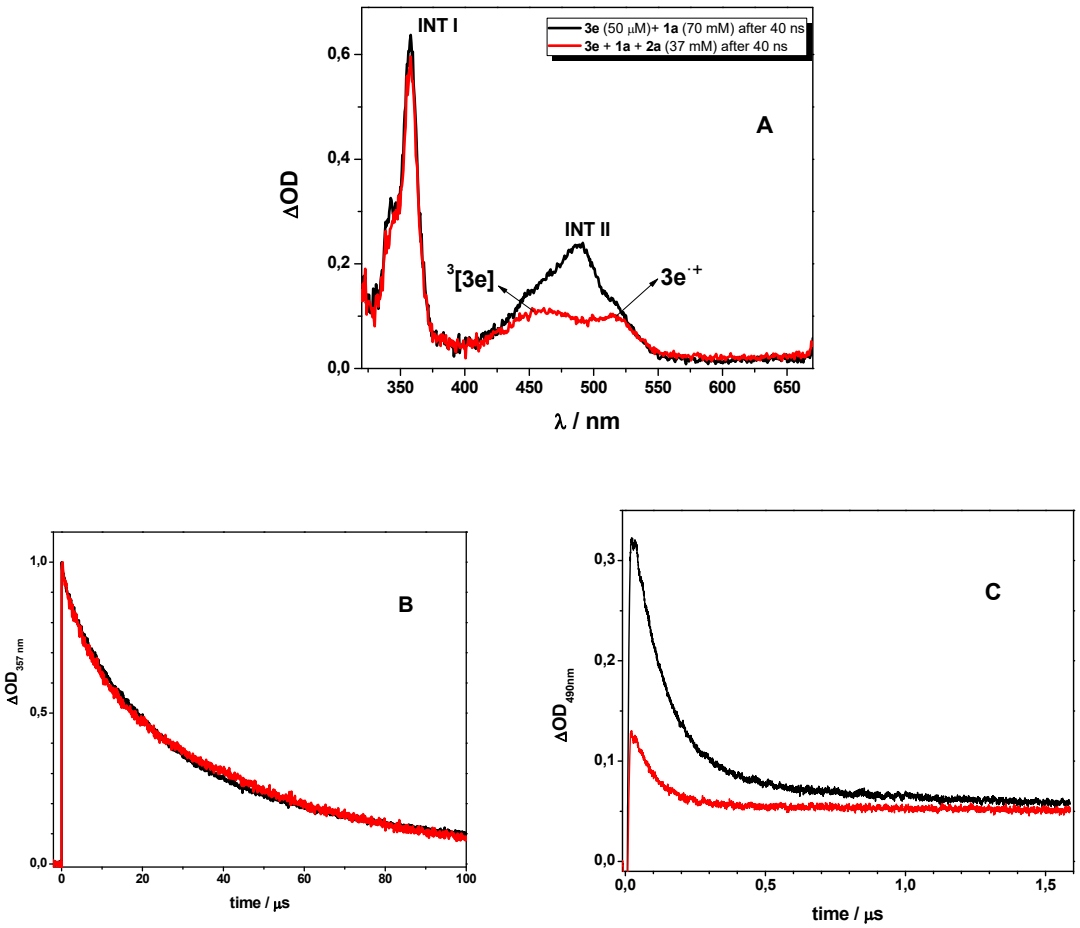

b) Reaction with *p*-toluidine **8b**

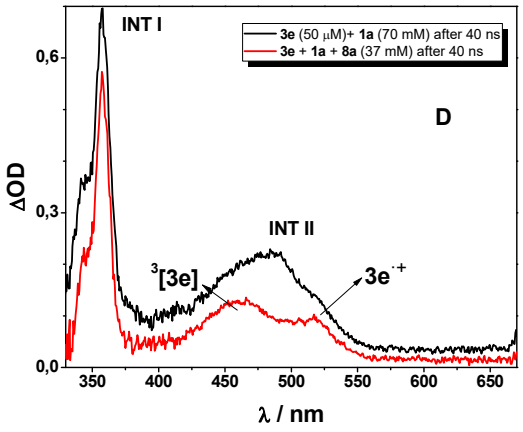

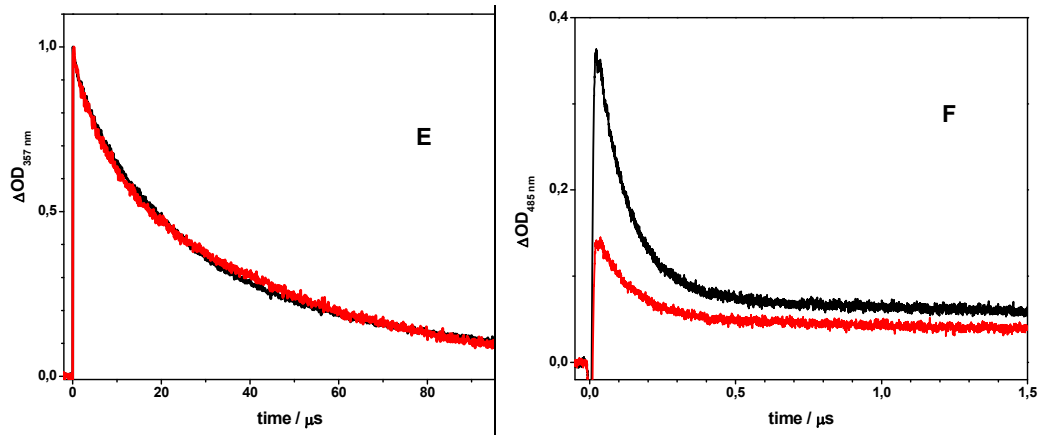

Supplementary Figure 7. a) LFP of the quenching with pyrrole **2a**: A: Transient absorption spectra recorded 40 ns after the laser pulse (λ_{exc} = 355 nm, MeCN/Ar) of **3e** (50 μM) with 70 mM of **1a** (black), and in the presence of **2a** (40 m M) (red). B: Decay at 357 nm of **3e** (50 mM) and **1a** (70 mM) (black) and in the presence of **2a** (37 mM) (red). C: Decay at 490 nm of **3e** (50 mM) and **1a** (70 mM) (black) and in the presence of **2a** (37 mM) (red); b) LFP of the quenching with *p*-toluidine **8b**: D: Transient absorption spectra recorded 40 ns after the laser pulse (λ_{exc} = 355 nm, MeCN/Ar) of **3e** (50 μM) with 70 mM of **1a** (black), and in the presence of **8b** (37 mM) (red). E: Decay at 357 nm of **3e** (50 mM) and **1a** (70 mM) (black) and in the presence of **8b** (37 mM) (red). F: Decay at 490 nm of **3e** (50 mM) and **1a** (70 mM) (black) and in the presence of **8b** (37 mM) (red).

Supplementary Notes 3:

Absorption spectrum of 1a, 3e and 3g:

The absorption spectrum of a solution of the different compounds in CH_3CN was measured using a quartz cuvette with 1 cm of optical pathway.

a) b)

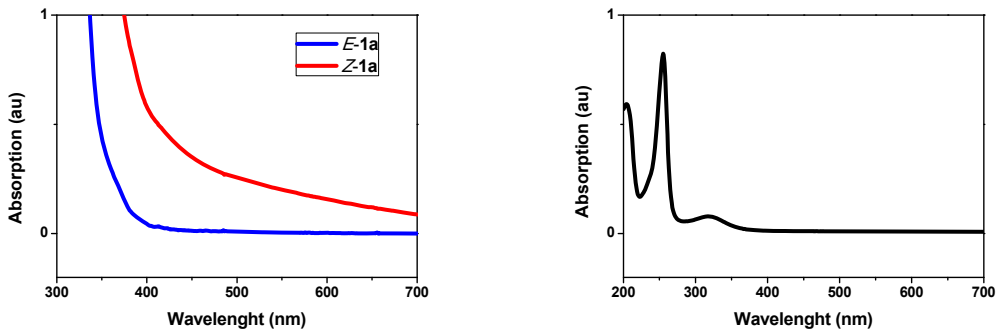

c)

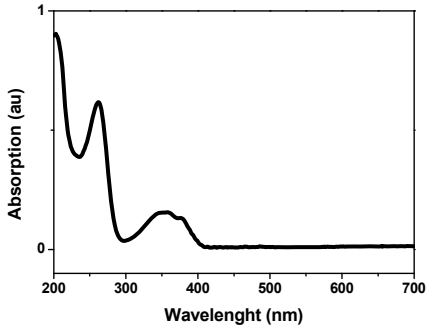

d)

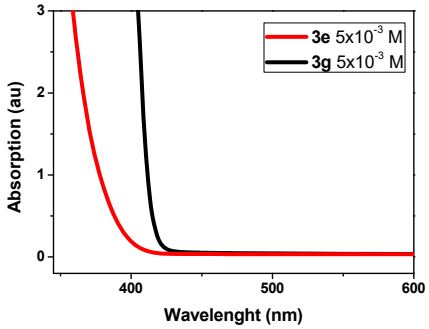

Supplementary Figure 8. a) Absorption spectrum of a 0.1 M solution of ***E*-1a** (blue line) and ***Z*-1a** (red line) in acetonitrile; b) Absorption spectrum of a 0.17 mM solution of **3e** in acetonitrile; c) Absorption spectrum of 0.1 mM solution of **3g** in acetonitrile; d) Absorption spectrum of **3e** and **3g** at the concentration of the reaction (5 mM) in acetonitrile.

Fluorescence quenching studies:

For the steady-state and time resolved fluorescence quenching studies with photocatalyst **3g**, increasing concentrations of quencher were added to a solution 100 μM of **3g** in CH_3CN under N_2 atmosphere (λ_{exc} = 372 nm).

a)

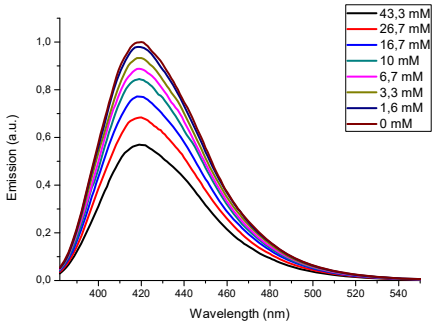

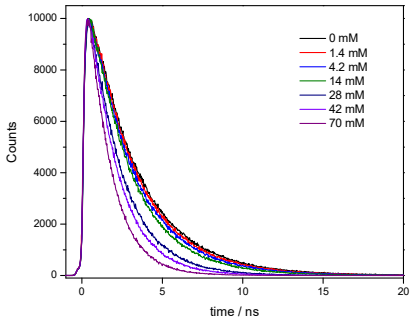

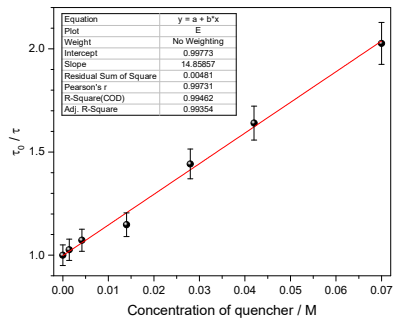

k_q **(S_1) = 4.7 x 10^9 M^{-1}s^{-1}**

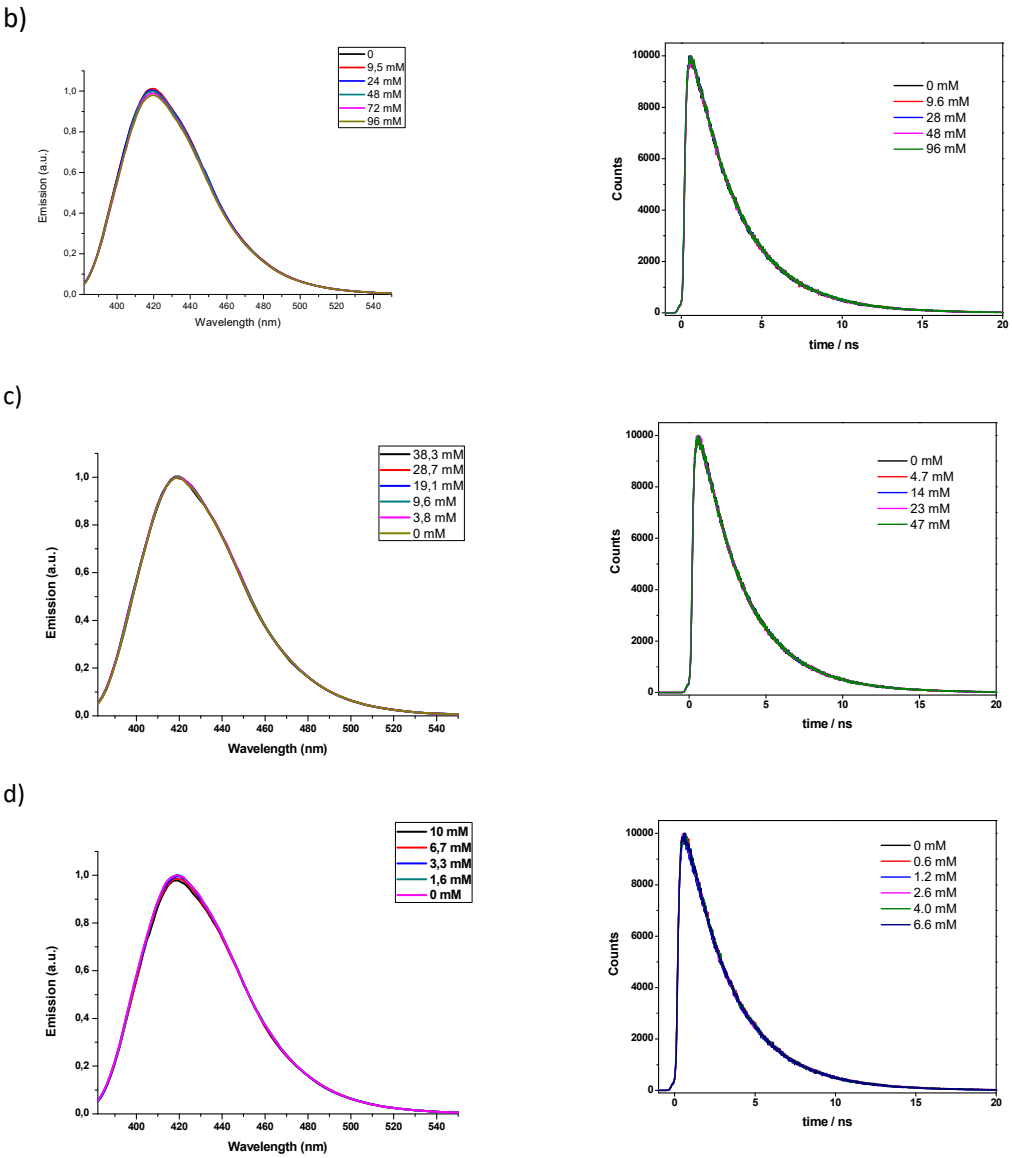

Supplementary Figure 9. Steady-state and time resolved fluorescence quenching of **3g** with increasing concentrations of a) ***E*-1a**, Stern-Volmer plot to obtain $k_q(S_1)$; b) **2a**; c) DIPA, d) *p*-Toluidine

For the steady-state fluorescence quenching studies with photocatalyst **3e** increasing concentrations of quencher were added (up to 5 x 10^{-4} M) to a solution of **3e** in CH_3CN with absorbance 0.1 at the excitation wavelength (λ_{exc} = 350 nm) under N_2 atmosphere.

a)

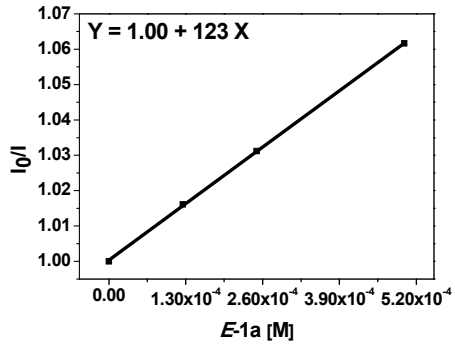

b)

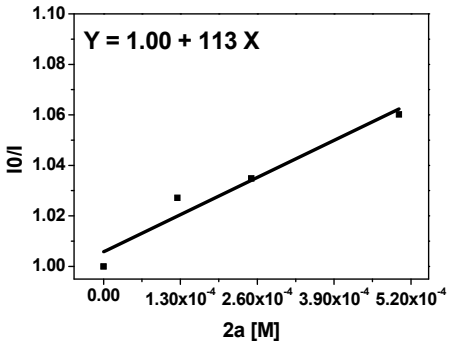

c)

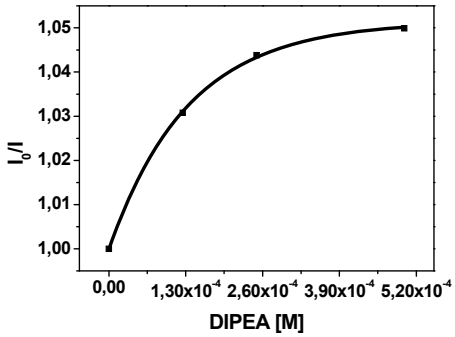

d)

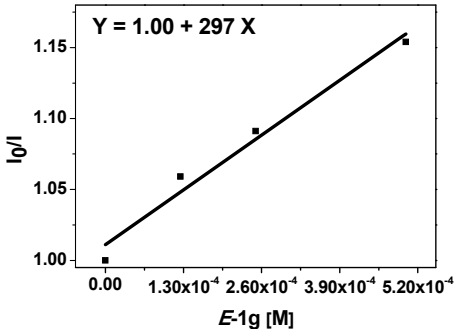

e)

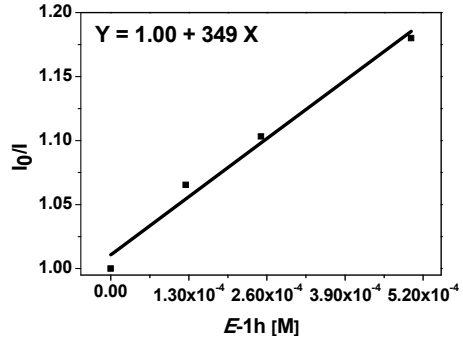

f)

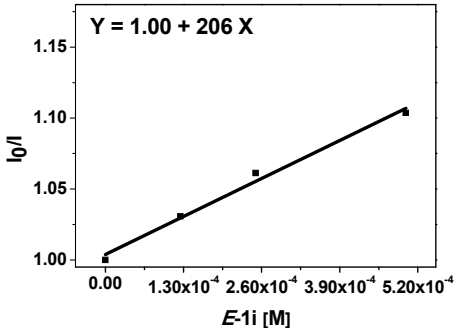

g)

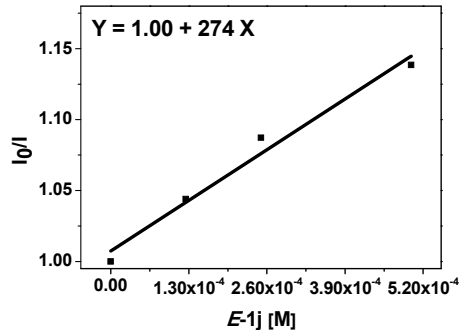

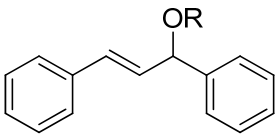

1f, R= COPh
1g, R= CO_2Et
1h, R= $CONMe_2$
1i, R= OH

Supplementary Figure 10. Stern-Volmer equations of the steady-state fluorescence quenching of **3e** with increasing concentrations of a) ***E*-1a**; b) **2a**; c) DIPEA; d) ***E*-1g**; e) ***E*-1h**; f) ***E*-1i**; g) ***E*-1j**.

Excited state energy of 3e and 3g:

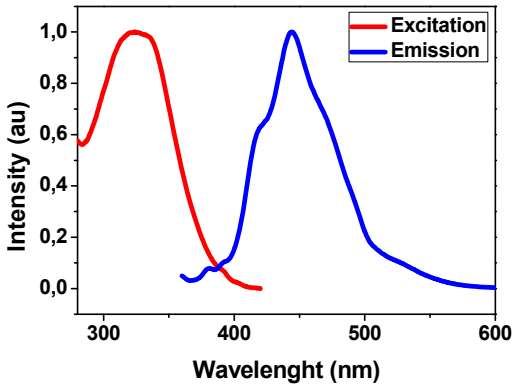

Supplementary Figure 11. Normalized emission and excitation spectrum of **3e**.

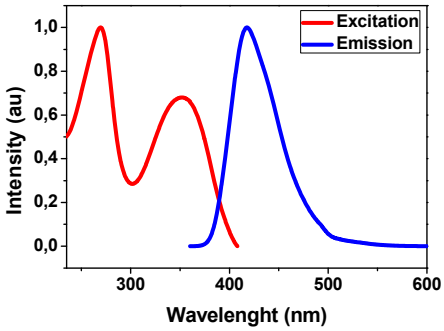

Supplementary Figure 12. Normalized emission and excitation spectrum of **3g**.

The singlet excited state energy of the photocatalysts [$E_{0\text{-}0}$(**3*/3**)] were calculated from the intersection between the emission and excitation spectrum applying the Supplementary Equation 1:

$$E = N * \frac{h\,c}{\lambda} = 6.022 * 10^{23} mol^{-1}\ \frac{6.63{\cdot}10^{-34} J{\cdot}s{*}3{\cdot}10^{8}(m/s)}{\lambda\,(m)}$$

Supplementary Equation 1

$E_{0\text{-}0}$ S_1(**3e*/3e**) = 73.7 Kcal/mol = 3.19 eV

$E_{0\text{-}0}$ S_1(**3g*/3g**) = 73.5 Kcal/mol = 3.18 eV

The triplet excited state energy of the photocatalysts [$E_{0\text{-}0}$(**3*/3**)] were obtained by DFT calculations (see section 13.3)

$E_{0\text{-}0}$ T_3(**3***/**3**) = -2.8 eV

Supplementary Notes 4.

Cyclic Voltametry

CV measurements were carried out under argon atmosphere. The measurement were performed in MeCN containing 0.1 M tetra *n*-butylammonium tetrafluoroborate. A glassy carbon electrode (working electrode), platinum wire counter electrode, and Ag/AgCl reference electrode was employed for the CV measurement. The scan rate was 50 mV/s, a step potential of 5.0 mV was applied.

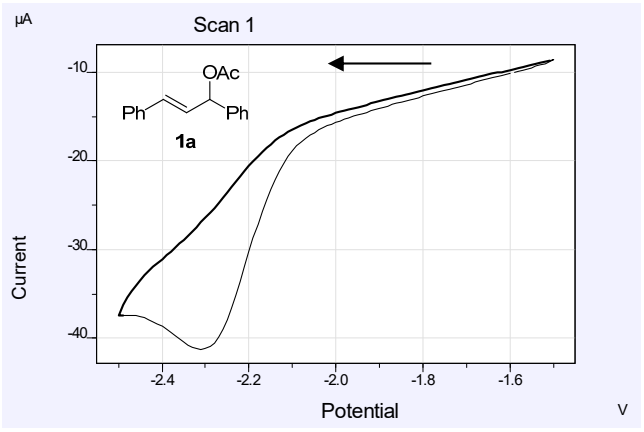

Supplementary Figure 13. Cyclic voltammetry of **1a**, E (**1a**/**1a**$^{\bullet-}$) = - 2.35 eV vs SCE.

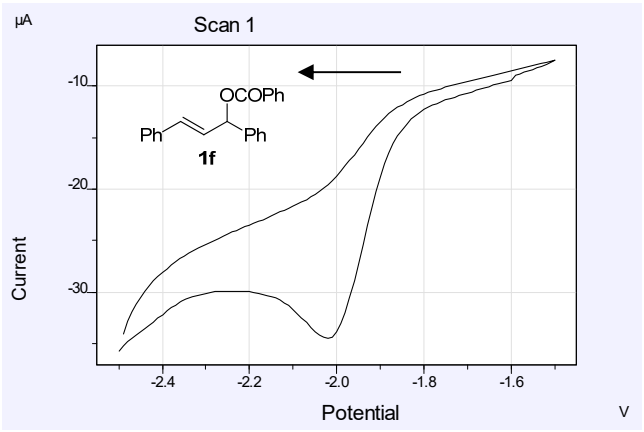

Supplementary Figure 14. Cyclic voltammetry of **1f**, E (**1f**/**1f**$^{\bullet-}$) = - 2.06 eV vs SCE.

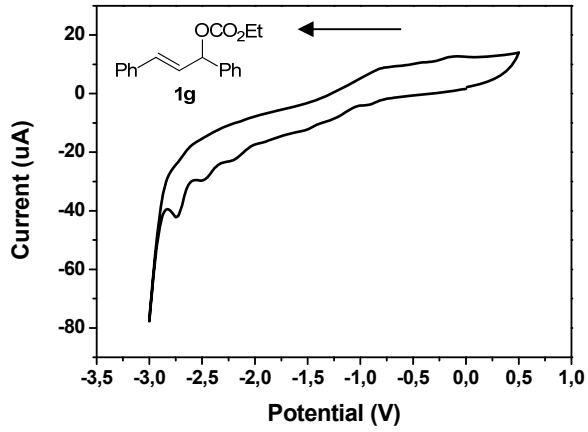

Supplementary Figure 15. Cyclic voltammetry of **1g**, E (**1g**/**1g**$^{\bullet-}$) = - 2.27 eV vs SCE.

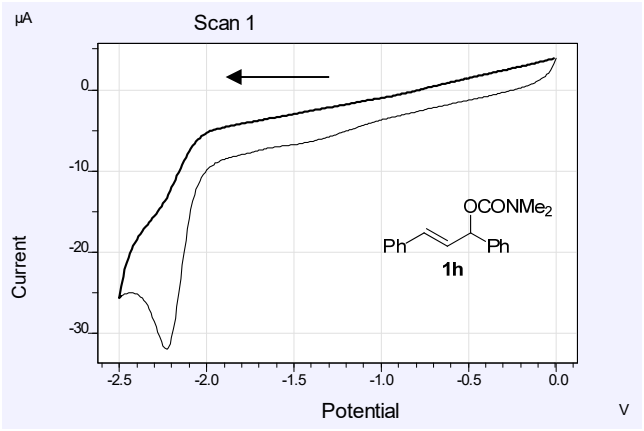

Supplementary Figure 16. Cyclic voltammetry of **1h**, E (**1h**/**1h**$^{\bullet-}$) = - 2.27 eV vs SCE.

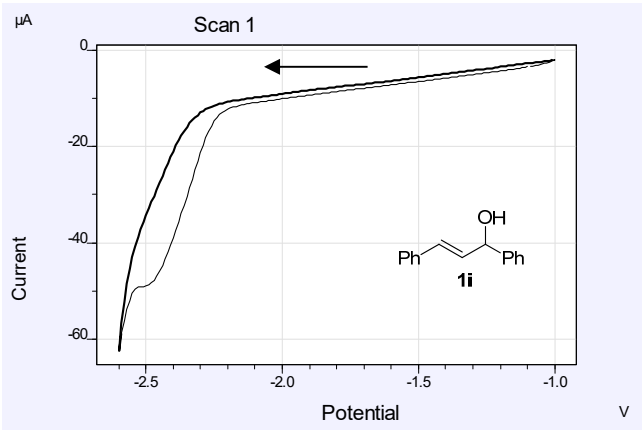

Supplementary Figure 17. Cyclic voltammetry of **1i**, E (**1i**/**1i**$^{\bullet-}$) = - 2.52 eV vs SCE.

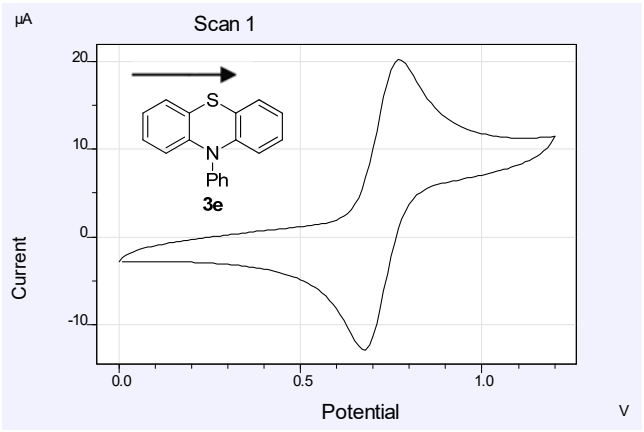

Supplementary Figure 18. Cyclic voltammetry of **3e**, E (**3e**$^{\bullet+}$/**3e**) = 0.68 eV vs SCE.

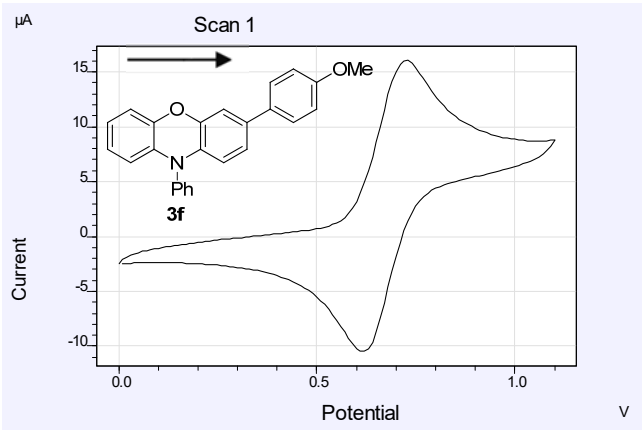

Supplementary Figure 19. Cyclic voltammetry of **3g**, E (**3g**$^{\bullet+}$/**3g**) = 0.63 eV vs SCE.

Determination of the reduction redox potential of the excited photocatalyst (E*red) and Rhem-Weller equation:

The reduction redox potential of the excited photocatalyst (**3e** and **3g**) was subsequently determined. Indeed, knowing the electrochemical oxidation peak potential and estimating spectroscopically the excited state energy of them [$E_{0\text{-}0}$(**3***/**3**)] from the intersection between the emission and excitation spectrum, the value of E^{*}red(**3**) = E(**3**$^{\bullet+}$/**3***) can be obtained from the Supplementary Equation 2.[34]

$$E(\mathbf{3}^{\bullet+}/\mathbf{3}^{*}) = E(\mathbf{3}^{\bullet+}/\mathbf{3}) - E_{0\text{-}0}\,S_1(\mathbf{3}^{*}/\mathbf{3})$$

Supplementary Equation 2

E*red(**3e**$^{\bullet+}$/**3e***) = 0.68 – 3.19 = -2.51 V (vs SCE)

E*red(**3g**$^{\bullet+}$/**3g***) = 0.63 – 3.18 = -2.55 V (vs SCE)

To calculate the free Gibbs energy of the reaction the Rhem-Weller equation was used:

$$\Delta G^{o}_{et}(eV) = (E^{o}_{red}(PC^{*}/PC^{\cdot -}) - E^{o}_{red}(D^{\cdot +}/D))$$

Supplementary Equation 3

$\Delta G_{\mathbf{1a/3e}}$ = -2.51 – (-2.35) = -0.16 eV = -3.6 Kcal/mol

$\Delta G_{\mathbf{1a/3g}}$ = -2.55 – (-2.35) = -0.2 eV = -4.6 Kcal/mol

The free Gibbs energy for the SET form the triplet excited state of **3** was also calculated:

$E_{0\text{-}0}\, T_3$(**3***/**3**) = -2.8 eV

E*red T_3 (**3e**$^{\cdot +}$/**3e***) = 0.68 – 2.8 = -2.12 V (vs SCE)

$\Delta G_{\mathbf{1a/3}}$ = -2.12 – (-2.35) = 0.23 eV = 3.6 Kcal/mol

According to the Rhem-Weller equation, the SET from the triplet excited state is an unfavourable process.

Supplementary Notes 5.

Determination of the Quantum Yield

A solution of ferrioxalate was chosen as actinometer following the procedure described by the IUPAC (subcommittee on photochemistry).[35] The procedure is based on the decomposition under irradiation of ferric ions to ferrous ions which are complexed by 1,10-phenanthroline. This photochemical transformation has a known quantum yield and the complexation of Fe^{2+} with 1,10-phenanthroline can be monitored by UV-Visible absorption since its extinction coefficient at 510 nm is known (=11100 M^{-1} cm^{-1}). Therefore, the moles transformed can be related with the moles of photons absorbed by the Supplementary Equation 4.

$$\Phi = \frac{mol\ transformed}{photons\ absorbed}$$

Supplementary Equation 4

The complete procedure should be done under a red safe-light environment. At 420 nm ferroxilate has a Φ = 1.05.[36] 0.006, 0.012, or 0.15 M solutions of $K_3[Fe(C_2O_4)_3]$ $3H_2O$ can be used for actinometry. In this case, we chose a concentration of 0.15 M. The solutions were prepared and stored in a dark laboratory:

1. Potassium ferrioxalate solution (0.15 M): 368.4 mg of $K_3[Fe(C_2O_4)_3]$ $3H_2O$ (commercially available) and 26.6 μL of H_2SO_4 were added into a 5 mL volumetric flask and filled to the mark with Milli-Q water.

2. Phenanthroline solution (0.15 M): 1.35 g of 1,10-phenantroline monohydrate were added to 50 mL volumetric flask and filled to the mark with MilliQ water.

3. Buffer solution: 4.94 g of NaOAc and 1 mL of H_2SO_4 were added to 100 mL volumetric flask and filled to the mark with MilliQ water.

4. Model reaction solution: A vial equipped with a magnetic stir bar was charged with the corresponding allylic compound **1** (0.1 mmol), pyrrole (0.2 mmol), **3g** (1.7 mg, 5 mol%), DIPA (86 μL, 0.5 mmol) and acetronitrile (1 mL) and fitted with a teflon screw cap septum. The reaction was degassed with three freeze-pump-thaw cycles. The vial was then backfilled with N_2 and stirred under 420 nm LED irradiation (18.3396 W/m^2 intensity; approximate distance was 2 cm from the vial) at 20ºC.

Actinometry procedure: Due to the reactor setup (Supplementary Figure 20), the simultaneous irradiation of both the actinometer solution and model reaction is not feasible. However, the stability of the irradiation light was checked through radiometer measurements (from spectro-radiometer equipment Stellarnet model Blue-Wave UV-NB50). Therefore, we assumed that consecutive measurements of both actinometer and model reaction are comparable. In addition, using the same spectrometer, the LED source spectrum was measured, detecting a maximum wavelength of emission of 418 nm (Supplementary Figure 21).

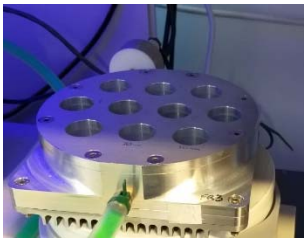

Supplementary Figure 20. LED setup of the reaction

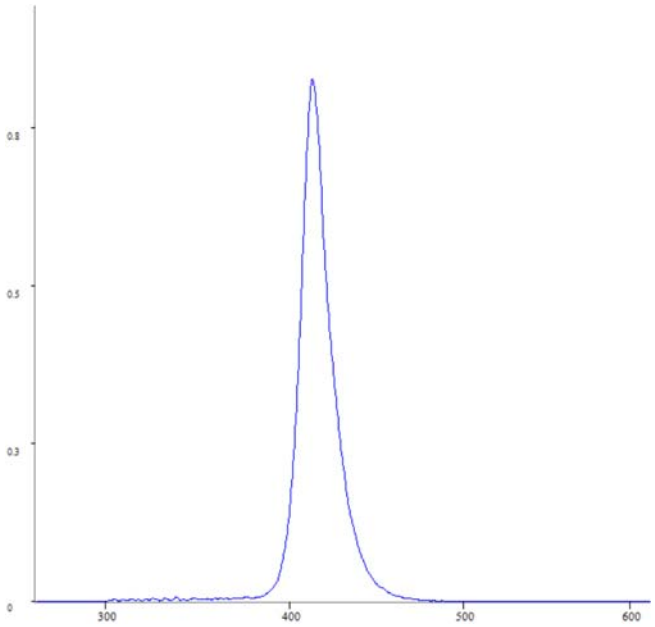

Supplementary Figure 21. Emission spectrum of the blue LED of the photochemical reactor (λ_{max}= 415 nm).

2 mL of potassium ferrioxalate solution (0.15 M) were introduced into the photoreactor under dark conditions while being stirred. Then, the LED was switched on. Every 10 s the light was switched off and a 0.1 mL aliquot was taken. To each aliquot, 2 mL of buffer solution and 0.5 mL of 1,10-phenanthroline 0.15 M were added and the final volume was raised to 10 mL with MilliQ water. Then 83 μL of this solution were diluted to 5 mL with MilliQ water. As a blank sample, a solution was prepared with 0.1 mL of potassium ferrioxalate solution (0.15 M) before irradiation, 2 mL of buffer solution and 0.5 mL of 1,10-phenanthroline 0.15 M in a 10 mL of volumetric flask filled with water until the mark, and 83 μL of this solution were diluted to 5 mL with MilliQ water. The absorbance spectrum of each sample was monitored at 510 nm. The absorbance to each time was related with the photochemically produced Fe^{2+} ions across the Lambert-Beer Law (Supplementary Equation 5), where V_1 is the irradiated volume (noting that the initial volume is 2 mL but it changes as the aliquots are taken); V_2 is the aliquot volume (0.1 mL), V_3 is the final volume after addition of 1,10-phenanthroline and buffer (10 mL). *b* is referred to the optical pathway (1 cm), ΔA (510 nm) is the difference in absorbance between the irradiated solution and the blank sample, ε (510 nm) is the extinction coefficient of the complex formed by Fe(II) and 1,10-phenanthroline (ca. 11100 M^{-1} cm^{-1}).

$$moles\ of\ Fe^{2+} = \frac{V_1 \cdot V_3 \cdot \Delta A_{(510\ nm)}}{10^3 \cdot V_2 \cdot b \cdot \varepsilon_{(510\ nm)}}$$

Supplementary Equation 5

The moles of Fe^{2+} formed (x) are plotted as a function of time (t) (Supplementary Figure 21).

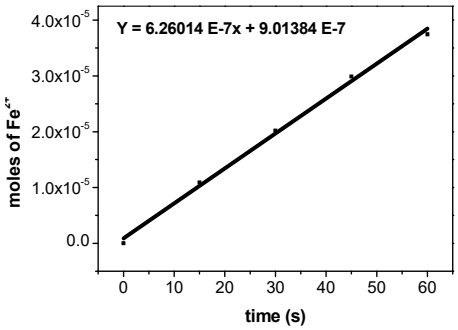

Supplementary Figure 22. Actinometer.

The slope of this line (*dx*/*dt*) was correlated to the moles of incident photons by unit of time ($q^0_{n,p}$) using the Supplementary Equation 6:

$$q^0_{n,p} = \frac{dx/dt}{\Phi_{(\lambda)} \cdot [1-10^{-A(\lambda)}]}$$

Supplementary Equation 6

Where $\Phi_{(\lambda)}$ is the quantum yield of the actinometer reaction at the irradiated wavelength, in this case being 1.05 at 420 nm for 0.15 M dilution[35] and $A_{(\lambda)}$ is the absorbance of the actinometer solution (ferrioxalate) at the irradiated wavelength (415 nm). The absorbance at 415 nm was measured with an Agilent 8453 UV-visible Spectroscopy System using a quartz cuvette with 1 cm of optical pathway.

Therefore, the moles of incident photons by unit of time ($q^0_{n,p}$) was determined as 5.96 10^{-7} einstein s^{-1}.

The kinetics of the reaction under study were done as follows: the photoreactor (blue LEDs) was switched on and the reaction mixture was stirred. At 60, 90, 120, 150, and 180 minutes an aliquot of 0.1 mL was taken from the reaction mixture under a positive flow of nitrogen, and diluted with 0.6 mL of $CDCl_3$. Thus, the conversion of the reaction at the different indicated time was determined by ^1H NMR. Knowing the initial molar concentration, the determination of the moles of photo-converted product is possible.

Plotting the moles of product versus the irradiation time, the slope *dx*/*dt* can be related with the quantum yield across the equation [4] being equal to time ($q^0_{n,p}$) $\Phi_{(\lambda)} \cdot [1\text{-}10\text{-}A_{(\lambda)}]$. Therefore, the quantum yield at the wavelength of irradiation Φ (420 nm) can be calculated once A (420 nm) is determined. To measure A (420 nm), a model reaction

solution was added to a 1 cm optical pathway cuvette and the UV-Visible spectrum was recorded obtaining an absorbance of 0.19288.

Therefore the quantum yield for the reaction is: Φ = 0.015 = 1.5 %.

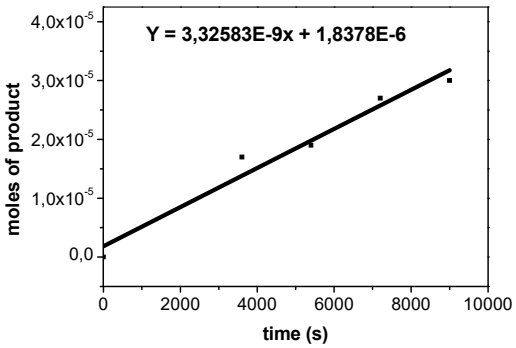

Supplementary Figure 23. Kinetic of the reaction.

Supplementary Notes 6.

General methods for DFT calculations:

Quantum chemistry calculations were carried out using the density functional theory (DFT). In particular, geometry optimizations were performed using the M06-2X functional[37] in combination with the 6-311G**[38] basis set including acetonitrile (ε = 37.5) solvent effects with the solvation model density (SMD).[39] All optimizations were performed without any geometrical constraint and harmonic vibrational frequencies have been also evaluated at the same level of theory to characterize minima and transition states in the potential energy surface. Transition states have been connected to products by optimization of geometries slightly modified from the transition states. All the calculations were performed using the Gaussian09 program.[40]

Calculation of redox potentials $E_{(Pc^*/Pc^-)}$.:

Redox potentials from excited state are calculated considering the potential value in the ground state, measured by electrochemical methods, and the energy of the S^1 excited state experimentally determined as the crossing point between the emission and the excitation spectrum. However, the reduction of photocatalysts in the ground state occur out of the practical range measurable with our experimental system. Therefore, we

theoretically estimated the energetics of reduction of **3e** and **3g** in acetonitrile by considering the energy differences between the photocatalyst in the ground state and its reduced form. The absolute potentials, expressed in eV, are shown bellow.

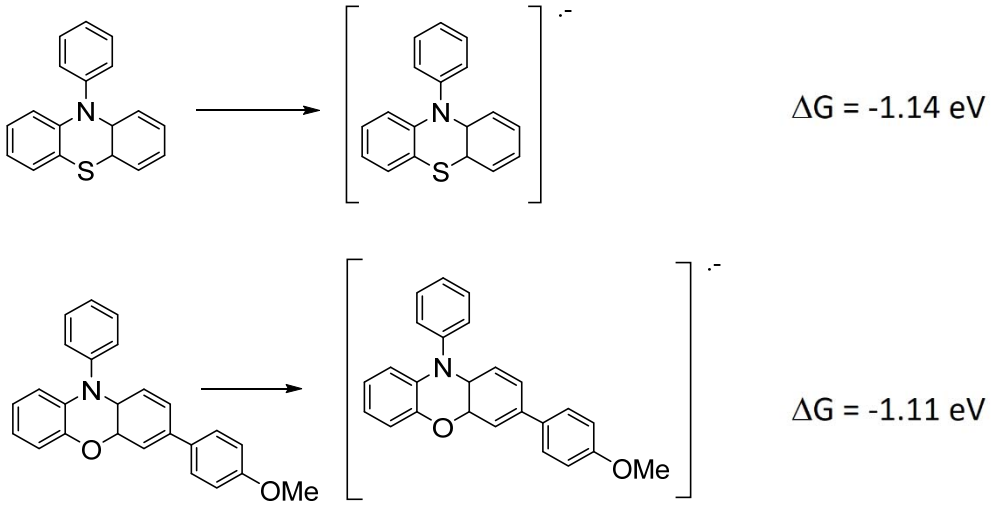

Supplementary Figure 24. Calculated redox potentials of **3e** and **3g**.

In order to convert the absolute potentials into values comparable to experimental results, we have to compare them with the known absolute potential of a common reference electrode. The IUPAC recommended absolute potential of NHE $E^{\ominus}(H^+/H_2)_{abs}$ value is 4.42 V.[41] Thus, redox potential for the reduction of **3e** and **3g** NHE are -3.28 V and -3.31V respectively. Considering that Saturated Calomel Electrode has a potential of +0.244 V vs NHE the values of reduction potentials of our photocatalysts vs SCE are: -3.52 V for **3e** and -3.55 V for **3g**. Effectively, such values are too negative and definitely should fall out of the measurable range in acetonitrile solution. Estimation of redox potential from excited state arise from consideration of the energy found for S_1. Such value is estimated to be 3.2 eV (see above), and therefore, the $E_{(Pc^*/Pc^-)}$ are found to be approximately -0.3 V vs SCE for both **3e** and **3g**.

Theoretical evaluation of the triplet excited state of 3e, 3g and 1a, and SOMO orbital of 1a.

The energy of the triplet excited state of **3e**, **3g** (Supplementary Figure 25A), *E*-**1a** and *Z*-**1a** (Supplementary Figure 25B) were calculated. According to the energies obtained, photosensitization of *E*-**1a** by both photocatalyst is feasible, while photosensitization of *Z*-**1a** cannot take place. Attending to the geometries of the excited states, the triplet excited state of *E*-**1a** presents an intermediate conformation between the *E*- and the *Z*-

isomer, and after relaxation its affords either the *E*- or the *Z*-**1a** in the ground state. However, the conformation of the *Z*-**1a** triplet excited state a does not change significantly compared to the ground state, therefore after relaxation its affords *Z*-**1a** exclusively. Therefore, under UV-light irradiation, there is an accumulation of the *Z*-**1a** isomer that cannot isomerize to the *E* isomer, and can only undergo the photoredox reaction.

Moreover, theoretical calculations show that the SOMO orbital either in the *E* or in the *Z* allylic acetate is centered in the double bond and the phenyl ring (Supplementary Figure 25C), confirming that the injection takes place in this part of the molecule. Here we attach the images to clear out the explanation.

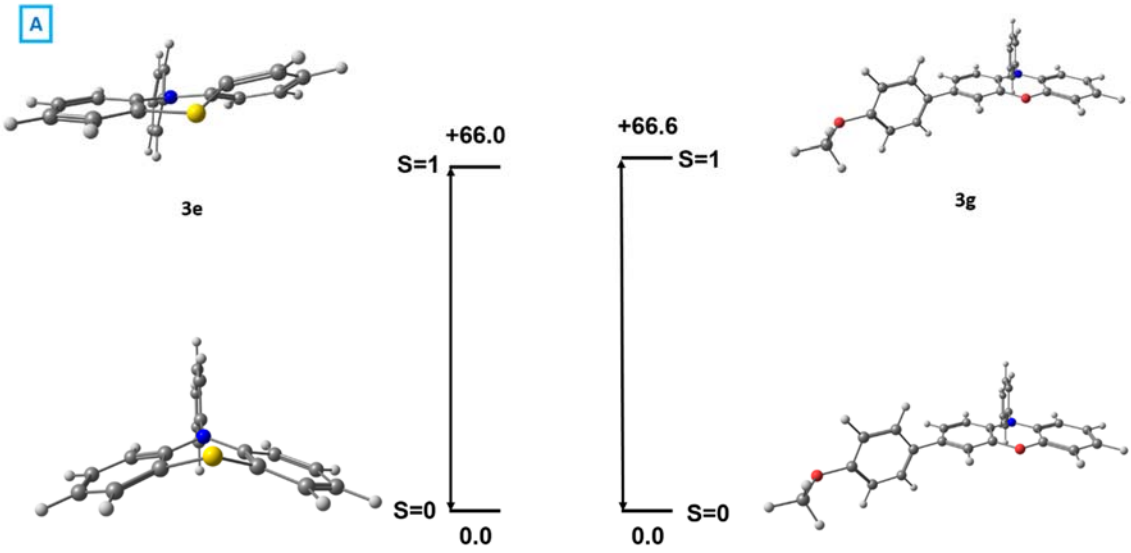

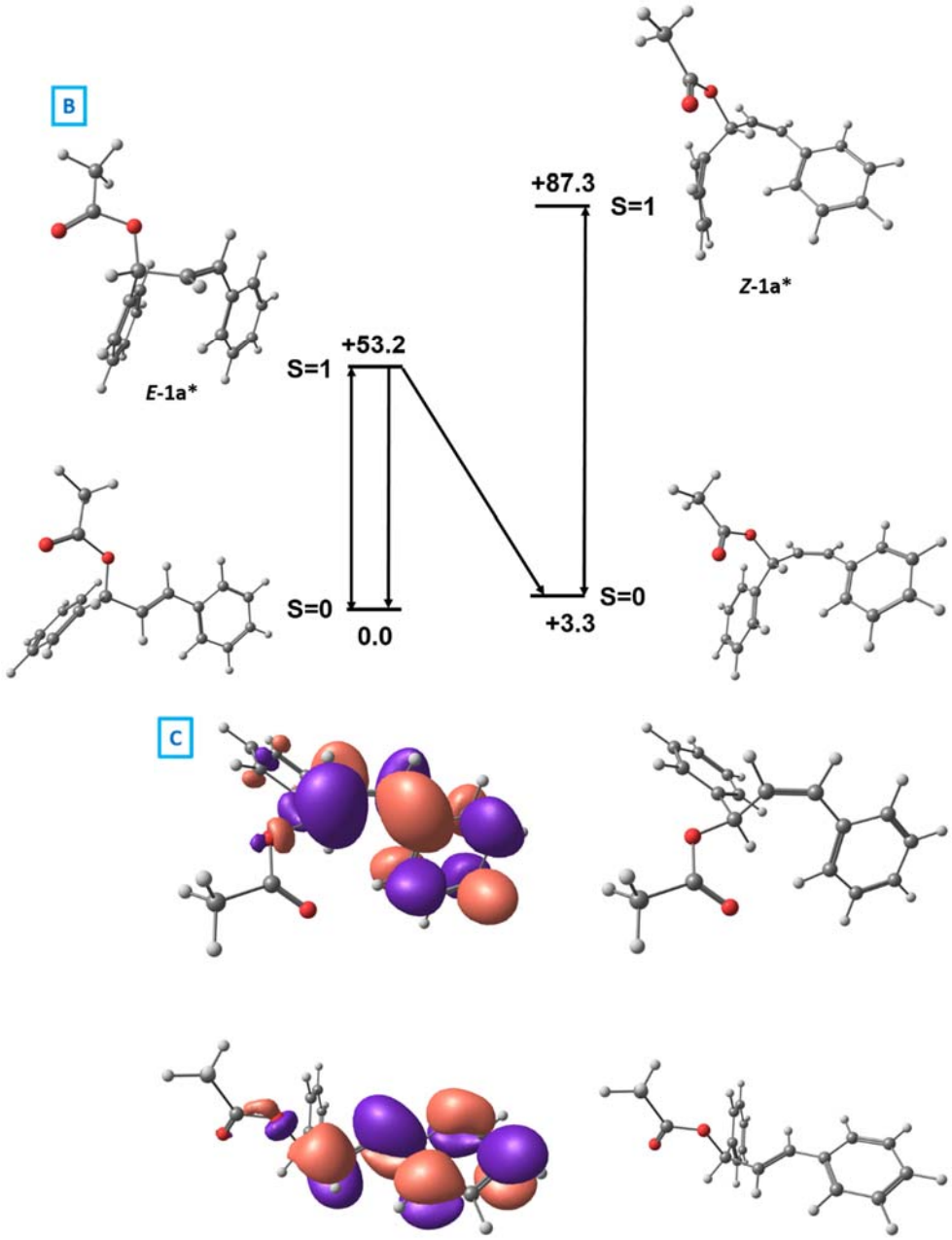

Supplementary Figure 25. A) Thermodynamic assesment of singlet-triplet gaps for both photocatalysts; B) Thermodynamic assesment of singlet-triplet gaps for Z and E substrates (energies in Kcal/mol); C) SOMO orbital in *E*-**1a** and *Z*-**1a.**

Theoretical evaluation of scission of acetate from anion radical generated from reduction of olefin 1a:

According experimental evidences, the photocatalyst undergoes a single electron transfer to **1a**, to afford the corresponding anion radical intermediate. According to theoretical results, such species evolves very fast through C-O bond scission to from the allyl radical and acetate anion. The very shallow kinetic barrier found ($\Delta G^{\ddagger}$ = 1.4 kcal/mol)

and the considerable thermodynamic driving force observed (ΔG = -22 kcal/mol), suggest that such process is, in practice, concerted to electron transfer process and a very important driving force that trigger the whole photocatalytic transformation.

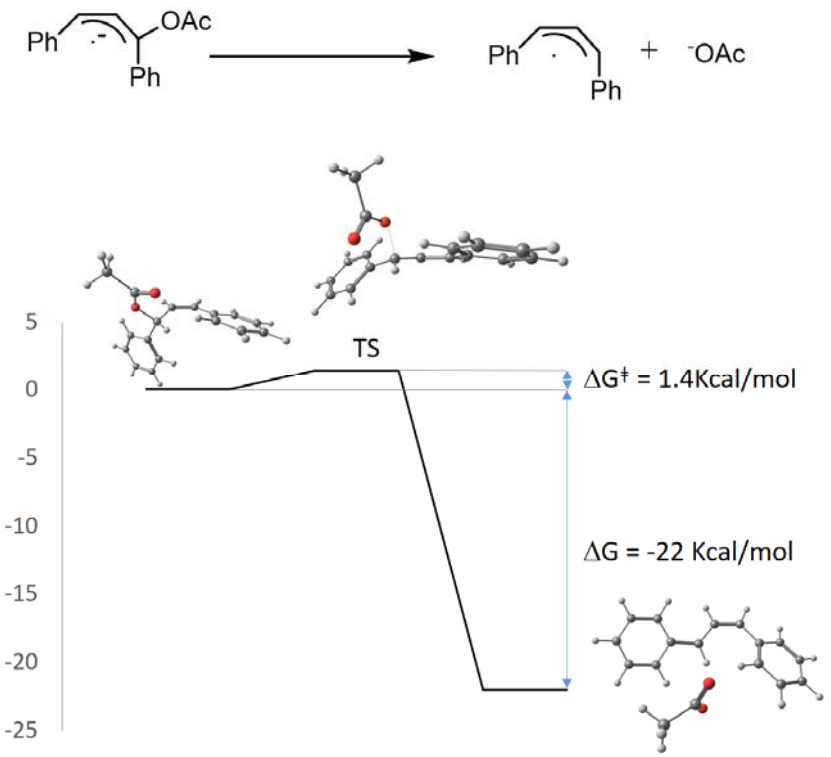

Supplementary Figure 26. Energetic profile for the scission of acetate from anion radical generated from **1a** reduction.

Calculation of energetics of redox reaction between allyl radical and oxidized photocatalysts:

Once allyl radical is formed by the scission of acetate, carbocation formation is the key step of the proposed mechanism. In accordance with experimental evidences for carbocation generation shown in the manuscript, calculations support the formation of such intermediate. Indeed, according to theoretical results the oxidation of allyl radical (**I**) by the oxidized photocatalyst (**PC**$^{+\cdot}$), results in the regeneration of the catalyst (**PC**) and formation of carbocationic intermediate (**II**). Such electron transfer has been evaluated by calculation of the different species involved separately. The thermodynamic balance shows that such process is favorable by -8.7 kcal/mol, for **3e** and -6.7 kcal/mol for **3g**.

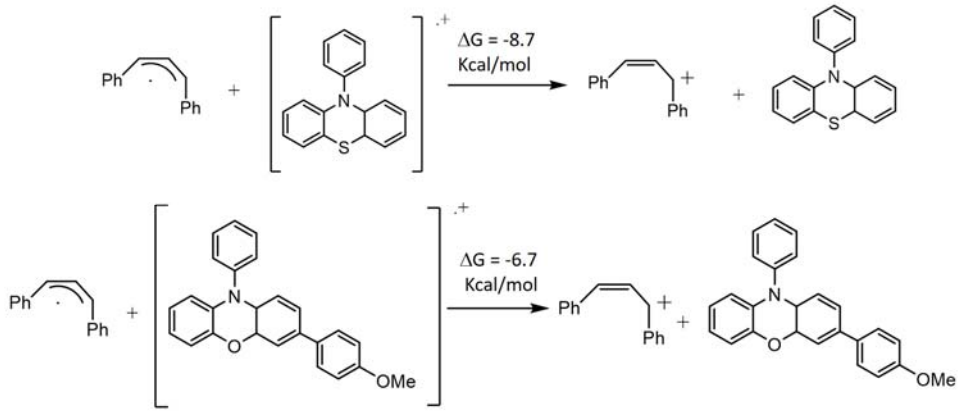

Supplementary Figure 27. Energetic profile for redox reaction between allyl radical and oxidized photocatalysts.

Theoretical evaluation of the isomerization of INT I and INT II:

In order to explain that the intermediate radical **I** or carbocation **II** can maintain its stereochemical information we have carried out additional calculations (Supplementary Figure 28). Although the energetic barriers are not very high (10.2-15.5 kcal/mol), they are significantly higher than the activation energy of the nucleophilic attack to the carbocation (4-5 kcal/mol). In addition, the ultrafast conversion of INT I at the sub-nanosecond scale to the carbocation via back electron transfer discards the isomerization of the radical intermediate. Therefore, the isomerization of these intermediates can be discarded.

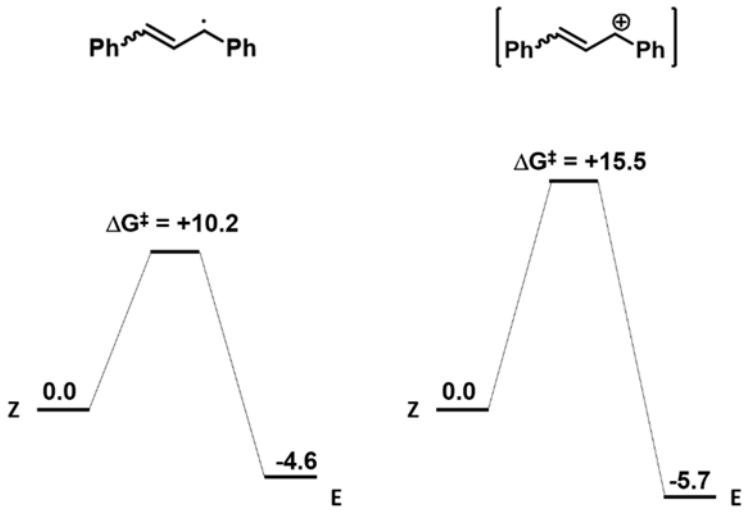

Supplementary Figure 28. Energetic profile for the isomerization of **INT I** and **INT II**.

Theoretical evaluation of reaction between carbocation and pyrrole:

Once the formation of a common carbocation intermediate is achieved, a Friedel-Crafts reaction between the carbocation and pyrrole takes place. Theoretical calculations

allowed to evaluate the thermodynamics and kinetics of such process. The first required step is the approaching of the reactants to generate an initial Van der Waals complex. The energetic difference between the initial complex and reactants calculated separately allows an estimation of the entropic cost of such approaching. In that case value of this cost is around 6 kcal/mol. From this initial complex, the system only has to overcome a barrier of 3.8 kcal/mol to produce the protonated intermediate **III**, that lays 14 kcal/mol below the reactants forming the initial Van der Waals complex. Thus, reaction between carbocation and pyrrole is a very favourable process from both thermodynamic and kinetic points of view.

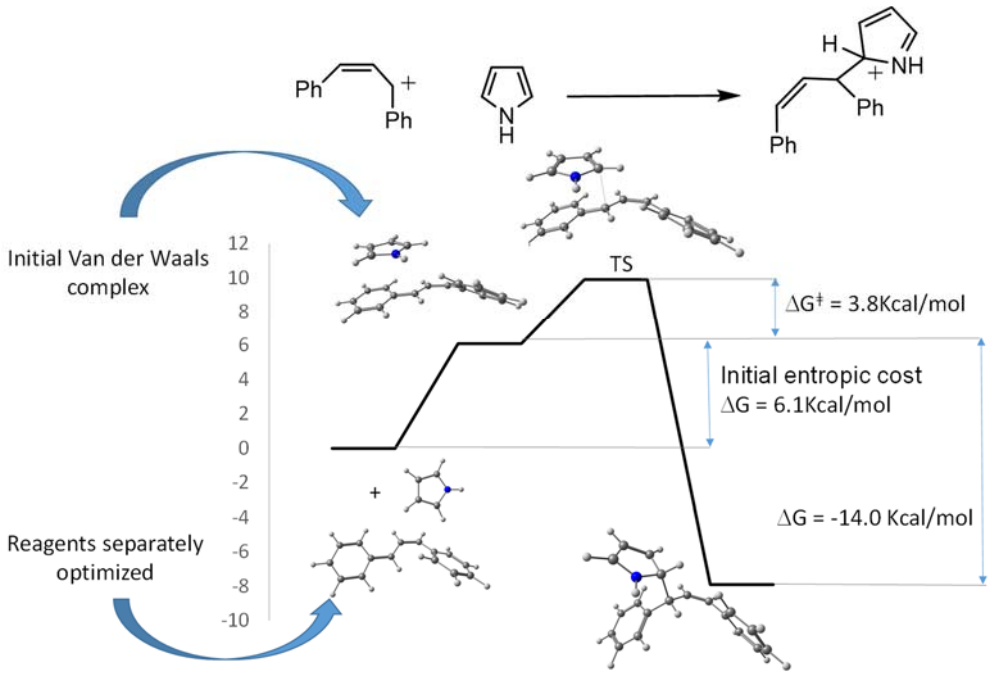

Supplementary Figure 29. Energetic profile for reaction between carbocation and pyrrole.

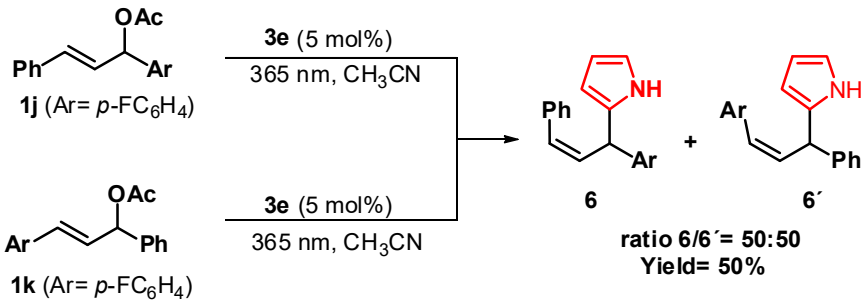

Supplementary Figure 30. The reaction of the two non-symmetric allylic derivatives bearing different aryl groups (**1j, 1k**) afforded the same equimolecular mixture of

products **6** and **6'** revealing that the reaction takes place through a common intermediate.,

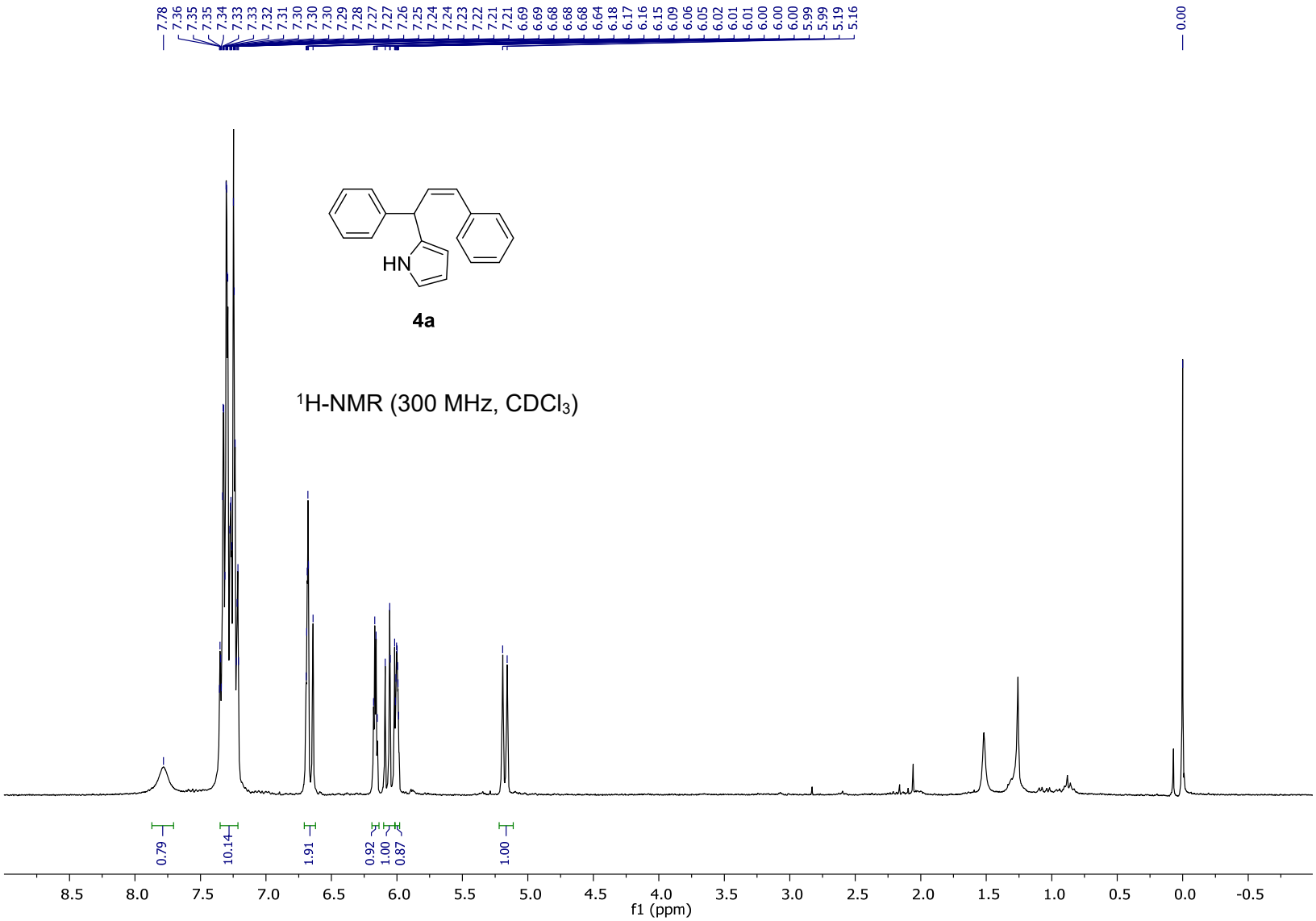

Supplementary Figure 46. ^{1}H-NMR spectra for compound **4a**

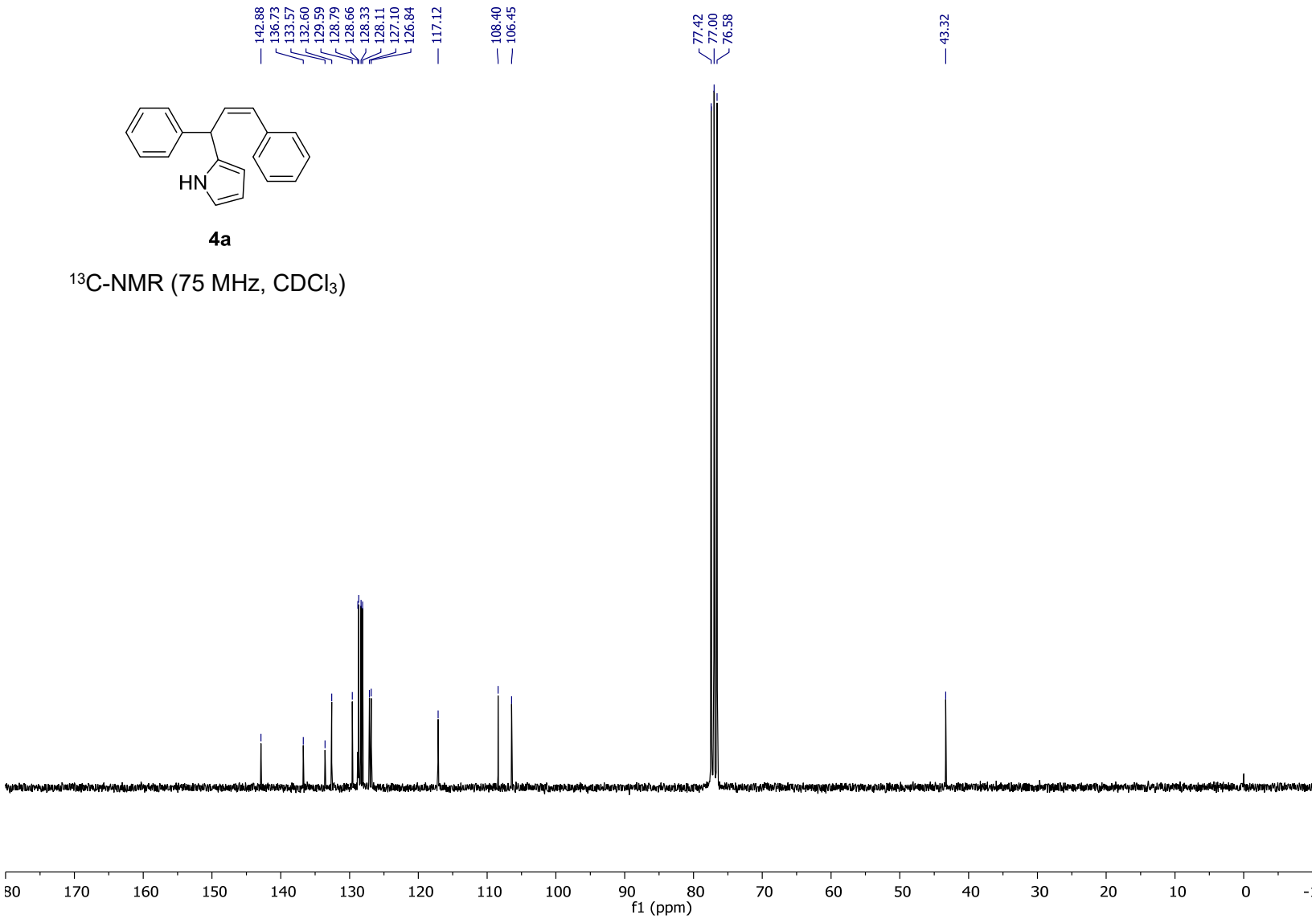

Supplementary Figure 47. ^{13}C-NMR spectra for compound **4a**

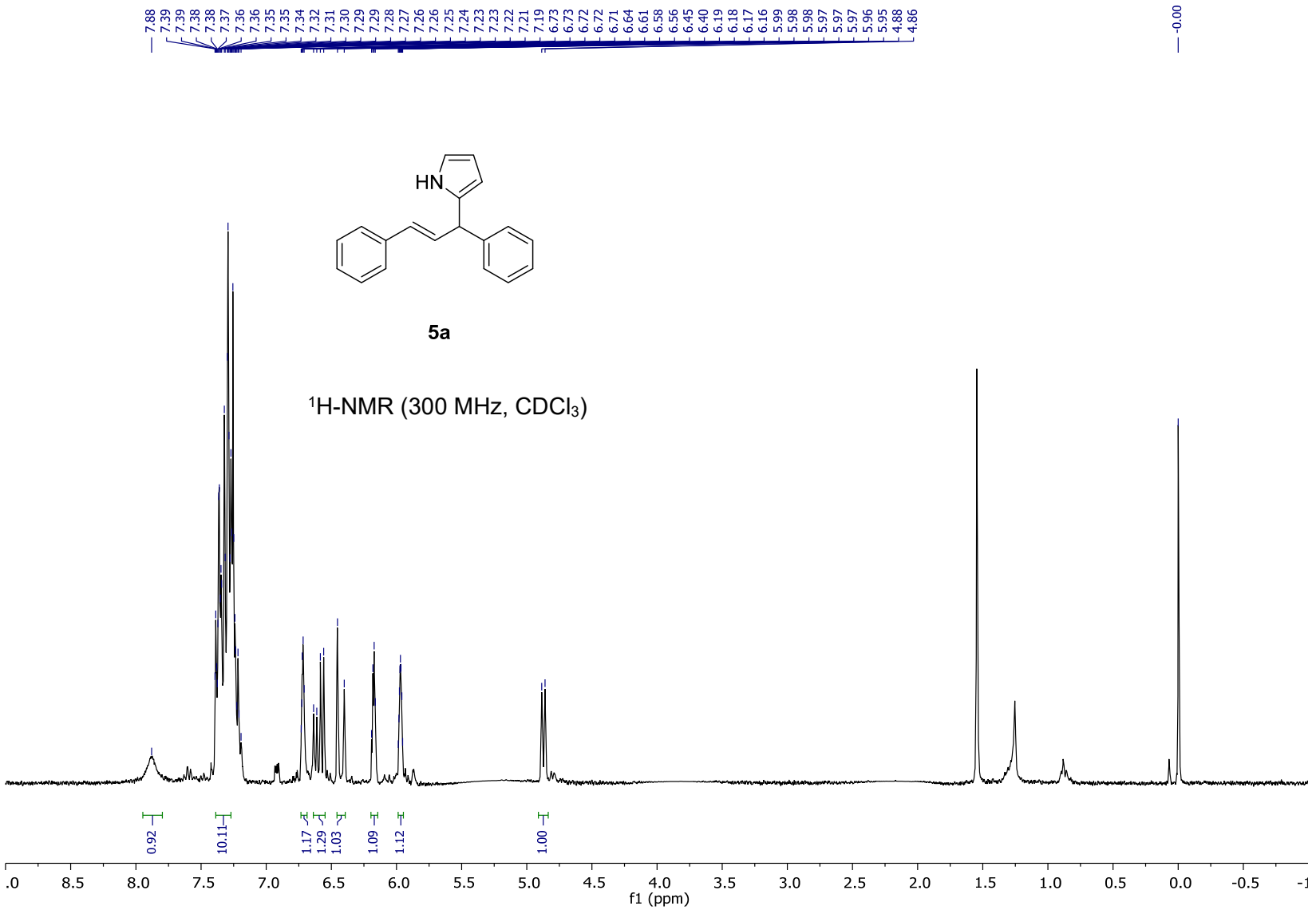

Supplementary Figure 84. ^{1}H-NMR spectra for compound **5a**

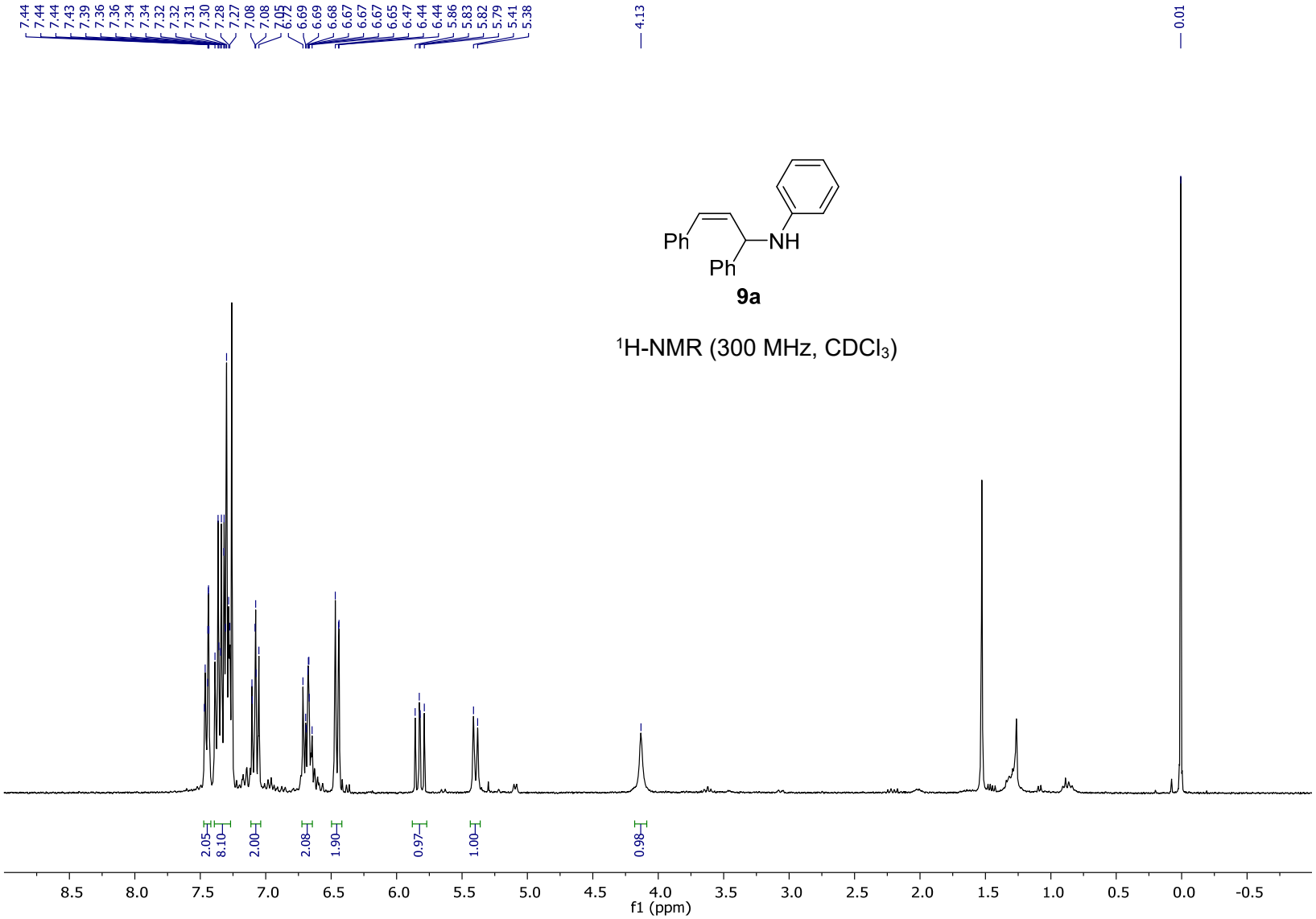

Supplementary Figure 104. ^{1}H-NMR spectra for compound **9a**

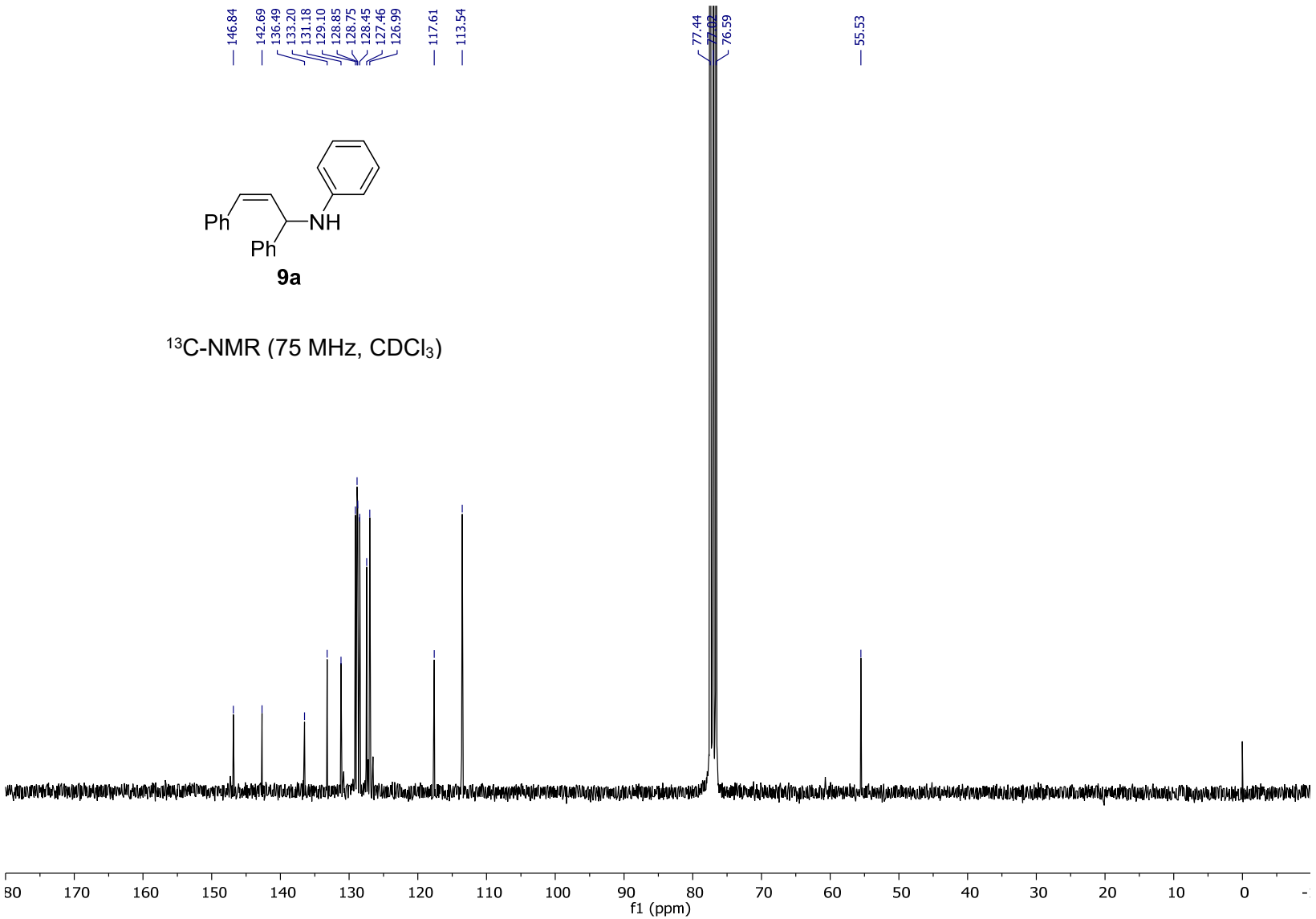

Supplementary Figure 105. ^{13}C-NMR spectra for compound **9a**

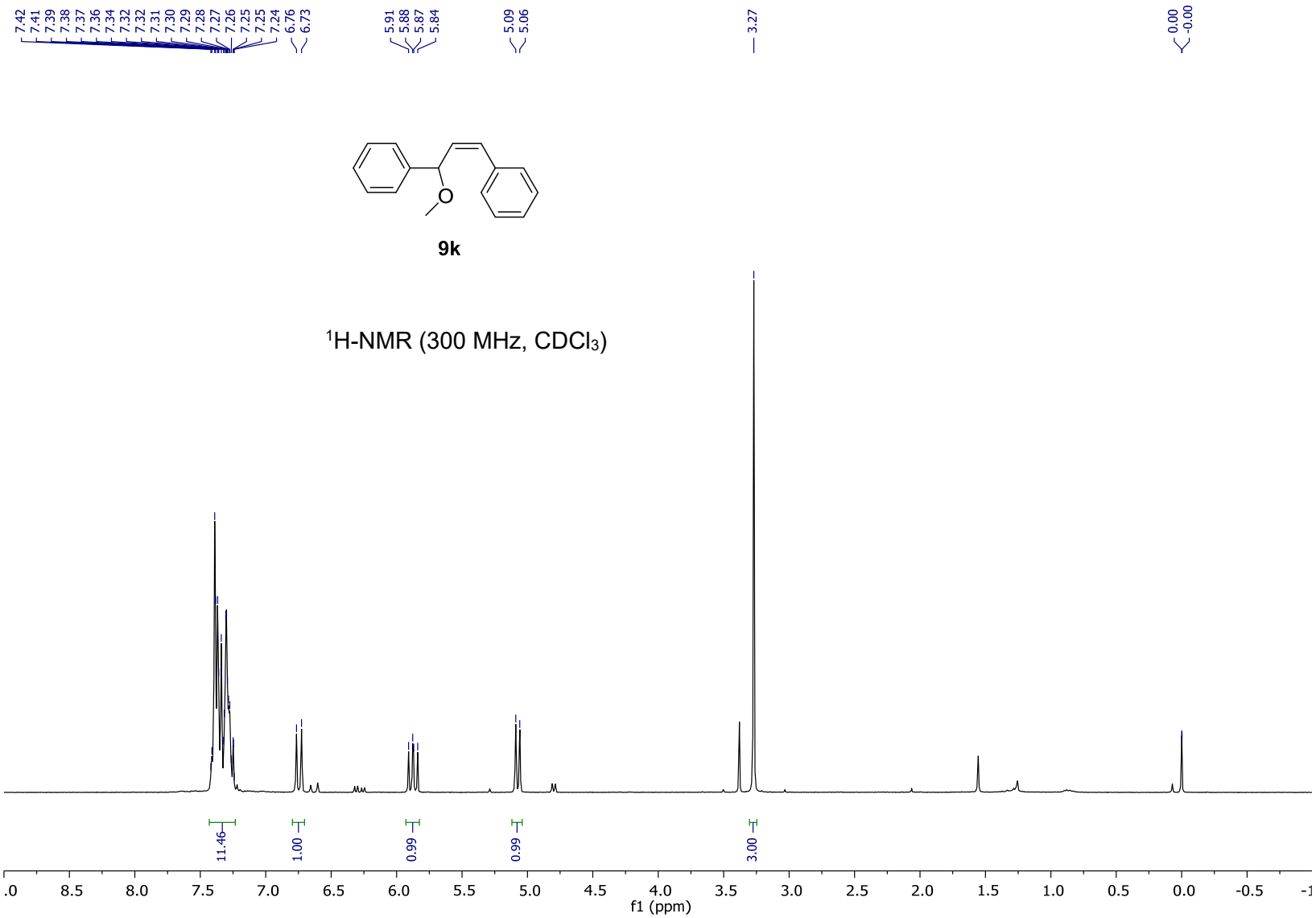

Supplementary Figure 123. ^{1}H-NMR spectra for compound **9k**

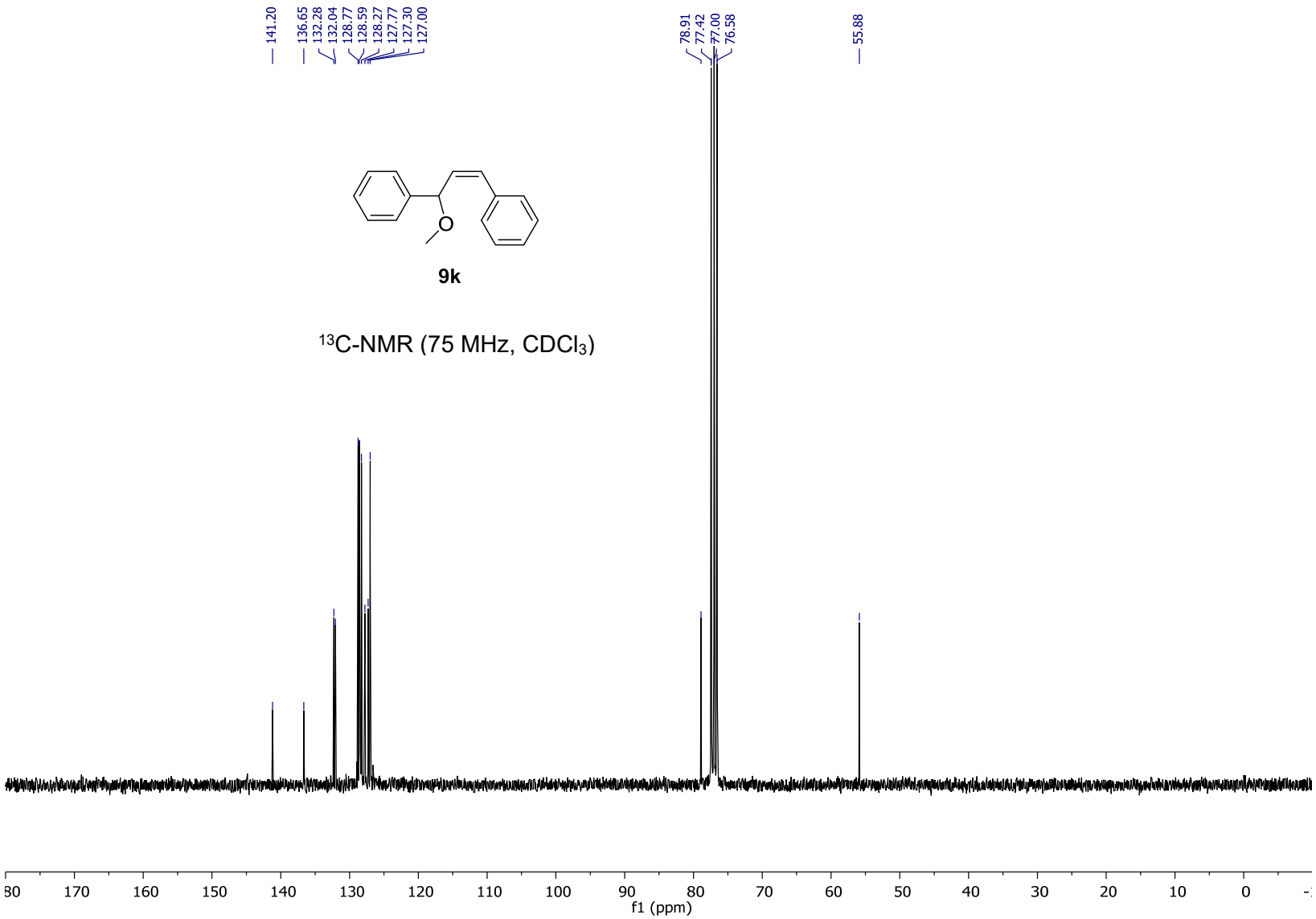

Supplementary Figure 124. ^{13}C-NMR spectra for compound **9k**

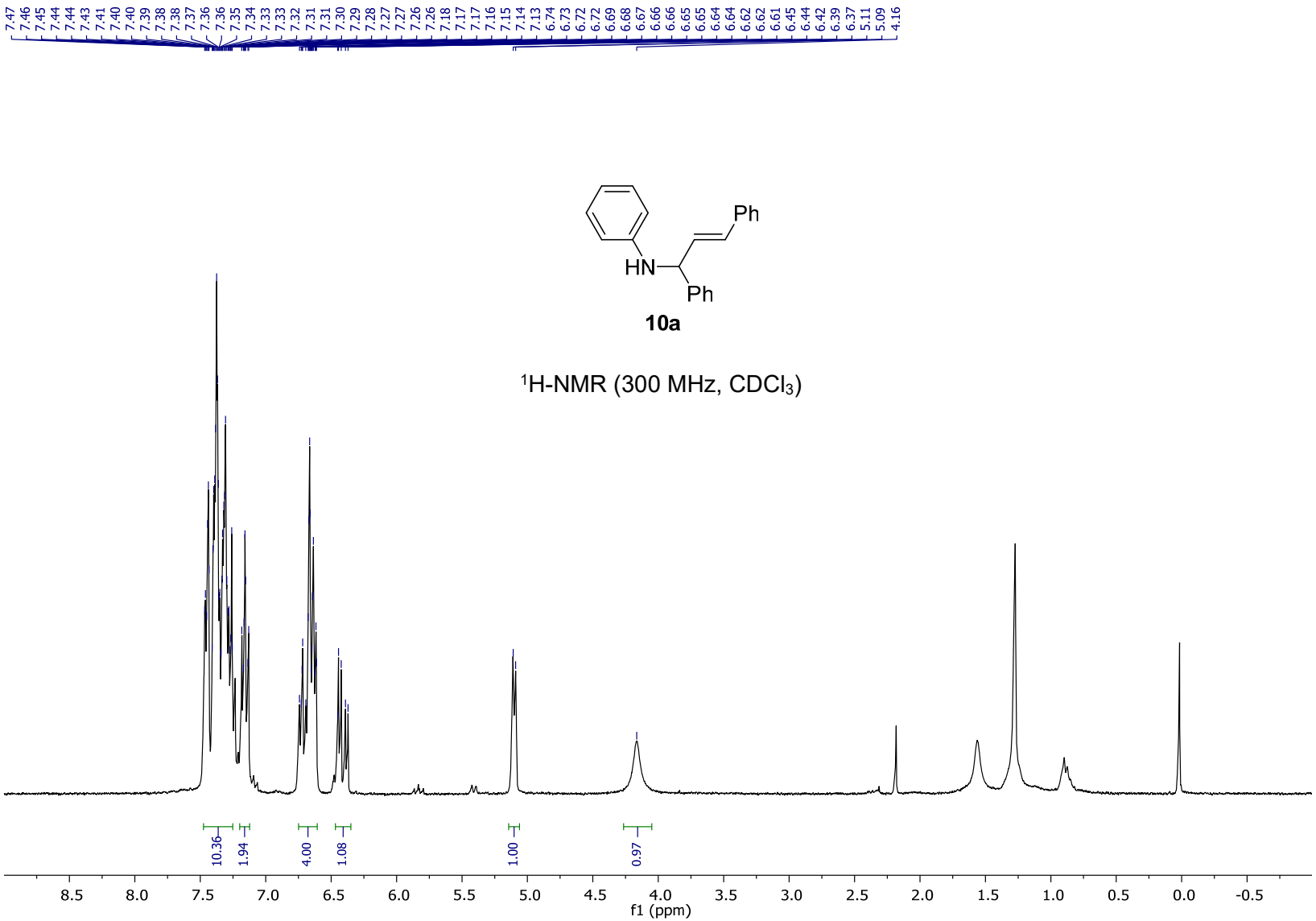

Supplementary Figure 129. ^{1}H-NMR spectra for compound **10a**

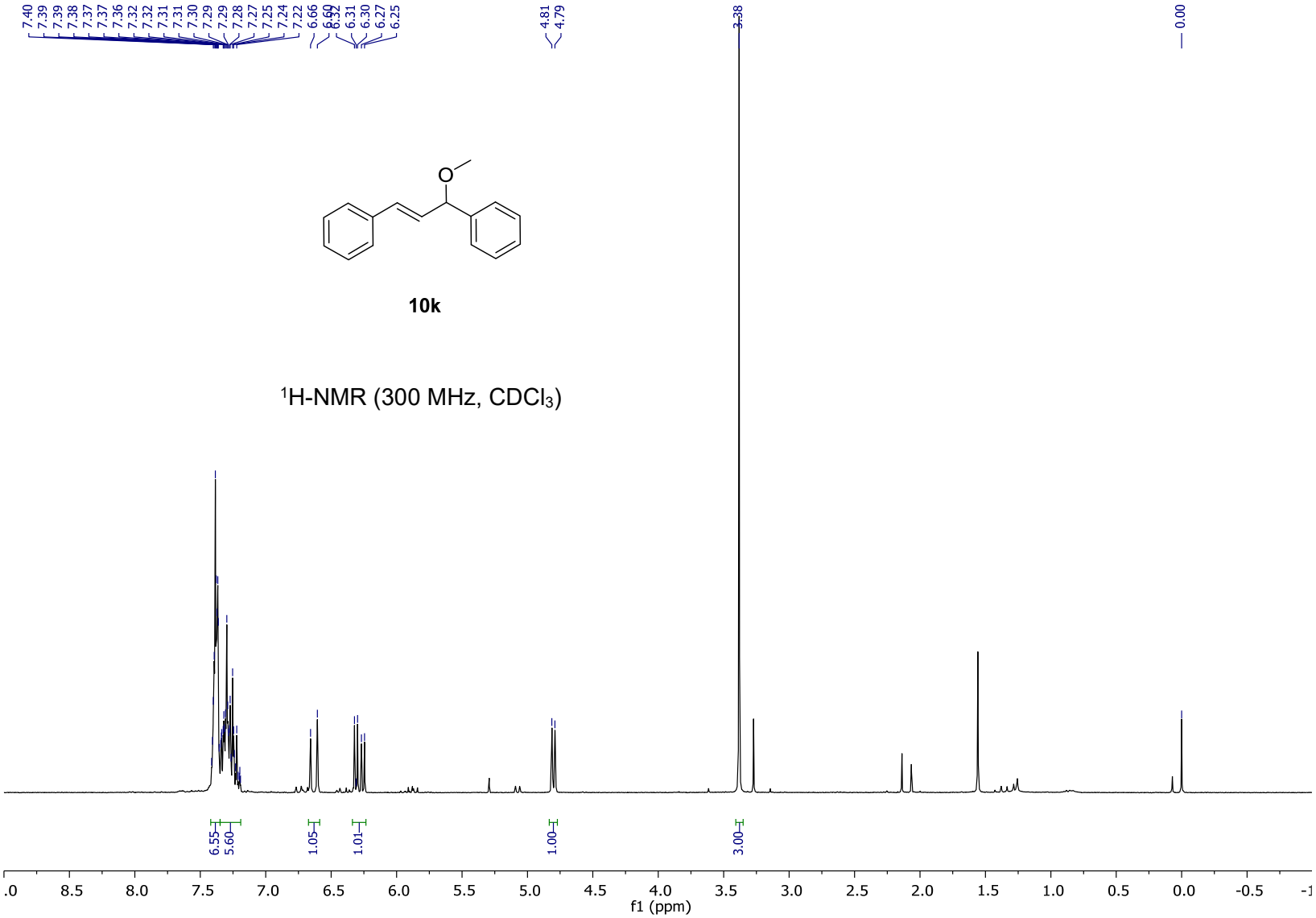

Supplementary Figure 142. ^{1}H-NMR spectra for compound **10k**

Supplementary References.

[1] Wang, Y.; Gu, M. The concept of spectral accuracy for MS. *Anal. Chem.* **82,** 7055–7062 (2010).
[2] Wang, Y. Methods for Operating MS Instruments Systems, United States Patent No. 6,983,213 (2006).
[3] Ochiaia, N.; Sasamoto, K.; MacNamara, K. Characterization of sulphur compounds in whisky by full evaporation dynamic headspace and selectable one-dimensional/two-dimensional retention time locked gas chromatography-mass spectrometry with simultaneous element-specific detection. *J. Chromatogr. A*, **1270**, 296–304 (2012).
[4] Ho, H.-P.; Lee, R.-Y.; Chen, C.-Y.; Wang, S.-R.; Li, Z.-G.; Lee, M.-R. Identification of new minor metabolites of penicillin G in human serum by multiple-stage tandem mass spectrometry. *Rapid Commun. Mass Spectrom.* **25**, 25–32 (2011).
[5] Gonda, Z.; Novák, Z. Transition-metal-free *N*-arylation of pyrazoles with diaryliodonium salts *Chem. - Eur. J.* **21**, 16801–16806 (2015).
[6] Li, X.-D.; Xie, L.-J.; Kong, D.-L.; Liu, L.; Cheng, L. Metal-free allylation of electron-rich heteroaryl boronic acids with allylic alcohols. *Tetrahedron* **72**, 1873–1880 (2016).
[7] Lee, B. H.; Choi, Y. L.; Shin, S.; Heo, J.-N. Stereoselective palladium-catalyzed α-arylation of 3-aryl-1-indanones: an asymmetric synthesis of (+)-pauciflorol. F *J. Org. Chem.* **76**, 6611–6618 (2011).
[8] Chan, C.-K.; Tsai, Y.-L.; Chang, M.-Y. $Bi(OTf)_3$ catalyzed disproportionation reaction of cinnamyl alcohols. *Tetrahedron* **73**, 3368–3376 (2017).
[9] Zhuang, M.; Du, H. Chiral Brønsted acid catalyzed enantioselective intermolecular allylic aminations. *Org. Biomol. Chem.* **12**, 4590–4593 (2014).
[10] Johnston, A. J. S.; McLaughlin, M. G.; Reid, J. P.; Cook, M. J. NaH mediated isomerisation–allylation reaction of 1,3-substituted propenols. *Org. Biomol. Chem.* **11**, 7662–7666 (2013).
[11] Kinoshita, N.; Kawabata, T.; Tsubaki, K.; Bando, M.; Fuji, K. Use of zinc enolate, free from other metals, in enantioselective palladium-catalyzed allylic alkylation. *Tetrahedron* **62**, 1756–1763 (2006).
[12] Shibatomi, K.; Muto, T.; Sumikawa, Y.; Narayama, A.; Iwasa, S. Development of a new chiral spiro oxazolinylpyridine ligand (Spymox) for asymmetric catalysis. *Synlett* 241–244 (2009).
[13] Mino, T.; Wakui, K.; Oishi, S.; Hattori, Y.; Sakamoto, M.; Fujita, T. Kinetic resolution of allylic esters in palladium-catalyzed asymmetric allylic alkylations using C–N bond axially chiral aminophosphine ligands. *Tetrahedron Asymmetry* **19**, 2711–2716 (2008).
[14] Caminiti, N. S.; Goodstein, M. B.; Leibler, I. N.-M.; Holtzman, B. S.; Jia, Z. B.; Martini, M. L.; Nelson, N. C.; Bunt, R. C. Reversible nucleophilic addition can lower the observed enantioselectivity in palladium-catalyzed allylic amination reactions with a variety of chiral ligands. *Tetrahedron Lett.* **56**, 5445–5448 (2015).
[15] Discekici, E. H.; Treat, N. J.; Poelma, S. O.; Mattson, K. M.; Hudson, Z. M.; Luo, Y.; Hawker, C. J.; Read de Alaniz, J. A highly reducing metal-free photoredox catalyst: design and application in radical dehalogenations. *Chem. Commun.* **51**, 11705–11708 (2015).
[16] McCarthy, B. G.; Pearson, R. M.; Lim, C.-H.; Sartor, S. M.; Damrauer, N. H.; Miyake, G. M. Structure–property relationships for tailoring phenoxazines as reducing photoredox catalysts *J. Am. Chem. Soc.* **140**, 5088–5101 (2018).
[17] Cao, Z.; Liu, Y.; Feng, X.; Zhuang, M.; Du, H. Pd-Catalyzed asymmetric allylic alkylation of indoles and pyrroles by chiral alkene-phosphine ligands. *Org. Lett.* **13**, 2164–2167 (2011).
[18] Trillo, P.; Baeza, A.; Nájera, C. Fluorinated alcohols as promoters for the metal-free direct substitution reaction of allylic alcohols with nitrogenated, silylated, and carbon nucleophiles. *J. Org. Chem.* **77**, 7344–7354 (2012).
[19] Shirakawa, S.; Kobayashi, S. Surfactant-type Brønsted acid catalyzed dehydrative nucleophilic substitutions of alcohols in water. *Org. Lett.* **9**, 311–314 (2007).
[20] Mino, T.; Nishikawa, K.; Asano, M.; Shima, Y.; Ebisawa, T.; Yoshida, Y.; Sakamoto, M. Chiral *N*-1-adamantyl-*N*-*trans*-cinnamylaniline type ligands: synthesis and application to palladium-catalyzed asymmetric allylic alkylation of indoles. *Org. Biomol. Chem.* **14**, 7509–7519 (2016).
[21] Feng, B.; Pu, X.-Y.; Liu, Z.-C.; Xiao, W.-J.; Chen, J.-R. Highly enantioselective Pd-catalyzed indole allylic alkylation using binaphthyl-based phosphoramidite-thioether ligands. *Org. Chem. Front.* **3**, 1246-1249 (2016).

[22] Cheung, H. Y.; Yu, W.-Y.; Lam, F. L.; Au-Yeung, T. T. L.; Zhou, Z.; Chan, T. H.; Chan. A. S. C. Enantioselective Pd-catalyzed allylic alkylation of indoles by a new class of chiral ferrocenyl P/S ligands. *Org. Lett.* **9**, 4295–4298 (2007).
[23] Liu, Z.; Cao, Z.; Du, H. Highly effective chiral phosphorus amidite–olefin ligands for palladium-catalyzed asymmetric allylic substitutions. *Org. Biomol. Chem.* **9**, 5369–5372 (2011).
[24] Sun, R.; Liu, J.; Yang, S.; Chen, M.; Sun, N.; Chen, H.; Xie, X.; You, X.; Li, S.; Liu, Y. Cp_2TiCl_2-catalyzed *cis*-hydroalumination of propargylic amines with Red-Al: stereoselective synthesis of *Z*-configured allylic amines. *Chem. Commun.* **51**, 6426−6429 (2015).
[25] Ohshima, T.; Miyamoto, Y.; Ipposhi, J.; Nakahara, Y.; Utsunomiya, M.; Mashima, K. Platinum-catalyzed direct amination of allylic alcohols under mild conditions: ligand and microwave effects, substrate scope, and mechanistic study. *J. Am. Chem. Soc.* **131**, 14317-14328 (2009).
[26] Wang, Z.; Mo, H.; Cheng, D.; Bao, W. Metal-free synthesis of allylic amines by cross-dehydrogenative-coupling of 1,3-diarylpropenes with anilines and amides under mild conditions. *Org. Biomol. Chem.* **10**, 4249-4255 (2012).
[27] Ohshima, T.; Nakahara, Y.; Ipposhi, J.; Miyamoto, Y.; Mashima, K. Direct substitution of the hydroxy group with highly functionalized nitrogen nucleophiles catalyzed by Au(III). *Chem. Commun.* **47**, 8322-8324 (2011).
[28] Concellón, J. M.; Suárez, J. R.; del Solar, V. Synthesis of enantiopure allylamines by reductive alkylation of amino epoxides with organolithium reagents. *Org. Lett.* **8**, 349-351 (2006).
[29] Baudoux, J.; Perrigaud, K.; Madec, P.-J.; Gaumont, A.-C.; Dez, I. Development of new SILP catalysts using chitosan as support. *Green Chem.* **9**, 1346−1351 (2007).
[30] Liu, Q.-L.; Chen, W.; Jiang, Q.-Y.; Bai, X.-F.; Li, Z.; Xu, Z.; Xu, L.-W. A D-Camphor-based Schiff base as a highly efficient N,P ligand for enantioselective palladium-catalyzed allylic substitutions. *ChemCatChem* **8**, 1495−1499 (2016).
[31] Thiemann, T. Etherification of (*E*)-1,3-diaryl- and (*E*)-1,3-diheteroaryl- prop-2-en-1-ols with primary and secondary alcohols over platinum on carbon. *J. Chem. Res.* 528−534 (2007).
[32] Miranda, M. A.; Perez-Prieto, J.; Font-Sanchis, E.; Kónya, K.; Scaiano, J. C. Flash photolysis of 1,3-Dichloro-1,3-diphenylpropane in polar solvents: generation of a stabilized *γ*-chloropropyl cation, subsequent formation of a propenyl cation, and nucleophilic trapping of both cations. *J. Phys. Chem. A* **102***,* 5724-5727 (1998).
[33] Mattay J., Vondenhof M. Contact and solvent-separated radical ion pairs in organic photochemistry. In: Photoinduced Electron Transfer III. Topics in Current Chemistry. Eds: Mattay J.; Springer, Berlin, Heidelberg, **159**, pag. 219-255 (1991).
[34] Silvi, M.; Arceo, E.; Jurberg, I. D.; Cassani, C.; Melchiorre, P. Enantioselective organocatalytic alkylation of aldehydes and enals driven by the direct photoexcitation of enamines. *J. Am. Chem. Soc.* **137**, 6120−6123 (2015).
[35] Kuhn, H. J.; Braslavsky, S. E.; Schmidt, R. Name and symbol of the element with atomic number 111. *Pure Appl. Chem.* **76**, 2105–2146 (2004).
[36] Hamai, S.; Hirayama, F. Actinometric determination of absolute fluorescence quantum yields. *J. Phys. Chem.* **87**, 83-89 (1983).
[37] Zhao Y.; Truhlar, D. G. The M06 suite of density functionals for main group thermochemistry, thermochemical kinetics, noncovalent interactions, excited states, and transition elements: two new functionals and systematic testing of four M06-class functionals and 12 other functionals. *Theor. Chem. Acc.* **120**, 215–241 (2008).
[38] Hehre W. J.; Ditchfield, R.; Pople, J. A. Self-consistent molecular orbital methods. XII. Further extensions of Gaussian-type basis sets for use in molecular orbital studies of organic molecules. *J. Chem. Phys.* **56**, 2257–2261 (1972).
[39] Marenich, A. V.; Cramer, C. J.; Truhlar, D. G. Universal solvation model based on solute electron density and on a continuum model of the solvent defined by the bulk dielectric constant and atomic surface tensions. *J. Phys. Chem. B* **113**, 6378–6396 (2009).
[40] Frisch, M. J.; Trucks, G. W.; Schlegel, H. B.; Scuseria, G. E.; Robb, M. A.; Cheeseman, J. R.; Scalmani, G.; Barone, V.; Mennucci, B.; Petersson, G. A. et al., Gaussian 09 Revision E.01, Wallingford CT: Gaussian, Inc., 2009.
[41] Fawcett, W. R. The ionic work function and its role in estimating absolute electrode potentials. *Langmuir* **24**, 9868-9875 (2008).

Part 2

…to Organocatalytic Materials

7. Introduction

7.1 Construction of catalytic MOFs and COFs

This part of the doctoral thesis has sought to develop organocatalytic processes using heterogeneous materials as platforms to support the catalytic centres. The selected materials to carry out this purpose are the Metal-organic frameworks (MOF, which is a class of coordination network, see below) and Covalent organic frameworks (COF, which is a class of porous organic polymer, see below) due to the great porosity of these two types of materials, which facilitates their use as catalysts, together with the possibility of designing active building blocks. This introduction aims to show why these frameworks are good candidates to be used in catalysis and a revision about some organocatalytic procedures using COFs and MOFs that have been done in the last years in order to contextualize the projects of this thesis.

7.1.1. General concepts of MOFs and COFs

A **coordination network** is a coordination compound extending, through repeating coordination entities, in 1 dimension, but with cross-links between two or more individual chains, or a coordination compound extending through repeating coordination entities in 2 or 3 dimensions.[84]

A **metal–organic framework**, abbreviated to MOF, is a coordination network with organic ligands containing potential voids,[84] in other words, a MOF is a coordination network with the special feature of being porous.

According to IUPAC, it is not necessary for a MOF to be crystalline for being considered as such,[84] since they are dynamic systems whose structure and porosity can change depending on temperature and pressure. However, big efforts are always done to obtain crystalline MOFs, since it enables the characterization of the materials by diffraction techniques, and crystalline ordered structures offer optimal pore sizes and surface areas. Solvothermal synthesis is usually required to obtain crystalline MOFs, since these conditions offer reversibility to the coordination bond formation, which is crucial for an ordered growth of the material.

The MOF-5 (also called IRMOF-1) is a good example to illustrate these concepts. When an appropriate carboxylic acid (like acetic, benzoic and pivalic acid), RCO_2H, is combined with the ion Zn^{2+}, it forms the tetranuclear supertetrahedral cluster motif shown in Figure 13A-B,[85] with formula $Zn_4(O)O_{12}C_6R_4$. The combination of 1,4-benzenedicarboxylic acid, BDC, which have two carboxylic acid moieties in linear distribution pointing to opposite sides (Figure 13C), with the ion Zn^{2+} in the appropriate conditions, gives the MOF-5. The MOF-5 is a crystalline material where these cluster motif is repeated in a three-dimensional framework, with high pore volume and therefore high surface (Figure 13D).[86] In this network, the entire metal-oxide clusters are the nodes. The use of longer dicarboxylic acids gives rise to isoreticular (with the same topology)

[84] S. R. Batten, N. R. Champness, X.-M. Chen, J. Garcia-Martinez, S. Kitagawa, L. Öhrström, M. O'Keeffe, M. Paik Suh, J. Reedijk, *Pure Appl. Chem.* **2013**, *85*, 1715–1724.
[85] W. Clegg, D. R. Harbron, C. D. Homan, P. A. Hunt, I. R. Little, B. P. Straughan, *Inorg. Chim. Acta*, **1991**, *186*, 51-60.
[86] H. Li, M. Eddaoudi, M. O'Keeffe, O. M. Yaghi, *Nature*, **1999**, *402*, 276-279.

MOFs with higher volume and surface, like the IRMOF-16 (Figure 13F),[87] formed from TPDC ligand (Figure 13E) and Zn^{2+}, which is a relevant MOF in this doctoral thesis.

As can be seen in the latter example, the MOFs are usually coordination networks whose nodes are metal oxide clusters.[88] These clusters are rigid structures, with the points of extension (the carboxylates of the ligands) with a well-defined geometry and directionality which is crucial to obtain ordered periodic structures, so these clusters define geometrical shapes referred to as secondary building units (SBUs).[89]

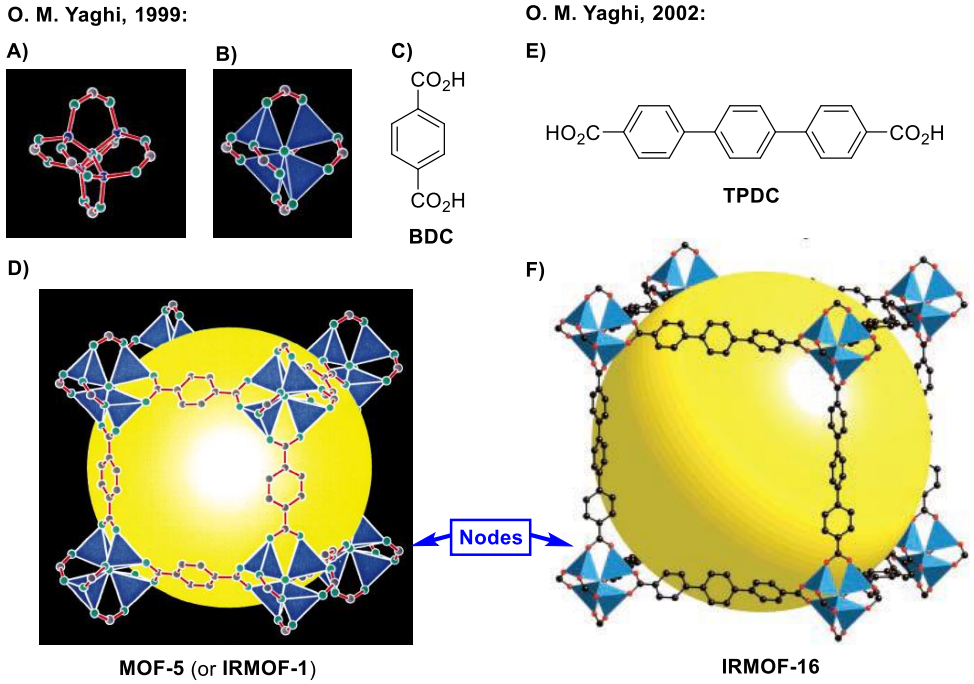

Figure 13. A) The $Zn_4(O)O_{12}C_6$ cluster (Zn, blue; O, green; C, grey). **B)** The same, with the ZnO_4 tetrahedra indicated in blue. **C)** The 1,4-benzenedicarboxylic acid ligand (BDC). **D)** One of the cavities of the MOF-5. **E)** [1,1':4',1''-terphenyl]-4,4''-dicarboxylic acid ligand (TPDC). **F)** One of the cavities of the IRMOF-16. In **D** and **F** the yellow sphere indicates the cavity. **Figures A**, **B** and **D** reprinted by permission from Springer Nature Customer Service Centre GmbH from Ref. 86. Copyright 1999. **Figure F** from Ref. 87. Reprinted with permission from The American Association for the Advancement of Science (AAAS).

The big porosity of MOFs makes them to have multiple applications in different fields,[118] such as gas sorption,[90a-b] molecular recognition,[90c] proton conductivity,[90d] and catalysis.[90e-f]

---

[87] M. Eddaoudi, J. Kim, N. Rosi, D. Vodak, J. Wachter, M. O'Keeffe, O. M. Yaghi, *Science*, **2002**, *295*, 469-472.

[88] There are MOFs which do not have these metal clusters in their structures: a) K. S. Park, Z. Ni, A. P. Côté, J. Y. Choi, R. Huang, F. J. Uribe-Romo, H. K. Chae, *PNAS*, **2006**, *103*, 10186-10191. b) A. J. Clough, J. M. Skelton, C. A. Downes, A. A. de la Rosa, J. W. Yoo, A. Walsh, B. C. Melot, S. C. Marinescu, M. O'Keeffe, O. M. Yaghi *J. Am. Chem. Soc.* **2017**, *139*, 10863−10867.

[89] O. M. Yaghi, M. O'Keeffe, N. W. Ockwig, H. K. Chae, M. Eddaoudi, J. Kim, *Nature* **2003**, *423*, 705-714.

[90] a) L. Du, Z. Lu, K. Zheng, J. Wang, X. Zheng, Y. Pan, X. You, J. Bai, *J. Am. Chem. Soc.* **2013**, *135*, 562−565. b) J. A. Mason, J. Oktawiec, M. K. Taylor, M. R. Hudson, J. Rodriguez, J. E. Bachman, M. I. Gonzalez, A. Cervellino, A. Guagliardi, C. M. Brown, P. L. Llewellyn, N. Masciocchi, J. R. Long, *Nature* **2015**, *527*, 357–361. c) B. Chen, S. Xiang and G. Qian, *Acc. Chem. Res.* **2010**, *43*, 1115–1124. d) N. T. T. Nguyen, H. Furukawa, F. Gándara, C. A. Trickett, H. M. Jeong, K. E. Cordova, O. M. Yaghi, *J. Am. Chem. Soc.* **2015**, *137*,

Porous organic polymers (POPs) are organic materials with covalently bonded thermally stable backbones exhibiting high and accessible surface areas.[91] **Covalent organic frameworks (COFs)** are a class of porous organic polymer with a crystalline structure.[92] Until 2005, all the examples of POPs are amorphous non-ordered structures; the synthesis of crystalline organic polymers required reversibility in the formation of the covalent bonds between the building blocks to ensure an ordered crystal growth. This was achieved for first time by Yaghi and co-workers in 2005 by reversible condensation of ditopic aromatic boronic acids, which formed a Covalent Organic Framework (COF) with boroxine bonds, named COF -1.[93]

In a more wide definition, COFs are well-defined 2D and 3D periodic networks that are completely made up of light elements (i.e. oxygen, boron, nitrogen) and are connected by strong covalent bonds to form rigid, crystalline, porous structures with pore sizes ranging between 7-27 Å.[94] Scheme 41 shows as example the COF-300, developed by Yaghi *et al.* in 2009.[95] The aniline and the benzaldehyde condenses, forming an imine bond (Scheme 41A), which is a reversible reaction. The condensation between tetra-(4-anilyl)methane, which have anilines in the vertexes of a tetrahedron, and terephtaldehyde, which have two aldehyde groups in opposite extremes of the molecule, forms the COF-300, a network with a diamond-type topology where the imine bonds are repeated periodically (Scheme 41B-C).

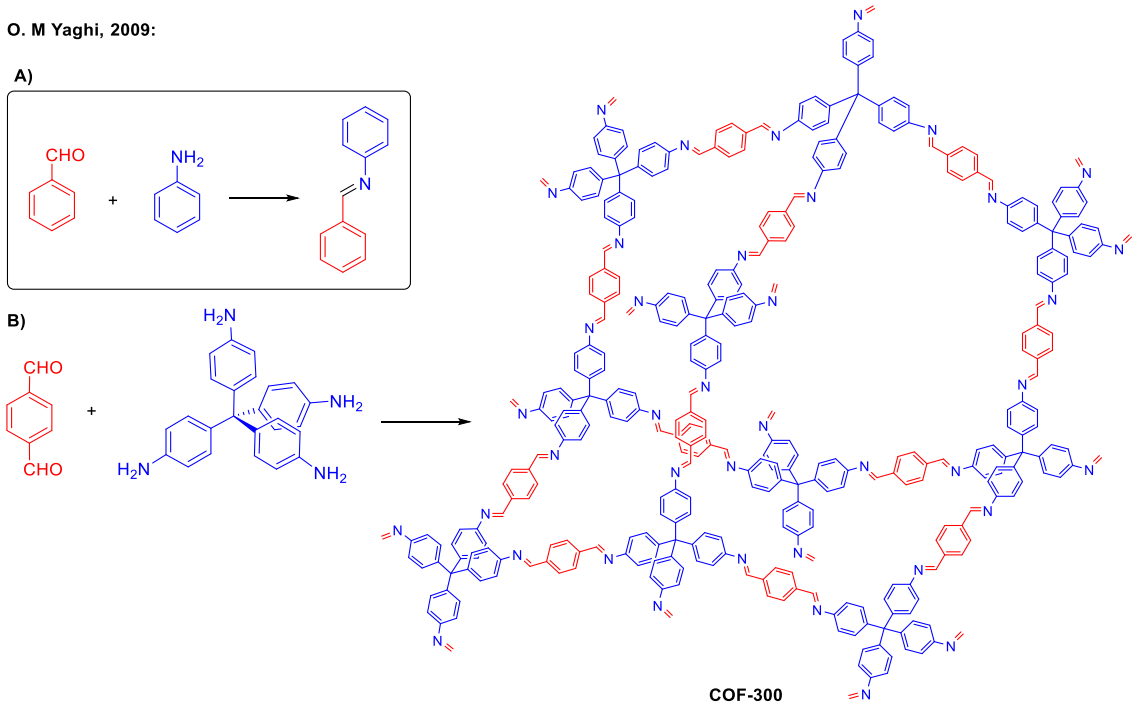

Scheme 41. A) Imine bond formation. **B)** COF-300 assembly by imine bond formation.

15394−15397. e) C.-D. Wu, M. Zhao, *Adv. Mater.* **2017**, *29*, 1605446. f) L. Jiao, Y. Wang, H.-L. Jiang, Q. Xu, *Adv. Mater.* **2018**, *30*, 1703663.

[91] H. Bildirir, V. G. Gregoriou, A. Avgeropoulos, U. Scherfd, C. L. Chochos, *Mater. Horiz.* **2017**, *4*, 546—556.

[92] a) X. Feng, X. Dinga, D. Jiang, *Chem. Soc. Rev.* **2012**, *41*, 6010–6022. b) S.-Y. Ding, W. Wang, *Chem. Soc. Rev.* **2013**, *42*, 548—568.

[93] A. P. Côté, A. I. Benin, N. W. Ockwig, M. O'Keeffe, A. J. Matzger, O. M. Yaghi, *Science*, **2005**, *310*, 1166-1170.

[94] Metal-organic Frameworks & Covalent Organic Frameworks, *ACS MATERIAL LLC*, Nov 15, **2017**.

[95] F. J. Uribe-Romo, J. R. Hunt, H. Furukawa, C. Klöck, M. O'Keeffe, O. M. Yaghi, *J. Am. Chem. Soc.* **2009**, *131*, 4570–4571.

Similarly to MOFs, COFs are characterized for being porous networks. COFs usually exhibits great thermal stability and can reach temperatures that exceeds 300 °C, since they are composed of strong covalent bonds. In general, they show enhanced stability compared to most MOFs. Another characteristic of COFs is their low density since they are composed of lightweight elements.[96] Their crystallinity enables the characterization using diffraction techniques.

Other common feature that COFs have with MOFs is that their great porosity can be exploited for different applications:[108c] gas storage,[97a] separations,[97b] smart sensors,[97c] optoelectronics,[97d] energy storage and catalysis.[98]

7.1.2. Considerations for developing catalytic MOFs and COFs

Once the general characteristics of MOFs and COFs have been exposed, one may wonder why it can be useful to use these materials as platforms for catalysis. These two types of materials, although would act as heterogeneous catalysts, combine the best features of both heterogeneous and homogeneous catalysts.[99]

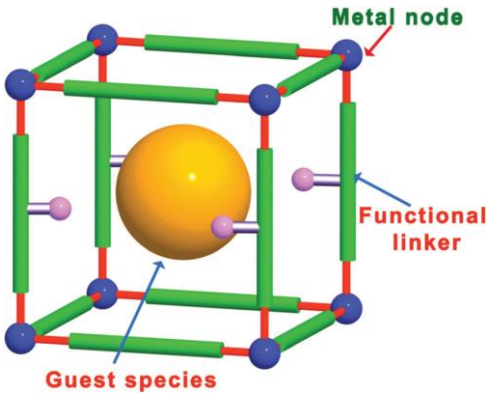

Figure 14. Possible catalytic sites in a MOF. Reproduced from Ref. 100 with permission from The Royal Society of Chemistry.

As heterogeneous catalysts, they are solid-state materials which do not solubilize in the reaction media so they can be easily separated from the mixture once the reaction is finished, allowing not only an easiest purification of the product, but also a reutilization of the catalyst. In many cases the MOF and COF catalysts could be recycled more than five times without losing catalytic effectivity.[108d, 130]

MOFs and COFs can be easily chemically tuned to the same level of detail as a homogeneous catalyst.[99] The building blocks can be chemically modified to incorporate different types of catalytic active sites and, in the case of MOFs, the metal ion can be selected and the second coordination sphere interactions can be manipulated.

MOFs and COFs are complex structures with different sites that can serve as catalytic centres. Figure 14 shows all possible active sites that a MOF can have[100] and some of them are applicable to COF:

---

[96] R. P. Bisbey, W. R. Dichtel, *ACS Cent. Sci.* **2017**, *3*, 533−543.

[97] a) J. Dong, Y. Wang, G. Liu, Y. Cheng, D. Zhao*, CrystEngComm* **2017**, *19*, 4899–4904. b) Z. Kang, Y. Peng, Y. Qian, D. Yuan, M. A. Addicoat, T. Heine, Z. Hu, L. Tee, Z. Guo, D. Zhao, *Chem. Mater.* **2016**, *28*, 1277−1285. c) G. Lin, H. Ding, D. Yuan, B. Wang, C. Wang, *J. Am. Chem. Soc.* **2016**, *138*, 3302−3305. d) Y. Du, H. Yang, J. M. Whiteley, S. Wan, Y. Jin, S.-H. Lee, W. Zhang, *Angew. Chem. Int. Ed.* **2016**, *55*, 1737–1741. e) S. Wang, Q. Wang, P. Shao, Y. Han, X. Gao, L. Ma, S. Yuan, X. Ma, J. Zhou, X. Feng, B. Wang, *J. Am. Chem. Soc.* **2017**, *139*, 4258−4261.

[98] H. Hu, Q. Yan, R. Ge, Y. Gao, *Chinese J. Cat.* **2018**, *39*, 1167–1179.

[99] S. M. Cohen, Z. Zhang, J. A. Boissonnault, *Inorg. Chem.* **2016**, *55*, 7281−7290.

[100] Y.-B. Huang, J. Liang, X.-S. Wang, R. Cao, *Chem. Soc. Rev.* **2017**, *46*, 126—157.

- Functional linker: The organic ligand or organic building block can have a functional group able to catalyse a reaction.
- Metal nodes (only applicable to MOFs): The metallic centres or metallic clusters can have coordinatively unsaturated metal sites (CUSs) that can act directly as metallic catalysts or can serve to coordinate extra ligands to the MOF than can have catalytic activity.
- Covalent bond linkages (only applicable to COF, not shown in Figure 14). Sometimes, the functional groups that are formed to bond the building blocks in a COF can act as catalytic centres. For example, the imine bonds can act as basic catalysts or to coordinate catalytic metallic centres or the boroxine bonds can act as acidic centres.
- Guest species: The porosity of these materials allows to accommodate discrete catalytic molecules inside the porous than only have weak interaction with the walls of the material.

There are several strategies (Scheme 42) to construct MOFs or COFs with catalytic activity:[99]

- Bottom-up strategy: it consists in synthesising building blocks which contains directly the catalytic centre and using them to construct the MOF or COF. Therefore, once the MOF or COF is formed, it is ready for the catalysis.[98]
- Post-synthetic modification (PSM):[101] It is the chemical transformation of an already formed COF or MOF to modify the functional groups presented in the structure. It results in a material that is still a COF or a MOF but with different structure. In can be used to introduce catalytic active sites. There are many types of post-synthetic modification, some of them are:
    - Post-synthetic deprotection (PSD): Some functional groups must be introduced in the material in their protected forms and a process of deprotection must be carried out once the material has been synthesised.
    - Post-synthetic exchange. This process is more typical for MOF. It is the exchange of the metal ions or the ligands of the MOF for others, maintaining the topology of the MOF.
    - Functionalization of coordinatively unsaturated sites (CUSs). Some MOFs have CUSs, that is, some of their metal centres have free coordination positions. Terminal ligands with catalytic functional groups can be coordinated to these sites. Normally, the CUSs must be previously activated to remove solvent molecule anchored to them.

Although the bottom-up strategy can seem the easiest way, sometimes it is not possible to follow such approach. Some catalytic functional groups can interfere with the self-assembly of the MOF or COF, since they can modify the optimal acid-base conditions for their formation or they can compete for the formation of the bonds presented in COFs and MOFs. For instance, the pyrrolidines must be always be protected in the building blocks of the material and once the material is formed a process of post-synthetic deprotection must be carried out.

[101] K. K. Tanabe, S. M. Cohen, *Chem. Soc. Rev.* **2011**, *40*, 498–519.

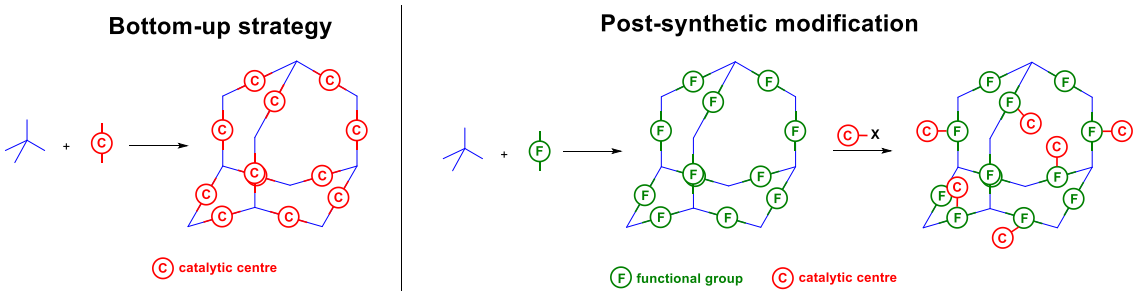

Scheme 42. Bottom-up strategy vs Post-synthetic modification in the synthesis of a hypothetical catalytic COF. These concepts can also be applied to MOFs.

Other problems associated with the bottom-up strategy are that bulky functional groups presented in the building blocks can make difficult to achieve crystallinity in the final material. Furthermore, the harsh solvothermal conditions for the synthesis can damage the catalytic groups present in the building blocks. These two problems can be solved with post-synthetic modification strategies.

On the other hand, the post-modification strategy has also some associated problems. Since it consists in a heterogeneous reaction to a solid material, the active sites inside the pores are less accessible than the sites of the surface; therefore, it is possible that the process yields a partially irregularly post-modified material. Since COFs and MOFs are insoluble solids, it is difficult to know the grade of post-modified sites, and only indirect techniques can be applied for it (for example, XPS can be applied to know if some element is presented in the material), which can derive in irreproducible results.

Constructing a catalytic MOF or COF is not only a question of attaching catalytic centres into the material, but also the material must be designed to tolerate the reactions conditions.[99] For example, if the reaction needs to be heated up, the material must withstand this temperature. Attention also must be paid to the chemical conditions; for example, some MOFs, like MOF-5, are sensitive to water or other proton sources because they are believed to protonate the carboxylate linkages, so other platform must be selected if the reaction requires the addition of acid. Other MOFs based in Zr^{4+}, like the UiO,[109] are more chemical stable.

Another very important consideration to be taken into account is the pore size[99] since the majority of the surface area of the MOF inside its pores. To maximize the efficiency of these materials as catalysts the reactants must be able to flow inside the channels in order they can interact with all the catalytic centres of the material. A small pore would imply a hindered mass transport or, if the reactants cannot even to go inside, a catalysis limited to the surface of the material. Reactions whose reactants are relatively big organic molecules would need materials with bigger pores than those required for reactions where only molecules like CO_2, H_2O or H_2 are involved. It is very important to consider that the synthesis of some MOF and COF can result into two concatenated frameworks, what reduces the theoretical pore size considerably. In some cases, like in the biggest IRMOF, the concatenation can be avoided by carrying out the solvothermal synthesis in diluted conditions.[87]

7.2. MOFs and COFs as organocatalytic platforms

7.2.1. General concepts about Organocatalysis

Organocatalysis is the use of small organic molecules to catalyse organic transformations.[102] These small catalysts are called organocatalysts and they are classified by the mode that they have to bond to the substrate and activate it:[103]

- **Activation by covalent bond**: The organocatalyst forms a covalent bond with one of the substrates, making it more reactive. Once the reaction takes place the organocatayst is released. There are two main families of organocatalysts within this type of activation: the **aminocatalysts**, that are primary or secondary amines that are able to activate aldehydes and ketones through condensation with them, and the **N-heterocyclic carbenes**,[104] that are stabilized carbenes than can form reactive intermediates with aldehydes, esters, heterocycles, silylated nucleophiles…
- **Activation by non-covalent interactions**: The organocatalysts are organic bases or organic acids that activates the substrates by acid-base interactions. Depending of the strength of the acid or the base, the type of the interaction can vary. For example, a weak protic organic acid can form a hydrogen bond with the substrate, and the stronger the acid is, the more transferred the proton is to the substrate in this interaction (Figure 15); a protic organic acid with enough strength transfers completely the proton to the base, which can be defined as a Brønsted-Lowry acid. Making a simplification of this scale, this type of organocatalysts can be classified in:
    - **Activation by hydrogen bond**: They are usually weak protic acids, like ureas or squaramides, that catalyse the reaction forming hydrogen bonds with the substrates, activating them as electrophiles or stabilizing negatively charged intermediates.
    - **Activation by proton exchange**: They are organic acids or bases with enough strength to transfer or accept a proton to the substrate in order to activated it, for example, carboxylic acids or tertiary amines. A proton exchange yields a positively charged molecule and a negatively charged molecule, so the catalyst and the intermediates can be associated by ionic interactions during the course of the reaction.

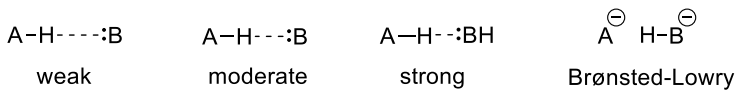

Figure 15. Hydrogen bond as a function of the acid strength.

The main role of an organocatalyst is activating the substrate to increase the reaction rate. Furthermore, in the last decades, more complex organocatalyst have been developed with a second role: promoting enantioselective reactions. These organocatalysts are optically pure chiral molecules and, since they are linked to the substrates through covalent or non-covalent bonds during the course of the reaction, they create a chiral atmosphere in the intermediates, favouring the formation of only one enantiomer.

---

[102] D. W. C. MacMillan, *Nature*, **2008**, *455*, 304-308.
[103] a) J. Alemán, S. Cabrera, *An. Quím.* **2009**, *105*, 189−197. b) J. Alemán, S. Cabrera, *Chem. Soc. Rev.* **2013**, 42, 774-793.
[104] M. Fèvre, J. Pinaud, Y. Gnanou, J. Vignolle, D. Taton, *Chem. Soc. Rev.* **2013**, *42*, 2142—2172.

In the last years, great efforts have been made to move the organocatalysts to the field of COF and MOF, introducing them as subunits in the structure of these porous materials. As was related before, the organocatalytic MOFs and COFs maintain the advantages of a heterogeneous catalyst, such as the easy separation of the reaction media and recyclability, but also have the advantages of homogeneous organocatalysts, like the broad range of activation modes or their easy modulation.

The next sections (Sections 7.2.2 – 7.2.8) will show representative examples of organocatalytic porous materials. The examples are classified by the activation mode of the organocatalytic subunit and the strategy to construct the catalytic porous material will be emphasised. In this classification the examples of MOF and COF will be treated equally.

7.2.2. Activation by covalent bond

The most employed strategy to do covalent organocatalysis with both COF and MOF is to incorporate pyrrolidine moieties as pending arms of the backbone of these structures. These pyrrolidines (and other aminocatalysts) have different modes to activate aldehydes and ketones. The two most frequent activation modes are the **via enamine** and the **via iminium ion**.[103] In the **via enamine** (Scheme 43A) the pyrrolidine moiety condenses with an aldehyde (or ketone) and the α proton of the condensed intermediate undergoes tautomerization to form the enamine intermediate; in this enamine intermediate the α position is activated to give a nucleophilic attack to an electrophile. In the **via iminium ion** (Scheme 43B), the pyrrolidine condenses with and α,β-unsaturated aldehyde to form an iminium ion intermediate; this iminium ion is activated as electrophile to suffer a nucleophilic attack to the β-carbon or to undergo a cycloaddition with a dipolarophile. In both vias, in the bond formation step (addition of enamine to E^+ in Scheme 43A and addition of Nu^- to iminium ion in Scheme 43B), since the chiral aminocatalyst is covalently bonded to the substrate, one of the substrate faces is blocked by the R group, favouring the formation of one enantiomer. These two modes of activation have been carried out with MOFs and COFs containing aminocatalytic moieties. In these functionalized materials, the R group of the pyrrolidine moiety would be the walls of the MOF or COF. Therefore, a correct selection of the material platform can favour that the walls block one of the faces of the enamine or iminium ion intermediates in the addition of electrophiles or nucleophiles to obtain optically pure products.

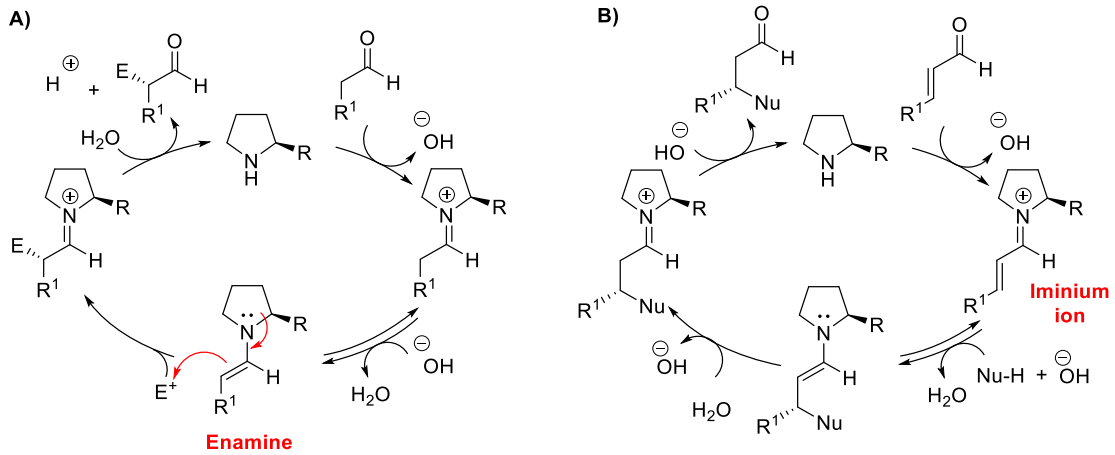

Scheme 43. Mechanisms of action of aminocatalysts: **A)** Via enamine **B)** Via iminium ion.

Telfer's group was one of the first in achieving this purpose in 2011. They used enantiopure chiral ligands functionalized with protected pyrrolydine in the synthesis of a MOF-5 analogue[86] and, once the MOF was formed, they performed a thermolytic deprotection to unveil the pyrrolidines (Scheme 44A).[105] This MOF, named IRMOF-Pro, catalysed the aldol condensation of the acetone or the pentanone to the *para*-nitrobenzaldehyde, reaction which proceeds via enamine, although with very low enantiomeric excess.

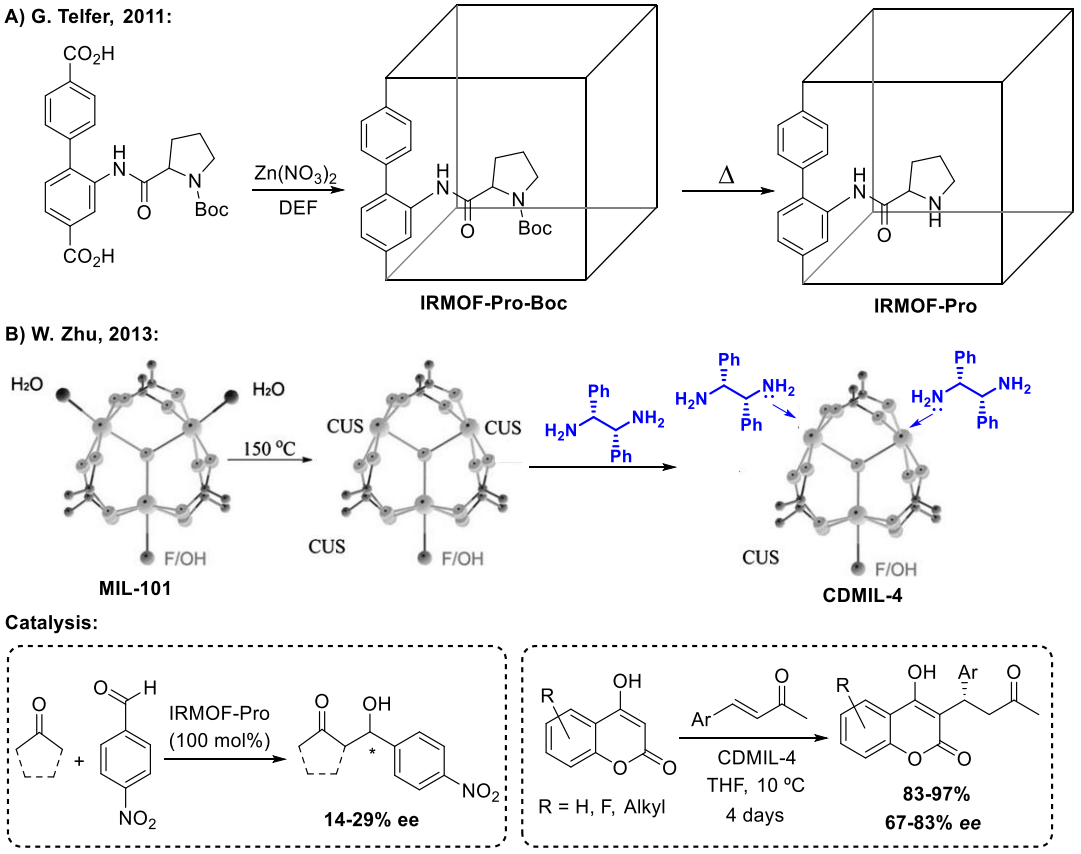

Scheme 44. MOFs with pyrrolidine catalytic centres. Scheme B adapted from Ref. 106 with permission from John Wiley and Sons.

In 2013 Zhu *et al.* used another type of post-synthetic strategy to incorporate aminocatalytic centres in the MIL-101 (Scheme 44B).[106] In this MIL-101 MOF[107] each chromium atom of the clusters is coordinated to four carboxylate oxygen, one μ_3–O, and a terminal ligand that can be a water molecule or a fluorine atom (coming from the HF in the synthesis). They carried out a dehydration process to this MOF, applying vacuum at 150 °C, to remove the molecules of water, leaving coordinatively unsaturated metal sites (CUSs). Then, they added (1*R*,2*R*)-1,2-diphenylethylenediamine, which coordinates to the CUSs by one nitrogen atom, so the other amino group was free to make catalytic processes. This functionalized MOF, called CDMIL-4, successfully catalysed the addition of hydroxycoumarines to α,β-unsaturated ketones with moderate enantiomeric excess. In this reaction, the amine catalytic centre condensates with the α,β-unsaturated ketones, forming an iminium ion, which is activated to suffer the addition (in a similar way to the one shown in Scheme 43B). Using this process with the CDMIL-

[105] D. J. Lun, G. I. N. Waterhouse, S. G. Telfer, *J. Am. Chem. Soc.* **2011**, *133*, 5806–5809.
[106] T. Shi, Z. Guo, H. Yu, J. Xie, Y. Zhong, W. Zhu, *Adv. Synth. Catal.* **2013**, *355*, 2538 – 2543.
[107] G. Férey, C. Mellot-Draznieks, C. Serre, F. Millange, J. Dutour, S. Surblé, I. Margiolaki, *Science* **2005**, *309*, 2040-2042.

4, they obtained the anticoagulant drug Warfarine (R_1 = H, Ar = Ph) in gram scale (2.8 g, 82% *ee*, >99% *ee* after recrystallization), demonstrating that the catalysis with MOF has potential applications.

The pyrrolidine moiety has been incorporated to COF materials too.[108a-d] In 2015 Jiang *et al.* developed the TPB-DMTP-COF, a 2D COF, formed by imine bonds between the building blocks triphenylbenzene (TPB) and dimethoxyterephthaldehyde (DMTP) (Scheme 45A).[108b] The methoxy lone electron pairs delocalize in the central phenyl ring, reinforcing the interlayer interactions, which aids in its crystallization and in increasing the porosity. They synthesised other analogues of this COF in which they mixed the DMTP building block with 2,5-bis(2-propynyloxy)terephthalaldehyde (BPTA) in different proportions, obtaining the $[HC\equiv C]_x$-TPB-DMTP-COF, a COF which contains a controlled amount of terminal alkynes in its structure. Post-synthetic modifications allowed to incorporate pyrrolidine moieties to the alkyne sites of the COF by click chemistry, obtaining $[(S)\text{-Py}]_x$-TPB-DMTP-COFs, a series of COFs with controlled amount of pyrrolidines as pending arms. This COFs successfully catalysed the the Michael addition of ketones to nitrostyrenes with good enantioselectivities. They concluded than when the channels of COF were saturated of pyrrolydines pending arms, it was deleterious for the yield and enantiomeric excess of the reactions, since the reactants did not flow smoothly through the channels of the COF. On the other hand, the use of a COF with a [(*S*)-Py]/DMTP ratio of 17% achieved the best results of yields and enantioselectivity.

Two years later Cui and co-workers designed a series of analogue of the TPB-DMTP-COF, but in this case they incorporated the protected pyrrolidine moieties in the TBP building block and then made a post-synthetic deprotection (Scheme 45B). [108d] They did a series of this COF varying the structure of the pyrrolidine (or imidazolidine) motif and found that they could catalyse enantioselectively the α-aminoxilation of aldehydes and the aldol reaction, which occurs via enamine, and the Diels-Alder reaction of cinammaldehyde, which occurs via iminium ion. They could check and select which of the variants of the pyrrolidine COF was the best for each reaction, demonstrating the great versatility of COFs in modulating their catalytic properties.

[108] a) H. Xu, X. Chen, J. Gao, J. Lin, M. Addicoat, S. Irleb, D. Jiang, *Chem. Commun.* **2014**, *50*, 1292—1294. b) H. Xu, J. Gao, D. Jiang, *Nat. Chem.* **2015**, *7*, 905–912. c) H.-S. Xu, S.-Y. Ding, W.-K. An, H. Wu, W. Wang, *J. Am. Chem. Soc.* **2016**, *138*, 11489−11492. d) J. Zhang, X. Han, X. Wu, Y. Liu, Y. Cui, *J. Am. Chem. Soc.* **2017**, *139*, 8277−8285.

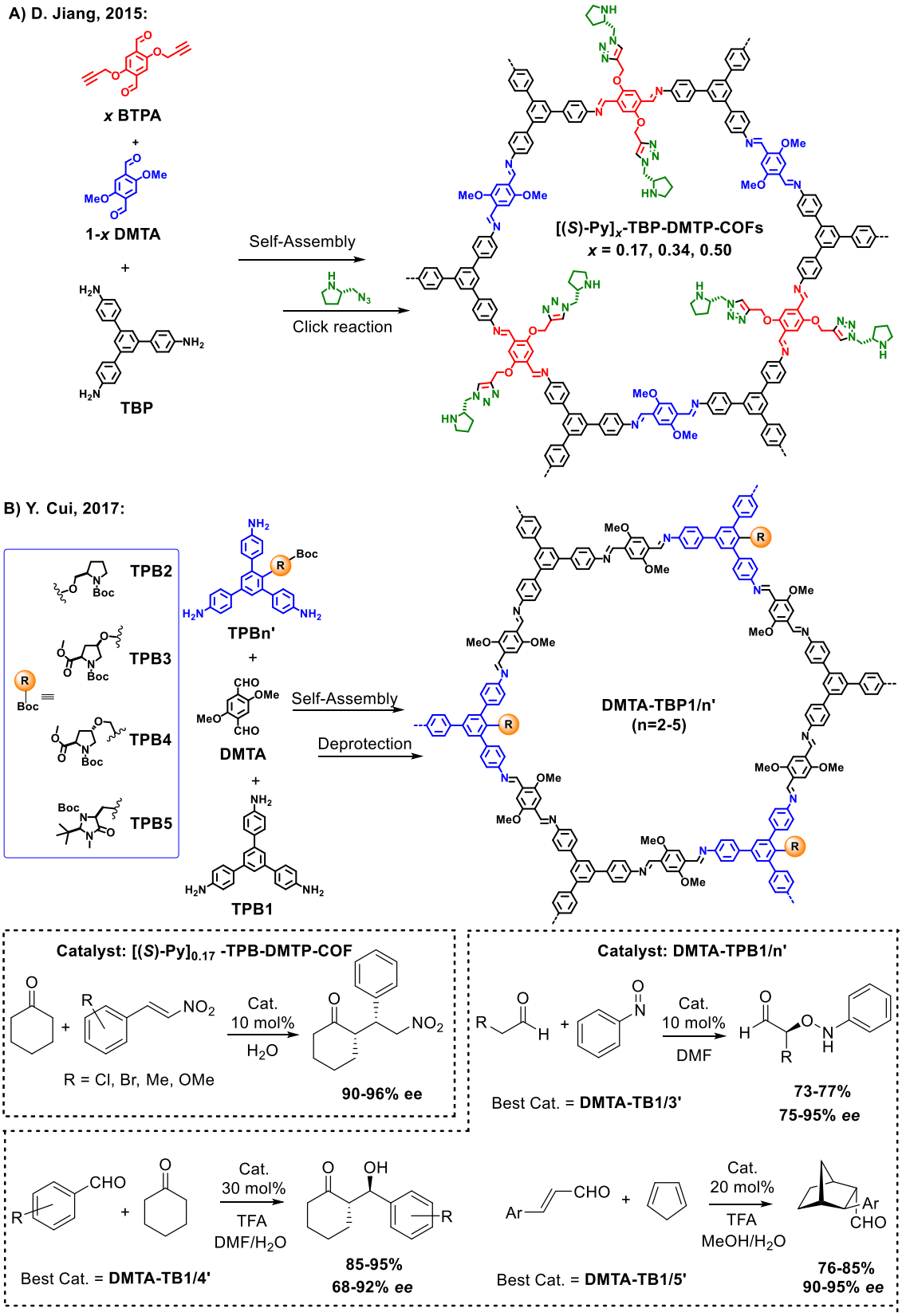

Scheme 45. COFs with pyrrolidine catalytic centres.

Aminocatalysis is not the only strategy within the covalent organocatalysis field that has been incorporated to MOF or COF, but *N*-heterocyclic carbenes has also been combined with these materials. In 2016, Perry *et al.* designed a UiO-67 MOF analogue[109] with *N*-heterocyclic carbenes in which they incorporated the heterocycles by bottom-up strategy and activated them with LDA by post-synthetic modification (Scheme 46).[110] The transesterification was the reaction selected to check the activity of this MOF with good results. In this reaction the *N*-heterocycle carbene can either activate the ester or the alcohol.[104] In the first pathway, the carbene undergoes nucleophilic attack to ester, binding to it covalently. In the second pathway the carbene plays the role of a base, interacting with the alcohol by hydrogen bond.

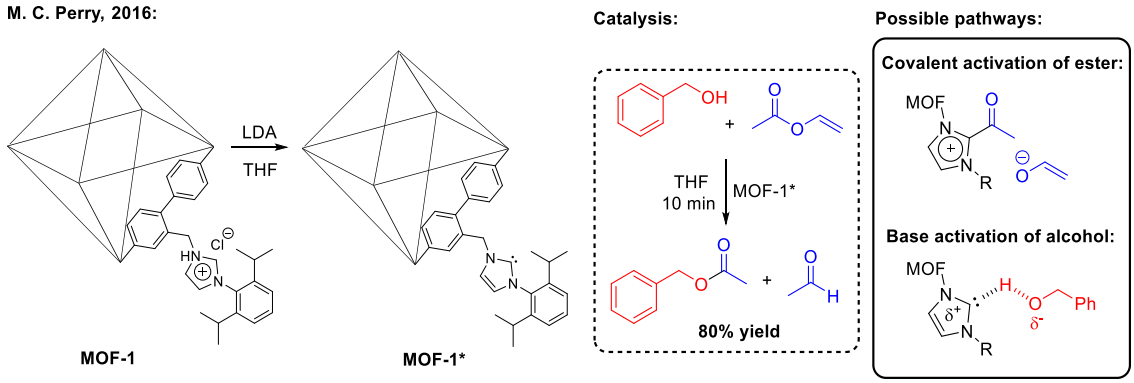

Scheme 46. MOF with N-heterocycle carbene catalytic centres.

7.2.3. Hydrogen bond organocatalysis

Some very frequent moieties used as hydrogen bond donors in organocatalysis are the ureas,[111a] thioureas[111a-f] and squaramides[111g]. These subunits are weak Lewis acids, which are capable of donating two hydrogen bonds to a substrate in order to activate it. For example, a thiourea can bind to the oxygen of an epoxide, which polarizes the C-O bond of the epoxide, weakening the bond and making the carbon more electrophilicic to suffer a nucleophilic attack and subsequent ring opening (Scheme 47B).[112a] Other similar example is the coordination of the thiourea to the nitro group of nitrostyrenes, which polarizes the molecule, activating it for a Michael addition (Scheme 47C).[112b] Although these subunits are efficient catalysts, they can undergo self-assembly (especially ureas and squaramides), decreasing their solubility and blocking their catalytic centre (Scheme 47A),[99,113] which leads to a reduction of the catalytic

[109] J. H. Cavka, S. Jakobsen, U. Olsbye, N. Guillou, C. Lamberti, S. Bordiga, K. P. Lillerud, *J. Am. Chem. Soc.* **2008**, *130*, 13850–13851.
[110] W. T. Schumacher, M. J. Mathews, S. A. Larson, C. E. Lemmon, K. A. Campbell, B. T. Crabb, B. J.-A. Chicoine, L. G. Beauvais, M. C. Perry, *Polyhedron*, **2016**, *114*, 422–427.
[111] a) S. J. Connon, *Chem. Commun*. **2008**, 2499–2510. b) P. R. Schreiner, *Chem. Soc. Rev.* **2003**, *32*, 289-296. c) Y. Takemoto, *Chem. Pharm. Bull.* **2010**, *58*, 593-601. d) E. Marqués-López y R. P. Herrera, *An. Quím.* **2009**, 10, 05−12 e) S. Beckendorf, S. Asmus, O. García Mancheño, *ChemCatChem* **2012**, *4*, 926 – 936 f) Z. Zhang, Z. Bao, H. Xing, *Org. Biomol. Chem.* **2014**, *12*, 3151–3162. g) R. I. Storer, C. Aciroa, L. H. Jones, *Chem. Soc. Rev*. **2011**, *40*, 2330–2346.
[112] a) S. S. Chimni, N. Bala, V. A. Dixit, P. V. Bharatam, *Tetrahedron*, **2010**, 66, 3042–3049. b) G. Dessole, R. P. Herrera, A. Ricci, *Synlett* **2004**, *13*, 2374–2378.
[113] a) I. G. Sonsona, E. Marqués-López, M. Häring, D. Díaz Díaz, R. P. Herrera, *Catalysts* **2018**, *8*, 305. b) A. Berkessel, F. Cleemann, S. Mukherjee, T. N. Müller, J. Lex, *Angew. Chem. Int. Ed.* **2005**, *44*, 807 –811.

activity. Immobilizing these moieties in porous materials as MOF[114] could avoid this "self-quenching", so the catalytic centres would be free to activate the reagents that flow through the pores.

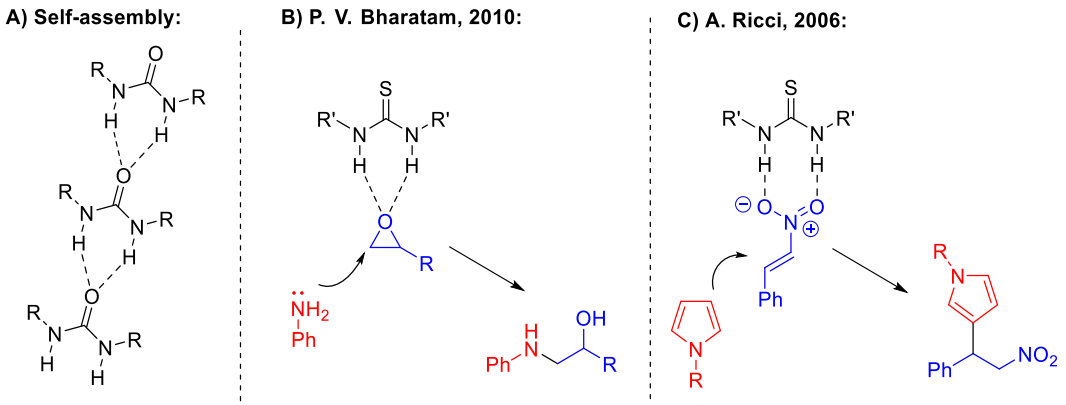

Scheme 47. A) Self-assembly of urea derivative. **B** and **C)** Activation of electrophiles by thiourea hydrogen bond.

The urea is normally incorporated to the MOFs by bottom-up strategy and does not need a post-synthetic deprotection or activation.[114, 115] In the literature there are some examples where the urea is presented attached to the ligands as a pending arm,[115b,e] (in a similar way than the pyrrolidines attached to the MOF and COF shown in the previous section). However, other important strategy to incorporate this unit is the design of a ligand where the catalytic unit is longitudinally part of the ligand itself and not a bifurcation.[115a,c,d] A representative example of this concept is the ditopic ligand H_2-urea shown in Scheme 48A, which was used by Junk *et al.* in 2015 in combination with Zn^{2+} and the pilar ligands bipy or bpe to create the TMU-18 and the TMU-19. In these two MOFs, the catalytic unit, the urea, is part of the backbone of the MOF (Scheme 48A).[115c] Although in a relaxed conformation of the ligand H_2-urea, the directionality of the two carboxylic acids is not linear, the angles of the ligand are flexible enough to adopt an almost linear conformation when is part of the MOF. The aperture of epoxides by alcohols was catalysed by these MOFs more efficiently than using the molecular urea as catalyst.

A different approach had to be used for the incorporation of thiourea to the MOF, since this functional group is more thermally unstable than urea and it does not tolerate the harsh conditions of a solvothermal synthesis. In 2014 Wang's group followed a post-synthetic modification strategy of IRMOF-3,[87] which is an analogue of MOF-5 that contains one amine group in each aromatic ring. In this strategy they added isothiocyanate in basic conditions to the IRMOF-3, which reacted with the amine groups forming thiourea moieties as pending arms. (Scheme 48B).[116] This MOF activated efficiently the benzaldehyde for the acetalisation and the Morita–Baylis–Hillman reactions.

---

[114] J. V. Alegre-Requena, E. Marqués-López, R. P. Herrera, D. Díaz Díaz, *CrystEngComm*, **2016**, *18*, 3985–3995.

[115] a) J. M. Roberts, B. M. Fini, A. A. Sarjeant, O. K. Farha, J. T. Hupp, K. A. Scheidt, *J. Am. Chem. Soc.* **2012**, *134*, 3334−3337. b) P. W. Siu, Z. J. Brown, O. K. Farha, J. T. Hupp, K. A. Scheidt, *Chem. Commun.* **2013**, *49*, 10920—10922. c) A. A. Tehrani, S. Abedi, A. Morsali, J. Wang, P. C. Junk, *J. Mater. Chem. A* **2015**, *3*, 20408–20415. d) X.-J. Wang, J. Li, Q.-Y. Li, P.-Z. Li, H. Lu, Q. Lao, R. Ni, Y. Shia, Y. Zhao, *CrystEngComm*, **2015**, *17*, 4632–4636. e) Incorporation of urea by post-synthetic modification: X.-W. Dong, T. Liu, Y.-Z. Hu, X.-Y. Liu, C.-M. Che, *Chem. Commun.* **2013**, *49*, 7681—7683.

[116] Y. Luan, N. Zheng, Y. Qi, J. Tang, G. Wang, *Catal. Sci. Technol.* **2014**, *4*, 925–929.

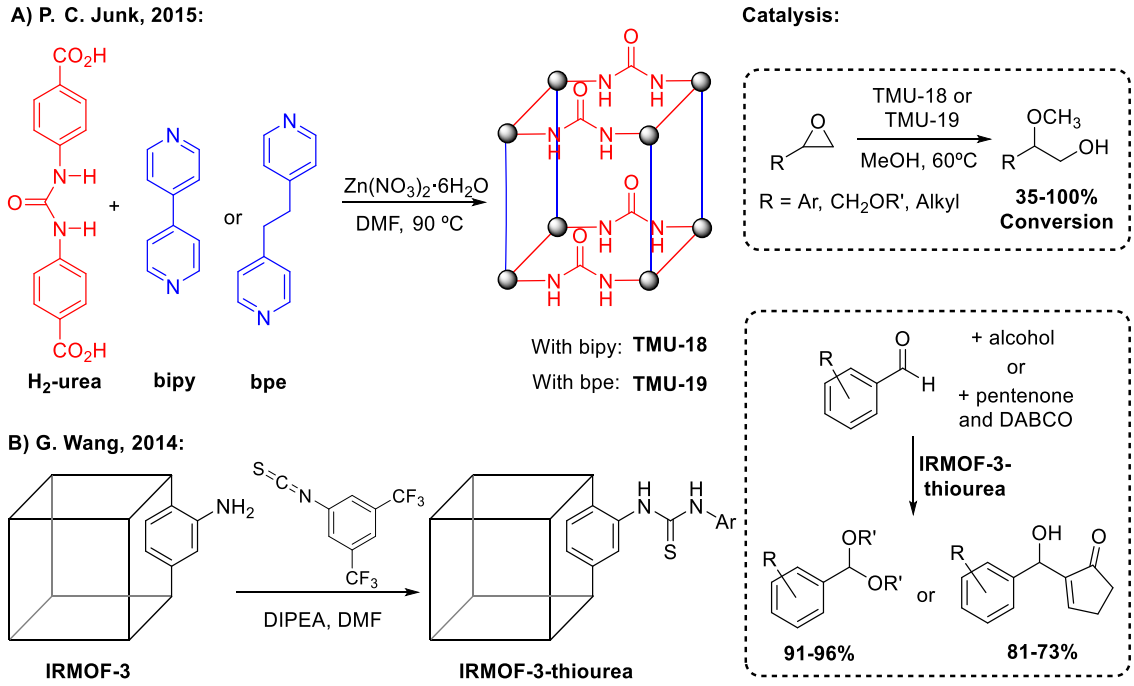

Scheme 48. MOFs with urea and thiourea moieties.

There are some works where squaramide has been attached to MOFs, which are especially relevant in this doctoral thesis, and were published during our investigations. In the two works shown in Scheme 49 the squaramide moiety is incorporated by bottom-up strategy. In 2015 Mirkin *et al.* created an analogue of MOF UiO-67[109] mixing the usual ligands of this MOF (the H_2-bpdc) with H_2-squar, a similar ligand with a squaramide moiety as a bifurcation, creating the UiO-67-Squar/bpdc (Scheme 49A).[117] Taking as model reaction the Friedel-Crafts of indols with nitrostyrenes, they carried out very interesting kinetic studies and demonstrated that the UiO-67-Squar/bpdc catalysed the reaction more efficiently than the same MOF with attached ureas or without any hydrogen bond donor. Very similar to the example shown is Scheme 45A, the more efficient MOF was the one that was synthesised mixing the ligands H_2-bpdc and H_2-squar in a 1/1 ratio. However, when the MOF was made entirely with the ligand H_2-squar it was a worse catalyst, because the channels were saturated with the squaramide pending arms and the reactants did not flow properly inside the MOF.

In 2016 Cohen *et al.* designed a ligand called "dbda" where the squaramide was longitudinally part of it, to create the Zn(dbda), a MOF in which the squaramide was part of the backbone (Scheme 49B).[118] The author also chose the Friedel-Crafts for testing the catalytic activity of the MOF. This MOF, whose metal was the Zn(II), was unstable in the reaction conditions and did not succeed in the catalysis. They carried out a post synthetic exchange of these metal centres by cupper centres, obtaining the Cu(dbda), a MOF which was structurally similar. They checked that a 99% of the metal centres had been exchanged and, curiously, the Cu(dbda) could not be directly synthesised by solvothermal conditions. The Cu(dbda) was stable under the reaction conditions and could catalyse successfully the Friedel-Crafts reaction.

[117] C. M. McGuirk, M. J. Katz, C. L. Stern, A. A. Sarjeant, J. T. Hupp, O. K. Farha, C. A. Mirkin, *J. Am. Chem. Soc.* **2015**, *137*, 919−925.
[118] X. Zhang, Z. Zhang, J. Boissonnaulta S. M. Cohen, *Chem. Commun.* **2016**, *52*, 8585−8588.

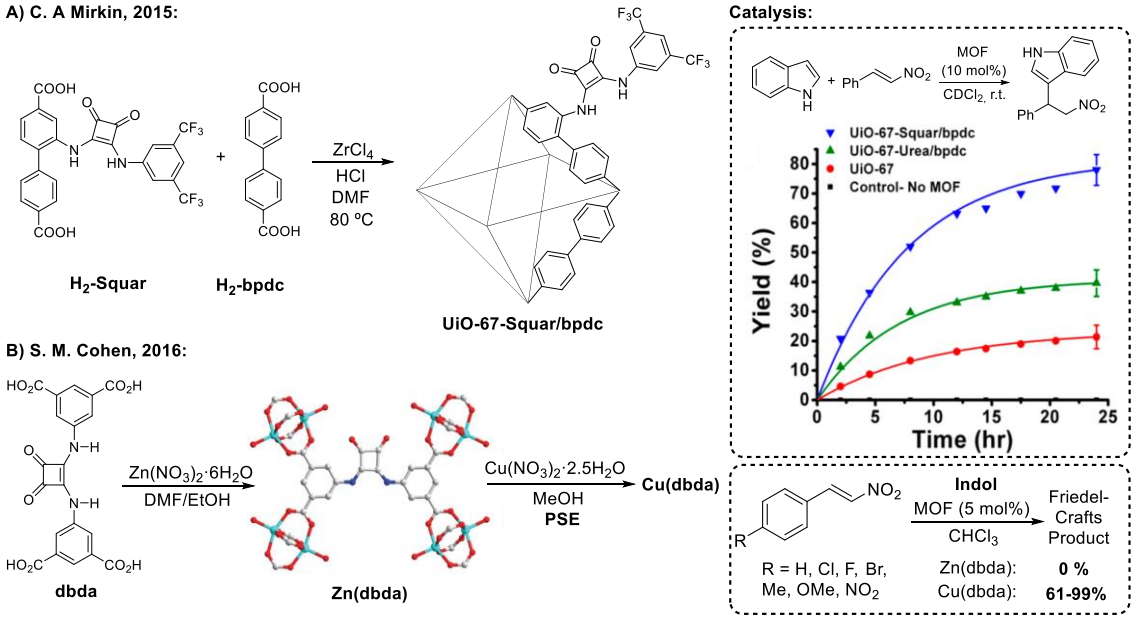

Scheme 49. MOFs with squaramide moieties. Kinetics plot reprinted with permission from Ref. 117. Copyright 2015 American Chemical Society. Structure of Zn(dbda) reproduced from Ref. 118 – Published by the Royal Society of Chemistry.

In the field of COFs, the hydrogen bond catalysis has not been so extensively developed as in the field of MOF. However, some interesting examples can be found. Two COFs containing ureas as a part of their backbone, the COF-117 and the COF-118, have been synthesised by Yaghi *et al.* in 2018, but the catalytic activity was not checked.[119] After the works made in this doctoral thesis, a new work about COF functionalized with squaramides was published, synthesised by Zhang and co-workers in 2019. They incorporated the squaramide by bottom-up strategy to a layerd COF (analogue of $2DP_{1+5}$),[120] which was called COF-SQ (Scheme 50).[121] The COF-SQ catalysed the Michael addition of 1,3-dicarbonyl compounds to nitrostyrenes with good yields.

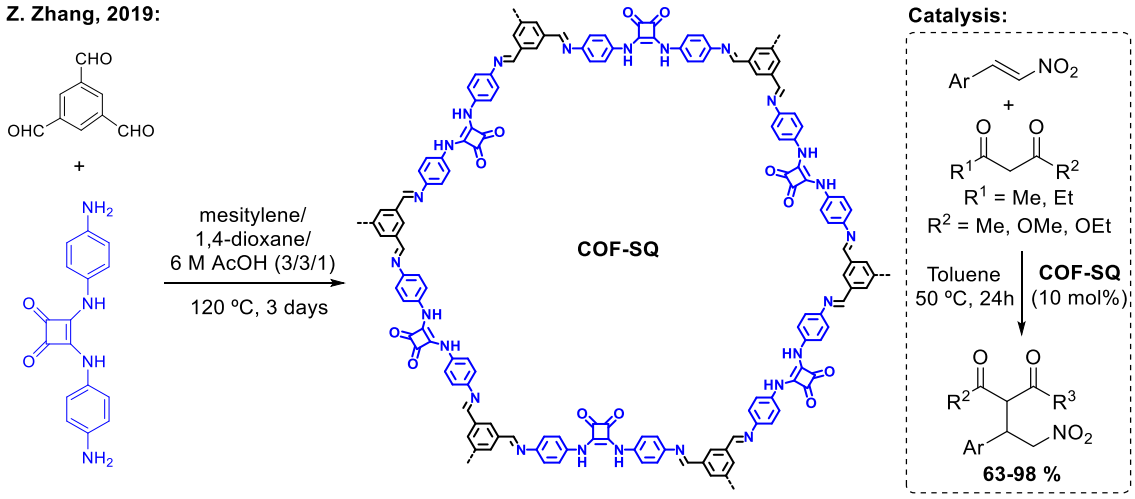

Scheme 50. COF with squaramide moieties.

[119] C. Zhao, C. S. Diercks, C. Zhu, N. Hanikel, X. Pei, O. M. Yaghi, *J. Am. Chem. Soc.* **2018**, *140*, 16438−16441.
[120] Y. Yu, J. Lin, Y. Wang, Q. Zengd, S. Lei, *Chem. Commun.* **2016**, *52*, 6609—6612.
[121] X. Li, Z. Wang, J. Sun, J. Gao, Y. Zhao, P. Cheng, B. Aguila, S. Ma, Y. Chen, Z. Zhang, *Chem. Commun.* **2019**, *55*, 5423—5426.

7.2.4. Activation by proton exchange organocatalysis

There are a variety of works where different MOF with basic centres have been used for catalysis.[122] One of the most recent examples is a novel MOF based in europium and the ligand 4,4',4''-((1,3,5-triazine-2,4,6-triyl)tris(azanediyl))tribenzoic acid, synthesised by Zhao *et al.* in 2018 (Scheme 51A),[123] which in this text will be referred as Eu-MOF. The triamine-triazine core of the ligand provides a great number of basic centres to the MOF.

COFs materials with basic centres have been also used in catalysis, being a recent example the LZU-301.[124] This COF has the same topology than COF-300[95] and, like this, the ligands are linked by imine bonds (Scheme 51B). This imine functional groups and the pyridine motifs of the ligands are basic centres that can act together in catalysis.

The Knoevenagel condensation between benzaldehyde derivatives and malonitrile is a reaction commonly used to check the catalytic power of basic materials, since the malonitrile needs to be deprotonated for the reaction to take place (Scheme 51A-B). The Eu-MOF catalysed efficiently this reaction for several benzaldehyde derivatives in three hours. The LZU-301 COF also catalysed the reaction, and it was discovered that the bigger the benzaldehyde was, the lower yield was obtained, which demonstrated that there was a size selectivity and the big reactants did not fit properly into the channels of the COF.

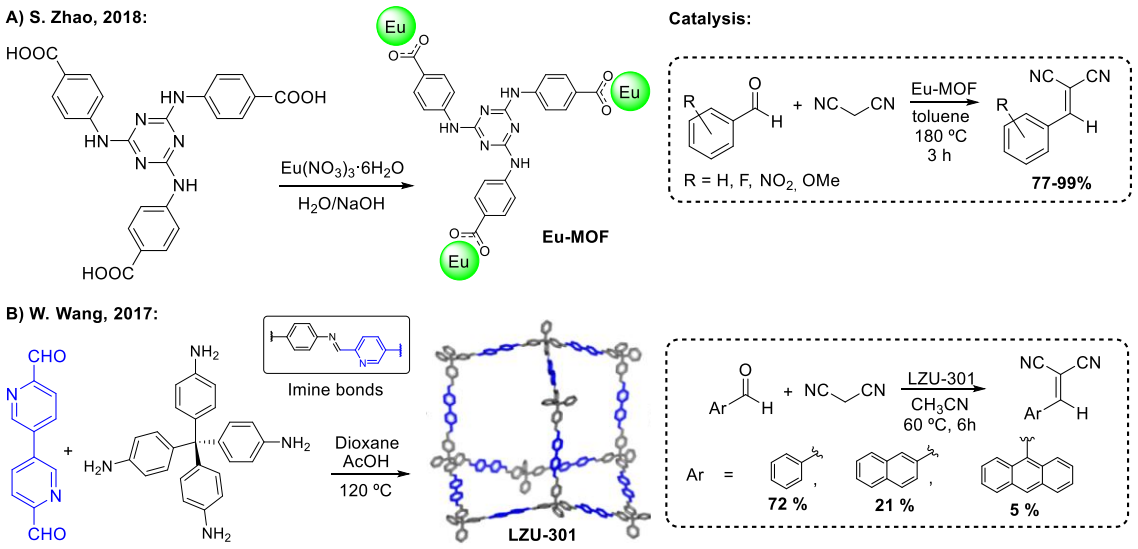

Scheme 51. MOF and COF with basic catalytic activity. Structure of LZU-301 adapted with permission from Ref. 124. Copyright 2017 American Chemical Society.

There are diverse works about catalysis with MOFs in which the catalytic centres are the metal centres that are unsaturated and can act as Lewis acid.[90e-f] However, it is possible to find works in the literature about MOFs with catalytic Brønsted organic acids in the ligands.[125a-b] For example, in 2014, Jiang *et al.* used the 2-sulfoterephthalic acid to constructed an analogue of MIL-101,[107] the MIL-101-SO_3H (Scheme 52A).[125b] The two carboxylic acids of the ligand are

[122] L. Zhu, X.-Q. Liu, H.-L. Jiang, L.-B. Sun, *Chem. Rev.* **2017**, *117*, 8129−8176.
[123] S. Zhao, *J. Mol. Struct.* **2018**, *1167*, 11-15.
[124] Y.-X. Ma, Z.-J. Li, L. Wei, S.-Y. Ding, Y.-B. Zhang, W. Wang, *J. Am. Chem. Soc.* **2017**, *139*, 4995−4998.
[125] a) G. Akiyama, R. Matsuda, H. Sato, M. Takata, S. Kitagawa, *Adv. Mater.* **2011**, *23*, 3294–3297. b) Y.-X. Zhou, Y.-Z. Chen, Y. Hu, G. Huang, S.-H. Yu, H.-L. Jiang, *Chem. Eur. J.* **2014**, *20*, 14976 – 14980.

coordinating the chromium centres, but the sulfonic group is free to act as catalyst. The authors proved satisfactorily its activity in the aperture of epoxides in methanol.

There are several works in the literature in which metal ions are coordinated to basic centres of the COF in a post-synthetic modification, and these metal act as Lewis acid in catalysed reactions.[98] Parallel to MOFs, there are also some examples where organic Brønsted acids are attached to the material. The ligand 2,5-diaminobenzenesulfonic acid was utilized to make the TFP-DABA (Scheme 52B),[126] an analogue of TpPa-1,[127] in which the sulfonic acids are free, for example, to catalyse the dehydration of fructose into 5-hydroxymethylfurfural.

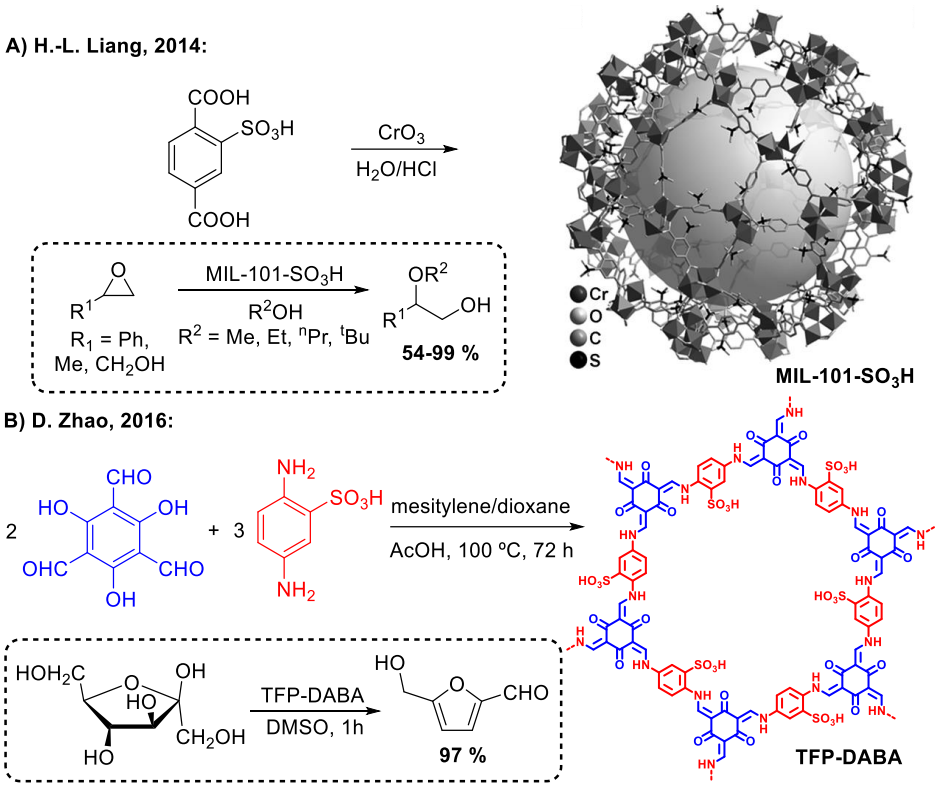

Scheme 52. MOF and COF with acidic catalytic activity. Structure of MIL-101-SO_3H reproduced from Ref. 125b with permission from John Wiley and Sons.

7.2.5. Bifunctional catalysis

The great versatility in preparing tailored MOFs and COFs allows to introduce more than one catalytic centres in these materials. Selecting a material platform with suitable dimensions is critical to carry out bifunctional catalysis, since the different catalytic centres must be in an appropriate distance to each other to act cooperatively. This target has been accomplished in both MOF and COF fields.

The ligand TBP (Scheme 53A, left) is a photoactive species and can undergo processes of single electron transfer when it is excited with light. In 2007 Lee *et al.* demonstrated that the MOF resulting of the mixture of this ligand with Zn^{2+} in ethanol under solvothermal condition,

[126] Y. Peng, Z. Hu, Y. Gao, D. Yuan, Z. Kang, Y. Qian, N. Yan, D. Zhao, *ChemSusChem* **2015**, *8*, 3208 – 3212.
[127] S. Kandambeth, A. Mallick, B. Lukose, M. V. Mane, T. Heine, R. Banerjee, *J. Am. Chem. Soc.* **2012**, *134*, 19524−19527.

the $[Zn_3(ntb)_2(EtOH)_2]_n{\cdot}4n$EtOH, had very versatile coordinatively unsaturated metal sites (CUSs),[128] since they could remove and anchor again molecules of ethanol to the Zn atoms of the MOF clusters (not shown). In 2012, Duan and co-workers made a solvothermal synthesis with the TBP ligand and $Zn(NO_3)_3{\cdot}6H_2O$ in the presence of *L*-BCIP, which is a chiral pyrrolidine bonded to an imidazole ring (Scheme 53A).[129] This synthesis yielded a MOF in which the TBP was the bridge between the clusters and de *L*-BCIP was a terminal ligand, bonded by the imidazole nitrogen. A post synthetic deprotection of the pyrrolidine gave the final MOF Zn-PYI1. The two catalytic centres could act cooperatively and allow to perform light-driven α-alkylation of aldehydes: the excited triphenylamine reduces the bromomalonitrile by single electron transfer (SET), provoking the scission between the bromine anion and the radical malonitrile. This radical attacks to the enamine formed by the condensation of the aldehyde and the pyrrolydine centre.

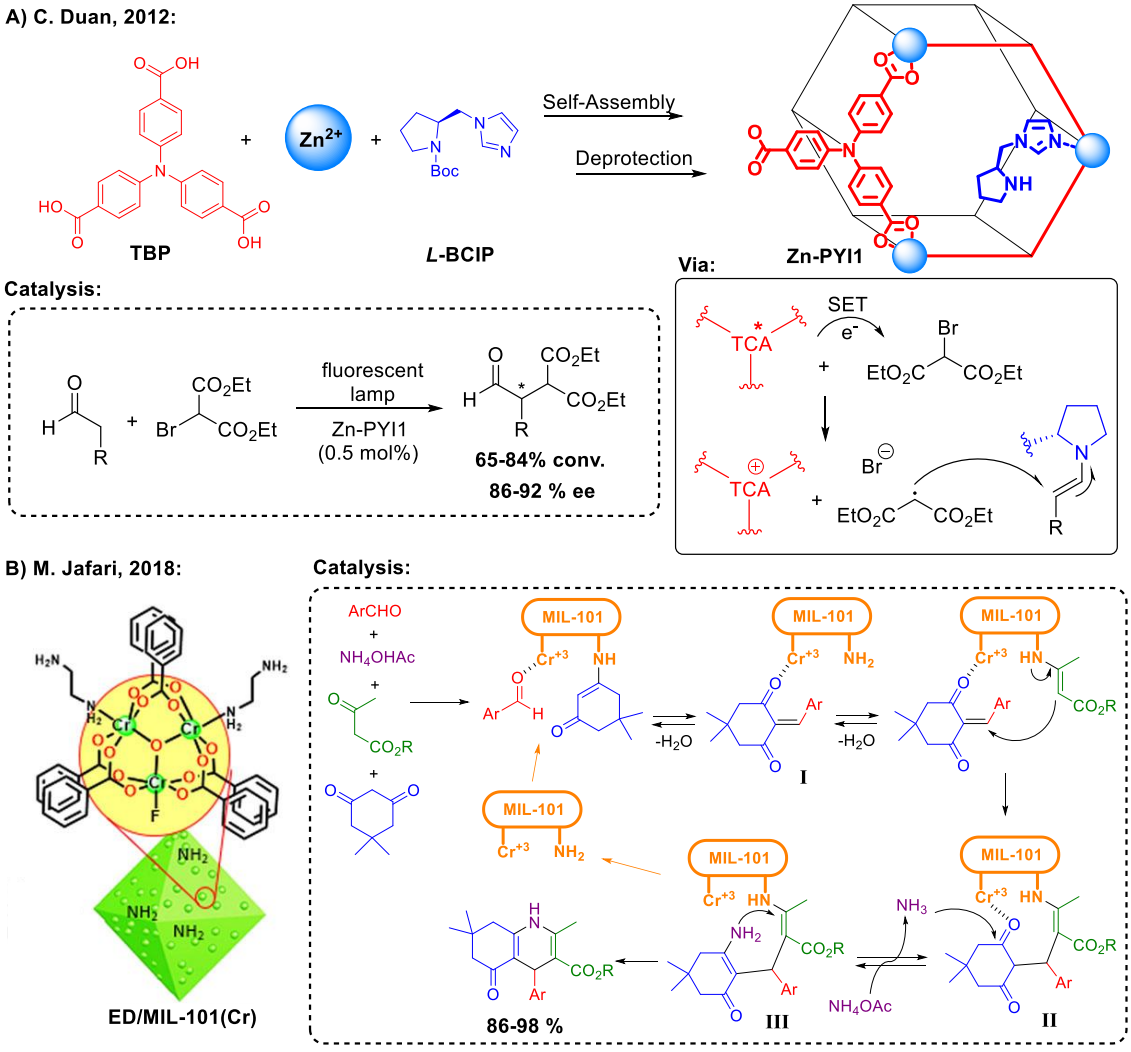

Scheme 53. Bifunctional catalytic MOFs. Structure of ED/MIL-101(Cr) reproduced from Ref. 130 with permission from John Wiley and Sons.

In 2018 Jafari *et al.* synthesised the ED/MIL(Cr), a very similar MOF to the one shown in Scheme 44B (the CDMIL-4),[106] with ethylene diamine (NH_2-CH_2-CH_2-NH_2) anchored to the CUSs of the MIL-101.[107] They demonstrated that the free amines and the chromium metal centres of

[128] M. P. Suh, Y. E. Cheon, E. Y. Lee, *Chem. Eur. J.* **2007**, *13*, 4208 – 4215.
[129] P. Wu, C. He, J. Wang, X. Peng, X. Li, Y. An, C. Duan, *J. Am. Chem. Soc.* **2012**, *134*, 14991−14999.

this MOF could act cooperatively catalysing the multicomponent Hantzsch reaction between dimedone, benzaldehyde, a β-ketoester, and an ammonia salt (Scheme 53B).[130] The first step in the condensation of the benzaldehyde, activated by coordination to the Cr^{3+}, and the dimedone, activated via enamine to give intermediate **I**. This intermediate **I** is attacked by the enamine formed by the β-ketoester and the amine of the ED/MIL(Cr), forming intermediate **II**. Then, intermediate **II** is activated by coordination to Cr^{3+} and is converted to **III** by addition of ammonia. Finally, intermediate **III** affords final polyhydroquinoline by intermolecular nucleophilic cyclization process. This reaction has been catalysed with different homogeneous and heterogeneous catalysts and the authors assert that they obtained the highest yield (>98 %) with the ED/MIL(Cr).

A simple strategy to develop bifunctional catalytic structures is to construct a material with both acidic and basic centres. However, opposite to MOFs, the COFs do not have metal centres that can act as Lewis acids, so it is important to make strategies to incorporate both centres. A representative example is the 2,3-DhaTph, synthesised by Banerjee *et al.* in 2015, which is 2D COF (analogue of COF-366)[131] that linked porphyrins and 2,3-dihydroxyterephtaldehyde by imine bonds (Scheme 54A).[132] This COF could catalyse the one-pot synthesis of 2-benzylidenemalononitrile (**3**), beginning from benzaldehydedimethylacetal (**1**): the two aromatic hydroxyl groups were acid enough to carry out the deacetalization of benzaldehydedimethylacetal (**1**) into benzaldehyde (**2**), and the basic porphyrins deprotonates the malonitrile to undergo a Knoevenagel condensation with benzaldehyde (**2**) to yield the final product (**3**). The immobilization of the acidic and basic catalytic groups in the material avoids that they neutralize to each other, which would nullify the catalysis.

To demonstrate that the 2,3-DhaTph was acting actually as a bifunctional catalyst they synthesised the 2,3-DmaTph, an analogue COF with methoxyl groups instead of hydroxyl groups and used it in the same one-pot reactions. In the same reaction time, the conversions with 2,3-DmaTph were always the half of the conversion obtained with 2,3-DhaTph, approximately, demonstrating that both functional groups, the hydroxyls and the porphyrins were necessary for an optimal catalytic process.

In 2016 Qiu and co-workers designed the DL-COFs, which were a series of 3D COF whose ligands were linked by imine bond, which is a basic subunit, and by boroxine bond, which is an acidic subunit (Scheme 54B).[133] The presence of these two moieties allowed this COF to catalyse the same one-pot synthesis of 2-benzylidenemalononitrile described in the previous paragraph and they also monitored the evolution of reactant, intermediate and final product. The interest of this work is that they took advantage of both types of chemical bonds that linked the ligands and did not have to add extra functional groups.

[130] S. Rostamnia, H. Alamgholiloo, M. Jafari*, Appl. Organomet. Chem.* **2018**, *32*, e4370.
[131] S. Wan, F. Gándara, A. Asano, H. Furukawa, A. Saeki, S. K. Dey, L. Liao, M. W. Ambrogio, Y. Y. Botros, X. Duan, S. Seki, J. F. Stoddart, O. M. Yaghi, *Chem. Mater.* **2011**, *23*, 4094–4097.
[132] D. B. Shinde, S. Kandambeth, P. Pachfule, R. R. Kumar, R. Banerjee, *Chem. Commun.* **2015**, *51*, 310—313.
[133] H. Li, Q. Pan, Y. Ma, X. Guan, M. Xue, Q. Fang, Y. Yan, V. Valtchev, S. Qiu, *J. Am. Chem. Soc.* **2016**, *138*, 14783−14788.

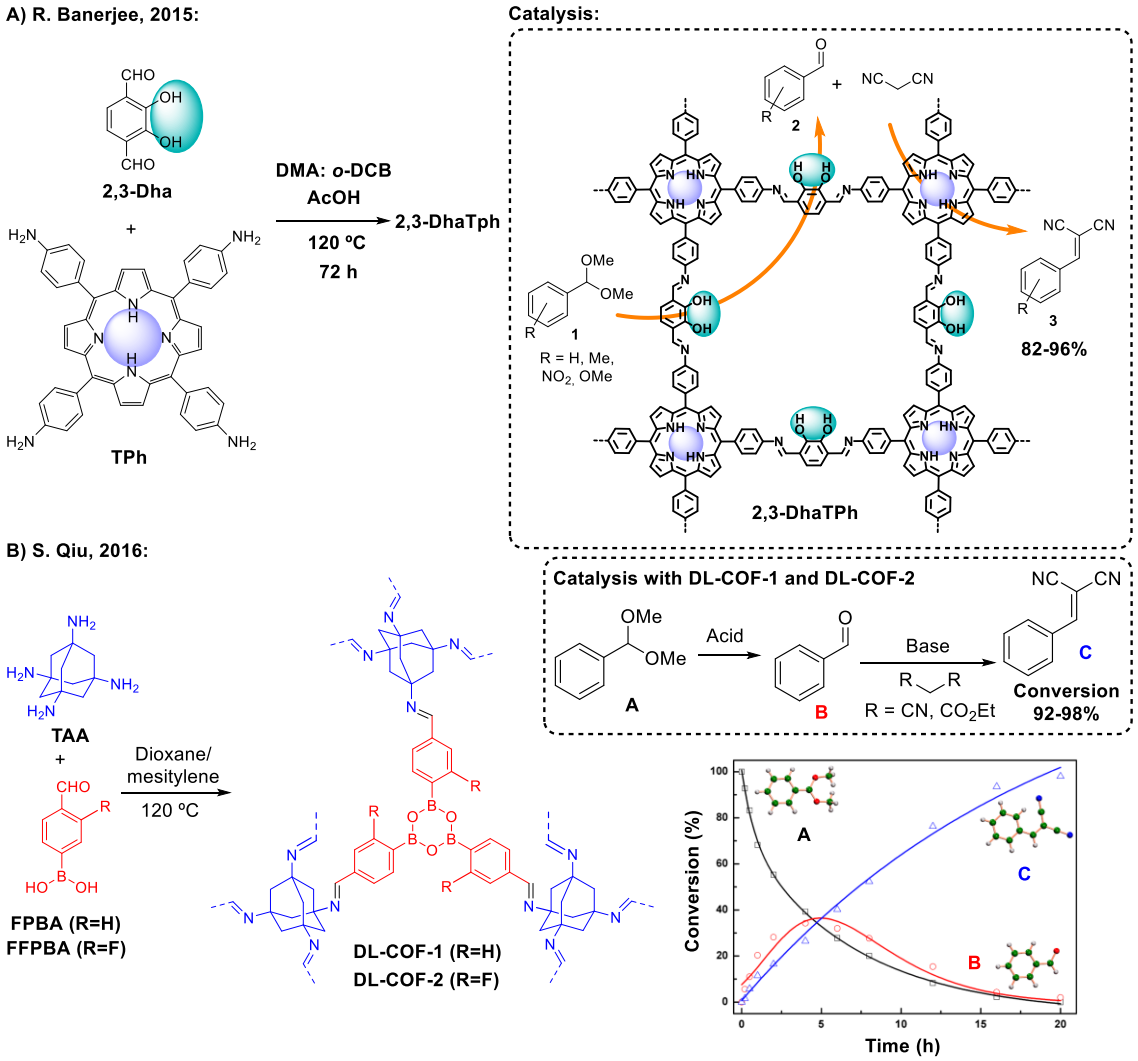

Scheme 54. Bifunctional catalytic COFs. Kinetics plot reprinted with permission from Ref. 133. Copyright 2016 American Chemical Society.

7.2.6. Confinement effects

There are some cases in which the use of a MOF or a COF as catalyst can present great advantages, not only for having the catalytic centres attached to a heterogeneous platform, but rather for carrying out the reaction in confined spaces, *i.e.*, inside the pores of the materials. This confinement can be responsible of changes in the chemical selectivity of the reaction. Scheme 55 gathers works where the confinement of the reactants and intermediates inside the pores of materials are especially relevant.

In 2012 Lin *et al.* developed a MOF which contains chiral phosphoric acid in its structure and checked its catalytic activity with the Friedel-Crafts reaction between the indol and imines (Scheme 55A).[134] Curiously, the product that they obtained using this MOF was the *R* enantiomer, but when they used a structurally similar homogeneous phosphoric acid with the same configuration of the one inside the MOF, they obtained the *S* enantiomer. Computational studies revealed the origin of this change in the enantioselectivity. In Scheme 55A (right, top), it

[134] M. Zheng, Y. Liu, C. Wang, S. Liu, W. Lin, *Chem. Sci.* **2012**, *3*, 2623–2627.

can be seen the calculated less energetic transition state of the reactions with the homogeneous catalyst, which leads the reaction to the *S* product. However, when an equivalent transition state is calculated inside the MOF material, the reactants do not fit properly inside the channel and there is steric hindrance with the walls of the MOF, making the transition state very high in energy, so the reactants must achieve other arrangement. Scheme 55A (right, bottom) shows the less energetic transition state inside the channel, which leads to the *R* enantiomer.

Ranocchiari, Bokhoven and co-workers have several works in which they study confinement effects in MOF.[135] In 2014 they synthesised the LSK-3, an IRMOF-9 analogue,[87] which have attached phosphine groups to some of the ligands (Scheme 55B).[135b] They checked its catalytic power with several reactions which were well-known to be catalysed by phosphines by covalent interactions, such as the coumarin synthesis from alkynes and the umpolung addition. Interestingly, some reactions were efficiently catalysed by the LSK-3, such as the coumarin synthesis (reaction I), but the LSK-3 was not able to catalyse at all other reactions, like the umpolung addition (reaction II), although both reactions were totally catalysed by molecular PPh_3. They studied these reactions in greater depth to understand this effect. In the coumarin synthesis (reaction I) the first step is the formation of a zwitterionic species between the alkyne and the phosphine moiety. The next step is the deprotonation of the phenol by the zwitterion; subsequent nucleophilic attack, release of the catalyst and cycle closure leads to the coumarin. The umpolung reaction shares a similar mechanism (reaction II): it begins with the attack of the phosphine moiety to the allene to form the zwitterion, which then deprotonates the malonitrile and leads to subsequent reaction until the addition product formation. Experimental studies show that when these two reactions are set up using the LSK-3 as catalyst the zwitterion is formed in both cases, but only in the case of coumarin formation the deprotonation and subsequent reactions takes places. Computational calculations explain this chemical selectivity. Scheme 55B (bottom) shows the most stable structures for the zwitterionic intermediates attached to the MOF of both reactions. In the case of the coumarin formation (**intermediate I**), the negative carbon is fully available for the access of the phenol for the deprotonation step (the yellow arrow indicates the access place for the base). However, in the case of the umpolung addition, in the zwitterion (**intermediate II**) the negative charge is oriented to the walls of the MOF and the access of the malonitrile to be deprotonated would suffer high steric hindrance. Other orientation of the zwitterion is much higher in energy. Therefore, although there is enough space inside the channel of MOF for all the reactants to fit, the imposition of the orientation of the intermediates by the MOF and the steric hindrance of the walls of the channel avoids the reaction.

[135] a) X. Xu, J. A. van Bokhoven, M. Ranocchiari, *ChemCatChem* **2014**, *6*, 1887 – 1891. b) X. Xu, S. M. Rummelt, F. L. Morel, M. Ranocchiari, J. A. van Bokhoven, *Chem. Eur. J.* **2014**, *20*, 15467 – 15472 c) G. Bauer, D. Ongari, X. Xu, D. Tiana, B. Smit, M. Ranocchiari, *J. Am. Chem. Soc.* **2017**, *139*, 18166−18169.

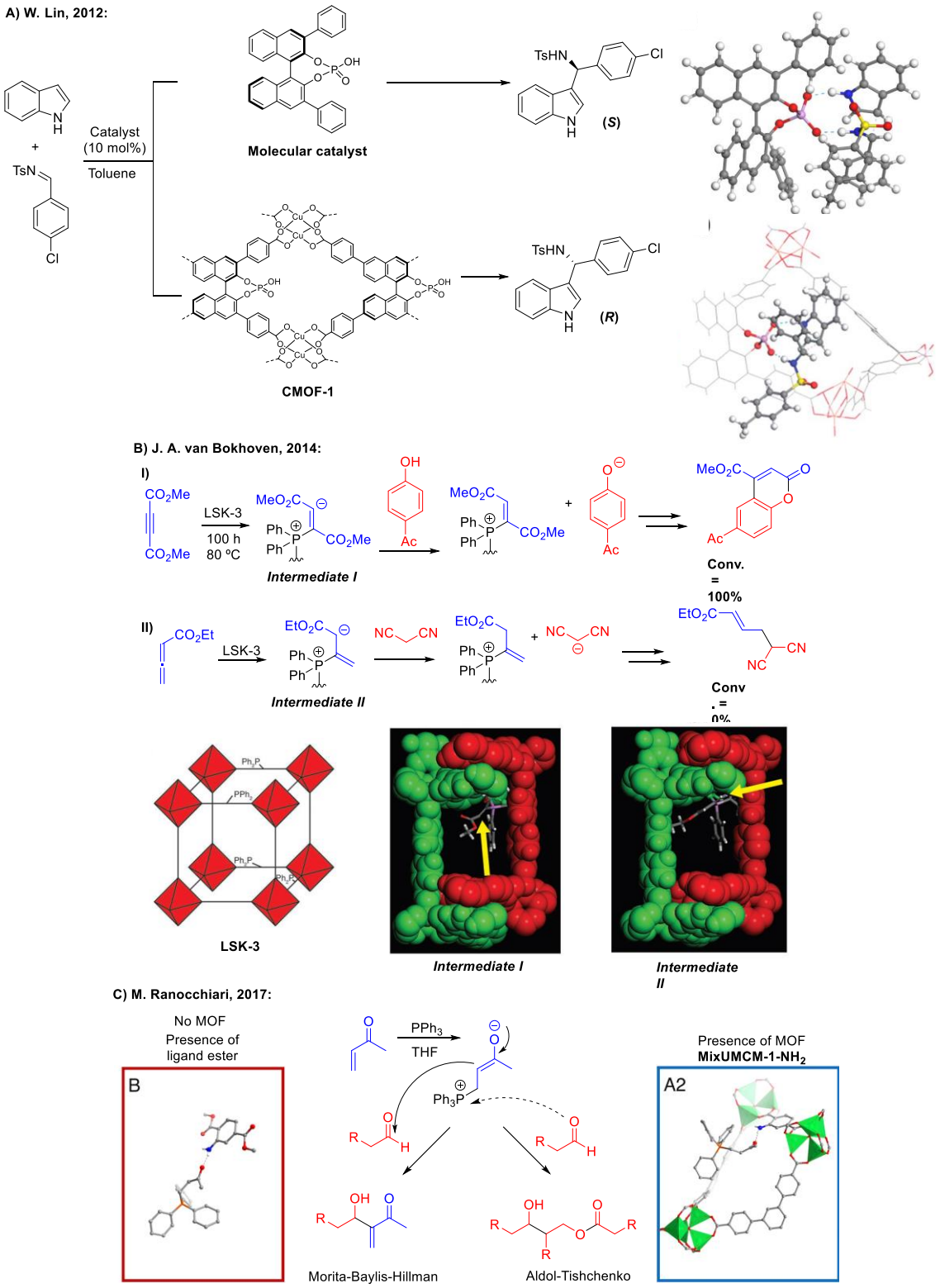

Scheme 55. Confinement effects in MOFs. Calculated structures of Scheme A reproduced from Ref. 134 with permission from The Royal Society of Chemistry. Structures of Scheme B reproduced from Ref. 135b with permission from John Wiley and Sons. Structures of Scheme C adapted from Ref. 135c Copyright 2017 American Chemical Society, ACS AuthorChoice (Open access).

Another very interesting example was carried out by Ranocchiari *et al.* in 2017, who studied confinement effects of the Morita-Baylis-Hillman reaction between the methyl vinyl ketone and aliphatic aldehydes catalysed by molecular triphenyl phosphines (Scheme 55C).[135c] In a first step, the molecular phosphine and the methyl vinyl ketone forms an zwitterionic intermediate. The α carbon of the zwitterion attacks to the carbonyl carbon of the aldehyde and subsequent steps leads to the release of the catalyst and the product formation. In the absence of MOF the expected product was obtained. However, in the presence of MixUMCM-1-NH_2 (a UMCM-1 analogue[136] with amine groups in some of the ligands), the Aldol-Tishchenko reaction took place instead of the Morita-Baylis-Hillman. In the Aldol-Tishchenko the zwitterion acts just as catalyst: The aldehyde is activated through coordination of its carbonyl oxygen with the phosphonium cation of the zwitterion, which leads to an aldol reaction and a Tishchenko reaction, yielding a product which gathers three aldehyde molecules. Control experiments shows that the zwitterion anchored to the MOF is the catalyst of the reactions. However, in the absence of MixUMCM-1-NH_2 and the presence of the aminated ligand, the zwitterion anchored to the ligand evolves to the Morita-Baylis-Hillman, showing that the Aldol-Tishchenko only happened inside the MOF. Molecular dynamics could explain the origin of this change of reactivity. Outside the MOF, the three phenyl groups shield the phosphorus of the zwitterion by steric hindrance, so the probability of the attack of the zwitterion α carbon to the aldehyde carbonyl carbon (solid arrow) is much higher than the attack of the aldehyde carbonyl oxygen to the zwitterion phosphorus (dashed line). However, the MixUMCM-1-NH_2 limits the freedom of movement of the zwitterion, distorting the tetrahedral configuration of the phosphonium moiety, increasing the probability of the attack of the aldehyde carbonyl oxygen to the zwitterion phosphorus (dashed line), which allows the Aldol-Tishchenko reaction.

In the COF field there are also works where the confinement effects gain relevance. In 2015 Jiang *et al.* designed a 2D imine-linked COF whose ligands contained pyrene and anthracene subunits and called it Py-An COF (Scheme 56).[137] It catalysed the Diels-Alder between 9-hydroxymethylanthracene and *N*-substituted maleimides. Based on crystallographic data,[138] they explained that the interaction involved in the acceleration of the reaction is a perpendicular π-π interaction (in other words, a C-H···π interaction) between the anthracene walls of the COF and the anthracene reactant. These interactions accumulate the planar reactants into the channels and lower the energetic barriers for the Diels-Alder reaction. When the reaction takes place, the product decreases in aromaticity and adapts a bent conformation, what weakens the C-H··· π interactions between the products and the π-walls and facilitates the exit of the product to be substituted for other planar and more aromatic reactant. Therefore, this is a COF in which the flow of molecules that go into the pores as reactants and leave the COF as product is especially favoured.

[136] K. Koh, A. G. Wong-Foy, A. J. Matzger, *Angew. Chem. Int. Ed.* **2008**, *47*, 677 –680.
[137] Y. Wu, H. Xu, X. Chen, J. Gao, D. Jiang, *Chem. Commun.* **2015**, *51*, 10096—10098.
[138] M. Ramos Silva, A. Matos Beja, J. A. Paixão, L. Alte da Veiga, A. J. F. N. Sobral, N. G. C. L. Rebanda, A. M. d'A. Rocha Gonsalves*, Acta Crystallogr., Sect. C: Cryst. Struct. Commun.* **2000**, *56*, 1136-1138.

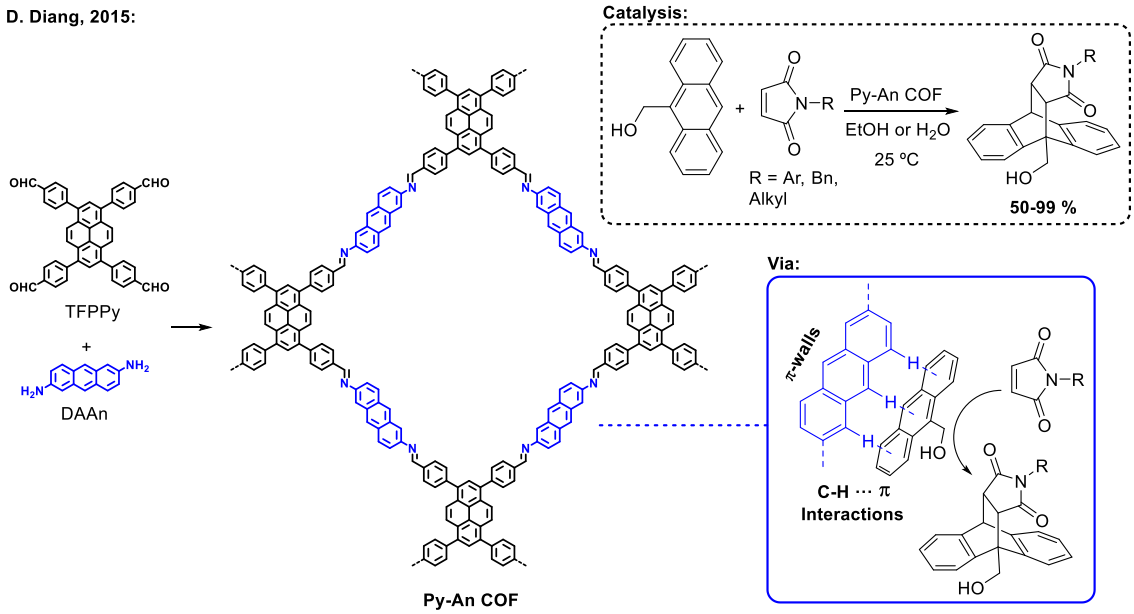

Scheme 56. Confinement effects in COFs.

As it was mentioned in the beginning of this introduction, the incorporation of organocatalytic units in the structure of MOFs and COFs seeks to maintain the properties and advantages of homogeneous organocatalysis and, at the same time, to add the advantages of the heterogeneous catalysts like the easy separation and recyclability. For this reason, these examples are very inspiring, since these materials do not only maintain the chemical activity of the organocatalytic centres that they contain, but the fact that the catalysis occurs in confinement environment confers to the catalytic processes new selectivities and even a change in the reactivity. This shows the importance of the scientific research in the emerging fields of MOFs and COFs. There are many things to discover in these versatile materials, and the investigation of new structures and new applications of COFs and MOFs can bring new concepts to the Chemistry.

7.2.7. Initial hypothesis about squaramide catalysis in MOFs

In their work, Cohen and co-workers (see above, section 7.2.3) made a comparison between the Cu(dbda) and the UiO-67-Squar/bpdc (the two MOFs with squaramides in their structures, Scheme 49) and checked that both MOFs catalysed the Friedel-Crafts reactions with approximately the same efficiency. They draw a very interesting conclusion: in Cu(dbda) the catalytic group is part of the ligand 'backbone' and in UiO-67-Squar/bpdc the catalytic squaramide is a dangling component, what make them have features that compliment and distinguish to each other. Therefore, "depending on catalyst design, one can envision scenarios where one or the other functional group arrangement might be preferable".[118]

Since the squaramide moiety is so broadly used in organocatalysis and in other fields of the Chemistry like as "ion receptors", it is very important to continue investigating these porous materials containing this functional group. It would be valuable to develop more MOFs containing squaramides with different structure to have a wider range of these materials, since each structure can be useful in different scenarios. Moreover, the works of Mirkin and Cohen

are focused in using their catalytic MOFs in the Friedel-Crafts reactions of indols to nitrostyrenes, so it is also desirable to investigate other reactions in which these frameworks can have a catalytic role.

The main advantage that the Cu(dbda) offers is that it has a 100% functional ligand incorporation without loss of surface area, as opposite to UiO-67-Squar/bpdc which only has a 50 % of ligand incorporation and the ligand pending arms represents obstacles in the flow of the reactants. On the other hand, one important disadvantage of the Cu(dbda) is that it needs a post-synthetic modification, since the original Zn atoms must be exchange by Cu to increase the stability, complicating the synthesis. A noteworthy advance would be the synthesis of a MOF containing squaramide that, as Cu(dbda), the squaramide would be part of the backbone of the MOF, but that could be synthesised in one step without post-synthetic modifications.

The objectives of this part are detailed in Section 8.1.

7.2.8. Initial hypothesis about proton exchange organocatalysis in COFs

As can be seen, the MOF and COF that catalyse reactions by acid-base proton exchange are structurally simpler that other organocatalytic materials (see above, Section 7.2.4.). For example, they do not need post-synthetic modifications and in the case of the acidic MIL-101-SO_3H (Scheme 52A) and TFP-DABA (Scheme 52B) it is only required a bottom-up strategy to use building blocks with sulfonic acids groups. The case of the basic COFs is even simpler because the basic imine bonds between the building blocks of the COF are very usual. Moreover, the building blocks with basic pyridine moieties are very frequent in both MOF and COF (for example, Scheme 51B), so it could be said that the design of catalytic basic materials does not even need a bottom-up strategy. In this sense, this type of organocatalytic MOF and COF which act by proton exchange offers a lot of possibilities and can be very useful, due to their easy synthesis and manipulation.

As can be seen during this introduction, the organocatalytic centres of MOF and COF are functional groups bonded covalently to the materials that have been incorporated by bottom-up strategy or by post-functionalization. However, it is uncommon to find MOFs or COFs where the organocatalytic centres are guest species inside the pores of the materials (as depicted as a yellow sphere in Figure 14). Therefore, it would be an interesting goal the design of porous materials with small catalytic centres inside the pores, anchored to the walls of the material by non-covalent interactions. This concept would have the advantage that one material could be used to harbour different types of catalytic molecules depending of the requirements of the catalysed reactions.

Due to the simplicity of these organic acid-base proton exchange processes, we hypothesised about anchoring small organic acids or bases as starting point for this investigation. A good candidate material to harbour small organic molecules by non-covalent interactions into the pores is the COF-300 since it is a simple material to synthesise and there are precedents in which catalytic metal centres or inorganic compounds are anchored to the pores. In 2015, Jia *et al.*, using a impregnation method, introduced phosphomolybdic acid (PMA) in COF-300 (Scheme 57A);[139] the PMA protonated the imine groups of COF-300 and the

[139] W. Gao, X. Sun, H. Niu, X. Song, K. Li, H. Gao, W. Zhang, J. Yu, M. Jia, *Microporous and Mesoporous Materials* **2015**, *213*, 59-67.

interaction between the protonated imine groups and the anions of PMA helped to disperse the PMA for all the surfaces and cavities of the material. The resulted COF, the PMA@COF-300, successfully catalysed the epoxidation of alkenes. In 2016, Esteves and co-workers functionalized the pores of COF-300 with $Pd(OAc)_2$ by coordination bond between the imine groups and the metallic centres (Scheme 57B).[140] $Pd(OAc)_2$@COF-300 was able to catalyse cross-coupling reactions, such as Suzuki–Miyaura, Heck, and Sonogashira reactions.

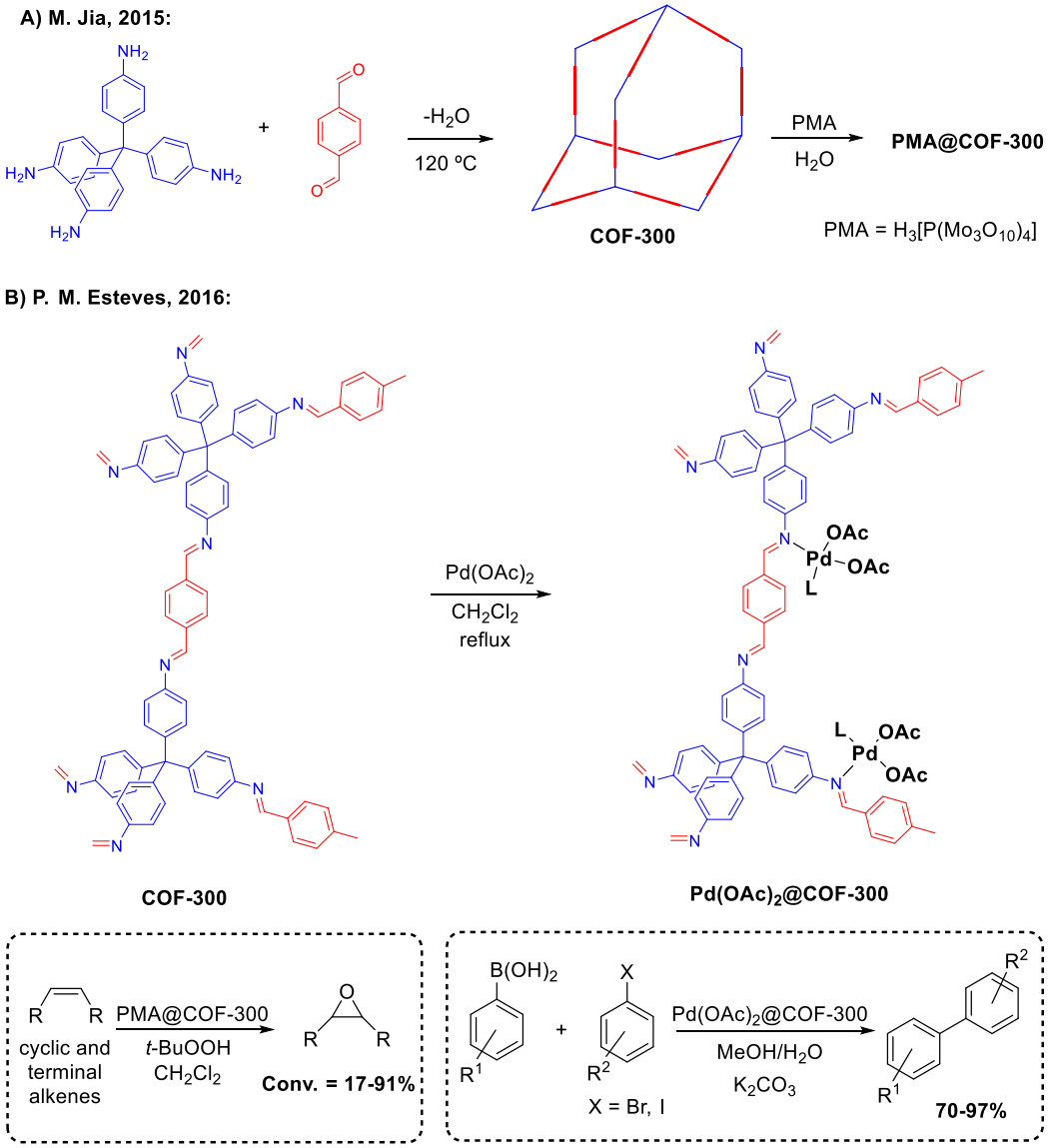

Scheme 57. Catalytic guest species in COF-300.

[140] R. S. B. Gonçalves, A. B. V. de Oliveira, H. C. Sindra, Bráulio S. Archanjo, M. E. Mendoza, L. S. A. Carneiro, C. D. Buarque, P. M. Esteves, *ChemCatChem* **2016**, *8*, 743 – 750.

These two examples show that the imine groups of COF-300, through different types of interactions, can stabilize and disperse guest species inside the pores of the material, and these species can act as catalysts. Our proposal is trying to do a parallel organocatalytic process, introducing small organic acids and bases, such as the acetic acid and the trimethylamine, inside the COF-300, which can interact with the material by non-covalent interactions. We would like to examine if one material, in this case the COF-300, can act as an acidic catalyst and/or as a basic catalyst, depending of the guest species that are in its interior (Scheme 58).

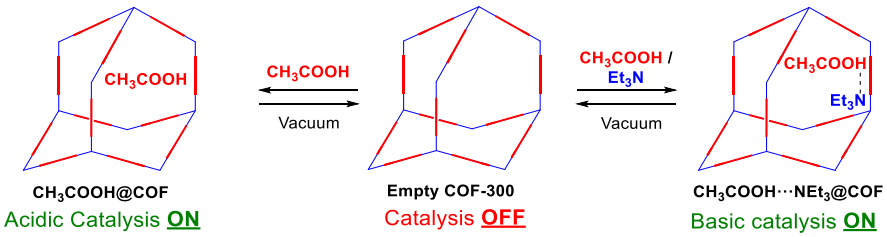

Scheme 58. Proposal of introducing catalytic small organic acids and bases inside COF-300.

The objectives related with this part can be found in Section 8.2.

8. Objectives

8.1. Squaramide-IRMOF-16 Analogue for Catalysis of Epoxide Opening

The objectives for this part are the following:

1) Synthesis of a new MOF material with squaramide groups in its backbone which does not require a post-synthetic modification.

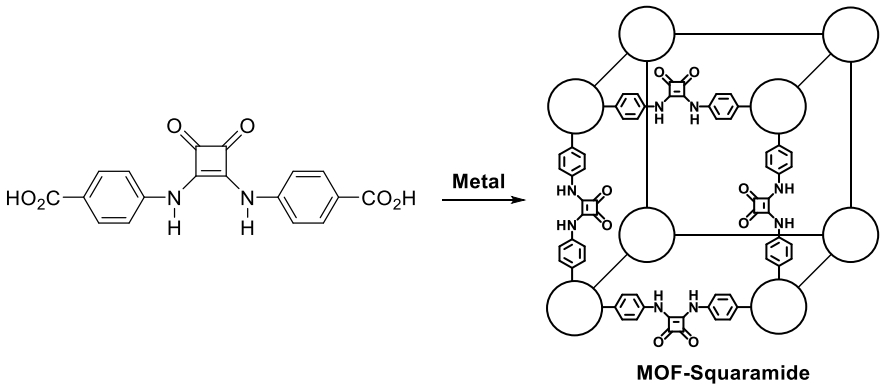

2) Characterization and structure resolution trough techniques like powder X-ray diffraction.

3) Kinetic studies of the epoxide opening by anilines catalysed by the new material. Comparison of reaction rates as a function of the size of the epoxides and anilines to study a possible size selectivity. Comparison of reaction rates between the reaction catalysed by the new material and the reaction catalysed by molecular squaramide to test the advantages of the heterogeneous catalysis versus the homogeneous catalysis.

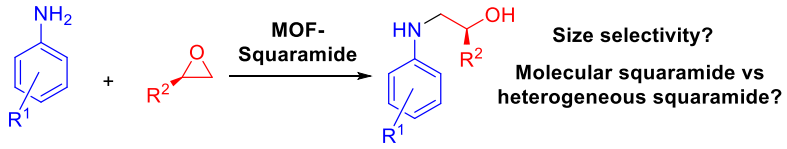

4) Use of the new catalytic material in the epoxide opening reaction with synthetic purposes. Synthesis, isolation and purification of products coming from tandem and one-pot reactions catalysed by the new MOF.

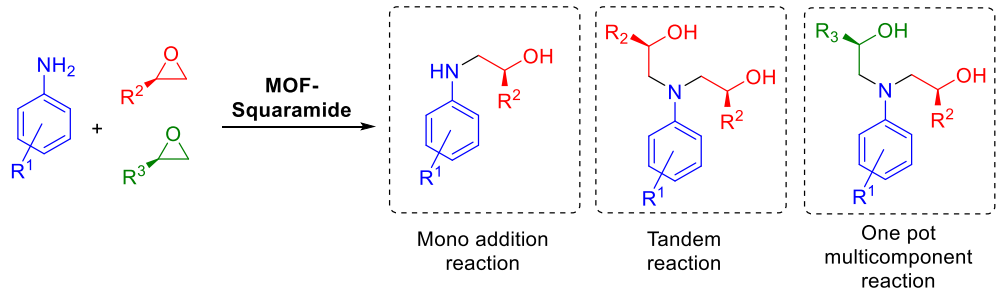

8.2 Switching Acidic and Basic Catalysis through Supramolecular Functionalization

The objectives for this part are the following:

1) Incorporation of small catalytic organic molecules in the pores of COF-300 material, like triethylamine and acetic acid.

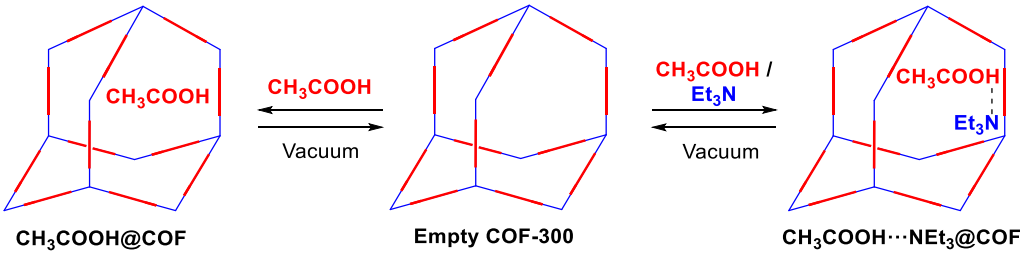

2) Characterization of these materials and verification of the presence of these molecules through different techniques, like SEM microscopy, NMR of solid state, isotopic labeling, thermogravimetric analysis…

3) Study of the catalytic effect of these materials in organic reactions: The catalytic activity of the COF with acidic centres will be tested in the epoxide opening reaction and the catalytic activity of the COF with basic centres will be tested in the Knoevenagel reaction of malonitrile and aromatic aldehydes.

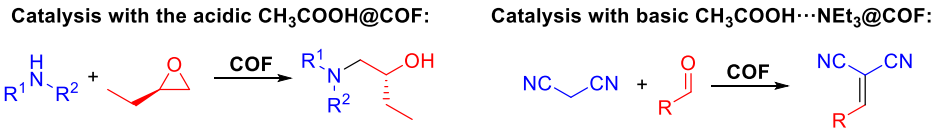

4) Leaching studies to check that the catalytic molecules act and stay inside the material throughout the course of the reaction and stability studies.

5) DFT calculation for the study of the interaction between the small organic molecules and the COF backbone and elucidation of the reaction mechanism inside the pores of the COF.

9. Publications

The works done in this doctoral thesis related to organocatalytic materials are described in the publications shown in this sections. They will appear in this order:

4. Squaramide-IRMOF-16 Analogue for Catalysis of Solvent-Free, Epoxide Ring-Opening Tandem and Multicomponent Reactions

C. Vignatti, J. Luis-Barrera, V. Guillerm, I. Imaz, R. Mas-Ballesté, J. Alemán, D. Maspoch, *ChemCatChem* **2018**, *10*, 3995– 3998.

Reprinted with permission from John Wiley and Sons.

5. Switching Acidic and Basic Catalysis in a Three-Dimensional Covalent Imine Structure through Supramolecular Functionalization

J. Luis-Barrerra, G. Imani-Shakibaei, J. Heras-Domingo, R. Cano, J. Pérez-Carvajal, I. Imaz, D. Maspoch, X. Solans-Monfort, J. Alemán, R. Mas-Ballesté, 2019, submitted to *Journal of Catalysis*.

The publication 5 has been Submitted to *Journal of Catalysis* but it has not been published yet. In this doctoral thesis the submitted version is presented.

NOTE: The publication 4 has two indicators for the number of the pages. One of the them indicates the number of the page within the journal. The other one indicates the number of the page within the doctoral thesis.

ChemPubSoc Europe

DOI: 10.1002/cctc.201801127

CHEMCATCHEM Communications

Squaramide-IRMOF-16 Analogue for Catalysis of Solvent-Free, Epoxide Ring-Opening Tandem and Multicomponent Reactions

Claudia Vignatti[+],[a] Javier Luis-Barrera[+],[b] Vincent Guillerm,[a] Inhar Imaz,*[a] Rubén Mas-Ballesté,*[c, d] José Alemán,*[b, d] and Daniel Maspoch*[a, e]

Tandem and multicomponent one-pot reactions are highly attractive because they enable synthesis of target molecules in a single reaction vessel. However, they are difficult to control, as they can lead to the formation of many undesired side-products. Herein we report the use of metal-organic framework (MOF) pores decorated with organocatalytic squaramide moieties to confine ring-opening epoxide reactions of diverse substrates. Controlled mono-addition or tandem reactions inside the pores yield 1,2-aminoalcohols or 1,2,2′-aminodialcohols, respectively, in good yields. In addition, this squaramide-functionalised MOF enables catalysis of higher-complexity multicomponent reactions such as the catalytic ring-opening of two different epoxides by a single amine to afford 1,2,2′-aminodialcohols.

Tandem reactions are among the best strategies to achieve molecular complexity in a single process.[1] They comprise two or more consecutive independent reactions, which are catalysed by one or more catalysts. Each catalyst produces an intermediate that is further transformed by a second catalytic cycle to give the final product. This translates to lower requirements for solvent, time and energy and to less waste relative to traditional processes. Consequently, tandem reactions have peaked the interest of numerous industries,[2] especially in their solvent-free form.[3]

1,2-amino alcohols (**3**) and 1,2,2′-aminodialcohols (**4**) are structural subunits that are widespread in natural products of industrial relevance.[4] Some of these natural products include (*S*,*R*,*R*,*R*)-Nebivolol, which is a β_1-adrenergic receptor blocker;[4e] Bestatin, which is an aminopeptidase inhibitor that exhibits immunomodulatory activity;[4d] Sphingosine, which is a a class of cell membrane lipids;[4d] and Cytoxazone, which is an immunomodulatory.[4d] They are also important synthetic intermediates for biologically active compounds,[4] stationary phases in HPLC,[5] and chiral ligands (e.g. Oxazaborolidine derivatives)[6a] or auxiliaries in asymmetric reactions.[6] 1,2-aminoalcohols and 1,2,2′-aminodialcohols can each be readily prepared via ring-opening of epoxides by amines. However, controlling the reaction of the amine (i.e. mono- vs. di-addition) to the epoxide is difficult, leading to mixtures of the two types of compounds.

Herein we show that confining the aforementioned reaction to metal-organic framework (MOF)[7] pores decorated with organocatalytic squaramide moieties enables control over the formation of the mono- or di- addition products (see below). Furthermore, it also allows for the selective synthesis of heterogeneous double-addition products via multicomponent reactions in which two different epoxides are opened by a single amine (see below). Recently, Hupp, Farha, Mirkin *et al.*[8] and Cohen *et al.*[9] demonstrated that squaramide moieties can be incorporated into MOFs by post-synthetic modification of UiO-67 and by using a tetracarboxylate squaramide-based linker to produce a new Cu(II)-based MOF showing a pore diameter of ~8 Å×8 Å. Both squaramide-functionalised MOFs[10] were successfully tested as catalysts for Friedel-Crafts reactions between indoles and β-nitroalkenes. For our targeted catalytic reactions, we constructed a squaramide-functionalised IRMOF-16 analogue (hereafter called **Sq_IRMOF-16**) because it shows a three-dimensional mesopore system in which the squaramide moieties are totally accessible in all three dimensions and are well separated to avoid any self-quenching phenomena. In addition, the pore diameter is ~17 Å×17 Å, which is sufficiently large to host the intermediates produced during the tandem reactions. The linker (3,4-dioxocyclobut-1-ene-1,2-diyl)bis(azanediyil)-*p*-dibenzoic acid, hereafter called **L1**) was designed to resemble, both in topology and in length, to the *p*,*p*′-terphenyl dicarboxylic acid (tpdc), which is the linker used to synthesise IRMOF-16 (Figure 1b).[11] Moreover, and in contrast to a previously reported linker[9] in which the squaramide moiety is in the *meta* position to the acid, in **L1** the squaramide moiety is

[a] C. Vignatti,[+] Dr. V. Guillerm, Dr. I. Imaz, Prof. D. Maspoch
Catalan Institute of Nanoscience and Nanotechnology (ICN2)
CSIC and The Barcelona Institute of Science and Technology
Campus UAB, Bellaterra, 08193 Barcelona, Spain
E-mail: inhar.imaz@icn2.cat
daniel.maspoch@icn2.cat
[b] J. Luis-Barrera,[+] Prof. Dr. J. Alemán
Organic Chemistry Department, Módulo 1
Universidad Autónoma de Madrid,
Madrid-28049, Spain
E-mail: jose.aleman@uam.es
[c] Prof. Dr. R. Mas-Ballesté
Inorganic Chemistry Department
Universidad Autónoma de Madrid,
Madrid-28049, Spain
E-mail: ruben.mas@uam.es
[d] Prof. Dr. R. Mas-Ballesté, Prof. Dr. J. Alemán
Institute for Advanced Research in Chemical Sciences (IAdChem)
Campus Universidad Autónoma de Madrid,
Madrid-28049, Spain
[e] Prof. Dr. D. Maspoch
Institució Catalana de Recerca i Estudis Avançats (ICREA)
08100 Barcelona, Spain
[+] These authors contributed equally to this work.

Supporting information for this article is available on the WWW under https://doi.org/10.1002/cctc.201801127

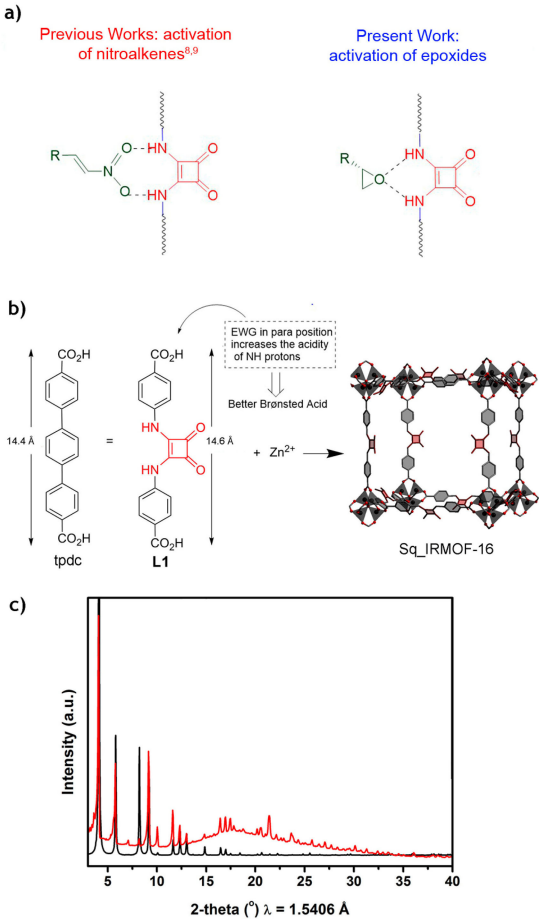

Figure 1. a) Schematic illustration of the introduction of squaramide moieties in MOFs for catalysing Friedel-Craft reactions with nitroalkanes (previous works) and simple, tandem and multicomponent epoxide ring-openings under solvent-free conditions (this work). b) Representation of the linkers tpdc and L_1, and of the structure of **Sq_IRMOF-16**, in which the squaramide moieties have been highlighted in red. EWG refers to electron withdrawing groups. c) XRPD diffractogram of **Sq_IRMOF-16** (red), compared with the simulated powder pattern obtained from the structural model (black).

para to the carboxylic group. Therefore, our design leads to a more acidic NH proton than in the *meta* case.

We began by synthesising **L1**, using slight modifications of previously reported procedures.[12] Then, **Sq_IRMOF-16** was synthesised by heating a mixture of **L1** and $Zn(NO_3)_2$ in *N*,*N*-dimethylformamide (DMF) at 85 °C for 7 days. After this period, yellow cubic crystals of **Sq_IRMOF-16** were harvested (yield = 53%). As expected, the experimental powder X-ray diffraction (PXRD) pattern of **Sq_IRMOF-16** was in excellent agreement with the one calculated from the envisioned squaramide-based IRMOF-16 (Figure 1c, see also Supporting Information, Figure S1). The squaramide-based IRMOF-16 model was constructed from the experimental IRMOF-16 structure[11] by ligand replacement, respecting the symmetry of IRMOF-16 (Pm-3m space group). This step was followed by a molecular mechanics energy minimisation to improve the geometry of the bonds within the framework using the Forcite tool of the Materials Studio software (Biovia).[13] Therefore, analogously to IRMOF-16, **Sq_IRMOF-16** comprises a zinc-metal cluster (Zn_4O) bridged by six dicarboxylate linkers that form a network with **pcu** topology. The network is a three-dimensional mesopore system (pore size: ~17 Å×17 Å) in which the squaramide moieties point towards the pores and therefore, are totally accessible in all three dimensions (Figure 1b).

For the catalytic experiments, we carefully dried **Sq_IRMOF-16** dried under inert atmosphere and then, immediately mixed it with the other reagents (Supporting Information, Figure S2). It is worth to mention that this drying step was critical, as **Sq_IRMOF-16** tends to become amorphous upon exposure to vacuum, and to transform into an unknown crystalline phase upon contact with water (Supporting Information, Figure S3). In order to verify that **Sq_IRMOF-16** remained stable during the catalytic processes, it was recovered from the reaction media after the catalytic runs and its crystalline phase was confirmed by XRPD (Supporting Information, Figure S4). Additional experiments proved that the catalytic activity of **Sq_IRMOF-16** was not related to the degradation or leaching of molecular species under the reaction conditions.[14]

As a first approach to studying the catalytic behaviour of **Sq_IRMOF-16**, we monitored the kinetics of the reactions of each amine (**1a**, R=Me, or **1b**, R = *t*-Bu) with each epoxide (**2a**, R = Et or **2b**, R = $C_{10}H_{21}$) at 60 °C (Figure 2b). We introduced to the reaction medium a 5 mol% content of catalytic centers, which are included in the structure of **Sq_IRMOF-16**; that is, 2.9 mg of **Sq_IRMOF-16** that corresponds to 0.005 mmol of catalytic units were used to catalyze the reaction of 0.1 mmol of the corresponding aniline with an excess of epoxide. Figure 2c is a plot of the kinetics for each mono-addition product, which was the major species at 8 hours of reaction. Here, the

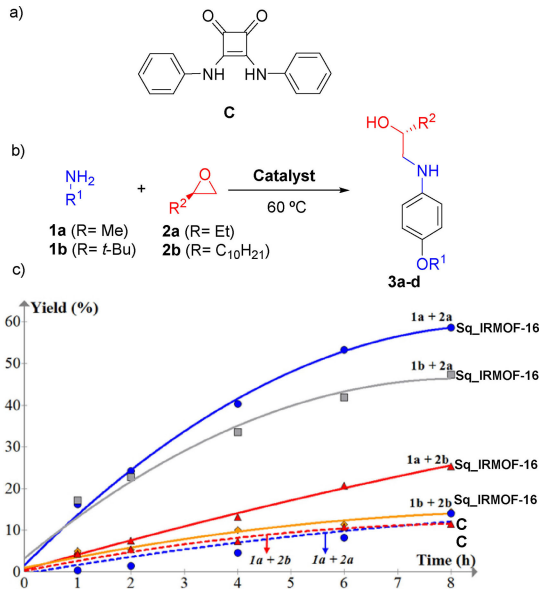

Figure 2. a) Representation of the molecular structure of catalyst **C**. b) Schematic representation of the epoxide ring-opening mono-addition reactions. c) Kinetics plots for ring-openings of an epoxide (**2a** or **2b**) by an amine (**1a** or **1b**), using either **MOF-Sq** (solid lines) or **C** (dashed lines) as catalyst (in both cases, 5 mol% of catalytic units). Reactions were run at 60 °C, using an excess of epoxide (200 μL) as solvent. Yield was measured by GC-MS and based on an internal standard.

performance of **Sq_IRMOF-16** was also compared with the molecular squaramide **C** as catalyst (Figure 2a). Using both catalysts, we studied the reaction of **1a** with **2a** (compare the blue dashed line with the blue solid one) and **2b** (compare the red dashed line with the red solid one). The reactions barely progressed when using **C**, probably due to the auto-self-aggregation and poor solubility of the catalyst. In quite contrast, the use of **Sq_IRMOF-16** enhanced both kinetics and yields of these reactions. Moreover, when using **Sq_IRMOF-16**, we observed that epoxide **2a** (R^2 = Et) appeared to react better than epoxide **2b** (R^2 = $C_{10}H_{21}$), as observed in Figure 2c (compare the solid blue line with the solid red one, or the solid grey line with the solid orange one). Likewise, amine **1a** (R^1 = Me) typically reacted faster than amine **1b** (R^1 = *t*-Bu), also evidenced in Figure 2c (compare the solid blue line to the solid grey one, or the solid red line to the solid orange one. Interestingly, in the case of the use of the smaller epoxide **2a** in their reaction with **1a** and **1b** (blue and greys lines), we also found a significant amount of the dialkylated products **4a** and **4b** (see Supporting Information). Altogether, these observations suggest that there is a size discrimination effect when **Sq_IRMOF-16** is used, which is probably due to the lower diffusion rates of the bulkier substrates. These differences confirm that the catalytic processes occur inside the pores of **Sq_IRMOF-16** rather than on its external crystal surfaces.

Interestingly, we observed that once the mono-addition products **3** were obtained, the bis-addition products, homo-disubstituted amino diols **4**, began to form. Figure 3 shows a series of tandem reactions of the amines **1a–b** and epoxides **2a–f** to form the diols **4a–g** catalysed by **Sq_IRMOF-16** (5 mol%) to test its catalytic utility. Remarkably, this reaction tolerated many combinations of reagents. The times required to obtain optimised yields of a series of diols **4** correlated to the size (**4a–4d**; Figure 3, top row) and/or polarity (**4e–4g**; Figure 3, bottom row) of the substrates. For example, comparing the synthesis of **4a** with that of **4b** reveals that ethyl-epoxide (**2a**) reacted faster with *para*-methoxy aniline (**1a**) than with *para*-*tert*-butyl aniline (**1b**). Similarly, to **4b**, the diols **4c** (from **1a** and **2b**) and **4d** (from **1b** and **2c**) required 3 days and 4 days, respectively, to reach moderate yields. We attributed these low reaction rates and moderate yields to the steric bulk and hydrophobicity of the alkyl chains in epoxides **2b** (R^2 = $C_{11}H_{23}$) and **2c** (R^2 = $C_{10}H_{21}$), which could hamper the diffusion of each epoxide through the pores of **Sq_IRMOF-16**.

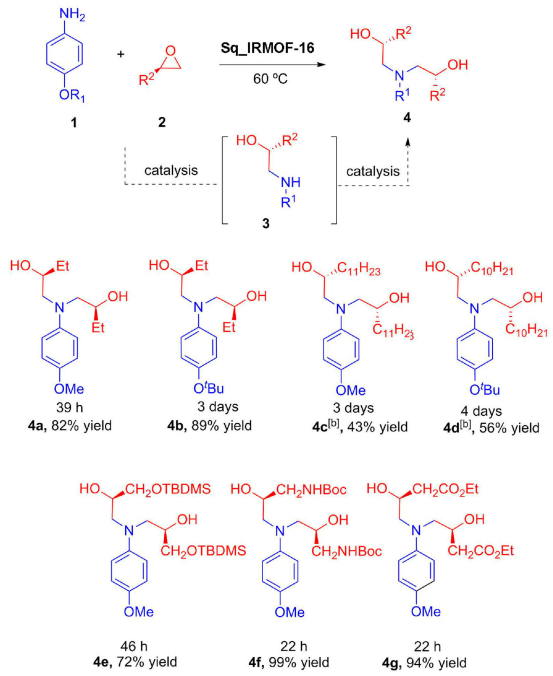

Figure 3. Schematic representation of the epoxide ring-opening tandem reaction (top) and representation of the molecular structures of the synthesized homo-disubstituted amino diols **4** (bottom). All the reactions were performed on a 0.1 mmol of aniline **1** and 1.0 mmol of epoxide **2**. In the case of **2b**, **2c** and **2e** were used 0.4 mmol of epoxide under solvent free conditions. [b] The corresponding mono-addition products were also detected in the crude mixture.

In the above reactions, we also found that the bulkier epoxide **2e** reacted at a similar reaction rate than did the smaller epoxide **2a**. We ascribed this fact to the greater polarity of the -CH_2OTBDMS group in **2e** relative to the -Et group in **2a**, which may help the diffusion of **2e** through the pores of **Sq_IRMOF-16**. Consistent with our hypothesis, the more polar epoxides **2f** (R^2 = CH_2HNBoc) and **2g** (R^2 = CH_2CO_2Et) gave near-total conversion (yields >90%) to their corresponding diols **4f** and **4g**, respectively, after only 22 h.

We next evaluated the capacity of **Sq_IRMOF-16** to catalyse multicomponent reactions of higher complexity. To this end, we used three reagents (one amine reacted sequentially with two epoxides) to generate heterogeneous diols in one-pot multi-component reactions. This approach typically requires less energy and generate less waste than step-reactions which needs multiple purification processes. However, a drawback of one-pot reactions for heterogeneous additions is that they demand strict control of the chemistry. In our case, to avoid the formation of undesired side-products, a single mono-addition intermediate **3** had to be generated first. Once **3** had been formed in the reaction media, via one pot process (i.e. without any purification), other epoxides can be added to obtain the desired hetero-disubstituted amino diols **5** (Figure 4).

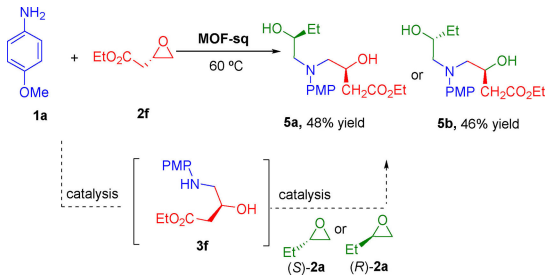

Figure 4. Schematic representation of the epoxide ring-opening multi-component reaction to form the amino diols **5**. All the reactions were performed on 0.1 mmol of aniline **1a** and 0.1 mmol of **3f** for the first step, followed by 1.0 mmol of epoxide **2a** for the second step.

We began by reacting *para*-methoxy aniline (**1a**) and epoxide (*S*)-**2f** in the presence of **Sq_IRMOF-16** for 8 hours to

produce the non-isolated intermediate **3f**. Then, the enantiopure epoxide (*S*)-**2a** was added to the reaction medium to give the desired amino-diol (*S,S*)-**5a**. Similarly, we synthesised the amino-diol (*S,R*)-**5b** using the same conditions as for **5a**, except that instead of (*S*)-**2a**, we used (*R*)-**2a**. In both cases, we found a substantial amount of the homo-substituted product **4g** (~ 20%) in the crude mixture. These results indicate that **Sq_IRMOF-16** can indeed catalyse multicomponent reactions, including diastereo-divergent ones.

In conclusion, we have synthesised a squaramide-functionalised IRMOF-16 analogue, **Sq_IRMOF-16,** for use as a catalyst in the ring-opening of epoxides by nucleophilic amines. **Sq_IRMOF-16** does not undergo the self-aggregation phenomena usually observed for squaramides in solution; in fact, this heterogeneous catalyst is superior to its molecular squaramide analogue. The pores in **Sq_IRMOF-16** are sufficiently large to catalyse the ring-opening of diverse epoxides using different amines. We have demonstrated the catalytic activity of **Sq_IRMOF-16** in the synthesis of simple, tandem and multicomponent epoxide ring-openings under solvent-free conditions and in good yields. The evidences suggest that these reactions are confined to the squaramide-functionalised pores, as **Sq_IRMOF-16** shows size- and polarity-discrimination effects. Given that many organocatalytic moieties can be introduced into MOF pores, we are confident that MOF-based catalysts such as **Sq_IRMOF-16** should help to expand the scope of heterogeneous catalysis in one-pot reactions.

Acknowledgements

This work was supported by the Spanish MINECO (projects PN MAT2015-65354-C2-1-R and CTQ2015-64561-R), the Catalan AGAUR (project 2014 SGR 80), the ERC under the EU FP7 (ERC–Co 615954 and ERC-CG 647550), and European Union's Horizon 2020 research and innovation programme under grant agreement No 685727. It was also funded by the CERCA Programme/Generalitat de Catalunya. ICN2 acknowledges the support of the Spanish MINECO through the Severo Ochoa Centers of Excellence Program, under Grant SEV-2013-0295.

Conflict of Interest

The authors declare no conflict of interest.

Keywords: Metal-organic frameworks · H-bond catalysis · Tandem and multicomponent reactions · Squaramide

[1] For selected reviews and books, see: a) A. Behr, A. J. Vorholt, K. A. Ostrowskia, T. Seidenstickera, *Green Chem.* **2014**, *16*, 982; b) Enantioselective Multicatalysed Tandem Reactions, Ed. H. Pellissier, RSC series; c) M. J. Climent, A. Corma, S. Iborra, M. J. Sabater, *ACS Catal.* **2014**, *4*, 870. d) T. L. Lohr, T. J. Marks, *Nat. Chem.* **2015**, *7*, 477.

[2] a) W. Zhao, F.-E. Chen, *Curr. Org. Synth.* **2012**, *9*, 873; b) O. G. Bhusnure, S. B. Gholve, P. S. Giram, T. A. Warad, V. S. Pangave, J. N. Sangshetti, *World J. Pharm. Res.* **2015**, *4*, 629; c) Multicomponent Reactions, Concepts and Applications for design and Synthesis, Ed. By R. P. Herrera and E. Marqués-López, J. Wiley & Sons, Hoboken, 2015; d) B. Ganem, *Acc. Chem. Res.* **2009**, *42*, 463; e) D. J. Ramon, M. Yus, *Angew. Chem. Int. Ed.* **2005**, *44*, 1602.

[3] W. C. Shearouse, D. C. Waddell, J. Mack, *Curr. Opin. Drug Discov. Devel.* **2009**, *12*, 772.

[4] For examples of bioactive naturally-occurring amino alcohols, see: a) K. C. Nikolau, H. J. Mitchel, F. L. van Delft, F. Rubsam, R. M. Rodriguez, *Angew. Chem. Int. Ed.* **1998**, *37*, 1871; b) T. D. Heightman, A. T. Vasella, *Angew. Chem. Int. Ed.* **1998**, *38*, 750; c) T. Kolter, K. Sandhoff, *Angew. Chem. Int. Ed.* **1998**, *38*, 1532; d) S. C. Bergmeier, *Tetrahedron* **2000**, *56*, 2561; e) C. W. Johannes, Mi. S. Visser, G. S. Weatherhead, A. H. Hoveyda, *J. Am. Chem. Soc.* **1998**, *120*, 8340.

[5] Y. Yuki, K. Saigo, K. Tachibana, M. Hasegava, *Chem. Lett.* **1986**, 1347.

[6] For recent reviews, see: a) D. J. Ager, I. Prakash, D. R. Schaad, *Chem. Rev.* **1996**, *96*, 835; b) R. Bloch, *Chem. Rev.* **1998**, *98*, 1407. c) M. T. Reetz, *Chem. Rev.* **1999**, *99*, 1121; d) *Comprehensive Asymmetric Catalyst*; E. N. Jacobsen, A. Pfaltz, H. Yamamoto Eds.; Springer-Verlag, Berlin, **1999**; e) I. Ojima, *Catalytic Asymmetric Synthesis*, 2nd ed.; VCH: New York, **2000**; f) S. C. Bergmeier, *Tetrahedron* **2000**, *56*, 2561; g) C. Bonini, G. Righi, *Tetrahedron* **2002**, *58*, 4981; h) Z. Tang, F. Jiang, L.-T. Yu, C. Xin, L.-Z. Gong, A.-Q. Mi, Y.-Z. Jiang, Y.-D. Wu, *J. Am. Chem. Soc.* **2003**, *125*, 5262.

[7] For a review of tandem reactions involving MOFs, see: a) Y.-B. Huang, J. Liang, X.-S. Wang, R. Cao, *Chem. Soc. Rev.* **2017**, *46*, 126. For review of MOF in catalytic reactions, see: b) A. Dhakshinamoorthy, A. M. Asiri, H. García, *Chem. Commun.* **2014**, *50*, 12800; c) J. Liu, L. Chen, H. Cui, J. Zhang, L. Zhang, C.-Y. Su, *Chem. Soc. Rev.* **2014**, *43*, 6011; d) G. Kumar, S. K Das, *Inorg. Chem. Front.* **2017**, *4*, 202; e) J. Gascon, A. Corma, F. Kapteijn, F. X. Llabrés i Xamena, *ACS Catal.* **2014**, *4*, 361. For other relevant works in this topic see: f) A. M. Rasero-Almansa, A. Corma, M. Iglesias, F. Sánchez, *ChemCatChem* **2014**, *6*, 1794; g) J. Gascon, U. Aktay, M. D. Hernandez-Alonso, G. P. M van Klink, F. Kapteijin, *J. Catal.* **2009**, *261*, 75; h) M. Tonigold, Y. Lu, B. Bredenköter, B. Rieger, S. Bahnmüller, J. Hitzbleck, G. Langstein, D. Volkmer, *Angew. Chem. Int. Ed.* **2009**, *48*, 7546.

[8] C. M. McGuirk, M. J. Katz, C. L. Stern, A. A. Sarjeant, J. T. Hupp, O. K. Farha, C. A. Mirkin, *J. Am. Chem. Soc.* **2015**, *137*, 919.

[9] X. Zhang, Z. Zhang, J. Boissonnault, S. M. Cohen, *Chem. Commun.* **2016**, *52*, 8585.

[10] For a critical perspective, see: S. M. Cohen, Z. Zhang, J. A. Boissonnault, *Inorg. Chem.* **2016**, *55*, 7281.

[11] M. Eddaoudi, J. Kim, N. Rosi, D. Vodak, J. Wachter, M. O'Keeffe, O. M. Yaghi, *Science* **2002**, *295*, 469.

[12] J. P. Malerich, K. Hagihara, V. H. Rawal, *J. Am. Chem. Soc.* **2008**, *130*, 14416.

[13] a) O. K. Farha, I. Eryazici, N. C. Jeong, B. G. Hauser, C. E. Wilmer, A. A. Sarjeant, R. Q. Snurr, S. T. Nguyen, A. Ö. Yazaydin, J. T. Hupp, *J. Am. Chem. Soc.* **2012**, *134*, 15016; b) H. Deng, S. Grunder, K. E. Cordova, C. Valente, H. Furukawa, M. Hmadeh, F. Gándara, A. C. Whalley, Z. Liu, S. Asahina, H. Kazumori, M. O'Keeffe, O. Terasaki, J. F. Stodddart, O. M. Yaghi, *Science* **2012**, *336*, 1018.

[14] To investigate any possible leaching of molecular catalytic species from **Sq_IRMOF-16**, we allowed the mixture of **1a**, **2a** and **Sq_IRMOF-16** to react for 2 hours. The mixture was then filtered and the filtrate was left to react for 2 more hours. This experiment revealed that after filtration, the catalytic activity was stopped. Therefore, the catalytic activity that we observed in this study is derived from the presence of heterogeneous material **Sq_IRMOF-16**, excluding the possibility that homogeneous catalytically active species underwent any leaching.

Manuscript received: July 12, 2018
Accepted Article published: July 20, 2018
Version of record online: August 1, 2018

Switching Acidic and Basic Catalysis in a Three-Dimensional Covalent Imine Structure through Supramolecular Functionalization

Javier Luis-Barrerra, Ghazaleh Imani-Shakibaei, Javier Heras-Domingo, Rafael Cano, Javier Pérez-Carvajal, Inhar Imaz, Daniel Maspoch, Xavier Solans-Monfort, José Alemán,* and Rubén Mas-Ballesté**

Prof. Dr. José Alemán, Dr. G. Imani-Shakibaei, J. Luis-Barrerra,
Department of Organic Chemistry (module 01)
Universidad Autónoma de Madrid,
E-mail: jose.aleman@uam.es
28049 Madrid, Spain.

J. Heras-Domingo, Prof. Dr. X. Solans-Monfort
Department of Chemistry
Facultat de Ciències, Universitat Autònoma de Barcelona
08191 – Bellaterra, Spain.
E-mail: xavier.solans@uab.cat

Prof. Dr. D. Maspoch, Dr. I. Imaz, Dr. J. Pérez-Carvajal
Catalan Institute of Nanoscience and Nanotechnology (ICN2), CSIC and BIST
08191 – Bellaterra, Spain.
E-mail: daniel.maspoch@icn2.cat

Prof. Dr. Daniel Maspoch
ICREA
Pg. Lluís Companys 23, Barcelona, 08010, Spain

Prof. Dr. R. Mas-Ballesté, Dr. Rafael Cano
Department of Inorganic Chemistry (module 07)
Facultad de Ciencias, Universidad Autónoma de Madrid
28049 Madrid, Spain.
E-mail: ruben.mas@uam.es

Prof. Dr. José Alemán, Prof. Dr. R. Mas-Ballesté
Institute for Advanced Research in Chemical Sciences (IAdChem),
Universidad Autónoma de Madrid,
28049 Madrid, Spain
www.uam.es/jose.aleman

Keywords: Covalent Organic Frameworks, Acid Catalysis, Basic Catalysis, Supramolecular functionalization

Abstract: Non-covalent inclusion of small acid and base molecules (CH_3COOH and NEt_3) in an imine structure based on micrometre COF-300 crystals and amorphous nanoparticles results on the facile modulation of its acid-base properties. Such strategy results in the triggering of acidic/basic catalytic activity of the otherwise inactive materials towards ring-opening epoxide and Knoevenagel condensation reactions. For both reactions, amorphous nanoparticles are better catalysts than micrometre crystals as they exhibit a higher external surface area. The found activities and stability of this supramolecular functionalization are modulated by confinement effects, which are rationalized with the help of DFT theoretical calculations. Furthermore, the chemical stability of these materials has been also experimentally evaluated, which is relevant in order to control assembly/disassembly processes.

1. Introduction

The development of molecules and materials with catalytic cavities, inspired on biological systems, such as enzymes, has been a main topic in modern chemistry. For instance, different molecules known as molecular flasks[1] are able to catalyse a variety of reactions in confined spaces. The outstanding performance of such molecular systems and other porous materials lays not only on the design of active catalytic centres, but also on the easy tuning of environment in a confined space, resulting on different regio-,[2] chemo-[3] and stereo-selectivities[4] in different reactions. In addition, the proximity between the different reactants in the confined space can result in an enhancement of the catalytic activity.[5] Furthermore, confined catalysis offers the possibility to perform size-selective reactions, specially important when working with mixtures of compounds with similar chemical and physical properties. During the last years, confinement effects have been particularly studied in different porous materials such as zeolites,[6] mesoporous silica[7] and metal-organic frameworks (MOFs).[8]

In 2005, Yaghi and co-workers described a new concept on the reticular chemistry field: the covalent-organic frameworks (COFs).[9] Their use as heterogeneous catalysts offers advantages compared to MOFs such as increased activity, durability and recyclability. COFs are based on the covalent linkage of organic subunits into two- or three-dimensional porous crystalline structures. Therefore, they show predictable composition, topology and porosity. As a consequence, COFs have been explored for applications related to gas storage and separation,[10] ultrasensitive sensing,[11] electronic applications,[12] and clean energy technologies.[13] However, only few recent studies initiated the exploration of their catalytic applications.[14] In 2014, Yan *et al.* described the intrinsic basic property of a three-dimensional (3D) imine-based COF useful for the catalytic Knoevenagel reaction.[15] After this achievement, other groups have employed two main covalent strategies in order to tune the catalytic activity of different COFs. The first one consisted in the post-functionalization of the material, attaching organic pending arms (top-left, **Scheme 1**)[16] or metal nano-particles,[14] which are both functionalizations irreversible processes. A second strategy relayed in the use of catalytic backbones, which often requires complex synthetic modifications of building blocks (top-right, **Scheme 1**).[17] Although these are interesting approaches, they require predetermined specific architectures or, in some cases, complicated post-functionalization processes.

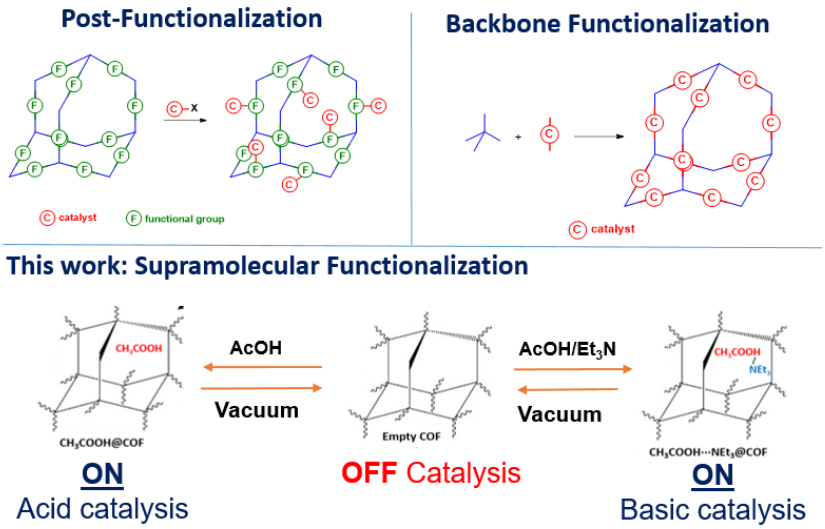

Scheme 1. Previous strategies for the catalytic functionalization materials and the supramolecular used in this work.

As an alternative to these strategies shown above, supramolecular functionalization appears as an easy way to modulate and direct several properties of COFs. In particular, hydrogen bonding interactions between COFs and small molecules have been recently demonstrated and applied to drug delivery and molecular recognition systems.[18] In addition, several porous materials with pre-designed structures that could make possible proton conduction mechanism have been applied to proton-exchange in fuel membranes.[19] Therefore, supramolecular hydrogen-bonding functionalization seems to be an straightforward strategy to modulate the properties of COF materials. However, to the best of our knowledge, such supramolecular functionalization strategy, to obtain catalytic COF-molecule confined systems, have never been applied to catalyse chemical organic transformations.

Herein we show that this latter strategy can be applied to functionalize COF-related materials for catalytic applications (bottom, **Scheme 1**). To this end, we selected the 3D COF-300[20] made of terepthalaldehyde (**1**) and tetra-(4-anilyl)-methane (**2**) (see **Figure 1**) as it is stable up to 490 °C, in water and common organic solvents. COF-300 was synthesized by a well-known two-step process:[21],[22] first, amorphous imine polymer nanoparticles (hereafter called amorphous-3 or **a-3**) were formed; and subsequently, these **a-3** nanoparticles were further reacted to form micrometre COF-300 crystals (hereafter called crystalline-3 or **c-3**). We demonstrate that both **a-3** and **c-3** can be reversibly functionalized through supramolecular interactions with two simple model molecules: a carboxylic acid (acetic acid) that has been used to catalyse ring-opening reactions of epoxides; and a Brønsted base (triethylamine) that has been used to catalyse Knoevenagel condensation.

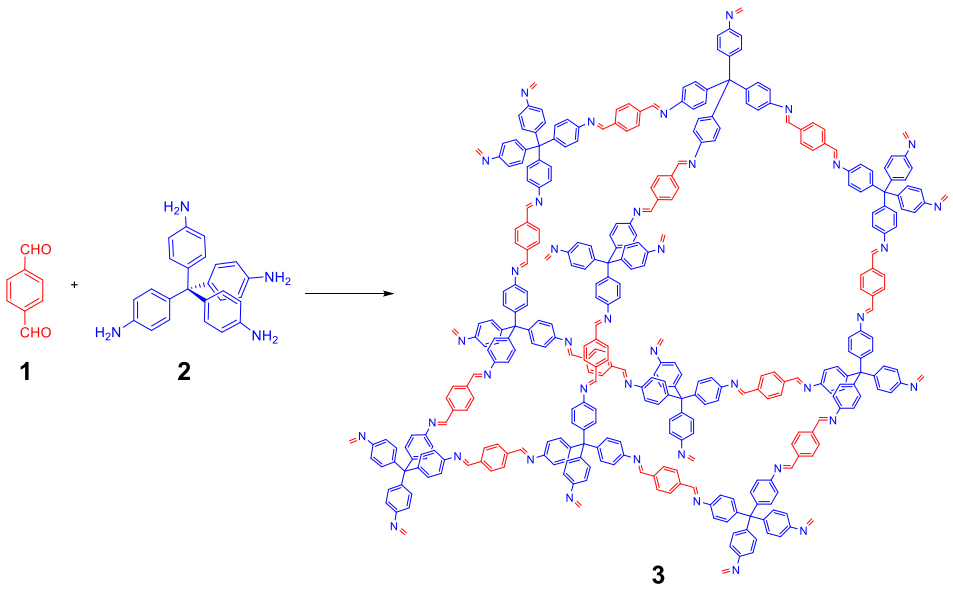

Figure 1. Structure of COF-300 based on the condensation of dialdehyde **1** and tetraamine derivative **2**.

2. Material and methods

All reagents for the synthesis of materials and for the catalyzed reactions and all organic solvents were acquired from commercial sources and used without further purification. Flash column chromatography was performed using pore 60 Å, 40-63 µm silica gel and compressed air. NMR spectra were acquired on a *Bruker Avance 300* spectrometer, running at 300 MHz for ^{1}H. Chemical shifts (δ) are reported in ppm relative to residual solvent signals ($CDCl_3$, 7.26 ppm for ^{1}H-NMR). The following abbreviations are used to describe peak patterns when appropriate: s (singlet), d (doublet), t (triplet), q (quartet), quint (quintet), m (multiplet), bs (broad singlet). Solid NMR spectra were acquired on a *Bruker AV 400 WB* spectrometer, running at 100 MHz for ^{13}C. Scanning Electron Microscopy (SEM) images were acquired in a *Philips XL30 S-FEG* microscope and the samples surfaces were previously metalated with chromium with a *Sputter Coater Quorum, Q150T-S*. Infra Red (IR) spectra were acquired in a *Agilent Technologies Cary 630 FTIR* spectrometer. PXRD patterns were collected with a *Bruker D8 Advance* X-ray diffractometer (Cu-Kα radiation; λ = 1.5418 Å) equipped with a Lynxeye detector. Samples were mounted on a flat glass plate. Patterns were collected in the 5°<2θ<100° range with a step size of 0.02° and exposure time of 0.5 s/step. Thermogravimetric analysis (TGA) was done in a *TGA Q500 TA Instruments* thermobalance coupled to a *ThermoStar* mass spectrometer. The yield of the catalyzed reactions was measured by gas chromatography (GC) using an *Agilent Technologies 7820A GC System* with a Flame Ionization Detector (FID). Volumetric N_2 sorption isotherms were collected at 77 K (liquid N_2) using an ASAP 2020 HD (Micromeritics). Temperature was controlled by using a liquid nitrogen bath.

2.1. Synthesis of the materials

2.1.1. Synthesis of CH_3COOH@a-3

A round-bottom flask was charged with 20 mL of dichloromethane, 3 mL of glacial acetic acid and 28.8 mg of tetrakis(4-aminophenyl)methane **2** (0.075 mmol), and the resulting mixture was stirred during 30 minutes. The solution was filtered through filter paper in order to remove particles that are not solved. In another flask, 20.1 mg of 1,4-benzendicarbaldehyde **1** (0.150 mmol) was dissolved in 15 mL of dichloromethane. The solution of 1,4-benzendicarbaldehyde **1** was added to the solution of tetrakis(4-aminophenyl)methane **2,** and it was stirred during 2 hours at room temperature. After this period, the precipitated yellow solid was filtrated through a membrane filter of 0.45 µm pores and washed with 10 mL of water, 10 mL of acetone and 5 x 10 mL of dichloromethane. It was obtained 40 mg of **CH_3COOH@a-3** (93%).

2.1.2. Synthesis of evacuated a-3

A round bottom flask was charged with 40 mg of **CH_3COOH@a-3**. Vacuum was then applied to the flask while heating at 80º C during 12 hours.

2.1.3. Synthesis of evacuated c-3

A solvothermal reactor was charged with 116 mg of **CH_3COOH@a-3**, 10.5 mL of 1,4-dioxane, 3.1 mL of glacial acetic acid, 2.1 mL of water and 2.1 mL of mesitylene. The mixture was heated under solvothermal conditions from 25 ºC to 120 ºC during 1 hour, and then to 120 ºC during 7 days. The solution was then cooled down to room temperature (from 120 ºC to 25 ºC in 1 hour). The precipitated solid was filtered through a membrane filter of 0.45 µm pores, washed with 10 mL of water, 10 mL of acetone and 5 x 10 mL of dichloromethane, and placed in a flask where it was heated at 80 ºC under vacuum for 12 hours to obtain 100 mg of evacuated **c-3** (88%).

2.1.4. Synthesis of crystalline CH_3COOH@c-3

100 mg of evacuated **c-3** were added to a mixture of dichloromethane (50 mL) and CH_3COOH (7.5 mL), and the resulting mixture was stirred during 12 hours. The solid was then filtrated through a membrane filter of 0.45 µm pores and washed with 10 mL of water, 10 mL of acetone and 5 x 10 mL of dichloromethane to obtain 104 mg of **CH_3COOH@c-3** (89%).

2.1.5. Synthesis of Et_3N@a-3 and Et_3N@c-3

A round-bottom flask was charged with 40 mg of evacuated **a-3** or **c-3** and 4 mL of NEt_3. The flask was connected to a water-cooled condenser and it was warmed to 80˚ C during 12 hours. The solid was filtrated through a membrane filter of 0.45 µm pores and washed with 10 mL of water, 10 mL of acetone and 5 x 10 mL of dichloromethane to obtain 35 mg of the material (86%).

2.1.6. Synthesis of $CH_3COOH\cdots NEt_3$@a-3 and $CH_3COOH\cdots NEt_3$@c-3

A round-bottom flask was charged with 40 mg of **CH_3COOH@a-3** or **CH_3COOH@c-3** and 4 mL of NEt_3. The flask was connected to a water-cooled condenser and it was warmed to 80˚ C during 12 hours. The solid was filtrated through a membrane filter of 0.45 µm pores and washed with 10 mL of water, 10 mL of acetone and 5 x 10 mL of dichloromethane to obtain 33 mg of the material (92%).

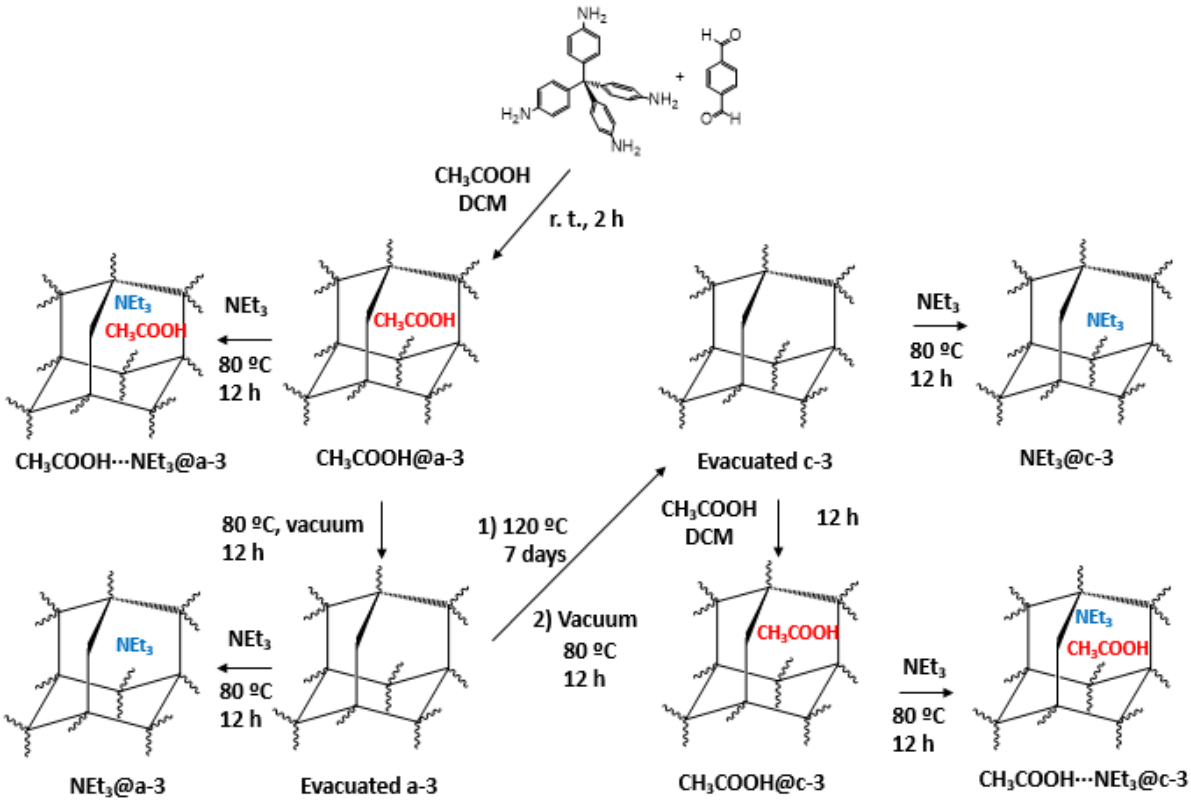

Figure 2. Schematic representation of the preparation of **a-3**, **c-3** and related supramolecular materials.

3. Results and Discussion

3.1. Preparation and characterization of a-3, c-3 and derivatized materials

The general rational followed in this work for the quest of differently functionalized **a-3** and **c-3** materials is shown in **Scheme 1** (bottom). Initially, the synthesis of crystalline **c-3** consisted in a two-step process. In a first step, a room temperature synthesis in the presence of acetic acid allowed the formation of the amorphous imine-based polymer nanoparticles **a-3**, which contains CH_3COOH molecules inside its structure.[23] Then, in a second step, these nanoparticles were subjected to a dynamic covalent chemistry to crystallize them under similar conditions to those reported by Dichtel *et al.*[22]

SEM images of the solid collected in the first step revealed the formation of amorphous-nanoparticles with diameters of nearly 100 nm (**Figure 3**; see S. I., Figures S1-3 for powder X-ray diffraction (PXRD) data). Solid-state MAS-^{13}C-NMR and FT-IR spectra confirmed the chemical identity of the material (see S. I., Figures S6 and S8-12, respectively). The FT-IR spectrum of COF-300 showed the C═N stretching modes characteristic for imines at 1620 and 1202 cm^{-1}. The solid-state MAS-^{13}C-NMR spectrum was also in agreement with the formation of the imine bonds since it shows: i) a resonance at 160 ppm that corresponds to the carbon atom of the C=N bond; and ii) a resonance at 70 ppm that corresponds to the quaternary Csp^{3}carbon atom. Thermogravimetric analysis (TGA) data revealed a 2.6 % of volatile molecules lost in the range of 50-400 ºC, which was consistent with the presence of acetic acid even after numerous washing procedures with distinct solvents (see S. I., Figure S13). The presence of acetic acid was further confirmed by mass spectrometry coupled to TGA analysis, which showed peaks at *m/z* = 15 and 43 that can be assigned to $[CH_3]^+$ and $[CH_3CO]^+$, respectively. Further evidence of the presence of acetic acid molecules inside **a-3** was acquired by solid-state MAS-^{13}C-NMR. To this end, **a-3** was synthesized in the presence of ^{13}C isotopically labelled acetic acid. Solid-state MAS-^{13}C-NMR of this newly synthesized **a-3** gave a clear evidence of the presence of ^{13}C-enriched acetic acid molecules by means of the CH_3 signal at 20 ppm (**Figure 4**). Altogether, these observations confirmed the formation of **CH_3COOH@a-3**.

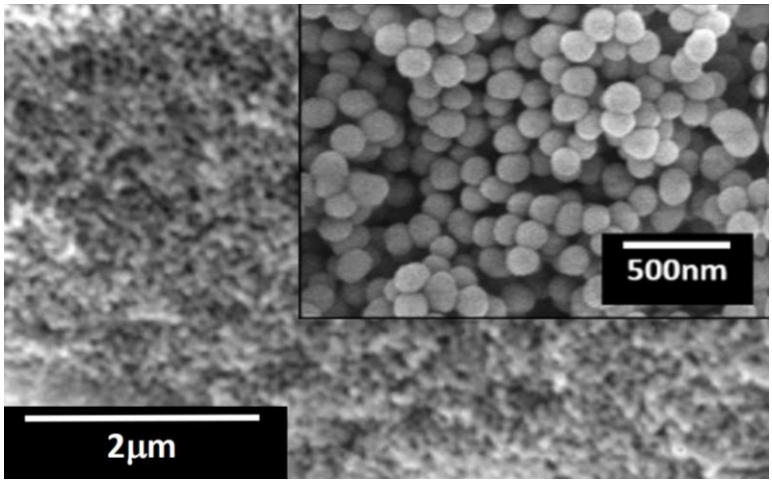

Figure 3. Representative SEM images of **CH_3COOH@a-3**.

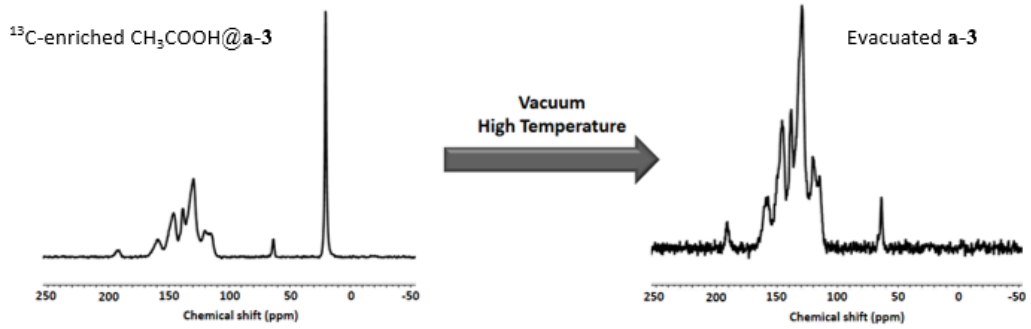

Figure 4. MAS-^{13}C solid NMR for **CH_3COOH@a-3** containing ^{13}C-enriched acetic acid. Characteristic signal of acetic acid (20 ppm) disappears after treatment of the sample under vacuum at high temperature.

The evacuation of all CH_3COOH molecules in **CH_3COOH@a-3** was achieved by heating it at 80 ºC during 12 hours under vacuum (1 mmHg). The resulting material showed the same morphology than its precursor (see S. I., Figure S5). First evidence of the evacuation of all acetic acid molecules was obtained by TGA analysis, from which no significant weight loss in the range of 50-400 ºC was observed (see S. I., Figure S14). We also demonstrated the removal of acetic acid molecules by performing solid-state MAS-^{13}C-NMR of a sample of ^{13}C enriched **CH_3COOH@a-3** exposed to identical activation conditions. Here, solid-state MAS-^{13}C-NMR spectrum showed that, while the peaks assigned to the COF-300 backbone remained identical, the characteristic signal due to acetic acid molecules at 20 ppm completely disappeared (see S. I., Figure S6).

In our quest of switching from acidic to basic properties of the material, a sample of **CH_3COOH@a-3** was treated with pure triethylamine (1 mL per 10 mg of **CH_3COOH@a-3**) overnight at 80 ºC. Thereafter, the solid (hereafter called **$CH_3COOH\cdots NEt_3$@a-3**) was filtrated and washed several times with water, acetone and dichloromethane. Again, SEM images confirmed the retention of the size and morphology of the nanoparticles after both amine treatments (see S. I., Figure S5). TGA analysis of **$CH_3COOH\cdots NEt_3$@a-3** showed a larger weight loss from 50 ºC to 400 ºC in comparison to **CH_3COOH@a-3** (4.6 % versus 2.6 %). Here, at this temperature range, mass spectrometry coupled to TGA revealed peaks at *m/z* = 43 and 51 in the ionization cell, which were assigned to $[CH_3CO]^+$ and $[HNEt_3]^{2+}$, respectively, thereby confirming the presence of both acetic acid and triethylamine molecules (see S. I., Figure S16). For both samples, solid-state MAS-^{13}C-NMR also demonstrated the incorporation of NEt_3 molecules by the appearance of a new signal at 47 ppm (see S. I., Figure S6), which are assigned to methylenic carbons.

In order to quest the reversibility of the functionalization of this material, we performed vacuum in a sample of **$CH_3COOH\cdots NEt_3$@a-3**, recovering the **evacuated a-3**, as revealed by TGA. It is worth mentioning that direct reaction of **evacuated a-3** with pure Et_3N results on a functionalized material in which the interactions between the imine structure and the guest molecules are very weak. Therefore, such functionalized material resulted in massive leaching of Et_3N molecules under catalytic conditions (*vide infra*). Consequently, such strategy was not useful to achieve confined catalysis.

In a subsequent synthetic step, amorphous **a-3** nanoparticles were converted to micrometre crystalline **c-3** particles by heating them at 120 ºC for 7 days in a mixture of dioxane, mesitylene and acetic acid. After exposing the treated solid under vacuum conditions, evacuated **c-3** was obtained in the form of microcrystals with dimensions of nearly 1 μm in diameter (**Figure 5a**). PXRD showed the characteristic pattern of COF-300 (**Figure 5b**).[20] Moreover, **c-3** did not show significant spectroscopic changes in both FT-IR and solid-state ^{13}C MAS NMR spectra in comparison to those seen for **a-3** (see S. I. Figures S10 and S7, respectively). TGA analysis for the **c-3** did not display any significant weight loss in the range of 50-400 ºC, confirming the evacuation of guest molecules from its framework (see S. I., Figure S17). This observation was further corroborated by N_2 sorption measurements at 77 K. As shown in **Figure 5c**, evacuated **c-3** showed to be porous after mild activation conditions (2 hours of primary vacuum at room temperature). The propierties of this material matched with the previously reported data:[24] the adsorption isotherm presented a S-shape (Type V) centered at 0.1 P/P_0 and with a plateau at 400 $cm^3\ g^{-1}$.

Then, evacuated **c-3** was functionalized with CH_3COOH by treating the material with CH_3COOH and dichloromethane at room temperature during 12 hours. TGA data revealed a 14.9 % of volatile molecules lost in the range of 50-400 ºC, which was consistent with the presence of acetic acid even after numerous washing procedures with distinct solvents. Accordingly, mass spectrometry coupled to TGA analysis presented evidences that volatile molecules produce ions in the ionization cell with *m/z* values of 60, which can be assigned to $[CH_3COOH]^+$ (see S. I. Figure S18).

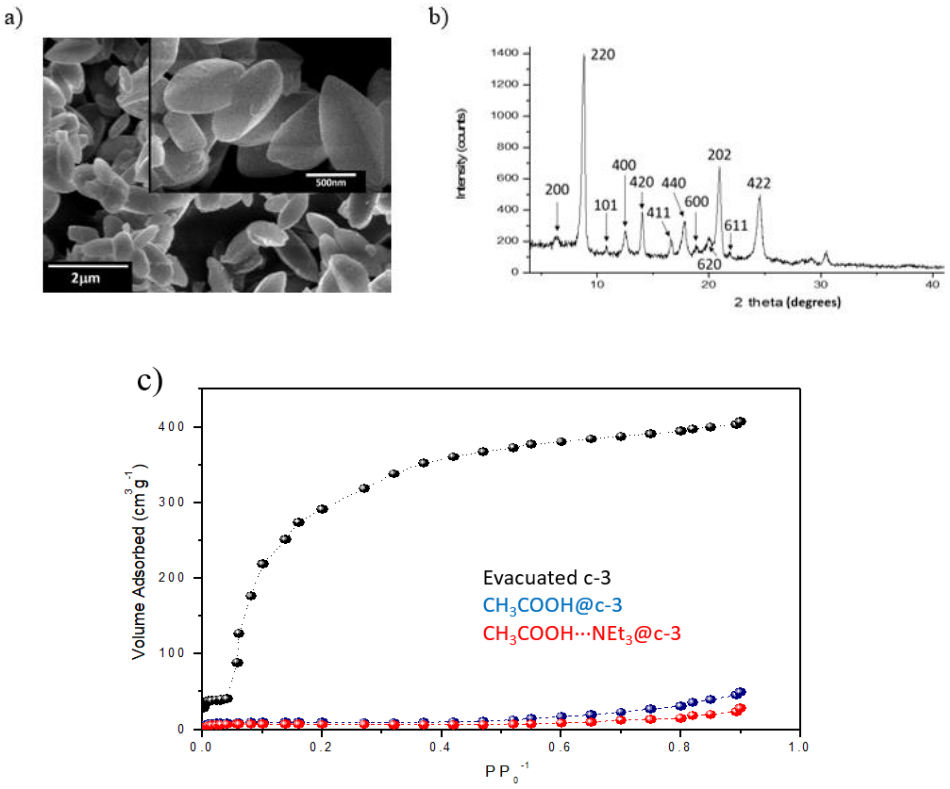

Figure 5. Characterization of **c-3** and derivatized materials**.** a) Representative SEM image of **c-3**; b) PXRD pattern of **c-3**; c) Nitrogen adsorption analysis of **c-3** (black), crystalline **CH_3COOH@c-3** (red) and crystalline **$CH_3COOH\cdots NEt_3$@c-3** (blue).

Similar to **CH_3COOH@a-3**, **CH_3COOH@c-3** was also functionalized with NEt_3 by treating it with NEt_3 (1 mL per 10 mg of **CH_3COOH@c-3**) overnight at 80 ºC. After this treatment, the resulting **$CH_3COOH\cdots NEt_3$@c-3** was filtrated and washed several times with water, acetone and dichloromethane. TGA data revealed a 4.4 % of volatile molecules that are lost in the range 50-400 ºC (see S. I., Figure S19). Moreover, mass spectrometry coupled to TGA revealed peaks at *m/z* = 60 and 86, which could be assigned to $[CH_3COOH]^+$, and $[C_5H_{12}N]^+$, respectively, thereby confirming the presence of both CH_3COOH and NEt_3 molecules. Important to highlight here is that N_2 sorption measurements in both **CH_3COOH@c-3** and **$CH_3COOH\cdots NEt_3$@c-3** showed a dramatic loss of porosity, with total uptakes decreasing below 50 $cm^3\ g^{-1}$ (49 $cm^3\ g^{-1}$ for **CH_3COOH@ c-3**, and 23 $cm^3\ g^{-1}$ for **CH_3COOH-NEt_3@c-3**. Moreover, addition of CH_3COOH or $CH_3COOH\cdots$ NEt_3 adduct resulted on the change of the isotherms observed to Type III. These changes in the isotherm trend and uptake were indicative of the blocking of the pores by the post-synthetic inclusion of CH_3COOH and NEt_3 molecules.

3.2. Catalysis

3.2.1. Comparison of the catalytic activity of amorphous a-3 and crystalline c-3 based materials

We started evaluating the catalytic activity of crystalline evacuated **c-3** and amorphous evacuated **a-3** and the corresponding functionalized materials in two model reactions: the ring-opening epoxide reaction of **4a** with epoxide **5** obtaining product **6a** under acidic conditions and the Knoevenagel reaction between malononitrile **7** and aldehyde **8a**, obtaining product **9a** under basic conditions.[25] The results obtained are summarized in **Scheme 2**.

The evacuated materials **a-3** and **c-3** showed a negligible catalytic activity for the two processes studied, being observed amounts of product similar to those obtained in control experiments without catalyst. On the contrary, crystalline acidic **CH_3COOH@c-3** and basic **$CH_3COOH\cdots NEt_3$@c-3** materials showed a moderate catalytic performance for both ring opening epoxide and Knoevenagel reactions, respectively. These first results confirmed that the inclusion of acidic and basic molecules in a COF is an efficient way to impart it with catalytic activity. However, this catalytic activity was moderate. We attributed this moderate activity to the fact that inclusion of these molecules dramatically reduces the porosity of **c-3** (as confirmed by sorption N_2 measurements, *vide supra*), thereby limiting the access of reagents to the internal parts of material. Therefore, catalysis using these materials, although confined, should be restricted to superficial pores. According to this hypothesis, we decided to study the catalytic activity of both amorphous **CH_3COOH@a-3** and **$CH_3COOH\cdots NEt_3$@a-3**, because they show a much higher external surface area due to their nanosized character. Supporting this hypothesis, both materials showed a much higher catalytic activity than their crystalline analogues: 45 % **CH_3COOH@c-3** *vs* 73 % **CH_3COOH@a-3** for the ring opening epoxide reaction; and 28 % **$CH_3COOH\cdots NEt_3$@c-3** *vs* 71 % **$CH_3COOH\cdots NEt_3$@a-3** for the Knoevenagel reaction.

For both reactions, we also discarded the possibility of leaching of molecular catalytic species (ie. CH_3COOH and NEt_3) from **a-3**. In the ring-opening epoxide reaction, as it is performed under solvent free conditions, leaching of CH_3COOH molecules hardly could result on catalytic activity because the small amount of acid (*ca* 125 μg per catalytic run) would immediately vaporize at 60 ºC. In the case of the Knoevenagel process, the reaction between benzaldehyde **8a** and malononitrile **7** in toluene was allowed to evolve during several hours in presence of **$CH_3COOH\cdots NEt_3$@a-3**. Thereafter, the system was filtered, additional amounts of reagents were added to the filtrated solution, and it was left to react during some additional hours (see S. I., section 9). The filtrated solution was found to have only a minor catalytic activity (19%) that corresponded to the combination of background reactivity (4%) and leaching effect (15%). Therefore, the main activities found for both **CH_3COOH@a-3** and **$CH_3COOH\cdots NEt_3$@a-3** in this work were a consequence of the presence of the catalytic heterogeneous material.

Note also here that model Knoevenagel reaction between benzaldehyde and malononitrile resulted in good yields of condensation products using **NEt_3@a-3** and **NEt_3@c-3**. However, the weakness of the interaction between the amine molecule (Et_3N) and the porous material, either crystalline or amorphous, resulted in complete leaching of catalytic molecules. Thus, we found that the filtered solution resulting from a first catalytic run, once separated from porous material, showed a significant catalytic activity. Therefore, confined catalysis was compromised using these materials because NEt_3 easily migrates out of porous network. This

is consistent with DFT calculations, which suggested that the interaction between NEt_3 and the organic material is only by Van der Waals interactions (see DFT calculations below).

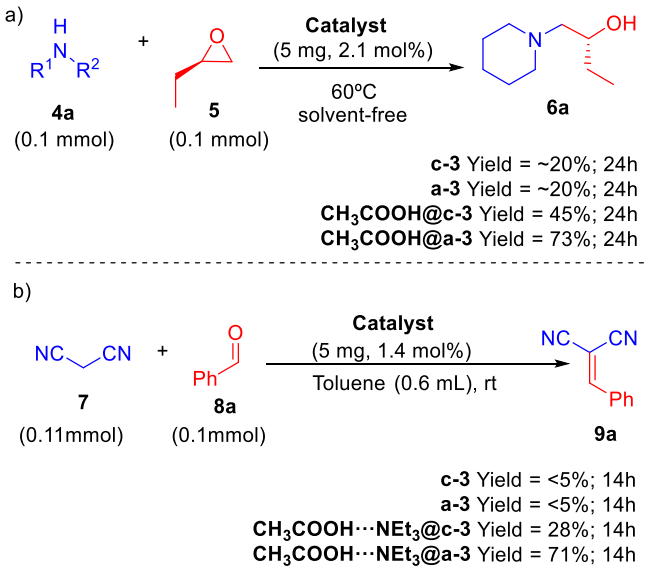

Scheme 2. Catalytic activity of the prepared materials for a) ring-opening epoxide reaction and b) Knoevenagel reaction.

3.2.2. Acid Catalysis: Ring-Opening Epoxide Reaction using CH_3COOH@a-3

To generalize the use of **CH_3COOH@a-3** to catalyse opening epoxide reactions, we performed different reactions with secondary amines (**4b** and **4c**) following a solvent free procedure. Under these reaction conditions, **CH_3COOH@a-3** catalysed the formation of product **6b** with a 55 % yield (**Scheme 3**). Moreover, it could also catalysed the formation of **6c** in low yields from Et_2NH (**4c**). Accordingly, while we observed a 20% of conversion that corresponds to the background reaction in the case of **4a** and **4b**, the uncatalyzed reaction did not generate a measurable amount of product when **4c** was used as reagent. (see. S. I., section 6).

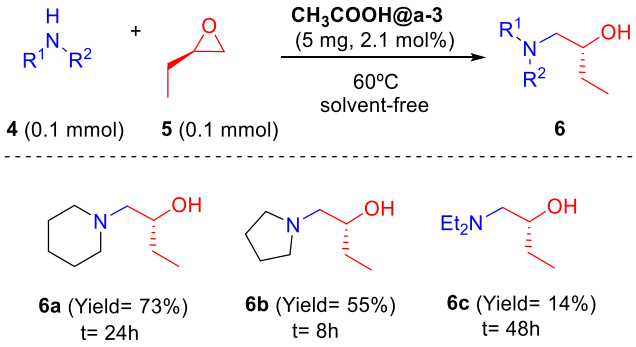

Scheme 3. Scope of epoxide ring opening reactions explored in this work catalysed by **CH_3COOH@a-3**.

3.2.3. Basic Catalysis: Knoevenagel Reaction using $CH_3COOH\cdots NEt_3$@a-3

We next expanded the scope of Knoevenagel reaction using different aldehydes **8b-g** (**Scheme 4**). We found an excellent catalytic outcome, which was maintained with electron donating groups, such as methyl or methoxy groups (**9b-c**), alkyl groups (**9d**), and more sterically demanding aldehydes (**9e** and **9f**). However, further increase of the steric hindrance in reagent **8g** resulted in null conversion to the Knoevenagel product **9g**. Considering that product **9g** could be obtained in homogenous catalysis using NEt_3 (see S. I., section 6), the null reactivity observed using **$CH_3COOH\cdots NEt_3$@a-3** can be understood by a size discrimination effect. In these Knoevenagel process, the background reactions were not significant (less than 5%, see S. I., see section 6).

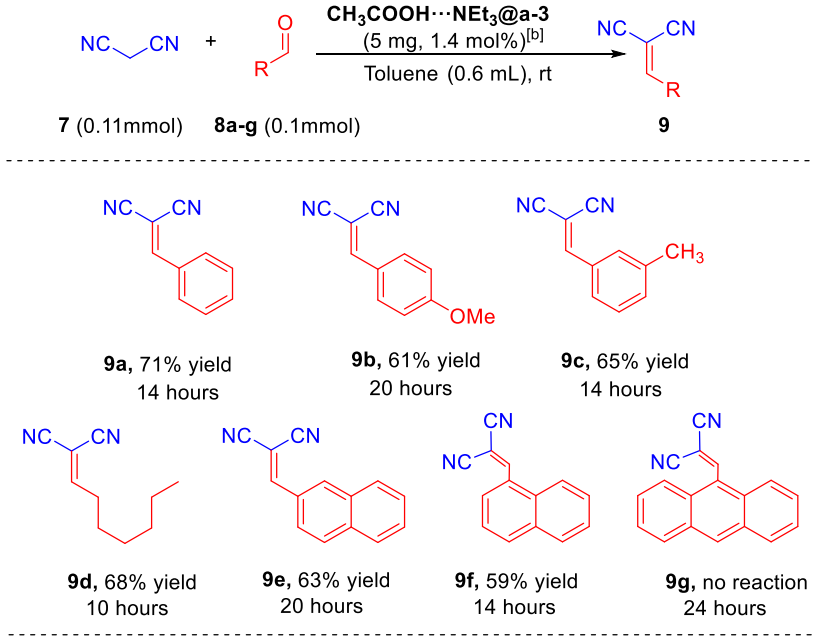

Scheme 4. Knoevenagel reactions explored in this work between malononitrile and aldehydes catalysed by **$CH_3COOH\cdots NEt_3$@a-3**. All the reactions were performed using 0.11 mmol of acetonitrile **7**, 0.1 mmol of aldehyde **8** and 5 mg of **$CH_3COOH\cdots NEt_3$@a-3** in 0.6 mL of toluene at room temperature. [b] mol% obtained from TGA analysis (4.6 % of total mass).

3.3. DFT analysis of the interactions between the imine structure and adsorbed molecules and the influence of confinement on the catalytic activity

3.3.1. DFT calculations for the imine structure-adsorbed molecules interactions

With the aim of further characterizing these materials and supporting the experimental data, DFT calculations with periodic boundary conditions were used to evaluate the interaction between the imine structure of **a-3/c-3** and CH_3COOH, NEt_3 and $CH_3COOH\cdots NEt_3$ adduct (see S.I., section 11). Note here that we considered that this methodology allows to investigate confined phenomena on both **a-3** and **c-3**. In fact, even though **a-3** has an amorphous character it should present many cavities such as the calculated, because its imine structure is similar to that of **c-3**, as confirmed by ^{13}C-NMR and FT-IR. Calculations were performed at the PBE-D2

level of theory with an energy cut-off of 400 eV. Results are presented in **Figure 6**, showing the optimized geometries, selected geometrical parameters and the adsorption energies of these imine structures functionalized with CH_3COOH, NEt_3 and $CH_3COOH\cdots NEt_3$ adducts. At this point, it is worth mentioning that we explored a limited number of relative orientations between the imine structure and the adsorbed molecule, as well as different conformations of the adsorbed molecules. The computed adsorption energies did not present large differences and therefore, we assumed that main trends would be conserved, even if more favorable minima were overlooked.

The interaction between acetic acid and the imine structure is stablished through hydrogen bonding between the acidic proton of the acetic acid and the imine group of the structure (**Figure 6**, top). The OH···N distance is 1.66 Å, which is indicative of a strong hydrogen bond. The associated adsorption energy is -79.4 kJ mol^{-1}.

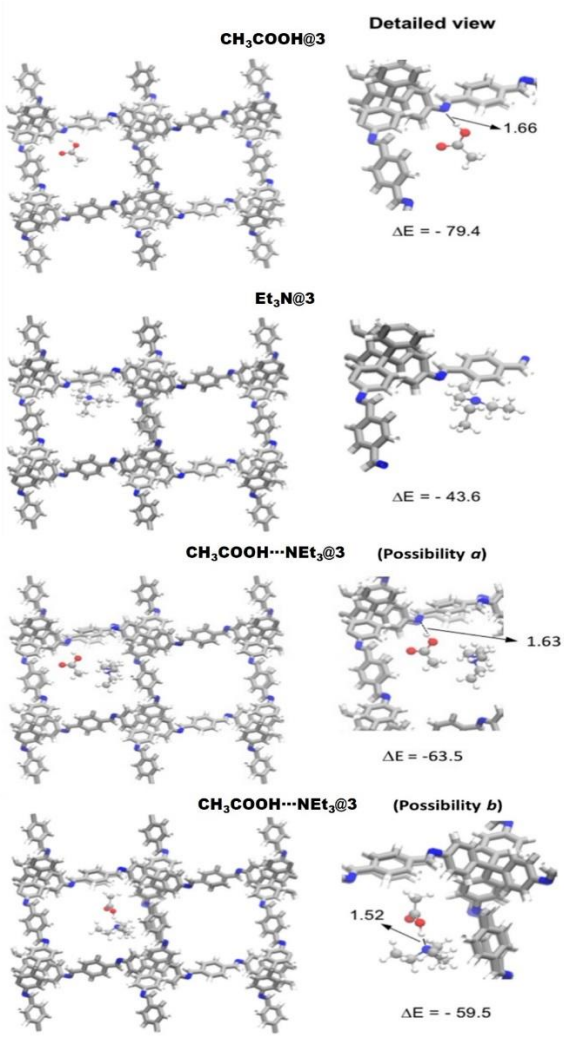

Figure 6. Optimized imine structures where CH_3COOH, NEt_3 and $CH_3COOH\cdots NEt_3$ adducts are included (distances in Å), and interaction energies (kJ mol^{-1}) between imine structure and the incorporated molecules.

On the other hand, the imine of the structure and the adsorbed amine (NEt_3) are both basic and no hydrogen bonding is possible between them. In this context, the adsorption takes place only through Van der Waals interactions and the preferred structure presents the NEt_3

close to the walls of the imine material. The shortest distances between atoms of NEt_3 and those of the imine structure are smaller than 4 Å (**Figure 6**, middle). The resulting adsorption energy is -43.6 kJ mol^{-1}.

Finally, we studied the interaction of the $CH_3COOH\cdots NEt_3$ mixture with the imine structure, considering a 1 to 1 relationship between CH_3COOH and NEt_3 (**Figure 6**, middle). Three possibilities were considered (see **Figure 6** and S21 of the Supporting Information): *a*) The interaction between CH_3COOH and the imine structure through hydrogen bonding with the presence of a NEt_3 molecule in the channel; *b*) The formation of a $CH_3COOH\cdots NEt_3$ complex interacting with the imine structure through Van der Waals interactions; and *c)* The interaction between a protonated triethylammonium ion with the imine group of the structure through hydrogen bonding and an acetate anion inside the channel. [26]

Within these initial structures, possibilities *a)* and *b)* almost equally raised as the most favorable situations. The first one can be described as an CH_3COOH molecule interacting with the imine structure through hydrogen bonding, while the remaining NEt_3 molecule interacts with the imine structure and CH_3COOH through van der Waals interactions. Such structure presents a strong N···HO hydrogen bond as evidenced by a short distance of around 1.52 Å. The second one implies the formation of a neutral $CH_3COOH\cdots NEt_3$ aggregate, interacting with the imine structure through van der Waals interactions, being the shortest distances between the guest molecules and the imine structure around 2.5 Å (**Figure 6**, bottom). Therefore, the mixture CH_3COOH + NEt_3 in the imine structure shows a combination of intermolecular and molecule-imine structure interactions that enhance the adsorption of the base molecule. For this material, we evaluated the thermodynamic cost of leaching one molecule of NEt_3 (47 kJ mol^{-1}) or the whole $CH_3COOH\cdots NEt_3$ aggregate (59.5 kJ mol^{-1}). Therefore, the most probable leaching process will correspond to the liberation of NEt_3 from **$CH_3COOH\cdots$ NEt_3@a-3/c-3**.

Overall, the computed adsorption energies suggested that NEt_3 will be more easily released from the imine structure when no CH_3COOH is present in the material (by 15.9 kJ mol^{-1}). Moreover, CH_3COOH in **CH_3COOH@a-3/c-3** was adsorbed more strongly than $CH_3COOH\cdots NEt_3$ aggregate in **$NEt_3\cdots CH_3COOH$@a-3/c-3**, suggesting that their removal would require harder conditions.

3.3.2. Analysis of Influence of Confinement of the Active Site by DFT Calculations

With the aim of further analysing the influence of the imine structure in the catalytic processes, we performed DFT calculations of the ring opening epoxide reaction catalysed by **CH_3COOH@a-3/c-3** and the Knoevenagel reaction catalysed by **$CH_3COOH\cdots NEt_3$@a-3/c-3**. Although CH_3COOH is needed to prevent NEt_3 leaching in the latter process, the base is the active catalytic centre. Therefore, we did not include CH_3COOH in the modelling in order to decrease the computational cost. The computational study was focused on understanding if the reaction can take place in a cavity defined by the imine structure as well as on determining the possible origin of the size selectivity. For that, we considered both the molecular systems and calculations with periodic boundary conditions, including the whole imine structure (see S. I., section 11 for the computational details). In each reaction, we explored the elementary step in which the new C-N or C-C bonds are formed (**Scheme 5**), assuming that the protonation/deprotonation steps as well as those for dehydration would be kinetically easier.

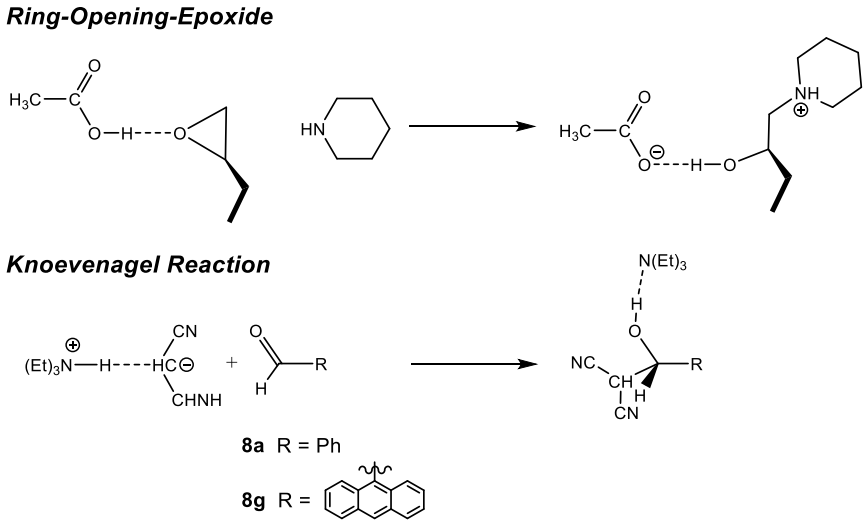

Scheme 5. Reaction steps studied computationally for the epoxide ring opening and Knoevenagel reactions.

3.3.2.1. Ring-Opening-Epoxide

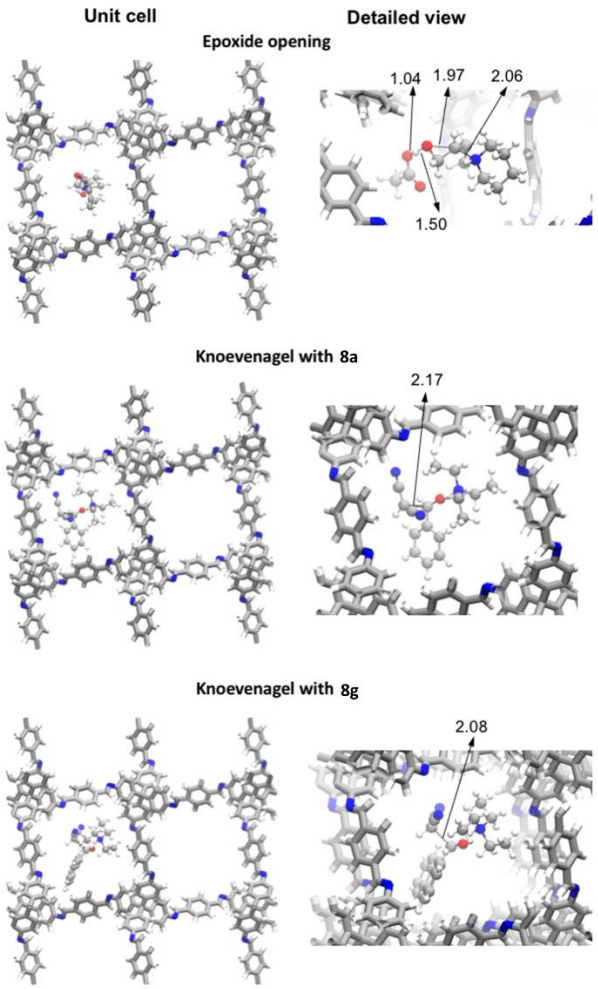

Figure 7. Optimized structures of the transition states associated to the ring opening epoxide and Knoevenagel reactions in the cavity defined by the imine structure. All distances are in Åmstrongs.

Regarding to the homogenous conditions, M06 calculations in gas phase and solution suggested that the reaction is concerted and once the epoxide ring is opened, the C-N bond is formed, and the proton of CH_3COOH is simultaneously transferred to the geminal alkoxide (see **Scheme 5** and **Figure 7**). In solution, this concerted process is exothermic in terms of potential energy (-118.6 kJ mol^{-1}) and it presents a relatively low energy barrier of 73.8 kJ mol^{-1} with respect to the reactants together forming the initial complex (**Figure 8**). It is worth mentioning that the main difficulty to perform the reaction is to approach the three reactants. Indeed, entropic effects are highly unfavourable and once thermal corrections are considered, the energy barrier becomes significantly higher ($\Delta G^{\ddagger}$ = 135.1 kJ mol^{-1}, see S.I.).

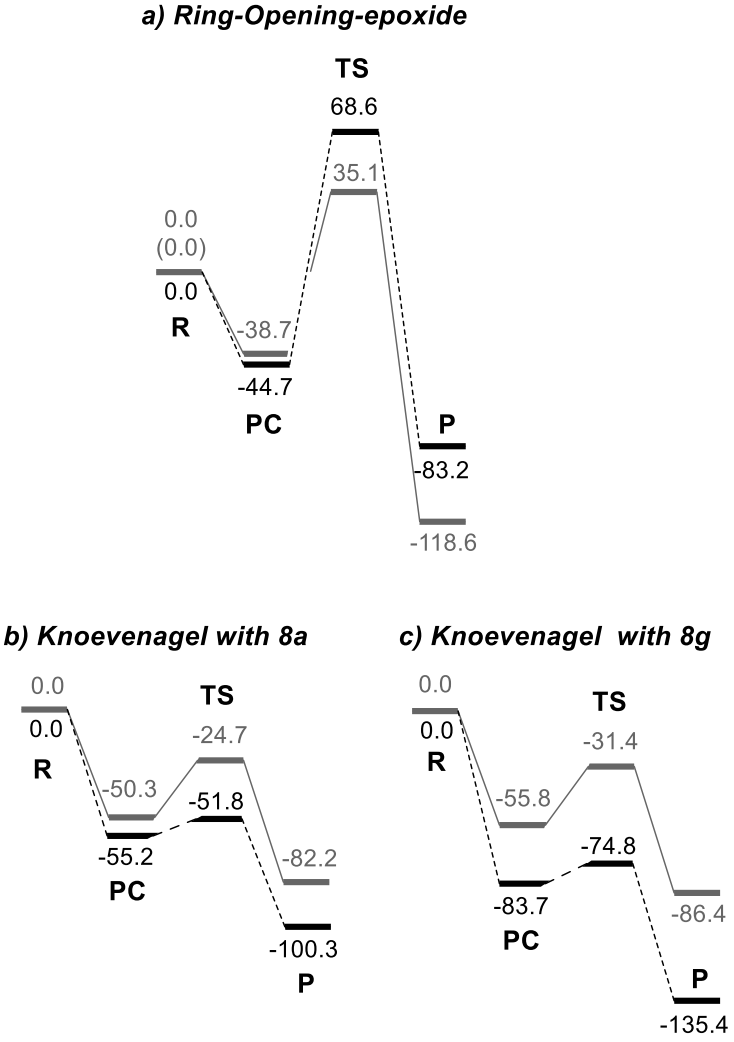

Figure 8. Energy profile in kJ mol^{-1} of Ring-Opening-Epoxide (a) and Knoevenagel with **8a** (b) and **8g** (c). Grey curves correspond to the M06/6-311+G(d,p) values associated with reaction in solution, while values in black correspond to the best estimated values for the reactions inside a cavity defined by the imine structure. **R** stands for separated reactants, **PC** for the reacting precomplex, **TS** for transition state and **P** for the products of the elementary step considered

Inclusion of the imine structure has little influence on the reaction energetics. Comparison between the molecular M06 values with those obtained with the best estimation considering the whole materials show little differences. In general, the imine structure marginally destabilizes the transition state. This suggests that the process would be slightly more energetically demanding inside the channels than in solution, but the computed energy barriers agree well with a feasible process requiring heating and large reaction times. The analysis of the structure of the transition state in the imine structure (**Figure 7**) shows that the

transition state perfectly fits inside the channel. The imine structure is around 4-5 Å far from the reacting species. Moreover, it suggests that cyclic secondary amines should in general react inside the imine structure, since their width (< 5 Å in the case of piperidine) is significantly smaller than the section of the cavity defined by the imine structure (around 11 Å).

3.3.2.2. Knoevenagel Reaction

We next explored the reaction considering two different aldehydes: benzaldehyde (**8a**) and anthracene-9-carbaldehyde (**8g**). The reaction of **8a** inside the cavity defined by the imine structure led to the formation of **9a** with a 71% yield, but **8g** did not react inside this cavity. Therefore, these two reactions are ideal examples to study the size selectivity.

Considering the homogenous system, molecular calculations in gas phase and solution showed that, regardless the reacting aldehyde, the nucleophilic attack to the carbonyl carbon (see **Scheme 5** and **Figure 8**) directly leads to the formation of the alcohol product, resulting from the addition of the deprotonated malononitrile (see S. I.). Indeed, the triethylammonium cation moved during this step from the malononitrile to the alkoxide group in a concerted manner (see **Scheme 5** and **Figure 7**). In solution, the global process is energetically highly favourable (ΔE = -82.2 and -86.4 kJ mol^{-1} for **8a** and **8g** respectively). The energy barrier with respect to the pre-complex are very low in these two cases (less than 26 kJ mol^{-1}). Therefore, although the entropic contribution approaching the three molecules together is again highly disfavoured. However, the global activation Gibbs energies are consistent with a feasible process ($\Delta G^{\ddagger}$ = 96.8 and 87.6 KJ mol^{-1} for the **8a** and **8g** respectively, see S. I., Figures S23-24). This is consistent with a relatively fast reaction, taking place at room temperature.

Several key features appeared when analysing the reactivity of **8a** and **8g** inside the cavity defined by the imine structure. In particular, aldehyde **8a** is sufficiently small to be accommodated inside the cavity either with the phenyl ring placed along or perpendicular to the channels of the material. This is due to the fact that the width of the phenyl ring is less than half of the cavity section. In contrast, aldehyde **8g** is significantly wider than **8a**. In fact, hydrogen atoms in positions 2 and 7 of the anthracene ring are separated by 9.2 Å, while the cavity section is smaller than 11 Å. Therefore, this imposes that the anthracene aldehyde **8g** can only diffuse in the less hindered orientation. Moreover, although several arrangements of the transition state of **8a** without steric hindrance from the cavity could be envisaged, we could only find two possibilities to settle the transition state associated to **8g**, but with severe geometrical constrictions (**Figure 7** and S. I., Figure S24). Therefore, diffusion of the reactants and products along the material seems to be much more favourable for **8a/9a** than for **8g/9g**. Overall, although the best estimated energies of the transition states inside the cavity are similar to those in solution, computations suggest that the system involving **8g** has much less flexibility inside the cavity and it would require a very specific orientation, which suggest that this would impose a high entropic penalization. This is especially relevant considering that the model used does not include neither the acetic acid needed to trap the triethylamine nor the solvent. Therefore, the diffusion of the resulting product **9g** would be challenging if ever formed. All this data together suggest that while **8a** and **8g** should react similarly in solution, the reaction of **8g** becomes more difficult inside the cavity. This reinforces the fact that the reaction takes place inside the material and that size selectivity would appear when the reactant is wider than 9 – 10 Å, such is the case of the three fused aromatic rings.

3.4 Stability of a-3 and derivatized materials under the reaction conditions: Disassembly pathways

In addition to the reactions shown above, we carried out the reaction between *para*-methoxyaniline (**4d**) and ethyl epoxide **5** (**Scheme 6**).[27] When **CH_3COOH@a-3** was used as catalyst, this reaction resulted on selective formation of mono-substituted product **6d** in a low yield (20 %; Scheme 6). This low yield was due to the disassembly of **CH_3COOH@a-3**, as we detected the formation of the corresponding imine **10** in the crude mixture (**Scheme 6**). Indeed, a strong change in the morphology of **CH_3COOH@a-3** was found by SEM (see bottom, **Scheme 6** and compare with **Figure 4**). The fact that the catalytic activity was stopped because of the disassembly of material was a clear indication that catalysis depended on the integrity of **CH_3COOH@a-3**. Therefore, CH_3COOH molecules act as catalytic centres only when they are associated to the porous framework, otherwise they easily vaporise.

Scheme 6. Initial ring opening epoxide explored in this work catalysed by **CH_3COOH@a-3**. Inset shows SEM image of the solid residue after the catalytic run. [a] mol% obtained from TGA analysis (2.57% of total mass). [b]Yield related to the consumption of **4d**.

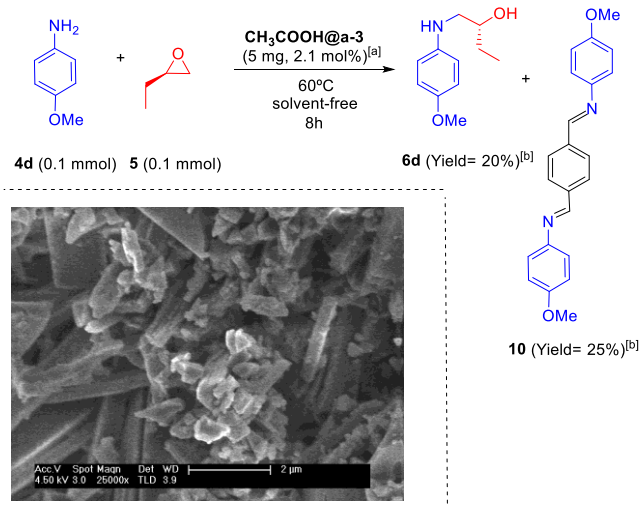

Scheme 6. Initial ring opening epoxide explored in this work catalysed by **CH_3COOH@a-3**. Inset shows SEM image of the solid residue after the catalytic run. [a] mol% obtained from TGA analysis (2.57% of total mass). [b]Yield related to the consumption of **4d**.

In the quest to obtain further insights on the reasons for the scarce yield obtained in the reaction between ethyl epoxide and methoxy aniline (see **Scheme 6**), we examined the stability of **CH_3COOH@a-3** towards the aniline, secondary amine and epoxide reagents. Epoxide reagent **5** did not show any reactivity with **CH_3COOH@a-3** (Equation a, **Scheme 7**), whereas methoxyaniline **4d** decomposed the imine structure through nucleophilic attack, resulting in the formation of a molecular diimine **10** (Equation b, **Scheme 7**). Such decomposition was followed by the presence of a ^{1}H-NMR signal in $CDCl_3$ at 8.54 pm (due to N=CH- protons). In contrast, the secondary amine did not react at all (Equation c, **Scheme 7**).

We extended this evaluation to the reaction conditions of a typical Knoevenagel condensation (see above, **Scheme 4**). To this end, we analysed the stability of **$CH_3COOH\cdots NEt_3$@a-3** towards malononitrile (**7**) and benzaldehyde (**8a**) (Equation d and e,

Scheme 7). While benzaldehyde reagent was inert towards the imine structure, malononitrile reacted with it through nucleophilic attack (Equation e). The generation of the molecular product from such decomposition was also followed by the presence of the ^{1}H-NMR signals in $CDCl_3$ at 8.05 and 7.82 ppm (C_6H_4 ring and $(CN)_2C$=CH- proton, respectively, see S. I., section 7).

The results presented above clearly indicated that **a-3** was reactive in presence of strong nucleophiles (**7** and **4d**) producing stable products. Therefore, imine structures are sensitive to the nucleophilic attack that result in erosion of the organic framework as a consequence of the reversible nature of the imine bond. Such decomposition reactivity competes with the catalysed reaction. Thus, in the case of Knoevenagel reactions, catalytic conditions (excess of aldehyde with respect to material) disfavour such reactivity. Indeed, examination by ^{1}H-NMR of the reaction mixture between benzaldehyde and malononitrile revealed that, while 5% of malononitrile reacted with the catalytic material (which corresponds to a 14% of the material), the remaining 95% of such substrate reacted with the benzaldehyde to produce the expected Knoevenagel product **9a**. Nevertheless, imine structure reactivity limits the output of the catalytic reaction and the recyclability of the corresponding material (see S. I., section 7).

Scheme 7. Stability studies performed on catalytically active **a-3** used in this work. [a] NMR yield related to decomposed material being other reagents in large excess, see S.I. for details.

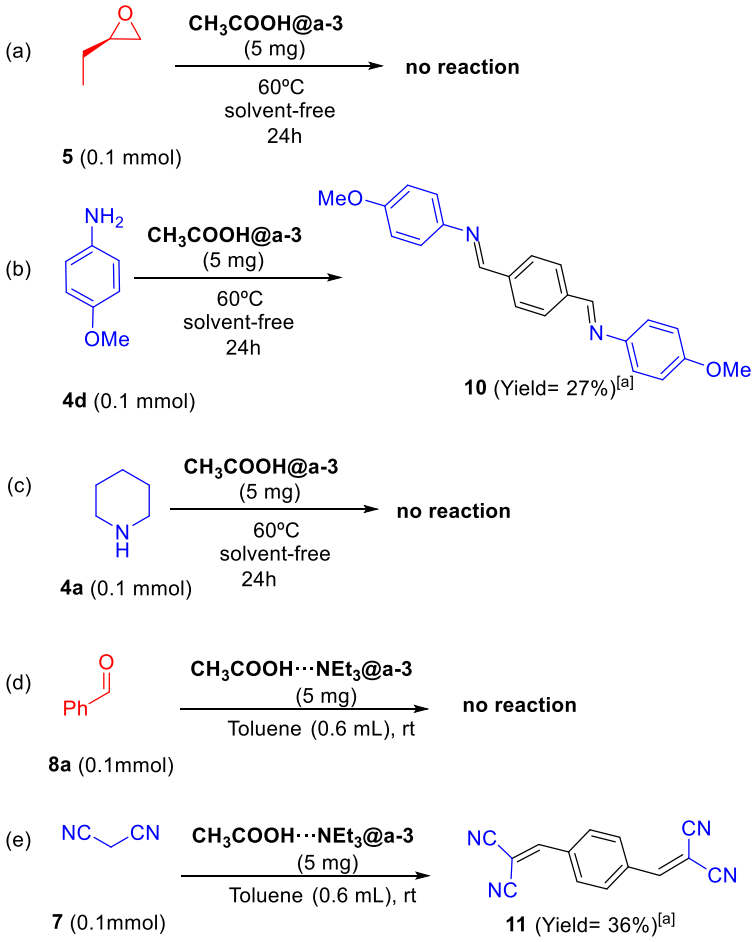

Scheme 7. Stability studies performed on catalytically active **a-3** used in this work. [a] NMR yield related to decomposed material being other reagents in large excess, see S.I. for details.

4. Conclusions

In this work we successfully carried out the supramolecular functionalization of crystalline COF-300 and related amorphous imine polymer nanoparticles with CH_3COOH molecules and the adduct $CH_3COOH\cdots NEt_3$. Gas adsorption experiments on crystalline samples corroborated the partial blocking of the porosity by the inclusion of CH_3COOH molecules or $CH_3COOH\cdots NEt_3$ adducts. Such inclusion dramatically reduced the porosity of such materials, avoiding the access of reagents to the internal parts of the framework. Therefore, catalysis using these functionalized COFs was moderate and restricted to their external surface area. Considering this, we increased the acid/base catalytic activity of these materials by using amorphous imine polymer nanoparticles, whose external surface area is higher than that of the micrometer crystals. Despite that these nanoparticles are amorphous and non-porous, its functionalization with CH_3COOH molecules and $CH_3COOH\cdots NEt_3$ adducts allowed use them as efficient catalysts for acidic ring opening epoxide and basic Knoevenagel reactions, respectively. Moreover, this catalysis exhibited size selectivity in Knoevenagel transformations, suggesting that reactions must take place into cavities of the imine structure located on the nanoparticle surface. Consistently, periodic boundary condition DFT calculations confirmed that the reaction can take place in cavities defined by the imine framework. Moreover, decomposition pathways were found when the imine-based organic framework reacts with a strong nucleophile, compromising the catalytic output and recyclability of these systems. These processes should definitively be considered for future designs of catalytic organic frameworks and for other applications where assembly/disassembly phenomena are crucial. Overall, this work presents a new alternative to modulate the catalytic properties of organic porous materials relying on non-covalent encapsulation of small acidic or basic molecules. Altogether, this approach provides several unique advantages and expands the scope of reactions mediated by organic materials.

Supporting Information

Supporting Information is available from the Wiley Online Library or from the author.

Acknowledgements

This work was supported by Spanish Ministerio de Economia y Competitividad (MINECO) (CTQ2015-64561-R; CTQ2017-89132-P; RTI2018-095038-B-I00) and “Comunidad de Madrid” and European Structural Funds (S2018/NMT-4367). It was also supported by the Generalitat de Catalunya (SGR XSM is grateful for the Professor Agregat Serra Húnter position). R. C. thanks to CAM for the “Atracción de Talento” fellowship.

[1] a) M. Yoshizawa, J. K. Klosterman, M. Fujita, Angew. Chem., Int. Ed. 48 (2009), 3418−3438. b) J. M. Wiester, P. A. Ulmann, C. A. Mirkin, Angew. Chem., Int. Ed. 50 (2011), 114−137. c) S. H. A. M. Leenders, R.Gramage-Doria, B. de Bruin, J. N. H. Reek, Chem. Soc. Rev. 44 (2015), 433−448.
[2] a) M. Yoshizawa, M. Tamura, M. Fujita, Science 312 (2006), 251−254. b) A. Cavarzan, A. Scarso, P. Sgarbossa, G. Strukul, J. N. H. Reek, J. Am. Chem. Soc. 133 (2011), 2848−2851. c) R. Gramage-Doria, J. Hessels, S. H. M. Leenders, O. Tröppner, M. Dürr, I. Ivanović-Burmazović, J. N. H. Reek, Angew. Chem., Int. Ed. 53 (2014), 13380−13384.
[3] D. M. Dalton, S. R. Ellis, E. M. Nichols, R. A. Mathies, F. D. Toste, R. G. Bergman, K. N. Raymond, J. Am. Chem. Soc. 137 (2015), 10128−10131.
[4] a) P. Thordarson, E. J. A. Bijsterveld, A. E. Rowan, R. J. M. Nolte, Nature 424 (2003), 915−918. b) C. J. Brown, R. G. Bergman, K. N. Raymond, J. Am. Chem. Soc. 131 (2009), 17530−17531. c) C. García-Simón, R. Gramage-Doria, S. Raoufmoghaddam, T. Parella, M. Costas, X. Ribas, J. N. H. Reek, J. Am. Chem. Soc. 137 (2015), 2680−2687.
[5] a) J. Chen, J. J. Rebek, Org. Lett. 4 (2002), 327−329. b) P.Howlader, P. Das, E. Zangrando, P. S. Mukherjee, J. Am. Chem. Soc. 138 (2016), 138, 1668−1676.
[6] See for instance: C. Martínez, A. Corma Coord. Chem. Rev. 255 (2011), 1558-1580.
[7] C. Perego, R. Millini, Chem Soc. Rev. 42 (2013), 3956-3976
[8] A. Kamakar, A. V. Desai, S. K. Ghosh, Chem. Rev. 307 (2016), 313-341.
[9] A. P. Coté, A. I. Benin, N. W. Ockwig, M.O'Keeffe, A. J. Matzger, O. M. Yaghi, Science 310 (2005), 1166-1170.
[10] a) M. G. Rabbani, A. K. Sekizkardes, Z. Kahveci, T. E. Reich, R. Ding, Chem. Eur. J. 19 (2013), 3324–3328. b) B. Ashourirad, A. K. Sekizkardes, S. Altarawneh, H. M. El-Kaderi, Chem. Mater. 27 (2015), 1349–1358.
[11] a) D. Kaleeswaran, P. Vishnoi, R. Murugavel, J. Mater. Chem. C 3 (2015), 7159–7171. b) S. Dalapati, S. Jin, J. Gao, Y. Xu, A. Nagai, D. Jiang, J. Am. Chem. Soc. 135 (2013), 17310–17313.
[12] a) M. Dogru, M. Handloser, F. Auras, T. Kunz, D. Medina, A. Hartschuh, P. Knochel, T. Bein, Angew. Chem., Int. Ed. 52 (2013), 2920–2924. b) S. Wan, F. Gándara, A. Asano, H. Furukawa, A. Saeki, S. K. Dey, L. Liao, M. W. Ambrogio, Y. Y. Botros, X. Duan, S. Seki, J. F. Stoddart, O. M. Yaghi, Chem. Mater. 23 (2011), 4094–4097.
[13] a) L. Stegbauer, K. Schwinghammer, B. V. Lotsch, Chem. Sci. 5 (2014), 2789–2793. b) V. S. Vyas, F. Haase, L. Stegbauer, G. Savasci, F. Podjaski, C. Ochsenfeld, B. V. Lotsch, Nat. Commun. 6 (2015), 8508. c) H. Yang, S. Zhang, L. Han, Z. Zhang, Z. Xue, ACS Appl. Mater. Interfaces 8 (2016), 5366–5375
[14] a) J. Thote, H. B. Aiyappa, A. Deshpande, D. D. Díaz, S. Kurungot, Chem. Eur. J. 20 (2014), 15961–15965. b) S. Ding, J. Gao, Q. Wang, Y. Zhang, W. Song, C. Su, W. Wang, J. Am. Chem. Soc. 133 (2011), 19816–19822. c) P. Pachfule, S. Kandambeth, D. D. Díaz, R. Banerjee, Chem. Commun. 50 (2014), 3169–3172. d) P. Pachfule, M. Panda, S. Kandambeth, S. M. Shivaprasad, D. Diaz, J. Mater. Chem. A 2 (2014), 7944–7952.
[15] Q. Fang, S. Gu, J. Zheng, Z. Zhuang, S. Qiu, Y. Yan, Angew. Chem. Int. Ed. 53 (2014), 2878 –2882.
[16] a) H. Xu, J. Gao, D. Jiang, Nat. Chem. 7 (2015), 905–912. b) H.-L. Qian, C.-X. Yang, X.-P. Yan, Nat. Commun. 7 (2016), article number: 12104.
[17] a) X. Han , Q. Xia, J. Huang, Y. Liu , C. Tan, Y. Cui, J. Am. Chem. Soc. 139 (2017), 8693–8697 b) Y. Zhi, P. Shao, X. Feng, H. Xia, Y. Zhang, Z. Shi, Y. Mua , X. Liu, J. Mater. Chem. A 6 (2018), 374.
[18] a) V. S. Vyas, M. Vishwakarma, I. Moudrakovski, F. Haase, G. Savasci, C. Ochsenfeld, J. P. Spatz,, B. V. Lotsch, Adv. Mater. 28 (2016), 8749-8754. b) S. Royuela, E. García-Garrido, M. Martín Arroyo, M. J. Mancheño, M. M. Ramos, D. González-Rodríguez, A. Somoza, F. Zamora, J. L. Segura, Chem. Commun. 2018, DOI: 10.1039/C8CC04346A.
[19] C. Montoro, D. Rodríguez-San-Miguel, E. Polo, R. Escudero-Cid, M. L. Ruiz-Gonzalez, J. A. R. Navarro, P. Ocón, F. Zamora, J. Am. Chem. Soc. 139 (2017), 10079−10086.
[20] F. J. Uribe-Romo, J. R. Hunt, H.Furukawa, C. Klöck, M.O'Keeffe, O. M. Yaghi, J. Am. Chem. Soc. 131 (2009), 4570–4571.

[21] A. de la Peña-Ruigómez, D. Rodríguez-San-Miguel, K. C. Stylianou, M. Cavallini, D, Gentili, F. Liscio, S. Milita, O. M. Roscioni, M. L. Ruiz-González, C. Carbonell, D. Maspoch, R. Mas-Ballesté, J. L. Segura, F. Zamora, Chem. Eur. J. 21 (2015), 10666-10670.
22 M. C. Daugherty, E, Vitaku, R. L. Li, A. M. Evans, A. M. Evans, A. D. Chavez, W. R. Ditchel, Chem. Commun. 55 (2019), 2680-2683.
[23] A. de la Peña-Ruigómez, D. Rodríguez-San-Miguel, K. C. Stylianou, M. Cavallini, D, Gentili, F. Liscio, S. Milita, O. M. Roscioni, M. L. Ruiz-González, C. Carbonell, D. Maspoch, R. Mas-Ballesté, J. L. Segura, F. Zamora, Chem. Eur. J. 21 (2015), 10666-10670.
[24] T. Ma, J. Li, J. Niu, L. Zhang, A. S. Etman, C. Lin, D. Shi, P. Chen, L.-H. Li, X. Du, J. Sun, W. Wang, J. Am. Chem. Soc. 140 (2018), 6763-6766.
[25] All the catalytic experiments were performed during a two weeks period from the synthesis of material, because we observed that storage of the materials for longer periods results in the decrease of catalytic activity, probably due to loss CH_3COOH and/or NEt_3 volatile molecules.
[26] In this latter case, we also explored the possibility of an ion pair formation $CH_3COO^{-}\cdots{}^{+}HNEt_3$, but the optimization evolved to the structure without charge separation.
[27] We carried out this reaction, using as a catalyst the **CH_3COOH@COF** under the conditions that we found optimal for epoxide-ring opening by reaction with aniline catalyzed by MOF containing squaramides (solvent-less at 60 ºC). See: C. Vignatti, J. Luis-Barrera, V. Guillerm, I. Imaz, R. Mas-Balleste, J. Alemán, D. Maspoch, ChemCatChem, 2018, DOI: 10.1002/cctc.201801127.

10. Experimental Section

The experimental section is directly taken from the documents “Supporting Information” of each publication.

Each Supporting Information appears in the same order as the publications.

NMR spectra are only shown for representative compounds.

The complete documents “Supporting Information”, with all NMR spectra are compiled on the CD enclosed. The Cartesian coordinates of DFT calculation of publication 5 are also enclosed on the CD.

Supporting Information

Squaramide-IRMOF-16 Analogue for Catalysis of Solvent-Free, Epoxide Ring-Opening Tandem and Multicomponent Reactions

Claudia Vignatti[+], Javier Luis-Barrera[+], Vincent Guillerm, Inhar Imaz,* Rubén Mas-Ballesté,* José Alemán,* and Daniel Maspoch*

Electronic Supplementary Information

Squaramide-IRMOF-16 Analogue for Catalysis of Solvent-Free, Epoxide Ring-Opening Tandem and Multicomponent Reactions

Claudia Vignatti, Javier Luis-Barrera, Vincent Guillerm, Inhar Imaz, Rubén Mas-Ballesté, José Alemán and Daniel Maspoch

Table of Contents

S1. Materials and General Methods

Zinc(II) nitrate hexahydrate, dimethyl squarate, 4-aminobenzoic acid, trimethylamine, anilines **1a**-**1b** and epoxides **2a-2f** were purchased from commercial sources and used as received without further purification. Molecular squaramide **C** was synthesized following a described procedure in the literature[1].

Purity of all bulk materials was confirmed through X-Ray powder diffraction measurements (XRPD) collected on an *X'Pert PRO MPD analytical diffractometer Panalytical* at 45 kV and 40 mA using Cu Kα radiation (λ= 1.5419 Å) and compared with single crystal simulated patterns. Elemental analyses were obtained by using a *CarboErba EA1108 microanalyzer*. NMR spectra were acquired on a *Bruker Avance 300 MHz spectrometer*, running at 300 and 75 MHz for ^{1}H and ^{13}C, respectively (In some indicated cases they were acquired in a *Bruker Avance 250 MHz spectrometer*). Chemical shifts (δ) are reported in ppm relative to residual solvent signals (**$CDCl_3$**, 7.26 ppm for ^{1}H-NMR and 77.16 ppm for ^{13}C-NMR; **DMSO-d_6**, 2.50 ppm for ^{1}H-NMR and 39.52 ppm for ^{13}C-NMR). Coupling constants are reported in Hertz and the following abbreviations are used to describe peak patterns: s (singlet), d (doublet), t (triplet), q (quartet), m (multiplet), bs (broad singlet). Different methods have been used for measuring the exact mass (indicated for each case): **MS (ESI)** (Electrospray mass spectroscopy) acquired with an *Agilent Technologies 6120 Quadrupole LC/MS*; **MS (EI)** (Electron Ionization mass spectroscopy) acquired with an *Agilent Technologies 5977B MSD*, in these two techniques *MassWorks software ver. 4.0.0.0 (Cerno Bioscience*) was used for the formula identification. (*MassWorks* is a MS calibration software which calibrates for isotope profile as well as for mass accuracy allowing highly accurate comparisons between calibrated and theoretical spectra[2]); **MS (TOF-ESI)** (Electrospray mass spectroscopy with Time-of-flight detector) acquired with *microTOF-Q Bruker Daltonics* spectrometer. Optical rotation was recorded in cells with 10 cm path length; the solvents and concentrations (in g/100 mL) are indicated in each case. Flash column chromatography was performed using pore 60 Å, 40-63 μm silica gel. The kinetics studies were performed following the progress of the reaction by gas chromatography using an *Agilent Technologies 7820A GC System* with a Flame Ionization Detector (FID).

[1] N. Fu, A. D. Allen, S. Kobayashi, T. T. Tidwell, S. Vukovic, *J. Org. Chem.* **2007**, *72*, 1951-1956.

[2] a) Y. Wang, M. Gu, *Anal. Chem.* **2010**, *82*, 7055-7062. b) Y. Wang, Methods for Operating MS Instrument Systems, United States Patent No. 6,983,213, **2006**. c) N. Ochiaia, K. Sasamoto, K. MacNamara, *Journal of Chromatography A*, **2012**, *1270*, 296-304. d) H.-P. Ho, R.-Y. Lee, C.-Y. Chen, S.-R. Wang, Z.-G. Li, M.-R. Lee, *Rapid Commun. Mass Spectrom.* **2011**, *25*, 25-32.

S2. Synthesis of Ligand L1 and Sq_IRMOF-16

S2.1. Synthesis of L1

4-((2-Methoxy-3,4-dioxocyclobut-1-en-1-yl)amino)benzoic acid (c)

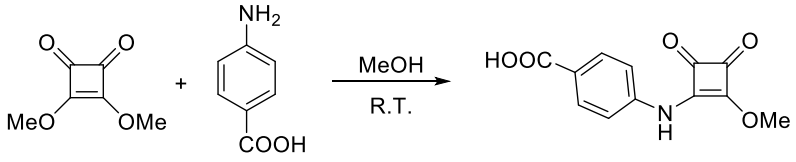

a **b** **c**

A white suspension of dimethyl squarate **a** (1.00 gr, 7.00 mmol) and 4-aminobenzoic acid **b** (0.960 g, 7.00 mmol) in 20 mL of dry MeOH was stirred 24 h at room temperature. The resulting yellow suspension was filtered, washed with MeOH and Et_2O and dried under vacuum to afford the desired pure compound **c** (1.30 g, 75% yield). **^{1}H-NMR (300 MHz, DMSO-d$_6$):** δ 12.71 (bs, 1H), 10.96 (s, 1H), 7.94 – 7.86 (m, 2H), 7.50 – 7.40 (m, 2H), 4.40 (s, 3H). **^{13}C-NMR (75 MHz, DMSO-d$_6$):** δ 187.6, 184.4, 179.5, 169.1, 166.8, 142.0, 130.6, 125.7, 118.7, 60.7.

4,4'-((3,4-Dioxocyclobut-1-ene-1,2-diyl)bis(azanediyl))dibenzoic acid (L1)

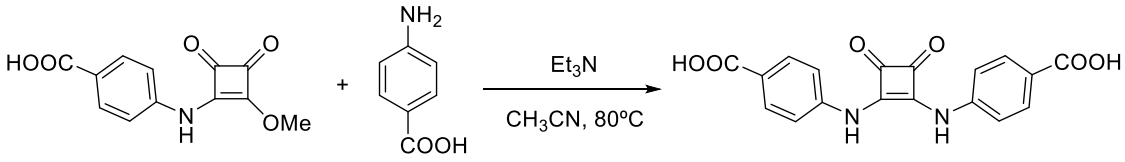

c **b** **L1**

Then, a mixture of **c** (0.90 gr, 3.60 mmol), 4-aminobenzoic acid **b** (0.497 g, 3.60 mmol) and Et_3N (0.503 mL, 3.60 mmol) in 18 mL of dry CH_3CN was heated at 80 ºC during 24 h in a sealed tube. The resulting suspension was concentrated up to *ca.* 9 mL. Then, H_2O (20 mL) was added and the pH was adjusted to 1 using HCl conc. The solid was filtered and washed thoroughly with H_2O until neutral pH and then with Et_2O, and dried under vacuum to afford pure squaramide **L1** (1.01 g, 80% yield). **^{1}H-NMR (250 MHz, DMSO-d$_6$):** δ 12.72 (bs, 2H), 10.31 (bs, 2H), 7.94 (d, J = 8.4 Hz, 4H), 7.57 (d, J = 8.4 Hz, 4H). **^{13}C-NMR (63 MHz, DMSO-d$_6$):** δ 182.0, 166.8, 165.9, 142.4, 130.9, 125.1, 118.0. **MS (TOF-ESI$^-$)**: Calcd. for $C_{18}H_{11}N_2O_6^-$ $[M-H]^-$: 351.0623. Found: 351.0614.

S2.2. Synthesis of Sq_IRMOF-16.

$Zn(NO_3)_2{\cdot}6H_2O$ (0.017 g, 0.057 mmol) and **L1** (0.020 g, 0.057 mmol) were dissolved in 4.8 mL DMF and heated to 85 ºC during 7 days. After this period, yellow cube crystals were collected in 53% yield and stored in DMF. FT-IR (ATR; cm^{-1}): 1650 (C=O from carboxylate) selected band. Anal. Calcd. for ($[Zn_4O(L1)_3]{\cdot}6H_2O{\cdot}4DMF$; $Zn_4C_{66}H_{70}N_{10}O_{29}$): C, 45.85; H, 4.08; N, 8.10, found: C, 45.00; H, 4.08; N, 9.00.

S3. XRPD diffractograms

Figure S1. Comparison of the experimental XRPD of **Sq_IRMOF-16** with simulated **IRMOF-16**.

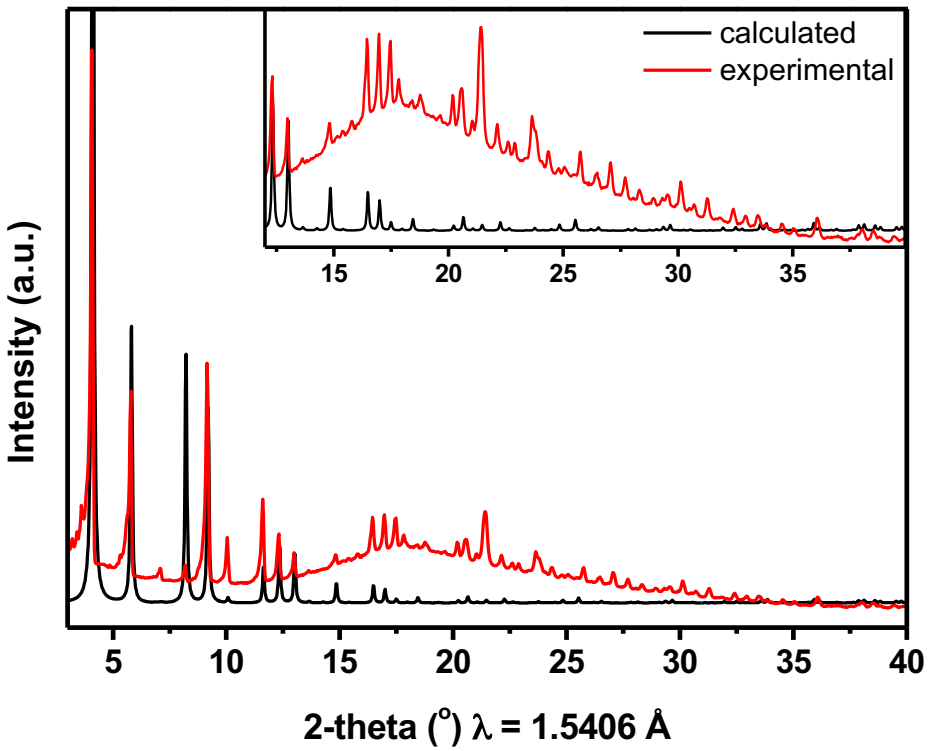

Figure S2. Comparison of the XRPD diffractograms of as-synthesized **Sq_IRMOF-16** (black) and after drying it under N_2 (blue).

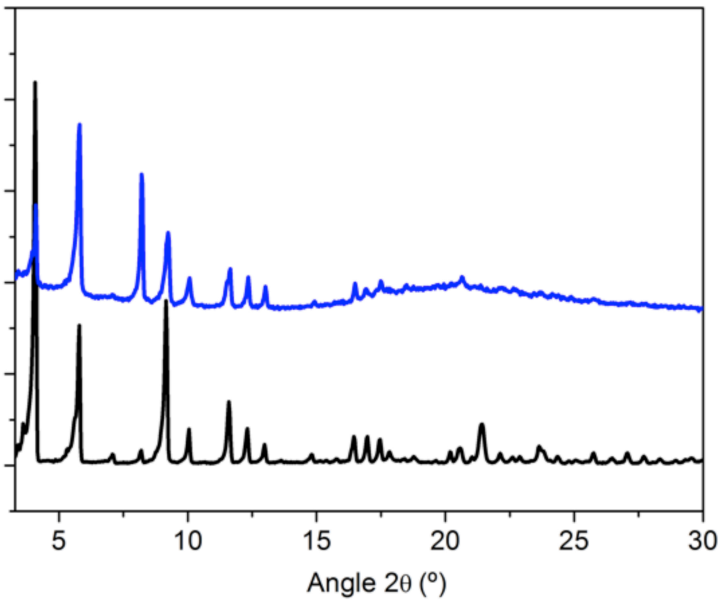

Figure S3. Comparison of the XRPD diffractograms of the synthesized **Sq-IRMOF-16** (black) and after exposing it to vacuum (red) and upon contact with water (blue).

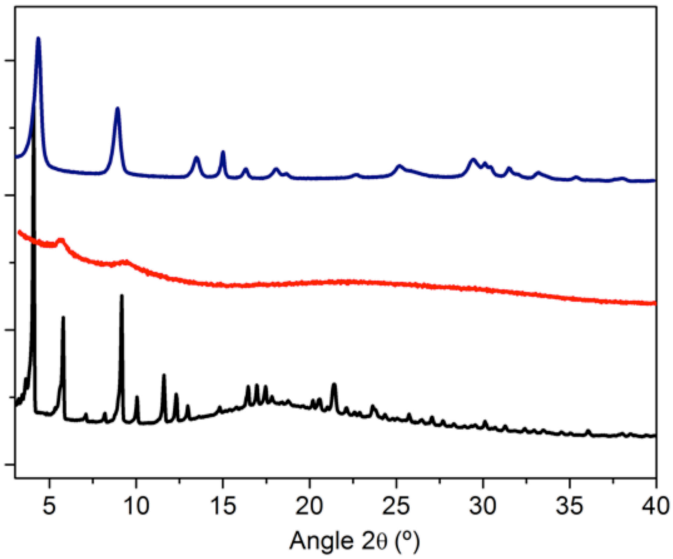

Figure S4. Comparison of the XRPD diffractograms of the synthesized **Sq-IRMOF-16** (black) and after using it as a catalyst for the epoxide ring-opening tandem (blue) and multicomponent (red) reactions.

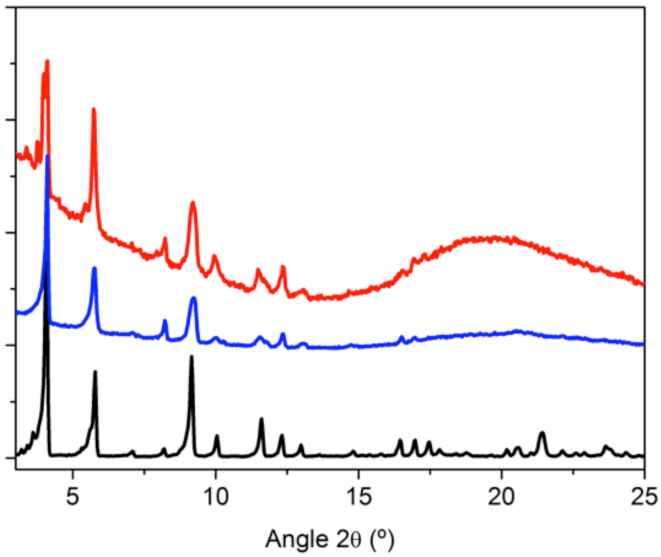

S4. Procedure and Data of kinetic studies

General procedure for the catalysis experiments

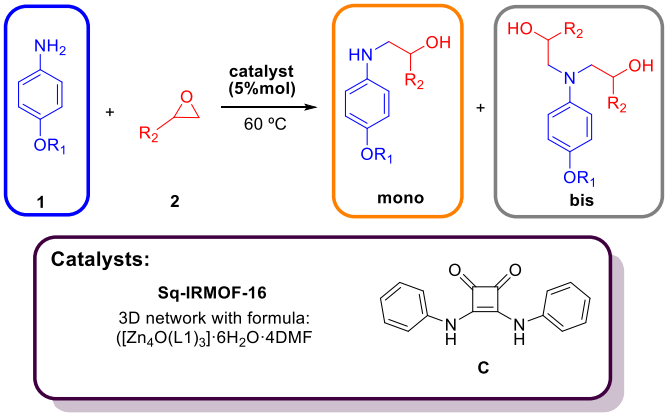

When **Sq_IRMOF-16** was used as catalyst, the required amount was dried under a nitrogen current during 2 h. 2.9 mg of dried **Sq_IRMOF-16** corresponded to 0.005 mmol of squaramide units. The catalyst **C** did not need any previous treatment.

The catalyst (0.005 mmol of squaramide units: 2.9 mg of **Sq_IRMOF-16** or 1.3 mg of **C**), 0.1 mmol of the corresponding aniline **1** and a stirring bar were transferred to a vial with septum and a nitrogen current was allowed to pass through the vial during 15 min. Then, 200 µL of the corresponding epoxide **2** was added (for the kinetics studies, racemic mixtures of epoxides **2** were used). The mixture was heated to 60 °C and it was stirred during 8 h. At different periods of time (1 h, 2 h, 4 h, 6 h and 8 h), an aliquot of 20 µL of the reaction mixture was taken and 500 µL of a 0.005 M solution of 2-methylnaphthalene (the standard for GC) in toluene was added to the aliquot. The aliquot was analysed by gas chromatography with FID detector.

Reaction 1a + 2a

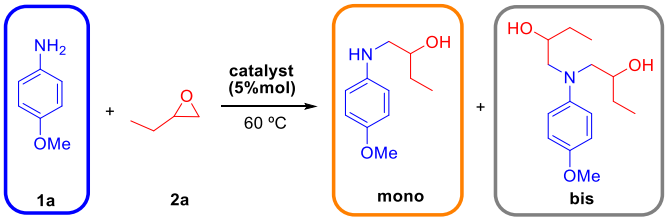

Sq_IRMOF-16

Time (h)	Aniline (%)	Mono (%)	Bis (%)
1	81	16	3
2	72	24	3
4	54	40	6
6	36	53	11
8	23	59	18

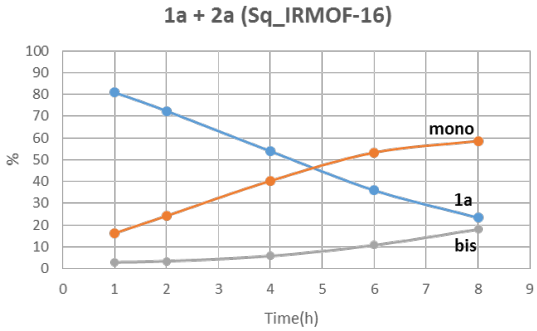

Catalyst C (Molecular Squaramide)

Time (h)	Aniline (%)	Mono (%)	Bis (%)
1	100	0	0
2	99	1	0
4	95	5	0
6	92	8	0
8	84	14	2

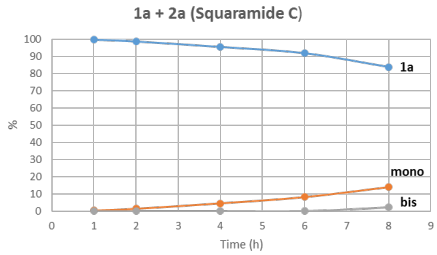

Without any catalyst

Time (h)	Aniline (%)	Mono (%)	Bis (%)
1	100	0	0
2	100	0	0
4	99	1	0
6	99	1	0
8	98	2	0

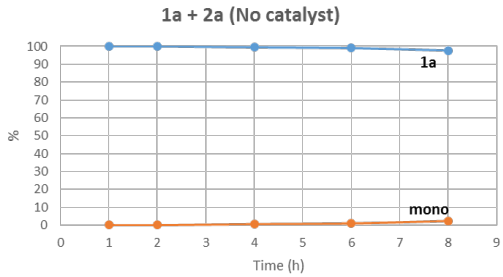

Reaction 1b + 2a

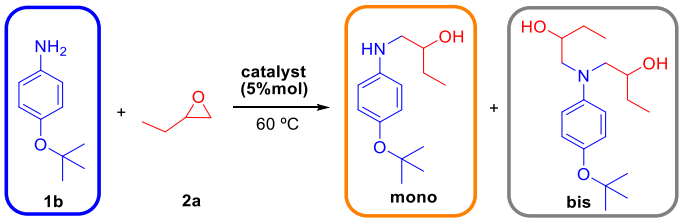

Sq_IRMOF-16

Time (h)	Aniline (%)	Mono (%)	Bis (%)
1	78	17	5
2	72	23	5
4	59	33	8
6	47	42	11
8	38	47	15

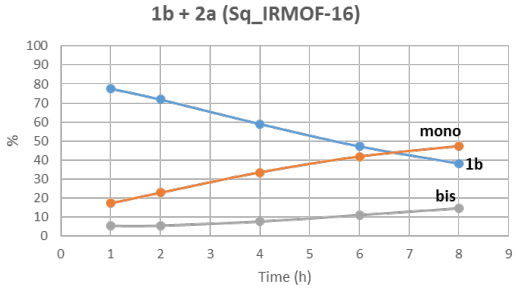

Catalyst C (Molecular Squaramide)

Time (h)	Aniline (%)	Mono (%)	Bis (%)
1	91	9	0
2	91	9	0
4	90	10	0
6	89	11	0
8	88	12	0

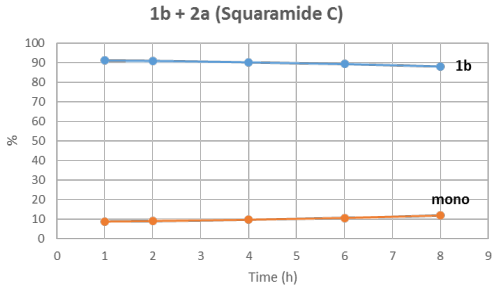

Without any catalyst

Time (h)	Aniline (%)	Mono (%)	Bis (%)
1	92	8	0
2	92	8	0
4	92	8	0
6	92	8	0
8	91	9	0

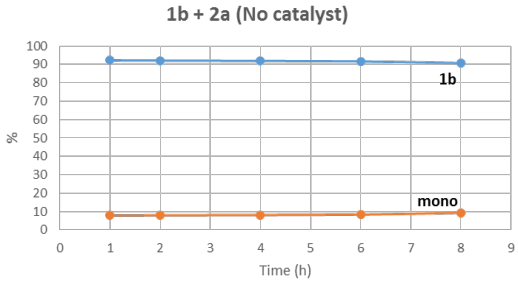

Reaction 1a + 2b

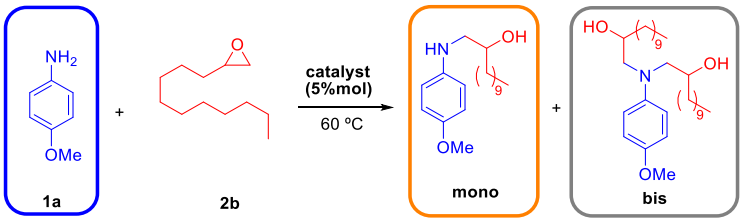

Sq_IRMOF-16

Time (h)	Aniline (%)	Mono (%)	Bis (%)
1	95	5	0
2	93	7	0
4	87	13	0
6	79	21	0
8	75	25	0

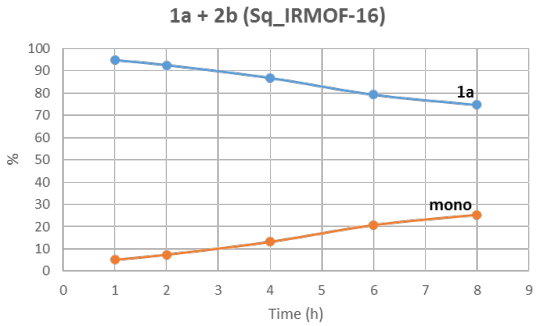

Catalyst C (Molecular Squaramide)

Time (h)	Aniline (%)	Mono (%)	Bis (%)
1	96	4	0
2	95	5	0
4	93	7	0
6	89	11	0
8	88	12	0

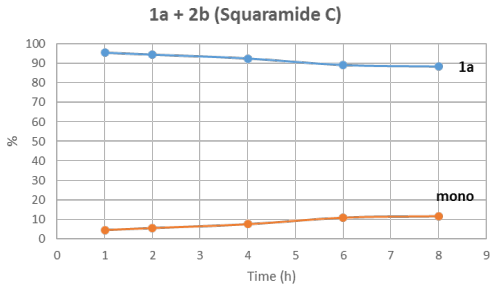

Without any catalyst

Time (h)	Aniline (%)	Mono (%)	Bis (%)
1	97	3	0
2	96	4	0
4	94	6	0
6	93	7	0
8	92	8	0

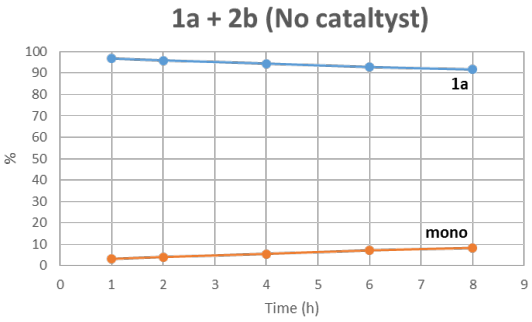

Reaction 1b + 2b

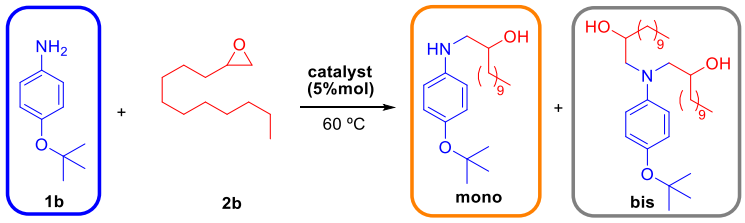

Sq_IRMOF-16

Time (h)	Aniline (%)	Mono (%)	Bis (%)
1	95	5	0
2	95	5	0
4	90	10	0
6	89	11	0
8	86	14	0

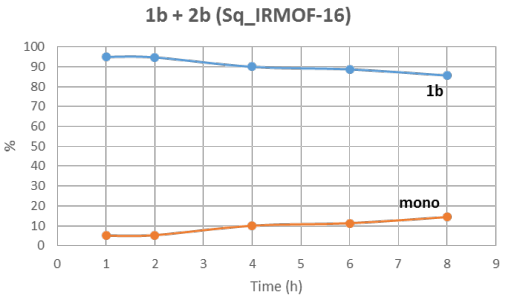

Without any catalyst

Time (h)	Aniline (%)	Mono (%)	Bis (%)
1	95	5	0
2	94	6	0
4	93	7	0
6	92	8	0
8	91	9	0

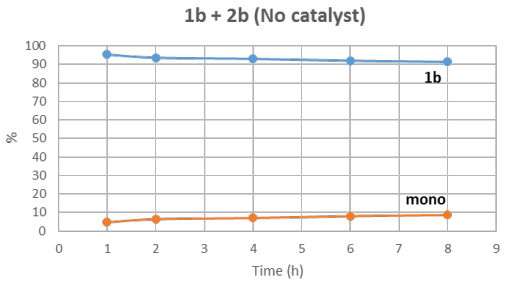

S5. Synthesis and characterization of aminodialcohols

S5.1 General procedure for the synthesis of homo-aminodialcohols 4 under Sq-IRMOF-16 catalysis.

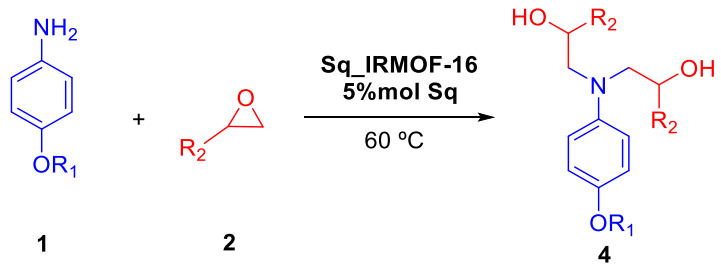

The required amount of **Sq_IRMOF-16** was dried under a nitrogen current during 2 h. 2.9 mg of dried **Sq_IRMOF-16** (0.005 mmol of squaramide units), 0.1 mmol of the corresponding aniline **1** and a stirring bar were transferred to a vial with septum and a nitrogen current was allowed to pass through the vial during 15 min. Then, 1 mmol of the corresponding optically pure epoxide **2** was added (in some indicated cases only 0.4 mmol was added). The mixture was heated to 60°C and it was stirred during the indicated time in each case. The progress of the reaction was controlled by ^{1}H-NMR. Once the reaction was finished, the product was purified by flash chromatography.

(2*S*,2'*S*)-1,1'-((4-Methoxyphenyl)azanediyl)bis(butan-2-ol) (4a)

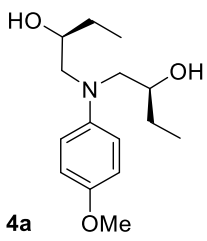

4a

The product was obtained following the described procedure after 39 h of stirring (Yield = 82%). The crude was purified by flash chromatography (cyclohexane: ethyl acetate 75:25 → 65:35). **$[\alpha]^{20}_{D}$** = -3.2 (c = 0.5, $CHCl_3$). **^{1}H-NMR (300 MHz, $CDCl_3$):** δ 6.92 – 6.78 (m, 4H), 3.80 – 3.70 (m, 2H), 3.76 (s, 3H), 3.31 (dd, *J* = 14.2, 2.7 Hz, 2H), 3.01 (dd, *J* = 14.2, 9.9 Hz, 2H), 2.76 (bs, 2H), 1.56 – 1.43 (m, 4H), 1.00 (t, *J* = 7.4 Hz, 6H). **^{13}C-NMR (75 MHz, CDCl3):** δ 153.5, 143.9, 118.5, 114.8, 69.9, 60.1, 55.8, 27.7, 10.1. **MS(EI$^+$):** Calculated for $C_{15}H_{25}NO_3^+$ $[M]^+$:267.1829; found: 267.1831.

(2*S*,2'*S*)-1,1'-((4-(*tert*-Butoxy)phenyl)azanediyl)bis(butan-2-ol) (4b)

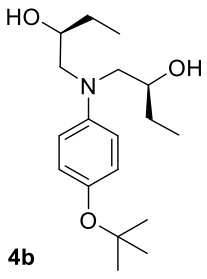

4b

The product was obtained following the described procedure after 3 days of stirring (Yield = 89%). The crude was purified by flash chromatography (cyclohexane: ethyl acetate 95:05 → 75:25). **$[\alpha]^{20}_{D}$** = -3.2 (c = 3.4, $CHCl_3$). **^{1}H-NMR (300 MHz, $CDCl_3$):** δ 6.86 – 6.77 (m, 2H), 6.72 – 6.64 (m, 2H), 3.83 – 3.70 (m, 2H), 3.34 (bs, 2H), 3.31 (dd, *J* = 14.5, 2.6 Hz, 2H), 3.05 (dd, *J* = 14.5, 9.7 Hz, 2H), 1.54 – 1.39 (m, 4H), 1.27 (s, 9H), 0.98 (t, *J* = 7.4 Hz, 6H). **^{13}C-NMR (75 MHz, $CDCl_3$):** δ 147.1, 145.9, 125.2, 115.6, 78.1, 70.0, 59.4, 28.8, 27.7, 10.1. **MS(EI$^+$):** Calculated for $C_{18}H_{31}NO_3^+$ $[M]^+$: 309.2298; found: 309.2298.

(2*R*,2'*R*)-1,1'-((4-Methoxyphenyl)azanediyl)bis(tridecan-2-ol) (4c)

The product was obtained following the described procedure using 0.4 mmol of epoxide **2c** after 3 days of stirring (Yield = 43%). The crude was purified by flash chromatography (cyclohexane: ethyl acetate 90:10 → 76:24). **$[\alpha]^{20}_D$** = +8.2 (c = 1.8, $CHCl_3$). **^{1}H-NMR (300 MHz, $CDCl_3$):** δ 6.90 – 6.77 (m, 4H), 3.86 – 3.70 (m, 2H), 3.76 (s, 3H), 3.30 (dd, *J* = 14.2, 2.7 Hz, 2H), 3.00 (dd, *J* = 14.1, 9.8 Hz, 2H), 2.71 (bs, 2H), 1.52 – 1.18 (m, 40H), 0.88 (t, *J* = 6.5 Hz, 6H). **^{13}C-NMR (75 MHz, $CDCl_3$):** δ 153.5, 144.0, 118.6, 114.8, 68.7, 60.4, 55.8, 34.9, 32.1, 29.9, 29.8, 29.8, 29.8 (x2), 29.5, 25.9, 22.8, 14.3. **MS(ESI$^+$):** Calculated for $C_{33}H_{62}NO_3^+$ $[M+H]^+$:520.4724; found: 520.4720.

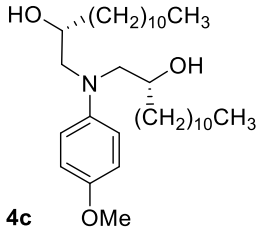

4c

1,1'-((4-(*tert*-Butoxy)phenyl)azanediyl)bis(dodecan-2-ol) (**4d**)

The product was obtained following the described procedure using 0.4 mmol of the epoxide **2b** (in this case a racemic mixture of the epoxide was used) after 4 days of stirring (Yield = 56%). The crude was purified by flash chromatography (cyclohexane: ethyl acetate 90:10 → 78:22). The spectroscopic data is given as a mixture of two diastereoisomers. **^{1}H-NMR (300 MHz, $CDCl_3$):** δ 6.90 – 6.82 (m, 4H), 6.76 – 6.69 (m, 2H), 6.53 – 6.44 (m, 2H), 4.03 – 3.93 (m, 2H), 4.03 – 3.93 (m, 2H), 3.69 (bs, 2H), 3.62 (dd, *J* = 15.1, 1.9 Hz, 2H), 3.35 (dd, *J* = 14.5, 2.6 Hz, 2H), 3.08 (dd, *J* = 14.6, 9.9 Hz, 2H), 2.99 (dd, *J* = 15.0, 9.7 Hz, 2H), 2.76 (bs, 2H), 1.53 – 1.21 (m, 90H), 0.88 (t, *J* = 6.5 Hz, 12H). **^{13}C-NMR (75 MHz, $CDCl_3$):** δ 147.3, 146.3, 145.9, 145.0, 125.4, 125.2, 115.7, 113.0, 78.0, 78.0, 70.3, 68.8, 62.1, 59.7, 35.0, 34.9, 32.1 (x2), 30.0 (x2), 29.8 (x2), 29.8 (x2), 29.8 (x2), 29.5 (x2), 28.9, 28.9, 25.9, 25.6, 22.8 (x2), 14.3 (x2). **MS(EI$^+$):** Calculated for $C_{34}H_{63}NO_3^+$ $[M]^+$: 533.4802; found: 533.4800.

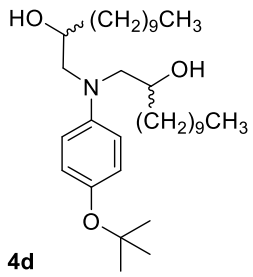

4d

(6*R*,10*R*)-8-(4-Methoxyphenyl)-2,2,3,3,13,13,14,14-octamethyl-4,12-dioxa-8-aza-3,13-disilapentadecane-6,10-diol (4e)

The product was obtained following the described procedure after 46 h of stirring (Yield = 72%). The crude was purified by flash chromatography (cyclohexane: ethyl acetate 90:10 → 75:25). **$[\alpha]^{20}_D$** = -11.7 (c = 2.8, $CHCl_3$). **^{1}H-NMR (300 MHz, $CDCl_3$):** δ 6.92-6.75 (m, 4H), 3.95-3.48 (m, 2H), 3.76 (s, 3H), 3.66 (dd, *J* = 10.1, 5.1 Hz, 2H), 3.59 (dd, *J* = 10.1, 5.5 Hz, 2H), 3.42 (dd, *J* = 14.6, 4.0 Hz, 2H), 3.29 (dd, *J* = 14.7, 7.7 Hz, 2H), 3.13 (s, 2H), 0.92 (s, 18H), 0.08 (d, *J* = 2.6 Hz, 12H). **^{13}C-NMR (75 MHz, CDCl3):** δ 152.6, 143.8, 116.5, 114.8, 69.9, 65.1, 56.3, 55.9, 26.0, 18.4, -5.3. **MS(ESI$^+$):** Calculated for $C_{25}H_{50}NO_5Si_2^+$ $[M+H]^+$:500.3222; found: 500.3240.

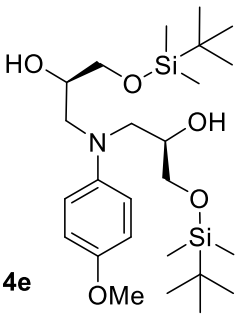

4e

Di-*tert*-Butyl ((2*S*,2'*S*)-((4-methoxyphenyl)azanediyl)bis(2-hydroxypropane-3,1-diyl))dicarbamate (4f)

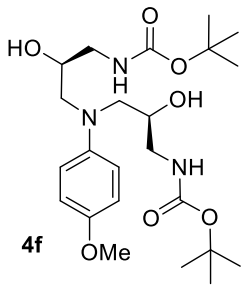

The product was obtained following the described procedure using 0.4 mmol of the epoxide **2e** after 22 hours of stirring (Yield = 99%). The crude was purified by flash chromatography (cyclohexane: ethyl acetate 70:30 → 20:80). **$[\alpha]^{20}_D$** = -18.9 (c = 1.9, $CHCl_3$). **^{1}H-NMR (300 MHz, $CDCl_3$):** δ 6.89-6.76 (m, 4H), 5.14 (bs, 2H), 4.00 (s, 2H), 3.87 (ddt, *J* = 10.1, 6.8, 3.4 Hz, 2H), 3.74 (s, 3H), 3.38-3.26 (m, 2H), 3.27 (dd, *J* = 14.3, 3.6 Hz, 2H), 3.16 – 3.00 (m, 4H), 1.43 (s, 18H). **^{13}C-NMR (75 MHz, $CDCl_3$):** δ 157.0, 153.8, 143.5, 118.6, 114.9, 79.9, 68.9, 57.9, 55.8, 44.4, 28.5. **MS(ESI$^+$):** Calculated for $C_{23}H_{40}N_3O_7^+$ $[M+H]^+$:470.2861; found: 470.2875.

Diethyl 4,4'-((4-methoxyphenyl)azanediyl)(3*S*,3'*S*)-bis(3-hydroxybutanoate) (4g)

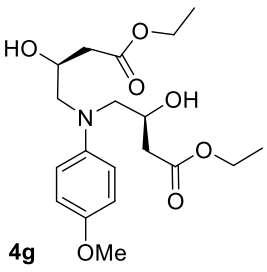

The product was obtained following the described procedure after 22 h of stirring (Yield = 94%). The crude was purified by flash chromatography (cyclohexane: ethyl acetate 90:10 → 85:15). **$[\alpha]^{20}_D$** = -23.2 (c = 1.2, $CHCl_3$). **^{1}H-NMR (300 MHz, $CDCl_3$):** δ 6.90 – 6.76 (m, 4H), 4.33 – 4.18 (m, 2H), 4.16 (q, *J* = 7.1 Hz, 4H), 3.75 (s, 3H), 3.68 (bs, 2H), 3.39 (dd, *J* = 14.5, 3.3 Hz, 2H), 3.21 (dd, *J* = 14.5, 8.9 Hz, 2H), 2.54 – 2.45 (m, 4H), 1.27 (t, *J* = 7.1 Hz, 6H) . **^{13}C-NMR (75 MHz, CDCl3):** δ 172.3, 153.3, 143.2, 117.6, 114.9, 66.0, 61.0, 59.2, 55.9, 39.2, 14.3. **MS(ESI$^+$):** Calculated for $C_{19}H_{30}NO_7^+$ $[M+H]^+$: 384.2017; found: 384.2019.

S5.2 General procedure for the synthesis of hetero-aminodialcohols 5 under Sq_IRMOF-16 catalysis.

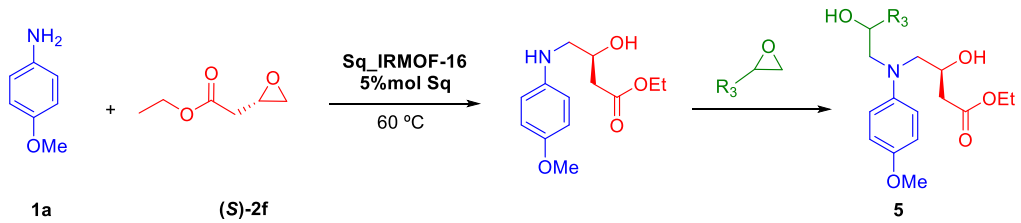

The required amount of **Sq_IRMOF-16** was dried under a nitrogen current during 2 h. 2.9 mg of dried **Sq_IRMOF-16** (0.005 mmol of squaramide units), 0.1 mmol of 4-methoxyaniline **1a** and a stirring bar were transferred to a vial with septum and a nitrogen current was allowed to pass through the vial during 15 min. Then, 0.1 mmol of ethyl (*S*)-2-(oxiran-2-yl)acetate **(*S*)-2f** was added. The mixture was heated to 60°C and it was stirred during 8 h. Then, in a second step, 10 mmol of the indicated epoxide was added. The mixture was heated to 60°C and it was stirred during the indicated time in each case. The progress of the reaction was controlled by ^{1}H-NMR. Once the reaction was finished, the product was purified by flash chromatography.

Ethyl (*S*)-3-hydroxy-4-(((*S*)-2-hydroxybutyl)(4-methoxyphenyl)amino)butanoate (5a)

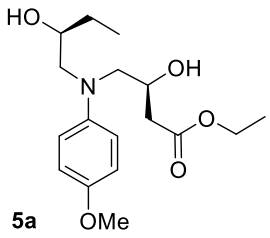

5a

The product was obtained following the described procedure for the synthesis of hetero-aminodialcoholes, adding in the second step 10 mmol of (*S*)-2-ethyloxirane **(*S*)-2a** and allowing the mixture to react during 3 days (Yield = 48%). The crude was purified by flash chromatography (cyclohexane: ethyl acetate 85:15 → 60:40). **$[\alpha]^{20}_D$** = -19.8 (c = 1.7, $CHCl_3$). **^{1}H-NMR (300 MHz, $CDCl_3$):** δ 6.89 – 6.78 (m, 4H), 4.24 (dtd, *J* = 9.1, 6.1, 3.1 Hz, 1H), 4.16 (q, *J* = 7.1 Hz, 2H), 3.81 – 3.67 (m, 1H), 3.76 (s, 3H), 3.52 (bs, 1H), 3.36 (dd, *J* = 14.4, 3.4 Hz, 1H), 3.33 (dd, *J* = 14.3, 2.7 Hz, 1H), 3.16 (dd, *J* = 14.4, 9.0 Hz, 1H), 3.04 (dd, *J* = 14.3, 9.8 Hz, 1H), 2.49 (d, *J* = 6.3 Hz, 2H), 1.57 – 1.41 (m, 2H), 1.27 (t, *J* = 7.1 Hz, 3H), 0.99 (t, *J* = 7.4 Hz, 3H) . **^{13}C-NMR (75 MHz, CDCl3):** δ 172.3, 153.4, 143.6, 118.0, 114.8, 70.1, 65.8, 61.0, 60.3, 58.9, 55.8, 39.2, 27.6, 14.3, 10.2. **MS(EI$^+$):** Calculated for $C_{17}H_{27}NO_5^+$ $[M]^+$: 325.1884; found: 325.1884.

Ethyl (*S*)-3-hydroxy-4-(((*R*)-2-hydroxybutyl)(4-methoxyphenyl)amino)butanoate (5b)

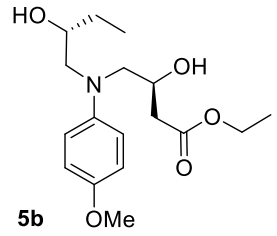

5b

The product was obtained following the described procedure for the synthesis of hetero-aminodialcoholes, adding in the second step 10 mmol of (*R*)-2-ethyloxirane **(*R*)-2a** and allowing the mixture to react during 3 days (Yield = 46%). The crude was purified by flash chromatography (cyclohexane: ethyl acetate 85:15 → 60:40). **$[\alpha]^{20}_D$** = -16.3 (c = 0.8, $CHCl_3$). **^{1}H-NMR (300 MHz, $CDCl_3$):** δ 6.87 – 6.79 (m, 2H), 6.71 – 6.64 (m, 2H), 4.36 (dtd, *J* = 9.2, 6.4, 2.8 Hz, 1H), 4.18 (q, *J* = 7.1 Hz, 2H), 3.92 – 3.81 (m, 1H), 3.76 (s, 3H), 3.58 (dd, *J* = 14.9, 2.6 Hz, 1H), 3.57 (dd, *J* = 14.9, 3.4 Hz, 1H), 3.12 (dd, *J* = 14.8, 9.3 Hz, 1H), 2.97 (dd, *J* = 14.8, 9.8 Hz, 1H), 2.49 (d, *J* = 6.4 Hz, 2H), 1.55 – 1.41 (m, 2H), 1.28 (t, *J* = 7.2 Hz, 3H), 1.01 (t, *J* = 7.4 Hz, 3H) **^{13}C-NMR (75 MHz, CDCl3):** δ 172.3, 152.6, 143.0, 115.4, 115.1, 71.3, 66.7, 62.0, 61.0, 60.7, 55.9, 39.2, 27.7, 14.3, 10.0. **MS(EI$^+$):** Calculated for $C_{17}H_{27}NO_5$ $[M]^+$: 325.1884; found: 325.1887.

S6. NMR spectra

S6.1 Ligand L1 and precursor

^{1}H-NMR (300 MHz, DMSO-d_6) (**c**)

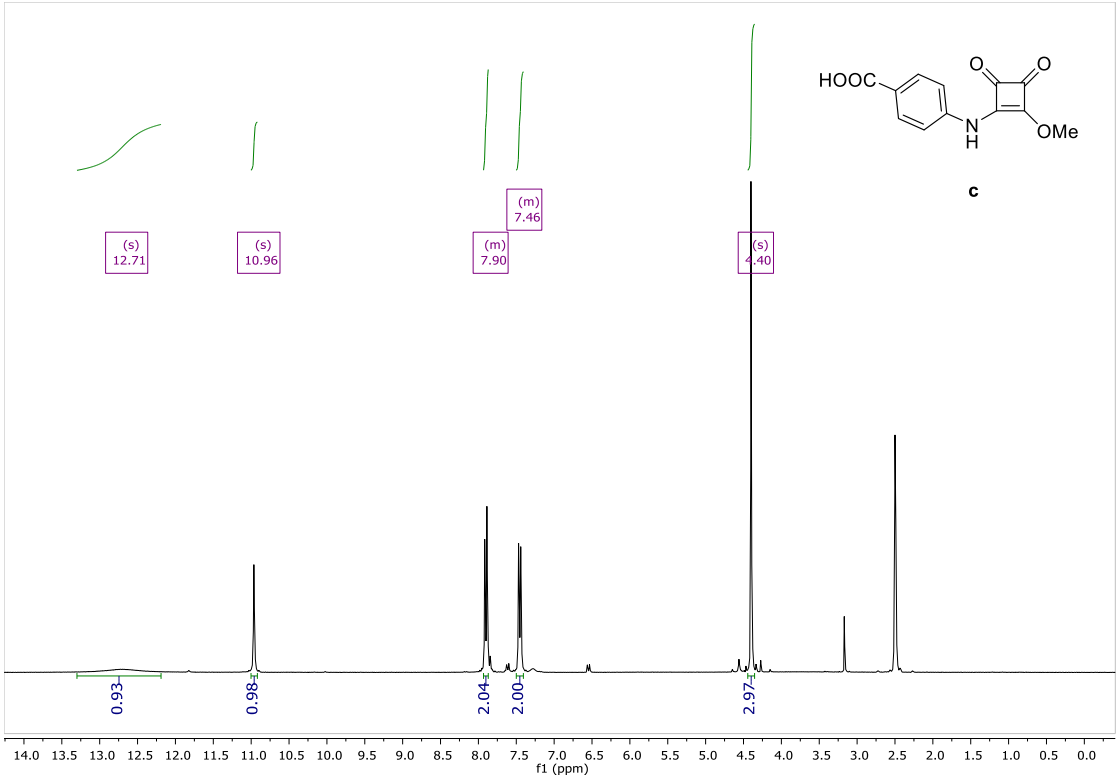

^{13}C-NMR (75 MHz, DMSO-d_6) (**c**)

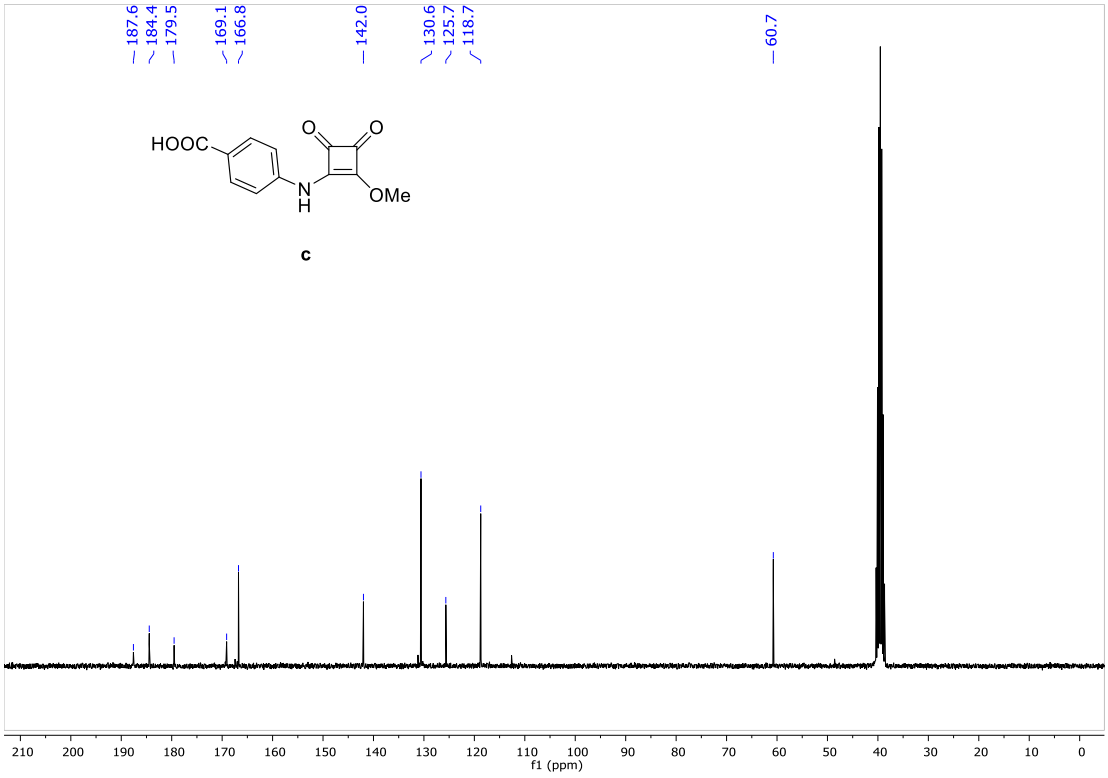

^{1}H-NMR (250 MHz, DMSO-d_6) (**L1**)

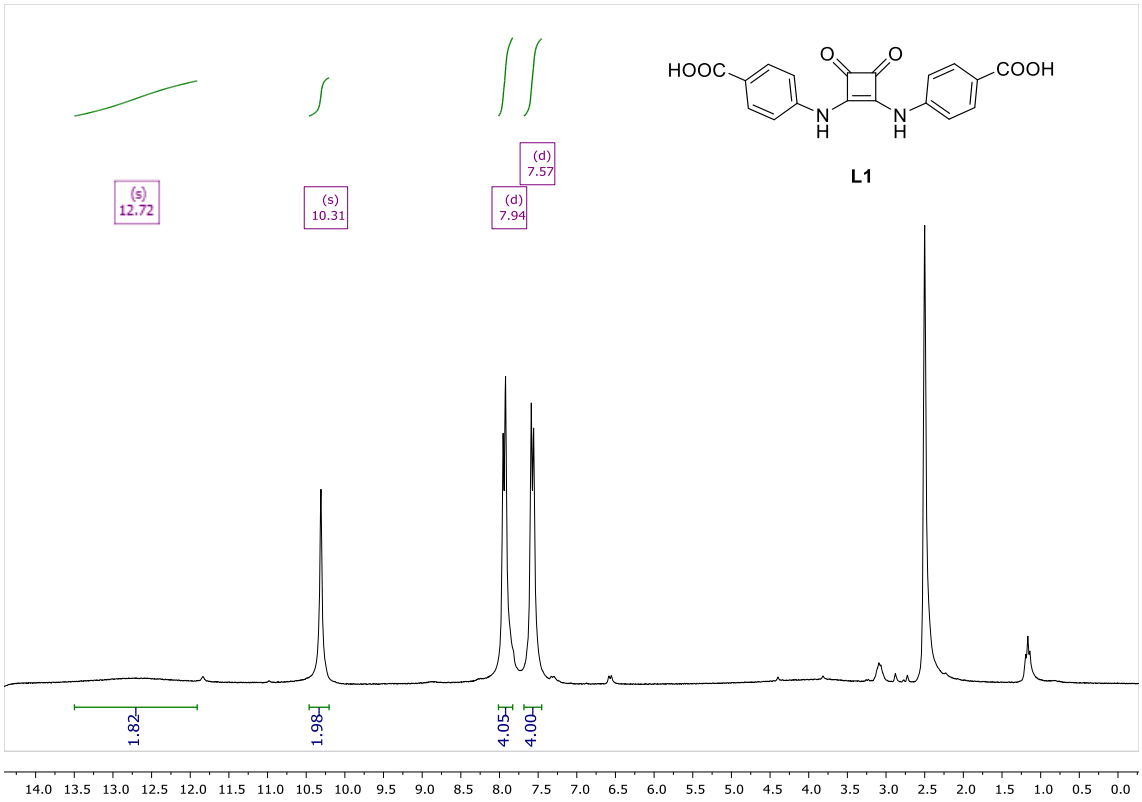

^{13}C-NMR (63 MHz, DMSO-d_6) (**L1**)

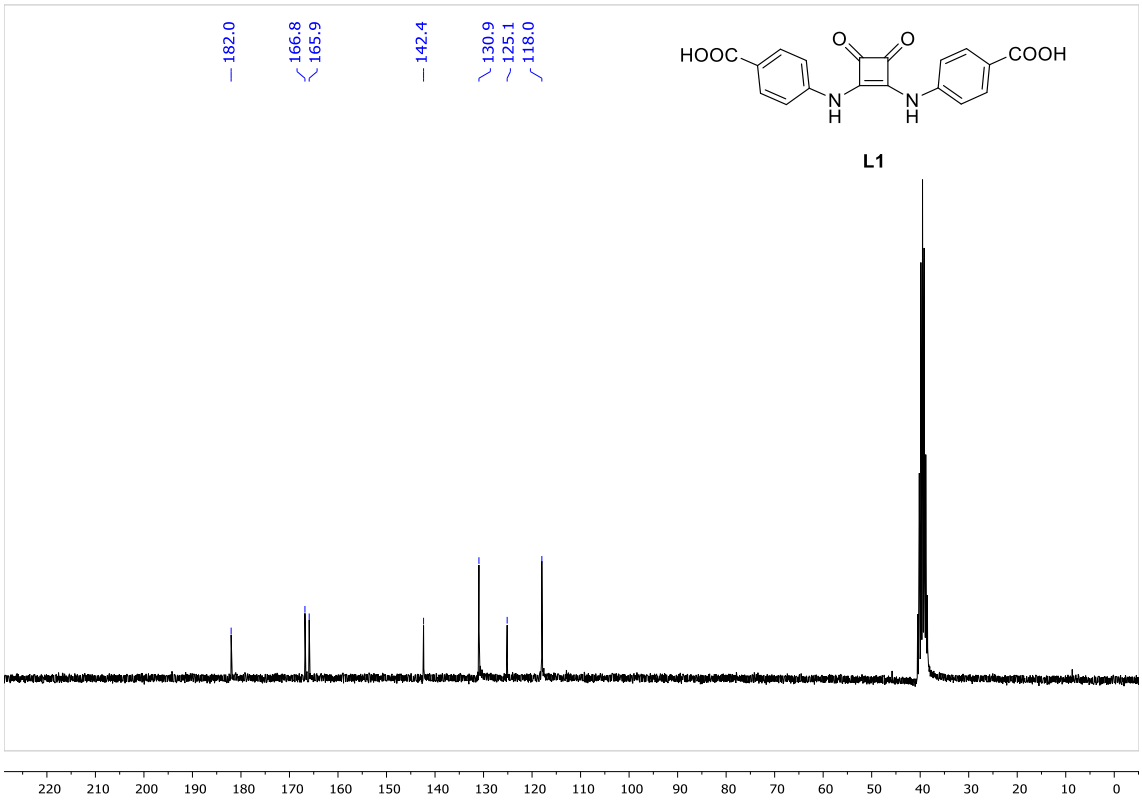

S6.1 Homo-aminodialcohols 4

^{1}H-NMR (300 MHz, $CDCl_3$) (**4a**)

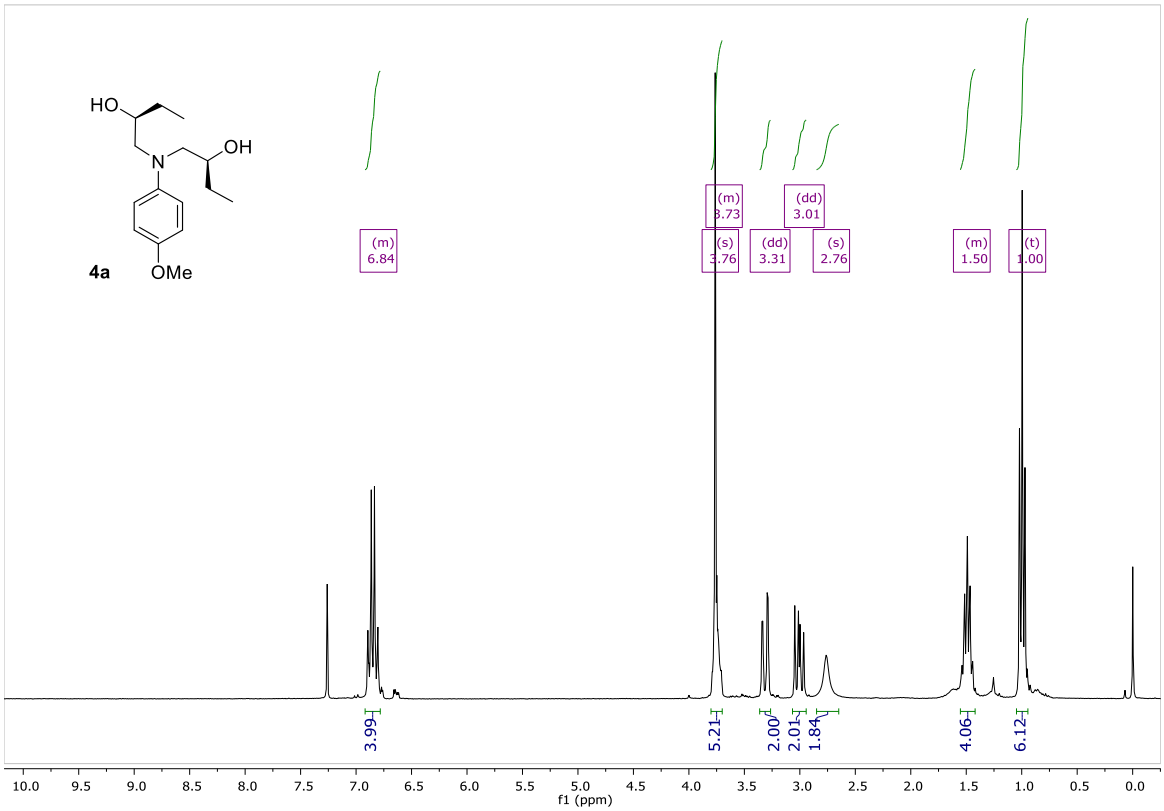

^{13}C-NMR (75 MHz, $CDCl_3$) (**4a**)

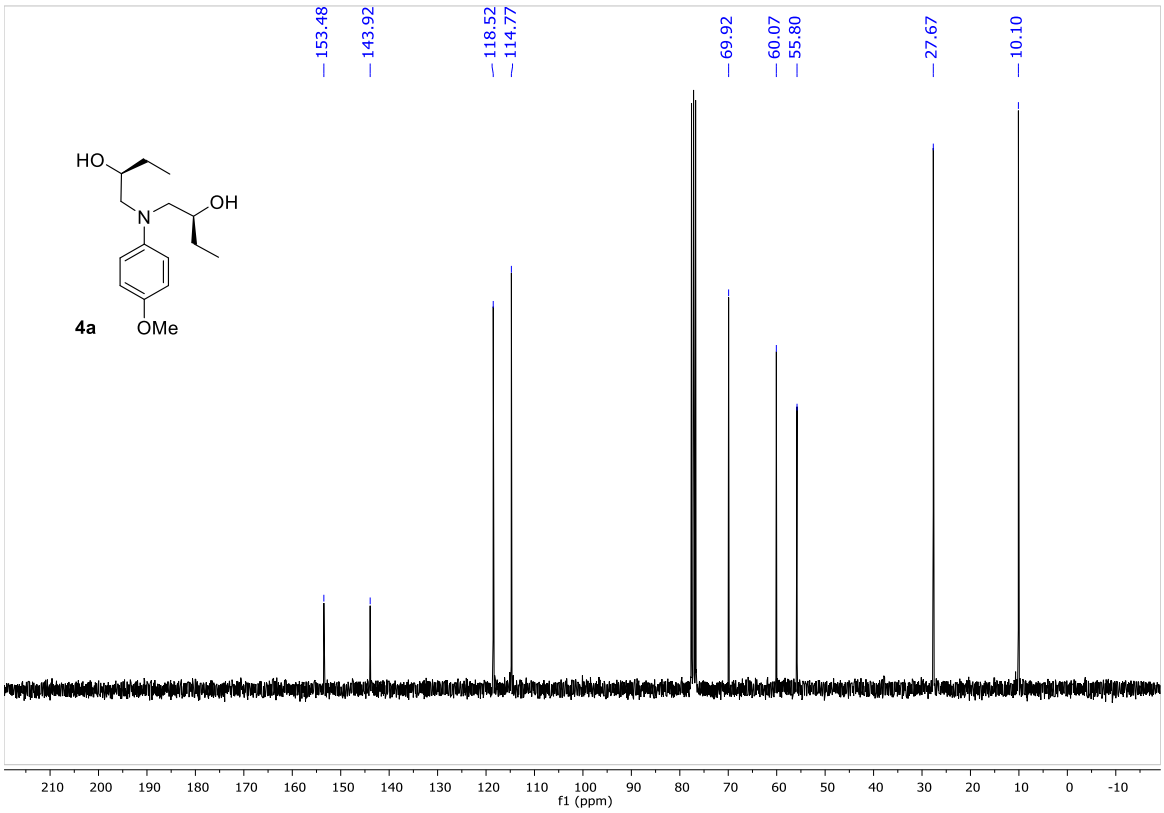

Supporting Information

Switching Acidic and Basic Catalysis in a Three-Dimensional Covalent Imine Structure through Supramolecular Functionalization

Javier Luis-Barrerra, Ghazaleh Imani-Shakibaei, Javier Heras-Domingo, Rafael Cano, Javier Pérez-Carvajal, Inhar Imaz, Daniel Maspoch, Xavier Solans-Monfort, José Alemán,* and Rubén Mas-Ballesté**

Table of Contents

1. Powder XRD diffractograms

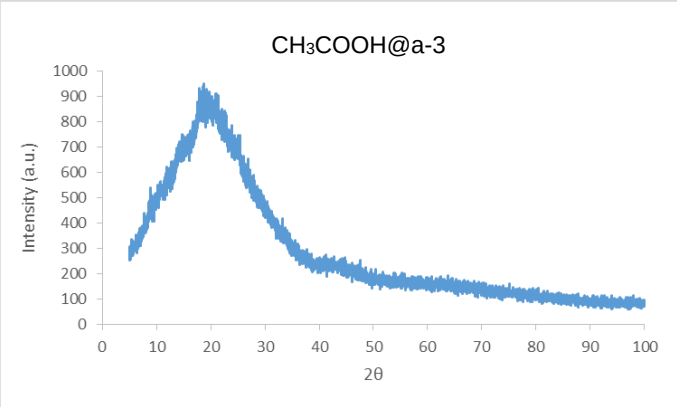

Figure S1. PXRD diffractogram for **CH_3COOH@a-3**

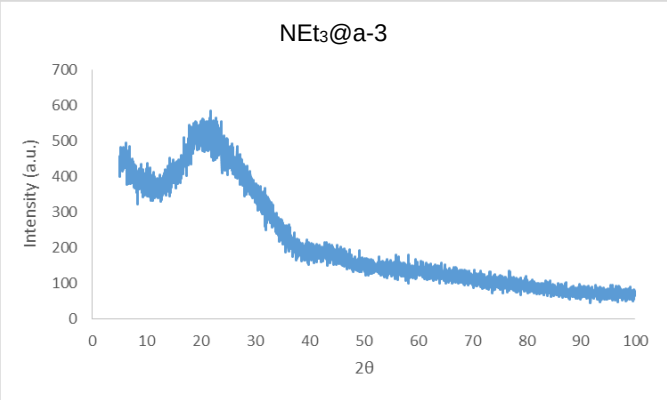

Figure S2. PXRD diffractogram for **Et_3N@a-3**

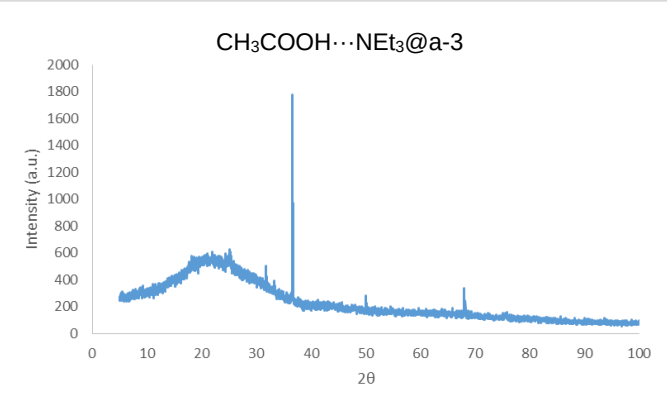

Figure S3. PXRD diffractogram for **$CH_3COOH\cdots Et_3N$@a-3**

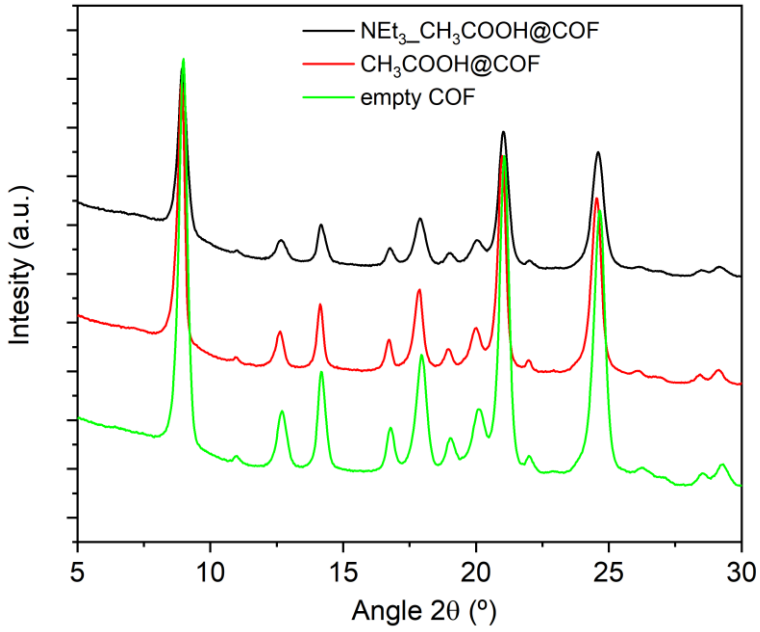

Figure S4. PXRD diffractogram **c-3** materials

2. SEM images for a-3 materials

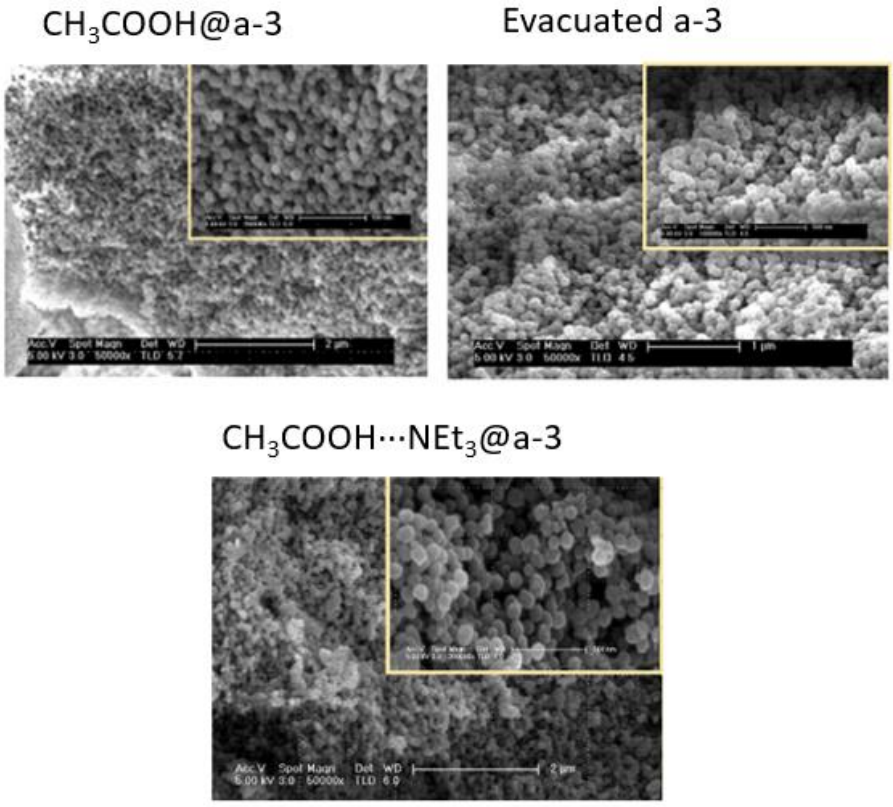

Figure S5. SEM images for **a-3** materials

3. NMR-Spectra

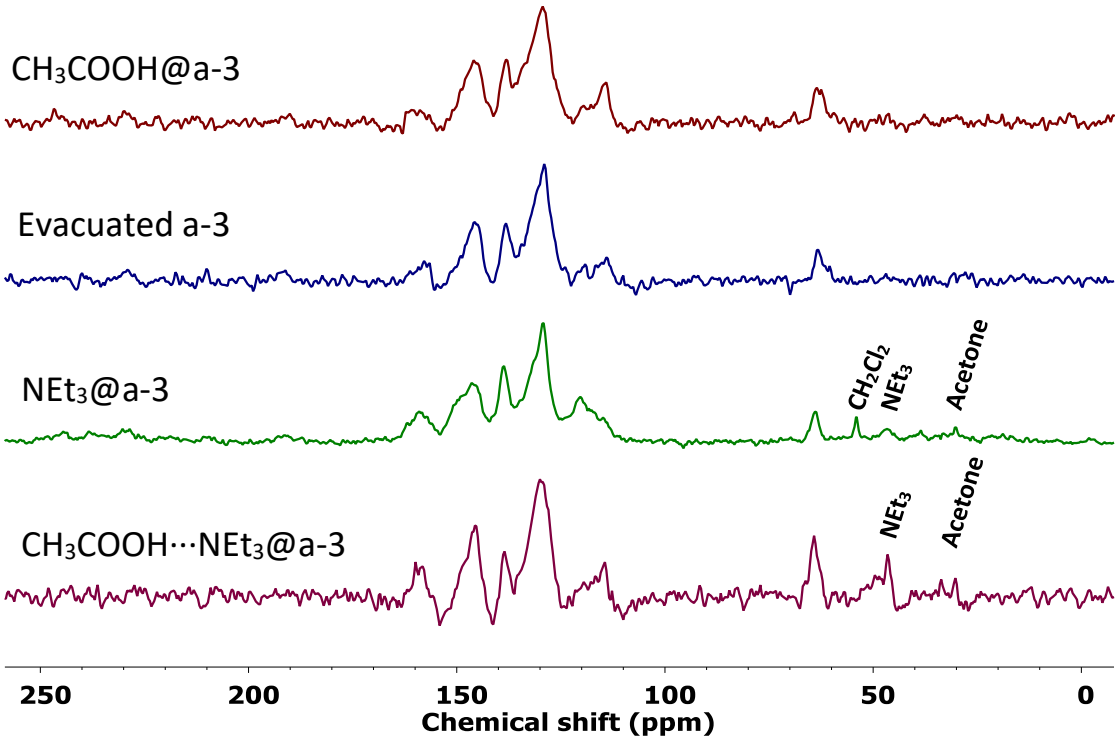

Figure S6. MAS-^{13}C NMR for **a-3** materials

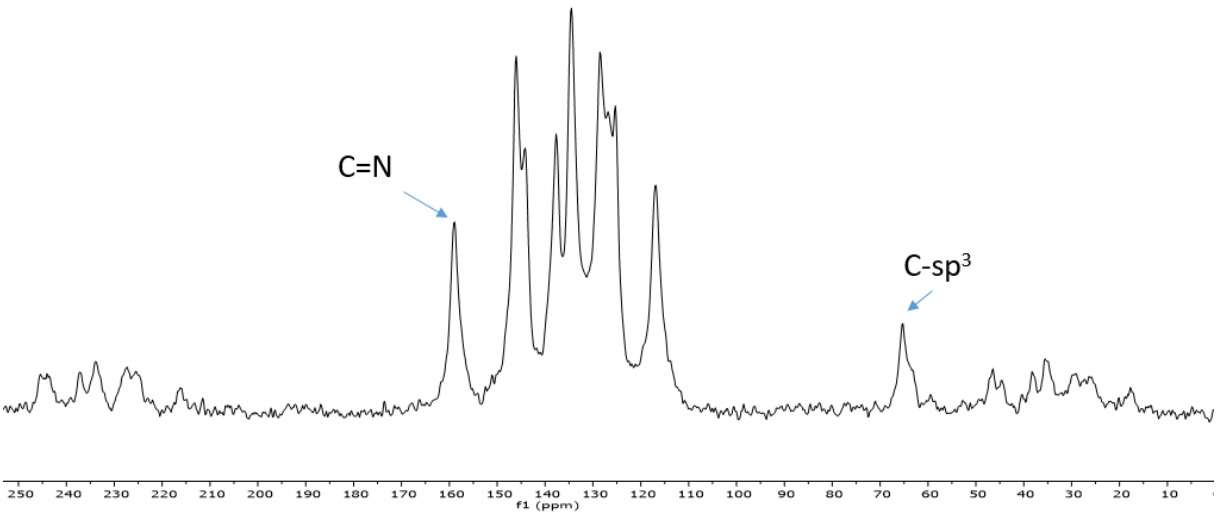

Figure S7. MAS-^{13}C NMR for **c-3**

4. IR spectra

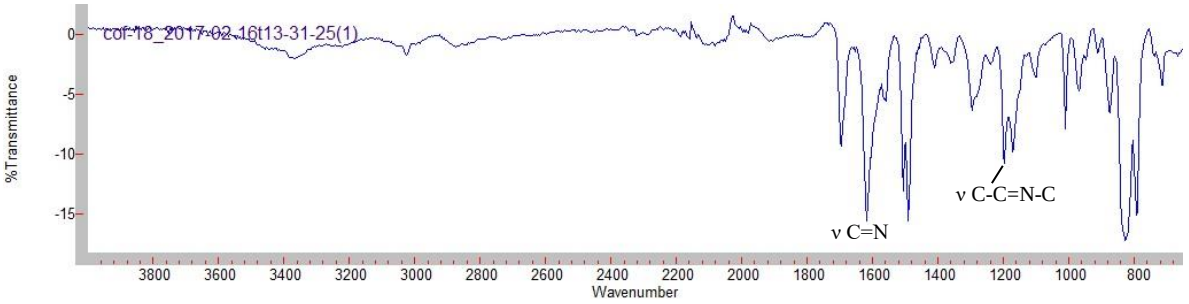

Figure S8. IR spectra for **CH_3COOH@a-3**

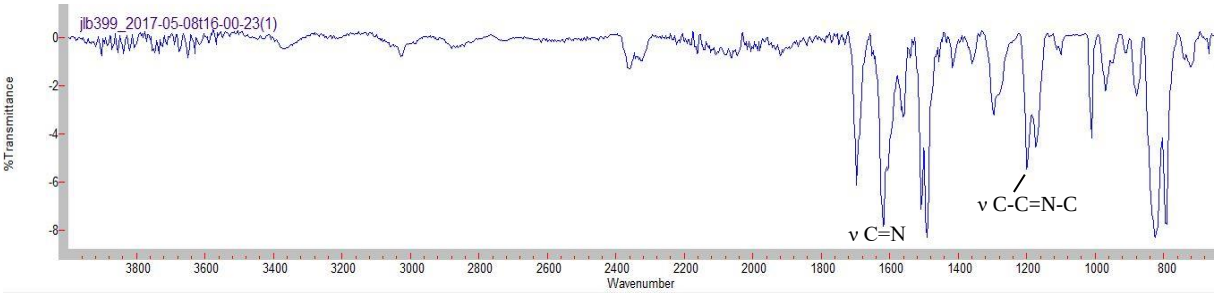

Figure S9. IR spectra for **Evacuated a-3**

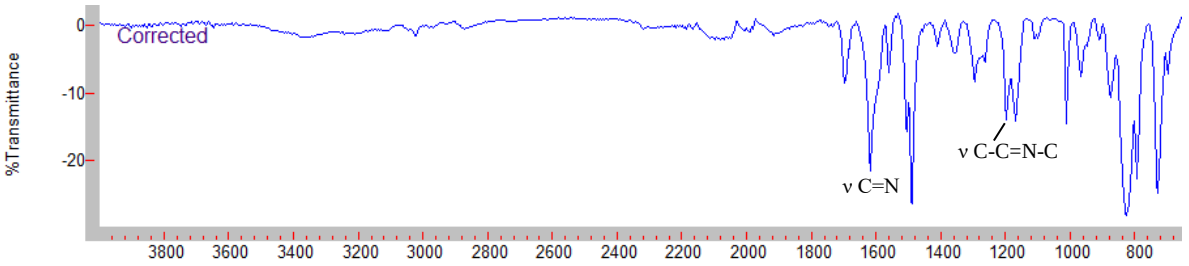

Figure S10. IR spectra for **Et_3N@a-3**

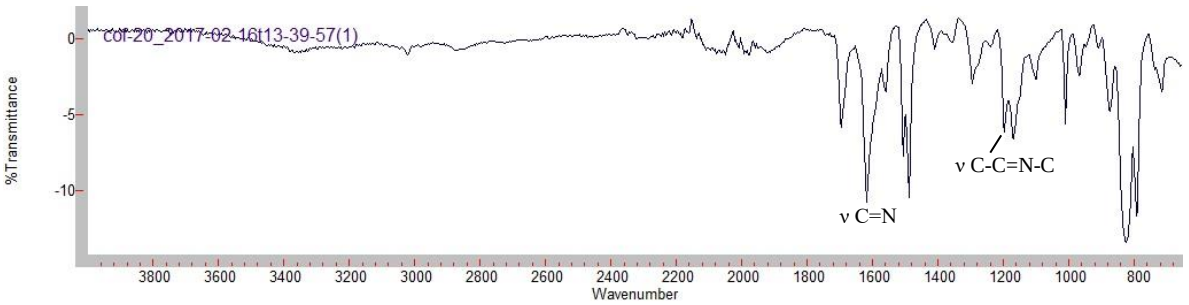

Figure S11. IR spectra for **$CH_3COOH\cdots Et_3N$@a-3**

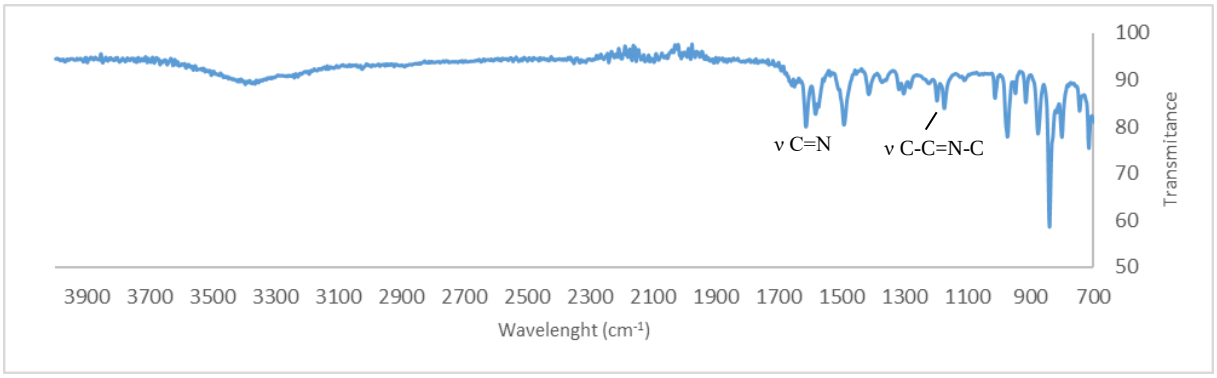

Figure S12. IR spectra for **Evacuated c-3**

5. TGA-MS

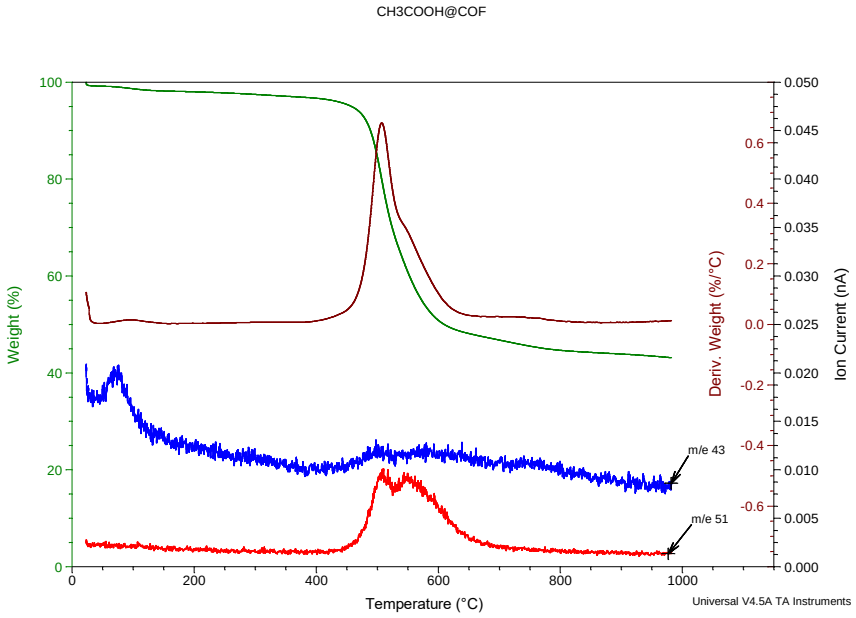
CH3COOH@COF
Weight (%)
Deriv. Weight (%/°C)
Ion Current (nA)
m/e 43
m/e 51
Temperature (°C)
Universal V4.5A TA Instruments

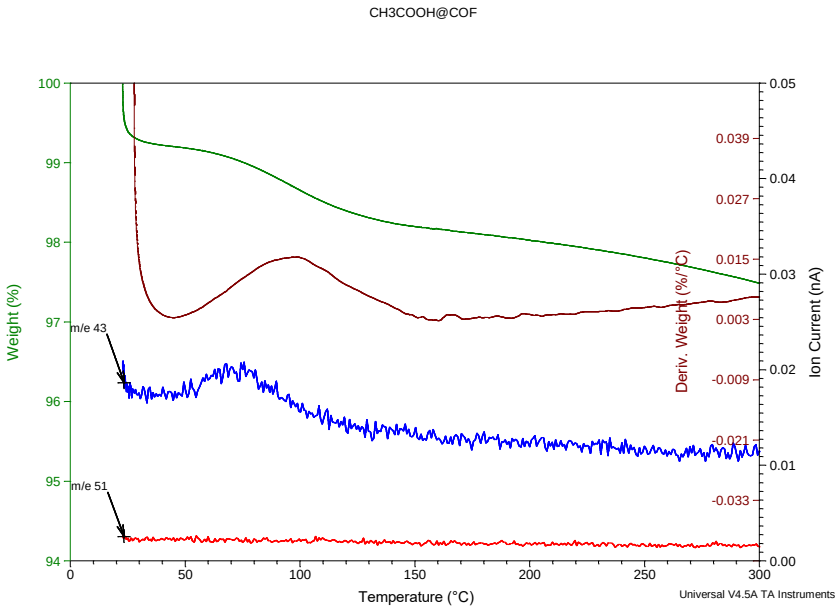
CH3COOH@COF
Weight (%)
Deriv. Weight (%/°C)
Ion Current (nA)
m/e 43
m/e 51
Temperature (°C)
Universal V4.5A TA Instruments

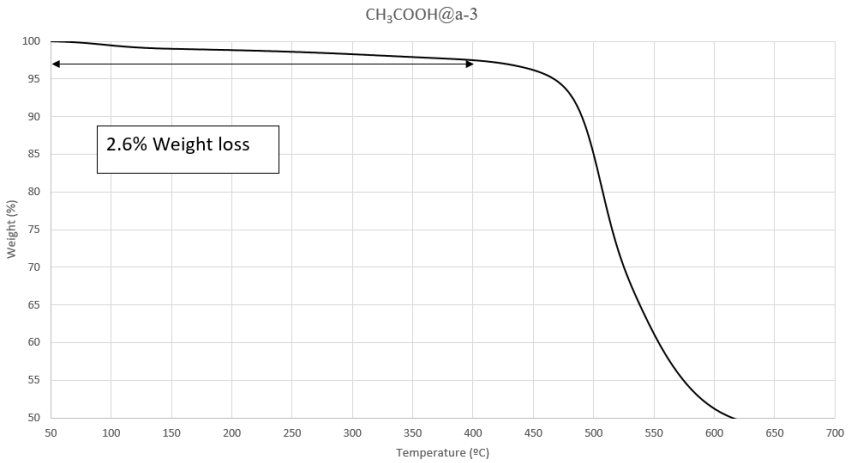

Figure S13. TGA-MS spectra for **CH_3COOH@a-3**

Empty COF

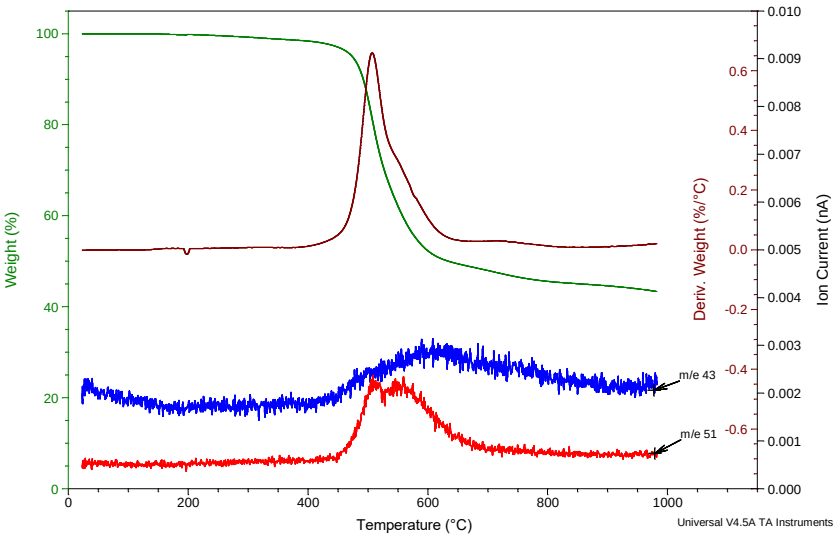

Empty COF

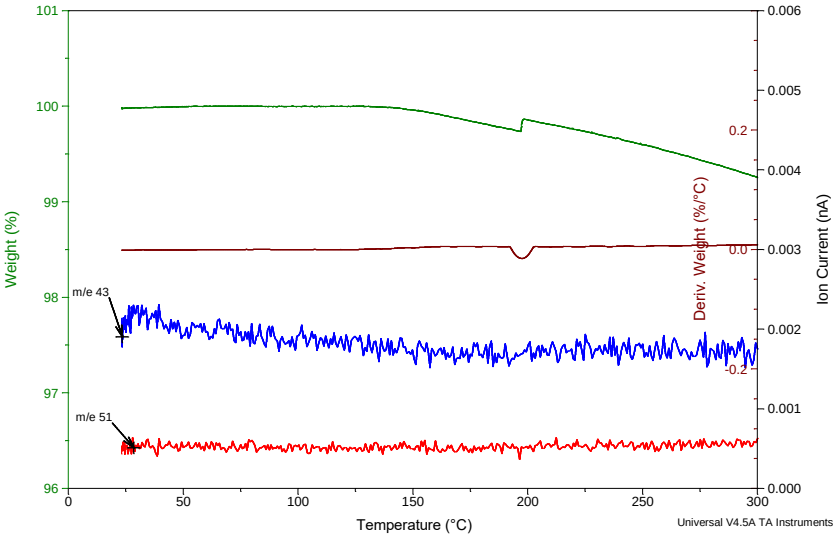

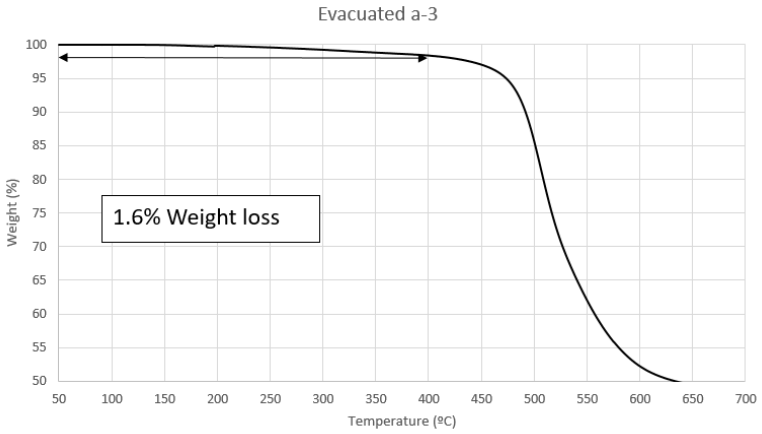

Figure S14. TGA-MS spectra for **Evacuated a-3**

NEt$_3$@a-3

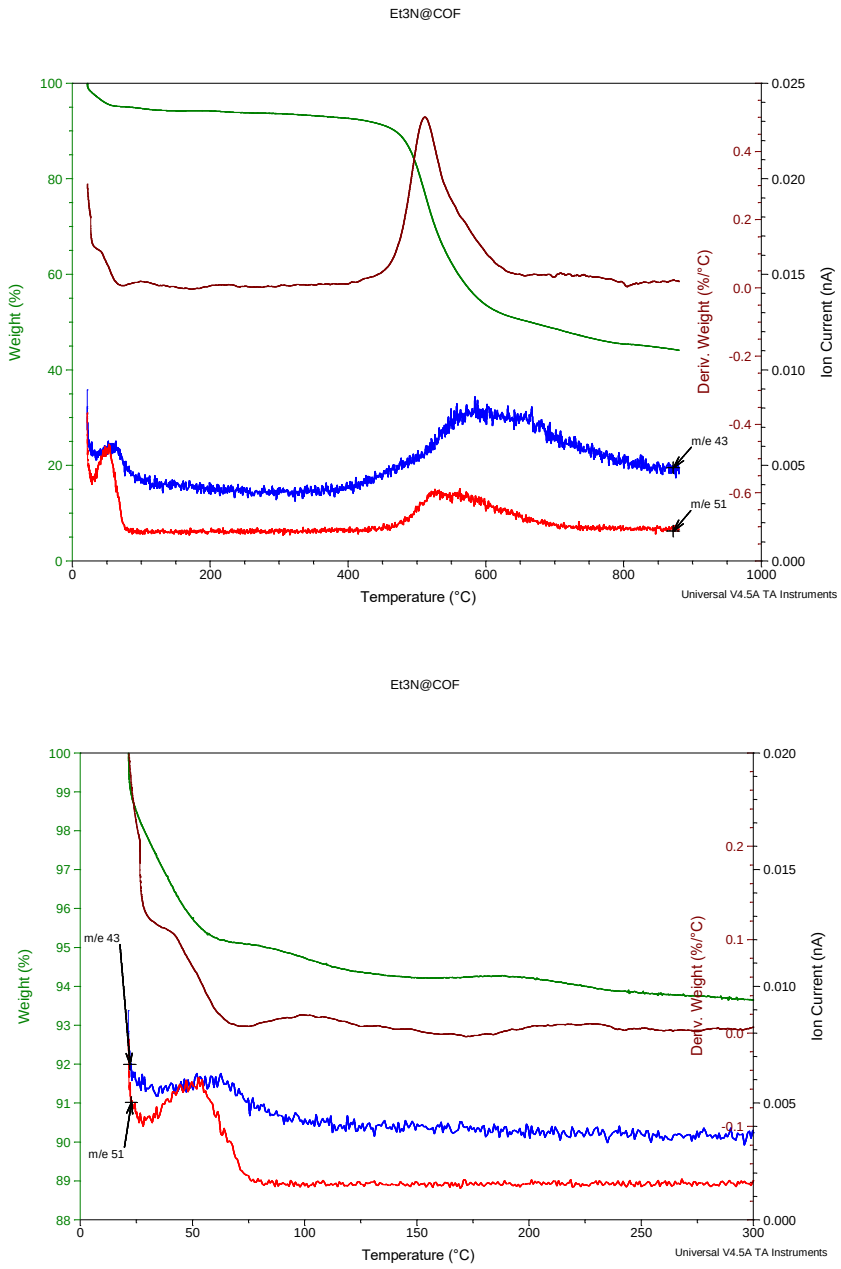

Figure S15. TGA-MS spectra for **Et$_3$N@a-3**

$CH_3COOH\cdots NEt_3$@a-3

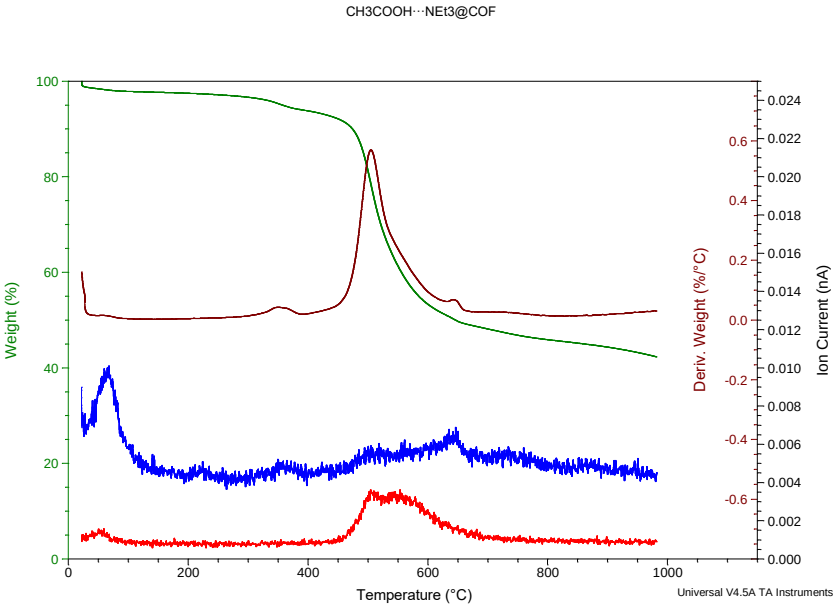

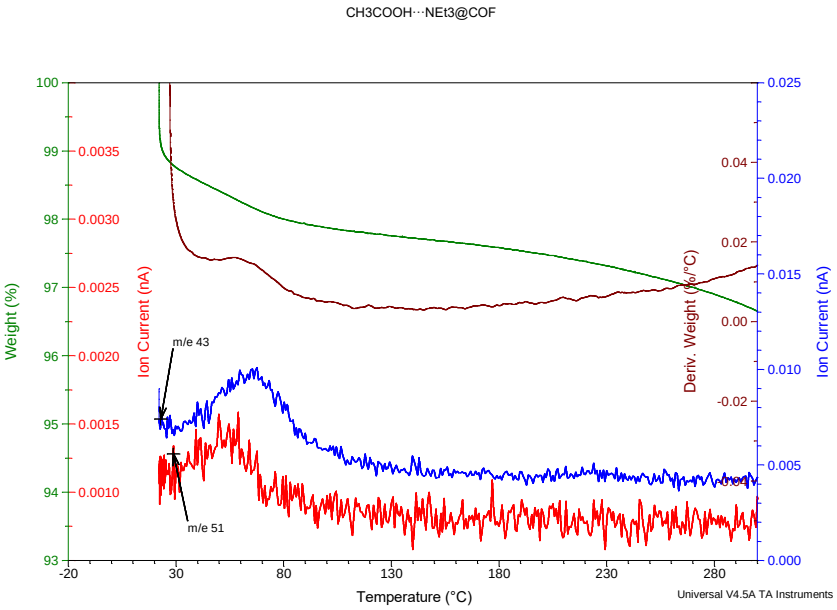

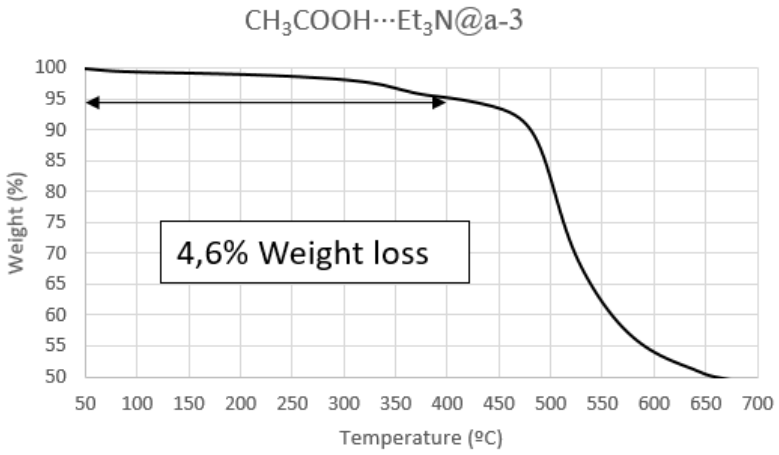

Figure S16. TGA-MS spectra for **$CH_3COOH\cdots Et_3N$@a-3**

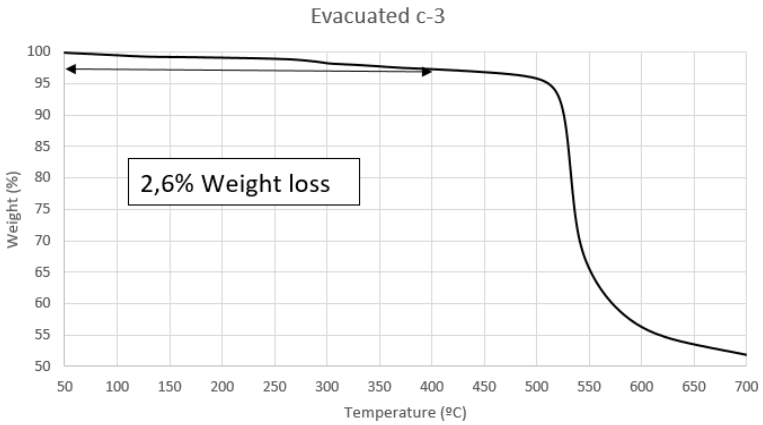

Figure S17. TGA-MS spectra for **Evacuated c-3**

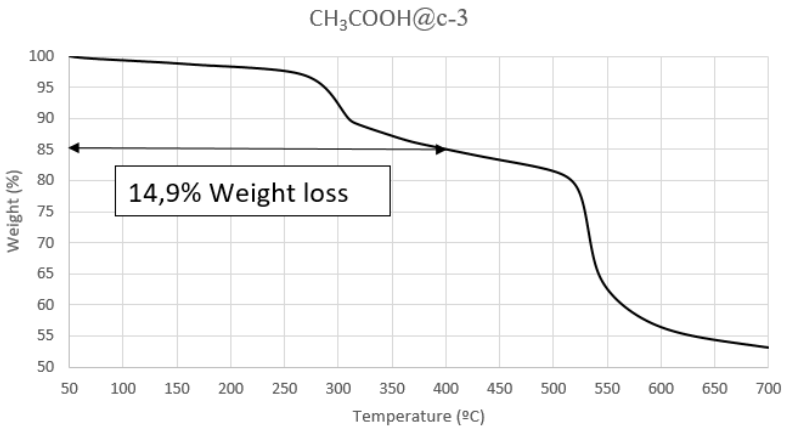

Figure S18. TGA-MS spectra for **CH_3COOH@c-3**

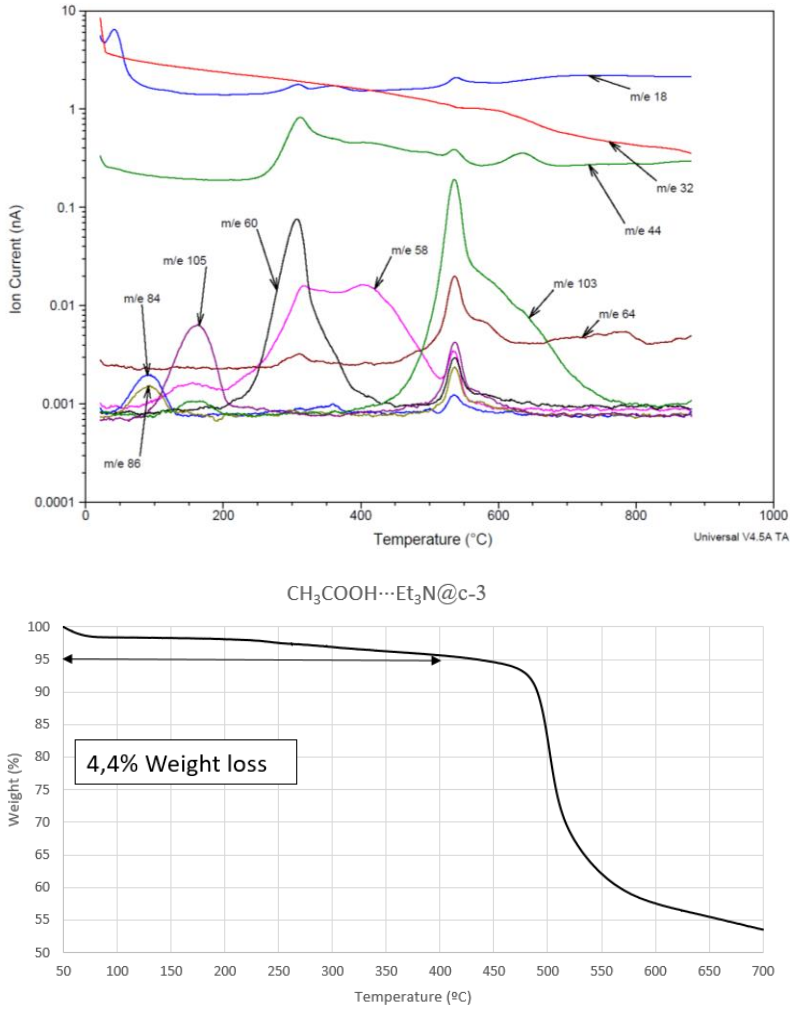

Figure S19. TGA-MS spectra for **$CH_3COOH\cdots Et_3N$@c-3**

Switching off the $CH_3COOH\cdots NEt_3$@a-3

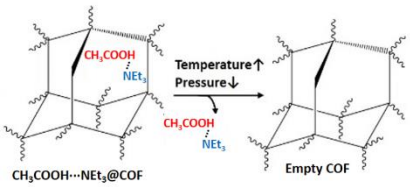

In order to demostrate that the switching of the **$CH_3COOH\cdots NEt_3$@a-3** can be done in any direction, a sample of this material was synthesized and the TGA-MS was measured. Then, the material was transferred to a 10 mL flask and vacuum was applied during twelve hours while the flask is in a bath at 80˚ C. A new TGA-MS analysis was done. Comparing both TGA, it can be confirmed that the material lost the $CH_3COOH\cdots NEt_3$, becoming "**Empty COF**"

Before Vacuum:

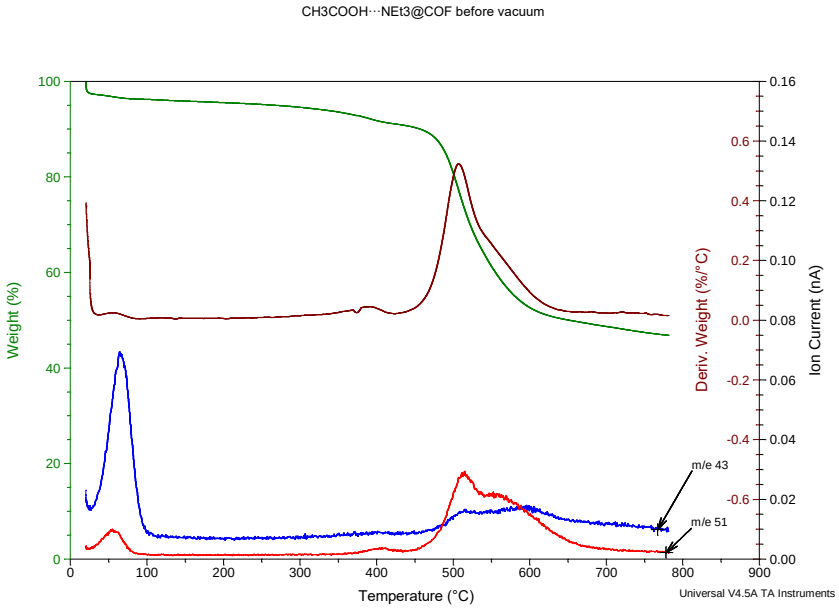

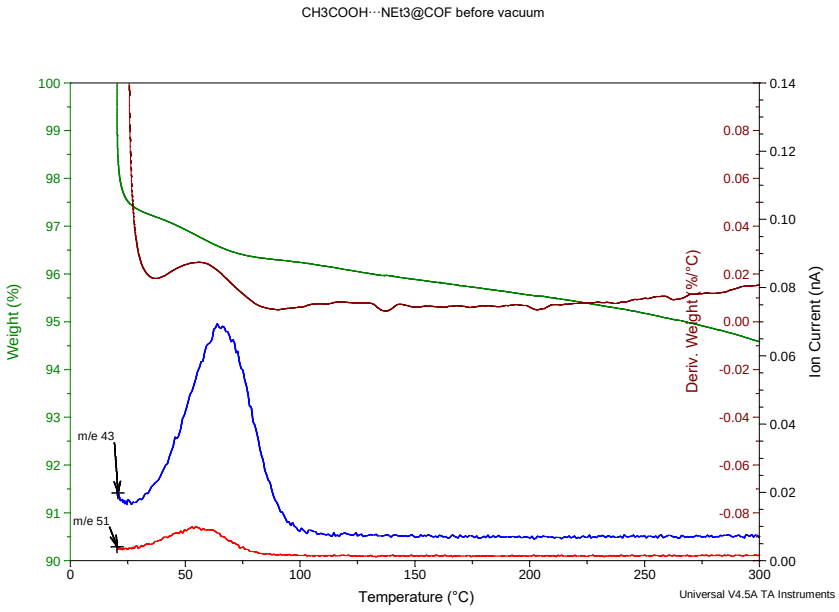

After Vacuum:

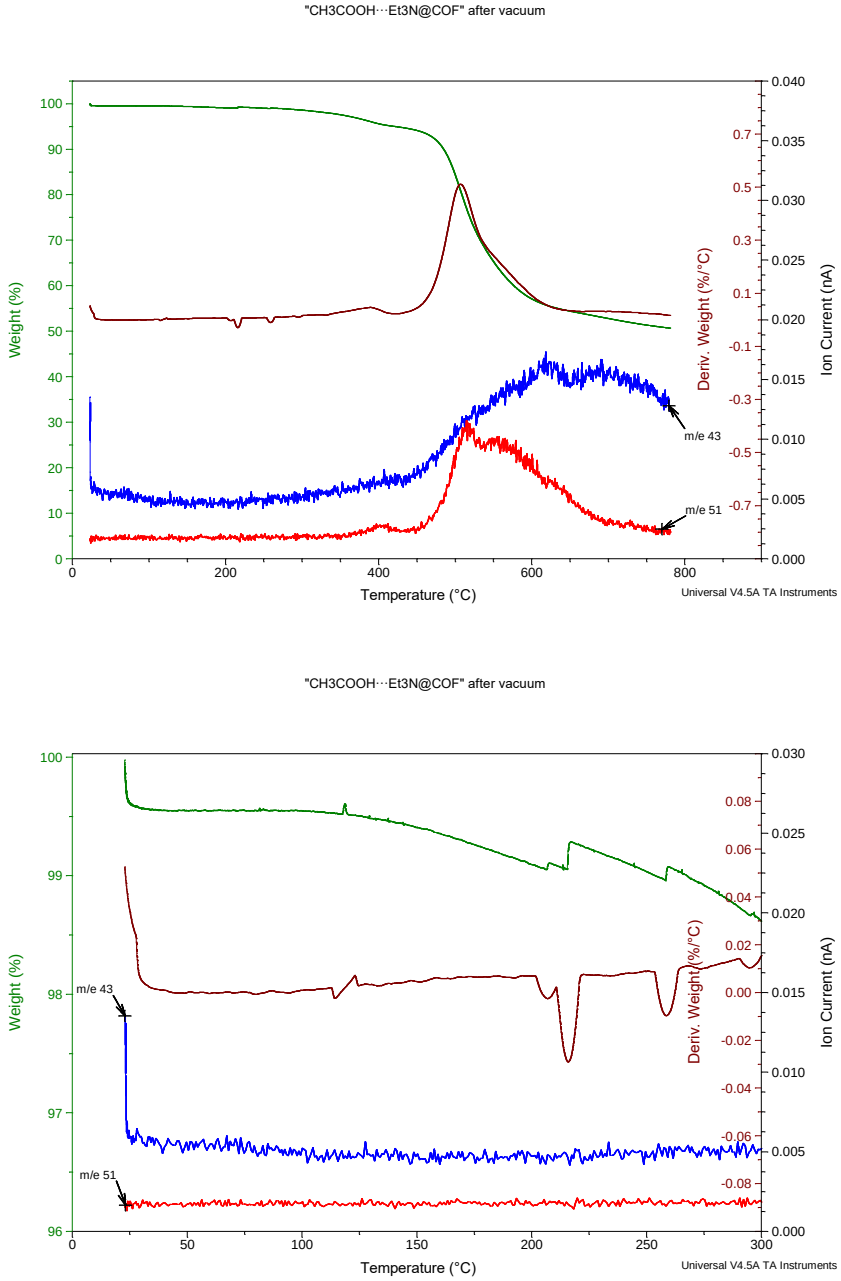

Figure S20. TGA-MS spectra for **$CH_3COOH\cdots Et_3N$@a-3** before and after vacuum

6. General procedure for the catalysis with the amorphous materials and characterization of products

All the catalytic experiments reported below were performed during a two weeks period from the synthesis of material, because we observed that storage of the materials for longer periods results in the decrease of catalytic activity, probably due to loss CH_3COOH and/or NEt_3 volatile molecules.

6.1 Epoxide opening catalyzed by CH_3COOH@a-3

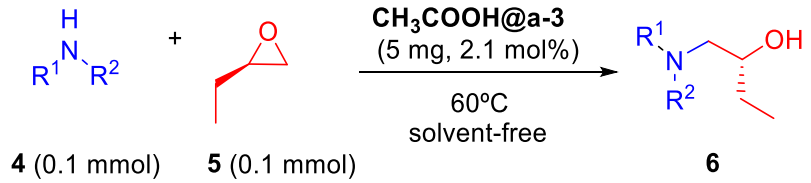

A screw cap with PTFE liner vial was charged with 0.1 mmol of the corresponding amine **4**, 0.1 mmol of the epoxide **5** and 5 mg of the **CH_3COOH@a-3**. The vial was warmed to 60° C during the corresponding time (see **Schemes 2** and **3** in the main text). To check the conversion, 1 mL of toluene is added to the vial. Then, an aliquot of 200 µL is taken and 500 µL of a 0.005 M solution of 2-methylnaphthalene (the standard for GC) in toluene was added to the aliquot. The aliquot in analyzed by gas chromatography with a flame ionization detector (FID).

The products of the reaction were previously synthesized using a reported procedure[1], in order to identify the retention time in the gas chromatography – FID and to make a calibration for quantitative analysis.

1-(Piperidin-1-yl)butan-2-ol (6a)

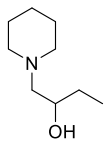

6a

^{1}H-NMR (300 MHz, $CDCl_3$): δ 3.74 (bs, 1H), 3.57 (dddd, J = 10.3, 7.0, 5.2, 3.3 Hz, 1H), 2.69-2.46 (m, 2H), 2.29 (dd, *J* = 12.2, 3.3 Hz, 1H), 2.28 – 2.22 (m, 2H), 2.16 (dd, *J* = 12.2, 10.5 Hz, 1H), 1.69 – 1.50 (m, 4H), 1.50 – 1.31 (m, 4H), 0.96 (t, *J* = 7.5 Hz, 3H). The product matched with the previous spectroscopic data described in the literature.[1,2]

[1] N. Azizi, M. R. Saidi, *Org. Lett.* **2005**, *7*, 3649-3651.
[2] S. R. Roy, A. Nijamudheen, A. Pariyar, A. Ghosh, P. K. Vardhanapu, P. K. Mandal, A. Datta, S. K. Mandal, *ACS Catal.* **2014**, *4*, 4307-4319.

1-(Pyrrolidin-1-yl)butan-2-ol (6b)

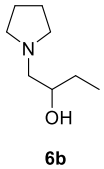

6b

^{1}H-NMR (300 MHz, $CDCl_3$): δ 3.64 – 3.49 (m, 1H), 3.48 (s, 1H), 2.72 – 2.63 (m, 2H), 2.56 (dd, *J* = 11.8, 10.7 Hz, 1H), 2.49 – 2.39 (m, 2H), 2.27 (dd, *J* = 11.9, 3.0 Hz, 1H), 1.80 – 1.74 (m, 4H), 1.53 – 1.38 (m, 2H), 0.97 (t, *J* = 7.5 Hz, 3H). The product matched with the previous spectroscopic data described in the literature.[1]

1-(Diethylamino)butan-2-ol (6c)

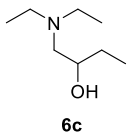

6c

^{1}H-NMR (300 MHz, $CDCl_3$): δ 3.50 (dddd, *J* = 10.4, 7.0, 5.2, 3.2 Hz, 1H), 2.64 (dq, *J* = 13.0, 7.3 Hz, 2H), 2.47 (dq, *J* = 13.0, 7.0 Hz, 2H), 2.42 (dd, *J* = 12.6, 3.2 Hz, 1H), 2.22 (dd, *J* = 12.6, 10.5 Hz, 1H), 1.52 – 1.36 (m, 2H), 1.02 (t, *J* = 7.1 Hz, 6H), 0.98 (t, *J* = 7.5 Hz, 3H). The product matched with the previous spectroscopic data described in the literature.[3]

1-((4-Methoxyphenyl)amino)butan-2-ol (6d)

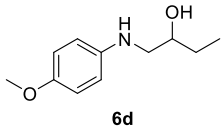

6d

^{1}H-NMR (300 MHz, $CDCl_3$): δ 6.84 – 6.75 (m, 2H), 6.68 – 6.59 (m, 2H), 3.81 – 3.68 (m, 1H), 3.75 (s, 3H), 3.22 (dd, *J* = 12.6, 3.1 Hz, 1H), 2.95 (dd, *J* = 12.6, 8.6 Hz, 1H), 1.65 – 1.48 (m, 2H), 1.01 (t, *J* = 7.5 Hz, 3H). The product matched with the previous spectroscopic data described in the literature.[4]

[3] S. J. Stropoli, M. J. Elrod, *J. Phys. Chem. A* **2015**, *119*, 10181−10189.
[4] P. C. Miller, T. J. Owen, J. M. Molyneaux, J. M. Curtis, C. R. Jones, *J. Comb. Chem.* **1999**, *1*, 223-234.

6.2 Knoevenagel condensation catalyzed by a-3

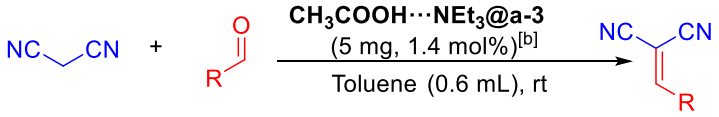

7 (0.11mmol) **8a-g** (0.1mmol) **9**

In a screw cap vial, 0.1 mmol of the corresponding aldehyde **8a-g** and 0.11 mmol of the malonitrile **7** were dissolved in 0.6 mL of toluene and 5 mg of **$CH_3COOH\cdots NEt_3$@a-3** was added. The mixture was stirred with a magnetic bar during the time indicated in **Table 1** in the main text. To check the conversion, an aliquot of 100 µL is taken and 500 µL of a 0.005 M solution of 2-methylnaphthalene (the standard for GC) in toluene is added to the aliquot. The aliquot is analyzed by gas chromatography with a flame ionization detector (FID).

The products of the reaction were previously synthesized using a reported procedure[5], in order to identify the retention time in the gas chromatography – FID and to make a calibration for quantitative analysis.

2-Benzylidenemalononitrile (9a)

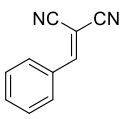

9a

^{1}H-NMR (300 MHz, $CDCl_3$): δ 7.95 – 7.88 (m, 2H), 7.78 (s, 1H), 7.68 – 7.60 (m, 1H), 7.59 – 7.50 (m, 2H). The product matched with the previous spectroscopic data described in the literature.[6]

2-(4-Methoxybenzylidene)malononitrile (9b)

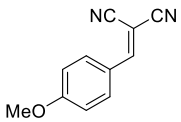

9b

^{1}H-NMR (300 MHz, $CDCl_3$): δ 7.96 – 7.88 (m, 2H), 7.65 (s, 1H), 7.06 – 6.98 (m, 2H), 3.92 (s, 3H). The product matched with the previous spectroscopic data described in the literature.[6]

2-(3-Methylbenzylidene)malononitrile (9c)

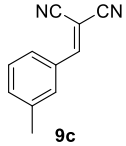

9c

^{1}H-NMR (300 MHz, $CDCl_3$): δ 8.14 – 8.06 (m, 2H), 7.54 – 7.46 (m, 1H), 7.41 – 7.30 (m, 2H), 2.45 (s, 3H). The product matched with the previous spectroscopic data described in the literature.[7]

[5] B Mohammadi, H. Kazemi, M. Shafieey, *Monatsh Chem*. **2014**, *145*, 1649-1652.
[6] J. B. M. de Resende Filho, G. P. Pires, J. M. G. de Oliveira Ferreira, E. E. S. Teotonio, J. A. Vale, *Catal. Lett.* **2017**, *147*, 167-180.
[7] M.M.H. Bhuiyan, M.I. Hossain, M. Ashraful Alam and M.M. Mahmud, *Chemistry Journal* **2012**, *2*, 31-37.

2-Octylidenemalononitrile (9d)

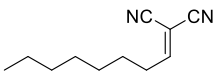

9d

^{1}H-NMR (300 MHz, $CDCl_3$): 7.33 (t, *J* = 8.0 Hz, 1H), 2.59 (q, *J* = 7.5 Hz, 2H), 1.56 (quint, *J* = 6.9 Hz, 2H), 1.44 – 1.20 (m, 8H), 0.97 – 0.83 (m, 3H). The product matched with the previous spectroscopic data described in the literature.[8]

2-(Naphthalen-2-ylmethylene)malononitrile (9e)

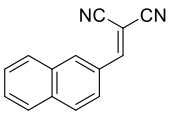

9e

^{1}H NMR (300 MHz, $CDCl_3$) δ 8.30 (s, 1H), 8.08 (dd, *J* = 8.7, 1.9 Hz, 1H), 7.96 (d, *J* = 8.5 Hz, 2H), 7.93 – 7.88 (m, 2H), 7.73 – 7.58 (m, 2H). The product matched with the previous spectroscopic data described in the literature.[6]

2-(Naphthalen-1-ylmethylene)malononitrile (9f)

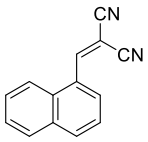

9f

^{1}H-NMR (300 MHz, $CDCl_3$): δ 8.66 (s, 1H), 8.28 (d, *J* = 7.3 Hz, 1H), 8.12 (d, *J* = 8.2 Hz, 1H), 7.97 (d, *J* = 7.9 Hz, 2H), 7.75 – 7.57 (m, 3H). The product matched with the previous spectroscopic data described in the literature.[7]

2-(Anthracen-9-ylmethylene)malononitrile (9g)

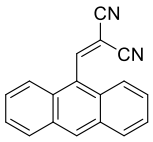

9g

^{1}H NMR (300 MHz, $CDCl_3$): δ 8.97 (s, 1H), 8.66 (s, 1H), 8.15 – 8.07 (m, 2H), 7.98 – 7.90 (m, 2H), 7.73 – 7.65 (m, 2H), 7.63 – 7.55 (m, 2H). The product matched with the previous spectroscopic data described in the literature.[7]

[8] Y. Jia, Y. Fang, Y. Zhang, H. N. Miras, Y.-F. Song, *Chem. Eur. J.* **2015**, *21*, 14862 –1487.

6.3 Formation of 9g catalyzed by COF and by NEt_3

Anthracene-9-carbaldehyde **8g** and 2-(anthracen-9-ylmethylene)malononitrile **9g** are not volatile enough to analyze them by Gas Chromatography (GC) so the conversion of this reaction was determined by ^{1}H-NMR spectrum of the reaction mixture. The reactions were set up following the general conditions for the catalyzed Knoevenagel condensation using the corresponding catalyst. At the indicated time, an aliquot of 100 μL was taken, the solvent was removed in the rotavap and it was analyzed by ^{1}H-NMR using $CDCl_3$ as solvent.

This reaction reached the 100 % of conversion with free triethylamine, indicating that the reaction can be catalyzed in basic conditions. However, using **$CH_3COOH\cdots NEt_3$@a-3** as catalyst, no formation of the product was observed (see ^{1}H-NMR spectra below) suggesting a size-selectivity in the pores of the COF.

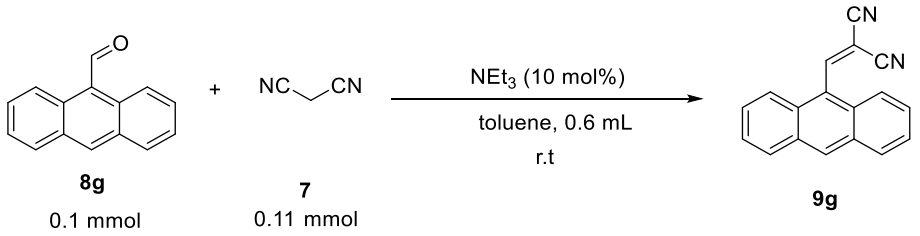

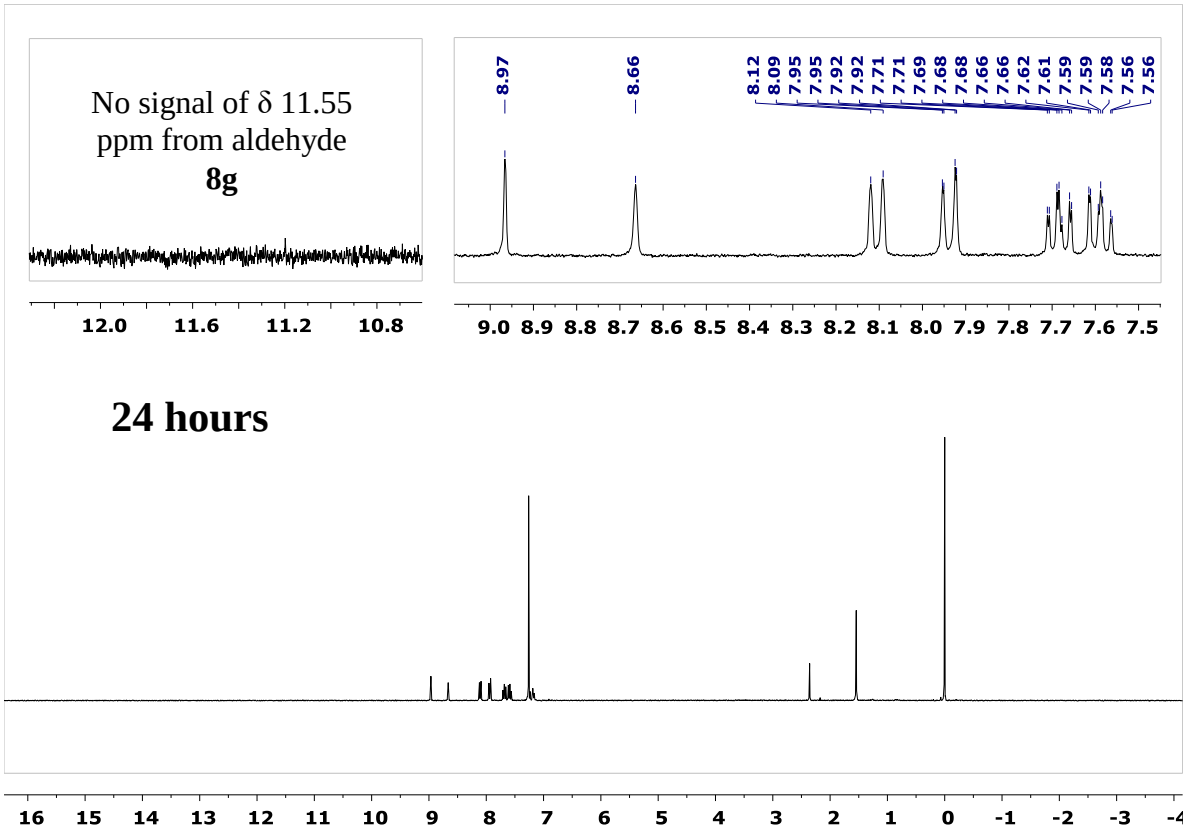

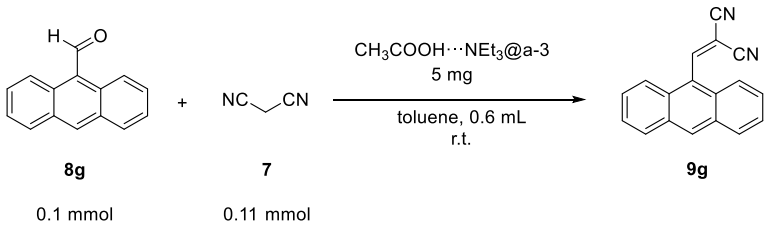

8g 0.1 mmol + **7** 0.11 mmol → **9g**

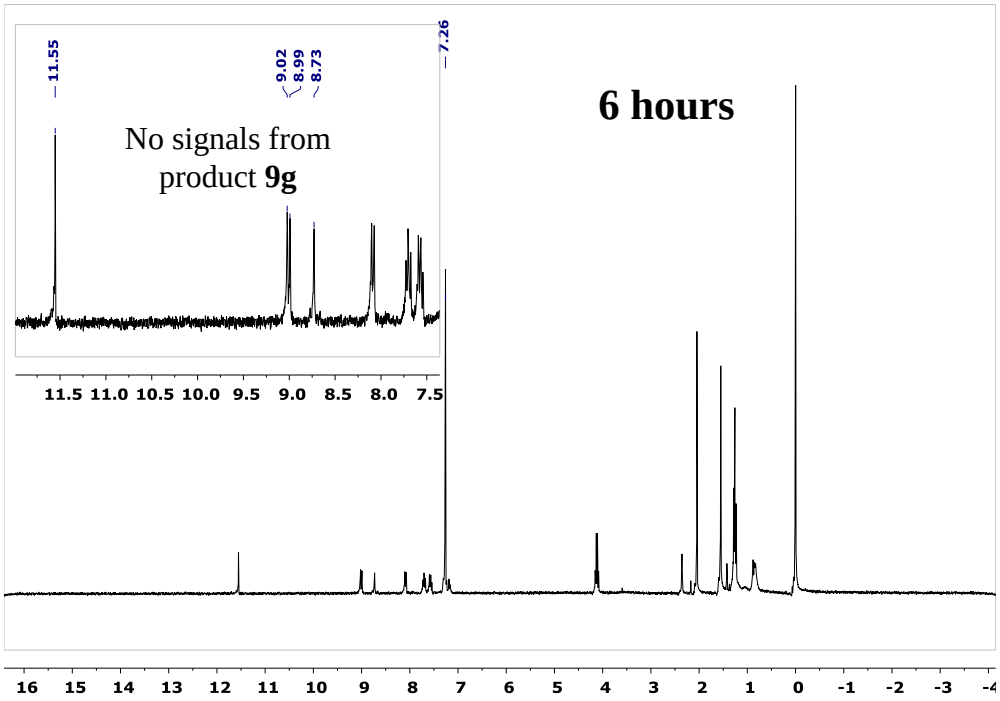

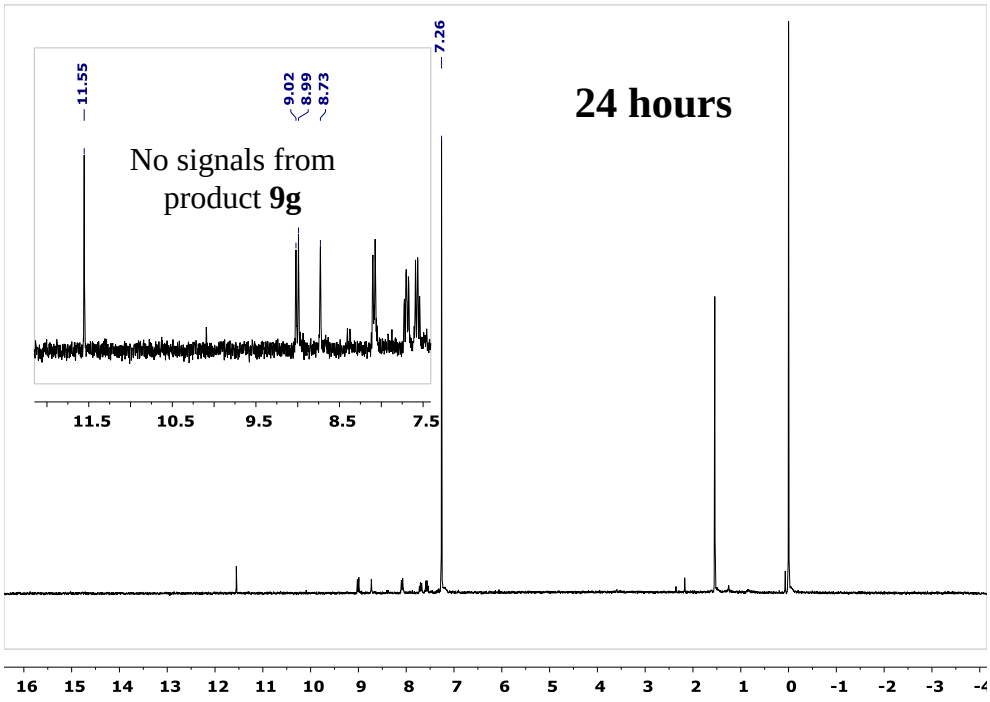

6.4 Epoxide opening and Knoevenagel background reactions

In order to verify that the reactions were catalyzed by the **CH_3COOH@a-3** or the **$CH_3COOH\cdots NEt_3$@a-3**, we always carried out all the reactions in the general conditions but without using a catalyst (Background reactions). In the next two tables the background yield of each reaction is shown to compare with the yield of the catalyzed reaction (both yields for the same time reaction).

Epoxide Opening:

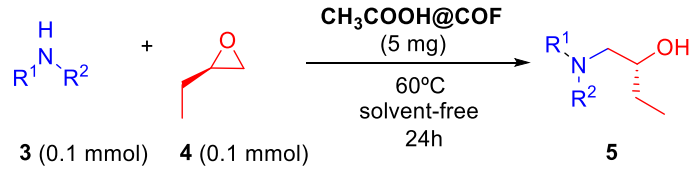

3 (0.1 mmol) **4** (0.1 mmol) **5**

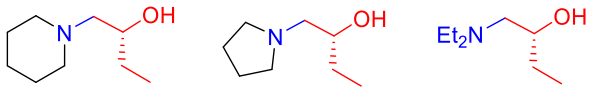

5b (Yield= 73%) t= 24h **(Background = 25%)**

5c (Yield= 55%) t= 8h **(Background = 20%)**

5d (Yield= 14%) t= 48h **(Background = 0%)**

Knoevenagel condensation:

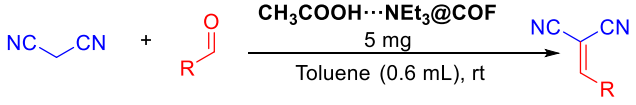

7 (0.11mmol) **8a-g** (0.1mmol) **9**

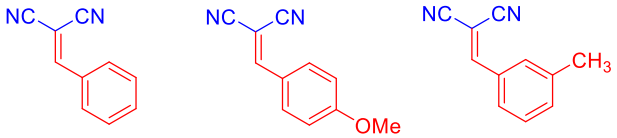

9a, 71% yield 14 hours **(Background = 2%)**

9b, 61% yield 20 hours **(Background = 5%)**

9c, 65% yield 14 hours **(Background < 1%)**

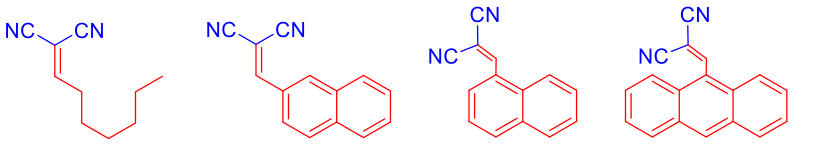

9d, 68% yield 10 hours **(Background < 1%)**

9e, 63% yield 20 hours **(Background < 1%)**

9f, 59% yield 14 hours **(Background = 17%)**

9g, no reaction 24 hours **(Background = 0%)**

7. Calculation of chemical erosion of COF

Some representative reactions of the Epoxide Opening or the Knoevenagel condensation were carried out following the general conditions but using only one of the two reagents, in order to check if the reagent reacts with the COF and to recognize possible byproducts.

In the case of the experiments carried out with the general conditions for the "Epoxide Opening", at the indicated time, $CDCl_3$ was directly added to the reaction mixture. Then the solution was analyzed by ^{1}H-NMR.

In the case of the experiments carried out with the general conditions for the "Knoevenagel condensation", at the indicated time, an aliquot of 100 µL was taken, the solvent was removed in the rotavap and it was analyzed by ^{1}H-NMR ($CDCl_3$). The reaction using both **8a** and **7** was also analyzed in this manner.

To calculate the amount of deteriorated COF is necessary to consider the amount of imine functional groups per 5 mg of material:

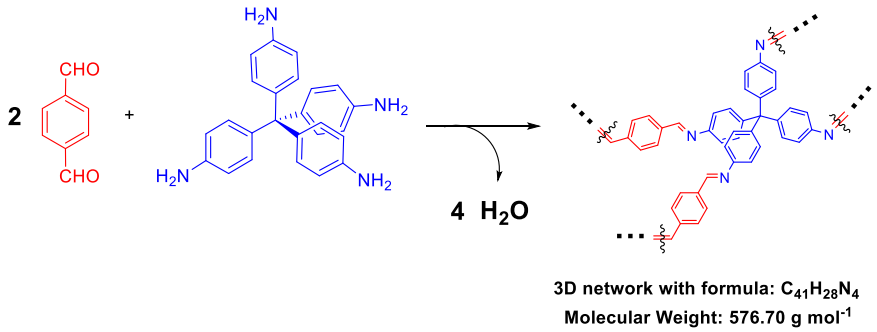

5 mg / 576.70 g mol^{-1} = 0.00867 mmol.

There is four imine functional groups in this subunit:

0.00867 mmol · 4 = 0.0347 mmol of imine functional groups in 5 mg of material.

Calculation of chemical erosion COF with Methoxyaniline 3a

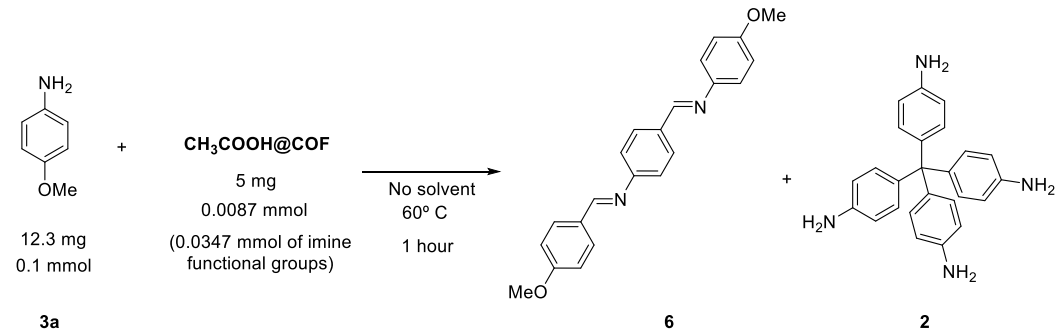

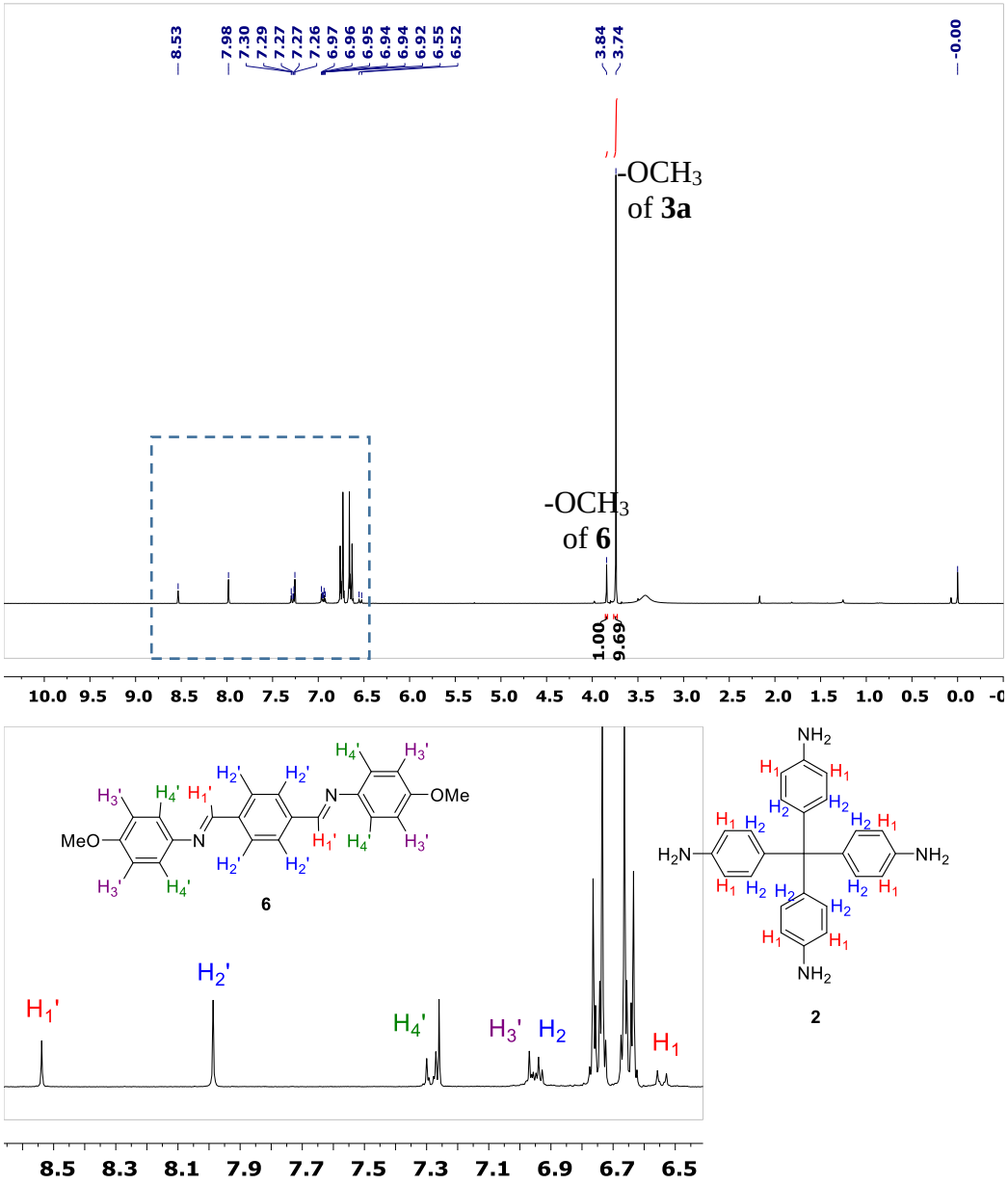

The signals of byproduct **6** matched with the previous spectroscopic data described in the literature.[9]

To calculate the ratio (byproduct **6** : methoxyanilne **3a**) we use the signal of 3.84 ppm for byproduct **6** and the signal at 3.74 ppm for methoxyanilne **3a**. The 3.84 ppm signal integrates for six protons, and the 3.74 ppm signal integrates for three protons, so the molar ratio is (0.50 : 9.69).

Considering the stoichiometry, two molecules of methoxyaniline **3a** are necessary for making one molecule of byproduct **6**, so the ratio of (reacted methoxyaniline: methoxyaniline left) is (1.00 : 9.69). In other words, 9.4 % of the initial methoxyaniline has reacted.

In the reaction, there was 0.1 mmol of initial methoxyaniline **3a**. Applying this percentage, 0.0094 mmol of the methoxyaniline has reacted with 0.0094 mmol of the imines functional groups of the COF. Therefore, the percentage of deteriorated COF is:

$$\%\ \text{chemical erosion COF} = \frac{0.0094\ \text{mmol reacted imines}}{0.0347\ \text{mmol total imines}} \cdot 100 = 27\ \%$$

[9] Z. Fang, C. Cao, J. Chen, X. Deng, *J. Mol. Struct.* **2014**, *1063*, 307-312

Calculation of chemical erosion of COF with piperidine 3b

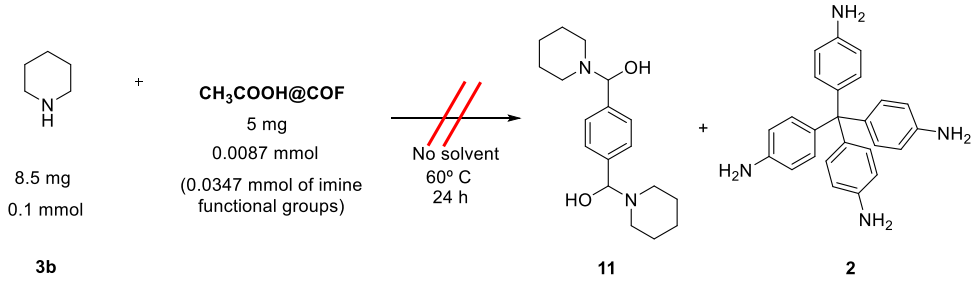

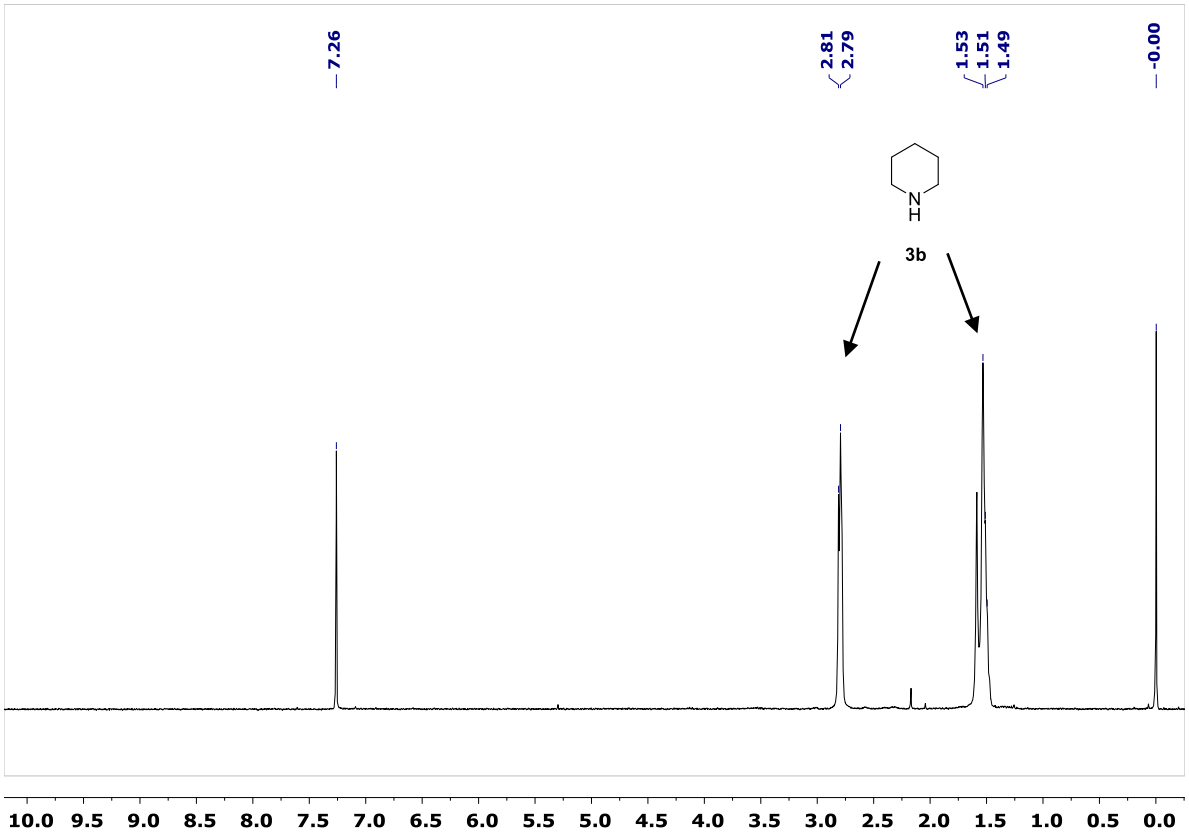

No byproducts from decomposition of COF were detected.

Calculation of chemical erosion of COF with epoxide 4

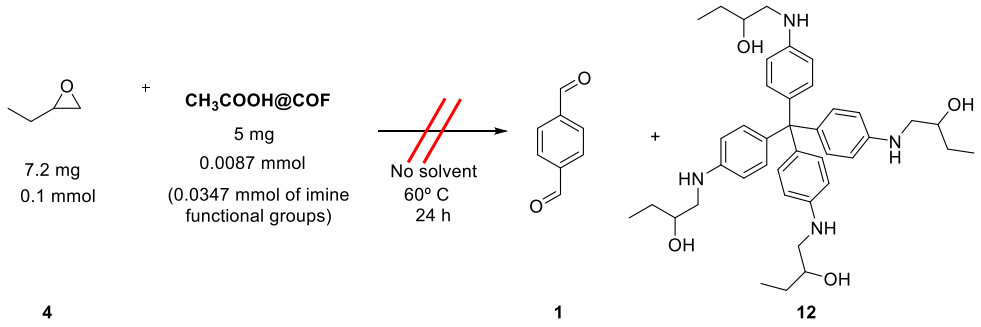

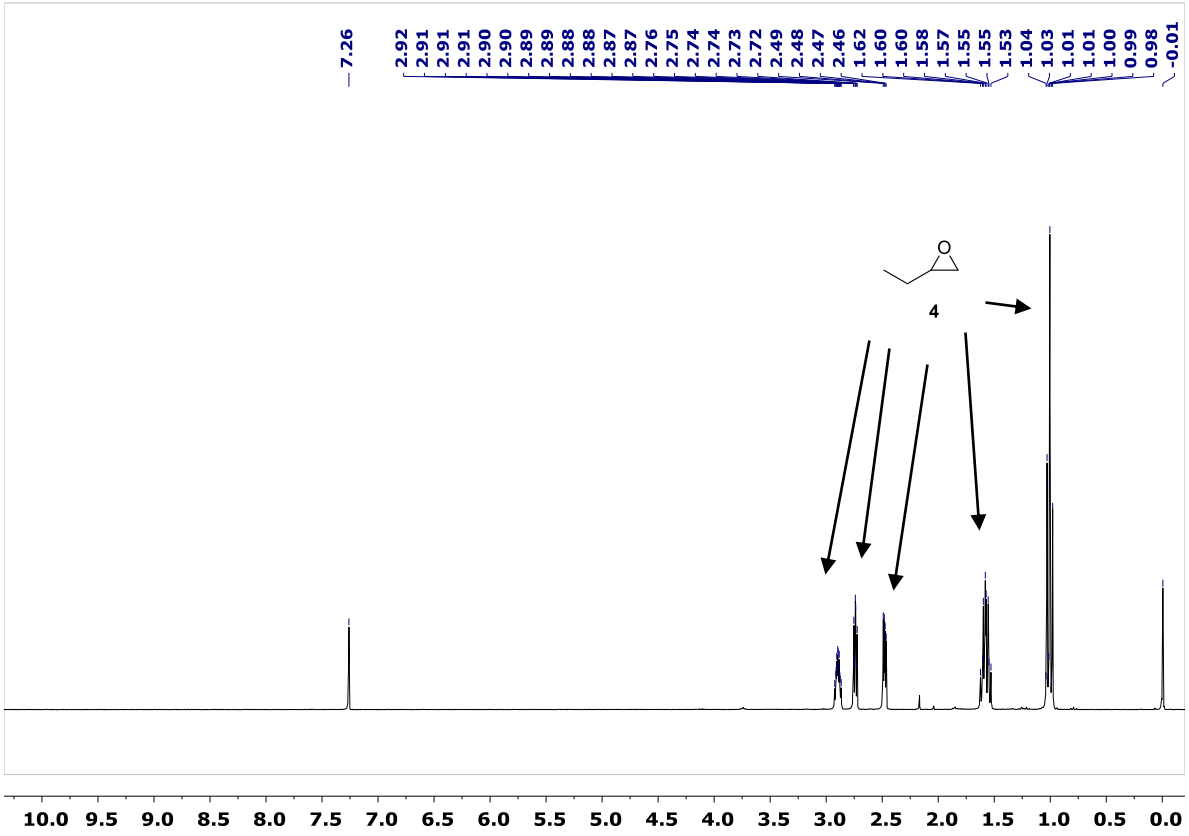

No byproducts from decomposition of COF were detected.

Calculation of chemical erosion of COF with malonitrile 7

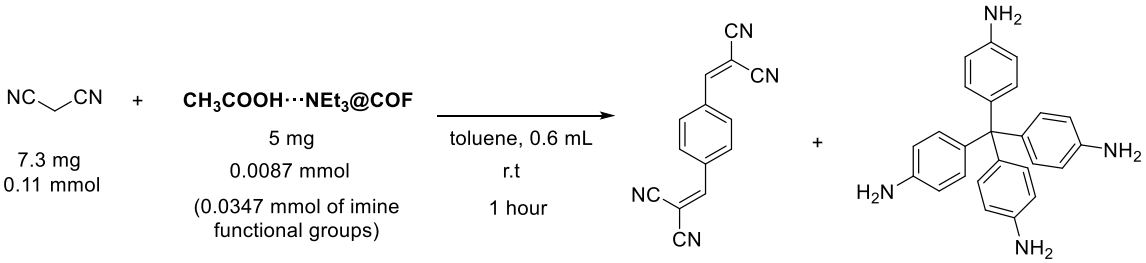

7.3 mg
0.11 mmol

7 **10** **2**

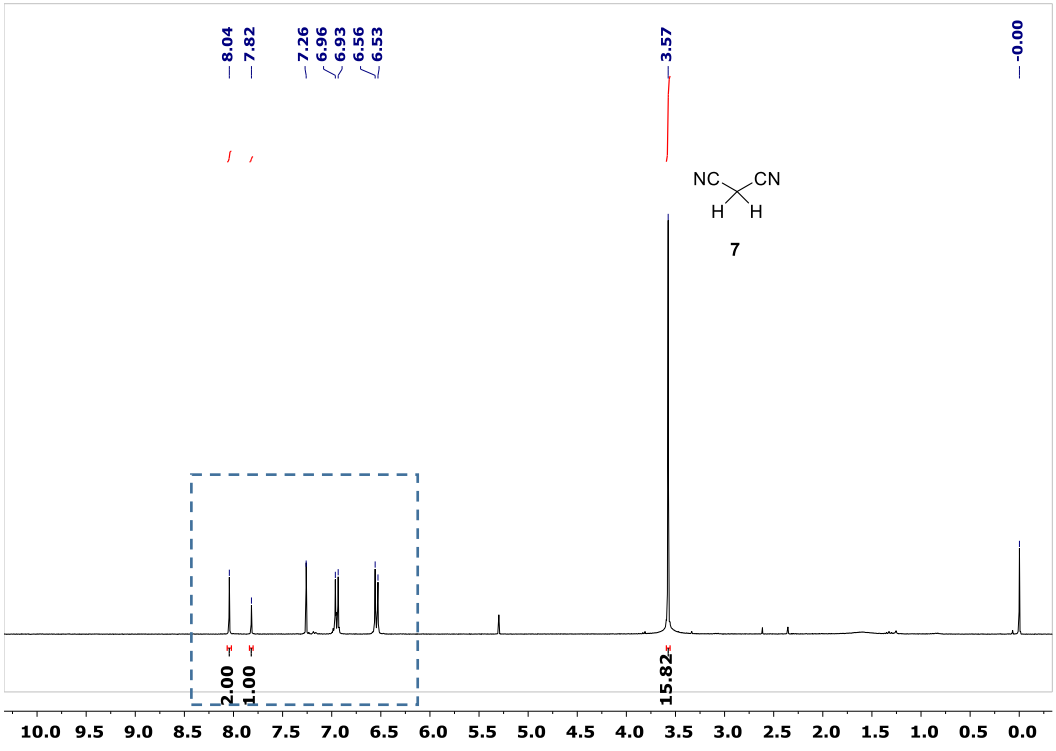

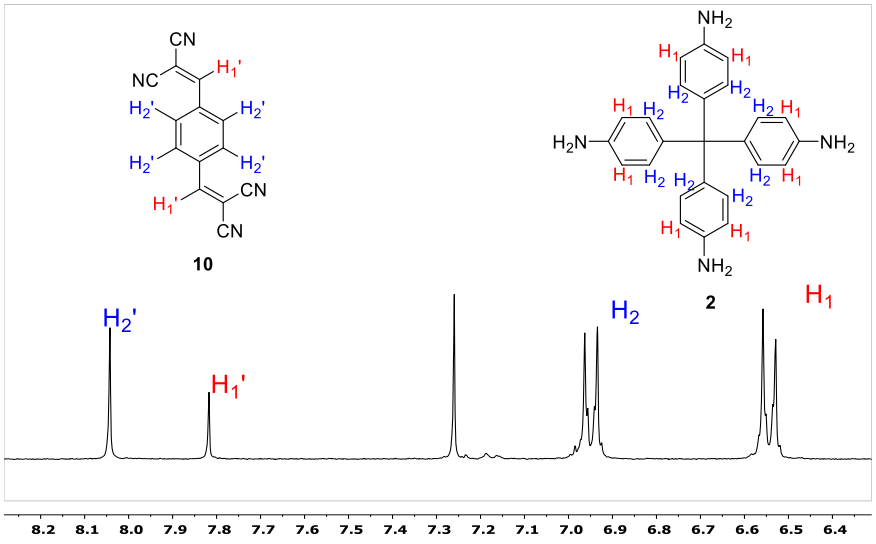

The signals of byproduct **10** matched with the previous spectroscopic data described in the literature.[10]

To calculate the ratio (byproduct **10** : malonitrile **7**) we use the signal of 7.82 ppm for byproduct **10** and the signal at 3.57 ppm for malonitrile **7**. Both signals integrate for 2 protons, so the ratio is (1.00 : 15.82).

Considering the stoichiometry, two molecules of malonitrile **7** are necessary for making one molecule of byproduct **10**, so the ratio of (reacted malonitrile: malonitrile left) is (2.00 : 15.82), in other words, 11.2 % of the initial malonitrile has reacted.

In the reaction, there was 0.11 mmol of initial malonitrile **7**. Applying this percentage, 0.012 mmol of the malonitrile has reacted with 0.012 mmol of the imines functional groups of the COF. Therefore, the percentage of deteriorated COF is:

$$\%\ \text{chemical erosion of COF} = \frac{0.012\ \text{mmol reacted imines}}{0.0347\ \text{mmol total imines}} \cdot 100 = 35.6\ \%$$

[10] S. K. Panja, N. Dwivedi, S. Saha, *RSC Adv*. **2015**, *5*, 65526-65531

Calculation of chemical erosion of COF with malonitrile 7 and benzaldehyde 8a

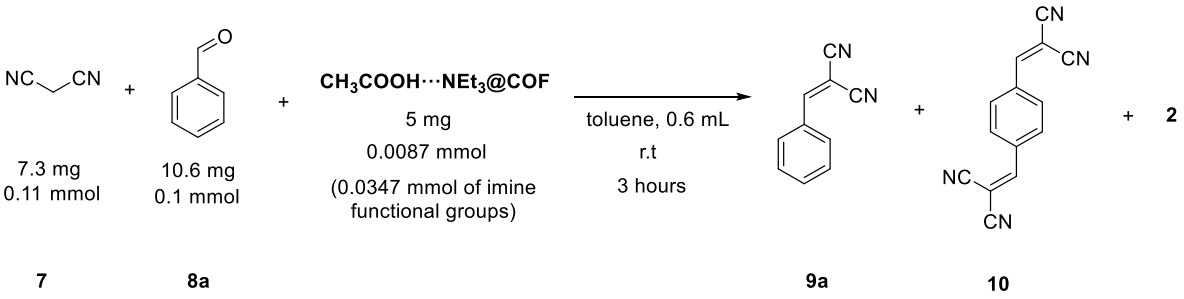

7.3 mg
0.11 mmol

10.6 mg
0.1 mmol

7 **8a** **9a** **10**

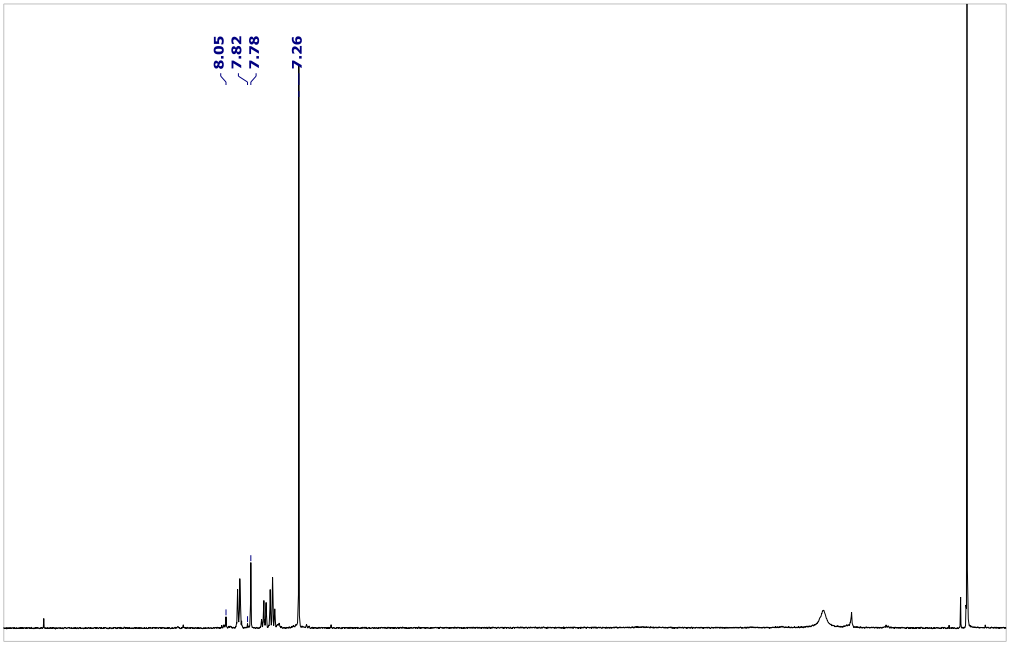

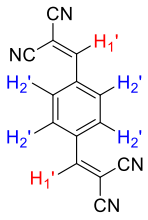

10

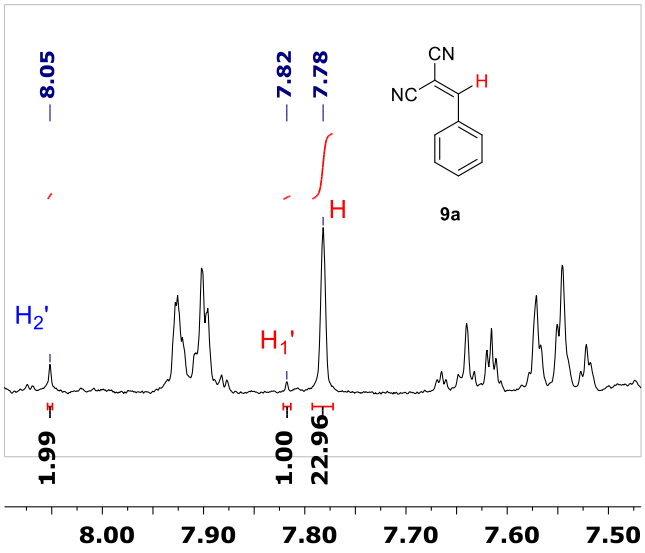

A crude of the catalyzed reaction with **$CH_3COOH\cdots NEt_3$@COF** was analyzed by ^{1}H-NMR in order to check the decomposition of the COF in the general conditions. The reaction has finished since the malonitrile (δ 3.57 ppm) has been completely consumed.

To calculate the ratio (byproduct **10** : product **9a**) we use and the signal at 7.82 ppm for byproduct **10** and the signal at 7.78 ppm for product **9a**. The signal at 7.82 ppm integrates by two protons, and the signal at 7.78 ppm integrates by one proton, so the molar ratio is (0.5 : 22.96).

Considering the stoichiometry, two molecules of malonitrile **7** are necessary for making one molecule of byproduct **10** but only one molecule of malonitrile **7** is necessary for making one molecule of product **9a**. Therefore the ratio of (malonitrile transformed in **10**: malonitrile transformed in **9a**) is (1.00 : 22.69), in other words, 4.2 % of the initial malonitrile has reacted with the COF and 95.8 % of the initial malonitrile has reacted with the benzaldehyde **8a**.

In the reaction, there was 0.11 mmol of initial malonitrile **7**. Applying this percentage, 0.0046 mmol of the malonitrile has reacted with 0.0046 mmol of the imines functional groups of the COF. Therefore, the percentage of deteriorated COF is

$$\%\ \text{chemical erosion of COF} = \frac{0.0046\ \text{mmol reacted imines}}{0.0347\ \text{mmol total imines}} \cdot 100 = 13.2\ \%$$

Calculation of deteriorated COF with benzaldehyde 8a

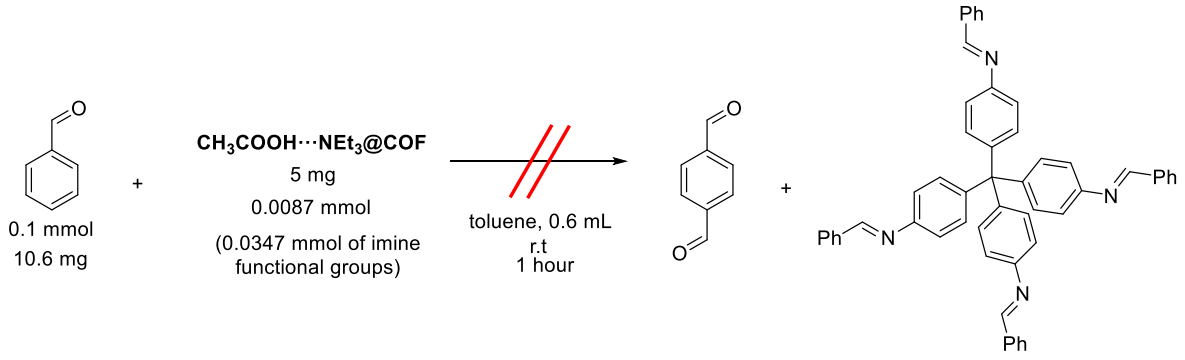

8a **1** **13**

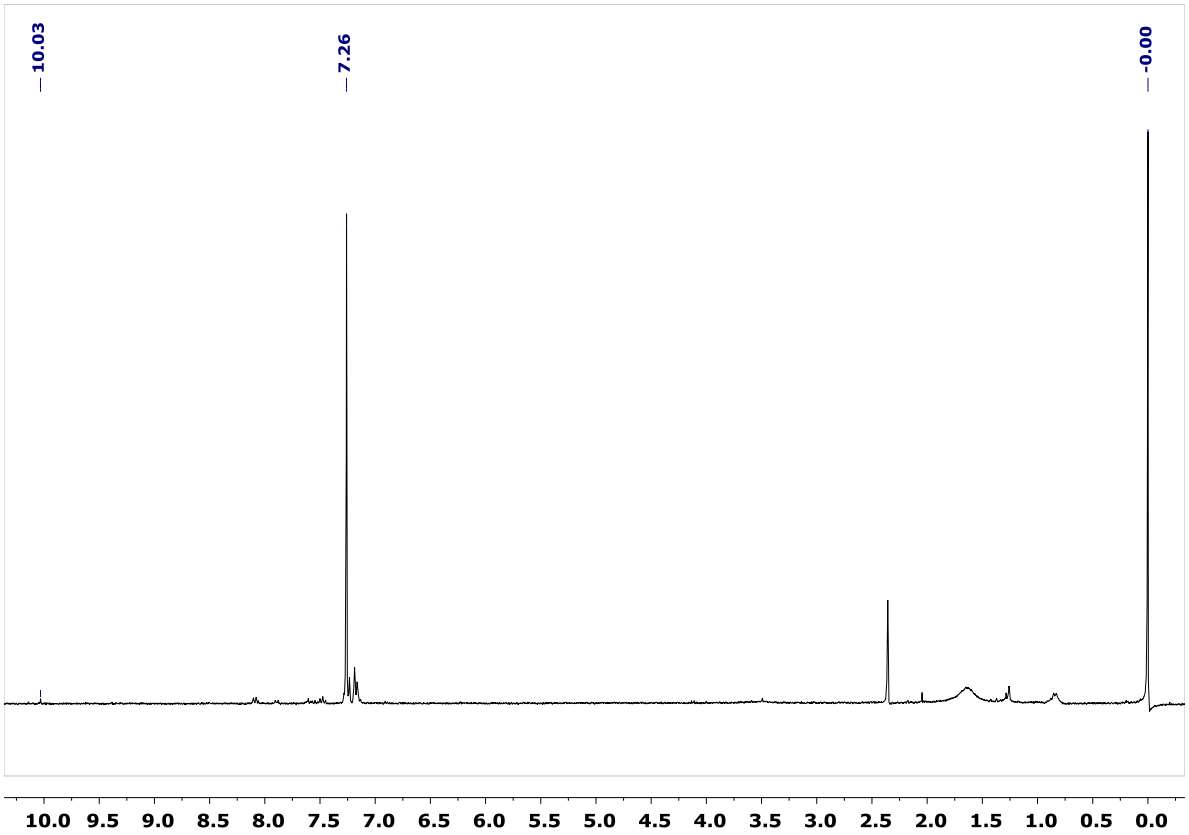

Before carrying out the spectrum, the toluene must be removed in the rotavap. The benzaldehyde **8a**, which is also volatile, is removed too. Some traces of benzaldehyde **8a** and toluene can be hardly seen in the spectrum. However, decomposition products of the COF, like terephthalaldehyde **1**, 4,4',4",4"'-methanetetrayltetraaniline **2** or byproduct **13** are not volatile and they should be observed in the case they had been formed. Since no traces of these products were found, it can be concluded that the benzaldehyde did not promote the decomposition of the COF.

8. COF stability after reactions

We carried out model reactions using COF as catalyst. After the indicated time, the reaction mixture was passed through a membrane filter of 0.45 μm pores and the solid was washed three times with 10 mL of CH_2Cl_2.

SEM images and IR spectra were taken from the solid to compare them with the images and spectra of the COF before the reaction.

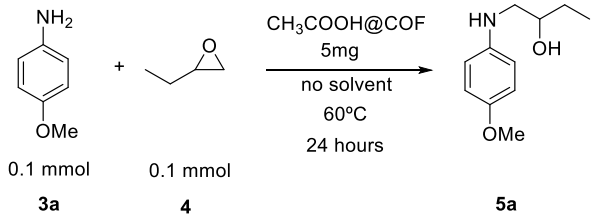

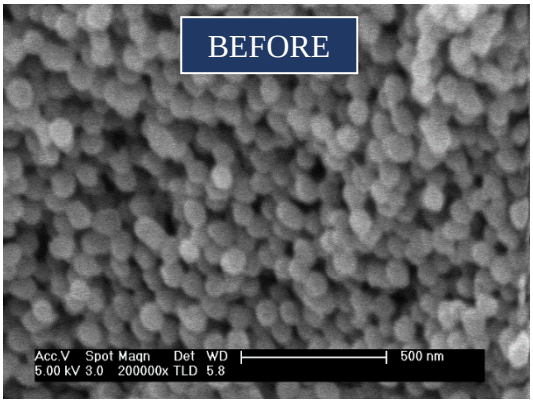

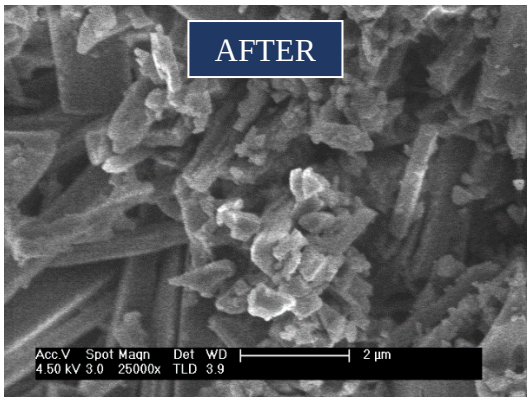

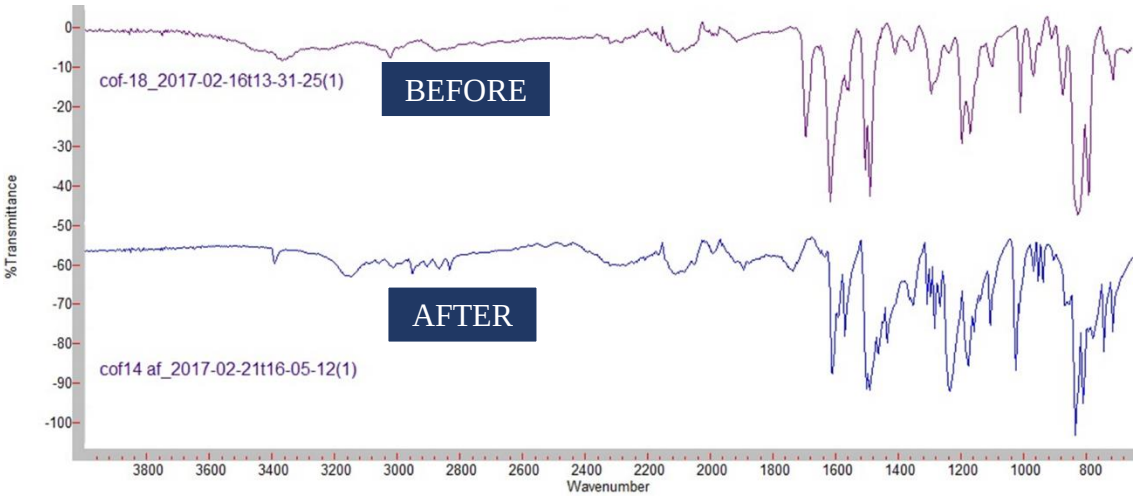

From the SEM images, it can be observed that the morphology of the solid was very different: the COF has been decomposed.

The IR spectra have different signals, which confirms that the solid has been transformed.

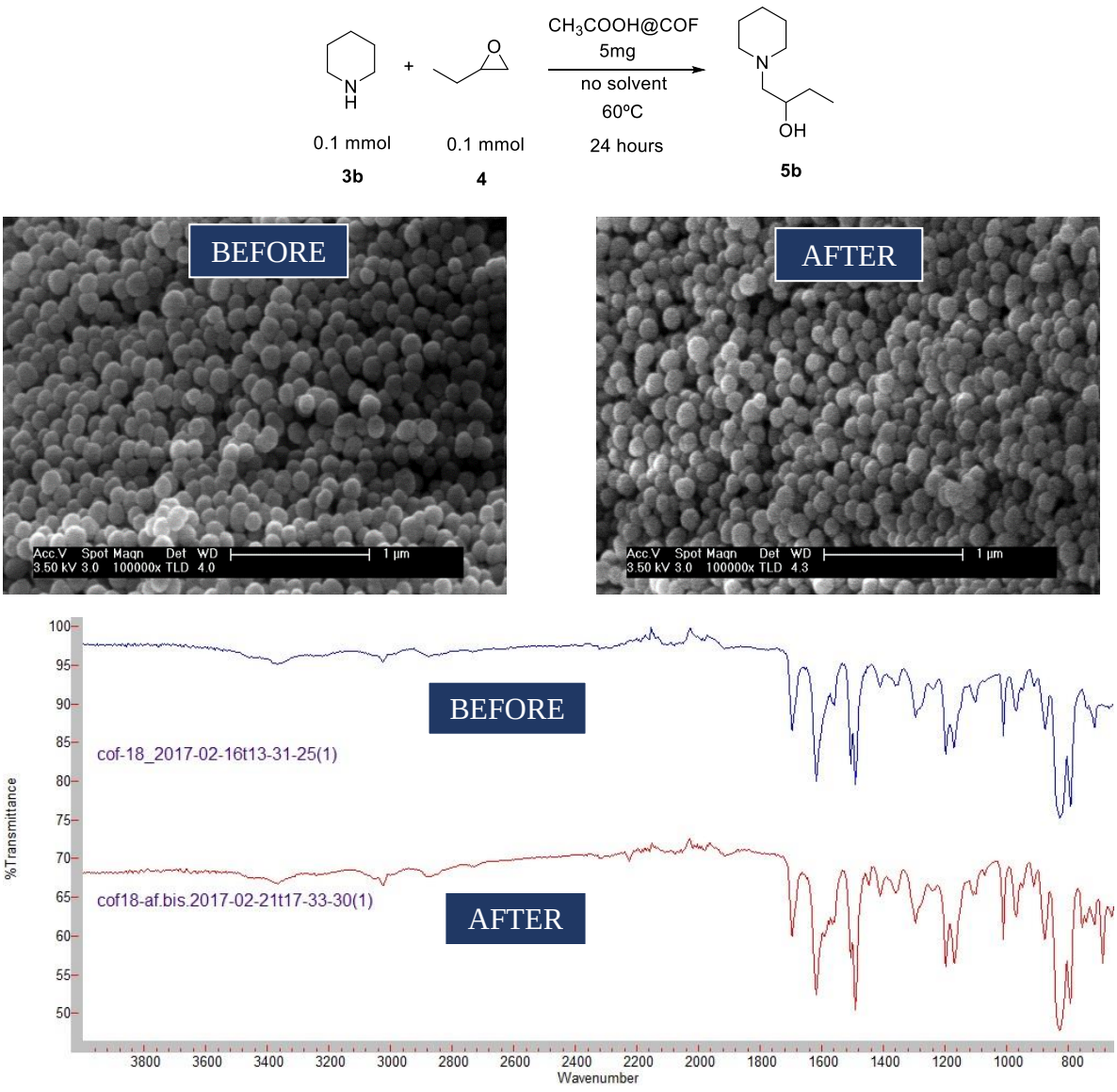

The reaction did not affect the morphology of the COF. The IR spectra show the same signals.

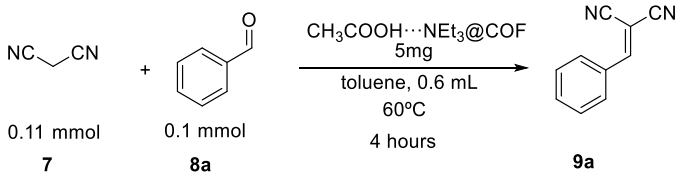

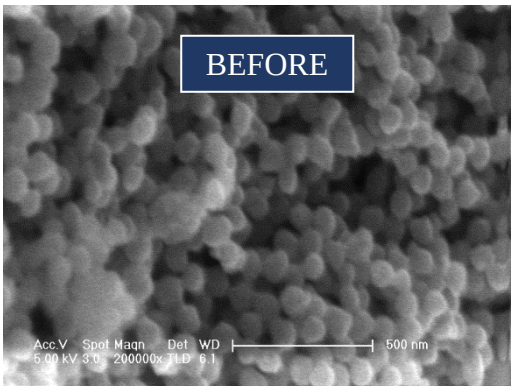

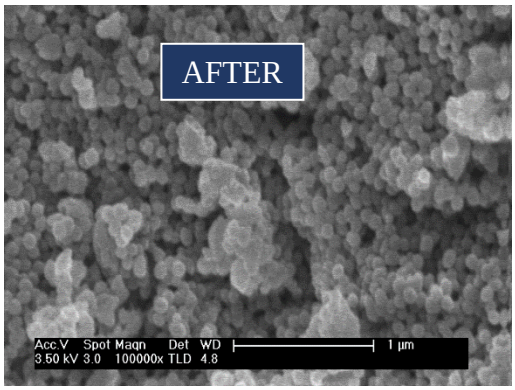

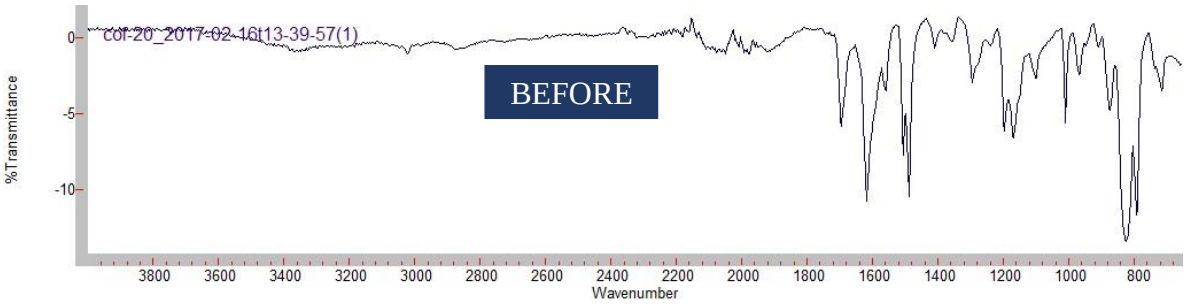

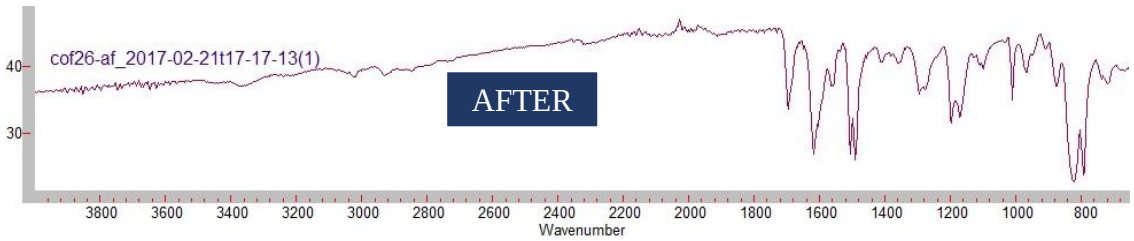

As described in the previous section, ^{1}H-NMR experiments indicated that malonitrile **7** reacted with the COF and decomposed a part of the material. However, the rest of the COF remained as a solid. From the SEM images and IR spectra, it could be observed that this solid presented the same morphology and the same IR signals.

9. Leaching tests

Leaching test of $CH_3COOH\cdots NEt_3$@COF

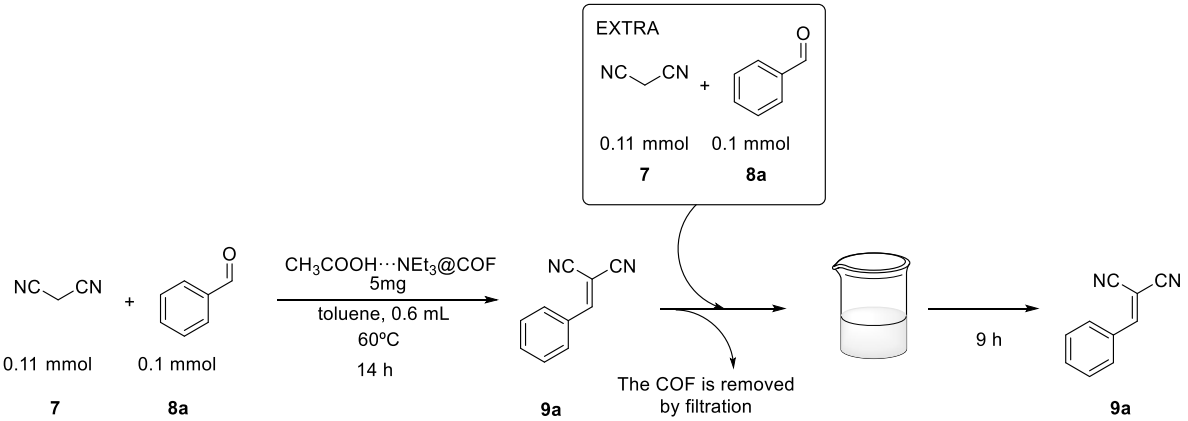

The reaction was set up following the general procedure for "Knoevenagel condensation catalyzed by COF" (see above) and the formation of the product **9a** was measured at 14 hours by GC-FID. There was 0.068 mmol of the product **9a** (Yield = 68%).

Then the reaction mixture was filtrated through membrane of 0.45 μm pores in order to remove the COF. Other 0.11 mmol of molonitrile **7** and 0.1 mmol of benzaldehyde **8a** were added to the reaction mixture. The mixture was allowed to react during 9 hours and the formation of the product was measured by GC-FID. There was 0.087 mmol of the product **9a**, therefore, 0.019 mmol had been formed in the second step (Yield in the second step = 19 %)

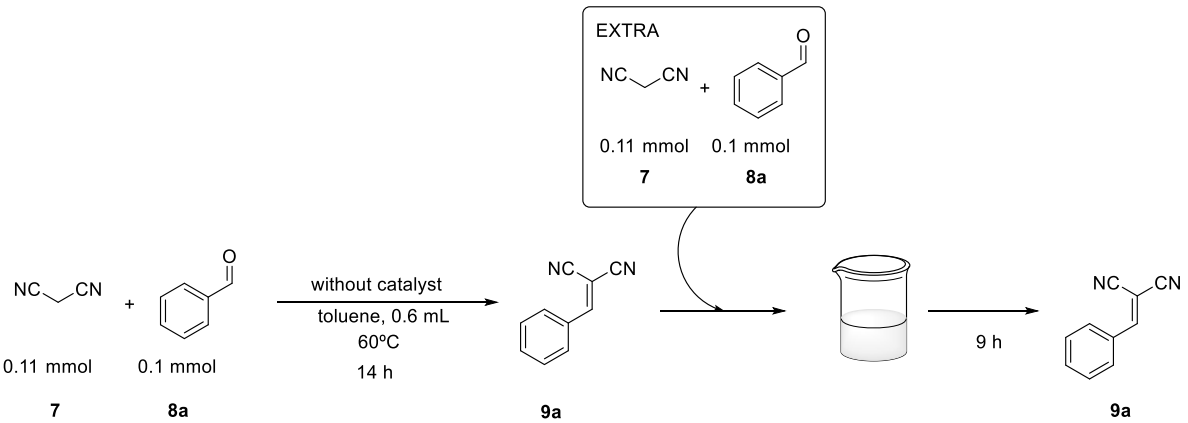

The same process was repeated but without COF: The reaction was set up following the general procedure for "Knoevenagel condensation catalyzed by COF" (see above) but without adding the COF and the formation of the product was measured at 14 hours by GC-FID. There was 0.008 mmol of the product **9a** (Yield = 8%).

Other 0.11 mmol of molonitrile **7** and 0.1 mmol of benzaldehyde **8a** was added to the reaction mixture. The mixture was allowed to react during 9 hours and the formation of the product was measured by GC-FID. There was 0.012 mmol of the product **9a**, therefore, 0.004 mmol had been formed in the second step (Yield in the second step = 4 %).

In the first experiment, when the **$CH_3COOH\cdots NEt_3$@COF** is presented in the reaction, the yield of the reaction is 68 %, but when the catalytic COF is removed and the reaction is repeated in the reaction media the yield decreases to 19 %. This indicates that the **$CH_3COOH\cdots NEt_3$@COF** acts as a solid heterogeneous catalyst.

However, comparing the second step of the two experiments, we observed that when there is not **$CH_3COOH\cdots NEt_3$@COF** from the beginning, the background reaction in the second step has a yield of 4%.

It can be conclude that the most of the catalytic activity is due to the heterogeneous **$CH_3COOH\cdots NEt_3$@COF**.

Leaching test of NEt_3@COF

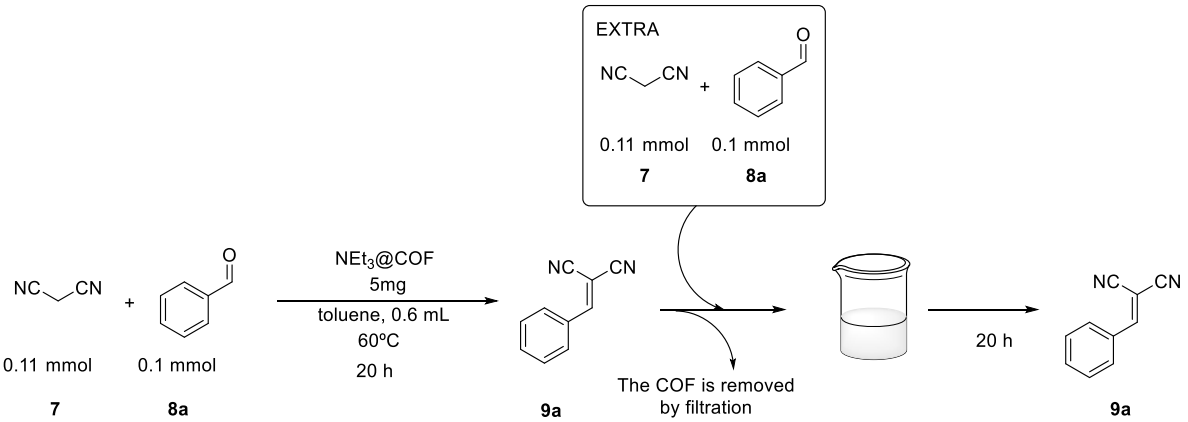

The reaction was performed following the general procedure for "Knoevenagel condensation catalyzed by COF" using as catalysis **NEt_3@COF** (see above). The formation of the product **9a** is measured at 14 hours by GC-FID (0.09 mmol of product **9a**, Yield = 90 %) and at 20 hours (0.1 mmol of product **9a**, Yield = 100 %).

Then, the reaction mixture was filtrated through membrane of 0.45 μm pores in order to remove the COF. Other 0.11 mmol of molonitrile **7** and 0.1 mmol of benzaldehyde **8a** was added to the reaction mixture. The mixture was allowed to react during 20 hours and the formation of the product was measured by GC-FID. There was 0.2 mmol of the product **9a**, indicating that 0.1 mmol had been formed in the second step (Yield in the second step = 100 %).

This leaching study indicates that the catalytic activity of **NEt_3@COF** is due to the molecules of Et_3N that are released from the COF and are dissolved in the reaction medium.

10. ^{1}H-NMR spectra

^{1}H-NMR ($CDCl_3$, 300 MHz) (5a)

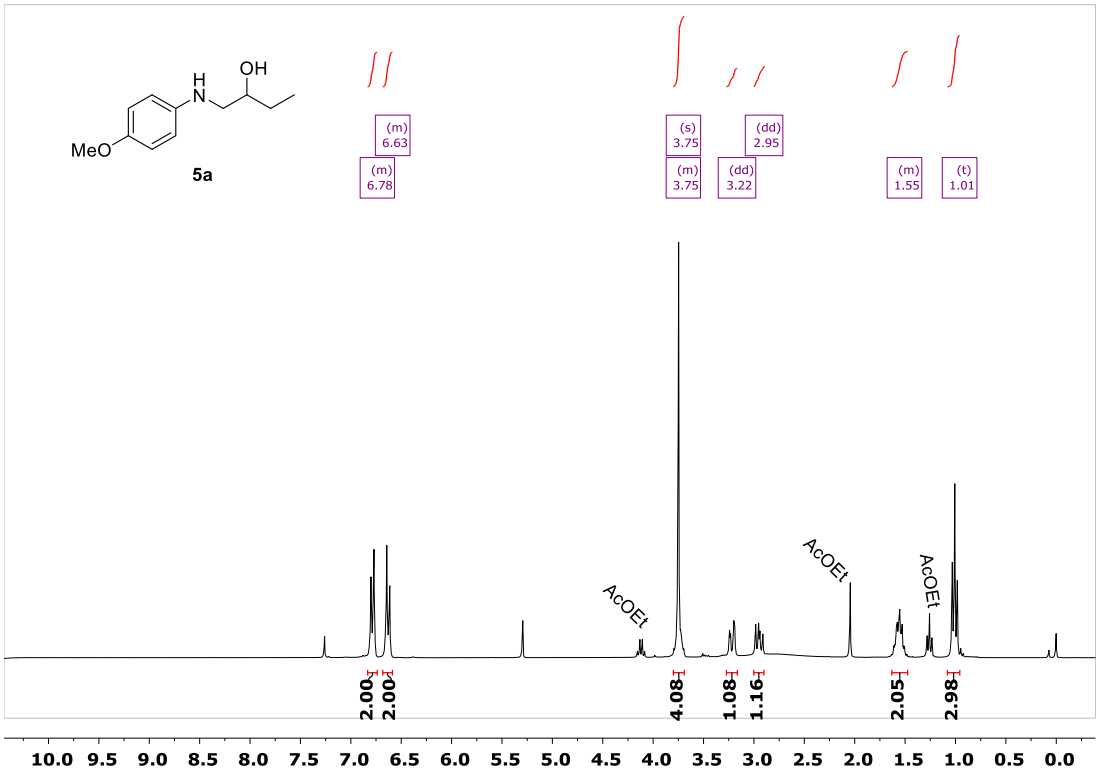

^{1}H-NMR ($CDCl_3$, 300 MHz) (5b)

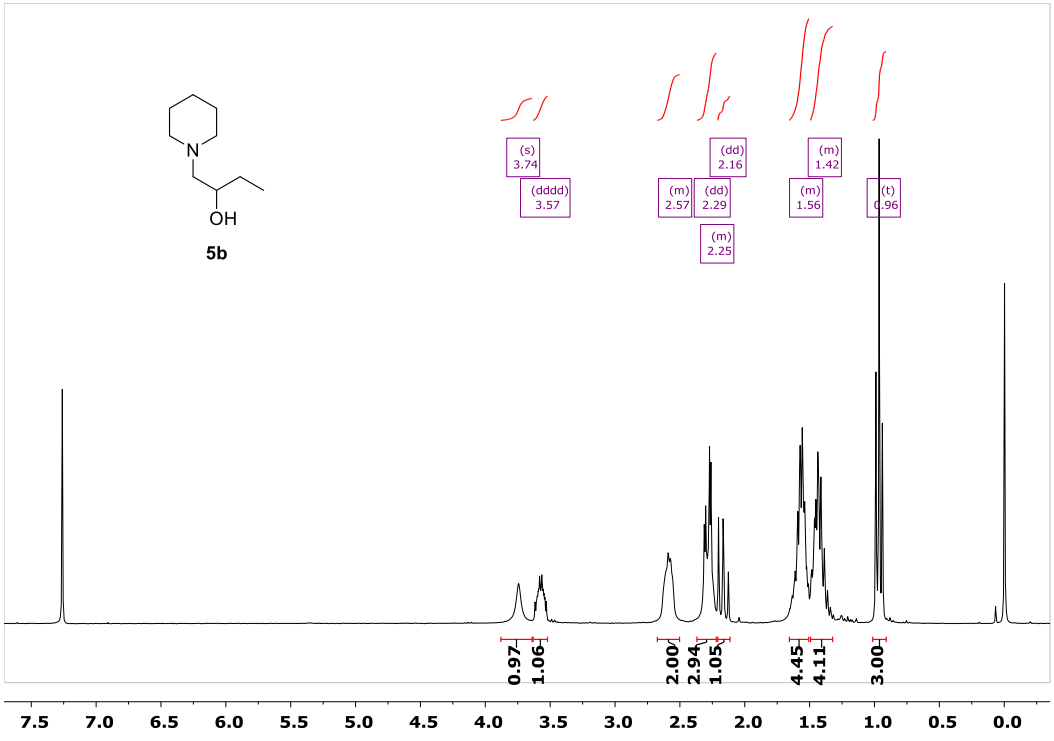

^{1}H-NMR ($CDCl_3$, 300 MHz) (9a)

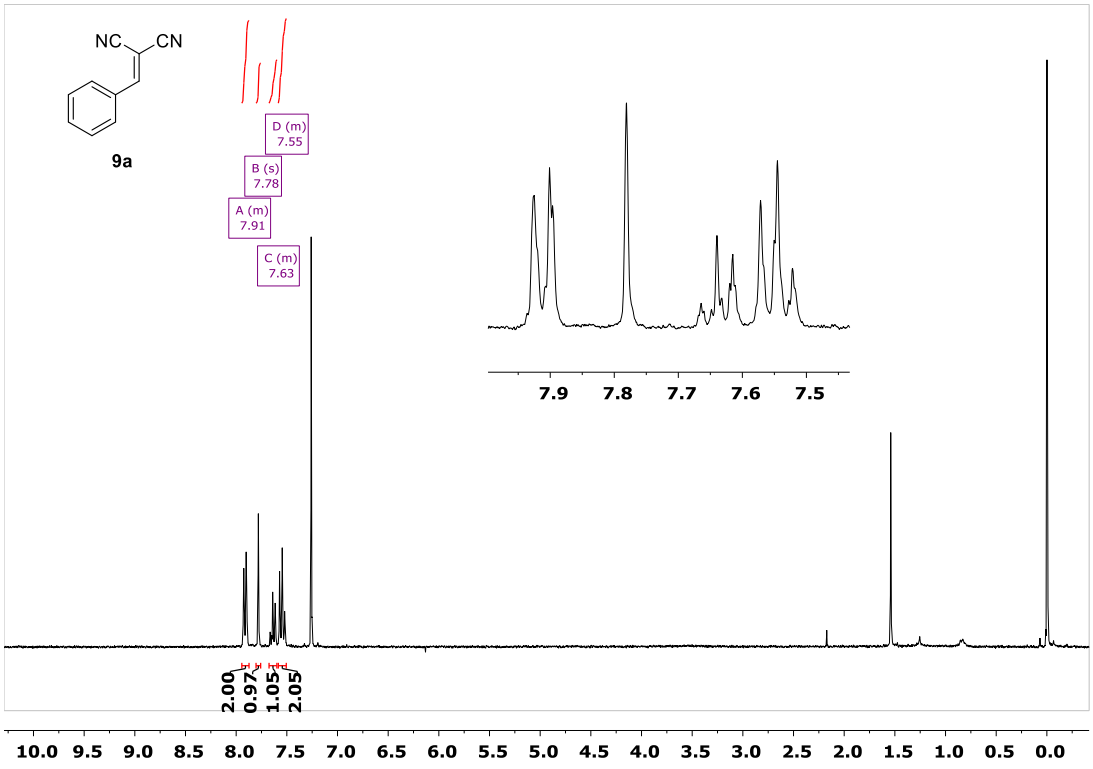

^{1}H-NMR ($CDCl_3$, 300 MHz) (9b)

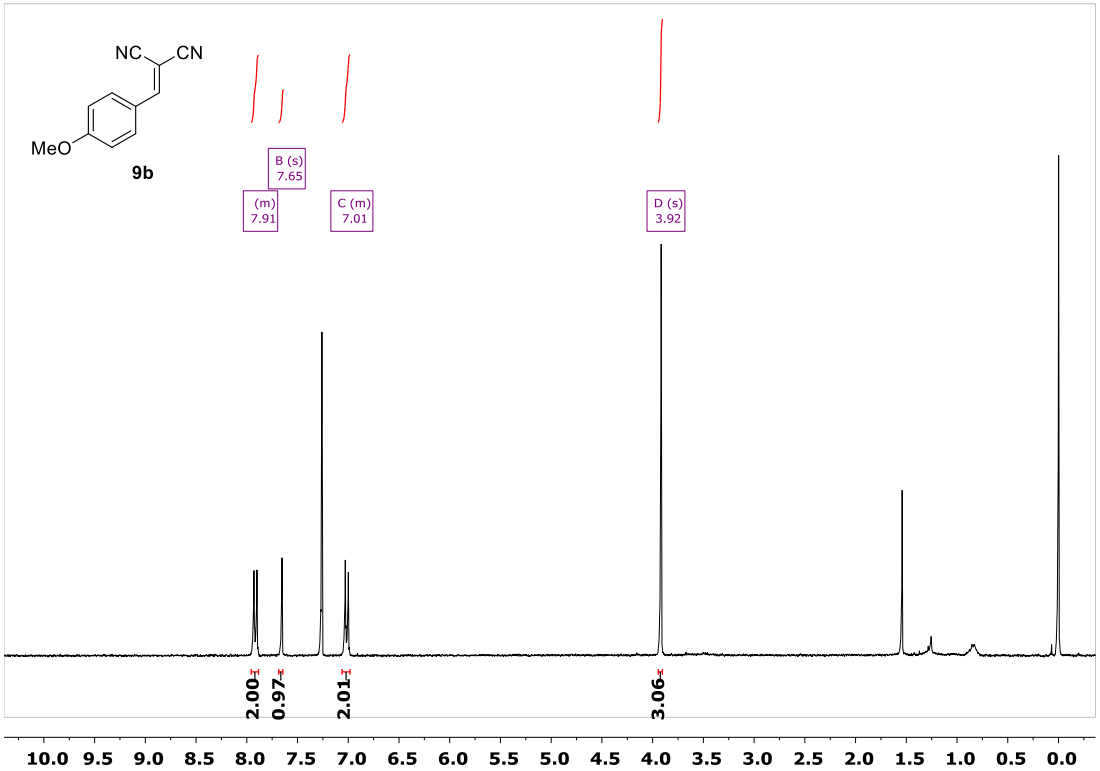

^{1}H-NMR ($CDCl_3$, 300 MHz) (9g)

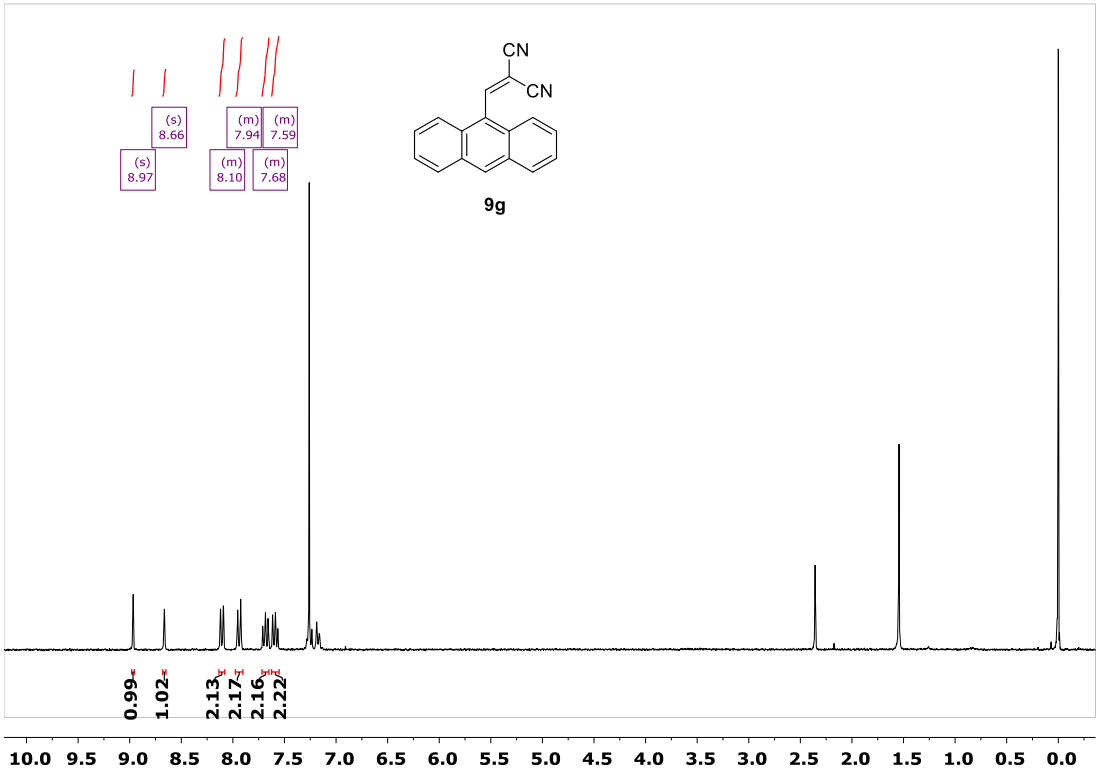

11. Computational details

Two sets of calculations have been performed to analyze computationally the interactions between acetic acid, triethylamine and the COF as well as the catalytic activity of the resulting material in the epoxide ring opening and the Knoevenagel reactions. On one hand, M06/6-311+G(d,p) molecular calculations have been performed with Gaussian09 package.[11] With these calculations we have explored the energetics of the studied reactions in gas phase and solution. Vibrational analysis has been used to ensure the nature of the stationary points (minima or transition state). Thermal effects have been computed assuming an ideal gas, the rigid rotor approximation and harmonic frequencies at T = 298 K and P = 1 atm. In addition, solvent effects have been included with the SMD implicit model.[12] For the case of the epoxide ring opening reaction, dichloromethane (ε =8.93) have been used as solvent since its dielectric constant is in between that of piperidine (ε =5.6) and several epoxides (ε =14.0 for ethylene oxide). In the Knoevenagel reaction, solvent effects are included considering the dielectric constant of toluene; the solvent used in experiments.

On the other hand, DFT periodic boundary condition calculations including the whole COF framework have been performed with VASP package.[13] These calculations have been used to study the reactivity inside the COF and to characterize the supramolecular interactions between the COF and acetic acid, triethylamine and a system formed by one acetic acid and one triethylamine molecule. The VASP packages uses plane-wave functions for describing the electronic wavefunction and it is very efficient when using GGA functionals. Unfortunately, the computational cost dramatically increases when using hybrid functionals and, in our particular case, the use of hybrid functionals is too expensive. In this context, all periodic calculations have been performed at the PBE level.[14] Dispersion forces were taken into account in the PBE calculations with the Grimme's empirical correction (D2).[15] We take the advantage that Grimme correction is added a posteriori to the DFT energy to estimate the contribution of the Van der Waals interactions in the global adsorption energies. This estimation is determined as the energy difference between the PBE-D2 and the PBE energies at the PBE-D2 optimized structure. The energy cutoff has been set to 400 eV. Geometry convergence criterion was fix to a change in energy of $1 \cdot 10^{-3}$ eV. The initial structure of the COF has been taken from the literature and the cell parameters (a = b = 28.127 Å; c = 17.758 Å and $\alpha = \beta = \gamma = 90°$) have been kept constant in all optimizations. All calculations have been performed considering only the gamma point of the reciprocal lattice. Initial structures have been constructed introducing manually the molecular fragments with the geometries obtained with Gaussian09 package. Several different starting points have been considered with the aim of exploring several local minima and analyze the energy difference between them. Several of these different minima are added in the results and discussion section. The

[11] Y. Zhao, D. G. Truhlar, *Theor. Chem. Acc.* **2008**, *120*, 215; Hariharan, P. C.; Pople, J. A. *Theor. Chim. Acta* **1973**, *28*, 213−222; Frisch, M. J. et al. Gaussian09.
[12] A. V. Marenich, C. J. Cramer, D. G. Truhlar, *J. Phys. Chem. B* **2009**, *113*, 6378.
[13] Kresse, G.; Hafner, *J. Phys. Rev. B: Condens. Matter Mater. Phys.* **1993**, *47*, 558−561; Kresse, G.; Hafner, *Phys. Rev. B: Condens. Matter Mater. Phys.* **1994**, *49*, 14251−14269; Kresse, G.; Furthmüller, *J. Phys. Rev. B: Condens. Matter Mater. Phys.* **1996**, *54*, 11169−11186; Kresse, G.; Furthmüller, *J. Comput. Mater. Sci.* **1996**, *6*, 15−50.
[14] Perdew, J. P.; Burke, K.; Ernzerhof, M. *Phys. Rev. Lett.* **1996**, *77*, 3865−3868
[15] S. Grimme, *J. Comput. Chem.* **2004**, *25*, 1463–1473; S. Grimme, *J. Comput. Chem.*, **2006**, *27*, 1787–1799.

differences between them do not change the major results of the computations. Remarkably, the energetics of the transition states have been obtained through a constrained optimization fixing the atoms involved in the formation and breaking of bonds. This imposed that the interatomic distances between the key atoms are kept constant to the values of the transition state obtained with the molecular calculations. This concerns the acidic hydrogen and the oxygen bonded to it of the acetic acid, the oxygen and the less substituted carbon bonded to the oxygen of the epoxide and the nitrogen atom of the piperidine in the ring opening reaction as well as the carbonyl carbon of the aldehyde and the central carbon of malononitrile in the Knoevenagel reaction.

At this point it is worth mentioning that we have also performed molecular calculations at the PBE-D2/6-311+G(d,p) level of theory with the aim of determining the effect of the functional on the energy barriers. The obtained results are all summarized in Table S1 (see above). Remarkably, the functional choice is crucial in determining the energy barriers, the PBE-D2/6-311+G(d,p) methodology predicting values that are around 40-50 kJ mol^{-1} lower than those predicted with M06/6-311+G(d,p). This underestimation of the energy barriers is a well-known drawback of pure GGA functionals, which stabilize structures where the electron density is largely delocalized. It is for this reason that we decided to add a correcting factor to the energetics of the species involved in the reactivity inside the COF (reacting precomplex, transition state and product). This correcting factor is determined by the difference between M06 and PBE-D2 values in the relative energies with respect separated reactants of each individual stationary point of the reaction in gas phase. As example, the transition state of the ring epoxide reaction in gas phase is predicted to be 43.5 kJ mol^{-1} above separated reactants with M06/6-311+G(d,p). The same transition state at PBE/6-311+G(d,p) level of theory is located -8.0 kJ mol^{-1} with respect to reactants. Therefore, the correcting factor for the energetics inside the COF is 51.5 kJ mol^{-1}.

Table S1. Relative energies in kJ mol^{-1} of the reactive pre-complex (reactant), transition state (TS) and product of the considered steps summarized in Scheme 4. Values in parenthesis corresponds to Gibbs energies.

Reaction[a]	Method	Reactant	TS	Product
1	$M06_{(Mol)}$[b]	-59.6 (30.6)	43.5 (144.3)	-15.6 (62.2)
1	$M06_{(Mol)solv}$[c]	-38.7 (51.1)	35.1 (135.1)	-118.6 (1.1)
1	$PBE_{(Mol)}$[d]	-70.1 (31.3)	-8.0 (93.9)	-89.0 (34.8)
1	$PBE_{(PBC)}$[e]	-55.0	17.7	-75.5
2 (8a)	$M06_{(Mol)}$[b]	-47.8 (57.4)	-28.9 (89.8)	-101.8 (26.2)
2 (8a)	$M06_{(Mol)solv}$[c]	-50.3 (56.3)	-24.8 (96.8)	-82.2 (36.3)
2 (8a)	$PBE_{(Mol)}$[d]	-84.7 (16.4)	-68.5 (48.3)	-119.3 (-2.7)
2 (8a)	$PBE_{(PBC)}$[e]	-92.5	-91.6	-136.9
2 (8g)	$M06_{(Mol)}$[b]	-56.2 (55.8)	-31.4 (87.6)	-110.8 (10.2)
2 (8g)	$M06_{(Mol)solv}$[c]	-55.8 (56.1)	-24.8 (96.8)	-86.4 (37.7)
2 (8g)	$PBE_{(Mol)}$[d]	-89.3(15.6)	-68.5 (48.3)	-132.5 (-10.7)
2 (8g)	$PBE_{(PBC)}$[e]	-117.1	-116.3	-157.0

[a] See Scheme 4 for reaction definition. [b] Molecular gas phase M06/6-311+G(d,p) calculations. [c] Molecular M06/6-311+G(d,p) calculations including solvent effects with implicit models [d] Molecular gas phase PBE-D2/6-311+G(d,p) calculations. [b] PBE-D2 periodic boundary conditions calculations including the whole COF framework.

$NEt_3\cdots CH_3COOH$@COF Adducts

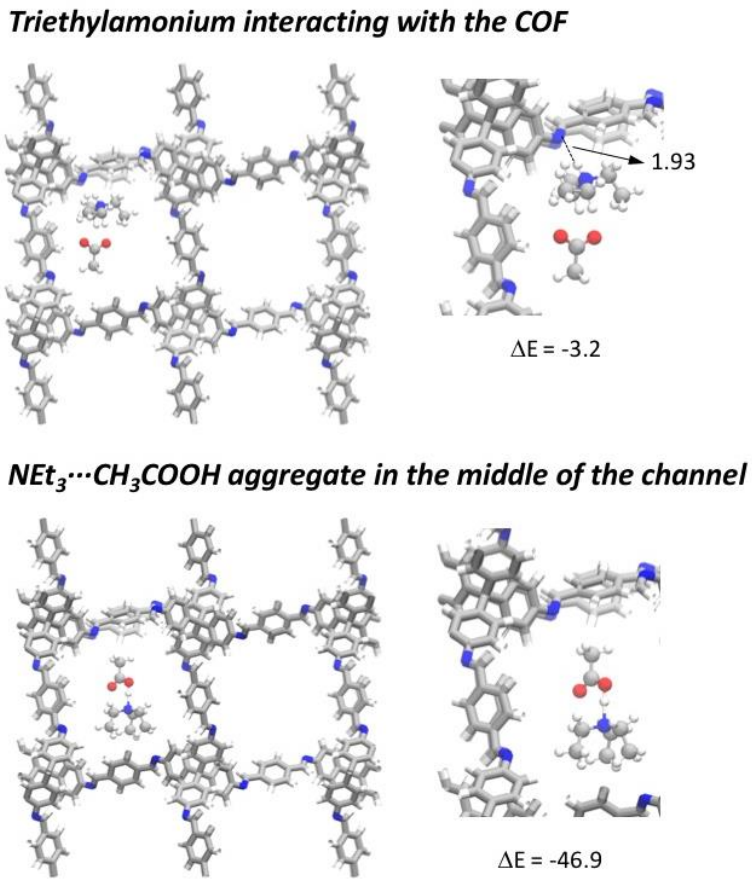

Figure S21. Optimized geometries of the $NEt_3\cdots CH_3COOH$@COF adducts not reported in the main text and their adsorption energies (ΔE) with respect to the $NEt_3\cdots CH_3COOH$ desorption. Distances are in Å and energies in kJ mol^{-1}.

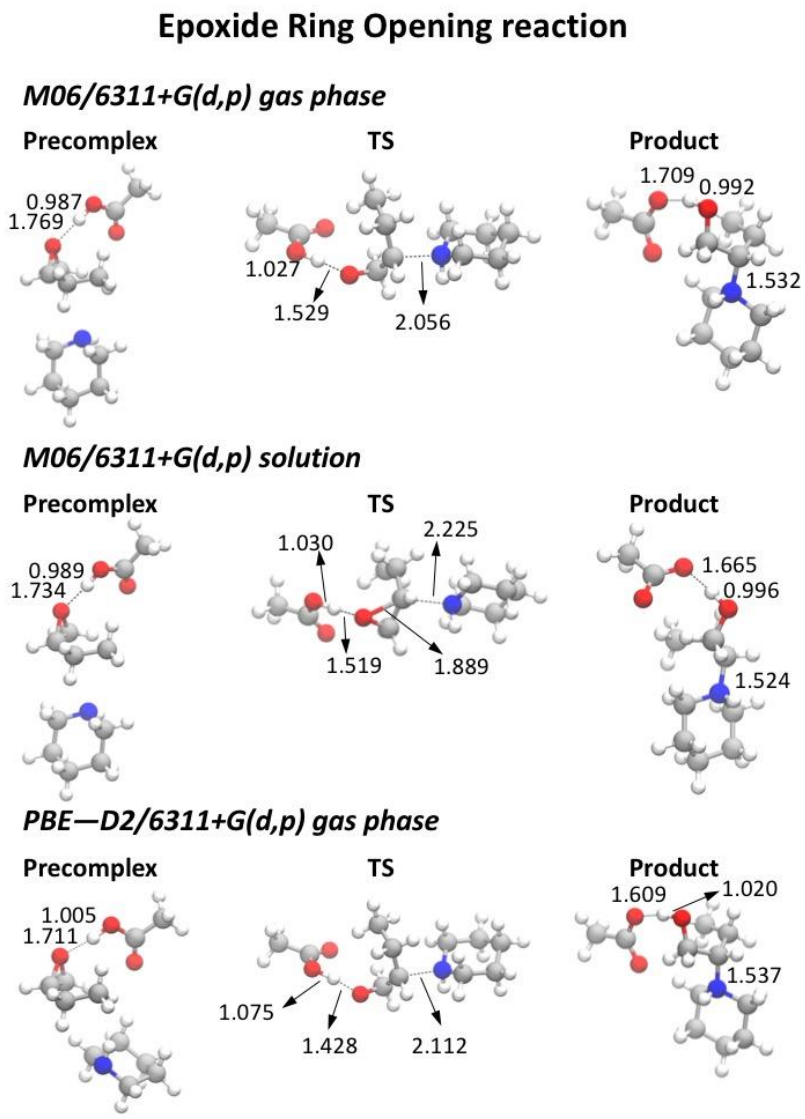

Figure S22. Optimized geometries of all intermediates and transition states found for the epoxide ring opening reaction involving **3b**. All distances are in Å.

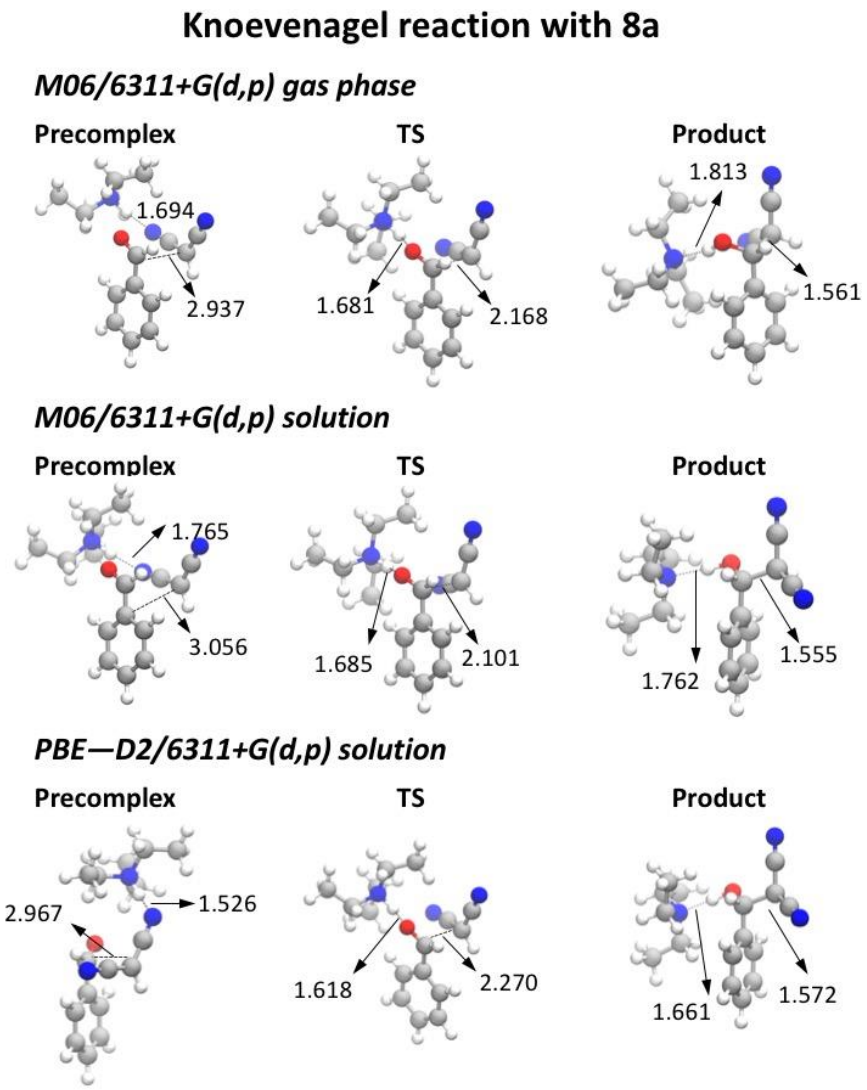

Figure S23. Optimized geometries of all intermediates and transition states found for the Knoevenagel reaction involving **8a**. All distances are in Å.

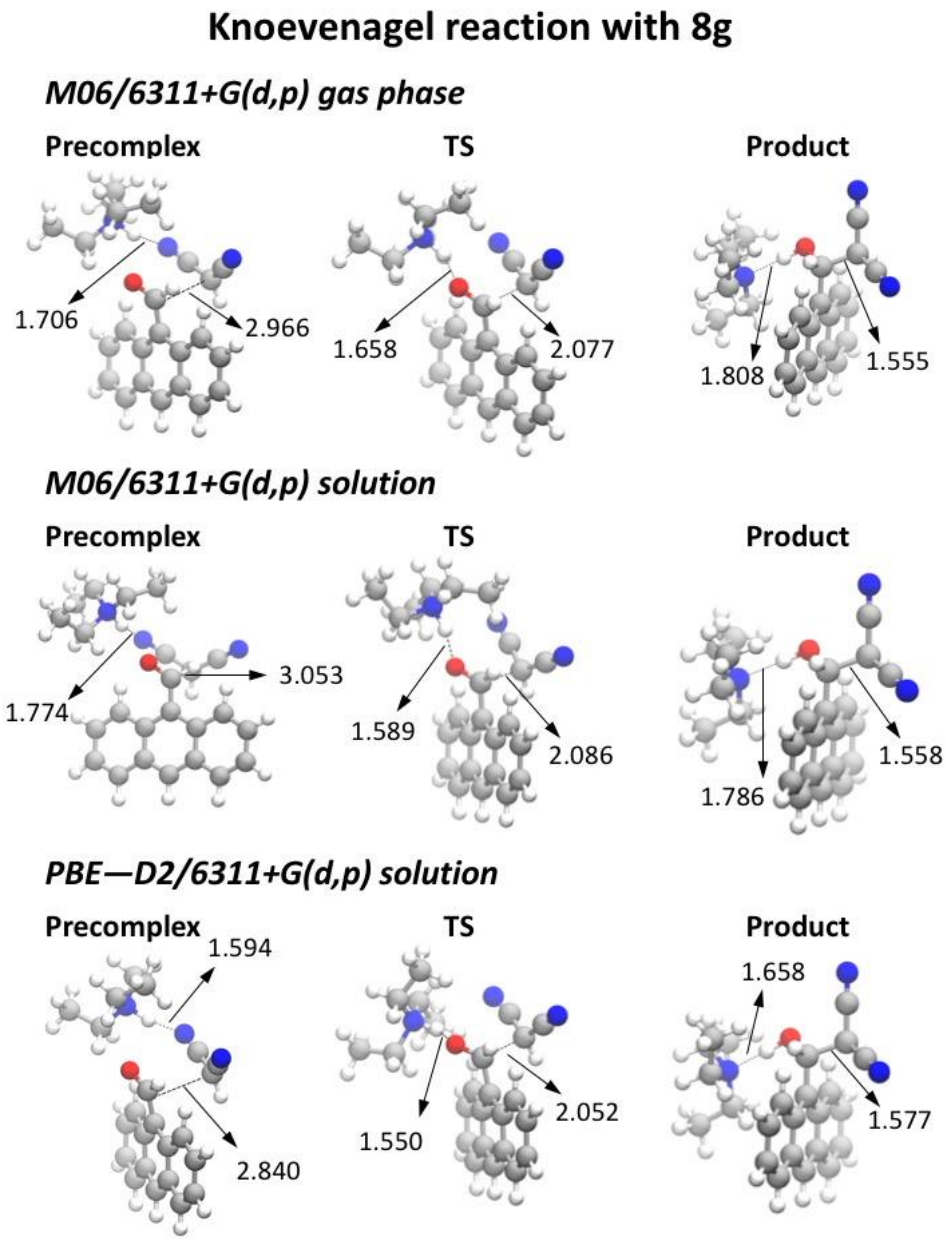

Figure S24. Optimized geometries of all intermediates and transition states found for the Knoevenagel reaction involving **8g**. All distances are in Å.

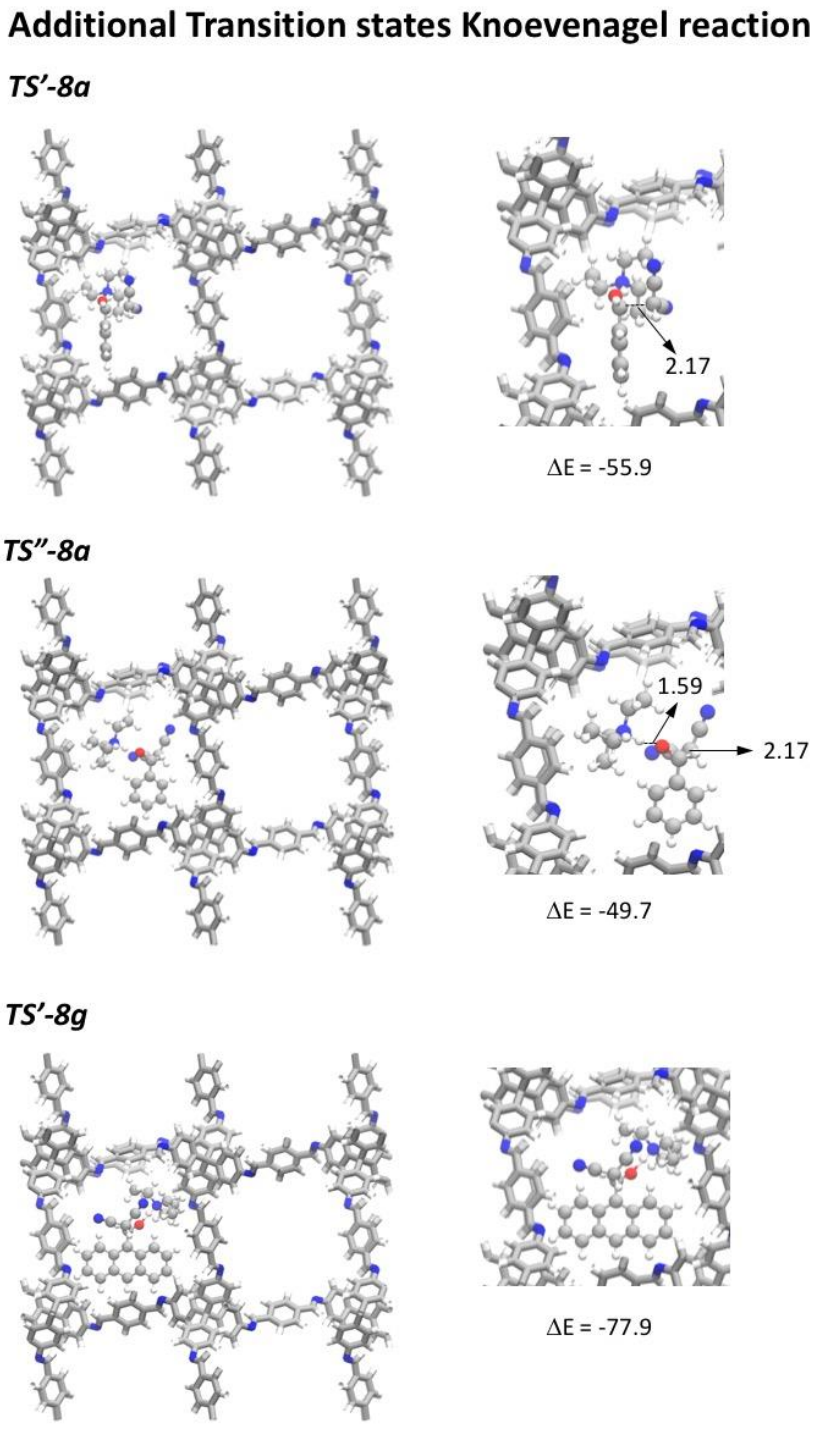

Figure S25. Optimized geometries of the transition states associated with the Knoevenagel reaction either with **8a** or **8g** not reported in the main text and their relative energies (□E) with respect to reactants (NEt_3@COF + $CH_2(CN)_2$ + RCHO. Distances are in Å and energies in kJ mol^{-1}.

11. Conclusiones finales de la presente tesis doctoral

La presente tesis doctoral ha profundizado en dos áreas diferentes de la catálisis en Química: la fotocatálisis molecular y la organocatálisis basada en materiales COF y MOF.

A continuación, se exponen las conclusiones de cada parte y unas conclusiones globales.

11.1. Fotocatálisis molecular.

Se ha desarrollado un método fotocatalítico mediado por luz visible para la transposición de ciclopropanos funcionalizados. El método tiene las siguientes características:

- Es un método suave, que solo requiere disolver el ciclopropano y el catalizador e irradiar la mezcla a temperatura ambiente con luz azul.
- Es válido tanto para formilciclipropanos (unidos a un enlace C=O) como para vinilciclipropanos (unidos a un enlace C=C) pudiendo obtener tanto 2,3-dihidrofuranos como ciclopentenos respectivamente. La importancia de este hecho radica en que los métodos de transposición descritos hasta la fecha solo suelen ser específicos para un doble enlace. Para ambos tipos de sustratos, se investigó el alcance de la reacción, viendo que era compatible con bastantes grupos funcionales
- Diferentes métodos experimentales y computacionales revelaron que se trata de un proceso de transferencia de energía. En este proceso juega un papel fundamental el grupo nitro unido al ciclopropano, ya que rebaja la energía de excitación de éste, equiparándola con la energía de triplete del catalizador. Así, el catalizador excitado transmite eficientemente la energía de triplete al ciclopropano, el cual sufre una ruptura homolítica y evoluciona hacia el producto de transposición.

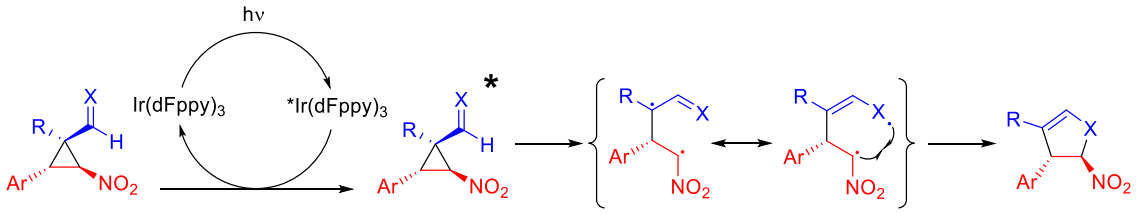

La fotocatálisis también ha sido usada para crear un nuevo método para la alilación de nuecleófilos como índoles, pirroles, aminas, alcoholes… El cuidadoso estudio de las condiciones de reacción y del proceso fotocatalítico ha llevado a desarrollar dicho método con dos importantes características, que son la selectividad *Z*/*E* y la ausencia de metales, además de que se han obtenido importantes conclusiones sobre el mecanismo:

- Ausencia de metales: La reacción se puede llevar a cabo con fotocatalizadores orgánicos como phenotiazinas y fenoxacinas, lo cual supone una ventaja frente a la mayoría de métodos de alilación de nucleófilos reportados hasta la fecha, que requieren el uso de catalizadores metálicos.
- Selectividad *Z*/*E*: La utilización del catalizador fenotiazina y la irradiación con luz ultravioleta (365 nm) lleva a la obtención del producto *Z*. Por otro lado, el uso del catalizador PMP-fenoxacina y la irradiación con luz azul (420 nm), lleva la obtención del isómero *E*, demostrando que la correcta manipulación del fotocatalizador y de sus propiedades fotofísicas juega un papel importante en la síntesis orgánica. Además, el estudio del alcance de la reacción demostró que la obtención de ambos isómeros es compatible con una amplia variedad de sustratos alílicos y de nucleófilos.
- Es un método muy general ya que permite la alilación de diversos nucleófilos: heterociclos, aminas alcoholes… permitiendo crear enlaces C-C, C-N y C-O respectivamente.
- La reacción transcurre por un proceso foto-rédox. Por transferencia de un único electrón, el catalizador excitado reduce al sustrato alílico, el cual expulsa el grupo saliente, resultando en un radical alílico. El catalizador oxidado toma un electrón del radical alilo, generándose un catión alilo, el cual es atacado finalmente por el nucleófilo. Además, en el caso de la obtención del isómero *Z*, el fotocatalizador tiene el papel de isomerizar el sustrato por un proceso de transferencia de energía. Se trata por tanto de un proceso en el cual el fotocatalizador puede actuar por los dos caminos principales de la fotocatálisis en un mismo proceso, demostrando la gran versatilidad de estas sustancias en el estado excitado.

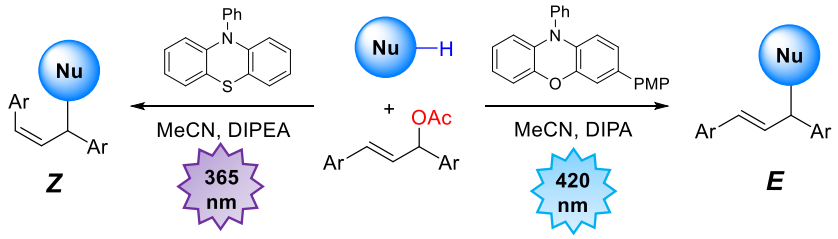

11.2. Materiales organocatalíticos.

Se ha sintetizado un MOF, análogo del IRMOF-16, que contiene el grupo funcional escuaramida en su estructura. El análisis de este MOF, llamado Sq_IRMOF-16, y los estudios catalíticos realizados con él llevan a concluir:

- La síntesis del Sq_IRMOF-16 no requiere ninguna modificación post-sintética y se trata de un material cristalino
- Cataliza la apertura de epóxidos por anilinas, de manera mucho más eficiente que la escuaramida molecular, demostrando que la distribución de las escuaramidas a lo largo de la estructura porosa del material evita la agregación de estos centros catalíticos.

- Dicho MOF tiene utilidad sintética, puesto que se llevaron a cabo varias reacciones “tándem” y “one-pot” catalizadas por dicho MOF, aislando los productos con buenos rendimientos.

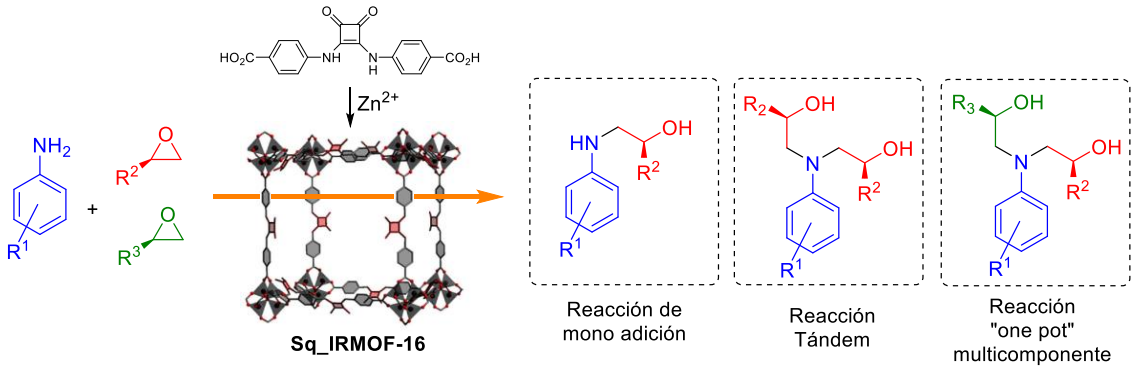

Partiendo de un COF ya descrito, el COF-300, se llevaron a cabo estudio de funcionalización de los poros por interacciones no covalentes, llegándose a las siguientes conclusiones:

- Es posible funcionalizar el material con pequeñas moléculas de ácido y de base, que quedan dentro de los poros del COF unidas al esqueleto de este mediante interacciones supramoleculares, como enlace de hidrógeno. Además, con la misma muestra de material, mediante técnicas de lavado y vacío, se puede cambiar la funcionalización de ácido a básica y viceversa.
- El material funcionalizado con centros básicos es capaz de catalizar eficientemente la condensación de Knoevenagel. Se observa una selección por tamaño en esta reacción.
- El material funcionalizado con centros ácidos fue empleado en catalizar la apertura de epóxidos. En este caso los resultados fueron moderados, obteniéndose rendimientos algo más bajos que en el caso de la catálisis básica y siendo más limitado el alcance de la reacción.
- Investigaciones experimentales y computacionales revelaron que la catálisis se produce dentro de poros del material, pero en los poros más superficiales. Por este motivo es más eficiente en este tipo de catálisis la versión amorfa del COF-300 que el propio COF-300 cristalino, ya que el primero tiene más superficie. También se comprobó que ciertos reactivos pueden degradar la estructura del COF, especialmente la anilina.

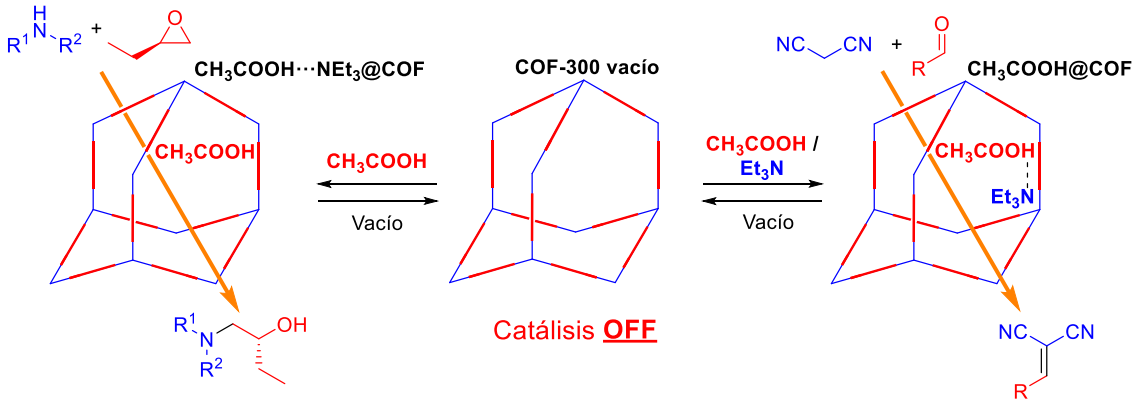

11.3. Conclusiones globales

La fotocatálisis se ha empleado satisfactoriamente para solucionar problemas dentro del campo de la síntesis orgánica y desarrollar nuevas metodologías. En los dos proyectos llevados a cabo en esta tesis doctoral dentro de este campo, se ha constatado que la fotocatálisis es una herramienta fundamental que permite llevar a cabo estrategias difíciles de realizar por métodos térmicos y conseguir nuevos resultados en la síntesis orgánica.

Así, en el proyecto de expansión de ciclopropanos, aunque existen numerosos artículos de transposiciones de ciclopropanos estructuralmente muy diversos, la fotocatálisis ha permitido el desarrollo de un método de transposición de ciclopropanos con otras estructuras, en condiciones más suaves que las descritas hasta la fecha y mucho más general. De la misma manera, si bien el proceso de alilación de nucleófilos es un proceso bastante descrito hasta la fecha, la fotocatálisis ha permitido desarrollar un método muy general de alilación de bastantes tipos de nucleófilos, sin la necesidad de usar catalizadores metálicos, y con una gran ventaja respecto a los métodos térmicos tradicionales, que es la posibilidad de acceder a los dos isómeros del doble enlace.

De esta manera, al igual que en muchas publicaciones en las últimas décadas, queda patente el gran potencial de la fotocatálisis y la necesidad de seguir investigando en ella. Además, es fundamental no solo usarla como herramienta, si no también investigar en detalle su funcionamiento y entender los procesos fotofísicos, ya que ello puede llevar a encontrar nuevas aplicaciones. Por ejemplo, el hallazgo del método que permite la alilación para la obtención del isómero *Z* o *E* en función del catalizador y la longitud de onda irradiada, nunca hubiera sido posible sin el estudio de cómo diversos grupos funcionales en los fotocatalizadores modifican sus propiedades fotofísicas y fotoquímicas.

Mientras que la fotocatálisis se ha empleado en solucionar problemas concretos de la síntesis orgánica, la investigación llevada a cabo en organocatálisis heterogénea, segunda parte de la tesis, ha sido llevada a cabo a un nivel más básico.

Desde la aparición de los MOF y los COF, se ha desarrollado una amplia investigación para encontrar diferentes aplicaciones a estos materiales, entre ellos la catálisis. Los dos proyectos realizados en esta tesis doctoral sobre materiales van dentro de esta línea. La investigación en catálisis con COF y MOF está en un momento en el que no se busca tanto en desarrollar nuevas reacciones orgánicas para la obtención de productos complejos si no en solucionar problemas más generales y conceptuales.

Ejemplo de esto es el proyecto desarrollado sobre el MOF con escuaramidas, o los antecedentes que existen sobre esto. La principal meta de estos proyectos es solucionar un problema bien conocido de la Organocatálisis homogénea, que es el auto-ensamblaje de ciertos catalizadores de enlace de hidrógeno y su pérdida de eficiencia. Aunque ya existían antecedentes, el trabajo de esta tesis se ha centrado en buscar más aplicaciones a este tipo de MOF, como la reacción de apertura de epóxidos.

En esta búsqueda de desarrollar nuevos conceptos en el campo de los materiales se desarrolló del proyecto de funcionalización supramolecular de COF. Como se ha comentado anteriormente, el proyecto no buscaba una gran complejidad en las reacciones llevadas a cabo, si no en desarrollar la idea de una funcionalización sencilla de catalizadores heterogéneos, aunque los resultados van de buenos, en el caso de la catálisis básica, a moderados, en el caso de la catálisis ácida.

De esta forma, la investigación de los materiales MOF y COF tiene un gran futuro y está lleno de posibilidades. La gran versatilidad en el diseño de estos materiales permitirá desarrollar nuevos conceptos y encontrar más aplicaciones.

Finalmente, cabe destacar que en los dos proyectos de materiales de la presente tesis doctoral, se han trasladado conceptos de Organocatálisis al campo de la catálisis heterogénea, el cual tiene mayor aplicabilidad en procesos industriales por la mayor facilidad para la purificación de los productos y la reutilización de los catalizadores.

Así, en los dos proyectos de catálisis heterogénea se han desarrollado metodologías para la obtención de productos complejos mientras que en los dos proyectos de catálisis homogénea se han desarrollado procesos más sencillos pero con una utilidad más práctica.

Apéndice

Durante el periodo de doctorado, además de las cinco publicaciones contenidas en esta tesis doctoral, se han desarrollado otros dos trabajos que se recogen en los siguientes artículos:

- L. Marzo, J. Luis-Barrera, R. Mas-Ballesté, J. L. García Ruano, J. Alemán, "Stereodivergent Aminocatalytic Synthesis of *Z*- and *E*-Trisubstituted Double Bonds from Alkynals", *Chem. Eur. J.* **2016**, *22*, 16467-16477 (destacado como Hot Paper).
- Gini, J. Bamberger, J. Luis-Barrera, M. Zurro, R. Mas-Ballesté, J. Alemán, O. García Mancheño, "Synthesis of 3-Benzazepines by Metal-Free Oxidative C–H Bond Functionalization Ring Expansion Tandem Reaction", *Adv. Synth. Catal.* **2016**, *358*, 4049-4056.

La última publicación derivó de una colaboración entre los grupos de investigación del Dr. José Alemán Lara y la Dra. Olga García Mancheño. Parte de este trabajo fue realizado durante una estancia en los meses de junio y julio del 2015 en el grupo de investigación de la Dra. Olga García Mancheño en la Universidad de Regensburg (Alemania).